

Winter 2007

I The synthesis and coordination chemistry of novel 1,1,1-tris(aminomethyl)ethane (TAME) derived ligands and their use as size selective fluorescent zinc(II) sensors II The synthesis of strongly and weakly binding ligands with nitrogen, oxygen, and sulfur-donor groups to be used as receptors in fluorescent ratiometric indicators for transition metal ions

Daniel Patrick Kennedy
University of New Hampshire, Durham

Follow this and additional works at: <https://scholars.unh.edu/dissertation>

Recommended Citation

Kennedy, Daniel Patrick, "I The synthesis and coordination chemistry of novel 1,1,1-tris(aminomethyl)ethane (TAME) derived ligands and their use as size selective fluorescent zinc(II) sensors II The synthesis of strongly and weakly binding ligands with nitrogen, oxygen, and sulfur-donor groups to be used as receptors in fluorescent ratiometric indicators for transition metal ions" (2007). *Doctoral Dissertations*. 410.
<https://scholars.unh.edu/dissertation/410>

This Dissertation is brought to you for free and open access by the Student Scholarship at University of New Hampshire Scholars' Repository. It has been accepted for inclusion in Doctoral Dissertations by an authorized administrator of University of New Hampshire Scholars' Repository. For more information, please contact nicole.hentz@unh.edu.

I. THE SYNTHESIS AND COORDINATION CHEMISTRY OF NOVEL 1,1,1-
TRIS(AMINOMETHYL)ETHANE (TAME) DERIVED LIGANDS AND THEIR USE
AS SIZE SELECTIVE FLUORESCENT ZN(II) SENSORS. II. THE SYNTHESIS
OF STRONGLY AND WEAKLY BINDING LIGANDS WITH N, O, AND S-DONOR
GROUPS TO BE USED AS RECEPTORS IN FLUORESCENT RATIOMETRIC
INDICATORS FOR TRANSITION METAL IONS.

BY

DANIEL PATRICK KENNEDY
B.S., University of New Hampshire, 2002

DISSERTATION

Submitted to the University of New Hampshire
in Partial Fulfillment of
the Requirements for the Degree of
Doctor of Philosophy
in
Chemistry

December, 2007

UMI Number: 3290103

INFORMATION TO USERS

The quality of this reproduction is dependent upon the quality of the copy submitted. Broken or indistinct print, colored or poor quality illustrations and photographs, print bleed-through, substandard margins, and improper alignment can adversely affect reproduction.

In the unlikely event that the author did not send a complete manuscript and there are missing pages, these will be noted. Also, if unauthorized copyright material had to be removed, a note will indicate the deletion.

UMI[®]

UMI Microform 3290103

Copyright 2008 by ProQuest Information and Learning Company.

All rights reserved. This microform edition is protected against unauthorized copying under Title 17, United States Code.

ProQuest Information and Learning Company
300 North Zeeb Road
P.O. Box 1346
Ann Arbor, MI 48106-1346

This dissertation has been examined and approved.

Dissertation Director, Roy Planalp,
Associate Professor of Inorganic Chemistry

N. Dennis Chasteen, Carpenter Professor of
Biophysical/Bioinorganic Marine Chemistry

W. Rudolph Seitz, Professor of Analytical
Chemistry

Edward H. Wong, Professor of Inorganic
Chemistry

Martin W. Brechbiel, Head of the Radioimmune
Inorganic Chemistry Section, National Cancer
Institute

Date

DEDICATION

Because of her love, patience and sense of humor I dedicate this dissertation to my wife Katie.

ACKNOWLEDGEMENTS

I would like to thank my advisor Dr. Roy Planalp for his guidance during my post-baccalaureate career at UNH. Scientific curiosity is the foundation of our professional relationship. Roy's flare for world music and culture, his penchant for travel and his ability to relate to diverse groups of people make him a truly unique and remarkable individual.

Our collaborators Dr. Arnold Rheingold, Dr. Antonio DiPasquale, Dr. W. Rudi Seitz, John Osambo, Dr. Shawn Burdette, Aaron Atkinson, Dr. N. Dennis Chasteen, Dr. Fadi Bou-Abdallah, Dr. Frank Torti, Dr. Suzi Torti and Dr. Martin Brechbiel have allowed us to keep many irons in the fire. Professional assistance from Dr. Robert Hancock and Dr. Christoph Fahrni is also appreciated.

I also must thank my committee Dr. Planalp, Dr. Edward Wong, Dr. Seitz, Dr. Chasteen and Dr. Brechbiel for taking the time to read this dissertation. It is an honor to have such a distinguished panel of scientists involved in my professional training.

Although many members of the UNH faculty have inspired me throughout the years, the teaching efforts of Dr. Wong, Dr. Gary Weisman and Dr. Chuck Zercher have greatly influenced my scientific thinking.

Help from Cindi Rohwer, Peg Torch, Kathy Gallagher, John Wilderman, Robert Constantine, Richard Haney and Allen Perkins is also much appreciated.

To present and past Planalp group members and to all of my friends at UNH: we have shared success, failure and tragedy. Don't let the grind empty your tanks.

Most importantly to my families Kennedy and Meehan: you have all been there for me when I needed you most...for that I am forever grateful.

TABLE OF CONTENTS

DEDICATION.....	iii
ACKNOWLEDGEMENTS.....	iv
LIST OF TABLES.....	ix
LIST OF FIGURES.....	xi
LIST OF SCHEMES.....	xx
ABSTRACT.....	xxiii

CHAPTER	PAGE
1: NOVEL LIGANDS DERIVED FROM THE 1,1,1- TRIS(AMINOMETHYL)ETHANE (TAME) FRAMEWORK: THE NI(II) MEDIATED TEMPLATE REACTION/TETRAHYDROBORATE REDUCTION	1
Summary.....	1
1.1 Introduction.....	2
1.2 Schiff base ligands and the template effect.....	3
1.3 Tripodal chelators.....	10
1.3.1 TACH systems.....	11
1.3.2 TACN systems.....	20
1.3.3 Cage ligands derived from sen.....	23
1.3.4 TREN ligands.....	26
1.3.5 1,3,5-Tris(aminomethyl)benzene ligands.....	31
1.4 Summary-The challenge of TAME.....	33
1.5 The preparation of the TAME framework.....	35
1.6 The Ni(II)-mediated template reaction of TAME.....	41
1.7 Tetrahydroborate reduction.....	47
1.8 Comparison of ligand field poperties of TAMEpyr and TAMEpyr- trisimine via Ni(II) complexes.....	49
1.9 Liberation of TAMEpyr I.60 and the preparation of benzyloxy- TAMEpyr I.64.....	56
1.10 Coordination Chemistry of TAMEpyr with various metal ions.....	60
1.11 Conclusions and future work.....	67

2. TAME DERIVED FLUORESCENT SENSORS FOR ZN(II)	68
Summary.....	68
2.1 Fluorescence: discussion adapted from reference (100).....	69
2.2 Applications of fluorescence: discussion adapted from reference (102).....	73
2.3 Photoinduced electron transfer.....	75
2.4 Proton PET sensors.....	79
2.5 Alkali and alkaline earth PET sensors.....	82
2.6 Zn(II), Cd(II), Hg(II) PET sensors.....	89
2.7 Metal-ion internal charge transfer (ICT) and twisted internal charge transfer (TICT) sensors.....	98
2.8 Electronic energy transfer (EET) metal-ion sensors (100).....	104
2.9 Excimer and exciplex metal sensors.....	109
2.10 Coordination-enhanced fluorescence metal-ion sensors.....	111
2.11 Novel TAME-based PET and CEF metal ion sensors.....	118
2.12 Synthesis of azaaromatic aldehydes.....	119
2.13 Synthesis of TAME-based ligands for metal-ion sensing via the template methodology.....	144
2.14 Photophysical properties of TAMEisoquin, and 6,7-DMTI: Zn(II) luminescent sensing.....	168
2.15 Conclusions and future work.....	180
3. FLUORESCENT RATIO-METRIC INDICATORS FOR TRANSITION METAL IONS: A GENERAL APPROACH	182
Summary.....	182
3.1 Introduction.....	184
3.2 Previous work within the Seitz group.....	188
3.3 Swelling polymeric networks for the detection of Cu(II).....	192
3.4 Preparation of metal ion receptors.....	195
3.5 Sensors prepared with the phenyl-IDA comonomer III.2 and bipyridyl comonomer III.1.....	204
3.6 Conclusions and future work.....	208
4. EXPERIMENTAL SECTIONS	210
4.1 General methods.....	210
4.2 Solvents.....	212
4.3 Reagents.....	214
4.4 Synthesis and characterization.....	217
4.4.1 Chapter 1 experimentals.....	218
4.4.2 Chapter 2 experimentals.....	234

4.4.3 Chapter 3 experimentals.....	269
APPENDIX. ASPECTS OF THE IRON COORDINATION CHEMISTRY OF CURCUMIN AND THE SYNTHETIC DERIVATIVE DMCU	282
Summary.....	282
Introduction.....	283
Reported Iron Coordination Chemistry of Curcumin.....	285
The Challenge of Curcumin.....	288
Ligand Preparation and Iron Complexation Experiments.....	288
Conclusions and Future Work.....	295
REFERENCES.....	298
SELECTED SPECTRA.....	322

LIST OF TABLES

Table 1 The six-coordinate ionic radii of selected main group metals	9
Table 2 Protonation and formation constants for the hexadentate tripodal ligand sen I.21.(57)	25
Table 3 Protonation and Zn(II)-formation constants of TRENpyr I.23.	28
Table 4 Formation constants ($\log\beta_{3,1,0}$) for ligands I.27 and I.26.	32
Table 5 Crystal data and structure refinement for $[\text{Fe}(\text{TACHTz})](\text{ClO}_4)_2$	45
Table 5 Crystal data and structure refinement for $[\text{Fe}(\text{TACHTz})](\text{ClO}_4)_2$	46
Table 6 Position of the <i>d-d</i> electronic transitions for I.50 and I.62. The spectra were collected at 25.0°C in MeCN. The exact position of the ${}^3\text{A}_{2g} \rightarrow {}^3\text{T}_{1g}(\text{F})$ transitions were obscured by the aforementioned MLCT band.	59
Table 7 The 1:1 M:L stoichiometry data. The air-sensitive nature of the Fe(II) and Co(II) complexes prevented ESI-MS analysis.	61
Table 8 Visible-near IR absorbance spectroscopy of $[\text{M}(\text{TAMEpyr})]^{2+}$	66
Table 9 Crystal data and structure refinement for $[\text{Ni}(\text{TAMEisoquin-}$ $\text{trisimine})](\text{ClO}_4)_2 \cdot \text{MeCN}$	151
Table 10 Selected bond lengths and bond angles for $[\text{Ni}(\text{TAMEisoquin-}$ $\text{trisimine})](\text{ClO}_4)_2 \cdot \text{MeCN}$	154
Table 11 Crystal data and structure refinement for $\text{Zn}(\text{TAMEisoquin})](\text{ClO}_4)_2 \cdot 5/3\text{MeCN}$	156
Table 12 Selected data from the structure of $[\text{Zn}(\text{TAMEisoquin})]^{2+}$	159
Table 13 Visible-near IR absorbance data for $[\text{Ni}(6,7\text{-DMTI-trisimine})](\text{ClO}_4)_2$ in MeCN at 25°C.	163

Table 14 Reagents used and their commercial sources	214
Table 15 Reported protonation and binding constants of curcumin with iron.(278)	286
Table 16 Measured magnetic moments for various solutions of curcumin and Fe(III).	294

LIST OF FIGURES

Figure 1. Formation of a Schiff base.....	3
Figure 2 The structures of some interesting acyclic Schiff base metal chelators ..	5
Figure 3 Examples of the thermodynamic and kinetic metal template effect.....	7
Figure 4 Template synthesis of Schiff base macrocycles.....	8
Figure 5 Ni(II)-mediated template reaction of 2,6-disubstituted pyridines.(30)	10
Figure 6 A selection of reported TACH-based chelators.....	11
Figure 7 Representation of the inner-coordination sphere of [Zn(TACHpy-trisimine)] ²⁺	12
Figure 8 Trigonal twist angle α for [M(TACHpyr-trisimine)] ²⁺	13
Figure 9 Representation of [Ga(TACHpyr)](NO ₃) ₃ ·DMF. The image was created from data obtained in the Cambridge Structural Database (CSD).....	14
Figure 10 Top-view down of [Hg(TACHpyr)](ClO ₄) ₂ highlighting the nearly trigonal prismatic geometry of this complex. The image was created from data obtained in the Cambridge Structural Database (CSD).	16
Figure 11 Fe(II)-mediated oxidation of TACHpyr under ambient conditions.(42) 17	
Figure 12 <i>N</i> -alkylated derivatives of TACHpyr.	18
Figure 13 Methylated and methoxylated derivatives of TACHpyr.(42) The structure in (a) is the open-form of apoTACH-x-Rpyr and the structure in (b) is the closed-form that occurs upon coordination.	19
Figure 14 The tripodal ligand TACNpyr I.20.....	20
Figure 15 Top-down view of the helical inversion of [Fe(TACNpyr)] ²⁺	21
Figure 16 The putative structure of [Na(TACNpyr)] ²⁺	22

Figure 17 Reversible and stereoselective N- to C-bonded rearrangement of (+)- [Co(TACNpyr)] ³⁺	22
Figure 18 The oxidation product (+)-[Co(TACNpyr-OH)] ³⁺	23
Figure 19 A select collection of the so-called “sarcophagines”	24
Figure 20 The structures of TREN I.22 TRENpyr I.23.....	27
Figure 21 Structures of [Mn(TRENpyr)](PF ₆) ₂ and [Zn(TRENpyr)](ClO ₄) ₂ . The images were created from data obtained in the Cambridge Structural Database (CSD).....	28
Figure 22 Preparation of [Fe(TRENpyr-trisimine)]X ₂	30
Figure 23 Structure of [Fe(TRENpyr-trisimine)](ClO ₄) ₂ . The image was created from data obtained in the Cambridge Structural Database (CSD).....	31
Figure 24 Chelators based on 1,3,5-tris(aminomethyl)benzene I.25.....	32
Figure 25 Putative structure of the ternary 3:1:3 M:L ¹ :L ² complex. In this case M=Cu(II), L ¹ =I.26, and L ² =o-phenanthroline.	33
Figure 26 The structure of [Fe(TAMEpyr-trisimine)](ClO ₄) ₂ . The image was created from data obtained in the Cambridge Structural Database (CSD).....	34
Figure 27 Proposed mechanism of ring-closure.....	40
Figure 28 Products isolated from the attempted direct preparation of TAMEpyr- trisimine.....	42
Figure 29 Preparation of the novel CrN ₃ O ₃ complex I.55.....	44
Figure 30 The ORTEP view of the cation [Fe(TACHTz)] ²⁺	47
Figure 31 Putative mechanism for tetrahydroborate reduction of [Ni(TAMEpyr- trisimine)] ²⁺ I.50.....	49

Figure 32 The visible absorbance spectra of [Ni(TAMEpyr-trisimine)] ²⁺ 1.50 and [Ni(TAMEpyr)] ²⁺ 1.58 in MeCN at 25°C.....	50
Figure 33 Splitting of metal <i>d</i> -orbitals in an octahedral field for a <i>d</i> ⁸ ion.(94)	51
Figure 34 Tanabe-Sugano diagram for a <i>d</i> ⁸ metal ion.	54
Figure 35 Assessment of Δ_o/B' for [Ni(TAMEpyr)] ²⁺ 1.58.	55
Figure 36 X-ray crystal structure of the cation [Zn(TAMEpyr)] ²⁺ 1.69.....	62
Figure 37 Partial ¹ H-NMR spectra for [Fe(TAMEpyr)] ²⁺ (top) in MeCN- <i>d</i> ₃ and [In(TAMEpyr)] ³⁺ (bottom) in DMSO- <i>d</i> ₆	65
Figure 38 The Jablonski diagram. The figure was borrowed from www.theochem.kth.se/people/orubiop/jablonski2.gif	69
Figure 39 Examples of fluorometric reagents for inorganic species from Skoog, Holler and Nieman.(102)	74
Figure 40 A fluorophore-spacer-receptor sensor turned “off” by PET in the absence of the analyte.....	76
Figure 41 A fluorophore-spacer-receptor sensor turned “on” by blocking the PET channel upon analyte recognition.....	77
Figure 42 Molecular orbital picture of PET when the receptor is vacant. The sensor will absorb light ($h\nu_{excite}$) but will not fluoresce.	78
Figure 43 Molecular orbital picture of PET when the receptor is occupied. The sensor is now “turned-on”.	79
Figure 44 The calculated superimposed HOMO and LUMO surfaces of a <i>p</i> -anilino-perylenetetracarboximide. Note the node that is collinear with the imide nitrogen atoms which serves to decouple the fluorophore from the anilino-	

receptor. The image was generated in Spartan at the semi-empirical PM3 level of theory.....	80
Figure 45 Examples of PET-H ⁺ sensor molecules.....	81
Figure 46 PET sensors for alkali and alkaline earth metals developed by Lincoln <i>et al.</i>	83
Figure 47 Examples of PET sensors for Na(I) and Li(I) respectively.....	85
Figure 48 A “turn-off” Ca(II) luminescent sensor. The starred sites in the figure are linked forming a conical-like structure.....	86
Figure 49 Gee’s novel Ca(II)-selective PET sensor.....	87
Figure 50 Pearson’s azacrown ether Mg(II) and Ca(II) sensors.....	88
Figure 51 Nakahara’s micellar Ba(II) PET sensor.....	89
Figure 52 Fluorescein-based Zn(II)-PET sensors. The identity of X can be H, Cl, or F.....	91
Figure 53 Coumarin-based PET sensors for Zn(II).....	92
Figure 54 Lippard’s ratiometric Zn(II) sensor.....	93
Figure 55 Pyrene-based mesoscopic Zn(II)-sensor.....	94
Figure 56 The structure of the non-ionic surfactant Triton X-100 II.25.....	95
Figure 57 Gunnlaugsson’s Zn(II)-sensor.....	95
Figure 58 Gunnlaugsson’s exciplex sensors for Zn(II) (left) and Cd(II) (right).....	96
Figure 59 Lippard and Nolan’s Hg(II)-sensor.....	97
Figure 60 Qian’s luminescent Hg(II)-sensor.....	98
Figure 61 Schematic of ICT metal ion sensing.....	99
Figure 62 ICT-based turn-off sensor for Zn(II).....	99

Figure 63 ICT-Hg(II) sensor.	100
Figure 64 An ICT Pb(II) sensor.	101
Figure 65 The structure of quinizarin II.34.....	102
Figure 66 A TICT-based sensor for Pb(II).	102
Figure 67 TICT-assisted luminescent metal-ion sensor.	103
Figure 68 TICT-based Ca(II) sensor.	104
Figure 69 An EET Al(III) sensor.	108
Figure 70 A hydroxamate turn-off sensor selective for Fe(III).	108
Figure 71 A hydrophobic anthracene fluorophore is attached to a novel Cu(II) receptor.....	109
Figure 72 Licchelli's <i>et al.</i> excimer-forming Zn(II) and Cd(II) sensor. The value of the n-ethyl units varies from 2-5.	110
Figure 73 Luminescent Ca(II) and Ba(II) sensors.....	111
Figure 74 Inversion of a nonluminescent $n\pi^*$ S ₁ state to an emissive $\pi\pi^*$ S ₁ state.	112
Figure 75 Quinoline-based CEF sensors for Zn(II).....	113
Figure 76 Mikata <i>et al.</i> 's TQEN II.48.	114
Figure 77 Representation of [Zn(TQEN)](ClO ₄) ₂ from the crystal structure data. The data was obtained from the Cambridge Structural Database (CSD).....	116
Figure 78 Mikata and coworkers' quinoline Zn(II) sensors.	117
Figure 79 Generic approach to TAME-based luminescent metal-ion sensors. .	119
Figure 80 The structure of the soluble hemiacetal-aluminate complex II.61.(191)	122

Figure 81 The structure of Fremy's salt in solution (left) and solid state (right).	128
Figure 82 UV-visible absorbance spectrum of Fremy's salt in 1M KOH.....	130
Figure 83 EPR spectrum of ca. 10^{-4} M Fremy's salt at 77K in 1M KOH.....	131
Figure 84 The energy levels for an unpaired electron in a magnetic field interacting with a nitrogen nucleus.....	132
Figure 85 Literature EPR spectrum of Fremy's salt.(217)	133
Figure 86 Thwarted homolytic aromatic substitution on substrate II.77.....	134
Figure 87 The feeble nucleophilic character of C6 likely prevents the desired regioselective acylation.....	137
Figure 88 The structure of 7-azacoumarin II.92.	138
Figure 89 The ORTEP views of $[\text{Zn}(\text{TACHquin})]^{2+}$ (two molecules A and B related by disorder) with 50% occupancy of C27 to C36.....	146
Figure 90 The visible-near IR absorbance spectrum of $[\text{Ni}(\text{TAMEquin-trisimine})](\text{ClO}_4)_2$ in MeCN (T=25°C).....	147
Figure 91 The visible-near IR absorbance spectra of $[\text{Ni}(\text{TAMEisoquin-trisimine})](\text{ClO}_4)_2$ II.113 (orange) and $[\text{Ni}(\text{TAMEquin-trisimine})](\text{ClO}_4)_2$ II.111 (yellow) in MeCN (T=25°C).	151
Figure 92 The ORTEP view of the cation $[\text{Ni}(\text{TAMEisoquin-trisimine})]^{2+}$. Note a C_3 axis that is co-linear with atoms C35, C34, and Ni1. The perchlorate anions and MeCN solvate have been eliminated for illustrative clarity.	153
Figure 93 The ORTEP view of cation A for $[\text{Zn}(\text{TAMEisoquin})]^{2+}$. The perchlorate anions and MeCN solvate have been removed for illustrative clarity.	158

Figure 94 Partial $^1\text{H-NMR}$ spectra of the Zn(II) and Cd(II) complexes of TAMEisoquin. The reader should direct their eyes to the spectral region between 3.0 and 5.0 ppm. Solvent impurities are indicated by an asterisk (*).....	160
Figure 95 Geometry optimized structure of $[\text{Cd}(\text{TAMEisoquin})]^{2+}$ at the B3LYP/LANL2DZ level of theory. Note the splaying of the isoquinoliny groups.	161
Figure 96 Putative structure of the bisazacoumarin complex II.121.....	167
Figure 97 UV spectra of 56 μM TAMEisoquin and $[\text{Zn}(\text{TAMEisoquin})]^{2+}$ in 50% aqueous DMF (v/v) at 25.0°C.....	169
Figure 98 Fluorescence spectra ($\lambda_{\text{ex}}=321$ nm) of 14 μM TAMEisoquin and $[\text{Zn}(\text{TAMEisoquin})]^{2+}$ in 50% aqueous DMF at 25.0°C.	170
Figure 99 The effect of concentration of $[\text{Zn}(\text{TAMEisoquin})]^{2+}$ on emission intensity (F) at $\lambda_{\text{em}}=355$ nm in 50% aqueous DMF at 25.0°C.....	171
Figure 100 Quantum yield determination of $[\text{Zn}(\text{TAMEisoquin})](\text{ClO}_4)_2$ in 50% aqueous DMF at 25.0°C. Serial dilutions of quinine were prepared in 1N H_2SO_4	172
Figure 101 Screening emission enhancements of TAMEisoquin in the presence of 1.0 equivalent of various cationic analytes. The experiments were conducted in 50% aqueous DMF at 25.0°C with $[\text{TAMEisoquin}]_{\text{Total}}=14\mu\text{M}$	174
Figure 102 UV spectra of 50 μM 6,7-DMTI and $[\text{Zn}(6,7\text{-DMTI})]^{2+}$ in 50% aqueous DMF at 25.0°C.	176
Figure 103 Fluorescence spectra ($\lambda_{\text{ex}}=326$ nm) of 5 μM 6,7-DMTI and $[\text{Zn}(6,7\text{-DMTI})]^{2+}$ in 50% aqueous DMF at 25.0°C.	177

Figure 104 The effect of concentration of $[Zn(6,7-DMTI)]^{2+}$ on emission intensity (F) at $\lambda_{em}=360$ nm in 50% aqueous DMF at 25.0°C.....	178
Figure 105 Quantum yield determination of $[Zn(6,7-DMTI)]^{2+}$ in 50% aqueous DMF at 25.0°C. Serial dilutions of quinine were prepared in 1 N H_2SO_4	179
Figure 106 Screening emission enhancements of 6,7-DMTI II.119 in the presence of 1.0 equivalent of various cationic analytes. The experiments were conducted in 50% aqueous DMF at 25.0°C with $[TAMEisoquin]_{Total}=20$ μM	180
Figure 107 Generic representation of a site-selective TAME-based luminescent sensor for the cellular analysis of Zn(II).	181
Figure 108 The structure of Holtz and Asher's Pb(II) polymeric sensor.	185
Figure 109 The structure of the luminescent dye PtOEP.	186
Figure 110 Fluorescence quenching of MPS-PPV with MV^{2+} . The figure was borrowed from reference (254).....	187
Figure 111 The reversal of MPS-PPV fluorescence quenching upon avidin binding. The functionality labeled "B" is a biotinylated residue on the polymer which has a large affinity for the analyte. The figure was borrowed from reference (254).....	188
Figure 112 Polymer sensor that detects changes in the ionic strength of aqueous solutions.....	189
Figure 113 Swelling/shrinking polymeric beads suspended in a hydrogel membrane.....	191
Figure 114 Representation of our novel Cu(II)-sensor.....	194
Figure 115 Ligating comonomers for FRET-based Cu(II) sensing.....	195

Figure 116 Monomeric FRET pair for incorporation into the swelling polyNIPA polymers. The naphthalene monomer acts as the donor and the anthracene monomer acts as the acceptor.....	205
Figure 117 Cu(II) titration of polyNIPA doped with compound III.1.....	207
Figure 118 Cu(II) titration of polyNIPA doped with compound III.2.....	208
Figure 119 Schematic of the homemade amperostatic coulometric titrator.....	249
Figure 120 The structure of curcumin.	283
Figure 121 Calculated pM values for curcumin with Fe(III) (blue curve) and Fe(II) (pink curve) as a function of pH.....	287
Figure 122 The MALDI-TOF MS of the isolated brown powder.	291
Figure 123 EPR spectra of standard Fe(III)-EDTA and Fe(III)-curcumin.	292
Figure 124 Proposed mechanism for curcumin mediated reduction of Fe(III)...	295

LIST OF SCHEMES

Scheme 1 The preparation of TAME·3HCl.....	35
Scheme 2 Dunn's preparation of TAME.....	37
Scheme 3 The preparation of TAME derivative I.43.....	38
Scheme 4 Attempted preparation of tetramine I.47.....	39
Scheme 5 Formation of azetidine I.48.....	40
Scheme 6 Preparation of TAME derivative I.49.	41
Scheme 7 The preparation of [Ni(TAMEpyr-trisimine)] ²⁺ I.50.....	41
Scheme 8 Schiff base condensations of TAME.	42
Scheme 9 The Ni(II)-mediated template reaction of TAME with five-membered ring heterocycles.	45
Scheme 10 The tetrahydroborate reduction of [Ni(TAMEpyr-trisimine)] ²⁺ I.50.	47
Scheme 11 Liberation of free TAMEpyr I.60.	57
Scheme 12 Failed attempts at the preparation of TAMEpyr I.60.....	58
Scheme 13 The preparation of benzyloxy-TAMEpyr I.64.....	60
Scheme 14 Preparation of a variety of TAMEpyr metal-complexes.	61
Scheme 15 Preparation of 2-quinolinecarboxaldehyde II.55.....	120
Scheme 16 Initial preparation of 1-isoquinolinecarboxaldehyde II.58.	120
Scheme 17 Alternative preparation of 1-isoquinolinecarboxaldehyde II.58.....	121
Scheme 18 The third approach to 1-isoquinolinecarboxaldehyde II.58.....	123
Scheme 19 Preparation of 1-benzothiazolecarboxaldehyde II.66.	124
Scheme 20 The attempted preparation of 1,2-benzisoxazole-3-carboxaldehyde II.71.....	124

Scheme 21 The preparation of 3,4-dimethoxy- β -phenethylamine II.75.....	126
Scheme 22 Attempt at preparing 6,7-dimethoxy-1-isoquinolinecarboxaldehyde II.84.....	127
Scheme 23 Electrochemical synthesis of Fremy's salt.....	129
Scheme 24 Preparation of 6,7-dimethoxy-1-isoquinolinecarboxaldehyde II.84.	135
Scheme 25 Preparation of 2,4-dimethoxy- β -phenethylamine II.88.....	136
Scheme 26 Failed Bischler-Napieralski reaction of II.88.....	136
Scheme 27 Retrosynthetic analysis of a 7-azacoumarin aldehyde.....	139
Scheme 28 The Bi(III)-mediated von Pechman reaction of resorcinol II.93.	139
Scheme 29 The failed Bi(III)-mediated von Pechmann reaction of 3-pyridinol II.95.....	140
Scheme 30 Two-pot preparation of a 7-azacoumarin II.100.	141
Scheme 31 The preparation of a 7-azacoumarin aldehyde II.102.....	142
Scheme 32 The preparation of a 6-azacoumarin II.108.	143
Scheme 33 The preparation of a 6-azacoumarin aldehyde II.109.....	144
Scheme 34 Preparation of [Ni(TAMEquin-trisimine)](ClO ₄) ₂ II.110.	144
Scheme 35 Preparation of TAMEquin II.112.....	149
Scheme 36 The preparation of [Ni(TAMEisoquin-trisimine)](ClO ₄) ₂ II.113.	150
Scheme 37 The preparation of TAMEisoquin II.115.....	155
Scheme 38 Preparation of [Zn(TAMEisoquin)](ClO ₄) ₂ II.116.....	156
Scheme 39 The preparation of [Cd(TAMEisoquin)](NO ₃) ₂ II.117.	161
Scheme 40 The preparation of [Ni(6,7-DMTI-trisimine)](ClO ₄) ₂ II.118.....	163
Scheme 41 The preparation of 6,7-DMTI II.119.....	165

Scheme 42 Failed attempts at the preparation of TAME-based trisimine complexes of bulky azaaromatic aldehydes.....	166
Scheme 43 The synthesis of the 6-azacoumarin trischelate complex of Fe(II).	168
Scheme 44 The preparation of allylated DPA III.5.	196
Scheme 45 Preparation of a lipophilic comonomer.....	198
Scheme 46 Preparation of acryloyl-IDA.	198
Scheme 47 Preparation of an acryloyl-thioether receptor for soft metal ions. ...	199
Scheme 48 Preparation of phenyl-IDA ligating comonomers.....	200
Scheme 49 The synthesis of Burdette and Atkinson's 2,2'-bipyridyl comonomer III.1.....	201
Scheme 50 Preparation of an N ₃ S ₂ macrocycle to serve as a Hg(II) or Pb(II) receptor.....	202
Scheme 51 Preparation of a model N ₄ S ₂ macrocycle.	204
Scheme 52 The preparation of curcumin.	289

ABSTRACT

I. THE SYNTHESIS AND COORDINATION CHEMISTRY OF NOVEL 1,1,1-TRIS(AMINOMETHYL)ETHANE (TAME) DERIVED LIGANDS AND THEIR USE AS SIZE SELECTIVE FLUORESCENT ZN(II) SENSORS. II. THE SYNTHESIS OF STRONGLY AND WEAKLY BINDING LIGANDS WITH N, O, AND S-DONOR GROUPS TO BE USED AS RECEPTORS IN FLUORESCENT RATIO-METRIC INDICATORS FOR TRANSITION METAL IONS.

By

Daniel Patrick Kennedy

University of New Hampshire, December, 2007

The Ni(II)-mediated template synthesis of the novel chelator TAMEpyr, where TAMEpyr = *N,N',N''*-tris(2-pyridylmethyl)-1,1,1-tris(aminomethyl)ethane, and its coordination chemistry with a host of metal ions is presented. Structural data for $[\text{Zn}(\text{TAMEpyr})]^{2+}$ show the propensity of the ligand for an octahedral coordination geometry. Solution studies of TAMEpyr further illustrate the chelator's flexibility. Lastly, the pyridyl groups of the parent ligand TAMEpyr were exchanged with a host of azaheterocycles affording a collection of novel TAME derived chelators.

The Ni(II)-template chemistry developed to prepare the novel chelator TAMEpyr was exploited in the preparation of novel Zn(II)-selective fluorescent sensors. The molecules TAMEisoquin and 6,7-DMTI possess the fluorophore-spacer-receptor design motif that is evident in many photoinduced electron transfer (PET) based metal-ion sensors. These molecules display exquisite spectroscopic selectivity for Zn(II) with target-induced fluorescence enhancements of ca. 14 and 17 respectively. The measured quantum yield for $[\text{Zn}(\text{TAMEisoquin})]^{2+}$ was a dismal 1.2%. This was improved, however, to 20% for $[\text{Zn}(6,7\text{-DMTI})]^{2+}$. The thermodynamic stability imparted to the target analyte from the polydentate N_6 -donor set was evidenced in the measured K_d' of 1.4 fM for $[\text{Zn}(\text{TAMEisoquin})]^{2+}$. Unlike many reported sensors, the TAME-based chelators display excellent selectivity for Zn(II) over Cd(II). Moreover, the synthetic flexibility of the TAME podand for additional functionalization may facilitate the development of novel bifunctional luminescent sensors. Work on TAME derived azacoumarins is presented.

Lastly, swelling polymeric networks built from N-isopropylacrylamide (NIPA) have been prepared toward the sensing of Cu(II). The candidate's role in this collaborative project was to synthesize strongly and weakly binding metal ion receptors to be copolymerized into the polyNIPA network. Fluorescent groups were also copolymerized into this network which acted as luminescent reporters upon analyte recognition. Depending on the charge of the bound metal-receptor complex the polymer either became swollen or shrank. Polymer shrinking brought the donor-acceptor pair closer together such that fluorescence

resonance energy transfer (FRET) increased. Conversely, reduction of like charges within the polymeric network caused the polymer to swell thus attenuating the measured FRET. This section describes the ligating systems chosen to be incorporated into the polyNIPA systems and the results obtained for the sensing of Cu(II) is presented.

CHAPTER 1

NOVEL LIGANDS DERIVED FROM THE 1,1,1-TRIS(AMINOMETHYL)ETHANE (TAME) FRAMEWORK: THE Ni(II) MEDIATED TEMPLATE REACTION/TETRAHYDROBORATE REDUCTION

Summary

In this chapter the synthetic chemistry of the tripodal triamine TAME will be discussed. Novel hexadentate ligands have been prepared and characterized using a tandem Ni(II) mediated template reaction/tetrahydroborate reduction and demetallation chemistry. The TAME derived systems proved to be flexible ligands for a host of transition and main group metal ions. This discussion will entail a description of the history of the template strategy in the synthesis of macrocyclic and acyclic ligating architectures. Tripodal ligands derived from TACH, TREN, TACN and sen will also be discussed. The synthesis of TAME derived ligands and the coordination chemistry of the novel ligand TAMEpyr will also be presented followed by conclusions and future work.

1.1. Introduction

Planar and tri-dimensional cyclic and acyclic Schiff bases, their polyamine homologues, and related derivatives have attracted interest due to their ability to shed light on molecular processes occurring in biochemistry, material science, magnetism, catalysis, encapsulation, activation, transport and separation phenomena.(1-8) In the bioinorganic arena many ligands have been designed to mimic the catalytic activity of naturally occurring metallo-enzymes.(9) A variety of planar macrocyclic and macroacyclic ligands have been prepared to better understand the role of different donor atoms, their relative position, the number and size of the chelating rings, flexibility and shape of the coordinating group toward selective binding of charged or neutral inorganic species.(10-12)

There has been considerable interest in our own research group in the preparation and study of hexadentate chelators based on the TACH framework **I.13**, where TACH=*cis,cis*-1,3,5-triaminocyclohexane (**Figure 6**). The picolyl derivative TACHpyr **I.14** (*ibid.*) was shown to have striking effects on cultured mammalian tumor cells. Interference with the cell growth cycle eventually led to apoptotic cell death.(13, 14) It is believed that the ligand targets biological iron, zinc, and copper which starves the cell of vital nutrients it needs to proliferate.(15)

The interest in TACH-tripodal N₆-donor systems is related to the rigidity of the framework and how that may relate to binding selectivity among the main

group and transition metal ions. Traditionally the TACH derived ligands were prepared via reductive amination procedures.(16) The author of this dissertation has a particular interest in template synthesis and has applied this to the tripodal framework TAME I.36, where TAME=1,1,1-tris(aminomethyl)ethane. Thus, in the following discussion the candidate describes the template synthesis of C=N bonded ligands, followed by an overview of the tripodal hexadentate ligands and related cage ligands derived from the TACH I.13, TACN I.19, TREN I.22 and 1,3,5-tris(aminomethyl)benzene I.25 frameworks.

1.2. Schiff base ligands and the template effect

Considerable progress has been made in the design and study of novel metal chelators.(17) The challenge of making elaborate chelators from simple starting materials has been overcome by employing self-assembling procedures, recognition processes, and taking advantage of the so-called “metal-template effect” (*vide post*). (18) Creation of polyfunctional ligating-architectures that contain additional coordinating sites, redox active groups (*e.g.* ferrocene), and IR active groups (*e.g.* arene-Cr(CO)₃) have often relied on Schiff-base forming reactions (**Figure 1**).

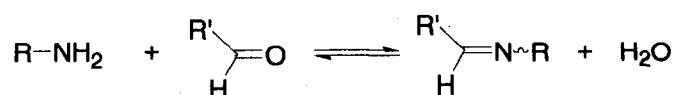


Figure 1. Formation of a Schiff base.

The importance of the C=N group in macrocyclic and macroacyclic chemistries is multifaceted and follows as:(18)

- 1) Often Schiff-bases are obtained by simple self-condensations of formyl- or keto- substrates with primary amine precursors (**Figure 1**). One-step multiple self-condensation processes can give rise to complex planar or tridimensional architectures.
- 2) Alternatively, templating with a metal-center often provides entry into otherwise inaccessible species.
- 3) Once the imine is formed reductive-demetalation reactions with an appropriate reducing agent affords the corresponding polyamine derivative. The derivative is less susceptible to hydrolysis and possesses greater flexibility than the imino-counterpart. The reduced compounds contain NH groups which may be further functionalized by appropriate synthetic methodologies.
- 4) There are many examples of metal-selective ligands (*e.g.* crown ethers for alkali and alkaline earth metals, macrocyclic thioethers for soft heavy metals, acyclic and macrocyclic polyaza ligands for first-row transition metals, etc.). The fusion of different coordinating entities (*e.g.* a Schiff-base and crown-ether moiety) into a unique ligating set can give rise to a very interesting system capable of multiple and/or different metal ion recognition processes.

Schiff bases do indeed form interesting metal complexes (**Figure 2**). For instance, the molecule pyridoxal isonicotonyl hydrazone (**PIH**) is an excellent

Fe(III) chelator that possesses desirable antitumor properties.(19) Chiral salen derivatives such as I.1 have been employed by Jacobsen *et al.* in the preparation of Co(III) complexes that catalyze the hydrolytic kinetic resolution of terminal epoxides.(20)

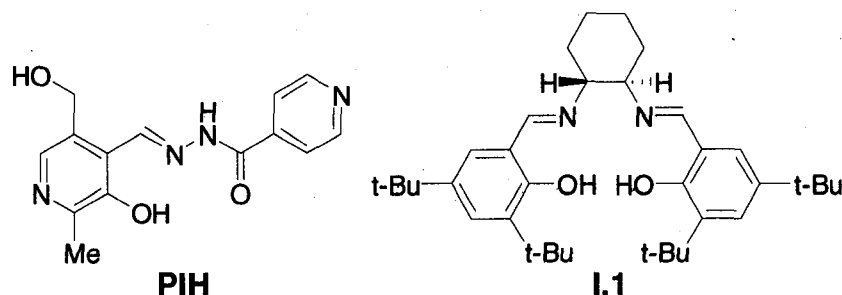


Figure 2 The structures of some interesting acyclic Schiff base metal chelators

However, the direct synthesis of structurally sophisticated Schiff base ligands (and subsequently the polyamine counterparts) is often complicated by competing polymerizations taking place concomitantly in the reaction milieu. In macrocyclic chemistry this phenomenon has been attributed to unfavorable entropy losses in the acyclic backbone upon the desired ring-closing step.(21) The side-products can be minimized by running the reaction at high dilution, thus reducing the likelihood of competing intermolecular processes. However, this strategy is often plagued by poor yields of the desired material. Another synthetic strategy is the inclusion of a metal ion that serves to direct the steric course of the reaction. The term 'metal template effect' coined by Daryle Busch in 1963 refers to the propensity of a metal ion to poise the reacting groups in such a fashion that otherwise energetically inaccessible reactions can take place.(22)

The metal template effect can be further categorized as either the “kinetic template effect” or “thermodynamic template effect.” Busch first described the kinetic template effect in the reaction of a diamagnetic Ni(II)-complex **I.2** with α,α' -dibromo-*o*-xylene **I.3** resulting in the production of a macrocyclic Ni(II)-complex **I.4** (**Figure 3**).⁽²³⁾ According to Busch the probability of ring-closure is assured by the presence of the metal ion, which holds the terminal mercapto groups in a *cis*-position such that a single rate-determining step occurs. Conversely, the so-called “thermodynamic template effect” refers to a reaction that will occur in the absence of the templating metal-ion.⁽²⁾ However, the metal promotes the formation of the desired product by removing it from competing equilibria. An example of this phenomenon was illustrated in the preparation of the aforementioned Ni(II)-complex **I.2**.⁽²⁾ In the absence of Ni(II), the reaction between β -mercaptoethylamine **I.6** and a generic α,α' -diketone **I.5** affords an equilibrating mixture of thiazoline **I.8** and the desired Schiff-base **I.7** (**Figure 3**). Upon addition of Ni(II) the yield of the desired Schiff-base as the Ni(II)-complex **I.2** was improved to ca. 70%.

Factors that influence the product slate of a metal template reaction include coordination preferences of the templating metal (*i.e.* hard or soft templates, geometry preferences, size selectivity, etc.), the chelate and/or macrocyclic effects, and the so-called negative template effect in which the templating metal holds reactive groups apart from one-another to encourage an intermolecular reaction.⁽²⁴⁾ Metal-mediated template reactions have been utilized in stubborn alkylations, Schiff-base condensations, Mannich

condensations, nitrile condensations, and self-assembly processes affording topologically rich molecules like the catenanes, rotaxanes, helicates and calixarenes.(24)

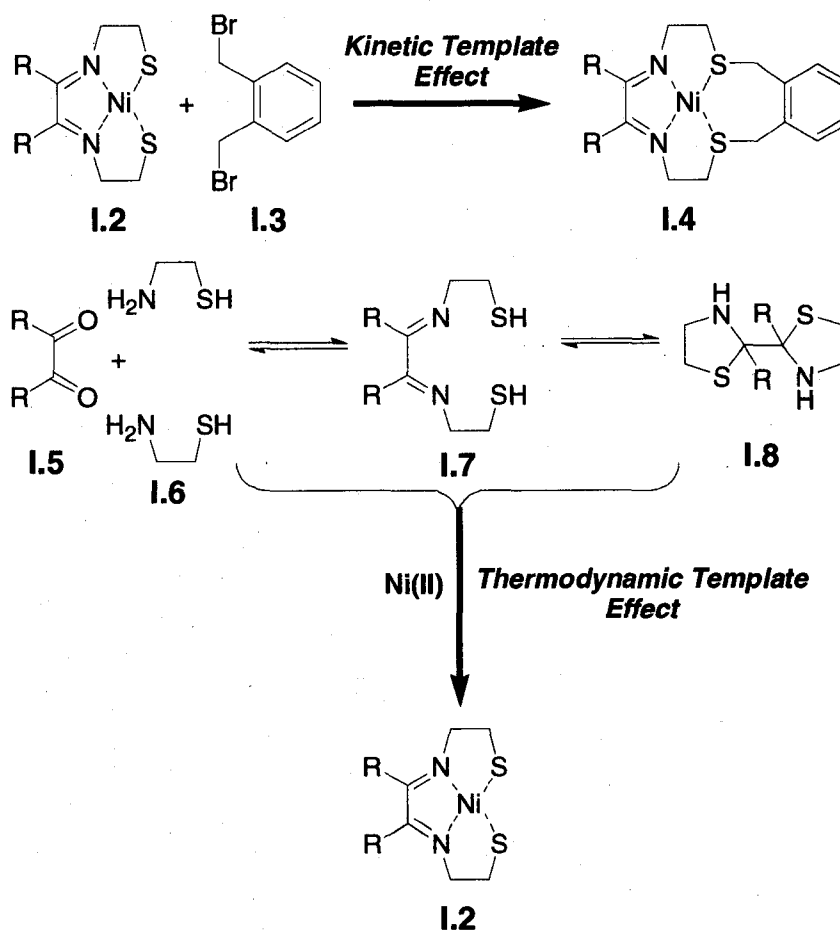


Figure 3 Examples of the thermodynamic and kinetic metal template effect.

An important feature of the metal template strategy is the effect of metal ion size and identity on the outcome of the reaction. This was illustrated in the reaction of 2,6-diformylpyridine with terminal amino-polyethylene glycols (**Figure 4**).(25-27)

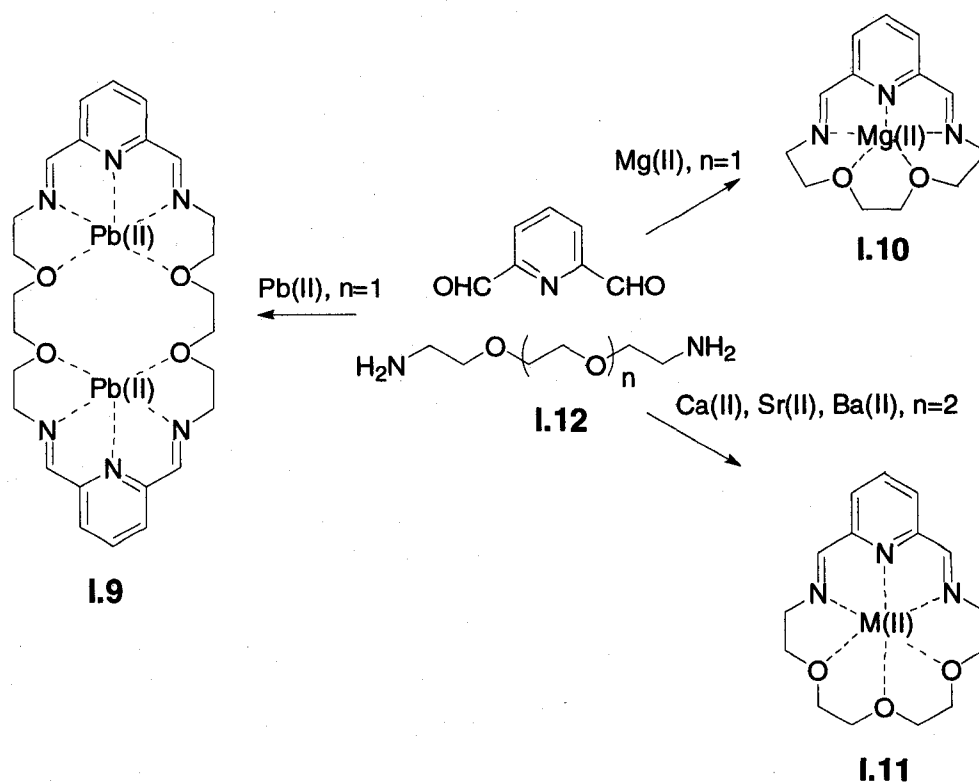


Figure 4 Template synthesis of Schiff base macrocycles

When $n=1$, the pentacoordinate product **I.10** was formed preferentially with Mg(II) due to an ideal fit between the macrocyclic binding cavity and ionic radius of the templating metal. This particular reaction is called a [1+1] condensation where the mole ratio of 2,6-diformylpyridine to the linear diamine **I.12** in the isolated product **I.10** was 1:1. The remaining alkaline earth metals reacted preferentially with the $n=2$ polyether giving the [1+1] hexacoordinate product **I.11**. However, when $n=1$, the presence of Pb(II) favors a [2+2] homobimetallic macrocyclic complex **I.9**. The Pb(II) -ion is relatively large with an ionic radius of 1.33 \AA which may favor the formation of a 30-membered ring.^(28, 29) This result highlights the importance of both size and identity of the metal ion in the outcome of these

reactions. The six-coordinate ionic radii of the templating metals are listed in

Table 1.(29)

Metal	Ionic Radius (Å)
Mg(II)	0.86
Ca(II)	1.14
Sr(II)	1.32
Ba(II)	1.49
Pb(II)	1.33

Table 1 The six-coordinate ionic radii of selected main group metals

A more recent example of a metal-assisted Schiff base condensation comes from the laboratory of Rybak-Akimova *et al.*(30) In the quest for novel-radiopharmaceuticals based on ^{67}Cu , the aim of this work was to develop macrocycles with acyclic pendant arms that would match the square-pyramidal geometry of Cu(II). The unique coordination and structural properties of such systems may also prove important in the development of enzyme mimics, new catalysts, MRI-contrast reagents and new fluorescent probes. The synthesis of five-coordinate Ni(II)-complexes with pendant arm-containing macrocycles was achieved by the Schiff-base condensation of 2,6-diacetyl- or 2,6-diformyl-pyridine with the tetra-amine trpn (where trpn= tris-(3-aminopropyl)amine) in the presence of $\text{Ni}(\text{ClO}_4)_2$ (**Figure 5**). The subsequent reductive demetallation afforded stable pentadentate ligands that were used to prepare the corresponding Cu(II)-complexes. Protonation of the pendant arm produced four-coordinate macrocyclic complexes. The treatment of $[\text{Ni}(\text{L2c})]^{2+}$ with either Ac_2O or BzCl resulted in the production of mono-functionalized Ni(II) complexes. After reductive demetallation these species were complexed to Cu(II) and were found to display a square-planar geometry in the solid state, as evidenced by X-ray

crystallography, and remained four-coordinate in aqueous solutions below pH=11.

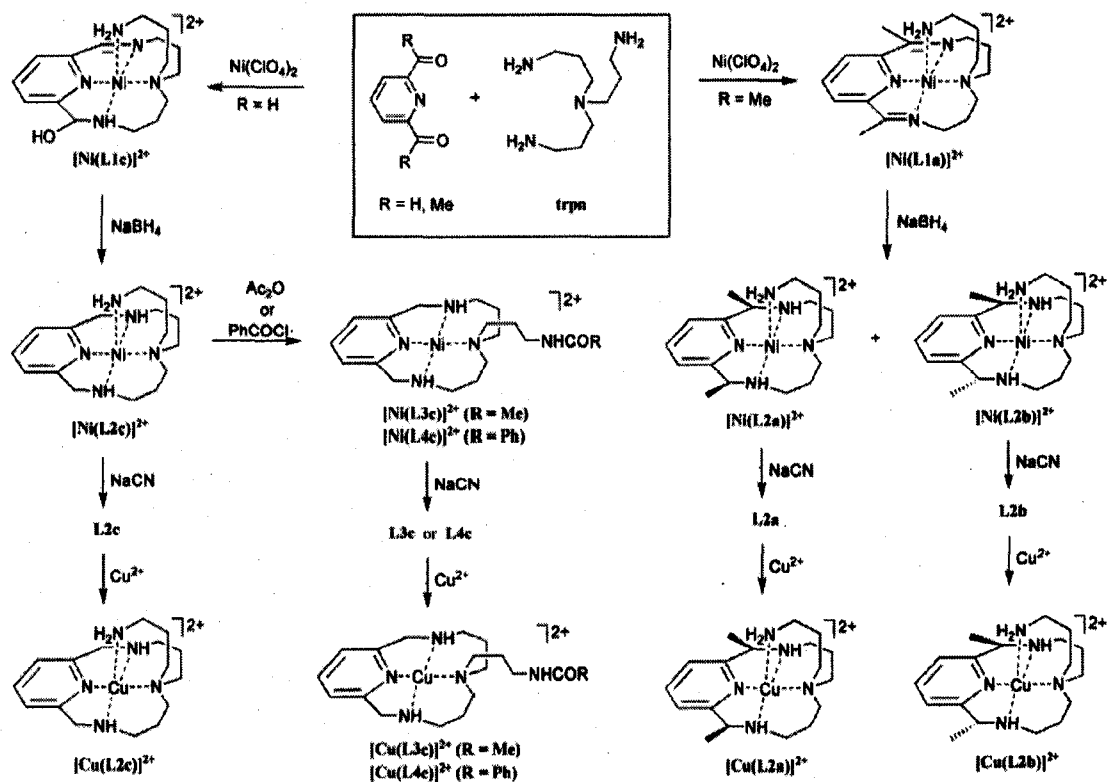


Figure 5 Ni(II)-mediated template reaction of 2,6-disubstituted pyridines.(30)

1.3. Tripodal chelators

There has been considerable interest toward the design and synthesis of a number of tripodal ligands. Researchers are actively pursuing tripods because of their inherent thermodynamic stability, kinetic inertness and interesting topological structures.(31) If appropriately sized, these frameworks will efficiently occupy a trigonal face of the bound metal-ion. The resulting framework can be further functionalized with additional donor groups to achieve novel ligating

architectures. The following discussion highlights some of the work that has been accomplished in the past on the TACH, TACN, sen, TREN, and TAME tripodal frameworks.

1.3.1. TACH Systems

Historically, the TACH-framework has been derivatized via metal-free Schiff-base condensations with 2-pyridinecarboxaldehyde (which ultimately led to the aforementioned ligand TACHpyr I.14) and salicylaldehyde to afford a small collection of hexadentate chelators (**Figure 6**).^(32, 33)

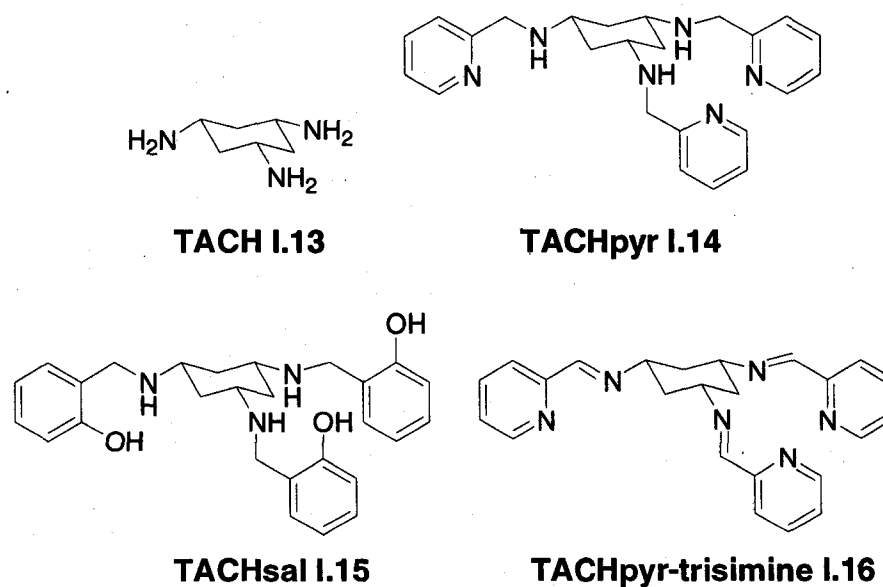


Figure 6 A selection of reported TACH-based chelators.

The lipophilic chelator TACHsal I.15 formed 1:1 M:L binding stoichiometries with Al(III), Ga(III), In(III) and Fe(III).⁽³²⁾ The resulting six-membered chelate rings are well-tailored for tricationic binding partners.⁽³⁴⁾

Likewise, the N_3O_3 donor set is adequate for trivalent metals according to HSAB theory.(35)

The Schiff-base TACHpyr-trisimine **I.16**, first reported in 1957 by Lions *et al.*, serves as a hexadentate ligand for a host of first-row divalent transition metal ions.(33, 36) According to Gillum *et al.* the ligand TACHpyr-trisimine **I.16** would prefer to coordinate a metal-ion in a trigonal prismatic geometry (**Figure 7**).

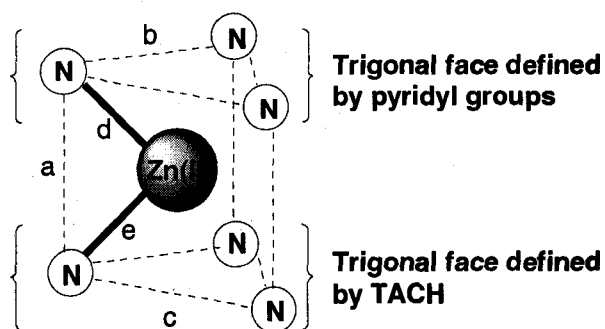


Figure 7 Representation of the inner-coordination sphere of $[Zn(TACHpyr-trisimine)]^{2+}$.

X-ray powder diffraction patterns for $[Mn(TACHpyr-trisimine)]^{2+}$, $[Co(TACHpyr-trisimine)]^{2+}$, and $[Zn(TACHpyr-trisimine)]^{2+}$ were very similar and supported slightly tapered trigonal prismatic geometries. The average dimensions from the structural data of $[Zn(TACHpyr-trisimine)]^{2+}$ follow as: $a=2.70\text{\AA}$, $b=2.85\text{\AA}$, $c=3.23\text{\AA}$, $d=2.15\text{\AA}$, $e=2.25\text{\AA}$ (**Figure 7**). For tris-chelates, like TACHpyr-trisimine **I.16**, a measure of the so-called twist angle (α) provides a quantitative measure of how octahedral or trigonal prismatic a six-coordinate metal-complex is (**Figure 8**). The average value of α , as calculated from Gillum's powder diffraction data, for Mn(II), Co(II), and Zn(II) was *ca.* 8° . An ideal octahedron possesses a twist

angle of 60° . If the two trigonal faces in **Figure 8** are completely eclipsed then the twist angle is 0° resulting in a trigonal prismatic geometry.

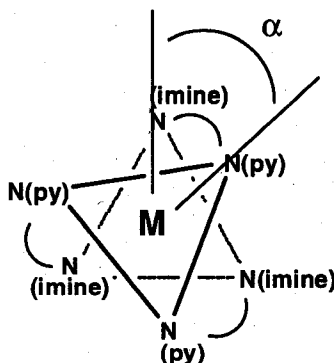


Figure 8 Trigonal twist angle α for $[M(\text{TACHpyr-trisimine})]^{2+}$.

X-ray powder diffraction data obtained for TACHpyr-trisimine **I.16** complexes of both Fe(II) and Ni(II) were not definitive. Absorbance spectroscopy, however, corroborated a near-octahedral geometry for $[\text{Fe}(\text{TACHpyr-trisimine})]^{2+}$. The work of Fleischer *et al.* later found that $[\text{Ni}(\text{TACHpyr-trisimine})]^{2+}$ possessed an intermediate geometry between trigonal prismatic and octahedral.⁽³⁷⁾ The twist angle was measured from single-crystal X-ray crystallography to be ca. 32° . It appears that the presence of the three-imino groups (C=N) in TACHpyr-trisimine restrict its ability to twist about the principal rotation axis (normal to the page in **Figure 8**) thus hindering the formation of octahedral metal complexes.

Improvements on the synthesis of the TACH **I.13** framework ultimately led to the preparation and study of the aforementioned chelator TACHpyr **I.14**.⁽¹⁶⁾ TACHpyr **I.14** was initially prepared to serve as a ligating scaffold for novel Ga(III)-radiopharmaceuticals. It was found that the ligand readily formed

complexes with "cold" Ga(III) and In(III) in methanol (Figure 9).(38) $^1\text{H-NMR}$ studies over a period of four weeks indicated that $[\text{Ga}(\text{TACHpy})]^{3+}$ was inert to

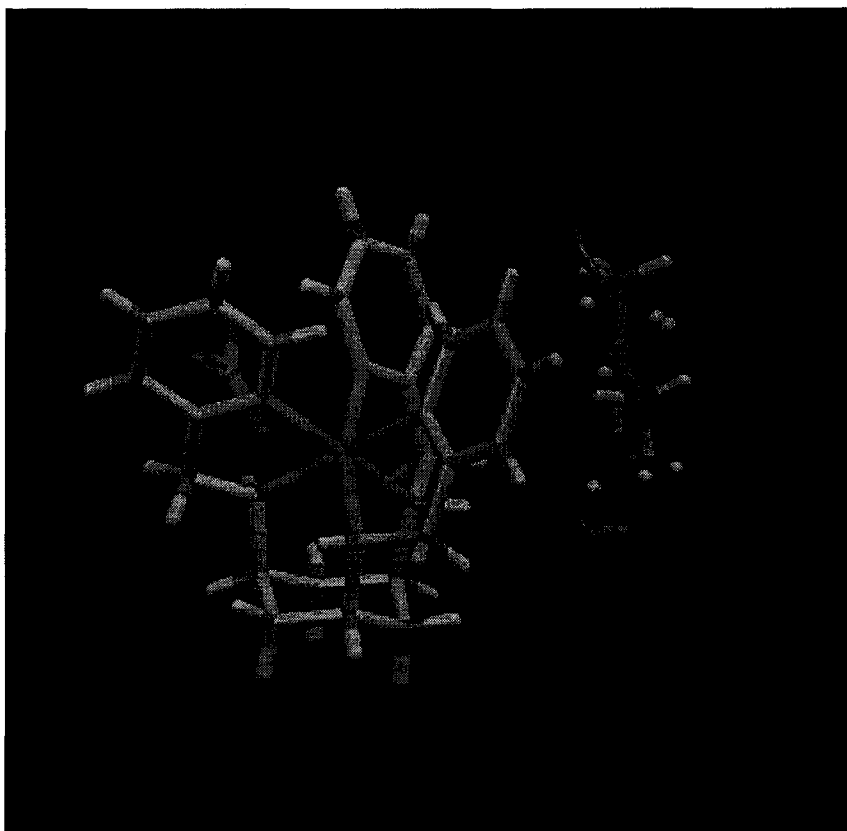


Figure 9 Representation of $[\text{Ga}(\text{TACHpy})](\text{NO}_3)_3 \cdot \text{DMF}$. The image was created from data obtained in the Cambridge Structural Database (CSD).

hydrolysis in aqueous solvent systems over a pH range of 2-8, while $[\text{In}(\text{TACHpy})]^{3+}$ was unstable in water at pH 5-7. The crystal structure of $[\text{In}(\text{TACHpy})][\text{NO}_3]_3 \cdot \text{DMSO}$ showed a greater distortion toward trigonal prismatic coordination geometry than $[\text{Ga}(\text{TACHpy})][\text{NO}_3]_3 \cdot \text{DMF}$. This was evidenced in the angles of twist ($\frac{\alpha}{2}$), which ranged from $21.98(22)^\circ$ to $22.66(22)^\circ$ in the Ga(III) complex and $17.93(11)^\circ$ to $19.04(10)^\circ$ in the In(III) complex. The cyclohexyl ring of the coordinated TACHpy I.14 ligand was also more distorted by the larger In(III) metal-ion. The distortions were evident in the splaying of the cyclohexyl

nitrogens from their ideal axial positions. Likewise, bloating within the binding cavity led to a reduction in the average C-C-C-C torsion angle of the cyclohexyl ring.

Group IIB metal complexes of TACHpyr **1.14** also illustrated the size selective nature of the chelator.⁽³⁹⁾ The complexes [Zn(TACHpyr)](ClO₄)₂·MeOH, [Cd(TACHpyr)](ClO₄)₂, and [Hg(TACHpyr)](ClO₄)₂ were isolated and their solid state structures were determined (**Figure 10**). The coordination sphere changed from an octahedral to a trigonal-prismatic geometry with increasing metal radius. The crystallographically measured twist angles (α) were 43.7(2)° for [Zn(TACHpyr)]²⁺, ranged between 11.0(4)° and 21.7(2)° for [Cd(TACHpyr)]²⁺, and ranged between 3.1(3)° and 5.5(2)° for [Hg(TACHpyr)]²⁺. As was noted for [In(TACHpyr)]³⁺, a slight outward expansion of the triaminocyclohexane nitrogens occurred with Cd(II) and Hg(II). This likewise led to a reduction in the cyclohexyl ring C-C-C-C torsion angles with concomitant flattening of the ring.

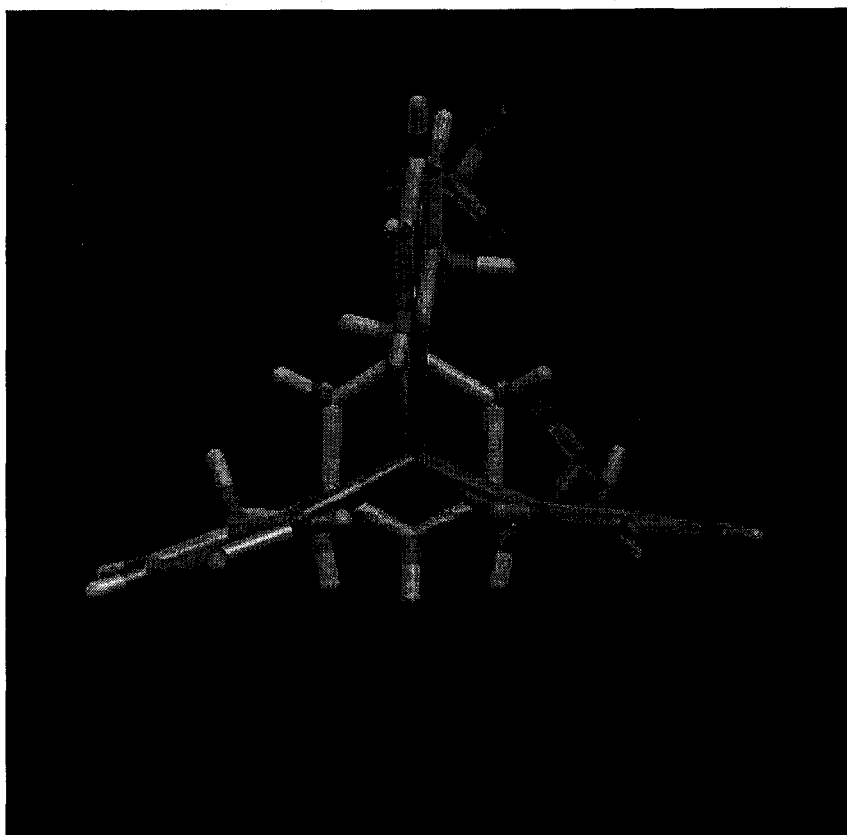


Figure 10 Top-view down of $[\text{Hg}(\text{TACHpyr})](\text{ClO}_4)_2$ highlighting the nearly trigonal prismatic geometry of this complex. The image was created from data obtained in the Cambridge Structural Database (CSD).

The interaction of Fe(II) and Fe(III) with TACHpyr **I.14** gave rise to six-coordinate, low-spin, cationic complexes of Fe(II).⁽⁴⁰⁾ The anaerobic reaction of TACHpyr **I.14** with Fe(II) salts afforded the bronze-colored $[\text{Fe}(\text{TACHpyr})]^{2+}$ complex, but under ambient conditions oxidative dehydrogenation of one or two of the aminomethylene group(s) of the ligand occurred (**Figure 11**). The resulting mono- and diimino Fe(II) complexes (denoted as $[\text{Fe}(\text{TACHpyr-ox-2})]^{2+}$ and $[\text{Fe}(\text{TACHpyr-ox-4})]^{2+}$ respectively) were an inseparable mixture, but could be collectively oxidized with H_2O_2 to the aforementioned complex $[\text{Fe}(\text{TACHpyr-trisimine})]^{2+}$ (which is indicated in **Figure 11** as $[\text{Fe}(\text{TACHpyr-ox-6})]^{2+}$). Similar

oxidations of secondary amines coordinated to Ru, Fe, Ni, Cu, Co, and Os centers have all been observed.(41) Cyclic voltammetry of the imino

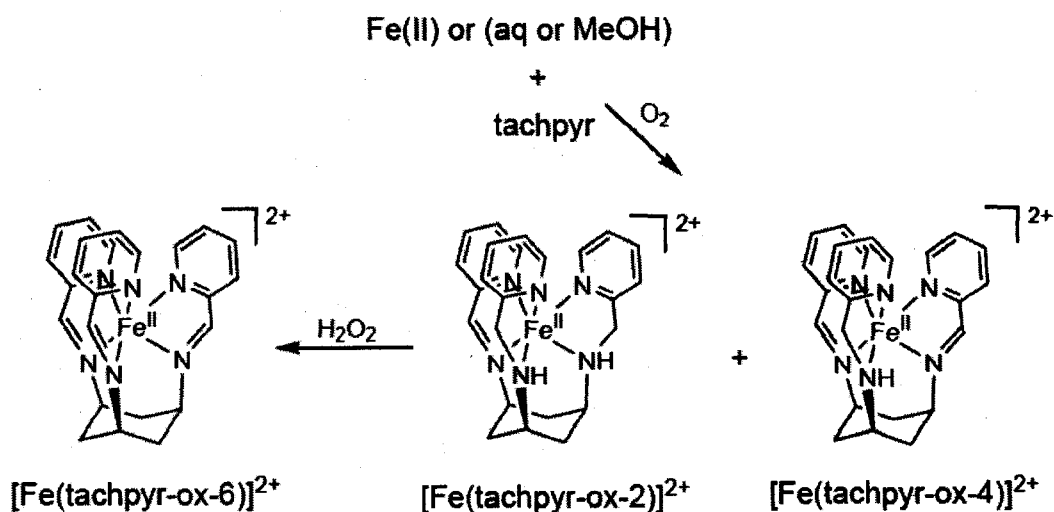
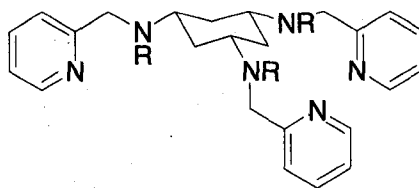


Figure 11 Fe(II)-mediated oxidation of TACHpyr under ambient conditions.(42)

complex mixture revealed an irreversible anodic wave at +0.78 V (vs. *N.H.E.*).

The experiment was carried out in water with 0.5M KCl as the supporting electrolyte. TACHpyr **I.14** likewise acted as a reducing agent toward Fe(III) salts, affording the mono- and diimino Fe(II) complexes as products. The chelator also reductively removed Fe(III) from an Fe(III)(ATP)₃ complex (which is a putative form of intracellular iron), producing the mono- and diimino Fe(II) complexes denoted in **Figure 11**.

The effects of steric hindrance on the complexation of Mn(II), Co(II), Ni(II), Cu(II) and Zn(II) were studied with *N*-alkylated analogs of TACHpyr **I.17** and **I.18** (**Figure 12**).⁽⁴³⁾



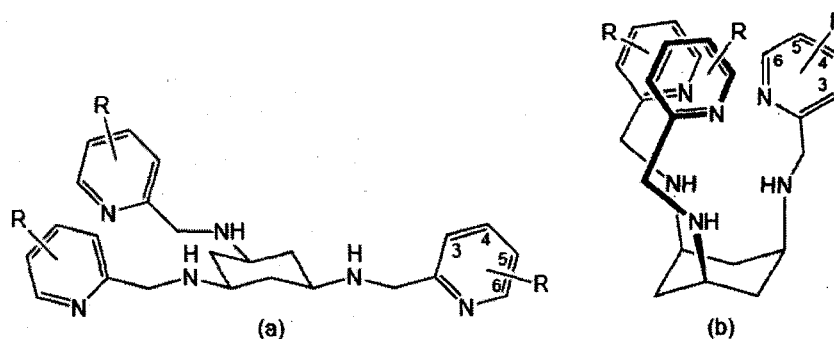
R=Me I.17

R=Et I.18

Figure 12 N-alkylated derivatives of TACHpyr.

The ligands (*N*-Me)3TACHpyr **I.17** and (*N*-Et)3TACHpyr **I.18** formed hexacoordinate complexes with Mn(II), Co(II), Ni(II), Cu(II), and Zn(II) in MeOH. The Mn(II) and Co(II) complexes possess high-spin electronic configurations, based on solution magnetic susceptibility, electronic spectroscopy and X-ray crystallographic studies. However, visible-near IR absorbance spectra and X-ray data demonstrated weakened bonding in the complexes of (*N*-R)3TACHpyr **I.17** and **I.18** relative to TACHpyr **I.14**. These observations have been attributed to the steric effects of the Me or Et groups on the coordinated TACH amines. Structures of [Zn(TACHpyr)]²⁺ and [Ni(TACHpyr)]²⁺ indicated a clear preference of TACHpyr **I.14** and its derivatives for octahedral geometry, while [Cu((*N*-Me)3TACHpyr)]²⁺ exhibited a classic Jahn-Teller tetragonal distortion. The [M(TACHpyr)]²⁺ complexes (where M = Co, Ni, Cu and Zn) were all inert in aqueous pH 5.5 media. However, all the metal complexes of the *N*-alkylated TACHpyr derivatives dissociated the metal ion at pH=5.5, consistent with the aforementioned reduced binding strength of the chelators.

Substitutions on the pyridyl rings of TACHpyr **I.14** afforded a collection of TACH-*x*-Rpyr chelators, where the ring substituents (R) are either methyl groups or methoxy groups (**Figure 13**).⁽⁴⁴⁾



$L^1 - L^4$, R = Me, tach-x-Mepyr ($x = 3 - 6$)
 L^5 , R = MeO, tach-x-MeOPyr ($x = 6$)

Figure 13 Methylated and methoxylated derivatives of TACHpyr.(42) The structure in (a) is the open-form of apoTACH-x-Rpyr and the structure in (b) is the closed-form that occurs upon coordination.

Dicationic complexes of the TACH-x-Rpyr family of chelators were prepared and studied in both the solid state and in solution. Striking features were seen in the 6-substituted complexes ($x=6$, R=Me or R=MeO), where steric repulsions between the 6-substituents at the 3-fold axis of the pseudo-octahedral coordination sphere resulted in substantially weakened metal-ligand bonding. Intraligand repulsions resulted in bond angle and length distortions, coordination unsaturation, and shifts of the *d-d* electronic transitions to lower energies. Aqueous lability studies by HPLC agreed with the spectroscopic findings. The bonding properties of the other TACH-x-Mepyr chelators (where $x = 3, 4, 5$) closely resembled the solution chemistry of the parent ligand TACHpyr **I.14**. Likewise, X-ray crystallography revealed that $[Zn(TACH-3-Mepyr)]^{2+}$ closely resembled $[Zn(TACHpyr)]^{2+}$. The cytotoxicities of the chelators toward human breast cancer cells (MCF7) at a fixed chelator concentration of 16 μ M showed time-dependent induction of cell death in the order TACH-3-Mepyr $>$ TACH-4-Mepyr $>$ TACH-5-Mepyr $>$ TACHpyr **I.14**, whereas TACH-6-Mepyr and TACH-6-

MeOpyr had no effect on the cells. The depressed cytotoxicities of the latter two were attributed to the inability of the chelators to bind Fe(II) or Zn(II) strongly.

In sum the TACH framework will ideally occupy the trigonal face of metal ions that have ionic radii that vary between *ca.* 0.7Å and 0.9Å. The size selective nature of TACH is related to its rigidity. Distortions that occur upon metal ion coordination are reflected in perturbations in the chair conformation of the cyclohexyl ring. The TACH podand can be functionalized with a host of donor groups using metal free synthetic methodology.

1.3.2. TACN Systems

The tripodal framework 1,4,7-triazacyclonane **I.19** (TACN) has been utilized in the hexadentate chelator TACNpyr **I.20**, where TACNpyr= 1,4,7-tris(2-pyridylmethyl)-1,4,7-triazacyclononane (**Figure 14**).

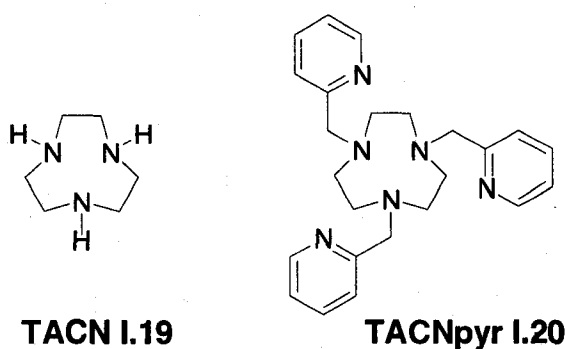


Figure 14 The tripodal ligand TACNpyr **I.20**.

Wieghardt *et al.* prepared and studied the Mn(II), Fe(II), Co(II), Ni(II), Cu(II), Ru(II) and Pd(II) complexes of TACNpyr **I.20**.⁽⁴⁵⁾ Crystallographic studies of [Mn(TACNpyr)]²⁺ revealed a distorted trigonal-prismatic geometry. This is

analogous to what was seen with $[\text{Mn}(\text{TACHpyr})]^{2+}$.⁽⁴³⁾ Like $[\text{Ni}(\text{TACHpyr})]^{2+}$, the complex $[\text{Ni}(\text{TACNpyr})]^{2+}$ possesses an octahedral geometry in solution and the solid state. In $[\text{Pd}(\text{TACNpyr})]^{2+}$, the ligand only offers the metal-center five donor atoms resulting in the “dangling” of one of the picolyl pendant arms. The cyclic voltammograms of the Mn(II), Fe(II), Co(II) and Ni(II) complexes of TACNpyr **I.20** showed reversible or quasi-reversible 1-electron-transfer processes in MeCN. Studies carried out by Christiansen *et al.* showed that $[\text{Fe}(\text{TACNpyr})]^{2+}$ undergoes rapid helical inversions between the Δ and Λ configurations (**Figure 15**).⁽⁴⁶⁾ The ^{13}C -NMR data was used to measure a rate constant for racemization which exceeded 150 s^{-1} at 90°C . According to the authors the racemization takes place via an intramolecular twisting mechanism (*i.e.* Bailar-twist) which is favored when the triplet excited state for an Fe(II)-complex is close in energy to the singlet ground state.^(46, 47) This process requires the intermediacy of a trigonal prismatic transition state.

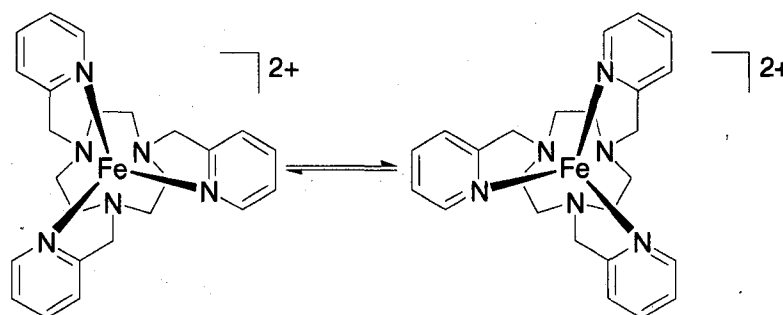


Figure 15 Top-down view of the helical inversion of $[\text{Fe}(\text{TACNpyr})]^{2+}$.

The work of Tsukube *et al.* showed that TACNpyr **I.20** is a highly selective and efficient membrane transporter of Na(I) (**Figure 16**).^(48, 49) The striking feature of this study is that the relatively soft TACNpyr **I.20** chelator, which is

recognized as a good ligand for heavy metal cations and transition metal ions, also shows specific "ionophoric" activity for a hard cation like Na(I).

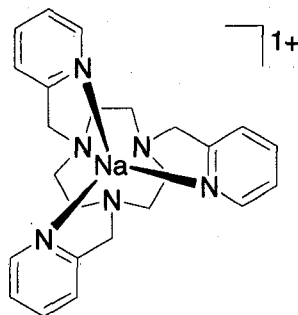


Figure 16 The putative structure of $[\text{Na}(\text{TACNpyr})]^{2+}$.

Very recently Jackson *et al.* reported a reversible and stereoselective N- to C-bonded rearrangement of $[\text{Co}(\text{TACNpyr})]^{3+}$ (Figure 17).⁽⁵⁰⁾

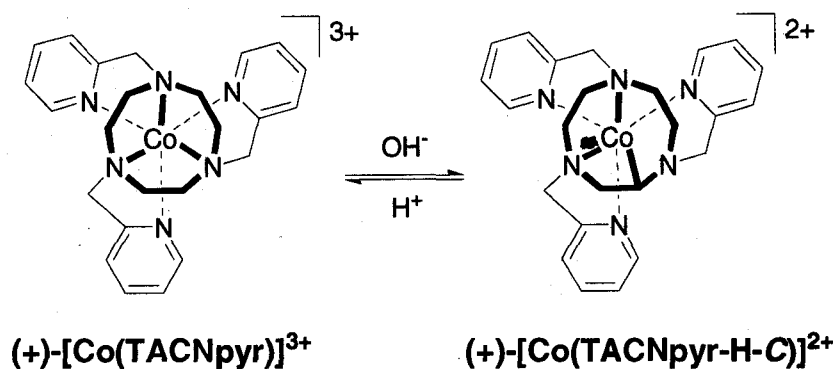
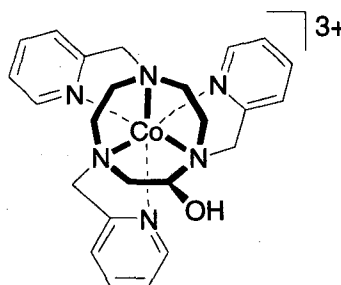


Figure 17 Reversible and stereoselective N- to C-bonded rearrangement of $(+)\text{-}[\text{Co}(\text{TACNpyr})]^{3+}$.

In this novel rearrangement a TACN nitrogen was displaced upon deprotonation of the relatively acidic α -carbon, which then binds to the metal ion as a carbanionic-donor. The kinetics for this process show retention of configuration of the resolved $(+)\text{-}[\text{Co}(\text{TACNpyr})]^{3+}$ reactant. The racemization between the (+) and (-)-forms of $[\text{Co}(\text{TACNpyr})]^{3+}$ (*i.e.* Δ and Λ) competes, as evidenced in the kinetics studies, with the donor-atom rearrangement. The reaction is also slowly

reversed in acidic media with retention of configuration. In pH=7 solutions of this complex an oxidation of the α -carbon competes with the rearrangement affording (+)-[Co(TACNpyr-OH)]³⁺ (Figure 18).



(+)-[Co(TACNpyr-OH)]³⁺

Figure 18 The oxidation product (+)-[Co(TACNpyr-OH)]³⁺.

In sum the TACN framework is unique in that the tridentate N₃ cap is embedded in a nine-membered ring which may add a degree of size selectivity for metal ions in TACN derived ligands. The acidity of the α -methylene units in the TACN ring is responsible for the interesting chemistry of the resolved [Co(TACNpyr)]³⁺ complex. Unlike the analogous TACH derived ligands TACNpyr shows promise as a novel ionophore.

1.3.3. Cage ligands derived from sen

Formaldehyde has been used in a remarkable variety of reactions with polyamines to give macrocyclic and macropolycyclic ligands. Polymacrocyclic formation with the Co(III)-complex of sen I.21, where sen=5-(4'-amino-2'-azabutane)-5-methyl-3,7-diazanonane-1,9-diamine, affords an array of sophisticated caged molecules collectively known as the "sarcophagines"

(Figure 19).(51-55) The reaction of $[\text{Co}(\text{sen})]^{3+}$ with paraformaldehyde and TEA is a unique metal-templating Mannich reaction.(56) The resulting tri-iminium cationic intermediate from this reaction will then participate in a multi-step condensation with a host of reaction partners, which include various aldehydes, phosphines, and arsines. The resulting sarcophagine ligand “entombs” the Co(III)-center thus hindering decomplexation.

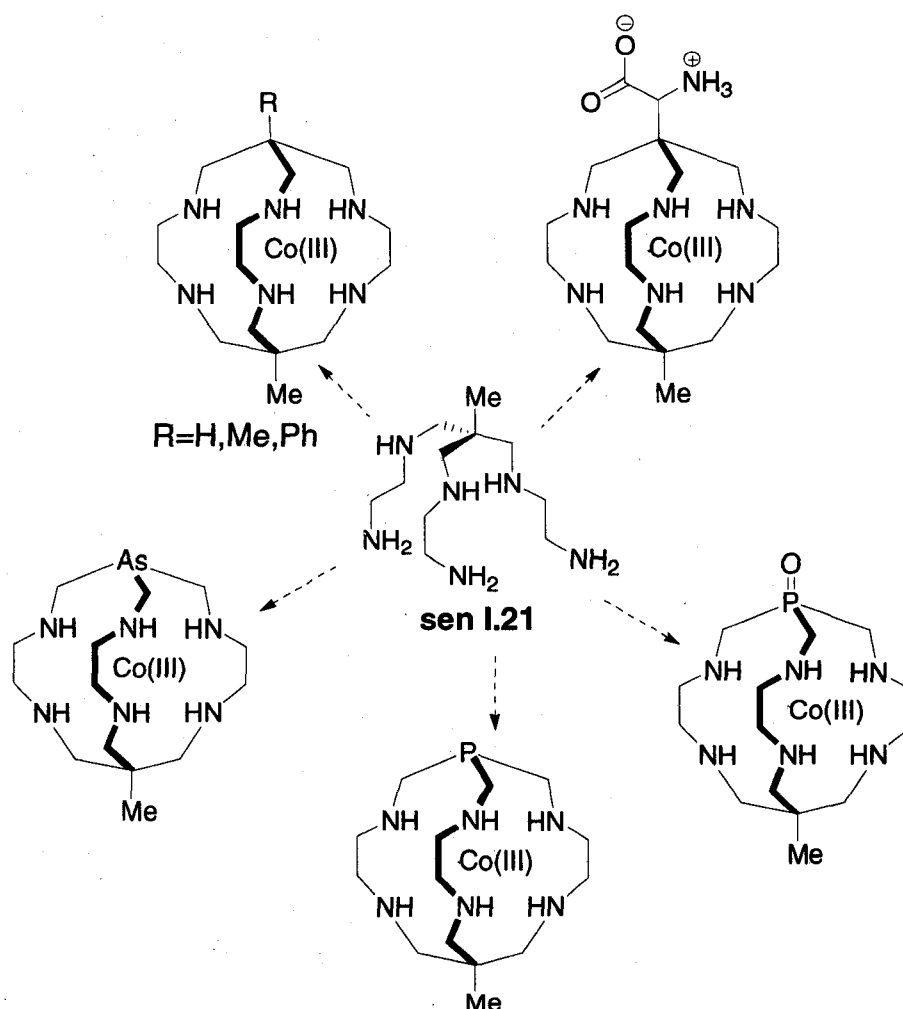


Figure 19 A select collection of the so-called “sarcophagines”.

The stability constants for the parent **sen I.21** were ascertained by Hollingshed *et al.* with a host of transition and main group metal ions (**Table**

2).(57) The authors claim that the complexation behavior of sen I.21 as compared to linear polyamines and polyazamacrocycles is associated with the steric properties of the chelator rather than the basicities of the ligand coordination sites. Sen I.21 forms the strongest complexes with first-row transition metals and weaker complexes with Cd(II) and Pb(II) because of a poor-size match within the binding cavity. The binding constant with In(III) was surprisingly high and was attributed to the size-selective nature of sen I.21. The relative stabilities of Mn(II)<Fe(II)<Co(II)<Cu(II)>Zn(II) is in accord with the Irving-Williams series.(58)

Table 2 Protonation and formation constants for the hexadentate tripodal ligand sen I.21.(57)

Equilibria (L=sen I.21, all metals are dicationic except for In which is tricationic)	LogK (25.0°C, $\mu=0.1$)
HL/L·H	10.76±0.01
H ₂ L/HL·H	10.08±0.01
H ₃ L/H ₂ L·H	9.40±0.01
H ₄ L/H ₃ L·H	7.20±0.01
H ₅ L/H ₄ L·H	5.19±0.01
H ₆ L/H ₅ L·H	2.73±0.01
MnL/Mn·L	8.6±0.1
MnLH/MnL·Mn	8.1±0.1
FeL/Fe·L	13.4±0.1
FeLH/FeL·H	7.0±0.1
CoL/Co·L	18.0±0.1
CoLH/CoL·H	5.9±0.1
CoLH ₂ /CoLH·H	5.6±0.1
CuL/Cu·L	26.2±0.3
CuLH/CuL·H	9.9±0.1
CuLH ₂ /CuLH·H	5.6±0.1
Cu ₂ L/Cu·Cu·L	33.5±0.1
Cu ₂ LH ₁ /Cu ₂ L·H ⁻¹	7.8±0.1
Cu ₂ LH ₂ /Cu ₂ LH·H ⁻¹	10.7±0.1
ZnL/Zn·L	17.0±0.1
ZnLH/ZnL·H	6.8±0.1
ZnLH ₂ /ZnLH·H	5.9±0.1
CdL/Cd·L	13.4±0.1

Table 2 continued...	
CdLH/CdL·H	8.0±0.1
CdLH ₂ /CdLH·H	6.3±0.1
PbL/Pb·L	9.2±0.1
PbLH/PbL·H	9.1±0.1
PbLH ₂ /PbLH·H	7.5±0.1
InL/In·L	15.1±0.1
InLH/InL·H	9.7±0.1
InLH ₂ /InLH·H	6.7±0.1
InLH ₁ /InL·H ⁻¹	10.4±0.1

To summarize the sen derived ligands are unique in that they afford a host of caged ligands in the presence of formaldehyde and Co(III). The sen ligand itself forms thermodynamically robust complexes with both transition block metal ions and main group metal ion as evidenced by large formation constants with these species. The tripodal cap is more flexible than the corresponding TACH and TACN frameworks because the anchoring methylene H's are free to twist about the principal rotation axis when they are engaged in coordination.

1.3.4. TREN ligands

The tripodal polyamine TREN **1.22** (where TREN=tris-(2-aminoethyl)amine) has been employed by many workers as a facial cap for a variety of metal-ions (**Figure 20**). Most notably Schrock and coworkers have utilized various derivatives of TREN **1.22** in the

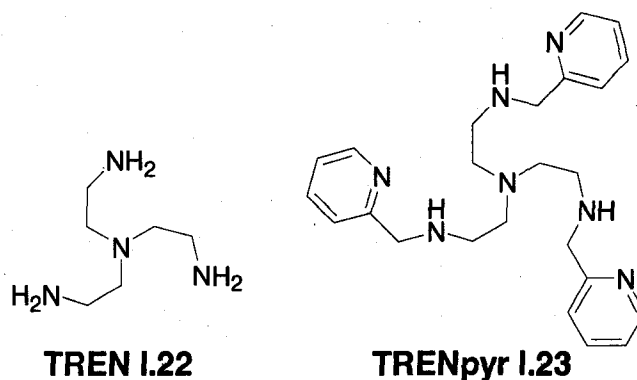


Figure 20 The structures of TREN I.22 TRENpyr I.23.

preparation of molybdenum-containing catalysts that effect the reductive splitting of N_2 to NH_3 under ambient temperatures and pressures.⁽⁵⁹⁾ Keeping in-stride with the previous examples the analogous ligand TRENpyr I.23 is unique in that it contains a seventh donor atom at the apex of the TREN-framework (**Figure 20**). Indeed, a seven-coordinate complex of TRENpyr I.23 exists with Mn(II) as evidenced in the crystallographic study carried out by Deroche *et al.* (**Figure 21**).⁽⁶⁰⁾ Moreover, $[Mn(TRENpyr)]^{2+}$ scavenges superoxide ($O_2^{\cdot -}$) which was also studied by Deroche and coworkers using the so-called xanthine-xanthine oxidase-cytochrome c assay. A few papers were published years earlier that were aimed at studying the superoxide dismutase (SOD) activity of Fe(II) complexes of both TRENpyr I.23 and the well-know hexadentate heavy-metal chelator TPEN, where TPEN=*N,N,N',N'*-tetrakis-(2-pyridylmethyl)ethylenediamine.⁽⁶¹⁻⁶³⁾ Superoxide dismutase is an enzyme which reduces cellular oxidative stress by converting $O_2^{\cdot -}$ into H_2O_2 . Both aminopyrdyl ligands readily disengage coordination of a picolyl group to the metal-center, which is hypothesized to play a role in the observed SOD activity. A later crystallographic study of $[Zn(TRENpyr)]^{2+}$ showed that the ligand only

offers the metal six donor-sites resulting in the dangling of one of the picolyl arms (Figure 21).(64)

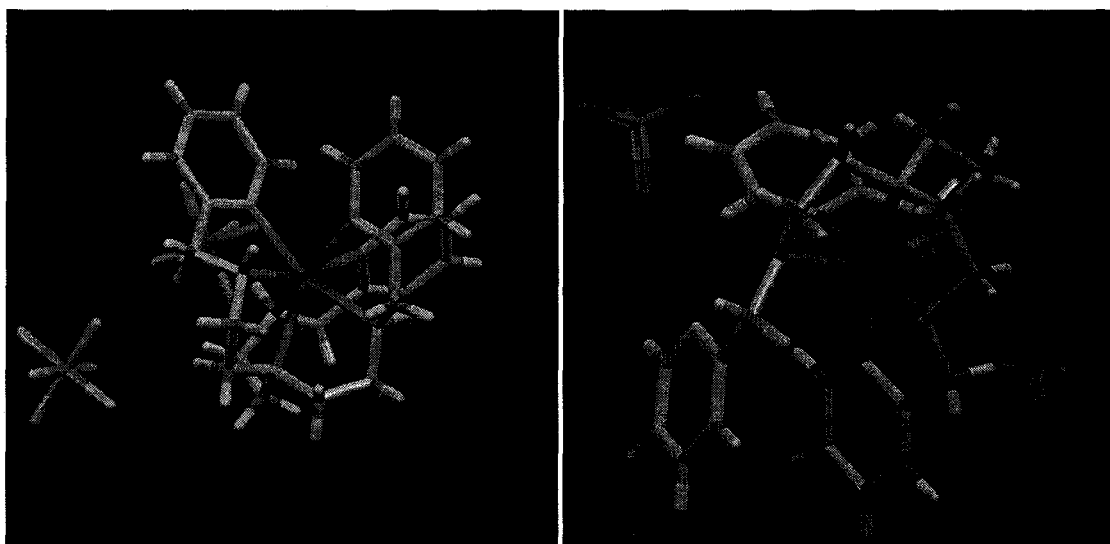


Figure 21 Structures of [Mn(TRENpyr)](PF₆)₂ and [Zn(TRENpyr)](ClO₄)₂. The images were created from data obtained in the Cambridge Structural Database (CSD).

In the same study (Mohamadou and Gérard) the protonation constants and binding constants of TRENpyr I.23 with Zn(II) were obtained potentiometrically (Table 3).

A small collection of papers by Hartmann and coworkers describe the gas (*i.e.* mass spectroscopy), solution, and solid state coordination environments of TRENpyr I.23 with Ni(II) and Cu(II).(65, 66) In the solid state the chelator binds two

Table 3 Protonation and Zn(II)-formation constants of TRENpyr I.23.

Equilibria (L=TRENpyr I.23)	LogK/β (25.0°C, μ=0.1), β for Zn(II) only
HL/L·H	9.12±0.01
H ₂ L/HL·H	8.14±0.01
H ₃ L/H ₂ L·H	6.91±0.01

Table 3 continued...	
H ₄ L/H ₃ L·H	2.50±0.01
H ₅ L/H ₄ L·H	1.0±0.3
ZnL/L·Zn	15.62±0.02
ZnLH/Zn·L·H	21.38±0.01
ZnLH ₂ /Zn·L·H ²	23.92±0.04

equivalents of Ni(II). The measured magnetic moment for this complex was 3.59BM, which is below the range expected for two paramagnetic Ni(II)-centers. The authors speculate that the complex cation contains one tetrahedrally bound Ni(II) ion, with experimental magnetic moments that range between 3.2-4.1BM, and one square planar Ni(II) ion, which does not contribute to the observed paramagnetism.⁽⁶⁷⁾ The authors admit that structural data for this species remains elusive. However, it is the opinion of the candidate that Hartmann and coworkers failed to account for the possibility of antiferromagnetic behavior within the dimetallic complex. From the elemental analysis data they report [Ni₂(TRENpyr)](BF₄)₂(OH)₂ which suggests the possibility that the hydroxyl groups are bridging the metal-centers. However, in solution and the gas phase a binding stoichiometry of 1:1 M:L was observed with Ni(II). The visible-near IR absorbance data supports Ni(II) in an octahedral environment. Similar behavior with Cu(II) was also observed, however solution and gas phase data indicated that TRENpyr **I.23** forms a tetragonally distorted monomeric complex with the metal.

Brewer *et al.* reported a reaction of Fe(III) with TREN **I.22** and three equivalents of 2-pyridinecarboxaldehyde that exclusively yields the Fe(II) complexes, [Fe(TRENpyr-trisimine)]X₂ (where X = ClO₄⁻ or PF₆⁻) (**Figure 22**).⁽⁶⁸⁾

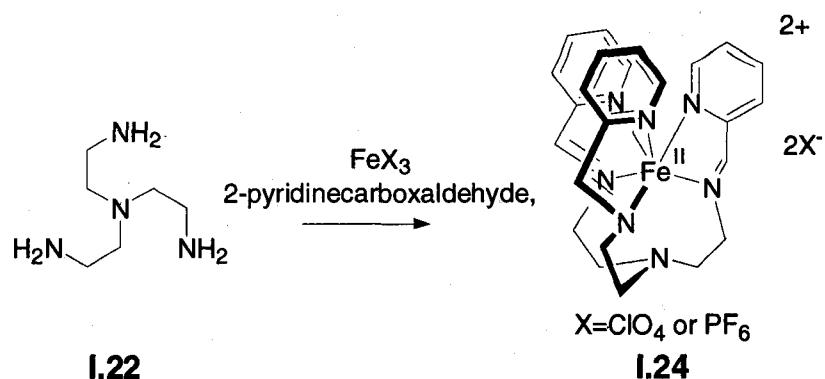


Figure 22 Preparation of $[\text{Fe}(\text{TRENpyr-trisimine})\text{X}_2]$.

The structure of $[\text{Fe}(\text{TRENpyr-trisimine})](\text{ClO}_4)_2$ **1.24** was determined with X-ray crystallography and features an octahedral Fe(II)-center with facial coordination of the pyridyl and imino N atoms (**Figure 23**). The short Fe-N bond distances (1.9747Å (Fe-N_{pyridyl}) and 1.9523Å (Fe-N_{imino})) support a low spin assignment for the Fe(II)-center. The apical N atom of the TREN **1.22** framework is nearly planar and is outside of bonding interactions with the metal at a distance of *ca.* 3.45Å. The low spin assignment is supported by Mössbauer spectroscopy, which reveals two low spin forms that are not in thermal equilibrium.

In sum the TREN framework is unique in that upon functionalization of the primary amines with additional donor groups the resulting ligand can offer its binding partner more than six coordinating atoms. This leads to interesting reactivity as evidenced by the SOD mimicry of $[\text{Fe}(\text{TRENpyr})]^{2+}$ and unique coordination geometries as illustrated by the seven coordinate complex $[\text{Mn}(\text{TRENpyr})]^{2+}$. Like sen derived ligands the TREN framework is more flexible than the corresponding TACH and TACN based ligating systems.

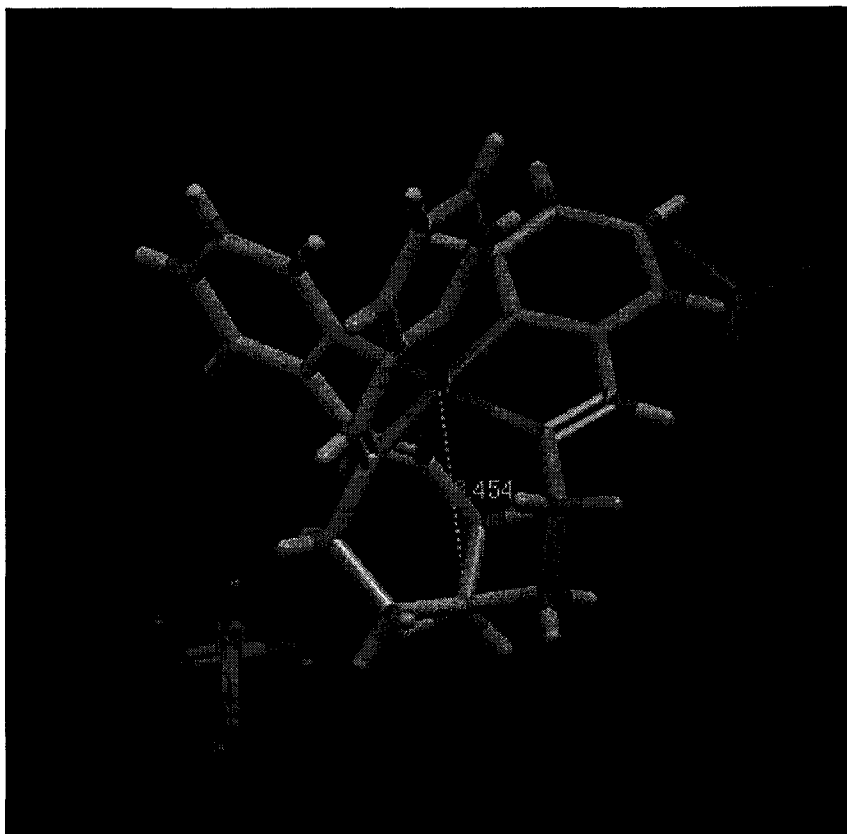


Figure 23 Structure of [Fe(TRENpyr-trisimine)](ClO₄)₂. The image was created from data obtained in the Cambridge Structural Database (CSD).

1.3.5. 1,3,5-Tris(aminomethyl)benzene ligands

Another class of tripodal chelators are based on the 1,3,5-*tris*-(aminomethyl)benzene framework **I.25** (Figure 24). This ligating group is more constrained than the aforementioned tripodal architectures. Lin and coworkers have prepared and characterized ligands **I.26** and **I.27**.(31, 69) Because of reduced flexibility within the arene-framework there was a tendency for the ligands to form trimetallic complexes with a host of divalent first-row transition metal ions.

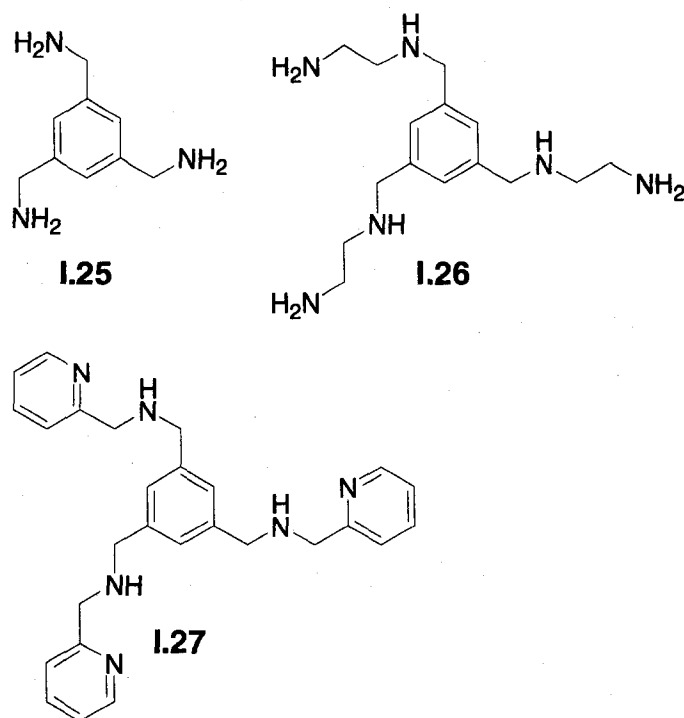


Figure 24 Chelators based on 1,3,5-tris(aminomethyl)benzene I.25.

The formation constants for the 3:1 M:L complexes are reported in **Table 4**.

Ligand	Co(II)	Ni(II)	Cu(II)	Zn(II)
I.27	16.97±0.12	22.35±0.16	24.07±0.06	23.00±0.07
I.26	28.44±0.06	28.57±0.13	29.17±0.09	28.49±0.06

Table 4 Formation constants ($\log\beta_{3,1,0}$) for ligands I.27 and I.26.

With the hexamine chelator **I.26** ternary complexes with *o*-phenanthroline were also studied (**Figure 25**). This study was aimed at better understanding the self-assembling processes that take place in the construction of coordination oligomers and polymers. In this case each branch of the tripod will bind a metal-center to afford a 3:1 M:L complex. The metal centers in each branch will be chemically and magnetically equivalent. The resulting thermodynamically robust and kinetically inert tripodal architecture can then be employed in the

construction of supramolecular systems that may possess interesting and useful physical properties.(70)

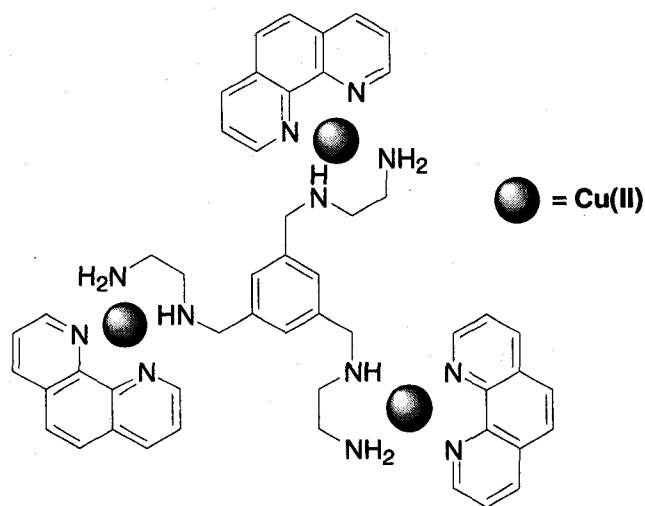


Figure 25 Putative structure of the ternary 3:1:3 M:L¹:L² complex. In this case M=Cu(II), L¹=1.26, and L²=o-phenanthroline.

1.4. Summary-The challenge of TAME

The tripodal framework TAME **1.36**, where TAME=1,1,1-tris(aminomethyl)ethane, has been under utilized in the preparation of new acyclic ligating architectures. Two reports in the literature describe the preparation and study of Mn(II), Fe(II), Co(II), and Zn(II) complexes of TAMEpyr-trisimine **1.51**, where TAMEpyr-trisimine= *N,N',N''*-tris(2-pyridylmethyl)-1,1,1-tris(iminomethyl)ethane.(71, 72) The structure of the complex [Fe(TAMEpyr-trisimine)]²⁺ was determined by crystallography and is indeed quite octahedral (Figure 26).

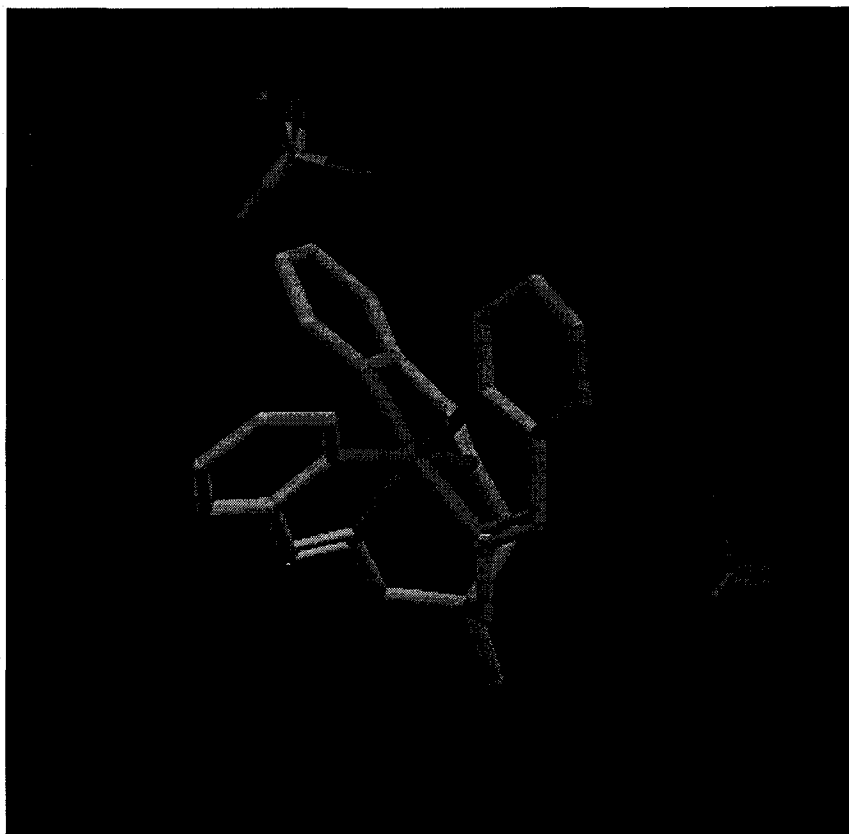


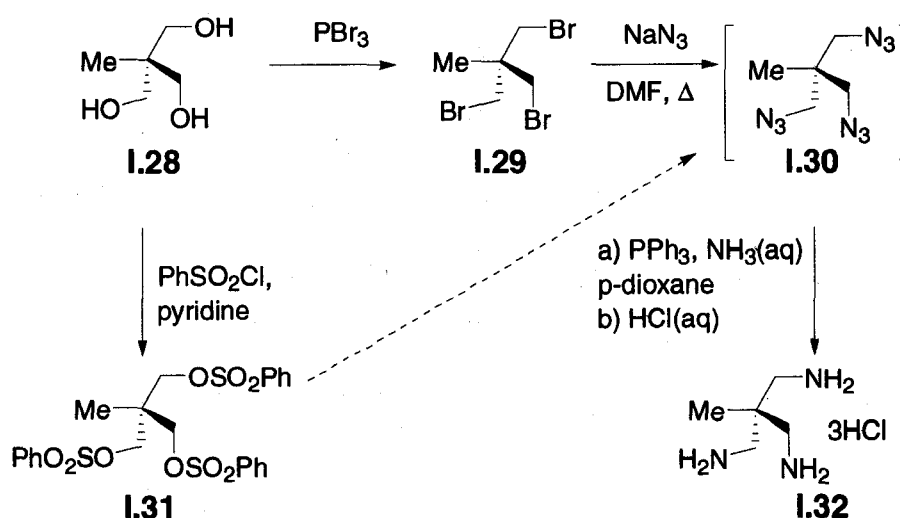
Figure 26 The structure of $[\text{Fe}(\text{TAMEpyr-trisimine})](\text{ClO}_4)_2$. The image was created from data obtained in the Cambridge Structural Database (CSD).

However, the hexahydro analogue TAMEpyr **I.60**, where TAMEpyr = N,N',N'' -tris(2-pyridylmethyl)-1,1,1-tris(aminomethyl)ethane, has not been prepared and studied until now. The following discussion describes the preparation and coordination chemistry of the novel hexadentate chelator TAMEpyr **I.60**. We utilized a Ni(II)-mediated Schiff base condensation of TAME **I.36** and TAME-derivatives with a variety of azaaromatic aldehydes to afford a new family of tripodal hexadentate chelators. The coordination chemistry of TAMEpyr **I.60** with various transition block and main group metal ions is presented and comparisons with our gold-standard chelator TACHpyr **I.14** are made. A portion of the following work has been published.(73)

Results and discussion

1.5. The preparation of the TAME framework

The preparation of the tripodal triamine TAME **I.36** began with the commercially available trialcohol **I.28** (Scheme 1). The hydroxyl groups in the starting material were converted into bromides via treatment with PBr_3 .^(74, 75)



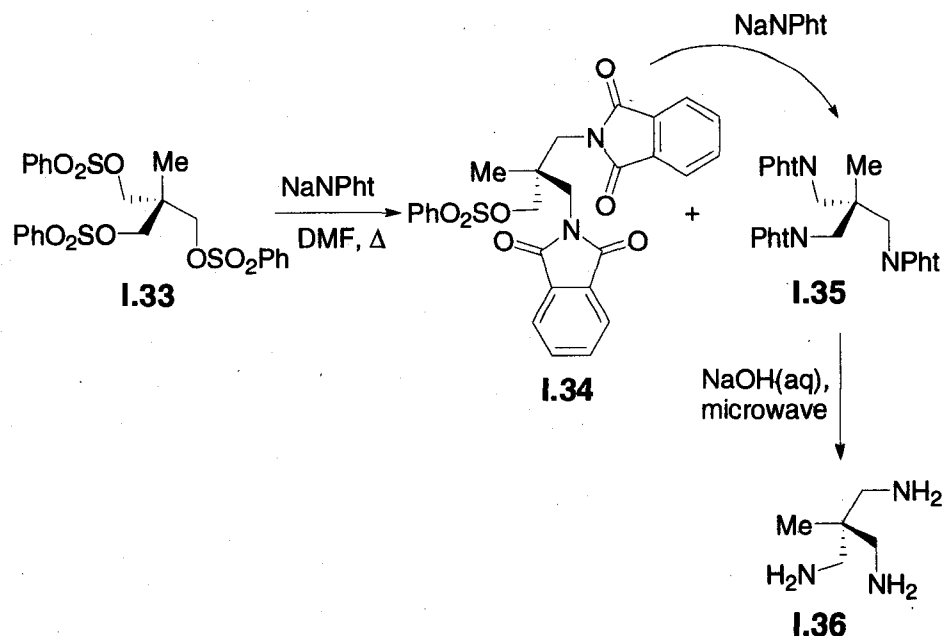
Scheme 1 The preparation of TAME-3HCl

The disadvantage of this reaction was the production of copious amounts of HBr during the addition of PBr_3 to the reaction pot. This by-product was scrubbed from the head-space of the reaction vessel by piping the evolving gas into a solution of NaOH . An alternative approach that avoids the production of caustic fumes is to convert the hydroxyl groups into an arenesulfonate via treatment of the starting material with the appropriate arenesulfonyl chloride. The tribromide **I.29** underwent a reaction with NaN_3 to afford the crude triazide **I.30**. Fleischer had isolated the triazide and partially characterized it (IR analysis). However,

due to the explosive nature of polyazides this material was generated *in situ* and then subsequently reduced via a Staudinger reaction with triphenylphosphine in $\text{NH}_3(\text{aq})$ and p-dioxane.(76, 77) This approach, initially developed by Martin *et al.*, is attractive because it does not require the use of LiAlH_4 whose reaction with water or air could cause an explosion. The desired triamine was then isolated from solution in moderate yield (40.2%) as the hydrochloride salt **I.32** via treatment with HCl and filtering the resulting precipitate.

Following the method of Fleischer *et al.* the starting material **I.28** was also converted into the corresponding benzenesulfonate **I.31**.(78) The particular advantage of this reaction was that the product could be recrystallized from EtOH/acetone in excellent yields (92.3%). Albeit trivial, compound **I.31** can then be converted into TAME·3HCl **I.32** via the same reaction sequence of the tribromide **I.29**.

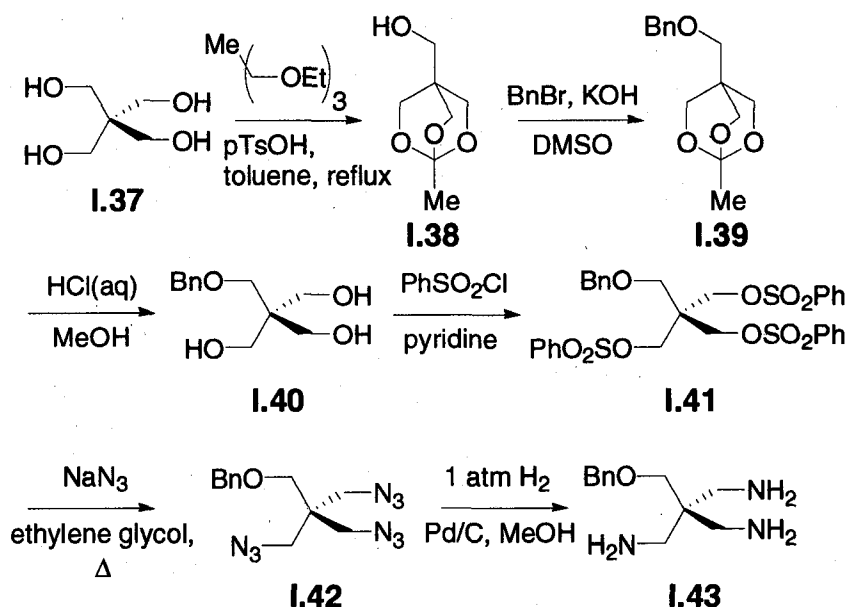
An alternative preparation of the free base TAME recently arose from the research efforts of Dunn *et al.* (**Scheme 2**). (79)



Scheme 2 Dunn's preparation of TAME.

Looking to avoid the preparation of polyazides, Dunn developed a strategy that initially relied on the so-called Gabriel reaction.⁽⁸⁰⁾ Starting with the aforementioned benzenesulfonate **I.33** the corresponding trisphthalimide **I.35** was prepared in poor yield (*ca.* 20%). The reduction in yield can be compensated for by simply running the reaction on larger scale and recovering the bisphthalimide by-product **I.34**. Geue and coworkers reported that the recovered material can be treated with additional sodium phthalimide (NaNPht) to afford the desired product **I.35**.⁽⁸⁰⁾ The subsequent reaction of **I.35** with NaOH as reported by Geue requires the use of a reaction bomb. Dunn avoided that step by carrying out the hydrolysis in a microwave oven in a closed vessel. The desired product was then extracted from the reaction liquor as the free base TAME **I.36** which was used as is in subsequent chemistries.

In order to explore polyfunctional TAME derivatives that could be used to link, immobilize, or target TAME chelators the differentiation of pentaerythritol **I.37** was studied (Scheme 3).⁽⁸¹⁾

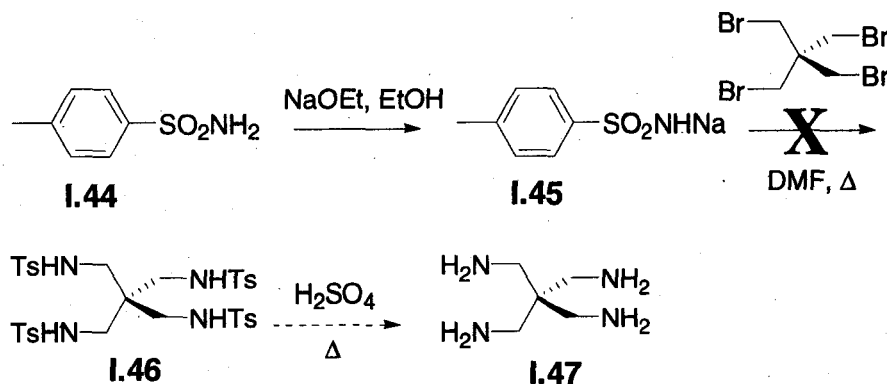


Scheme 3 The preparation of TAME derivative **I.43**.

The pentaerythritol starting material was converted into an orthoester **I.38** with triethyl orthoacetate and catalytic pTsOH. This step furnished the differentiated pentaerythritol derivative **I.38** that possessed a lone hydroxyl group. This particular compound was susceptible to low-pressure sublimation which greatly facilitated the purification of the crude product slate. The lone hydroxyl group was then converted into a benzyloxy group via a Williamson etherification reaction affording compound **I.39**. The orthoester functionality of compound **I.39** then underwent acid-mediated decomposition with dilute aqueous HCl yielding the trialcohol **I.40**. This key synthetic intermediate could be purified by trituration with Et₂O. The hydroxyl groups of **I.40** were converted into the corresponding

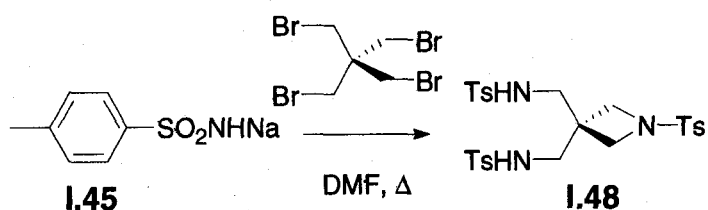
benzenesulfoxy groups using the aforementioned Fleischer chemistry.⁽⁷⁸⁾ The resulting compound **I.41** was then heated with NaN_3 in ethylene glycol affording the desired triazide **I.42**. The triazide **I.42** was isolated via a liquid-liquid extraction and partially characterized (IR analysis) to ensure that all the benzenesulfoxy leaving groups had departed. The isolated triazide **I.42** (*caution!*) was subsequently dissolved in MeOH and reduced with 1 atm of H_2 in the presence of catalytic Pd^0 . This reaction afforded the desired TAME derivative **I.43** in nearly quantitative yield.

An alternative approach to differentiated TAME derivatives came about serendipitously. Initial attempts at the preparation of tetraamine **I.47** were met with limited success (**Scheme 4**).



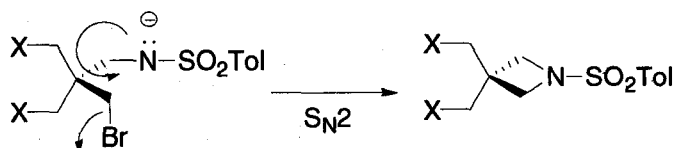
Scheme 4 Attempted preparation of tetraamine I.47.

The major by-product from the failed reaction was highly crystalline and could be recrystallized from boiling EtOH to afford the azetidine **I.48** in *ca.* 30% yield (**Scheme 5**).



Scheme 5 Formation of azetidine 1.48.

The close proximity of a nucleophilic sulfonamide to an adjacent electrophilic primary bromide on the same molecule creates a high local concentration of reacting partners thus facilitating an intramolecular ring closure via an S_N2 mechanism (**Figure 27**).

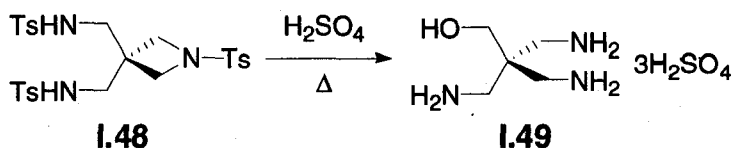


X=NHTs or Br

Figure 27 Proposed mechanism of ring-closure.

This would suggest that the reaction was carried out under kinetic control and the initially desired tetrasulfonamide **1.46** could possibly be accessed under more forcing conditions. Further attempts at the tetrasulfonamide were not carried out. Presumably a spiroazetidine would not form because of excessive ring-strain in the *spiro*[3.3]heptane skeleton.⁽²¹⁾

The azetidine **1.48** is still a synthetically useful reagent because it readily undergoes a detosylation/ring-opening reaction in refluxing 70% aqueous H_2SO_4 to afford the differentiated TAME derivative **1.49** as a hydrogen sulfate salt (**Scheme 6**).

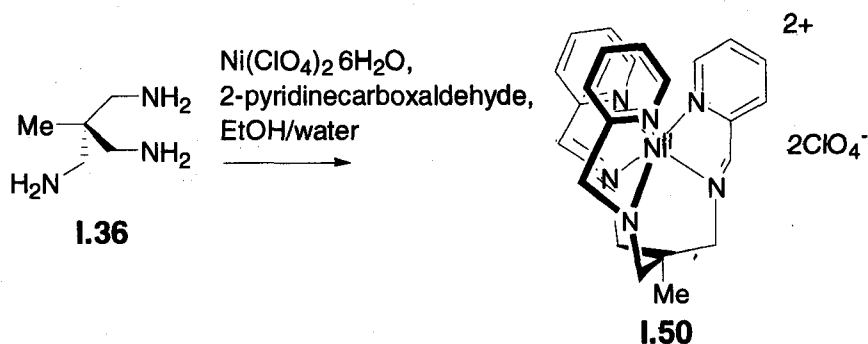


Scheme 6 Preparation of TAME derivative I.49.

The attractive feature of this reaction sequence is two-fold: reduction of the number of synthetic steps to gain access to the desired triamine scaffold (6 steps in **Scheme 3** as opposed to 2 steps); and there is no need to prepare and handle any explosive polyazides. It was later discovered that Litherland and Mann had already reported the azetidine **I.48** and the corresponding hydrolysis reaction to afford compound **I.49** in 1938.⁽⁸²⁾

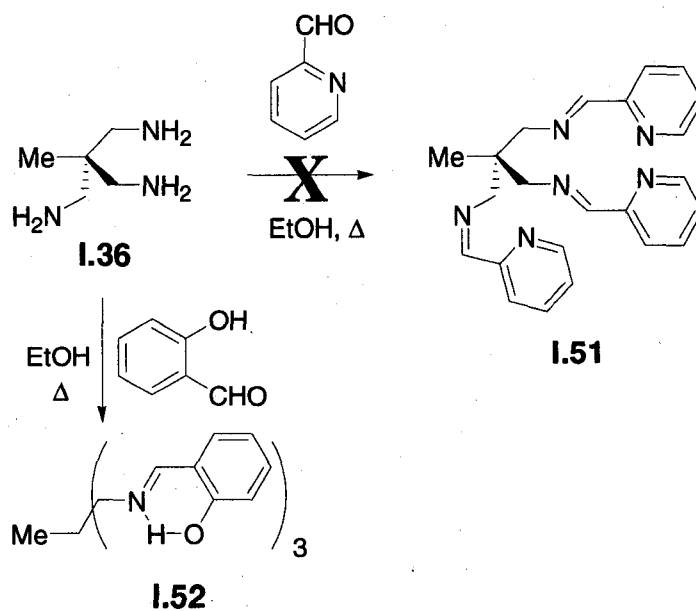
1.6. The Ni(II)-mediated template reaction of TAME

The tripodal triamine TAME **I.36** can be condensed with three equivalents of 2-pyridinecarboxaldehyde and one equivalent of a Ni(II) salt to cleanly afford the trisimine complex **I.50** (**Scheme 7**) in moderate yield (40.2% isolated yield).



Scheme 7 The preparation of [Ni(TAMEpyr-trisimine)]²⁺ I.50.

The advantage of the template methodology became apparent when attempts were made at the direct preparation of TAMEpyr-trisimine **I.51** via a metal-free Schiff base condensation (**Scheme 8**), which showed that



Scheme 8 Schiff base condensations of TAME.

the major products isolated from the direct reaction of TAME and 2-pyridinecarboxaldehyde were not the desired trisimine **I.51** but rather a mixture of amina **I.54** and the trisubstituted-triazaadamantane **I.53** (**Figure 28**).

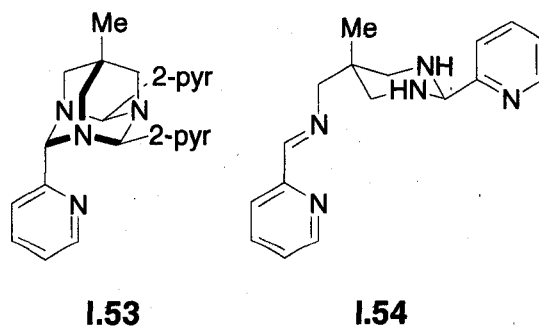


Figure 28 Products isolated from the attempted direct preparation of TAMEpyr-trisimine.

During the course of the reaction the close proximity of a primary amine and adjacent imine greatly increases the local concentration of reacting partners. This facilitates an intramolecular ring closure affording amina **1.54** as an intermediate. The amina then undergoes subsequent cyclization-reactions to afford the triazaadamantane **1.53**. The triazaadamantane **1.53** was first prepared in 1957 by Dwyer *et al.* but they incorrectly proposed the trisimine structure **1.51** (83). The development of NMR methods led to the discovery of the correct adamantyl-like structure **1.53** nearly a decade later (84). The assignment of the position of the 2-pyridyl groups was finally accomplished in 1978 by Webb and Edwards. (85) Their NMR data were consistent with the presence of a single isomer containing diequatorial and monoaxial pyridyl groups (**Figure 28**). This adamantyl structural motif was also seen by Webb and Edwards in the condensation product of TAME **1.36** and benzaldehyde.

As was discussed in the preparation of the differentiated TAME derivative **1.43** (**Scheme 3**) it appears that competing intramolecular cyclizations are a common reaction motif in this class of neopentyl derivatives. However, if TAME was reacted with salicylaldehyde no cyclization products were observed (**Scheme 8**). The trisimine **1.52** formed in excellent yield (93.6%), likely because the phenolic group can readily engage in a hydrogen bond (as shown in **Scheme 8**) with the pendant arm imine thus thwarting any intramolecular cyclizations.

The ligand donor set N_3O_3 in the ligand **1.52** is ideally suited for harder cations (*e.g.* Fe(III), Ga(III), Cr(III), *etc.*). To demonstrate this a 1:1 complex with

Cr(III) was prepared by reacting **I.52** with $\text{CrCl}_3 \cdot 6\text{H}_2\text{O}$ in the presence of Na_2CO_3 (Figure 29).

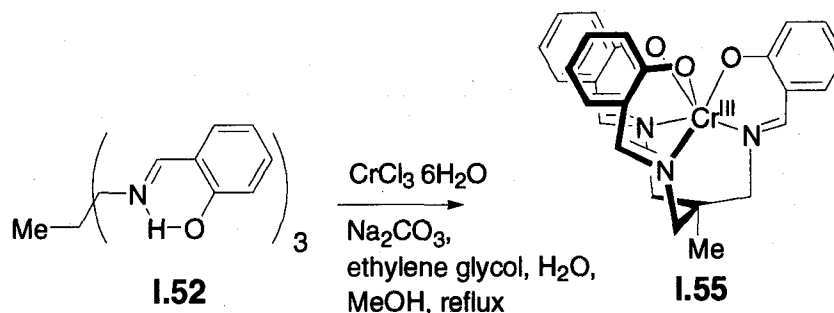
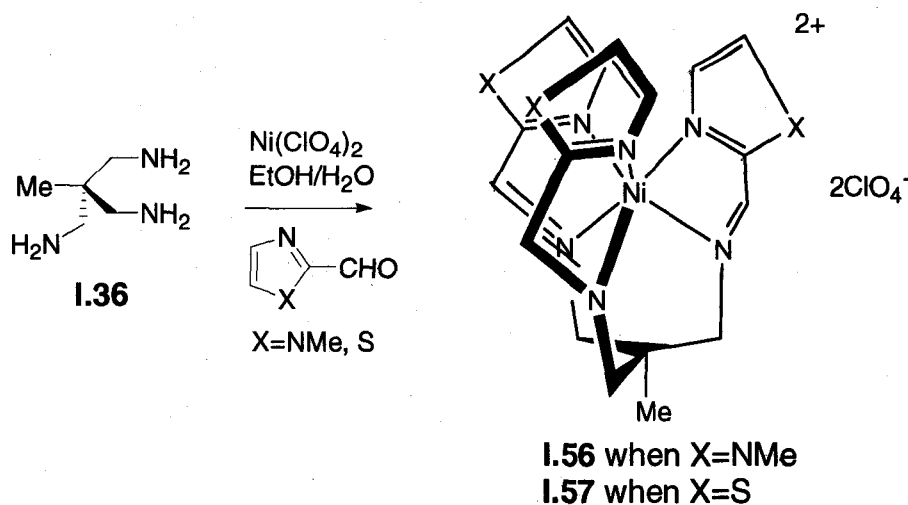


Figure 29 Preparation of the novel CrN_3O_3 complex **I.55**.

The reaction mixture needed to be refluxed with ethylene glycol because of the inert-nature of Cr(III). It is known that water-ligand exchange rates depend on both the charge and the ligand field stabilization energy (LFSE) of the cation.⁽⁸⁶⁾ The effect is most evident in Cr(III) and Co(III), both trivalent cations possessing local minima of LFSE amongst ions of the first row d-block with electronic configurations of d^3 and low-spin d^6 respectively. Because of this Cr(III) ligand substitution occurs through an associative mechanism (I_a) rather than a dissociative one (I_d).⁽⁸⁷⁾ Therefore, association of ligand **I.52** with Cr(III) will be hindered by unfavorable steric interactions within the inner coordination sphere, thus slowing the rate of complexation. The sluggish nature of the complexation allowed a competing hydrolysis of the Schiff base ligand to occur which drastically reduced the isolated yield of the complex to *ca.* 15%.

The template reaction also proceeds when the heterocycle is a five membered-ring. This was demonstrated by preparing trisimine complexes of TAME with 2-imidazolecarboxaldehyde and 2-thiazolecarboxaldehyde (Scheme 9).



Scheme 9 The Ni(II)-mediated template reaction of TAME with five-membered ring heterocycles.

This result is noteworthy because α -thiazolyl and α -imidazolyl groups, as claimed in the literature, are poorly oriented for chelation as compared to their six-membered counterparts (*e.g.* α -pyridyl). (88-91) The non-ideal chelating dispositions of these groups result in poor orbital overlap between the donor atom and the metal center.

A crystallographic study of the complex $[\text{Fe}(\text{TACHTz})](\text{ClO}_4)_2$, where $\text{TACHTz} = N,N',N''\text{-tris}(2\text{-thiazolylmethyl})\text{-cis,cis-1,3,5-triaminocyclohexane}$, showed that chelating thiazolyl groups will adequately bind Fe(II) when appended to a tripodal architecture (Table 5).

Table 5 Crystal data and structure refinement for $[\text{Fe}(\text{TACHTz})](\text{ClO}_4)_2$.

Compound	$[\text{Ni}(\text{TACHTz})](\text{ClO}_4)_2$
Color/shape	Red/block
Empirical formula	$\text{C}_{18}\text{H}_{24}\text{Cl}_2\text{FeN}_6\text{O}_8\text{S}_3$
Temperature	213(2) K
Crystal system	Monoclinic
Space group	$P2(1)/2$
Unit cell dimensions	$a=17.101(4)\text{\AA}$ $\alpha=90.00^\circ$

Table 5 continued...

	b=8.781(2)Å	β=92.098(3)°
	c=16.320(4)Å	γ=90.00°
Volume	2449.1(10)Å ³	
Z	4	
Density (calculated)	1.832 Mg/m ³	
Absorption coefficient	1.150mm ⁻¹	
Diffractometer/scan	Bruker SMART/CCD area detector	
Radiation/wavelength	Mo Kα (graphite monochrom.)/0.7107Å	
F(000)	1384	
Crystal size	0.40x0.30x0.20mm	
θ Range for data collection	1.19 to 28.18°	
Index ranges	-22≤h≤2, -11≤k≤10, -21≤l≤21	
Reflections collected	17824	
Independent reflections	5677	
Observed reflections	5677	
Data/restraints/parameters	5677/0/439	
Goodness-of-fit on F ²	1.030	
Final R indices [I>2σ(I)]	R ₁ =0.0371, wR ₂ =0.0937	
R indices (all data)	R ₁ =0.0453, wR ₂ =0.1011	
Largest diff. peak and hole	0.717 and -0.521e.Å ⁻³	

Table 6 Crystal data and structure refinement for [Fe(TACHtz)](ClO₄)₂.

The ORTEP view of the [Fe(TACHtz)]²⁺ complex cation clearly shows the Fe(II) center in a nearly perfect octahedral geometry (**Figure 30**). The measured average twist angle α was 52(1)°, which is very close to the ideal value of 60°.

The disposition of the thiazolyl groups toward the metal center was assessed by measuring the “bite” of the three 5-membered chelate rings. The average distance between the nitrogen donors in each of the pendant arms is 2.64(1)Å, which is accompanied by an average N(het.)-Fe-N(amine) bite-angle of 83.0(5)°.

When compared to the closely related complex [Fe(TACH-3-Mepyr)]Cl₂, with a measured intra-chelate nitrogen distance of 2.65(1)Å and a bite-angle of 83.6(4)°, it appears that chelating thiazolyl groups are efficient donors when appended to a tripodal framework (unpublished results). The author of this dissertation believes trigonal twisting about the C₃ principal rotation axis allows the thiazolyl groups to achieve adequate dispositions for good orbital overlap with the metal center.

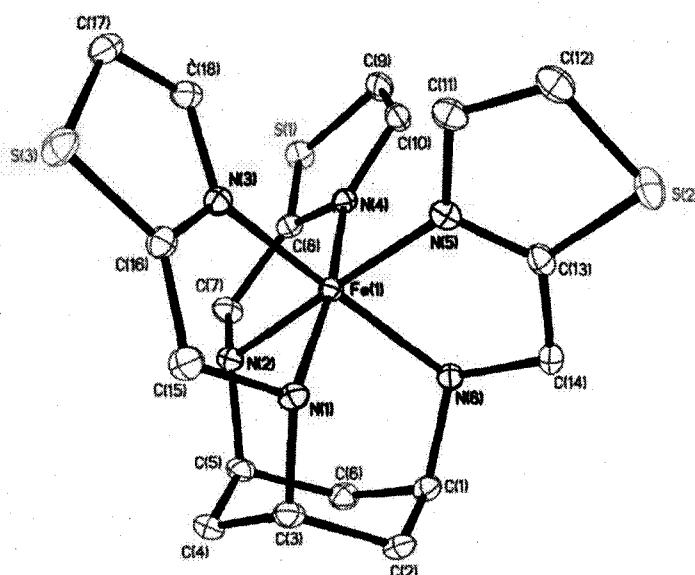
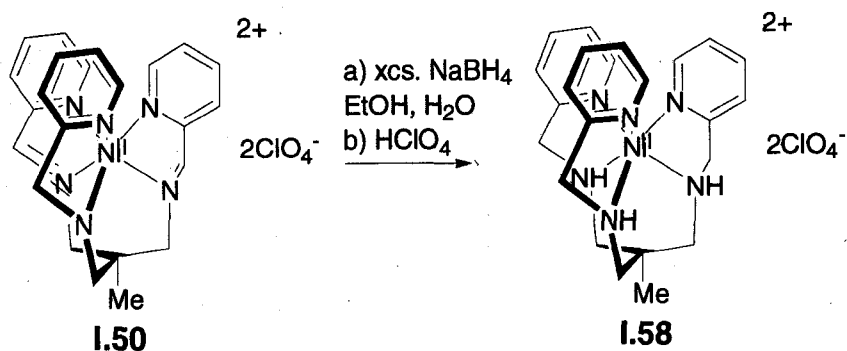


Figure 30 The ORTEP view of the cation $[\text{Fe}(\text{TACHTz})]^{2+}$.

1.7. Tetrahydroborate reduction

The versatility of the template reaction is evident from the subsequent tetrahydroborate reduction of $[\text{Ni}(\text{TAMEpyr-trisimine})]^{2+}$ **I.50**. The resulting triamino complex $[\text{Ni}(\text{TAMEpyr})]^{2+}$ **I.58** (Scheme 10) was generated cleanly. (73)



Scheme 10 The tetrahydroborate reduction of $[\text{Ni}(\text{TAMEpyr-trisimine})]^{2+}$ **I.50**.

This reaction proceeds through reductive demetallation initially producing metallic Ni⁰ (*i.e.* nickel-black) as a precipitate and putatively the free ligand TAMEpyr-trisimine **I.51** (Figure 31). The reaction mixture contains excess NaBH₄ which is free to reduce the triimino ligand **I.51** to the triamino ligand TAMEpyr **I.60**. The reaction is quenched by the addition of concentrated HClO₄ until a pH of approximately 6 is achieved (assessed with pH paper). The advantage of HClO₄ as a quenching reagent is three-fold: it will decompose the excess NaBH₄ into B(OH)₃ which prevents over reduction that would affect the heterocyclic rings(92), it will decompose the boron-amido complexes **I.59** liberating the free secondary polyamine **I.60**, and finally it will oxidize the nickel-black to Ni(II). The Ni(II) is subsequently captured by the emerging TAMEpyr to afford a pink [Ni(TAMEpyr)]²⁺ complex **I.58**. The generation of this complex provides the investigator with a colorimetric indicator signaling the completion of the reaction.

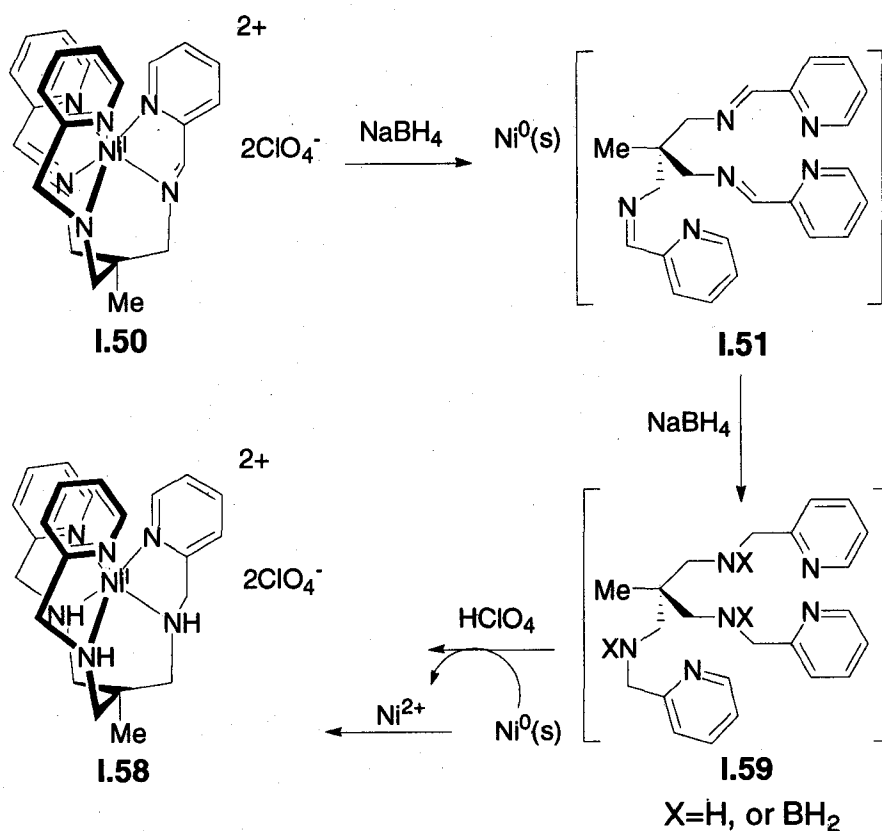


Figure 31 Putative mechanism for tetrahydroborate reduction of $[\text{Ni}(\text{TAMEpyr-trisimine})]^{2+}$ **1.50**.

1.8. Comparison of ligand field properties of TAMEpyr and TAMEpyr-trisimine via Ni(II) complexes

The orange complex $[\text{Ni}(\text{TAMEpyr-trisimine})]^{2+}$ **1.50** and the pink $[\text{Ni}(\text{TAMEpyr})]^{2+}$ complex **1.58** were studied with absorbance spectroscopy. In the visible-near IR spectrum of unreduced $[\text{Ni}(\text{TAMEpyr-trisimine})]^{2+}$ **1.50** (orange colored spectrum in **Figure 32**) the presence of a metal-to-ligand charge-transfer (MLCT) band starting at ca. 490 nm (20400 cm^{-1}) and proceeding into the UV region is characteristic of the pendant arm imino groups.⁽⁹³⁾ This band was

noticeably absent in the spectrum of $[\text{Ni}(\text{TAMEpyr})]^{2+}$ (pink colored spectra *ibid.*) indicating the desired reduction had occurred.

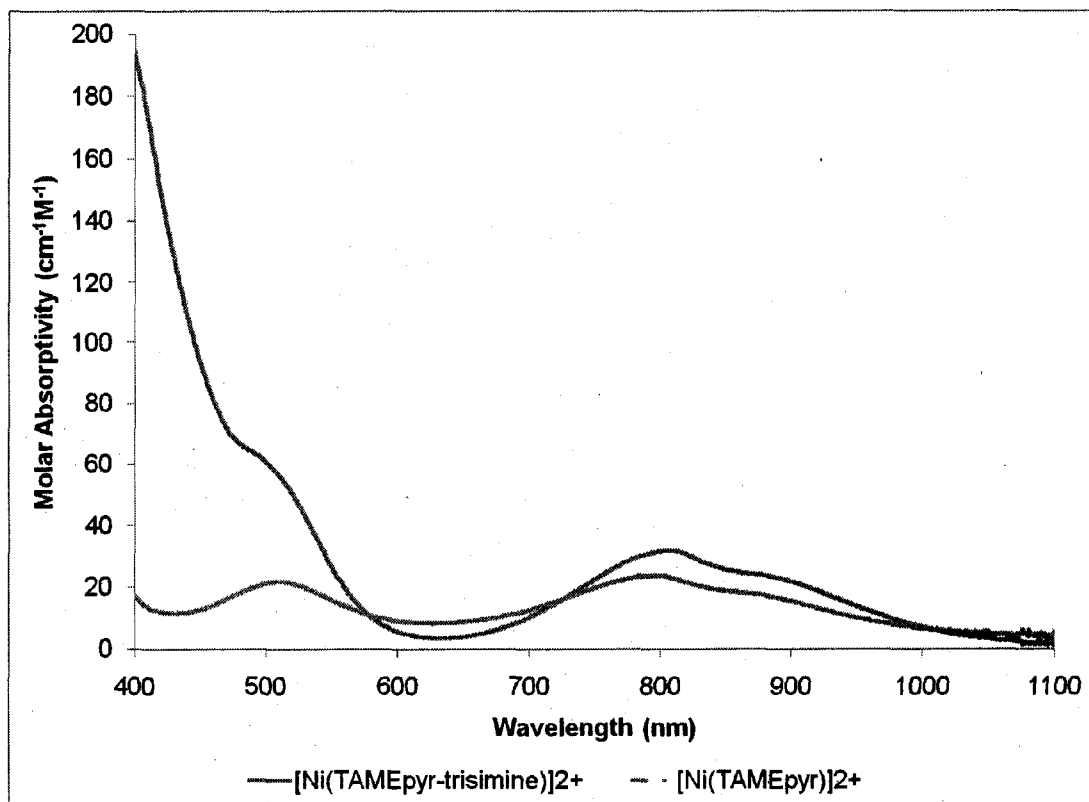


Figure 32 The visible absorbance spectra of $[\text{Ni}(\text{TAMEpyr-trisimine})]^{2+}$ **I.50** and $[\text{Ni}(\text{TAMEpyr})]^{2+}$ **I.58** in MeCN at 25°C.

The shoulder that appears at *ca.* 490 nm (20400 cm⁻¹, $\epsilon=65$ cm⁻¹M⁻¹) in the spectrum of **I.50** is the ${}^3A_{2g} \rightarrow {}^3T_{1g}(F)$ metal-centered *d-d* transition. This assignment suggests that this complex possesses a pseudo-octahedral geometry in solution.⁽⁴³⁾ This structural assignment is corroborated by the presence of a low-energy transition at 804 nm (12400 cm⁻¹, $\epsilon=32$ cm⁻¹M⁻¹) with a shoulder at *ca.* 865 nm (11600 cm⁻¹, $\epsilon=24$ cm⁻¹M⁻¹). This particular transition is assigned as the metal-centered ${}^3A_{2g} \rightarrow {}^3T_{2g}$ band envelope that is overlapping with a spin-forbidden ${}^3A_{2g} \rightarrow {}^1E_{1g}$ transition.⁽⁴²⁾ This electronic transition is rather

useful because it correlates well with the crystal field splitting parameter Δ_o .(28)

The value of Δ_o is a measure of the energy difference between the bonding t_{2g} and antibonding e_g metal-centered d -orbitals in an octahedral field (Figure 33).

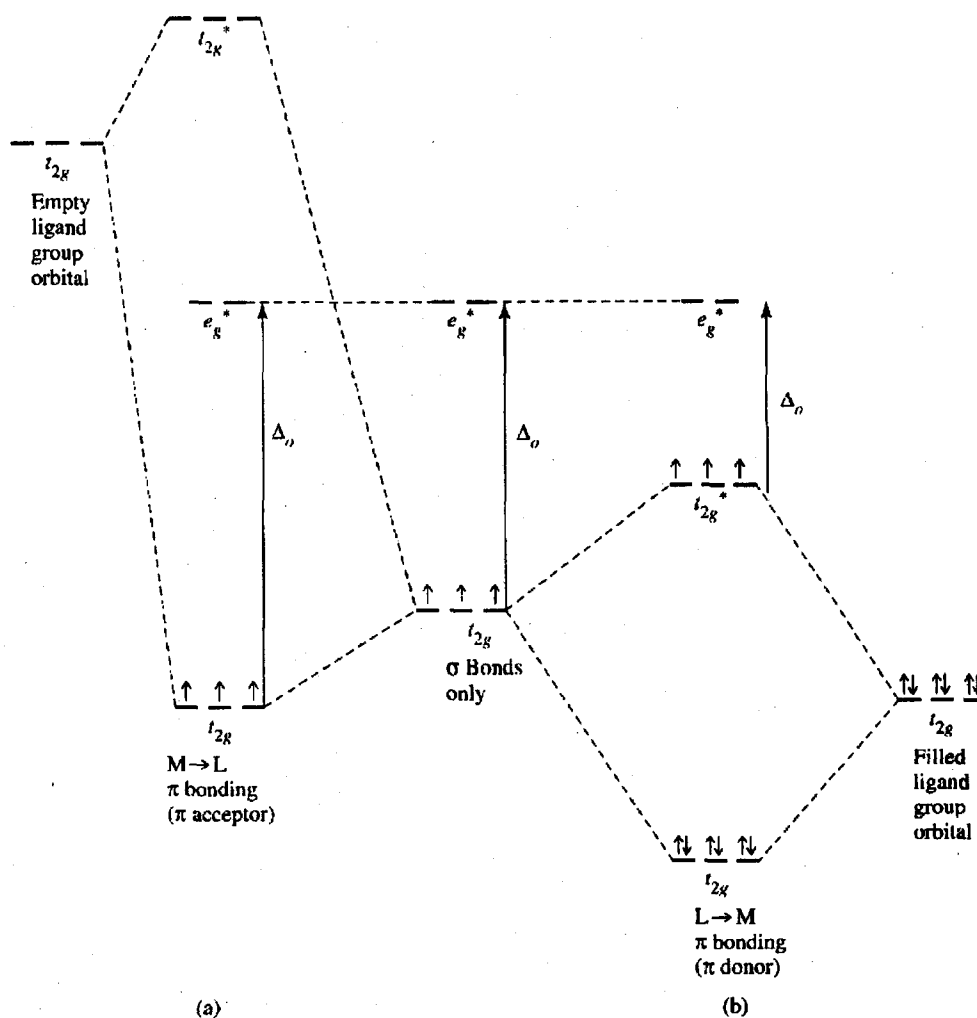


Figure 33 Splitting of metal d -orbitals in an octahedral field for a d^3 ion.(94)

If a ligand, like TAMEpyr-trisimine **1.51**, is a good σ -donor and π -acid then the metal will be highly stabilized in that ligand field resulting in a large Δ_o (to the left in Figure 33). The converse is true if the ligand is a poor donor/acceptor or

possesses a donor atom disposition that is incongruent with the metal-ion in the complex. This will cause a decrease in Δ_0 and a bathochromic shift in the ${}^3A_{2g} \rightarrow {}^3T_{2g}$ band envelope. The values of Δ_0 obtained from the spectra of a series of structurally related tris(α -diimine) complexes of Ni(II) tend to vary between 10400 and 12800 cm^{-1} .⁽⁹⁵⁾ The value of Δ_0 for complex **I.50** (12400 cm^{-1}) was approximated from the lowest energy transition in the absorbance spectrum. A reported low energy transition of 14000 cm^{-1} for the related complex $[\text{Ni}(\text{TACHpyr-trisimine})]^{2+}$ is far-removed from the expected range of Δ_0 .⁽⁹³⁾ This spectral aberration was rationalized by assuming a non-octahedral geometry in solution.

The exact value of Δ_0 and the so-called Racah ligand field parameter B' , which is a measure of the interelectronic repulsions of the metal d -electrons, can be obtained for a d^8 metal in an octahedral field if all three spin-allowed transitions are observed in the absorbance spectrum.⁽²⁸⁾ Unfortunately, the highest energy ${}^3A_{2g} \rightarrow {}^3T_{1g}(\text{P})$ $d-d$ transition was obscured in the spectrum of **I.50** by the presence of the aforementioned MLCT band. Moreover, the approximation/ratiometric method as explained in the text of Miessler and Tarr requires one to know the exact position of the ${}^3A_{2g} \rightarrow {}^3T_{1g}(\text{F})$ transition.⁽⁹⁴⁾ The symmetry labels located in the parentheses next to ${}^3T_{1g}$ (*i.e.* P or F) refer to the corresponding Russel-Saunders term symbols for the free-ion. Ascertaining that value proved challenging because of the overlap with the MLCT band. Furthermore, it appears that this band is artificially large ($\epsilon=65 \text{ cm}^{-1}\text{M}^{-1}$) because of intensity-borrowing with the adjacent MLCT band.

Interpretation of the spectrum of complex **I.58** was more straightforward because of the lack of the MLCT band upon reduction (pink spectrum in **Figure 32**). The higher energy ${}^3A_{2g} \rightarrow {}^3T_{1g}(F)$ transition in $[Ni(TAMEpyr)]^{2+}$ **I.58** occurred at 510 nm (19600 cm^{-1} , $\epsilon=21\text{ cm}^{-1}\text{M}^{-1}$) indicating that the complex maintains a pseudooctahedral geometry in solution. This claim was further corroborated by the presence of the low-energy transition at 794 nm (12600 cm^{-1} , $\epsilon=24\text{ cm}^{-1}\text{M}^{-1}$) and a shoulder at *ca.* 861 nm (11600 cm^{-1} , $\epsilon=18\text{ cm}^{-1}\text{M}^{-1}$), which has been assigned as the ${}^3A_{2g} \rightarrow {}^3T_{2g}$ band envelope overlapping with the ${}^3A_{2g} \rightarrow {}^1E_{1g}$ spin-forbidden transition. A pseudooctahedral structural assignment came as no surprise because it was anticipated that reduction of the imino groups to the amino groups in **I.58** would result in a more flexible ligating scaffold that could better accommodate the preferred octahedral geometry of six-coordinate Ni(II). It appears that the loss of the π -acidic imino groups in complex **I.50** was energetically compensated for by relaxing the strain within the chelator. In fact, a slight blue-shift of *ca.* 10 nm (160 cm^{-1}) in Δ_o upon C=N reduction suggests that the Ni(II)-is better stabilized by the triamino ligand TAMEpyr **I.60**.

The Racah ligand field parameter B' was calculated from the spectrum of $[Ni(TAMEpyr)]^{2+}$ **I.58** and the Tanabe-Sugano diagram (**Figure 34**) for a d^8 metal.⁽⁹⁴⁾

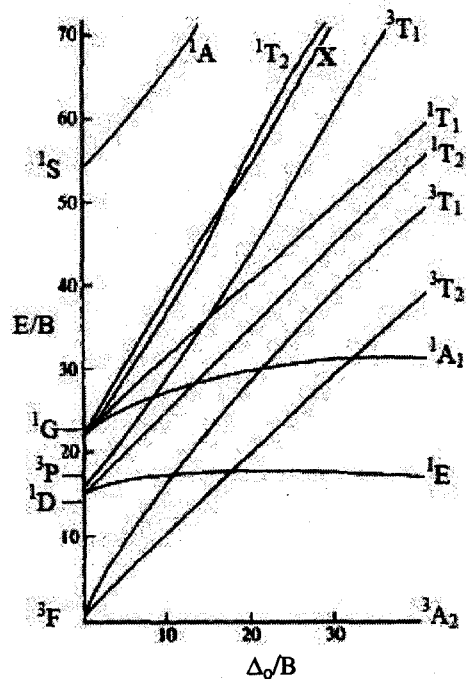


Figure 34 Tanabe-Sugano diagram for a d^6 metal ion.

A plot of the ratio of the ${}^3T_{1g}(F)$ and ${}^3T_{2g}$ transitions (ν_2/ν_1) as a function of Δ_0/B' was created from the Tanabe-Sugano diagram and exponentially fit (**Figure 35**). The spectrum of complex **1.58** was used to calculate the ν_2/ν_1 ratio ($\nu_2/\nu_1=1.56$). The value of Δ_0/B' for $[\text{Ni}(\text{TAMEpyr})]^{2+}$ **1.58** was then ascertained from **Figure 35** ($\Delta_0/B' = 24$) and used to calculate the Racah parameter ($B'=530 \text{ cm}^{-1}$) and a more accurate value of Δ_0 ($\Delta_0=12700 \text{ cm}^{-1}$).

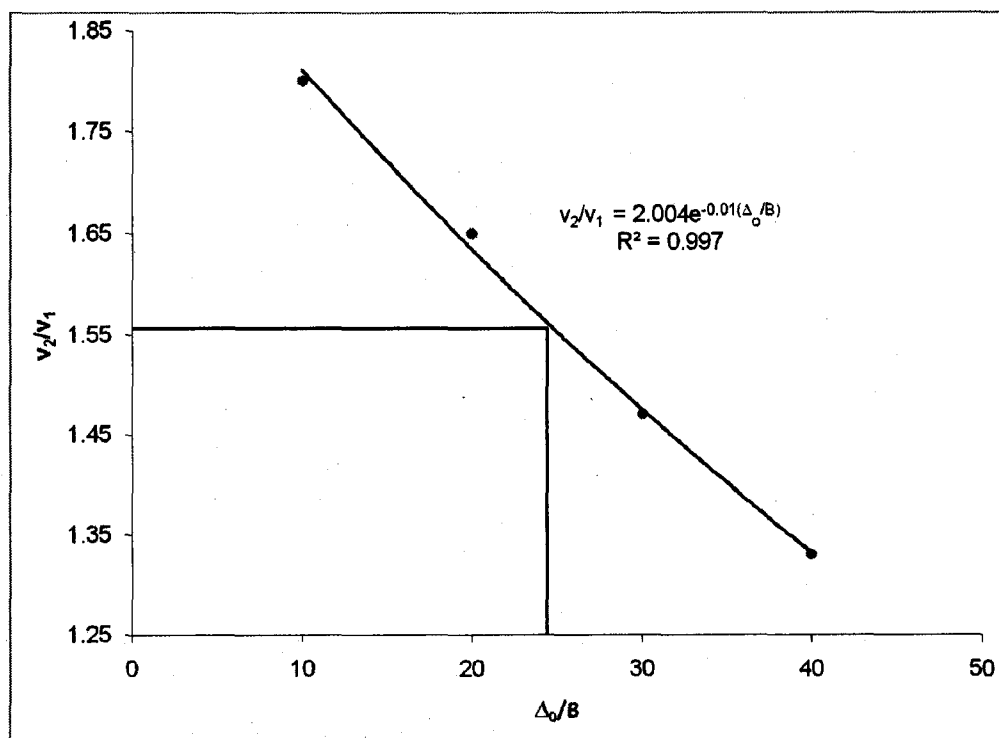


Figure 35 Assessment of Δ_o/B' for $[\text{Ni}(\text{TAMEpyr})]^{2+}$ I.58.

Unlike tris(α -diimine) Ni(II) complexes which have Racah parameters (B') that vary between 740 and 880 cm^{-1} , the triamino complex I.58 possesses enhanced covalent character as compared to the trisimine complex I.50 with a calculated value of $B'=530 \text{ cm}^{-1}$.⁽⁹⁵⁾ This came as a surprise because loss of the imino groups on reduction should reduce the π -acidity of the ligand concomitantly enhancing the interelectronic repulsions of the d -electrons due to reduced metal-to-ligand backdonation. The Racah parameter depends on both the π -acidity of the ligand and the ligand-metal fit, which might be perturbed by the presence of the imino groups in $[\text{Ni}(\text{TAMEpyr-trisimine})]^{2+}$.

A calculation of the so-called nephelauxetic parameter β , which is a ratio of the Racah parameter for the complex I.58 (B') and the Racah parameter for the gaseous free-ion (B) was carried out. This value is telling of how well the

ligand can reduce interelectronic repulsions on the metal upon coordination. A value of 1.00 tells the investigator that the metal-ligand bonding is purely electrostatic. A value of β less than 1.00 indicates increasing covalency within the metal-ligand coordinate bonds. The value of B for free Ni(II) is 1041cm^{-1} which results in a value of β for $[\text{Ni}(\text{TAMEpyr})]^{2+}$ **I.58** of 0.51.(28)

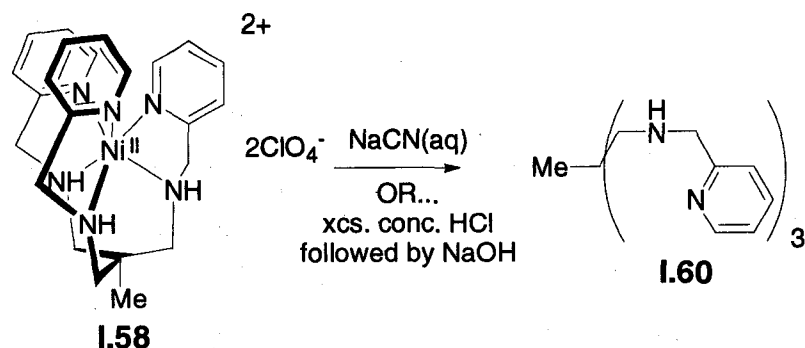
The more accurate ligand field splitting parameter Δ_o that was calculated from the Racah parameter B' allowed for the calculation of the f -factor for TAMEpyr **I.60** which could be used to place the chelator in the spectrochemical series. The relationship between Δ_o and the f -factor is as follows:

$$\Delta_o = g_{ion} \cdot f_{ligand} \tag{I.a}$$

where the g_{ion} for Ni(II) is 8700cm^{-1} and Δ_o for **I.58** is 12700cm^{-1} .(28) The calculation of the f -factor for the ligand resulted in a value of f_{TAMEpyr} of 1.46. This result placed TAMEpyr **I.60** at the higher end of the spectrochemical series thus classifying it as a strong-field ligand.

1.9. Liberation of TAMEpyr I.60 and the preparation of benzyloxy-TAMEpyr I.64

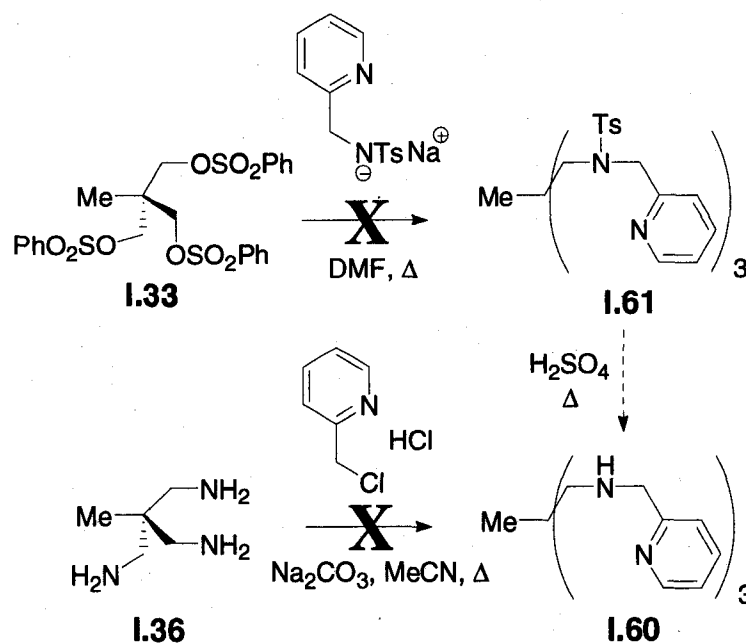
The liberation of TAMEpyr **I.60** from Ni(II) was accomplished by treating the isolated complex **I.58** with an aqueous solution of NaCN (**Scheme 11**).



Scheme 11 Liberation of free TAMEpyr I.60.

From the spectrochemical series the f -factor of CN^- is ca. 1.7 which is larger than the value calculated for TAMEpyr I.60 ($f_{\text{ligand}}=1.46$) suggesting that CN^- will outcompete TAMEpyr I.60 for the metal and form water soluble $[\text{Ni}(\text{CN})_4]^{2-}$. The completion of this particular reaction was monitored by noting the loss of the pink color and development of a yellow colored solution which is consistent with the formation of $[\text{Ni}(\text{CN})_4]^{2-}$. The freebase ligand was then extracted from the mother liquor with methylene chloride (DCM) and the solvent evaporated yielding the desired compound I.60 free of impurities in near quantitative yields. An alternative method of isolating free TAMEpyr I.60 involves acidifying an ethanol suspension of $[\text{Ni}(\text{TAMEpyr})](\text{ClO}_4)_2$ I.58 with excess concentrated HCl. The resulting white precipitate (presumably TAMEpyr·nHCl salt, where n can vary between 1 and 6) can be isolated via centrifugation and then treated with excess NaOH. The freebase TAMEpyr I.60 can then be extracted from the reaction mixture with DCM. With the liberated ligand in hand a systematic study of the coordination chemistry of TAMEpyr I.60 with a variety of metal ions ensued (*vide infra*).

Large-scale approaches (ca. 5-10 g) to the desired ligand were tentatively explored (**Scheme 12**).



Scheme 12 Failed attempts at the preparation of TAMEpyr I.60.

The first approach involved a reaction between the benzene sulfonate **I.33** and the sodium-salt of a 2-picolylsulfonamide. The reaction likely failed as a result of steric hindrance thus preventing the nucleophilic sulfonamide from reacting with the substrate **I.33**. The direct reaction of TAME **I.36** with 2-picolyl chloride also failed to produce the desired product **I.60**. The resulting product-slate was exceedingly complex as evidenced in the crude $^1\text{H-NMR}$ spectrum which indicated multiple alkylations on the primary amine of TAME **I.36** had taken place.

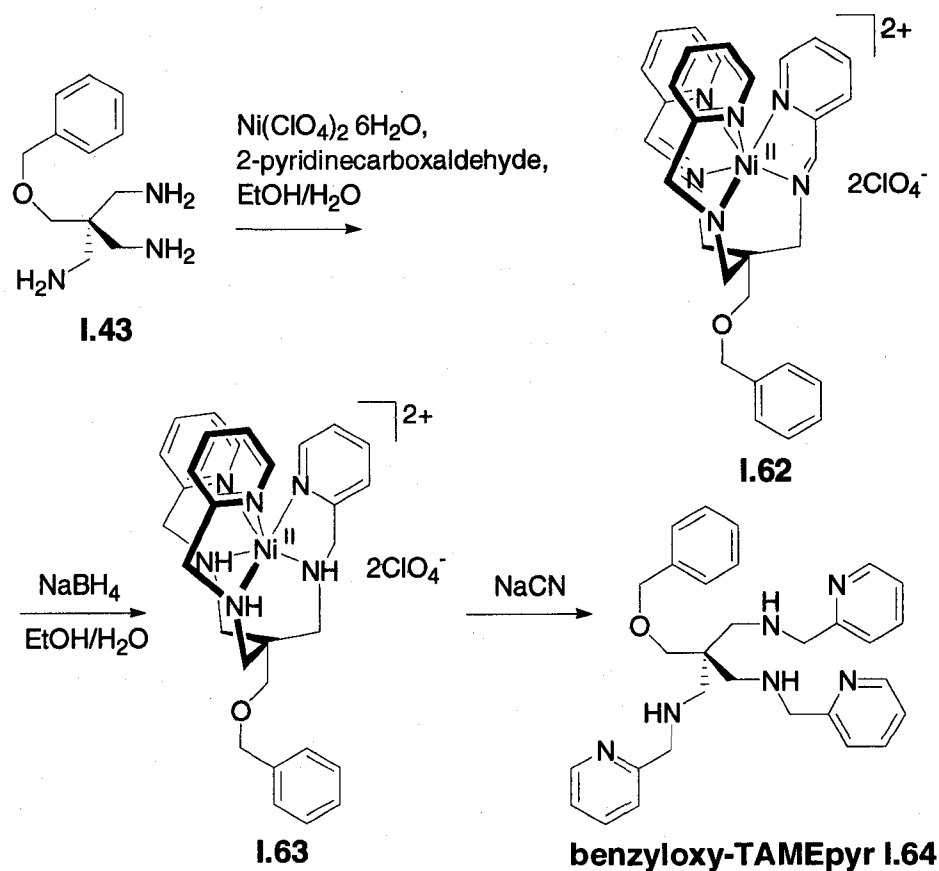
The benzyloxy differentiated TAME derivative **I.64** (*vide supra*) also underwent the Ni(II)-mediated template reaction with 2-pyridinecarboxaldehyde

affording the corresponding triimino complex **I.62** (Scheme 13). The visible-near IR absorbance spectrum of the isolated material was nearly identical to that of the parent complex [Ni(TAMEpyr-trisimine)](ClO₄)₂ **I.50** (Table 6).

$\bar{\nu}$ (cm ⁻¹) for [Ni(benzyloxy-TAMEpyr-trisimine)] ²⁺	Assignment	$\bar{\nu}$ (cm ⁻¹) for [Ni(TAMEpyr-trisimine)] ²⁺
12400	³ A _{2g} → ³ T _{2g}	12400
ca. 11300 (sh.)	³ A _{2g} → ¹ E _{1g}	ca. 11600 (sh.)
ca. 20000	³ A _{2g} → ³ T _{1g} (F)	ca. 20400

Table 7 Position of the *d-d* electronic transitions for **I.50** and **I.62**. The spectra were collected at 25.0°C in MeCN. The exact position of the ³A_{2g} → ³T_{1g}(F) transitions were obscured by the aforementioned MLCT band.

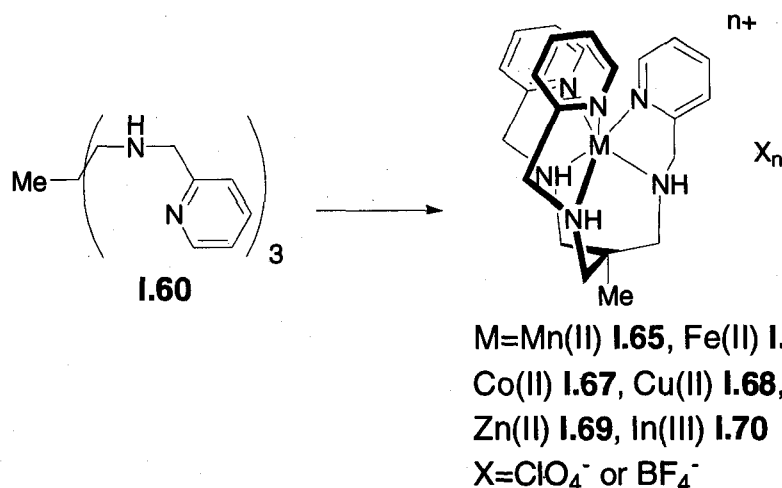
This result is important because introduction of additional functionality in the ligating scaffold does not interfere with the metal-binding site. In the future this will allow for the preparation of TAME-based bifunctional chelators which maintain the desirable metal binding properties of the parent TAMEpyr **I.60** ligand. This result highlights the utility of the peripheral methyl group in the TAME-framework. The isolated triimine complex **I.62** was then reduced with NaBH₄ in aqueous EtOH affording the desired triamino complex **I.63** in 35.0% isolated yield. The reduction was evidenced in the loss of a C=N stretch at 1648 cm⁻¹ and development of the N-H stretch at 3288 cm⁻¹ in the IR spectrum of the isolated complex **I.63**. The Ni(II)-center was subsequently removed with NaCN quantitatively affording the desired ligand benzyloxy-TAMEpyr **I.64**.



Scheme 13 The preparation of benzyloxy-TAMEpyr **I.64**.

1.10. Coordination Chemistry of TAMEpyr with various metal ions

The liberated ligand TAMEpyr **I.60** was used in the preparation of a variety of 1:1 metal complexes (**Scheme 14**). The analytical purity of the ligand was checked by elemental analysis and NMR spectroscopies prior to the complexation studies.



Scheme 14 Preparation of a variety of TAMEpyr metal-complexes.

The complexes were prepared straightforwardly by reactions of the metal salts and the ligand in MeOH with Et₂O as a cosolvent to induce precipitation and improve the yields of the desired material. The crude complexes were recrystallized from a MeCN/Et₂O solvent system and a 1:1 M:L composition was verified for all products by elemental analysis (*CHN*) and electrospray mass spectrometry (**Table 7**).

Complex	ESI-MS	<i>CHN</i> Data (calculated % on top and experimental % below)
[Mn(TAMEpyr)](ClO ₄) ₂ ·1/2H ₂ O	m/z=544, M-ClO ₄ ⁻	C, 42.3, H, 4.80, N, 12.8 C, 42.3, H, 4.78, N, 12.4
[Fe(TAMEpyr)](ClO ₄) ₂	-	C, 42.8 H, 4.69 N, 13.0 C, 43.1 H, 4.75 N, 13.1
[Co(TAMEpyr)](BF ₄) ₂	-	C, 44.3 H, 4.85 N, 13.5 C, 44.3 H, 5.05 N, 13.3
[Cu(TAMEpyr)](ClO ₄) ₂	m/z=552, M-ClO ₄ ⁻	C, 42.3 H, 4.63 N, 12.9 C, 42.2 H, 4.58 N, 12.8
[Zn(TAMEpyr)](ClO ₄) ₂	m/z=553, M-ClO ₄ ⁻	C, 42.2 H, 4.62 N, 12.8 C, 41.9 H, 4.60 N, 12.7
[In(TAMEpyr)](NO ₃) ₃ ·MeOH	m/z=629, M-NO ₃ ⁻	C, 39.8 H, 4.74 N, 17.4 C, 39.9 H, 4.47 N, 17.7

Table 8 The 1:1 M:L stoichiometry data. The air-sensitive nature of the Fe(II) and Co(II) complexes prevented ESI-MS analysis.

To gain insight into the geometry preferences of coordinated TAMEpyr **I.60** a crystallographic study of $[\text{Zn}(\text{TAMEpyr})]^{2+}$ **I.69** was carried out because Zn(II) has no electronic geometry preferences (**Figure 36**).⁽³⁹⁾ The cation possesses crystallographic C_3 symmetry where the C_3 axis passes through nuclei C9, C8 and Zn1. TAME **I.36** appears better suited to providing an octahedral geometry as compared to TACH **I.13**, because $[\text{Zn}(\text{TAMEpyr})]^{2+}$ **I.69** has a larger trigonal twist angle ($46.5(2)^\circ$) than the related complex $[\text{Zn}(\text{TACHpyr})]^{2+}$ ($43.7(2)^\circ$).⁽³⁹⁾

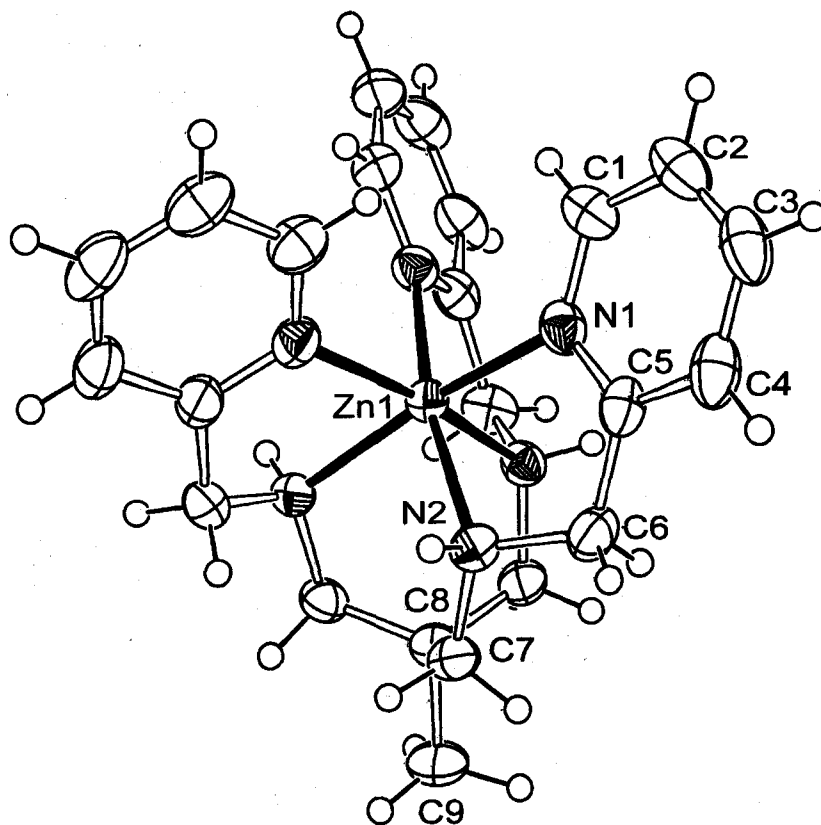


Figure 36 X-ray crystal structure of the cation $[\text{Zn}(\text{TAMEpyr})]^{2+}$ **I.69.**

Complex **I.69** also has significantly shorter Zn-N_{py} bond lengths than [Zn(TACHpyr)]²⁺ (2.128(2) Å versus 2.165(4) Å). A greater twist angle is consistent with shorter bond lengths to the metal ion because steric interactions between the coordinating pyridines were reduced. The other striking comparison is with [Fe(tptMeTAME)]²⁺, the Fe(II) complex of the tri-*N*-methylated TAMEpyr analog. This complex was structurally characterized at 153K, where the Fe(II) center is in the low-spin state and the trigonal twist angle is nearly octahedral at 51.0°.(96)

The ability of TAMEpyr **I.60** to attain a conformation close to octahedral is clearly attributable to twisting of the framework and so an analysis according to the formalisms that Al-Obaidi *et al.* applied to [Fe(tptMeTAME)]²⁺ is appropriate.(96) There are multiple conformational possibilities in TAMEpyr chelates because of left- or right-handed twists with respect to the C₃-axis of both the TAME cap (atoms C8, C7, C7A, C7B) and the three aminopyridyl arms. The twist configuration of the three six-membered rings in the TAME portion of [Zn(TAMEpyr)]²⁺ **I.69** was assigned by convention as δ^{CAP}. This assignment denotes a clockwise-twist about the C₃ axis. Furthermore, λ and δ configurations of the five-membered aminopyridyl chelate rings (*e.g.* Zn1-N2-C6-C5-N1) are possible. The three aminopyridyl arms may have an absolute configuration of Λ or Δ. In [Zn(TAMEpyr)]²⁺ **I.69** the conformation of the five-membered chelate rings are λλλ and the absolute configuration is Δ. The secondary nitrogens are rendered stereogenic upon coordination and in the structure of [Zn(TAMEpyr)]²⁺ **I.69** they were all found to possess the *S* configuration using the Cahn-Prelog-

Ingold nomenclature rules. The complex crystallizes in the chiral space group $P2_13$. Because the Flack parameter refined to a value of 0.015(14), the stereoisomer reported herein is correct. While the crystal studied is of the $\Delta\delta^{\text{CAP}}(\lambda\lambda\lambda)\text{SSS}$ isomer, crystals of the enantiomer $\Lambda\lambda^{\text{CAP}}(\delta\delta\delta)\text{RRR}$ are likely present somewhere in the sample but they were not studied.

The $^1\text{H-NMR}$ spectra of $[\text{Zn}(\text{TAMEpyr})]^{2+}$ **I.69**, $[\text{Fe}(\text{TAMEpyr})]^{2+}$ **I.66**, and $[\text{In}(\text{TAMEpyr})]^{3+}$ **I.70** show marked differences in appearance. The data illustrate that TAMEpyr maintains rigid pseudooctahedral geometry at room temperature when coordinated to a 3d metal ion, but as the size-fit worsens the inner coordination sphere becomes more elastic. The spectra of the Fe(II) and Zn(II) complexes display a sharp doublet-of-doublet spin pattern for the pseudobenzyl and TAME methylene protons indicating conformational rigidity in solution at room temperature. The corresponding methylene protons are no longer diastereotopic in the spectrum of $[\text{In}(\text{TAMEpyr})]^{3+}$ **I.70** and have collapsed into a doublet (**Figure 37**). The fluxional behavior observed in solution is consistent with a diastereomerization process taking place in solution. This spectral behavior was not observed in the closely related complex $[\text{In}(\text{TACHpyr})]^{3+}$ **I.70** until a temperature of 107° was achieved.⁽³⁸⁾ Presumably the complex **I.70** has a smaller twist angle because of the poor size match of the binding cavity with the relatively large In(III) ion (ionic radius=94pm).⁽²⁹⁾ This would reduce the energetic barrier to diastereomerization. Racemization between the Δ and the Λ forms would require configurational inversion of the secondary amines. The transition state for

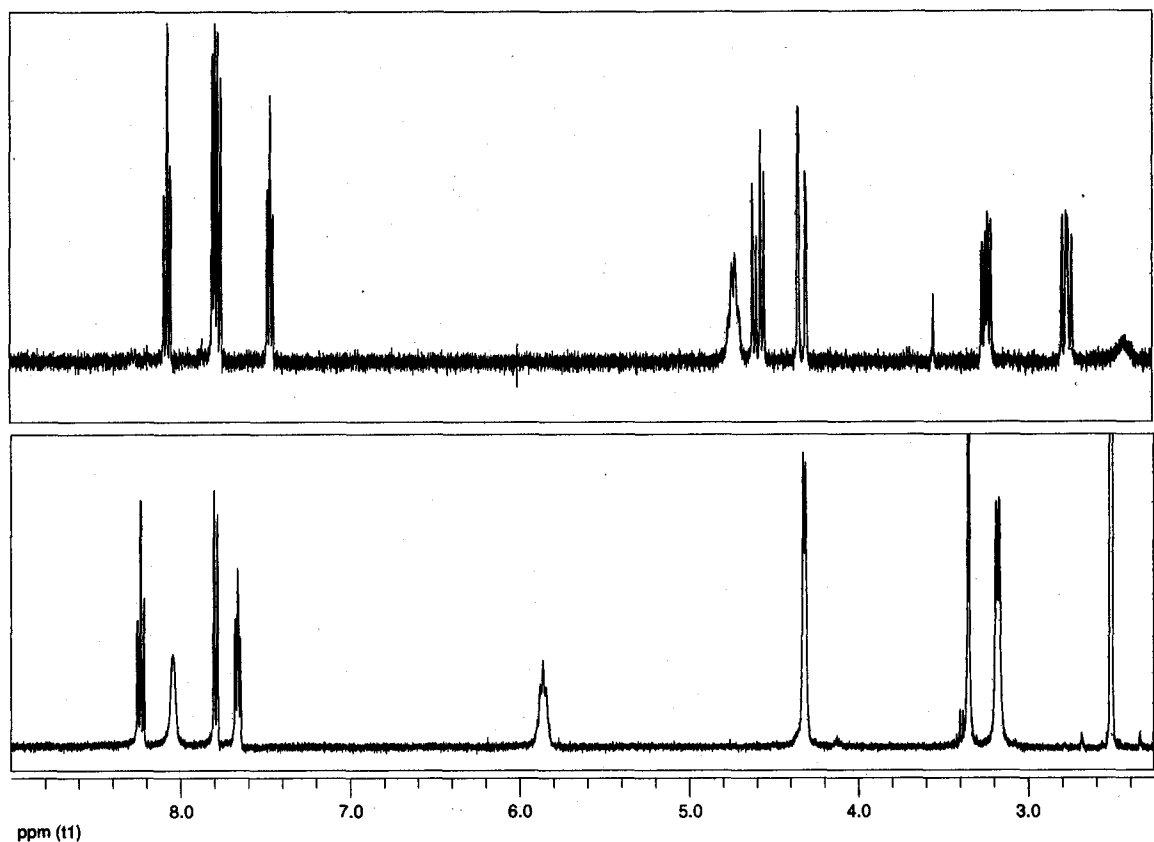


Figure 37 Partial $^1\text{H-NMR}$ spectra for $[\text{Fe}(\text{TAMEpyr})]^{2+}$ (top) in $\text{MeCN-}d_3$ and $[\text{In}(\text{TAMEpyr})]^{3+}$ (bottom) in $\text{DMSO-}d_6$.

such a process is a trigonal prismatic complex with a twist angle $\alpha=0^\circ$.⁽⁴⁷⁾ The energy barrier for a Bailar twisting mechanism for TAME based ligands should be lower than it is for TACH ligands because the TAME methylene carbons are not constrained to a ring. This in turn facilitates twisting about the C_3 axis. Variable temperature NMR experiments, which could be used to measure the activation energy for such a process, were not performed on the TAME derived metal complexes.

The visible-near IR absorbance spectra of all the colored complexes are fully consistent with a pseudooctahedral coordination geometry and strong metal-ligand interactions including effective $d\pi \rightarrow p\pi^*$ metal-ligand donation (**Table 8**).

M(II)	ν, cm^{-1} ($\epsilon, \text{cm}^{-1}\text{M}^{-1}$)	Transition	Color
Fe(II)	24000 (70000), 18000 (300)	MLCT	Bronze
Co(II)	21100 (63), 18400 (28), 10650 (21)	${}^4\text{T}_{1g} \rightarrow {}^4\text{A}_{2g}$, ${}^4\text{T}_{1g} \rightarrow {}^4\text{T}_{1g}(\text{P})$, ${}^4\text{T}_{1g} \rightarrow {}^4\text{T}_{2g}$,	Orange
Cu(II)	16100 (107)	${}^2\text{E}_g \rightarrow {}^2\text{T}_{2g}$	Blue

Table 9 Visible-near IR absorbance spectroscopy of $[\text{M}(\text{TAMEpyr})]^{2+}$.

The room temperature ${}^1\text{H-NMR}$ spectrum of $[\text{Fe}(\text{TAMEpyr})]^{2+}$ **I.66** (*vide supra*) is not paramagnetically shifted, indicating a low spin electronic configuration (${}^1\text{A}_{1g}$ ground state). An absorbance at 24000 cm^{-1} in this complex has therefore been assigned as a metal-to-ligand charge-transfer band (MLCT) characteristic of LS Fe(II) complexes.^(97, 98) This transition masks the *d-d* metal centered transitions except for a low energy shoulder (18000 cm^{-1} , $\epsilon=300 \text{ cm}^{-1}\text{M}^{-1}$), which is often assigned as an obscured ${}^1\text{A}_{1g} \rightarrow {}^1\text{T}_{1g}$ transition.⁽⁹⁷⁾ The spectrum of $[\text{Cu}(\text{TAMEpyr})]^{2+}$ **I.68** is typical of distorted octahedral complexes of Cu(II), with the presence of one asymmetric band at 16100 cm^{-1} .⁽⁹⁹⁾ The asymmetry is a result of a Jahn-Teller distortion invariably associated with d^9 metals. All three possible *d-d* transitions for a HS d^7 metal ion are seen in the spectrum of $[\text{Co}(\text{TAMEpyr})]^{2+}$ **I.67**. The ${}^4\text{T}_{1g} \rightarrow {}^4\text{A}_{2g}$ band often lies under the ${}^4\text{T}_{1g}(\text{P})$ transition, but in the case of **I.67** both transitions are seen at 21100 cm^{-1} and 18400 cm^{-1} respectively. The lowest energy transition, which is equal to Δ_0 , occurs at 10650 cm^{-1} . A ligand field strength $>15000 \text{ cm}^{-1}$ can cause Co(II) to be LS.⁽⁴⁷⁾ The resulting LS d^7 complex would then undergo Jahn-Teller distortions leading to additional strain within the complex thus disfavoring this electronic configuration. In fact, it is quite rare indeed to observe a LS Co(II) complex.

1.11. Conclusions and future work

In sum the Ni(II)-mediated template synthesis of the novel chelator TAMEpyr **I.60** and its coordination chemistry with a host of metal ions has been presented. Structural data for $[\text{Zn}(\text{TAMEpyr})]^{2+}$ **I.69** show the propensity of the ligand for an octahedral coordination geometry. This has been attributed to the flexibility of the framework in regard to trigonal twisting. Solution studies of TAMEpyr **I.60** demonstrate that the chelator possesses a great deal of flexibility which may be exploited in the future toward the preparation of metal-selective ligands. Moreover, the rich synthetic chemistry of the TAME framework will grant access to a host of bifunctional metal chelators without disturbing the binding pocket of the ligand. Lastly, the pyridyl groups can be exchanged with a host of azaheterocycles affording a new family of hexadentate chelators. The next chapter of this dissertation will describe how the Ni(II)-mediated template reaction of TAME **I.36** was exploited in the preparation of novel fluorescent Zn(II)-sensors.

CHAPTER 2

TAME DERIVED FLUORESCENT SENSORS FOR ZN(II)

Summary

In this chapter the candidate presents an application of TAME derived ligands for the PET/CEF fluorescent sensing of Zn(II). The discussion begins with a description of fluorescence and how fluorescent metal-chelates are used to detect a wide-variety of analytes. The literature precedence of fluorescent metal sensors has been restricted to the most recent examples because of the breadth of this field. This discussion then seques into the preparation of several azaaromatic aldehydes which serve as the fluorophores in the novel TAME derived luminescent sensors. The synthesis of the ligands via the Ni(II) mediated template reaction/tetrahydroborate reduction is discussed followed by a description of the photophysical properties of these systems.

2.1. Fluorescence: discussion adapted from reference (100)

Fluorescence is defined as the emission of light from an excited electronic state. When a molecule absorbs a photon of light it is excited to higher electronic and vibrational states. This process is illustrated in the so-called Jablonski diagram (Figure 38).

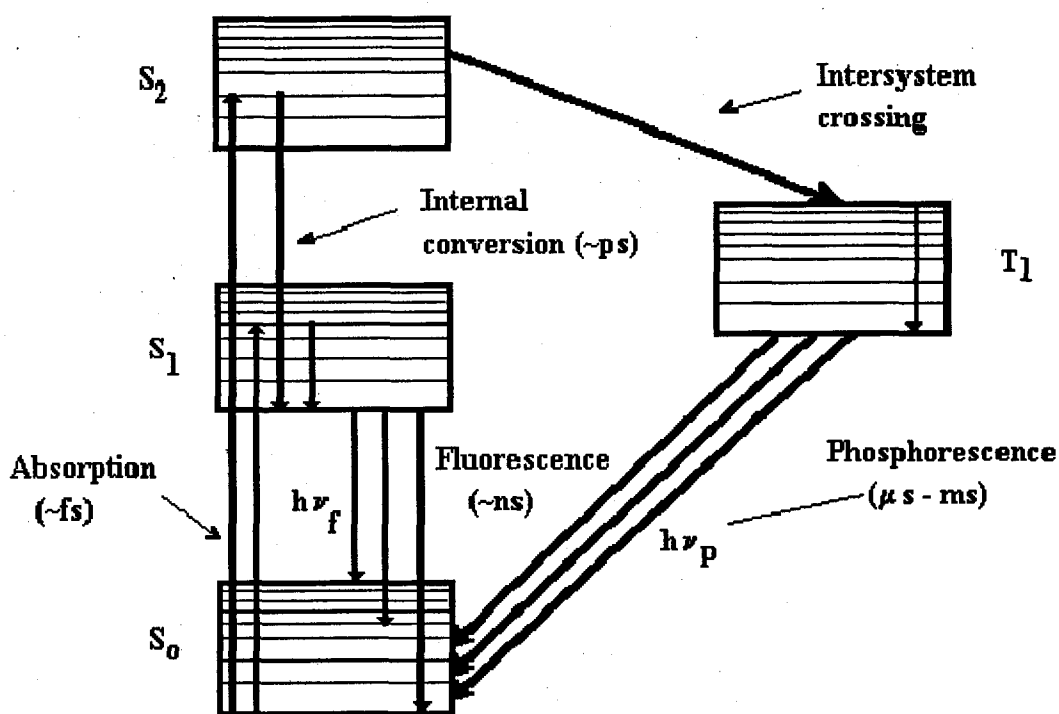


Figure 38 The Jablonski diagram. The figure was borrowed from www.theochem.kth.se/people/orubiop/jablonski2.gif.

The Frank-Condon principle states that electronic transitions are so fast compared to nuclear motion that nuclei have nearly the same position and momentum immediately before and after the electronic transition has occurred.(101) In the excited electronic state a valence electron will reside in either a non-bonding or antibonding molecular orbital. The excited state of the

molecule is then free to lose some of its vibrational energy and traverse to the lowest vibrational level of the first excited electronic state (S_1). This process is referred to as internal conversion. This rapid loss of energy is nonradiative (*i.e.* no photons are released) and therefore the emitted energy enters the surrounding environment as heat. The heat arises from collisions between the excited molecule and nearby solvent molecules. Once in the ground vibrational level of the S_1 state the molecule is free to relax to the ground electronic state (S_0) by emitting a photon ($h\nu_f$). This phenomenon is called fluorescence. The photon emitted is at lower frequency than the incident photon that enabled the excitation because of vibrational relaxation in the S_1 state prior to the emission. Often times the fluorescence-emission spectrum will resemble the absorbance spectrum because the same electronic and vibrational energy levels are involved in excitation and in emission.

Fluorescence spectra are influenced by the local environment of the excited molecule and as such can be useful in probing intermolecular interactions. The most sensitive indicators in such studies are the measurement of the lifetime of the excited state (τ) and the rate of relaxation (k_d). Upon excitation of a molecule the fluorescence from the excited state will decay. The rate law for this process is often first order and characterized by the following equation:

$$F \propto -\frac{d[M^*]}{dt} = k_d[M^*]$$

(II.a)

where F is the intensity of the fluorescence and $[M^*]$ is the concentration of the excited species M . The lifetime (τ) for this process is simply the inverse of the rate constant for deactivation ($\frac{1}{k_d}$). Measurements of fluorescence decay in dilute solutions can be achieved by impinging light on the sample, usually from a laser source, and observing the resulting fluorescence intensity over time. If the process is first-order then the decay will be exponential and a plot of $\log F$ versus time will be linear.

If fluorescence is the only pathway for deactivation (which may not be the case) then the aforementioned rate-law holds true and k_d is equal to k_f , which is defined as the first-order rate constant for fluorescence. However, competition from non-radiative processes, like thermal deactivation (k_t), photochemical reactions (k_p), and quenching reactions (k_Q) with other species in solution (Q) complicates the rate-law **II.a**. The overall rate of decay of the excited state is then the sum of the rates for the competing processes and follows as:

$$-\frac{d[M^*]}{dt} = k_f[M^*] + k_t[M^*] + k_p[M^*] + k_Q[M^*][Q] = k_d[M^*]$$

(II.b)

and, likewise, the observed lifetime is given as:

$$\tau = \frac{1}{k_f + k_t + k_p + k_Q[Q]}$$

(II.c)

The quantum yield (Φ) of fluorescence is defined as the fraction of absorbed photons that ultimately lead to emission via fluorescence. It is a ratio of the number of photons emitted to the total number of photons absorbed and varies in value between 0 and 1. Another way of representing the quantum yield is to create a ratio between k_f and k_d which leads to the following expression:

$$\Phi = \frac{\tau}{\tau_0}$$

(II.d)

where the natural fluorescence lifetime is represented by the variable τ_0 . This equation provides the relationship between quantum yield and fluorescence lifetime.

Fluorescence is almost always observed from the lowest excited state S_1 because of the exceedingly fast rates of internal conversion from the higher vibrational levels (see **Figure 38**). Internal conversion to the ground state also occurs and is the primary component of thermal deactivation which competes with the fluorescence. The rate for this process, however, is often slow because the difference in energy between S_1 and S_0 is large relative to the energy differences of the vibrational levels.

A decrease in the fluorescence emission intensity may be the result of several competing processes. Collisions with quenching molecules, excitation transfer to non-fluorescent species in solution, oligomerization resulting in non-

fluorescent species at high concentrations, and radiative migration leading to self-absorption are all reasons a decrease in the quantum yield occurs.

2.2. Applications of fluorescence: discussion adapted from reference (102)

Fluorescence techniques can be used to detect lower concentrations of a target analyte than the corresponding absorbance-based spectrophotometric methods. Fluorescence is one of the most sensitive analytical techniques available because the emission intensity (F) can be measured independent of the source power. Unlike absorbance measurements, which requires measuring *both* the incident (P_o) and emerging (P) light, fluorescence enjoys enhanced sensitivities because the power of the source can be increased. This source intensification leads to enhanced fluorescence emission intensities. In absorbance-based measurements, source intensification would result in a proportional change in P , which after creating the ratio ($\frac{P}{P_o}$), does not affect the measured absorbance. It is said that fluorometric methods have sensitivities that are one to three orders of magnitude better than the corresponding absorbance methods. However, precision and accuracy in fluorometric methods are two to five times worse.

Inorganic species can be detected with fluorometry either by forming a luminescent complex with a metal-ion or by quenching the natural fluorescence of a chelator via interactions with a paramagnetic species. It is the latter case that limits the fluorometric detection of many transition-metal ions. The open-

shell *d*-metals often prevent fluorescence by facilitating intersystem crossing of the excited singlet state to a triplet state (T_1). The T_1 state is free to relax by phosphorescence. A second limiting factor for the fluorometric detection of transition metals is the abundance of closely spaced vibrational levels which facilitates relaxation via internal conversion processes.

Several fluorometric reagents have been developed for non-transition metals because these species are less susceptible to the aforementioned deactivation processes. The most successful reagents for cation analysis possess aromatic groups with two or more donor atoms that serve to chelate the analyte. The structures of some well-known fluorometric reagents are given in

Figure 39.

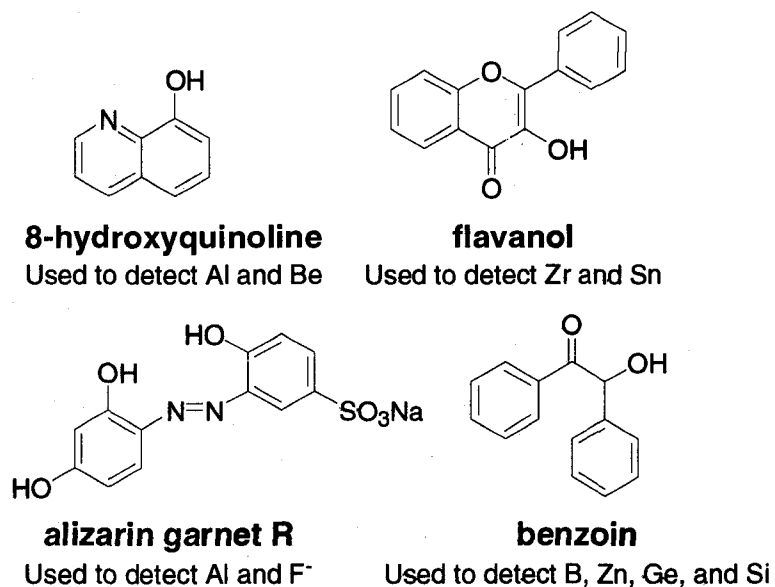


Figure 39 Examples of fluorometric reagents for inorganic species from Skoog, Holler and Nieman.(102)

The preceding discussion highlights the development of novel, selective, fluorometric reagents for metal-ion detection. These reagents are here-to-forth referred to as metal-sensors. Because of the breadth of this field the following discussion has been limited to recent advances in sensor chemistry citing examples that highlight sensor-design strategy. The reader should note that it is often difficult to fully identify and characterize all contributing mechanisms to the sensory action of a particular luminescent metal complex. It is the aim of the author of this dissertation to introduce some of the popular sensing mechanisms that have been exploited in the development of novel metal-ion sensors. This discussion will begin with photoinduced electron transfer metal sensors.

2.3. Photoinduced electron transfer

Luminescent sensors for a variety of analytes have been developed by taking advantage of the phenomenon of photoinduced electron transfer (PET).⁽¹⁰³⁻¹⁰⁶⁾ PET serves as the switching mechanism in the sensor between the “on” and “off” states. This strategy requires the preparation of a fluorophore covalently attached to an analyte-receptor via some spacer (**Figure 40**).

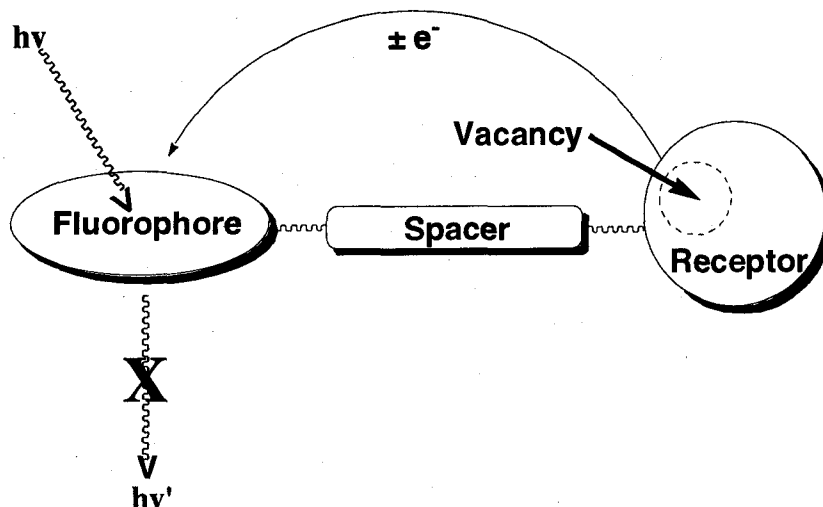


Figure 40 A fluorophore-spacer-receptor sensor turned “off” by PET in the absence of the analyte.

Known redox potentials are used to choose components so that the receptor will transfer an electron to-or-from the excited state of the fluorophore.(107) This effectively eliminates any emission in the absence of the target analyte and renders the sensor in the “off” state. When a diamagnetic analyte binds to the receptor this prevents the receptor mediated electron transfer to/from the excited state of the fluorophore (Figure 41). The sensor is then turned “on” and the excitation energy dumped into the surroundings as a detectable emission.

Alternatively, when a paramagnetic analyte binds to the receptor the fluorescence can be quenched via electron transfer from the metal center to the excited state of the fluorophore. This sensor design strategy has been referred to as “target-induced emission enhancement.”(108) The advantages of this strategy, according to Callan, de Silva, and Magri, is its quantitative design and the predictability of many observable parameters.

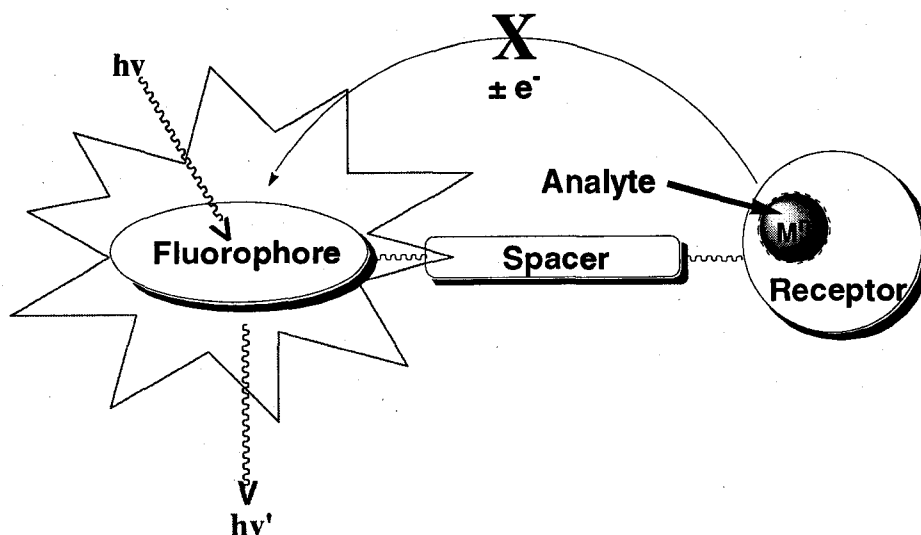


Figure 41 A fluorophore-spacer-receptor sensor turned “on” by blocking the PET channel upon analyte recognition.

Furthermore, intensity ratios between the “on” and “off” states are said to be useful at values of 2 and even visually dramatic (in the dark) at values of 10 or greater.(108)

Alternatively, one can view the PET process in terms of the frontier molecular orbitals of the fluorophore and receptor assembly (Figure 42).

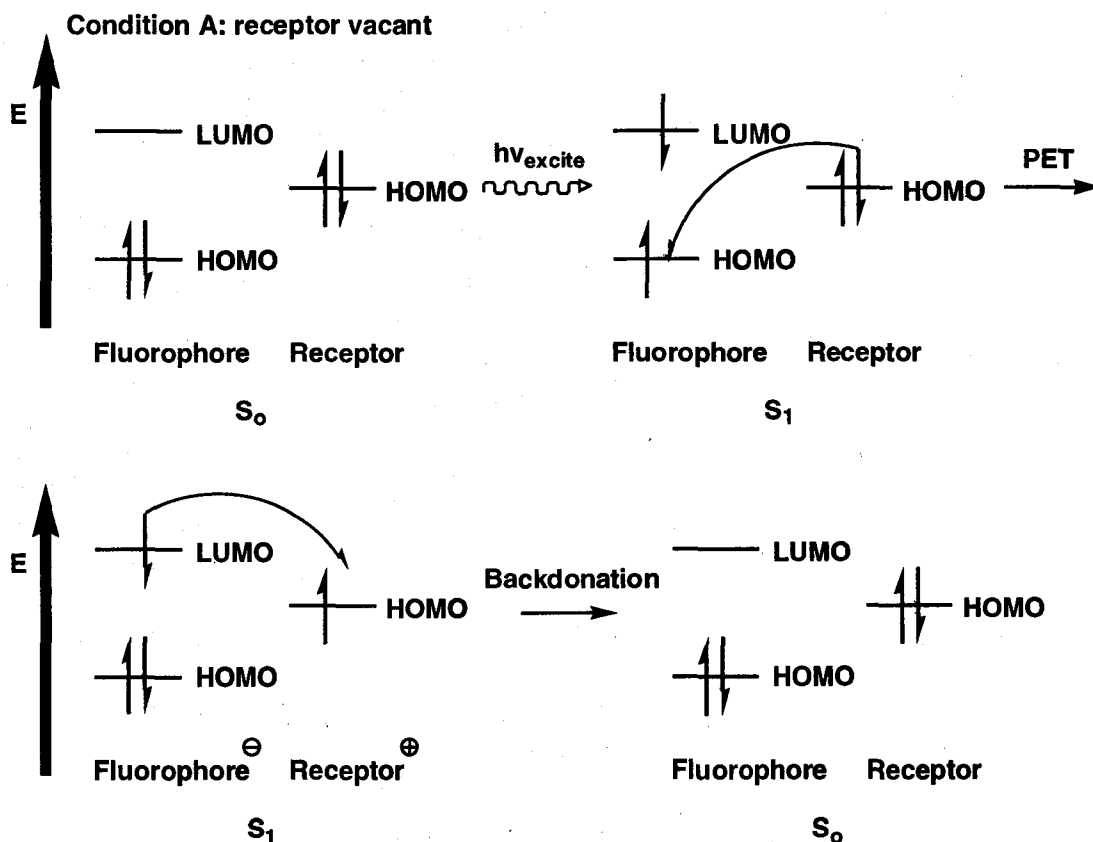


Figure 42 Molecular orbital picture of PET when the receptor is vacant. The sensor will absorb light ($h\nu_{excite}$) but will not fluoresce.

In **Condition A** where the receptor is vacant the excitation involves promotion of an electron from the highest occupied molecular orbital (HOMO) to the lowest unoccupied molecular orbital (LUMO) of the fluorophore. If the HOMO of the receptor lies in energy between the HOMO-LUMO pair for the fluorophore then the receptor is able to donate an electron to the half-filled HOMO of the fluorophore in the S_1 state. This is the photoinduced electron transfer event and results in a potentially damaging radical anion-cation pair. To repair itself the fluorophore can then thermally back-donate the electron that resides in its LUMO to the HOMO of the receptor resulting in the ground state of the assembly. This process does not involve fluorescence and as such the sensor is rendered silent.

In **Condition B** where the receptor is occupied by a cationic guest the HOMO of the receptor will be engaged in a coordinate covalent bond with the cation (**Figure 43**). This reduces the energy of the receptor's HOMO and as such the receptor will be less willing to participate in the aforementioned PET process. This phenomenon can be evidenced experimentally by measuring a cation-induced anodic shift in the cyclic voltammogram of the bound fluorophore-receptor assembly. The fluorophore is now "turned-on" and is free to relax through the usual fluorescence process.

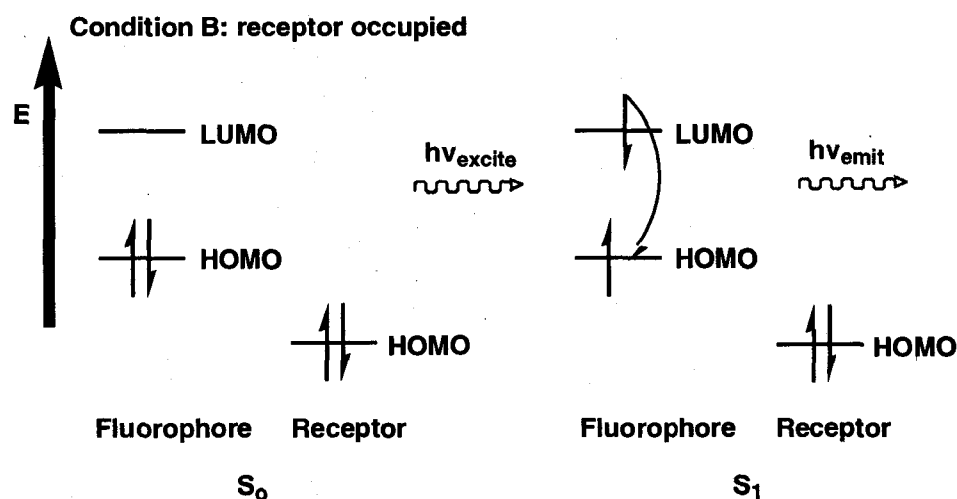


Figure 43 Molecular orbital picture of PET when the receptor is occupied. The sensor is now "turned-on".

2.4. Proton PET sensors

An example of the aforementioned "fluorophore-spacer-receptor" design strategy is illustrated in the H^+ -sensing molecule **II.1** developed by Zang and coworkers (**Figure 45**).⁽¹⁰⁹⁾ Unlike most PET sensors which employ a methylene spacer group, the imide nitrogen in compound **II.1** serves as a virtual

spacer between the receptor (aniline group) and the fluorophore (perylene-tetracarboximide) by creating a node in the molecular orbital system of the assembly (**Figure 44**). This breaks up any extended conjugation and as such PET from the anilinic unit to the perylene-tetracarboximide resulted in negligible fluorescence under basic conditions (*i.e.* the sensor is “off”). However, protonation of the anilino-nitrogen resulted in a strong fluorescence enhancement (FE). Other analytes that bind to the aniline group (*e.g.* ZnCl_2) also gave a similar effect.



Figure 44 The calculated superimposed HOMO and LUMO surfaces of a p-anilino-perylene-tetracarboximide. Note the node that is collinear with the imide nitrogen atoms which serves to decouple the fluorophore from the anilino-receptor. The image was generated in Spartan at the semi-empirical PM3 level of theory.

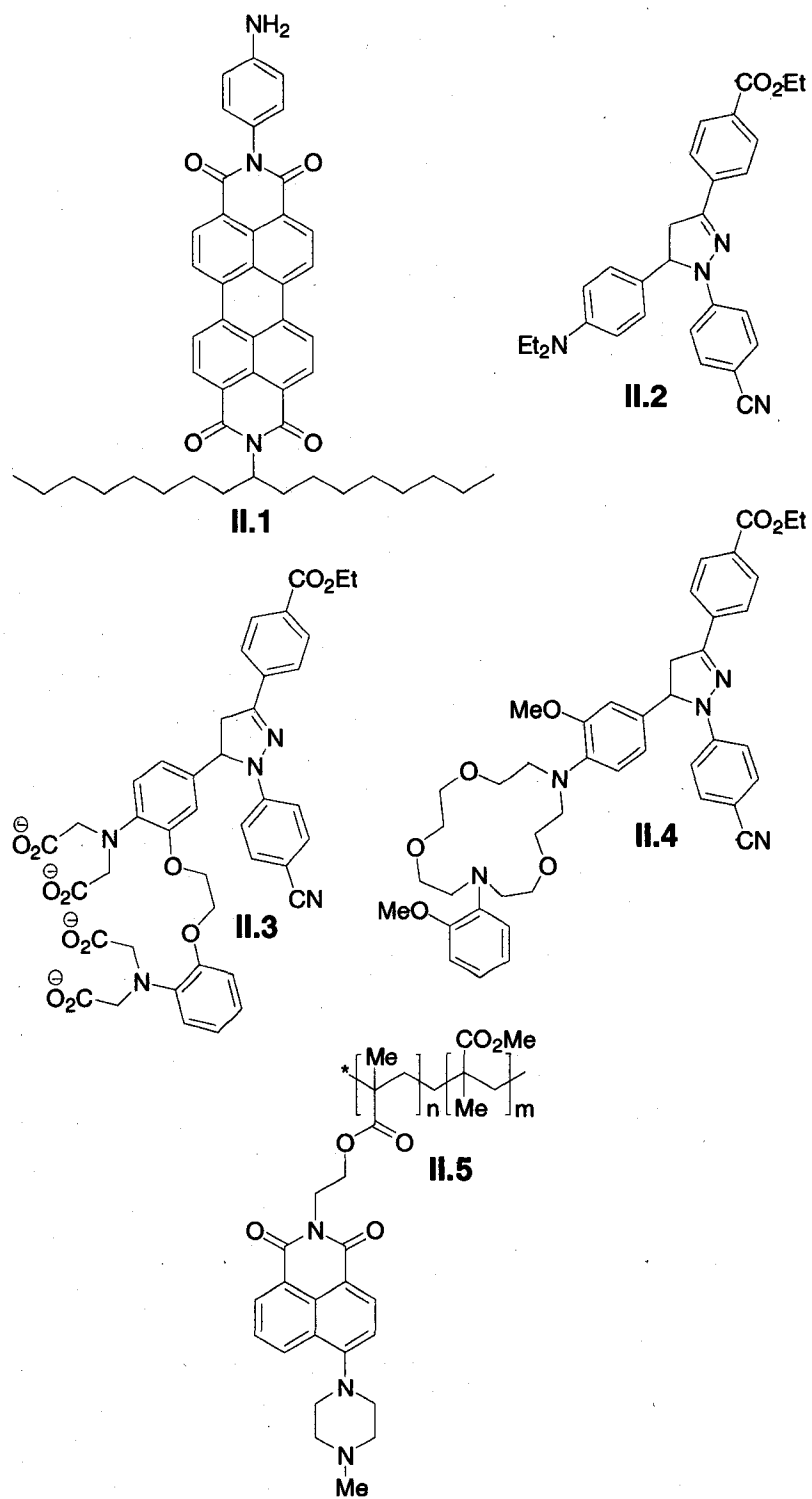


Figure 45 Examples of PET-H⁺ sensor molecules.

The fluorophore-spacer-receptor format was also utilized in compound **II.2** developed by Fahrni *et al* (Figure 45).⁽¹¹⁰⁾ Protonation of the dialkyl aniline unit

eliminates the PET to the pyrazoline fluorophore and a strong fluorescence enhancement was observed. This effect was also evidenced in compounds **II.3** and **II.4** which are designed as Ca(II) and Na(I) sensors respectively (**Figure 45**).^(111, 112)

The copolymer **II.5** developed by Tian *et al.* is another example of the fluorophore-spacer-receptor design motif.⁽¹¹³⁾ Protonation of the tertiary aliphatic amine inhibits PET thus switching “on” the emission from the naphthalimide unit.

2.5. Alkali and alkaline earth PET sensors

The detection of closed-shell alkali and alkaline earth metal ions with luminescent PET sensors has been achieved using the fluorophore-spacer-receptor design motif. A collection of anthracene-based PET sensors has been developed by Lincoln and coworkers (**Figure 46**).⁽¹¹⁴⁻¹¹⁶⁾

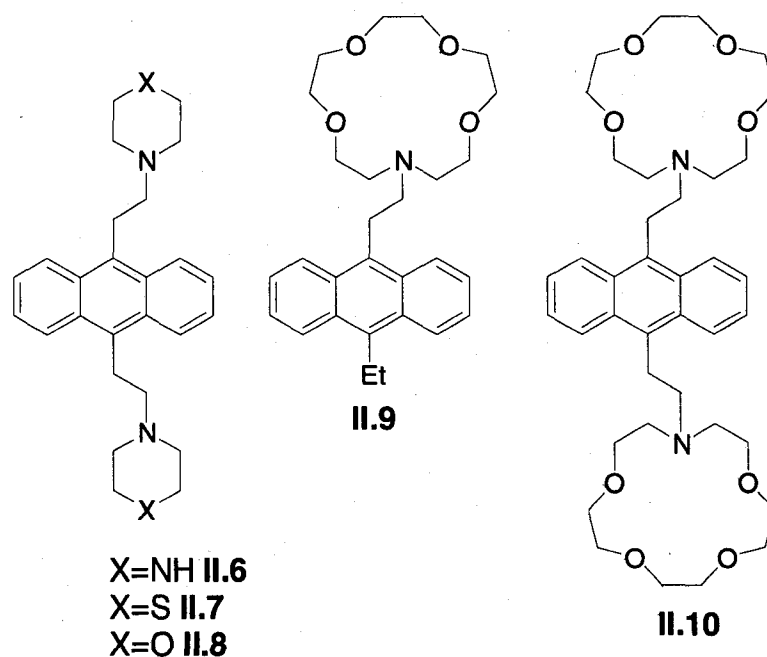


Figure 46 PET sensors for alkali and alkaline earth metals developed by Lincoln *et al.*

The presence of two-receptors in molecules II.6 through II.8 gives rise to three possible binding stoichiometries: namely 1:1 M:L (with 1 receptor empty and 1 receptor occupied); 2:1 M:L (both receptors occupied); and 1:1 M:L (both receptors engaged in a “sandwich” complex with 1 equivalent of the analyte). All three stoichiometries were observed with the alkaline earth metals. The alkali metals formed 1:1 and 2:1 binding stoichiometries but failed to form ‘sandwich’ complexes with the ligands. Fluorescence was only switched on when both tertiary nitrogens were engaged in coordination (*i.e.* binding stoichiometries of 2:1 M:L or 1:1 M:L sandwich complex). In the absence of the cations the authors note similar PET-mediated quenching events for all three X-molecules.

Unfortunately, the aim of selective binding for group I and group II metal ions within this set was not achieved. Moreover, the mono-azacoronand II.9, also developed by Lincoln *et al.* possessed an “off” quantum yield of 0.25 in the

absence of the analytes.(116) Even though the bis-azacoronand **II.10** maintains two binding sites, which may complicate the coordination chemistry, the off quantum yield (*i.e.* background fluorescence) was improved to 0.07. This result illustrates the quenching ability of two tertiary nitrogen lone pairs as compared to one. When both azacoronand receptor sites were occupied by the analyte the corresponding “on” quantum yields achieved values as high as 0.73. Unfortunately, poor analyte selectivity and limited water solubility reduces the utility of these molecules.

The crown-ether **II.11** introduced by Kenmoku *et al.* demonstrated a 5-fold fluorescence enhancement in the presence of Na(I) (**Figure 47**).⁽¹¹⁷⁾ This sensor is limited by a rather weak binding constant with Na(I) ($K_d=0.44M$) as measured at pH=7. The switching mechanism of this molecule is still PET-based even though there are no nitrogen-lone pairs contained in its structure. Likewise, the PET requisite Na(I)-induced anodic shift was observed in an electrochemical study of benzocrown ethers.⁽¹¹⁸⁾ The advantage of removing nitrogen from the sensor enhances receptor selectivity for the target Na(I) analyte over H⁺. This allows the sensor to be used in aqueous environments at pH=7.4.

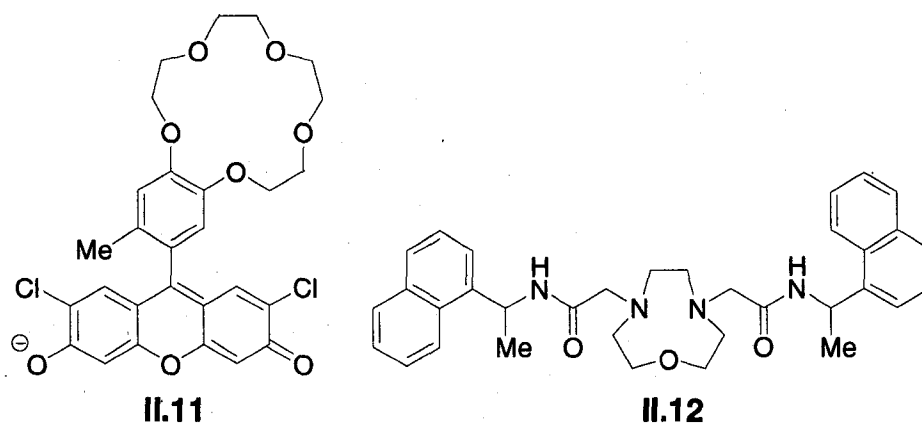


Figure 47 Examples of PET sensors for Na(I) and Li(I) respectively.

The development of sensors for Li(I) has proved to be challenging because of a lack of selective and strong receptors for the target analyte. One of the more strongly binding receptors is 1-oxy-4,7-diaza-9ane [N₂O]. Gunnlaugsson and coworkers have made progress toward Li(I) sensing by developing molecule **II.12** which operates in acetonitrile.⁽¹¹⁹⁾ This particular compound is an example of a “fluorophore-spacer-receptor-spacer-fluorophore” design motif. An observed fluorescence enhancement of 9 occurs when the Li(I) analyte binds to the diazacrown ether ($\Phi_{ON}=0.11$). A fluorescence enhancement was only observed with Li(I) and not with Na(I), K(I) and Ca(II). The disadvantage of this system is the relatively high pK_a of the receptor (pK_{a1}=7.2) in aqueous media limiting analyte selectivity over H⁺.

The boron-dipyrromethine fluorophore has become increasingly popular in the design of novel luminescent sensors.⁽¹²⁰⁻¹²²⁾ A recent example of a “turn-off” Ca(II) sensor (**Figure 48**) was reported by Cha *et al.*⁽¹²³⁾ The fluorescence of compound **II.13** switches off in the presence of the analyte because of the ease of oxidation of the resulting phenolate embedded in the calixcrown receptor.

In other words, a PET mechanism is invoked via the calixcrown phenolate oxygens to the adjacent dipyrromethine moiety upon analyte recognition thus extinguishing emission from the dye molecules.

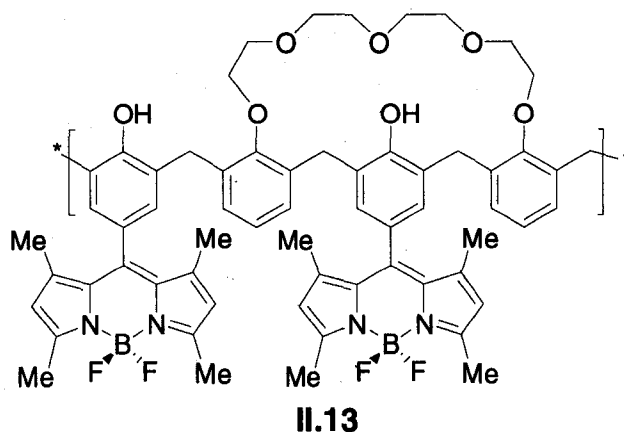


Figure 48 A “turn-off” Ca(II) luminescent sensor. The starred sites in the figure are linked forming a conical-like structure.

The sensor is selective for Ca(II) over other cations in methanolic solution, presumably because of a good size-match between the ionic radius of the analyte and the size of the calixcrown receptor. However, marked decreases in the quantum yield in aqueous media limits the utility of this sensor.

Additional examples of boron-dipyrromethine fluorophore-based metal sensors are highlighted in the work of Gee and coworkers.⁽¹²⁴⁾ The fluorophore was attached covalently to Roger Tsien’s Ca(II) receptor ‘BAPTA’ affording a new family of Ca(II)-selective turn-on sensors (**Figure 49**).⁽¹²⁵⁾

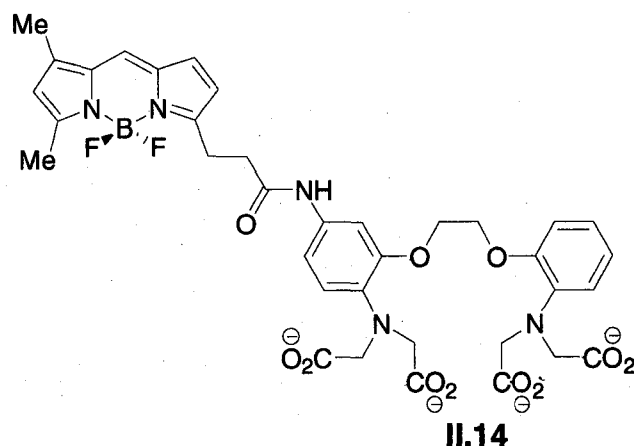
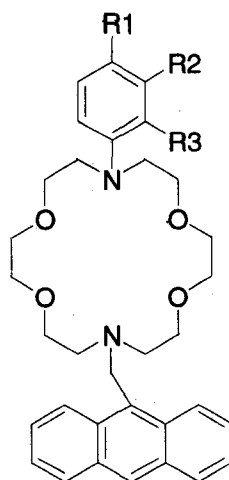


Figure 49 Gee's novel Ca(II)-selective PET sensor.

The acetate pendant arms in molecule **II.14** were converted into methyl esters to afford a cell permeable pro-chelator. Once in the cell the esters were saponified by trans-membrane esterases preventing the compound from exiting the cellular milieu.⁽¹²⁶⁾ This resulted in an order-of-magnitude increase in the observed fluorescence enhancement upon cellular Ca(II) recognition.

Another class of crown ether based sensors were developed by Pearson *et al.* (**Figure 50**).⁽¹²⁷⁻¹²⁹⁾ Metal ion selectivity for Mg(II) over Ca(II) is derived from changing the electronic properties of the *N*-aryl group appended to the azacrown ether receptor. The electron donating ability of the *N*-aryl group varies as follows: **II.18**>**II.15**>**II.16**=**II.17**. Compound **II.18** possesses enhanced selectivity for Mg(II) because the electron-rich phenylene diamine unit binds strongly to the charge-dense Mg(II) ion. NMR data suggested that Mg(II) resides in close proximity to the aliphatic amine portion of the azacrown ether receptor resulting in a large change in the chemical shifts derived from anthracene as compared to the free ligand.



R1,R2,R3=H II.15

R1=Cl,R2,R3=H II.16

R1,R3=H,R2=Cl II.17


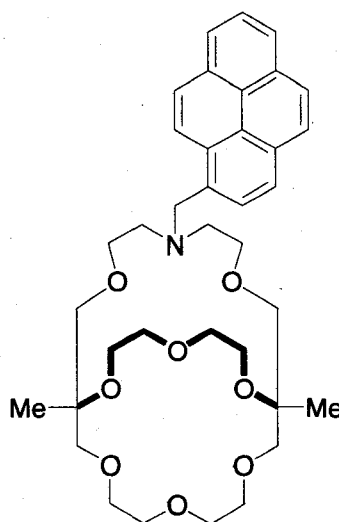
R2,R3=H,R1=  II.18

Figure 50 Pearson's azacrown ether Mg(II) and Ca(II) sensors.

In the remaining compounds II.15 to II.17 there was only a small fluorescence enhancement observed with Mg(II) suggesting the ion migrates to the *N*-aryl side of the receptor upon fluorophore excitation. This phenomenon is reminiscent of an internal-charge transfer (ICT) mechanism which would cause substantial positive charge density to accumulate at the aliphatic amine which may play a role in the sensory mechanism of this class of compounds.(130)

Barium has proven to be an elusive target for metal-ion sensing, also due to a lack of receptors with selectivity and affinity for Ba(II). The work of Nakahara and coworkers is perhaps the most significant contribution to this field to date.(131) The cryptand II.19, following the fluorophore-spacer-receptor format, shows poor binding to Ba(II) in water and thus a weak fluorescence enhancement. The reason for this is that water hydrates the ligand II.19 strongly

reducing its availability to the analyte. However, addition of the non-ionic detergent Triton X-100 to a solution of the sensor and Ba(II) caused the lipophilic chelator to migrate into a less polar micellar environment thus expelling water of hydration and enhancing analyte binding (see **Figure 56**).⁽¹³²⁾ This effect resulted in a strong fluorescence enhancement upon analyte recognition. The cryptand is size-selective for Ba(II) over the remaining alkaline earth metals, but analyte repulsions from the micellar environment limits the scope of this strategy. There is evidence in the literature that micellar environments can be useful when the receptor acts like a “periscope” and peaks into the solution and nabs nearby target cations.⁽¹³³⁾



II.19

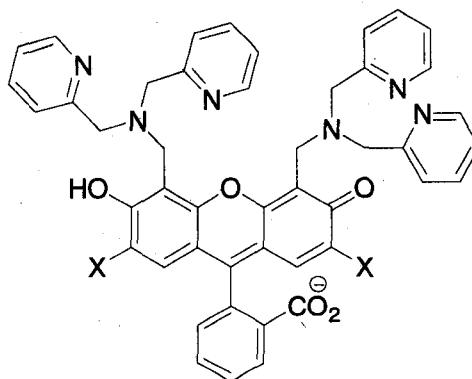
Figure 51 Nakahara's micellar Ba(II) PET sensor.

2.6. Zn(II), Cd(II), Hg(II) PET sensors

There are several criteria that must be met when developing metal ion sensors for biological applications: namely large molar absorptivities; a significant

fluorescent Stokes' shift to prevent self-quenching; large quantum yields; a shift in either/or both excitation and emission wavelengths upon analyte recognition; excitation wavelengths at or above 400nm to minimize background fluorescence of cellular components, tissue, and biological fluids; high selectivity for the target analyte; low toxicity; and if intracellular analytes are the desired target a high lipophilicity is needed so the fluorescent probe can diffuse across the lipid bilayer of the cell.(134)

Divalent zinc, an abundant metal ion found in biological systems, is an appropriate target analyte for PET-based sensors. The success of the following examples of Zn(II)-PET sensors can be partly attributed to the closed-shell nature of the analyte (d^{10}) and the availability of Zn(II)-selective receptors. The well-documented sensors developed concurrently in the laboratories of Lippard (MIT) and Tsien (UCSD) rely on the dipicolylamine (DPA) unit as the analyte receptor (**Figure 52**).(126, 135, 136) Burdette and Lippard strategically placed halogens (F or Cl) on the fluorophore to lower the pK_a of the tertiary nitrogens. This novel modification prevents protonation at this site under physiological pH thus reducing background fluorescence from the sensor in the absence of the analyte. Fluorescein is an attractive candidate for the fluorophore unit because of its visible excitation and emission wavelengths which reduces the possibility of



II.20

Figure 52 Fluorescein-based Zn(II)-PET sensors. The identity of X can be H, Cl, or F.

tissue damage in biological assays for Zn(II). The compound **II.20** in **Figure 52** follows the fluorophore-spacer-receptor format. When the analyte binds to the DPA receptor, PET from the tertiary amine to the fluorescein moiety is blocked causing a Zn(II)-induced fluorescence enhancement. This family of Zn(II) sensors has been implemented in the visualization of high levels of neuronal Zn(II), which has been implicated in Alzheimer's disease and other neurological disorders. Another attractive feature of this class of compounds is that neuron-sensor loading is achieved with passive diffusion without the need of acetoxymethyl ester derivatives.⁽¹²⁶⁾ The phenolate oxygen also binds to the Zn(II) contributing to the sensory mechanism via the aforementioned phenomenon of ICT.^(137, 138)

The DPA unit was also utilized in the development of coumarin based Zn(II)-PET sensors (**Figure 53**).⁽¹³⁹⁾ Compound **II.21** is another example of a fluorophore-spacer-receptor formatted sensor behaving straightforwardly in the presence of the analyte. Compound **II.22**,

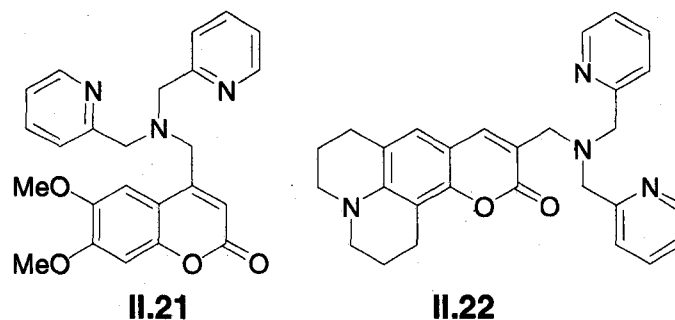


Figure 53 Coumarin-based PET sensors for Zn(II).

however, has a modicum of internal charge transfer character which contributes to the sensory mechanism. This is a result of the binding of the lactone oxygen of the coumarin to Zn(II). Metal-binding therefore perturbs the excited state of the chromophore causing the development of a shoulder in the emission spectrum. This effect resulted in a ratiometric sensor which may prove valuable in the quantitative analysis of Zn(II) in the intracellular milieu.(126) However, increasing the amount of water in the methanol solvent reduced the shift, suggesting that water is competing with the lactone oxygen for coordination to the metal. This does not bode-well for aqueous studies of compound **II.22** with the analyte. Likewise, the fluorescence enhancement of **II.22** is weak because of the background fluorescence of the free-ligand. Callan *et al.* speculate that the higher reduction potential of the aminocoumarin **II.22** as compared to the dimethoxycoumarin **II.21** which therefore prevents emission quenching (via PET) by the free-chelator.(108)

A recent example of a ratiometric sensor for Zn(II) came from Lippard's laboratory at MIT (**Figure 54**).⁽¹⁴⁰⁾ Woodroffe and Lippard couple the Zn(II)

sensitive DPA-fluorescein moiety to a Zn(II) insensitive coumarin unit producing compound **II.23**.

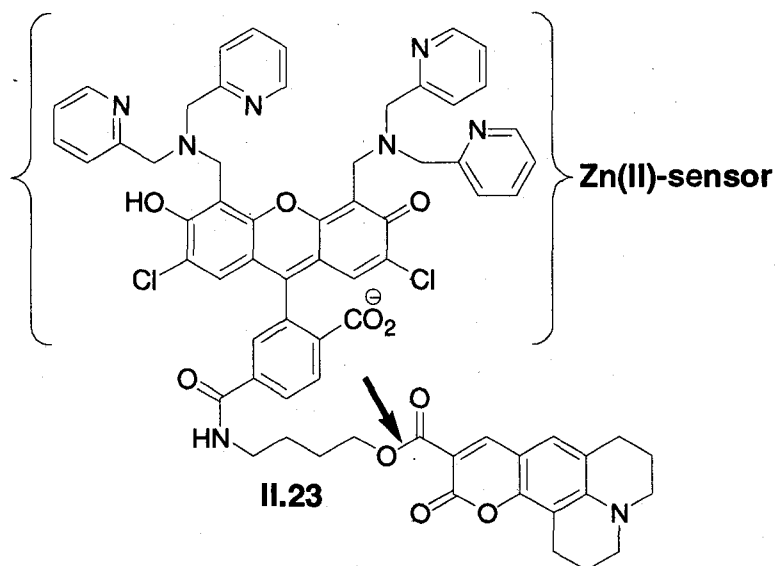
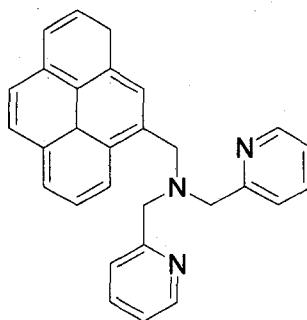


Figure 54 Lippard's ratiometric Zn(II) sensor.

Compound **II.23** undergoes saponification (at the arrow designated site in **Figure 54**) by the aforementioned esterases upon entry into a cellular environment. The liberated fluorescent molecules are subsequently observed at distinct wavelengths. The Zn(II) sensor portion of molecule **II.23** (indicated by parentheses in **Figure 54**) will bind Zn(II) and undergo a green fluorescence enhancement which can be quantified against the disparate blue coumarin fluorescence. This approach is only useful if the unconnected fluorophores are co-localized.

Simple PET sensors for Zn(II) based on pyrenyl-fluorophores are plagued by weak emissions due to aggregation of the ligands in bulk water (**Figure 55**).⁽¹⁴¹⁾ However, compound **II.24** can be dispersed in micelles and the

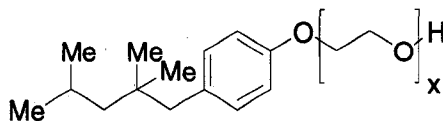
sensory action toward mesoscopic Zn(II) (*i.e.* Zn(II) near the surface of the micelle) enhanced.



II.24

Figure 55 Pyrene-based mesoscopic Zn(II)-sensor.

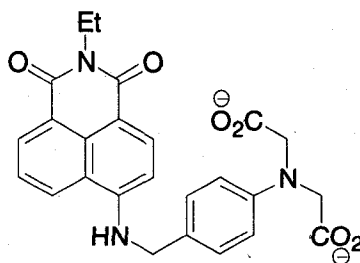
Furthermore, interference from H^+ is not an issue if the water the micellar vesicles are suspended in is buffered at pH=7. This is likely attributable to the dielectric effect of the micellar surface region disfavoring the presence of H^+ .⁽¹³³⁾ When the vesicles are created with an anionic surfactant (*e.g.* sodium dodecyl sulfate) then the negative charge density at the micellar surface enhances the presence of protons and concomitantly reduces the Zn(II)-induced fluorescence enhancement upon analyte recognition. When the surface of the micelles are positively charged, as they are with cetyltrimethylammonium bromide, then no Zn(II)-induced fluorescence enhancement was observed because the analyte is repelled from the vesicular surface via electrostatic forces. Therefore, non-ionic detergents emerge as the best choice for micellar-sensor assemblies, such as Triton-X-100 as was discussed in the special case of the Ba(II) sensor **II.19**.



II.25

Figure 56 The structure of the non-ionic surfactant Triton X-100 II.25.

A PET sensor for Zn(II) was developed by Gunnlaugsson *et al.* which contains a very simple iminodiacetate receptor (Figure 57).(142) This particular compound is insensitive to neutral pH and displays an “on” quantum yield of 21% (fluorescence enhancement=50). If the pH of the solution drops below *ca.* 5 protonation of the anilino-nitrogen attached to the carboximide resulted in a 100-fold enhancement of the emission intensity highlighting the unfavorable interference from H⁺.



II.26

Figure 57 Gunnlaugsson's Zn(II)-sensor.

Receptors designed for Zn(II) (*e.g.* DPA) often experience interference from Cd(II). Other examples of Gunnlaugsson's iminodiacetate PET sensors demonstrate exciplex emissions upon titration with Zn(II) or Cd(II) (Figure 58).(143, 144) The exciplex emission arises from a charge transfer between adjacent anthracenyl-fluorophores. The exciplex nature in the sensory mechanism manifested itself in the emission spectra, which show loss of the finer

features typical of anthracenyl fluorophores upon analyte binding. This was further evidenced by a large red-shift in the emission of the complex as compared to the free-ligand. The mono-substituted compound **II.27** forms an exciplex band at 468 nm upon Zn(II)-binding. Compound **II.28** has an enhanced affinity for Cd(II) relative to Zn(II) and produces exciplex emissions at 500 nm upon analyte binding.

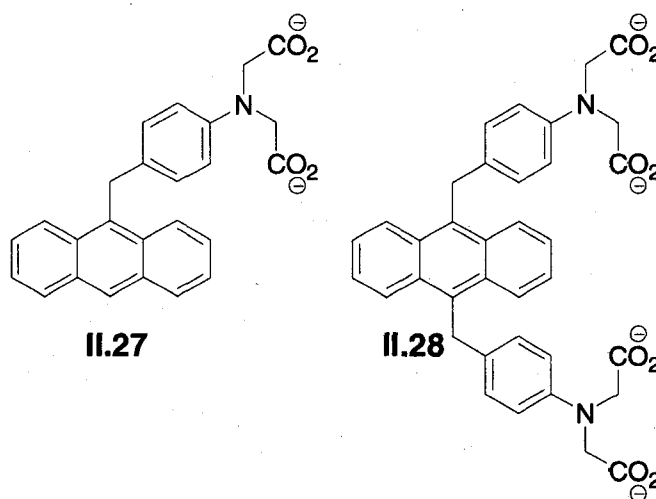
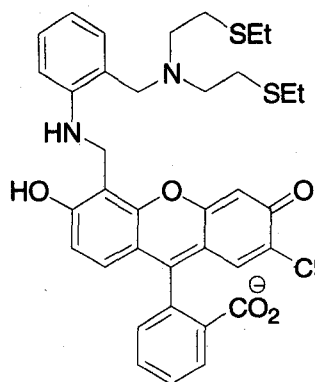


Figure 58 Gunnlaugsson's exciplex sensors for Zn(II) (left) and Cd(II) (right).

PET sensors for the toxic Hg(II) ion have also enjoyed recent success. Lippard and Nolan have developed a water soluble "on-off" sensor for Hg(II) that employs an N_2S_2 donor set (**Figure 59**).⁽¹⁴⁵⁾ The soft thioethers interact with the target analyte strongly effectively quenching the PET to the fluorescein-reporter.⁽¹⁴⁶⁾ However, this sensor is limited by a weak 5-fold fluorescence enhancement in the presence of 1.0 equivalent of the analyte. The background fluorescence of compound **II.29** under physiological conditions is a result of protonation at the aliphatic amine. The electron withdrawing nature of the protonated aminomethyl group raises the oxidation potential of the pendant

aniline unit sufficiently enough to hinder the PET process.(147) This will cause the sensor to be partially switched on in the absence of Hg(II).



II.29

Figure 59 Lippard and Nolan's Hg(II)-sensor.

Another example of a PET-based Hg(II) sensor comes from the laboratory of Qian (Figure 60).(148) The receptor of compound II.30 is a 2,6-bis(aminomethyl)pyridine group which also serves to anchor the aminonaphthalimide fluorophores. To improve water solubility two hydroxyethoxyethyl groups have been installed at the distal end of the sensor. The selectivity for the target analyte is excellent as evidenced by a fluorescence enhancement of 17 upon Hg(II) recognition, while other cations displayed feeble fluorescence enhancements in the presence of the sensor. The pK_a of the tertiary amine group was sufficiently low at a value of 5.2 to minimize interference from H^+ at neutral pH. The major advantage of this Hg(II)-sensor is the high affinity for Hg(II) that gives a detection limit of ca. 0.1nM Hg(II).

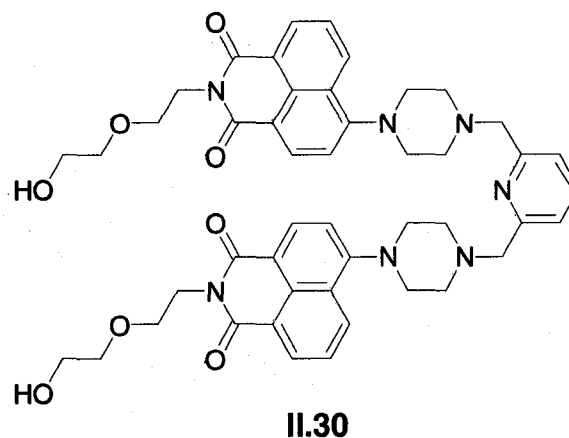


Figure 60 Qian's luminescent Hg(II)-sensor.

2.7. Metal-ion internal charge transfer (ICT) and twisted internal charge transfer (TICT) sensors

The fluorophore can be directly integrated into the receptor resulting in a seamless assembly of contiguous p-orbitals. These so-called internal charge transfer (ICT) metal sensors will possess an electron rich receptor and electron poor fluorophore.⁽¹⁴⁹⁾ A substantial redistribution of electron density occurs upon excitation resulting in a large dipole in the excited state. Binding of a charged species in the receptor perturbs the fluorophore upon excitation (**Figure 61**). Often the metal cation is ejected from the receptor in the excited state due to electrostatic repulsions within the receptor. The presence of the analyte, as **Figure 61** suggests, leads to blue-shifts in the absorbance spectra and red-shifts in the emission spectra as compared to the free-sensor.

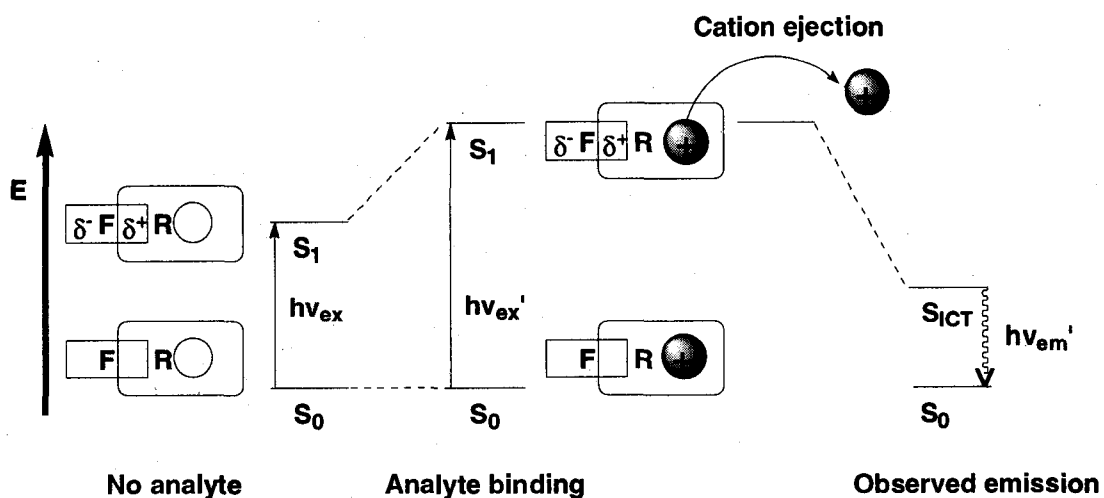


Figure 61 Schematic of ICT metal ion sensing.

An example of a “turn-off” Zn(II) sensor is compound **II.31** (Figure 62).⁽¹⁵⁰⁾ The extended conjugation between the pyrenyl-fluorophore and the terpyridine receptor via an dialkynyl thiophene conduit suggests that ICT is the major component of the sensory mechanism. Upon analyte binding fluorescence in acetonitrile of **II.31** is turned-off. Shifts in the UV-visible absorbance spectrum and cyclic voltammogram corroborate the affirmation of an ICT sensing mechanism.

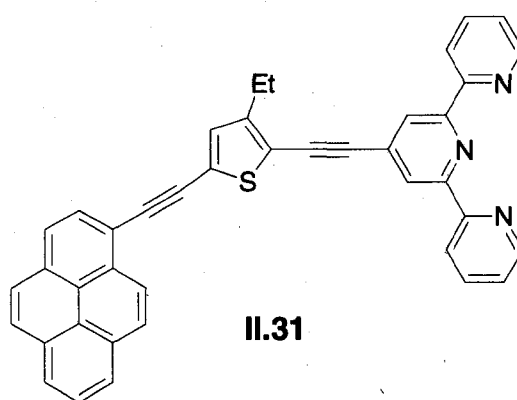


Figure 62 ICT-based turn-off sensor for Zn(II).

The NO₂S₂ coronand serves as the receptor for Hg(II) in sensor **II.32** (**Figure 63**).⁽¹⁵¹⁾ The selectivity for the target analyte is evidenced by a sub-micromolar detection limit (ca. 10⁻⁷M) of Hg(II). The ICT nature of **II.32** is revealed in a color change from pink to yellow upon Hg(II) binding. A small blue-shift was observed in the UV-visible absorbance spectrum.

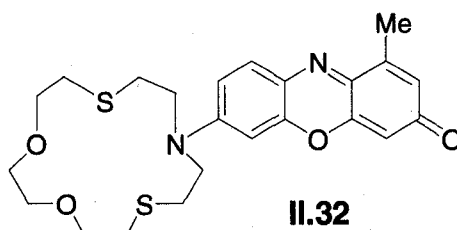
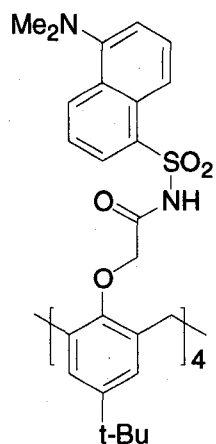


Figure 63 ICT-Hg(II) sensor.

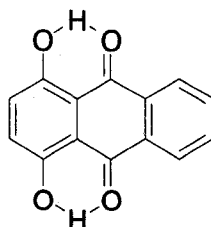
Métivier *et al.* have uncovered a useful Pb(II) sensor **II.33** by employing a calixarene receptor (**Figure 64**).⁽¹⁵²⁾ A blue-shift of 52 nm was observed in the UV-visible spectrum of **II.33** in the presence of the analyte. This result is noteworthy because the pH of the solution (40% aqueous MeCN) was 5.2 and protonation equilibria of the dansyl group normally effects the luminescent behavior through the usual PET processes. Likewise laudable, selectivity for Pb(II) was maintained over Cu(II), Zn(II), Cd(II), and Hg(II).



II.33

Figure 64 An ICT Pb(II) sensor.

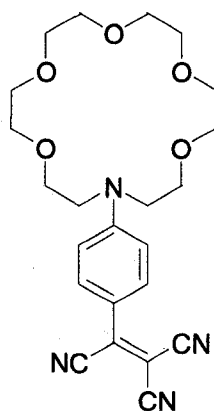
Quinizarin **II.34** has classically been utilized in the detection of B(III) and Be(II) (**Figure 65**).⁽¹⁵³⁾ Other hydroxyanthraquinones, like quinizarin-2-sulfonic acid, have also been used to detect Be(II) and Al(III).⁽¹⁵⁴⁾ It was recently recognized that these reagents are ICT fluorophores where intramolecular hydrogen bonds between the phenolic group and the adjacent carbonyl serve as de-excitation channels in the apo-ligand.⁽¹⁵⁵⁾ When the offending bonds are replaced with dative bonds to ionic analytes moderate fluorescence enhancements were observed. Tricationic guests, like Ga(III) or In(III), induce a seven-fold enhancement of the emission intensity of quinizarin **II.34**.



II.34

Figure 65 The structure of quinizarin **II.34**.

Pb(II) is a closed shell species and should be amenable to PET-based sensing. However, fluorescence quenching via intersystem crossing (*i.e.* “heavy-atom effect”) will plague such systems.(102) Jimenez *et al.* have avoided internal conversion deactivation by developing compound **II.35** which possesses a fluorescence enhancement with Pb(II) (**Figure 66**). (156) The structure of **II.35**



II.35

Figure 66 A TICT-based sensor for Pb(II).

suggests that this sensor contains an ICT fluorophore. However, twisting about the anilinic or aromatic C-vinyl bonds results in a so-called twisted internal charge transfer (TICT) state which is responsible for the observed fluorescence enhancement with Pb(II). An anodic shift was seen in the cyclic voltammogram

of the Pb(II)-**II.35** complex. This was due to destabilization of the sensor radical cation.(156)

Taking advantage of TICT Xiao and Qian developed compound **II.36** (**Figure 67**) (157) which features a cyclic piperazine receptor that resulted in a substantially twisted aromatic C-N bond because of the so-called *peri*-effect between the piperazine and the hydrogen at C8.(158)

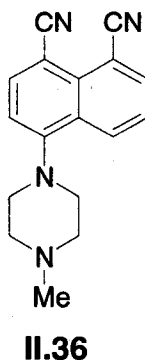


Figure 67 TICT-assisted luminescent metal-ion sensor.

The development of TICT states upon excitation prevented competing PET processes thus resulting in large fluorescence enhancements (>100) with the open-shell analytes Fe(III) and Cr(III) and smaller yet significant enhancements with Mn(II), Co(II), Ni(II), Cu(II), and Pb(II).(159) Interestingly, no enhancements were seen with Hg(II) or Zn(II).

The compound developed by Morozumi and coworkers **II.37** operates via an extreme case of the aforementioned TICT phenomenon (**Figure 68**).(160) The reader is encouraged to note that this system has the requisite structure for PET-based sensing by possessing the tried-and-true “fluorophore-spacer-receptor” design motif. Interestingly this compound exhibits a 37-fold

fluorescence enhancement upon interactions with Ca(II), but minimal to non-existent effects were observed with Sr(II), Ba(II), and Mg(II). The reason for this is that Ca(II) binds to the podand framework and both amido carbonyls facilitating the conformational twisting needed to achieve a TICT state. The structure of the complex thus gives rise to the desired emission. The selectivity for Ca(II) is clearly attributable to the size-selective nature of the polyether framework.

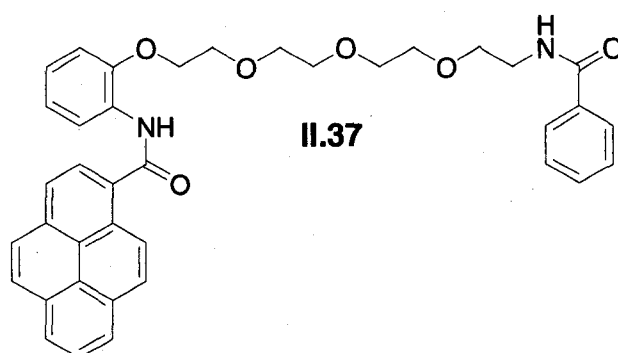
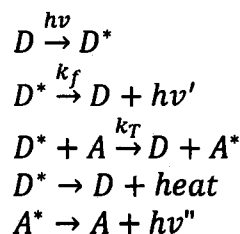


Figure 68 TICT-based Ca(II) sensor.

2.8. Electronic energy transfer (EET) metal-ion sensors (100)

Some of the most valuable applications of fluorescence involve the transfer of excitation energy from one fluorophore to another. This process is strongly dependent on the distance between the fluorophores and on their relative orientations. This phenomenon has been treated theoretically by a host of investigators and has been verified experimentally through the design of model systems.

The transfer of the excitation energy from a donor molecule (D^*) to an acceptor molecule (A) will ultimately lead to fluorescence from this species via the following collection of photochemical reactions:



The process begins with the donor undergoing excitation by absorbing a photon ($h\nu$). The donor can fluoresce (k_f), donate the excitation energy to the acceptor (k_T), or undergo internal conversion (evolve heat). If electronic energy transfer (EET) occurs then the excited acceptor (A^*) can fluoresce, as denoted in the last reaction by producing a photon ($h\nu''$). The transfer of excitation energy can be measured three ways: observing a decrease in the fluorescence quantum yield of the donor due to the presence of the acceptor; observing the decrease in the lifetime of the donor due to the presence of the acceptor; or noting the increase in fluorescence of the acceptor due to the presence of the donor. The efficiency for such a process is defined as the fraction of excited donor molecules that undergo deactivation via EET. It can be expressed in terms of the rate constant for EET (k_T) and the collective rate constants for all other deactivation pathways (k_d):

$$\text{efficiency} = \frac{k_T}{k_T + k_d}$$

(II.e)

The rate of energy transfer from a donor to an acceptor (k_T) is $k_T = \frac{1}{\tau_D} \left(\frac{R_0}{r}\right)^6$ where τ_D is the decay time of the donor alone, R_0 is the Förster distance, and r is the donor-acceptor distance (vide infra). The units for k_T are thus the same as the units for k_d (i.e. s^{-1}) leaving *efficiency* as a unitless quantity. Because the fluorescence quantum yield for the donor alone is $\frac{k_f}{k_d}$ and the quantum yield for the donor in the presence of the acceptor is $\frac{k_f}{k_d+k_T}$ the efficiency for EET can be expressed as the following:

$$efficiency = 1 - \frac{\Phi_{D+A}}{\Phi_D}$$

(II.f)

The efficiency of this transfer is heavily dependent on the distance between the donor and the acceptor. In the range of 1 to 10 nm EET is referred to as fluorescence resonance energy transfer (FRET). For each donor-acceptor pair the efficiency of EET depends on r^{-6} , where r is the distance between the FRET-pair. The relationship between r_0 , where r_0 is the distance at which the efficiency is 50%, and r is as follows:

$$efficiency = \frac{r_0^6}{r_0^6 + r^6}$$

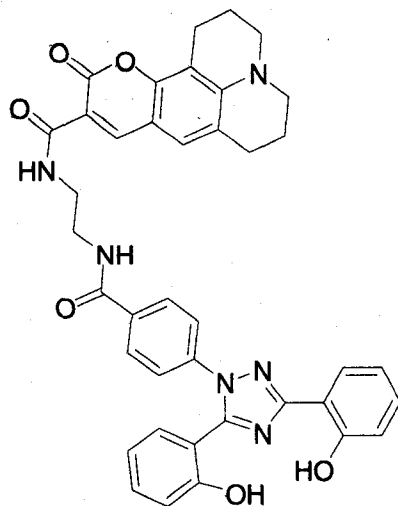
(II.g)

The variable r_0 is also termed the Förster distance.(161) Moreover, the value of r_0 depends on the amount of overlap between the fluorescence spectrum of the donor and absorbance spectrum of the acceptor. It also depends on the angular

orientation between the FRET pair, which is often unknown or difficult to ascertain. The orientations of the pair can be averaged, but caution needs to be exercised if the fluorophores are in a constrained environment.

Because each component possesses unique luminescent behavior a two-color sensory system can be developed and a ratio of the emission wavelengths for the *D-A* pair created. Therefore, the utilization of EET systems is particularly attractive in the sensing arena because the analyte can be quantitated in undefined environments. There has been success in the development of EET-based metal ion sensors which is evidenced in the following examples.

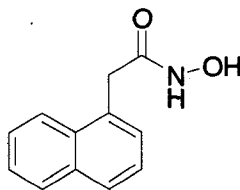
By coupling an aminocoumarin to the distal end of molecule **II.38** the EET mechanism was exploited in the sensing of Al(III) (**Figure 69**).⁽¹⁶²⁾ Upon analyte recognition the phenolic hydrogens are replaced with Al(III) which prevents vibrational coupling to the bulk water that would otherwise attenuate the emission intensity.⁽¹⁶³⁾ The resulting emission from the bound receptor overlaps with the absorbance of the aminocoumarin unit. The direct excitation of the aminocoumarin does not show Al(III)-induced fluorescence enhancement confirming that the aminocoumarin does not ligate the analyte. In the absence of the analyte the phenolic unit has a short excited lifetime due to vibrational coupling. This resulted in a feeble EET to the distal end of the molecule thus weak emissions were observed. On analyte recognition, however, the lifetime of the bound-receptor was extended giving rise to an excellent EET to the aminocoumarin.



II.38

Figure 69 An EET Al(III) sensor.

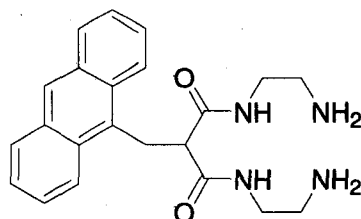
Often underutilized in receptor design, a hydroxamate is showcased in De Costa and coworkers compound **II.39** (Figure 70).⁽¹⁶⁴⁾ The structure possesses a fluorophore-spacer-receptor design motif seen in PET metal ion sensors and as such switches off the naphthalene fluorescence upon binding Fe(III) in 50% aqueous methanol under acidic pH. The appearance of a ligand-to-metal charge transfer absorption band at longer wavelengths suggests that EET deactivation may play a role in the turn-off sensory mechanism of this compound.



II.39

Figure 70 A hydroxamate turn-off sensor selective for Fe(III).

The hydrophobic PET sensor **II.40** relies on an EET-mediated quench of the anthracenyl unit upon Cu(II) binding (**Figure 71**).⁽¹⁶⁵⁾ The sensor **II.40** was integrated into Triton X-100 micelles. As was seen in the aforementioned examples, the micellular environment was not disturbed by the presence of small quantities of the sensor and the corresponding analyte.

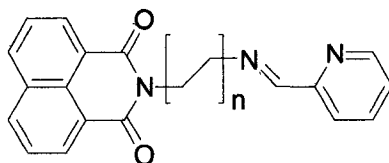


II.40

Figure 71 A hydrophobic anthracene fluorophore is attached to a novel Cu(II) receptor.

2.9. Excimer and exciplex metal sensors

Excited states possess half-filled orbitals which may interact with ground-state orbitals. The resulting π - π overlap results in extended delocalization of the states. This phenomenon manifests itself in broad red-shifts in the corresponding emission spectra of the excited-state complexes (termed exciplexes). The fluorophore-spacer-receptor system **II.41** developed by Licchelli *et al.* are designed to bring the π -systems of the naphthalimide fluorophores within close proximity to one another upon binding multiple molecules of **II.41** to one equivalent of analyte (**Figure 72**).⁽¹⁶⁶⁾



II.41

Figure 72 Licchelli's *et al.* excimer-forming Zn(II) and Cd(II) sensor. The value of the n-ethyl units varies from 2-5.

These fluorophores have enjoyed increasing use in exciplex-based sensors. Long-wavelength emissions were observed in the presence of small concentrations of Zn(II) or Cd(II), due to 1:3 M:L exciplexes. The exciplexes formed in solution when the poly(ethylene) linker unit was large enough ($n > 2$). Increasing the analyte concentration resulted in the formation of 1:2 and subsequently 1:1 M:L complexes which do not form exciplexes, and thus the long-wavelength emissions were extinguished. This result illustrated the lack of intraligand π - π interactions upon analyte binding. However, a fluorescence enhancement of 6 was seen with both Zn(II) and Cd(II) when conditions favoring 1:1 M:L binding stoichiometries were employed. The authors speculate that analyte interactions with the carbonyl groups of the fluorophore increases the energy of the $^1n\pi^*$ excited state thus preventing intersystem crossing which would ultimately extinguish the desired emission. (138, 167, 168)

Lastly, compounds II.42 through II.45 are designed to form exciplexes in the presence of Ca(II) or Ba(II). (169) By varying the length of the polyethylene glycol linker a suitable framework for the desired analyte was achieved causing the terminal naphthalene-units to overlap. The authors investigated the relationship between the substitution effects and the metal ion recognition. The

fluorescence quantum yields decreased as the electronegativity of the p-substituent of the acceptor benzoate increases. Compound **II.45** (where $n = 5, 6$) showed the most efficient quenching and exciplex emissions. When Li(I), Na(I), K(I) and Mg(II) were added to an acetonitrile solution of compounds **II.42** through **II.45** ($n = 5, 6$), the shape and intensity of the fluorescence spectra did not change. However, the spectra of all the compounds significantly changed with the addition of Ca(II) and Ba(II). In the absence of alkaline earth cations the emissions from the apo-ligand were moderated by the para-substituted benzoate via a PET mechanism.

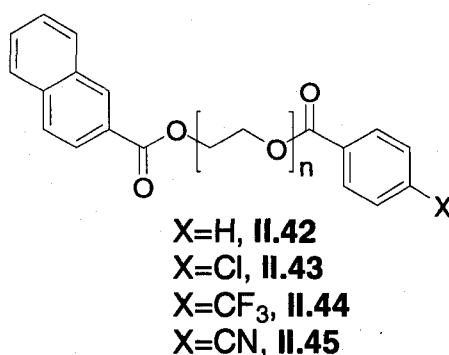


Figure 73 Luminescent Ca(II) and Ba(II) sensors.

2.10. Coordination-enhanced fluorescence (CEF) metal-ion sensors

Molecules with the lowest excited state of the ${}^1n\pi^*$ type are typically nonemissive in solution.^(168, 170, 171) This can be rationalized by two arguments.⁽¹⁰²⁾ The molar absorptivities for a $\pi\pi^*$ state are often 100 to 1000 times greater than they are for the $n\pi^*$ transition. Therefore, the lifetime associated with the $\pi\pi^*$ state is shorter (10^{-7} to 10^{-9} seconds) as compared to the

lifetime for the $n\pi^*$ state (10^{-5} to 10^{-7} seconds). Non-radiative deactivation channels will compete with fluorescence in $n\pi^*$ systems. The rate constant for intersystem crossing is smaller for $\pi\pi^*$ systems because the energy difference between the S_1 and T_1 states is larger. This reduces the likelihood for intersystem crossing so that fluorescence can occur. The fluorescence for such systems can be persuaded to switch "on" if the ${}^1n\pi^*$ state is perturbed such that the lowest energy singlet excited state is of the ${}^1\pi\pi^*$ type (**Figure 74**).

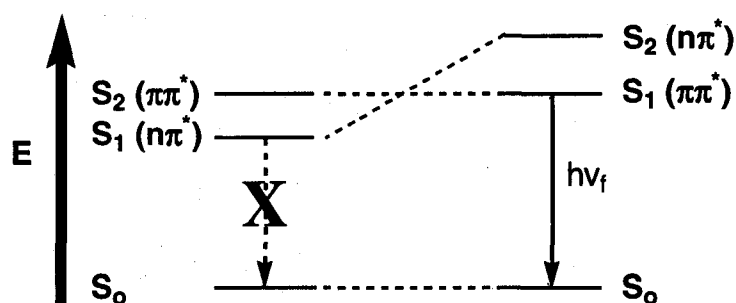


Figure 74 Inversion of a nonluminescent $n\pi^*$ S_1 state to an emissive $\pi\pi^*$ S_1 state.

Azaaromatics such as acridine, *o*-phenanthroline, and quinoline demonstrate this behavior in the presence of Lewis acids.⁽¹⁷²⁻¹⁷⁴⁾ Upon complexation to Zn(II) the ${}^1n\pi^*$ excited state of quinoline moves to higher energies. The inversion of the excited states affords a ${}^1\pi\pi^* \rightarrow S_0$ emission.⁽¹⁴⁹⁾ Several quinoline-based Zn(II) sensors have been developed around this principle (**Figure 75**).⁽¹⁷⁵⁻¹⁸⁰⁾

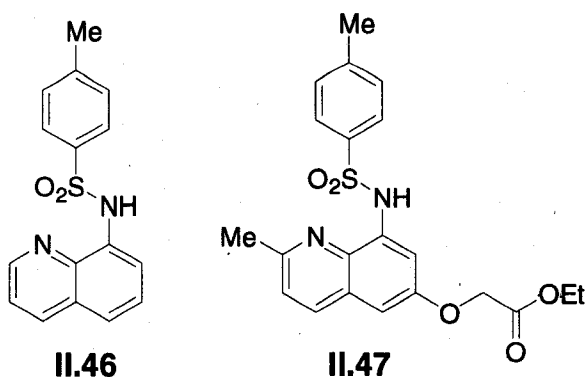
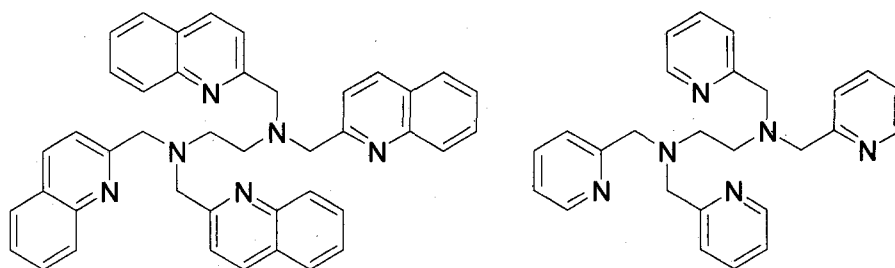


Figure 75 Quinoline-based CEF sensors for Zn(II).

Fredrickson's Zn(II)-sensor TSQ **II.46** is membrane permeable and selective for Zn(II) in the presence of physiological relevant concentrations of Ca(II) and Mg(II). Under pH 7.4 aqueous conditions TSQ forms the complex Zn(TSQ)₂ as the species for Zn(II) detection. One drawback of this sensor is that the intracellular Zn(II) chelator dithizone blocks the action of TSQ **II.46** by competing for the analyte.⁽¹⁸¹⁾ The closely related Zn(II)-sensor zinquin **II.47** is another quinoline-based sulfonamide, but the advantage of this particular chelator is the presence of an acetoxyethyl ester (**Figure 75**). Upon cellular loading of zinquin **II.47** ubiquitous intracellular esterases hydrolyze the acetoxyethyl group releasing the corresponding carboxylate into the cytosol. Hydrolysis hinders extracellular leakage of the sensor. However, extrusion of anionic fluorometric reagents from the cytosol via the action of organic ion transporters may limit the utility of this strategy.⁽¹⁸²⁾

A recent example of a quinoline based Zn(II)-sensor comes from the work of Mikata *et al.* (**Figure 76**).⁽¹⁸³⁾



TQEN II.48

TPEN II.49

Figure 76 Mikata *et al.*'s TQEN II.48.

Mikata's molecule **TQEN II.48** (where TQEN=*N,N,N',N'*-tetrakis(2-quinolylmethyl)ethylenediamine) is the first example of a **TPEN II.49** (where TPEN=*N,N,N',N'*-tetrakis(2-picoyl)ethylenediamine)-based fluorescent sensor. Unlike the aforementioned Zn(II)-sensors **TQEN II.48** possesses six-donor atoms which is the maximum number of donor atoms for Zn(II).⁽²⁸⁾ Maximizing donor atoms gives rise to very stable complexes with the analyte. By replacing the pyridine rings with quinoline groups, Mikata and coworkers have created a Zn(II)-sensor that relies on the concomitant operation of PET and CEF sensory mechanisms. The fluorophore-spacer-receptor design motif is embedded in each of the four chelate arms of **TQEN II.48** where the receptors are the tertiary amines and the spacers are the interstitial methylenes. The quinoline fluorophore also coordinates the analyte which raises the energy of the $^1n\pi^*$ state and affords a $\pi\pi^* \rightarrow S_0$ emission upon Zn(II)-recognition and excitation. In the absence of the analyte the amines launch PET at the four quinoliny groups rendering the sensor in the "off" state. **TQEN II.48** is soluble in chloroform, dichloromethane, and DMF and only slightly soluble in acetonitrile and DMSO. Unfortunately, **TQEN II.48** is insoluble in H₂O, acetone, methanol, and ethanol

limiting its utility in protic solvent systems. However, in DMF and 50% aqueous DMF TQEN II.48 yields a 23-fold emission enhancement in the presence of 1.0 equivalent of Zn(II). The response selectivity is only challenged by Cd(II), which exhibits *ca.* 60% of the emission intensity of $[\text{Zn}(\text{TQEN})]^{2+}$. Competition experiments with Na(I), K(I), Mg(II), Ca(II), Ni(II), and Mn(II) did not quench $[\text{Zn}(\text{TQEN})]^{2+}$, however the emission intensity was attenuated in the presence of Cu(II), Co(II), Cd(II), Ag(I) and excess Fe(III), giving an indication of the metal binding selectivity of TQEN II.48 relative to Zn(II). The crystal structure of $[\text{Zn}(\text{TQEN})]^{2+}$ shows that the chelator binds the analyte through all six of the nitrogens forming a distorted octahedral complex (**Figure 77**).

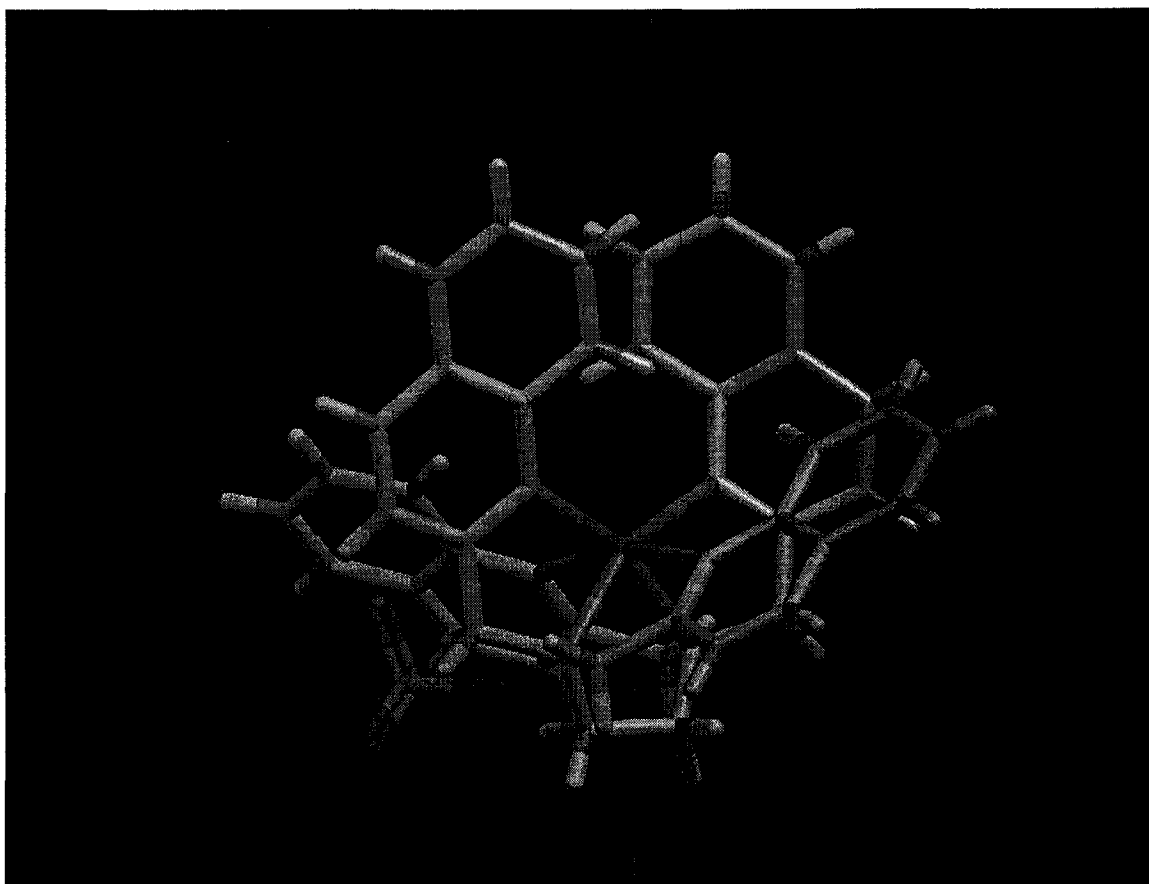
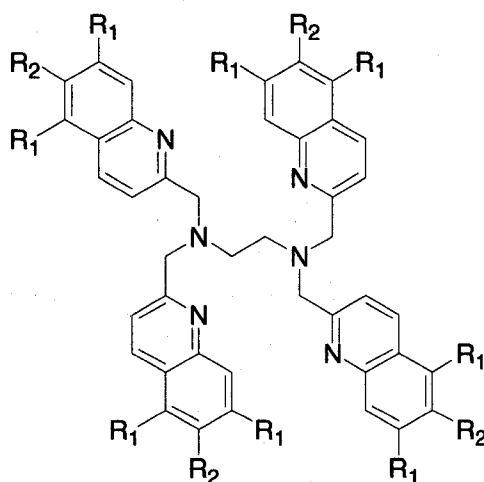


Figure 77 Representation of $[Zn(TQEN)](ClO_4)_2$ from the crystal structure data. The data was obtained from the Cambridge Structural Database (CSD).

Two unique aromatic ring environments occurred in this complex: two rings on the periphery of the complex, one coming forward and one going back, which cannot interact; and two rings pointing up in **Figure 77** which may give rise to π - π overlap between the benzo groups and cause excimer formation upon analyte binding and excitation. However, in this complex steric hindrance between the rings resulted in a twist forcing all four rings into a propeller-like configuration. The binding affinity of TQEN II.48 for Zn(II) in 50% aqueous DMF was measured to be $K_d = (7.0 \pm 3.2) \times 10^{-6} M$ which highlights the loss of thermodynamic stability of this complex relative to $[Zn(TPEN)]^{2+}$ which has a measured binding constant of approximately $K_d \sim 10^{-15} M$. This suggests that the quinolinyl groups are too close

together upon Zn(II)-binding resulting in a huge steric effect. A dim quantum yield of *ca.* 0.2% with the target analyte, unfortunately, limits the utility of this sensor.

Mikata improved on TQEN with the publication of the methoxy derivatives T(MQ)EN II.50 and T(TMQ)EN II.51 (Figure 78).⁽¹⁸⁴⁾



R1=R2=H: TQEN II.48

R1=H, R2=OMe: T(MQ)EN II.50

R1=R2=OMe: T(TMQ)EN II.51

Figure 78 Mikata and coworkers' quinoline Zn(II) sensors.

Installation of methoxy groups on the benzo-rings of TQEN II.48 not only improved the quantum yields of the sensor-Zn(II) complexes (2% for T(MQ)EN II.50 and 3% for T(TMQ)EN II.51) but long-wavelength emissions were evidenced in the fluorescence spectra. The unsubstituted ligand TQEN II.48 had an emission maximum at 383nm, whereas the methoxy derivatives had emission maxima at 408nm and 493nm for T(MQ)EN II.50 and T(TMQ)EN II.51 respectively. The crystal structure for [Zn(T(MQ)EN)]²⁺ revealed the possibility of excimer formation because of enhanced twisting of *ca.* 30° around the principal

rotation axis. Unfortunately, spectroscopic selectivity for Zn(II) over Cd(II) was lost when the methoxy groups were installed on the quinoline fluorophores. The sensor T(MQ)EN II.50 had a emission enhancement of *ca.* 11 in the presence of Zn(II) and an enhancement of *ca.* 14 in the presence of Cd(II). The sensor T(TMQ)EN II.51 suffers from considerable background emissions (*i.e.* the apo-ligand is partially turned “on” in 50% aqueous DMF) which reduced its enhancement to 2.8 in the presence of Zn(II) and *ca.* 4 in the presence of Cd(II). The authors did not speculate on the loss of Zn(II)/Cd(II) selectivity in the paper, however, the presence of the methoxy groups caused marked distortions in the inner coordination sphere of [Zn(T(MQ)EN)]²⁺ as evidenced in the structural data (not shown here). The increased steric interactions between the substituted quinolinyl groups may increase the size of the binding cavity of the ligand which could better accommodate Cd(II). Conversely, Cd(II) could distort the binding cavity in a manner that facilitates an excimer sensory mechanism, although no separate excimer emission signal was observed. Unfortunately, no structural data is available for these Cd(II) complexes.

2.11. Novel TAME-based PET and CEF metal ion sensors

The chemistry that was developed for the preparation of TAMEpyr I.60 as explained in Chapter 1 of this dissertation was exploited in the preparation of novel TAME-based PET/CEF metal ion sensors. The following discussion demonstrates the utility of the TAME framework in developing size-selective Zn(II)-luminescent sensors. The scope of this study was restricted to the

preparation and photophysical investigations of novel azaaromatic TAME-based luminescent metal-ion sensors (**Figure 79**).

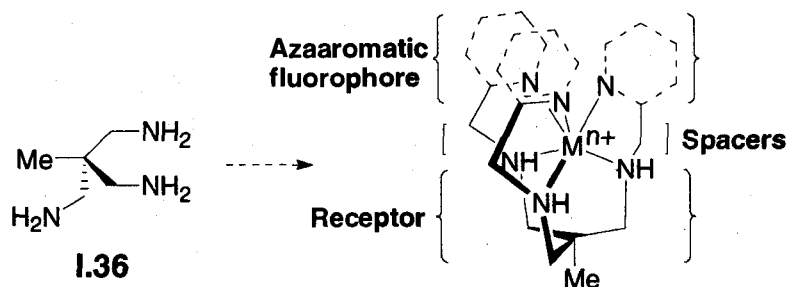


Figure 79 Generic approach to TAME-based luminescent metal-ion sensors.

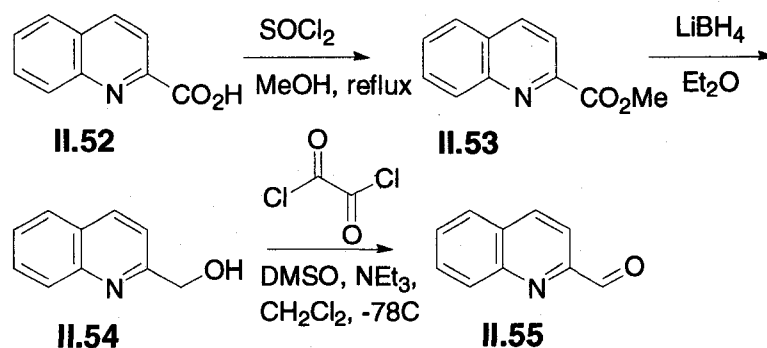
It was envisioned that the azaaromatic groups would serve as the fluorophore. Upon analyte binding the $^1n\pi^*$ state is expected to move to higher energies resulting in $\pi\pi^* \rightarrow S_0$ emissions. The TAME framework will serve as the receptor and render the sensor silent in the absence of the analyte. This will be due to PET via the interstitial methylene conduits. This discussion begins with the preparation of the requisite azaaromatic aldehydes.

Results and Discussion

2.12. Synthesis of azaaromatic aldehydes

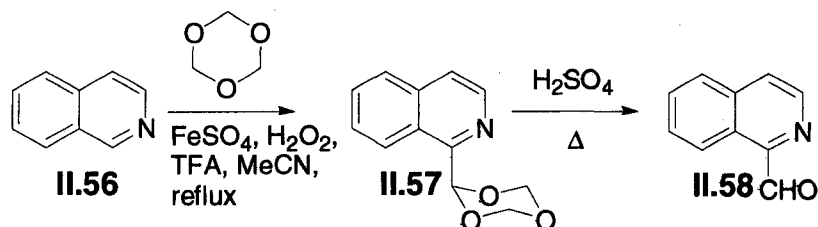
The reaction of 2-quinolinecarboxylic acid (quinaldic acid) **II.52** with thionyl chloride in refluxing MeOH cleanly afforded the corresponding methyl ester **II.53** in 80% yield (**Scheme 15**).⁽¹⁸⁵⁾ The ester was then reduced with LiBH_4 in Et_2O to afford the primary alcohol **II.54** in 90% yield. The alcohol **II.54** was used without any further purification in the subsequent Swern oxidation affording 2-

quinolinecarboxaldehyde **II.55**.(186-188) The disadvantage of the Swern oxidation was that the dimethyl sulfide by-product was not completely removed by chromatography and polluted the isolated material with a noxious odor.



Scheme 15 Preparation of 2-quinolinecarboxaldehyde II.55.

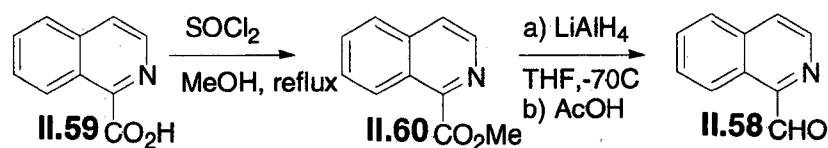
The isomeric compound 1-isoquinolinecarboxaldehyde **II.58** was initially prepared via formylation of the parent heterocycle isoquinoline **II.56** (Scheme 16).(189) This reaction, classified as a homolytic aromatic substitution, produced a trioxanyl derivative of isoquinoline **II.57**. According to Giordano *et al.* the first transformation is mediated by a Fenton reaction between the Fe(II) salt and H₂O₂ which subsequently produces a trioxanyl radical *in situ*.(189, 190) The resulting carbon-centered radical reacted regioselectively at C1 of the heterocycle affording compound **II.57**. The trioxanyl group is a mask for the desired aldehyde which was revealed upon treatment of **II.57** with sulfuric acid.



Scheme 16 Initial preparation of 1-isoquinolinecarboxaldehyde II.58.

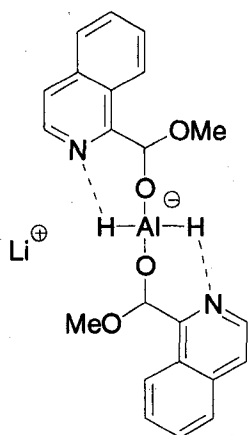
The major disadvantage of this strategy is the need for excess trioxane (e.g. 95 equiv.) in the preparation of the trioxanyl derivative **II.57**. During solvent removal in the workup the excess trioxane decomposed into formaldehyde gas and was deposited as paraformaldehyde $-(\text{CH}_2\text{O})_n-$ on the condenser of the employed rotary evaporator. The poisonous nature of formaldehyde and the tedium of cleaning the condenser prohibited the use of this strategy on larger scales.

An alternative synthesis of the desired aldehyde **II.58** was devised based on the chemistry that was performed on quinaldic acid **II.52** (Scheme 17). Commercially available 1-isoquinolinecarboxylic acid **II.59** was converted into the methyl ester **II.60** using thionyl chloride in refluxing MeOH.



Scheme 17 Alternative preparation of 1-isoquinolinecarboxaldehyde **II.58**.

The methyl ester **II.60** was then converted directly into the desired aldehyde **II.58** by treating the starting material with 0.50 equivalents of LiAlH_4 in THF at -70°C .⁽¹⁹¹⁾ Notably, the methyl ester **II.60** was not reduced to the corresponding 1° alcohol. The formation of a soluble hemiacetal-aluminate complex **II.61** reduces the reactivity of the anionic hydrogens thus preventing over reduction (Figure 80).

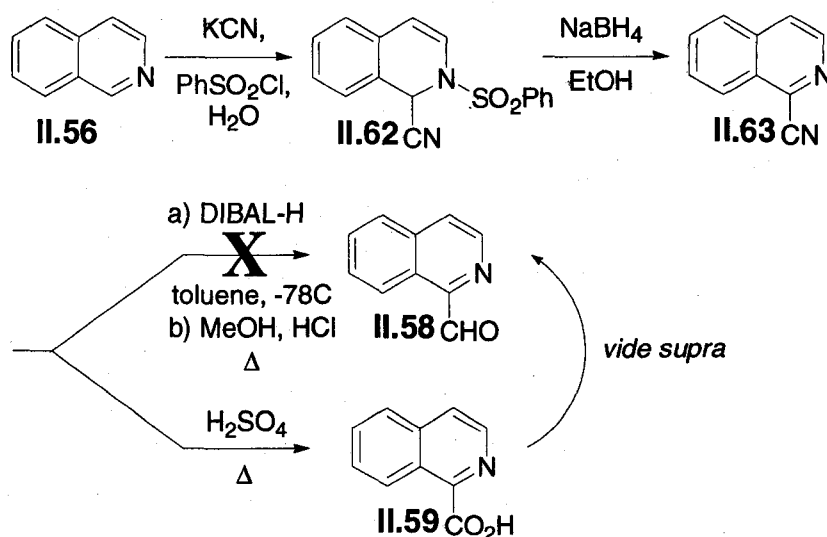


II.61

Figure 80 The structure of the soluble hemiacetal-aluminate complex II.61.(191)

The desired aldehyde **II.58** was liberated from the complex **II.61** upon treatment with AcOH. This reaction has been utilized by Rutner *et al.* in the preparation of otherwise inaccessible heterocyclic aldehydes (*e.g.* pyrazinealdehydes).

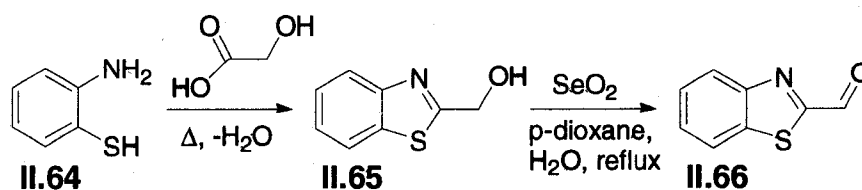
A third approach to 1-isoquinolinecarboxaldehyde **II.58** based on the so-called Reissert reaction (**Scheme 18**) was attempted.(192) Treatment of isoquinoline **II.56** with KCN, and benzene sulfonyl chloride (PhSO₂Cl) allowed for the regioselective installation of a nitrile functional group at C1 of the heterocycle.



Scheme 18 The third approach to 1-isoquinolinecarboxaldehyde II.58.

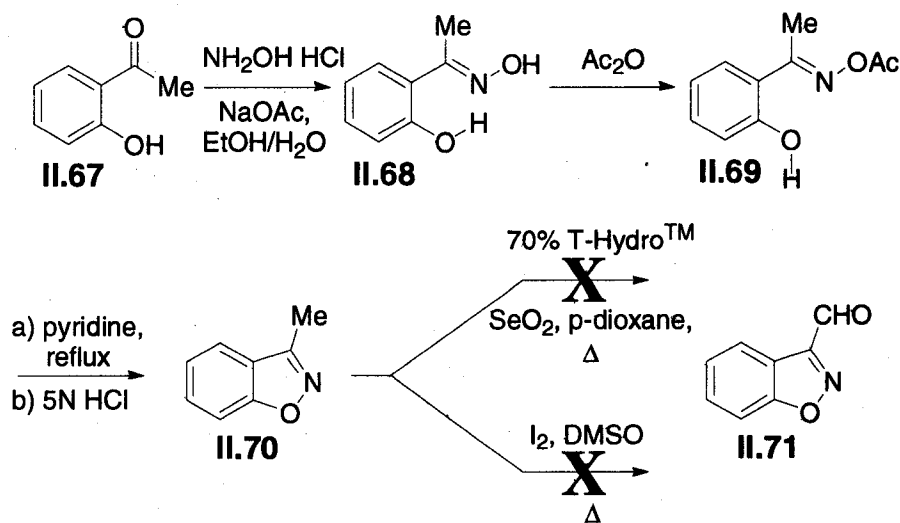
The resulting sulfonamide II.62 underwent elimination with NaBH₄ affording the nitrile II.63.(193) An attempt was made at reducing the nitrile with diisobutyl aluminum hydride (DIBAL-H) but competing reduction of the heterocycle to a 1,2-dihydroisoquinoline limited the scope of this approach.(92) Fortunately, the nitrile could be recycled by converting the remainder of the batch into the carboxylic acid II.59 which can be used in the preparation of the target (Scheme 17).

A small collection of benzo-fused five-membered heterocycles were also prepared. The benzo-fused thiazolecarboxaldehyde II.66 was prepared straightforwardly starting from 2-aminothiophenol II.64 and glycolic acid to afford the 1° alcohol II.65 (Scheme 19).(194) The advantages of this reaction are that it does not require a solvent and reaction completion is judged by the evolution of the stoichiometric amount of H₂O. The alcohol II.65 was then oxidized with SeO₂ and the resulting aldehyde II.66 was purified via sublimation.



Scheme 19 Preparation of 1-benzothiazolecarboxaldehyde II.66.

An attempt at the related 1,2-benzisoxazole-3-carboxaldehyde **II.71** was made starting with 2'-hydroxy acetophenone **II.67** (Scheme 20). The ketone **II.67** was converted into the oxime **II.68** via treatment with hydroxylamine·HCl and NaOAc.⁽¹⁹⁵⁾ The hydroxyl group of oxime **II.68** was then acetylated chemoselectively with acetic anhydride (Ac_2O) affording the acetoxy ketoxime **II.69**.⁽¹⁹⁶⁾

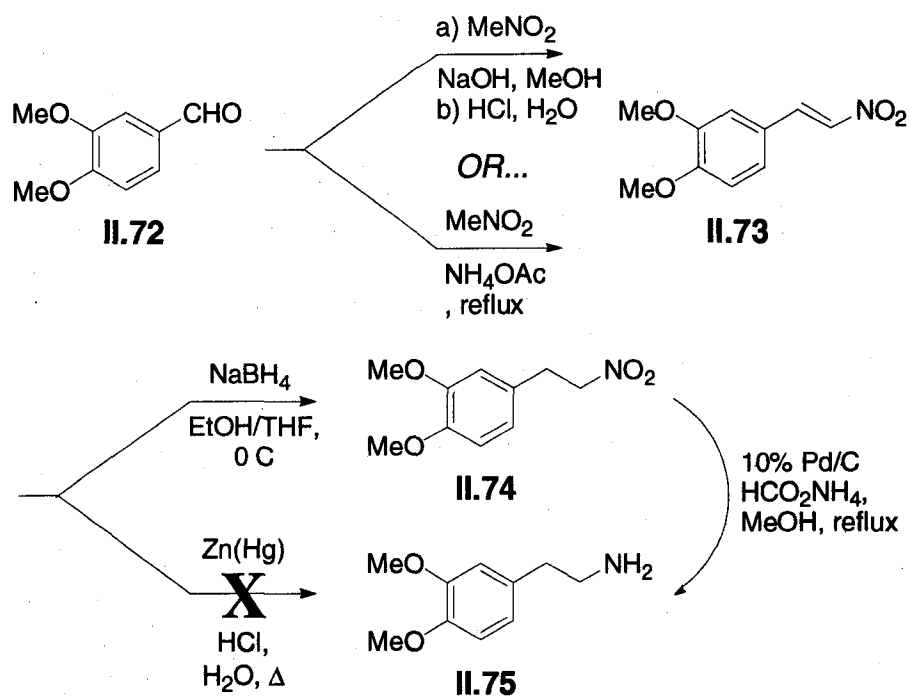


Scheme 20 The attempted preparation of 1,2-benzisoxazole-3-carboxaldehyde II.71.

The acetoxy group leaves via base-promoted intramolecular ring closure affording 3-methyl-1,2-benzisoxazole **II.70**.⁽¹⁹⁶⁾ Pure **II.70** was obtained by reduced-pressure distillation (bp=56°C, 210mTorr) and subjected to two oxidation attempts.

The first attempt at the desired aldehyde **II.71** was made by treating **II.70** with a mixture of 70% T-Hydro™ (where 70% T-Hydro™ is a 70% by weight aqueous solution of *t*-butyl hydrogen peroxide) and SeO₂ in *p*-dioxane.(197) No reaction occurred and only starting material was recovered and later subjected to a Kornblum oxidation with molecular iodine and methyl sulfoxide (DMSO), which again yielded only starting material after workup.(198, 199) It appears that the methyl group in compound **II.70** is not activated and will require a more powerful oxidant to achieve the desired transformation. No further attempts have been made at preparing aldehyde **II.71**.

Electron rich isoquinolinecarboxaldehydes have also been prepared. The inspiration for this stems from the methoxylated quinolines used by Mikata *et al* in the preparation of novel fluorescent Zn(II)-sensors (*vide supra*).(184) The first approach taken in the preparation of 6,7-dimethoxyisoquinoline-1-carboxaldehyde **II.84** started with the one-carbon homologation of commercially available 3,4-dimethoxybenzaldehyde **II.72** via a Henry nitro-aldol condensation (Scheme 21).(200, 201)

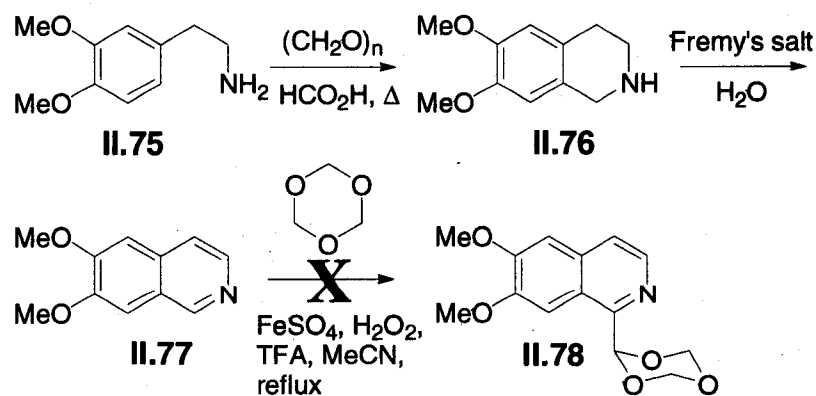


Scheme 21 The preparation of 3,4-dimethoxy-β-phenethylamine **II.75**.

This reaction was carried out with either NaOH or ammonium acetate (NH_4OAc) acting as the base. The method that utilized NaOH yielded the desired product **II.73**, after recrystallization, in 32.2% yield. The alternative method with NH_4OAc had an enhanced yield of 67.7% of compound **II.73** after recrystallization. Initial attempts at the global reduction of the β-nitrostyrene **II.73** were met with limited success. The first approach involved a Clemmensen reduction of the nitroalkene functionality to the aminoethyl group of the corresponding β-phenethylamine **II.75**.⁽²⁰²⁾ This reaction was accomplished only once on small scale (ca. 1 mmol of starting material) and could not be repeated successfully or scaled-up. The reason for the failure is, unbeknownst to the author of this dissertation but may be related to the batch-to-batch homogeneity of the zinc-mercury amalgam (Zn(Hg)). An alternative approach to the Clemmensen reduction, as described in

the literature, involves either $\text{H}_2/\text{Pd}/\text{C}$ or LiAlH_4 resulting in a global reduction of the nitroalkene to the desired β -phenethylamine **II.75**.(203-205) A safer, more facile approach to compound **II.75** involved a partial reduction of the substrate with NaBH_4 yielding the β -nitroethyl compound **II.74** in moderate yield (78.5%), followed directly by a catalytic transfer hydrogenation with 10% Pd/C and ammonium formate (HCO_2NH_4) affording an 86.7% yield of **II.75**. The advantages of this reaction are that no gaseous H_2 is needed to complete the transformation and the Pd/C catalyst also serves to decolorize the reaction mixture thus affording the desired compound free of impurities. The free base **II.75** can be used without any further purification in the next step of the synthesis of the isoquinoline target **II.84** or it can be stored for an indeterminate time as a hydrogen sulfate salt.

To construct the isoquinoline skeleton the β -phenethylamine **II.75** was first converted into the corresponding 1,2,3,4-tetrahydroisoquinoline **II.76** via a Pictet-Spengler reaction (**Scheme 22**). (206, 207)



Scheme 22 Attempt at preparing 6,7-dimethoxy-1-isoquinolinecarboxaldehyde **II.84**.

The resulting product **II.76** was purified by saturating an ethanolic solution with oxalic acid. The resulting oxalate salt of **II.76** was isolated in 94.0% yield and was spectroscopically pure. The tetrahydroisoquinoline **II.76** is a natural product bearing the trivial name *heliamine*.(208, 209) It is part of the alkaloid content of several giant columnar cacti including the species *Backebergia militaris*.

The literature oxidation of *heliamine* **II.76** occurs sequentially with T-Hydro™ and catalytic $\text{RuCl}_2(\text{PPh}_3)_4$ followed by refluxing the resulting 3,4-dihydroisoquinoline in *p*-cymene with catalytic Pd^0 .(210, 211) A potentially more convenient route is a single-pot two-step oxidation mediated by Fremy's salt.(212-214) In aqueous solution Fremy's salt exists as a purple monomeric nitrosodisulfonate radical **II.79** (Figure 81) (215)

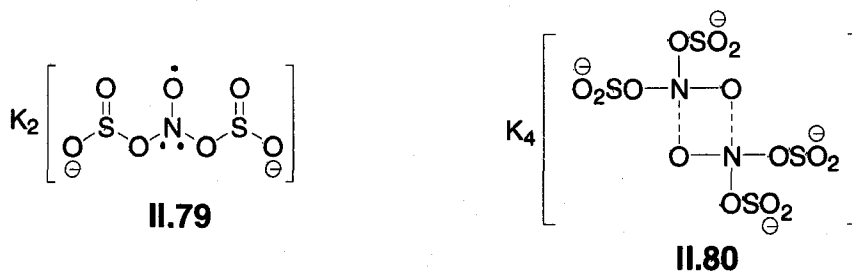
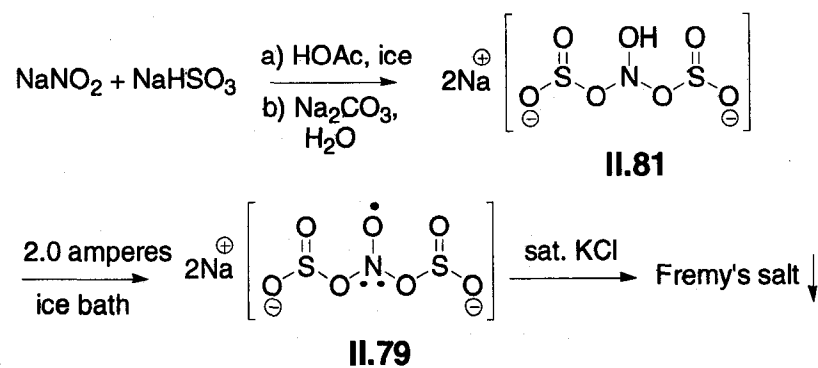


Figure 81 The structure of Fremy's salt in solution (left) and solid state (right).

which dimerizes in the solid state forming an explosive bright orange powder **II.80**. Fremy's salt was prepared electrochemically with a stainless steel electrode (see experimental) from the corresponding hydroxylamine disulfonate **II.81** (Scheme 23). Alternatively, a chemical means of oxidation of the hydroxylamine **II.81** can be done (*e.g.* KMnO_4) but this requires a subsequent purification of the isolated material.(213)



Scheme 23 Electrochemical synthesis of Fremy's salt.

A custom-designed amperostatic coulometric titrator was used to pass 2.0 amperes of current through the solution that contained the inorganic hydroxylamine **II.81**. The extent of the one-electron oxidation after *ca.* 3 hours was judged by UV-visible absorbance spectroscopy (**Figure 82**). The analytical wavelength selected for quantitation occurred at $\lambda=544\text{nm}$ and has a reported molar absorptivity of $14.5\text{cm}^{-1}\text{M}^{-1}$.⁽²¹³⁾ Quantitation of this band revealed the electrolysis was 83.7% complete after 3 hours.

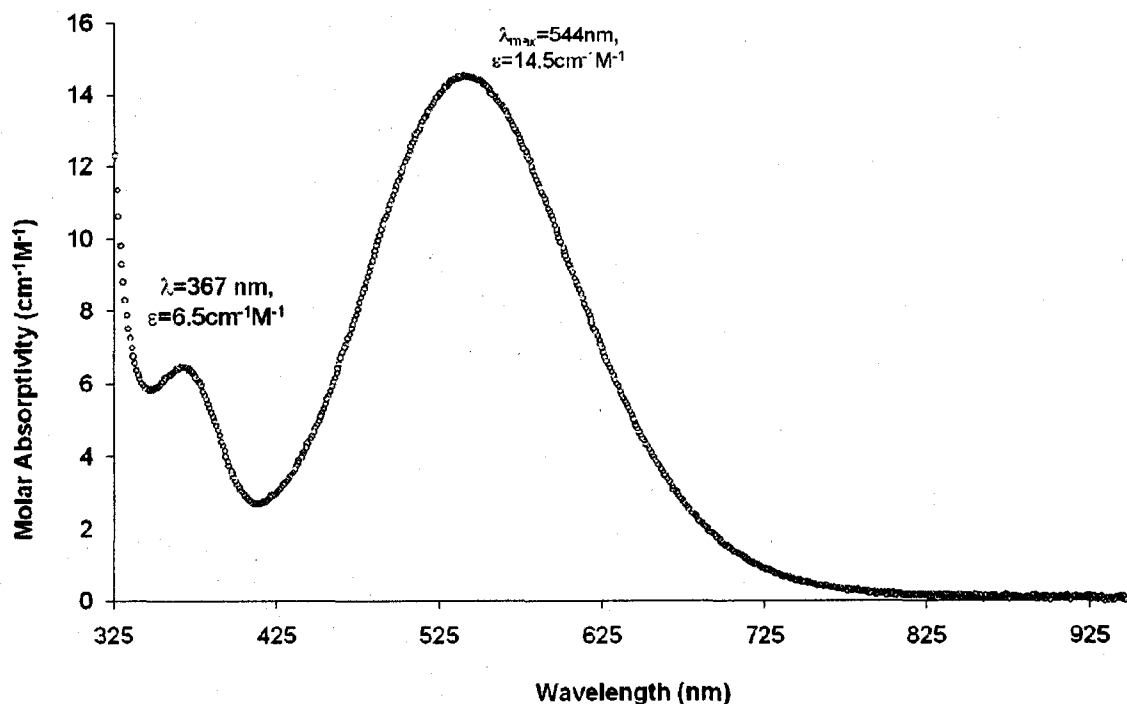


Figure 82 UV-visible absorbance spectrum of Fremy's salt in 1M KOH.

Fremy's salt was then precipitated from the reaction solution by addition of excess KCl. The precipitate was isolated via vacuum filtration and was stored damp in the refrigerator for several weeks without incident.

The identity of Fremy's salt was verified qualitatively by obtaining an EPR spectrum of a frozen (77K) 1M KOH solution of the isolated material (see experimental) (**Figure 83**).

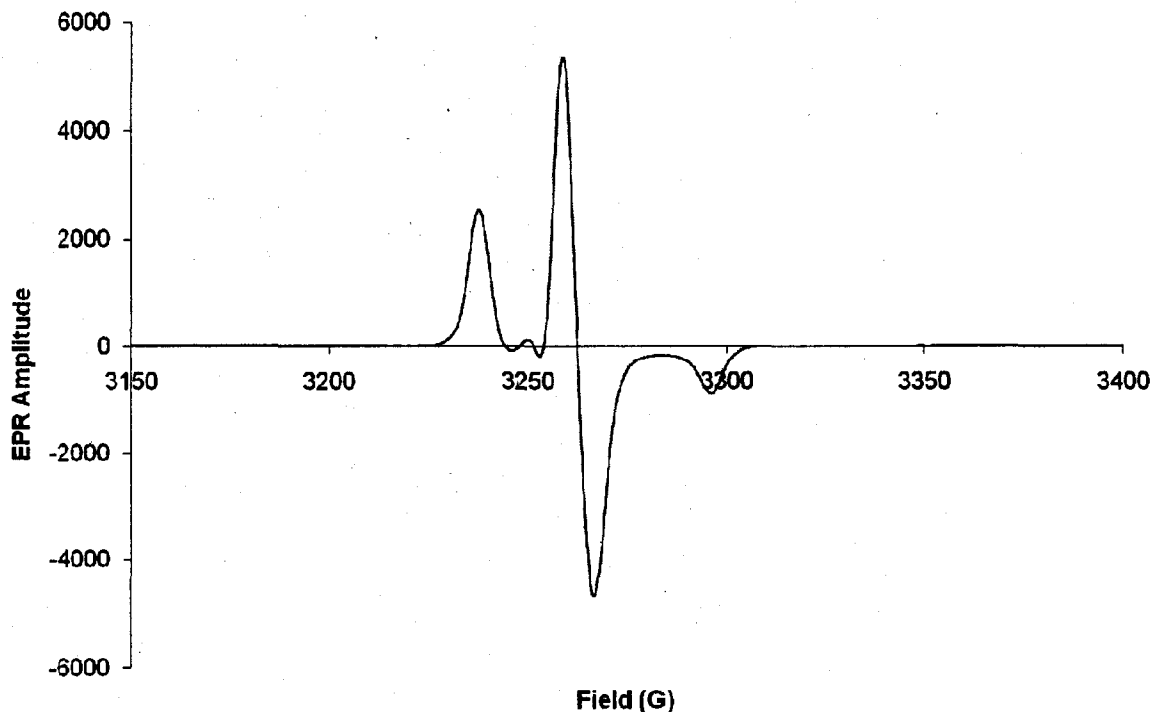


Figure 83 EPR spectrum of $ca. 10^{-4}M$ Fremy's salt at 77K in 1M KOH.

modulation frequency=10G; modulation amplitude=100kHz; receiver gain= 60dB; time constant=655.36ms; sweep time=335.54s; conversion time=81.92ms; power=17.09mW; attenuation=11dB; number of scans=1; centerfield=3275G, sweep-width=250G.

To interpret the EPR spectrum the appropriate spin-Hamiltonian for a nitroxide radical needed to be ascertained from the literature.(216) The energy E from the Hamiltonian contains a Zeeman splitting term ($m_s=-1/2$ or $+1/2$) and a single nitrogen ($I=1, m_N=-1,0,+1$) hyperfine term with nitrogen coupling A_N .

$$E = \beta g B_0 m_s + \beta \beta_N A_N m_s m_N$$

(II.h)

The variables for equation II.h are defined as:

β =Bohr magneton, which is equal to $9.274 \cdot 10^{-24}$ amperes-meter²

g =electron Zeeman factor and is dimensionless

B_o =applied magnetic field

m_s =spin of the electron

β_N =nuclear magneton

A_N =hyperfine coupling constant

m_N =nuclear angular momentum

In the presence of an external magnetic field (B_o) the energy levels for the unpaired electron interacting with the nitrogen nucleus are illustrated in **Figure 84**.

84.

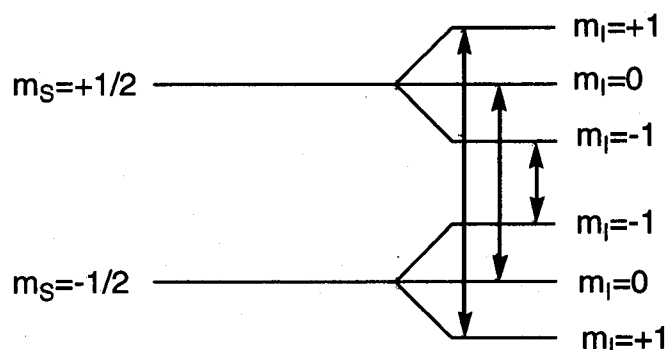


Figure 84 The energy levels for an unpaired electron in a magnetic field interacting with a nitrogen nucleus.

For a single photon transition m_N must remain the same ($\Delta m_N = 0$) which results in three allowed transitions (indicated by the double-headed arrows in **Figure 84**).

As the magnetic field is increased at constant frequency ($\nu \sim 9.5\text{GHz}$) the conditions of **Equation II.h** are fulfilled three times resulting in a triplet of lines in the energy absorption spectrum of a nitroxide radical.

$$\Delta E = h\nu = \beta g B - \beta \beta_N A_N m_N$$

(II.i)

The anisotropic behavior observed in the spectrum (**Figure 83**) was a result of dipolar hyperfine coupling and contact coupling within the frozen sample (contained within the **T** tensor of the spin Hamiltonian). However, the observed EPR spectrum of the synthetic material nearly matched a literature spectrum of authentic material (**Figure 85**).⁽²¹⁷⁾ The loss of fine structure in the experimental spectrum as compared to the literature spectrum can be attributed to differences in concentration of the analyte and the solvent system employed (literature conditions: 5 mM Fremy's salt in 0.5 M KNO_3 at 77K, experimental conditions: 10^{-4} M Fremy's salt in 1M KOH at 77K).⁽²¹⁸⁾

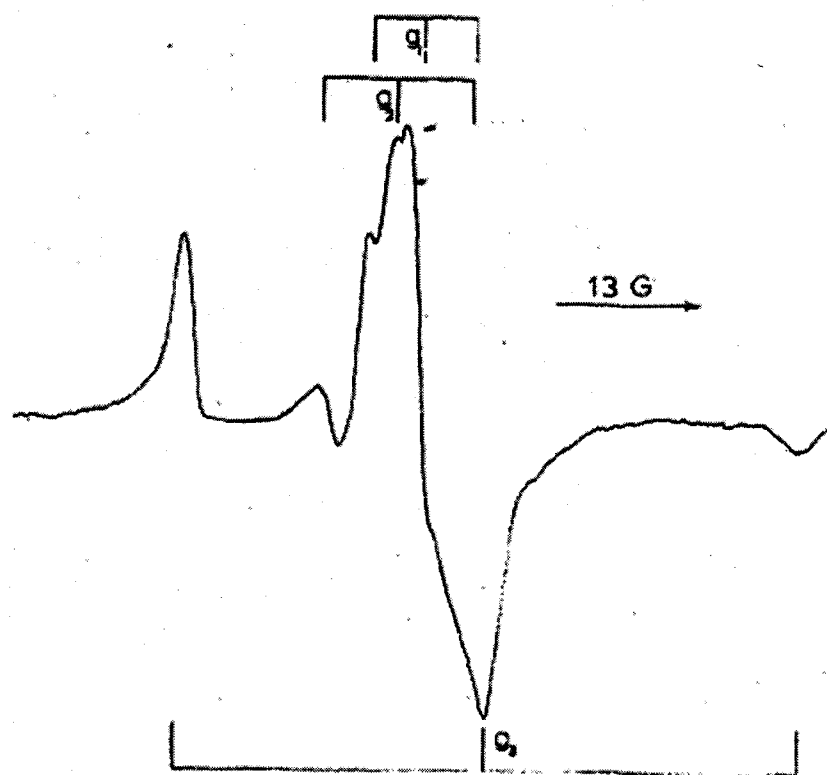


Figure 85 Literature EPR spectrum of Fremy's salt.⁽²¹⁷⁾

With the desired oxidant in hand the tetrahydroisoquinoline *heliamine* **II.76** was oxidized in an aqueous solution (**Scheme 22**). The reaction requires four-equivalents of Fremy's salt but thermal decomposition of the monomeric radical **II.79** needed to be compensated for by maintaining an excess of Fremy's salt in solution. Small aliquots of the damp orange powder were periodically added to the reaction flask and an excess of the reagent was judged by maintaining a purple solution. The isolated crude product was a mixture of the desired isoquinoline **II.77** and the corresponding 3,4-dihydroisoquinoline intermediate in a mole ratio of 8.9:1.1. The two compounds were separated via column chromatography affording the desired substrate **II.77** for subsequent chemistry.

Unfortunately, attempts at the homolytic aromatic substitution of compound **II.77** were not met with success (**Scheme 22**). Only starting material was evidenced by NMR likely indicative of the sluggish reaction between the electron-rich heterocyclic substrate **II.77** and the feebly nucleophilic carbon-centered trioxanyl radical (**Figure 86**).

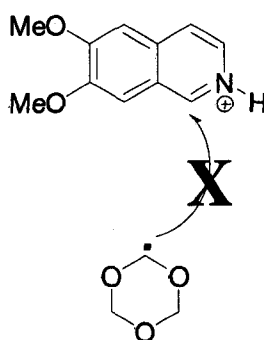
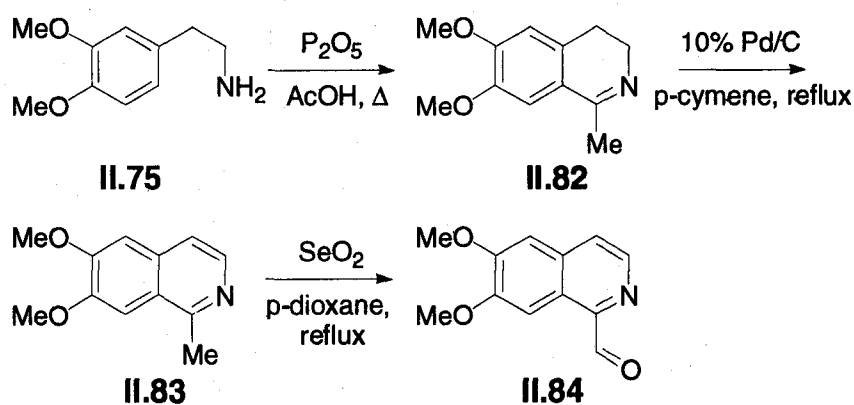


Figure 86 Thwarted homolytic aromatic substitution on substrate II.77.

An alternative entry into the desired 1-substituted 6,7-dimethoxyisoquinoline exploited a modified Bischler-Napieralski reaction

(Scheme 24).(219, 220) The advantage of this strategy is that the β -phenethylamine **II.75** prepared in the aforementioned synthesis (Scheme 22) can be reused. The first step in the reaction is a regioselective acylation at C6 of substrate **II.75** followed by a Schiff base condensation in the workup affording **II.82**. The resulting 1-methyl-3,4-dihydroisoquinoline **II.82** was then oxidized quantitatively (as evidenced by thin layer chromatography) with 10% Pd/C in refluxing p-cymene.(221) The resulting isoquinoline **II.83** possessed the active methyl group at C1 which underwent oxidation with SeO₂ in dry p-dioxane to afford the desired aldehyde **II.84** in nearly quantitative yield.(222)

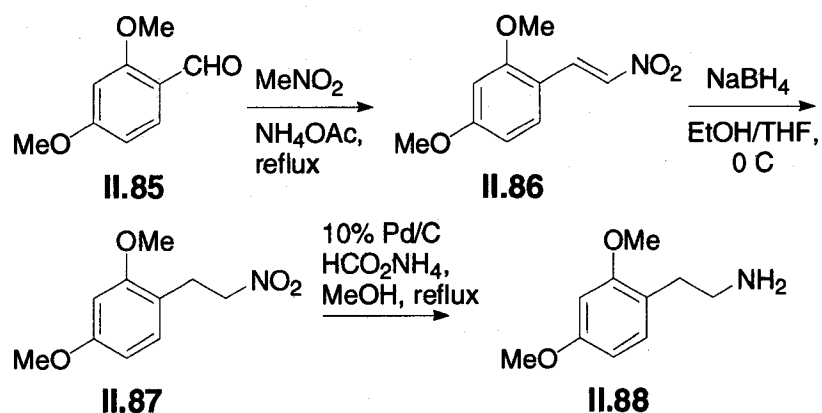


Scheme 24 Preparation of 6,7-dimethoxy-1-isoquinolinecarboxaldehyde **II.84.**

Care was taken to dry the p-dioxane prior to reaction by distilling the solvent from Na⁰ and storing the dry distillate over 4Å sieves. Any H₂O present in the solvent lengthens the reaction time resulting in oxidation of aldehyde **II.84** affording the corresponding carboxylic acid.

An attempt was made at preparing isoquinolines with varying substitution patterns of the distal methoxy groups (Scheme 25). The methodology developed for the preparation of 3,4-dimethoxy- β -phenethylamine **II.75** was

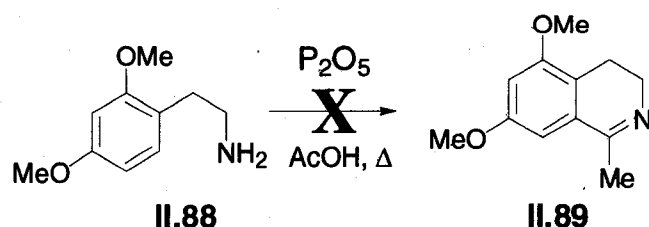
implemented in the preparation of the 2,4-dimethoxy analog **II.88** (see **Scheme 25**).



Scheme 25 Preparation of 2,4-dimethoxy- β -phenethylamine **II.88.**

Commercially available 2,4-dimethoxybenzaldehyde **II.85** was converted into the corresponding β -nitrostyrene **II.86** in 76.6% yield after recrystallization. The nitroalkene was reduced sequentially with NaBH_4 affording the β -nitroethyl compound **II.87** in 86.9% yield and then the nitro group reduced to the amine **II.88** via transfer hydrogenation in 88.2% yield. Once again the resulting β -phenethylamine **II.88** was promptly used as is in subsequent chemistries or stored long-term as the hydrogen sulfate salt.

Attempts at the cyclization of compound **II.88** via the Bischler-Napieralski reaction failed to produce the desired 3,4-dihydroisoquinoline **II.89** (**Scheme 26**).



Scheme 26 Failed Bischler-Napieralski reaction of **II.88.**

The disposition of the two methoxy groups with respect to C6 is the likely reason the Bischler-Napieralski reaction failed with this substrate (**Figure 87**). Electron donating groups only enhance the nucleophilic character of the *ortho* and *para* carbons within an aromatic ring.⁽²²³⁾ The regioselective acylation of **II.88** (which would lead to the desired 3,4-dihydroisoquinoline **II.89**) is likely hindered because C6 (*meta* to both methoxy groups) is suffering from an electron deficit rendering it feebly nucleophilic. The isolated material from this reaction was an intractable mixture of several compounds. It is speculated that acetylation at C3 and C5 complicated the product slate.

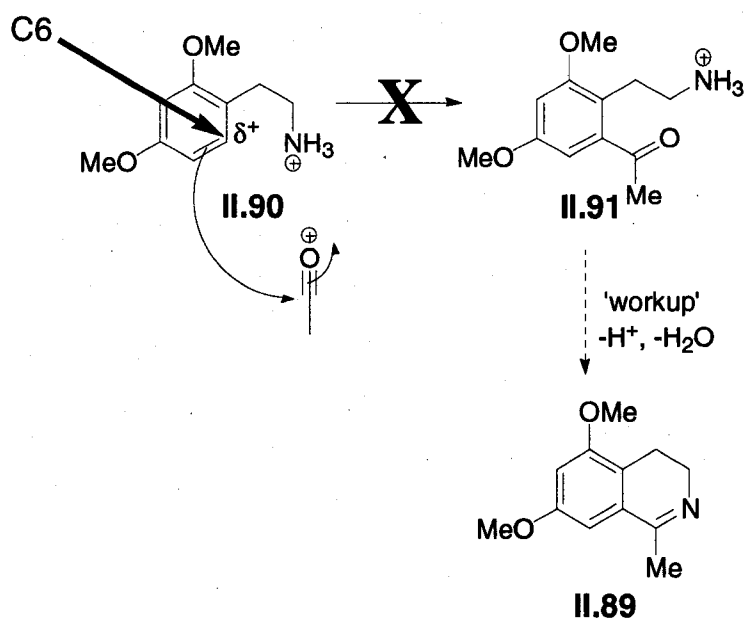
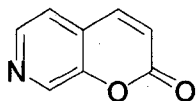


Figure 87 The feeble nucleophilic character of C6 likely prevents the desired regioselective acylation.

Efforts toward the preparation of coumarin derivatives granted access to another family of azaaromatic aldehydes. It was hypothesized that azacoumarins (**Figure 88**) would serve as excellent chromophores in the hunt for novel TAME based fluorescent metal sensors.

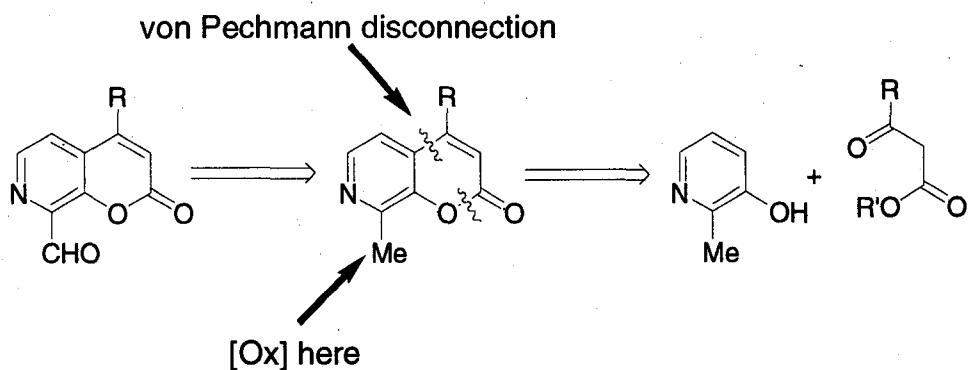


II.92

Figure 88 The structure of 7-azacoumarin II.92.

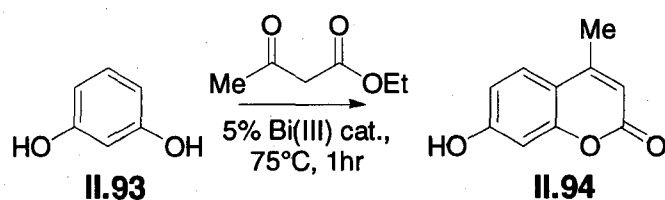
Coumarins are excellent fluorophores due to their photostability and long excitation and emission wavelengths.⁽²²⁴⁾ They also possess large Stoke's shifts thus preventing self-quenching.^(225, 226) Likewise, there are examples of coumarin-based main group metal sensors (*e.g.* K(I), Ca(II), Mg(II)) in the literature.⁽¹³⁴⁾ However, there appears to be a lack of any reports of azacoumarins serving this role. Moreover, there are no literature accounts of azacoumarins acting as ligands for metal ions. This provided a fertile ground for investigation.

Relying on what was learned from the preparation of 6,7-dimethoxy-1-isoquinolinecarboxaldehyde II.84 it was envisioned that preparation of an azacoumarin aldehyde would require the presence of an active methyl group adjacent to the heterocyclic nitrogen (**Scheme 27**). It was also envisioned that a von Pechmann-type reaction would serve to construct the pyranone ring around an appropriately substituted pyridinol.



Scheme 27 Retrosynthetic analysis of a 7-azacoumarin aldehyde.

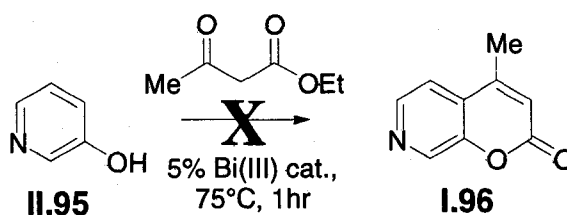
The von Pechmann reaction is an acid-mediated condensation of a phenol with a β -ketoester that yields a 4-substituted coumarin (hence the R group in **Scheme 27**). The acid catalysts typically used include AlCl_3 , P_2O_5 , and even trifluoroacetic acid, but a recent report by De and Gibbs demonstrates that BiCl_3 is also an efficient catalyst in the von Pechmann reaction (**Scheme 28**).⁽²²⁷⁾



Scheme 28 The Bi(III)-mediated von Pechman reaction of resorcinol II.93.

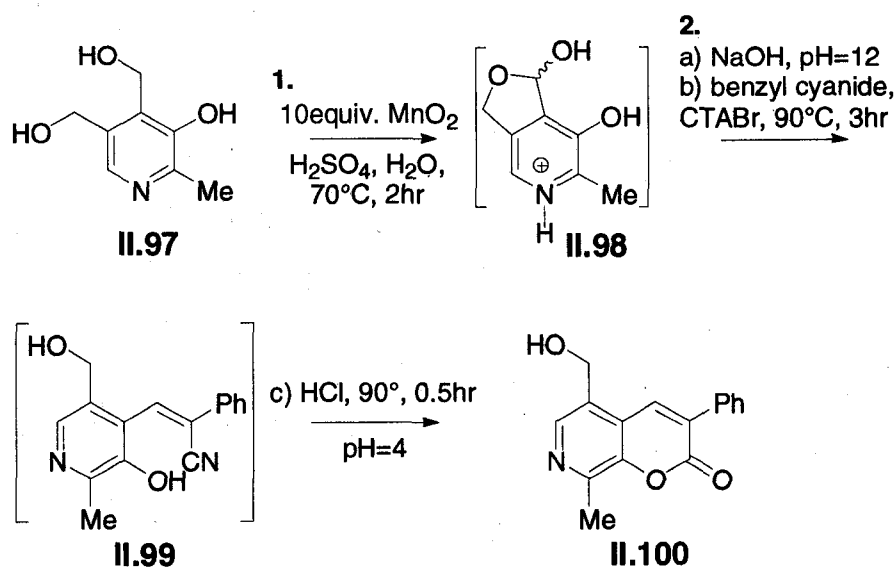
This particular catalyst was attractive because bismuth salts are relatively inexpensive, nontoxic and because of the ease with which the desired transformation can be effected. The methodology of De and Gibbs was tested with several Bi(III) salts (*i.e.* BiCl_3 , BiBr_3 , BiI_3 , Bi(OAc)_3 , and $\text{Bi(NO}_3)_3 \cdot 5\text{H}_2\text{O}$) and it was found that only BiCl_3 and $\text{Bi(NO}_3)_3 \cdot 5\text{H}_2\text{O}$ catalyzed the von Pechmann reaction of resorcinol **II.93**. However, all the reported substrates that underwent the Bi(III)-catalyzed von Pechmann reaction were electron-rich carbocycles.

Unfortunately, the transformation did not occur with the electron-poor substrate 3-pyridinol **II.95** (Scheme 29). Only starting materials were isolated upon workup.



Scheme 29 The failed Bi(III)-mediated von Pechmann reaction of 3-pyridinol **II.95**.

An alternative strategy for the construction of 7-azacoumarins was reported in 1997 by Brufola *et al.* which demonstrated a one-pot Knoevenagel condensation of the functionality rich substrate pyridoxal (one of the many forms of vitamin B6).⁽²²⁸⁾ Taking advantage of this methodology the closely related molecule pyridoxine **II.97** was converted into the corresponding 7-azacoumarin **II.100** in a two-pot four-step reaction sequence (Scheme 30).

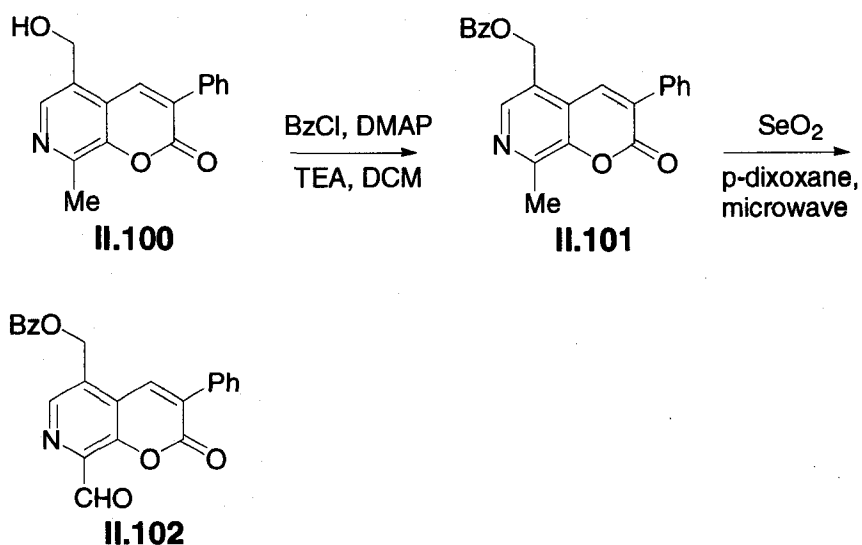


Scheme 30 Two-pot preparation of a 7-azacoumarin II.100.

The first step in the reaction sequence is a regioselective Mn(IV)-mediated oxidation of the alcohol located at C4 of the pyridoxine ring.⁽²²⁹⁾ The resulting aldehyde is in equilibrium with the corresponding hemiacetal **II.98** thus hindering further oxidation of the substrate. The second step involved a Knoevenagel condensation between the hemiacetal **II.98** and benzyl cyanide under basic conditions with cetyltrimethylammonium bromide (CTABr) acting as a phase transfer catalyst.⁽²³⁰⁾ The resulting terminal nitrile **II.99** was never isolated or characterized. Its existence as the diastereomer shown **II.99** was confirmed by the subsequent tandem acid hydrolysis-cyclization reaction affording the desired 7-azacoumarin **II.100** in 66.0% yield. The product was purified via recrystallization from boiling 1:1 acetone:EtOH (v/v).

The isolated 7-azacoumarin **II.100** contains the desired active methyl group adjacent to the heterocyclic nitrogen. However, the presence of the pseudobenzyl alcohol required protection of **II.100** before the methyl group could

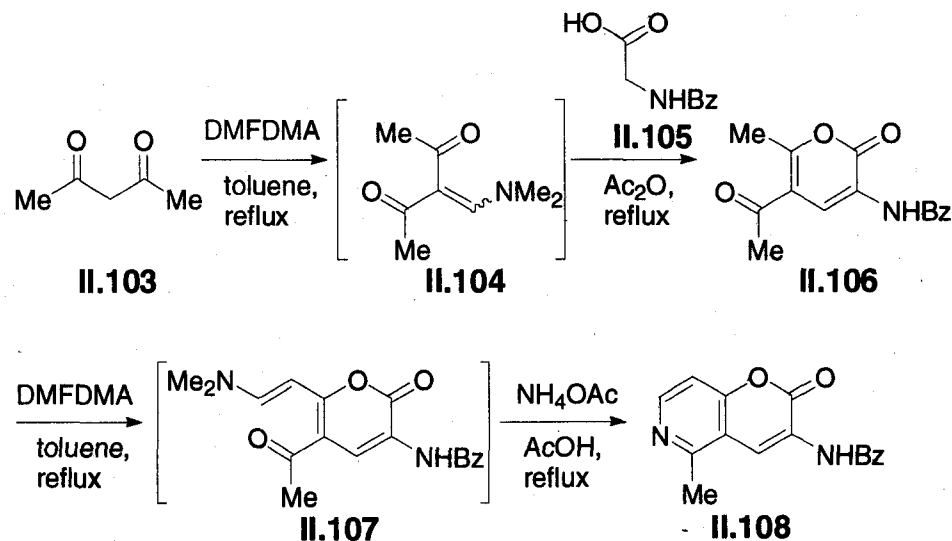
be oxidized. This was done with benzoyl chloride (BzCl) in dichloromethane (DCM), with a mixture of DMAP and triethylamine (TEA) acting as the base (**Scheme 31**). The TEA is a slightly stronger base and was co-employed with DMAP to achieve the desired transformation.



Scheme 31 The preparation of a 7-azacoumarin aldehyde II.102

The protected material **II.101** then underwent SeO_2 oxidation in dry p-dioxane with microwave irradiation. The ideal conditions for the quantitative formation of the desired aldehyde **II.102** (as evidenced by TLC) were achieved by maintaining a constant temperature of 175°C in a closed vessel for 0.5hr. The product **II.102** was chromatographed on silica to remove the selenium by-products.

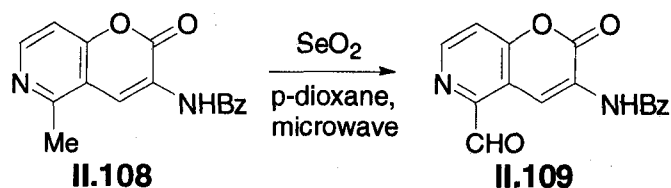
An alternative strategy in the synthesis of azacoumarins is the converse construction of a pyridine ring around an appropriately substituted pyranone ring (**Scheme 32**).



Scheme 32 The preparation of a 6-azacoumarin **II.108**.

By taking advantage of the chemistry developed by Svete *et al.* access was granted to a useful pyranone building block **II.106**.⁽²³¹⁾ The reaction sequence began with a Knoevenagel-condensation of 2,4-pentanedione **II.103** and dimethylformamide dimethylacetal (DMFDMA) affording compound **II.104**. The product was isolated without characterization and submitted to dehydrating conditions (Ac_2O) with hippuric acid **II.105** to give the desired pyranone **II.106** in 44.1% yield after recrystallization from boiling EtOH. The pyranone **II.106** contains an active methyl group which reacts with DMFDMA to afford the homologated amine **II.107**.⁽²³²⁾ The product was isolated without characterization and then converted into the corresponding 6-azacoumarin **II.108** in 22.0% yield after recrystallization from boiling EtOH/ H_2O .⁽²³³⁾ No attempts were made at optimizing the yields because the reactions employed were scalable (to ca. 5g). The product **II.108** from the previous reaction sequence contained the desired active methyl group adjacent to the heterocyclic nitrogen. This compound was then converted quantitatively into the corresponding

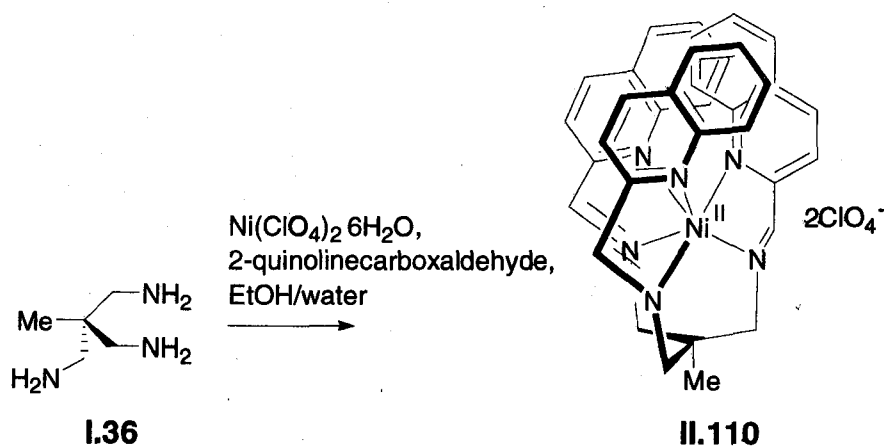
aldehyde **II.109** (evidenced by TLC) using the aforementioned microwave assisted SeO_2 oxidation (**Scheme 33**).



Scheme 33 The preparation of a 6-azacoumarin aldehyde **II.109**.

2.13. Synthesis of TAME-based ligands for metal-ion sensing via the template methodology

The Ni(II)-mediated template reaction of TAME **I.36** was first carried out with 2-quinolinecarboxaldehyde **II.55** affording the desired complex **II.110** in 30% yield after recrystallization (**Scheme 34**).



Scheme 34 Preparation of $[\text{Ni}(\text{TAMEquin-trisimine})](\text{ClO}_4)_2$ **II.110**.

It was somewhat of a surprise that the trisimine complex **II.110** formed at all because of foreseeable steric interactions between the benzo groups within the

inner coordination sphere. A report by Park describes structural preferences for the similar ligand TACHquin (where TACHquin=*N,N',N''*-tris(quinolinylmethyl)-*cis,cis*-1,3,5-triaminocyclohexane) with Zn(II) (**Figure 89**).⁽²³⁴⁾ X-ray crystallography elucidated a strong preference of TACHquin for an octahedral geometry ($\alpha=53.7(8)^\circ$). The reader is reminded that the ideal twist angle for a regular octahedron is $\alpha=60^\circ$, where α is the angle through which one trigonal face of the octahedron has been rotated with respect to the opposite trigonal face as viewed along the C_3 axis (see **Figure 8** in Chapter 1).⁽²³⁵⁾ Park speculated that enhanced trigonal twisting about the C_3 axis of the complex cation $[\text{Zn}(\text{TACHquin})]^{2+}$ is the mechanism taken by the chelator to reduce intraligand repulsions upon coordination to Zn(II). However, the substantial twisting within the cation resulted in the lengthening of the Zn-N3 bond (2.171(9)Å) with respect to the other two Zn-N(tach) bonds (2.124(9)Å and 2.135(9)Å). This phenomenon caused the Zn-N6 bond to shrink (2.198(10)Å) as compared to the other two Zn-N(quin) bonds (2.296(9)Å and 2.255(9)Å) thus bringing the three quinolinyl groups within close proximity. A crystallographic disorder of the single labeled pendant arm in **Figure 89** (with 50% occupancy of atoms C27 to C36) was ascribed to the crowding of the bulky heterocyclic groups

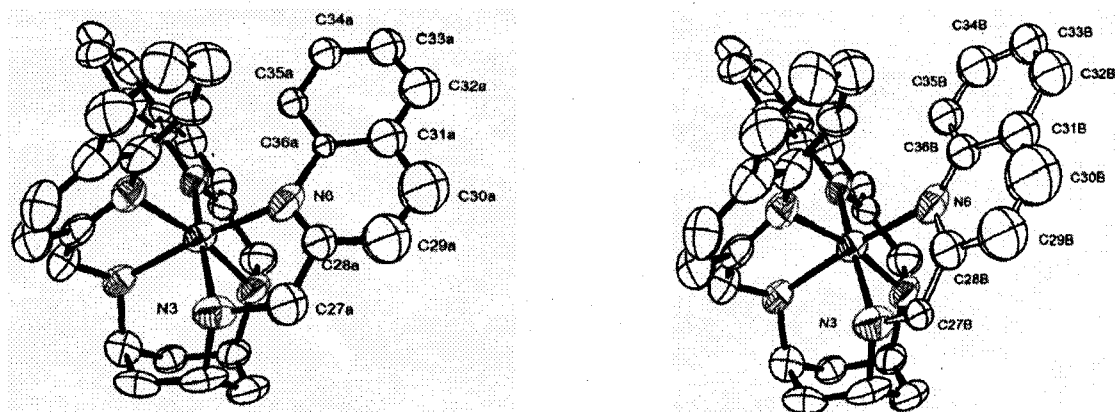


Figure 89 The ORTEP views of $[\text{Zn}(\text{TACHquin})]^{2+}$ (two molecules A and B related by disorder) with 50% occupancy of C27 to C36.

TAME can better accommodate the aforementioned twisting than TACH because the anchoring methylene groups within the TAME framework are not constrained to a six-membered ring. Therefore, TAME has more conformational flexibility than TACH facilitating the formation of the trisimine complex $[\text{Ni}(\text{TAMEquin-trisimine})]^{2+}$ **II.110** by reducing intraligand repulsions through adequate twisting about the C_3 axis.

The visible-near IR absorbance spectrum of complex **II.110** (**Figure 90**) illustrated the reduced ligand field strength of the TAMEquin-trisimine chelator as compared to TAMEpyr-trisimine **I.51** (see **Figure 32**).

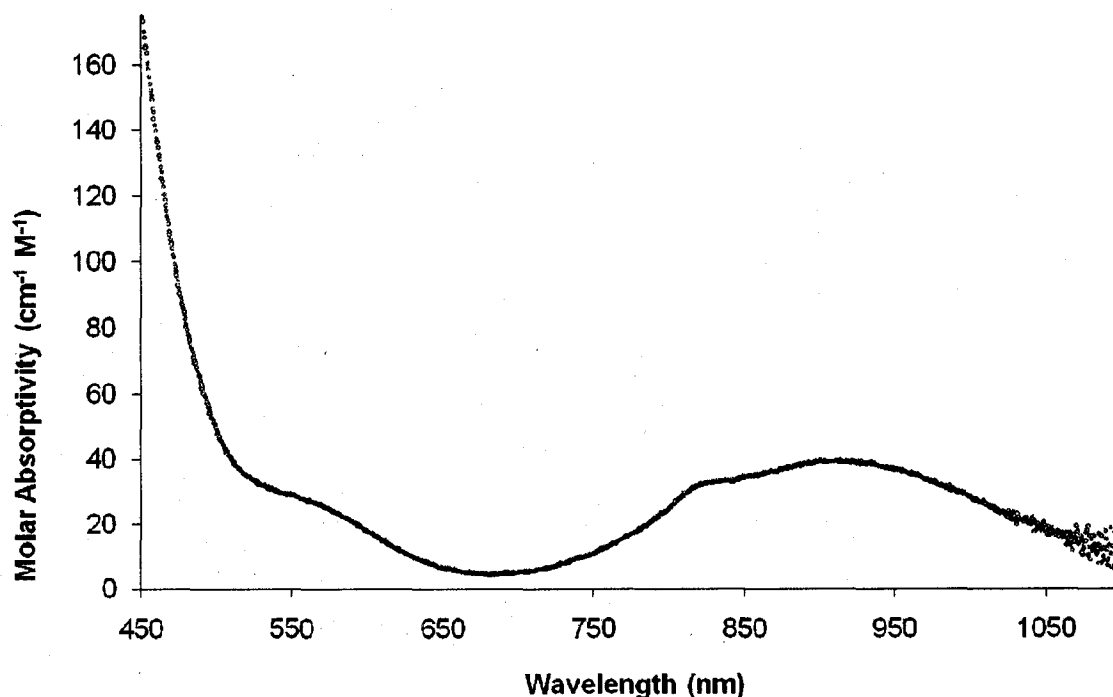
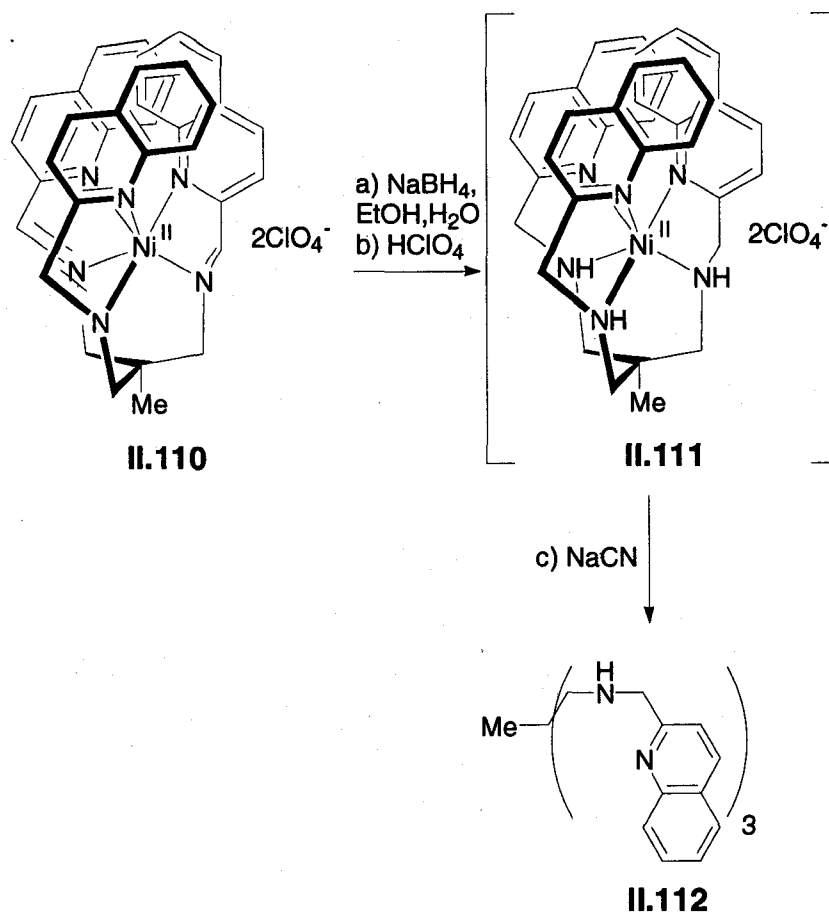


Figure 90 The visible-near IR absorbance spectrum of $[\text{Ni}(\text{TAMEquin-trisimine})](\text{ClO}_4)_2$ in MeCN ($T=25^\circ\text{C}$).

The most striking feature of the spectrum is the appearance of a high energy shoulder within the ${}^3\text{A}_{2g} \rightarrow {}^3\text{T}_{2g}$ band envelope (ca. 825nm (12100cm^{-1}), $\epsilon=32\text{cm}^{-1}\text{M}^{-1}$). This shoulder is assigned as the spin-forbidden ${}^3\text{A}_{2g} \rightarrow {}^1\text{E}_g$ $d-d$ transition. The position of the shoulder occurred at low energy within the spectrum of $[\text{Ni}(\text{TAMEpyr-trisimine})]^{2+}$ **I.50** (ca. 865nm (11600cm^{-1}), $\epsilon=24\text{cm}^{-1}\text{M}^{-1}$). This spectral pattern is consistent with a reduced ligand field strength of the chelator.⁽⁴⁴⁾ The approximate value of Δ_o for $[\text{Ni}(\text{TAMEquin-trisimine})]^{2+}$ **II.110** is 11050cm^{-1} (spectral feature at ca. 905nm, $\epsilon=39\text{cm}^{-1}\text{M}^{-1}$). A red-shift of 1350cm^{-1} as compared to the Δ_o of $[\text{Ni}(\text{TAMEpyr-trisimine})]^{2+}$ **I.50** (804nm (12400cm^{-1}), $32\text{cm}^{-1}\text{M}^{-1}$) corroborates the aforementioned non-bonding repulsions of the quinoliny groups. The reduced σ -donor ability of quinoline as compared to

pyridine fails to explain the marked decrease in Δ_o for [Ni(TAMEquin-trisimine)](ClO₄)₂ **II.110**.(183) Intraligand repulsions within the inner coordination sphere must exist in this complex despite the flexibility of the TAME framework. The planar C=N groups are inflexible and restrict additional twisting about the C₃ axis that is needed to relieve the quinolinyl crowding. The remaining *d-d* transition observed in the spectrum of [Ni(TAMEquin-trisimine)]²⁺ **II.110** is the ³A_{2g}→³T_{1g}(F) band (ca. 550nm (18000cm⁻¹) ε=28cm⁻¹M⁻¹) which was partially obscured by an overlapping MLCT band (ca. 540nm (18500cm⁻¹) ε>160cm⁻¹M⁻¹). There is also the possibility that the complex cation does not possess pseudooctahedral geometry in solution. Structural data, which unfortunately was not collected, could be used to confirm this suspicion.

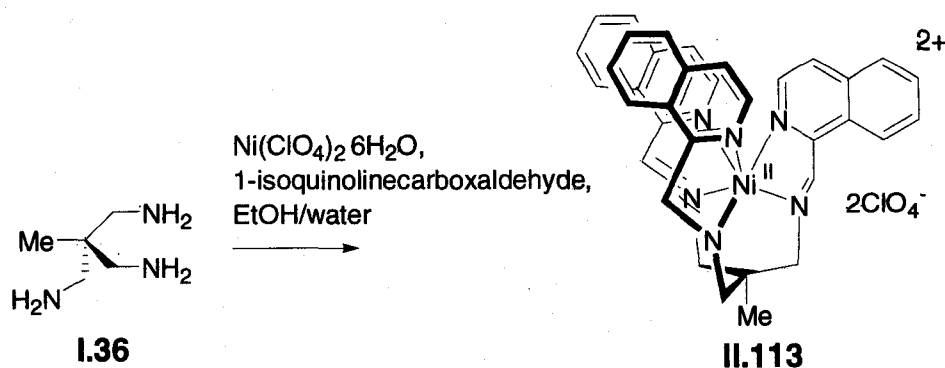
The complex [Ni(TAMEquin-trisimine)](ClO₄)₂ **II.110** was reduced with 70 equivalents of NaBH₄ to afford the corresponding Ni(II)-complex **II.111**. The desired ligand, TAMEquin **II.112**, was liberated from the Ni(II)-complex **II.111** with excess NaCN and isolated in 68.0% yield (**Scheme 35**).



Scheme 35 Preparation of TAMEquin II.112.

Over-reduction of the quinolinyll groups to the corresponding 1,2-dihydro-, or 1,2,3,4-tetrahydroquinolinyll groups was not an issue under these reaction conditions. This result further highlights the utility of the template strategy in the preparation of novel TAME-based chelators.

The Ni(II)-mediated template reaction of 1-isoquinolinecarboxaldehyde II.58 with TAME I.36 furnished the complex $[\text{Ni}(\text{TAMEisoquin-trisimine})](\text{ClO}_4)_2$ II.113 in 91.0% yield (Scheme 36).



Scheme 36 The preparation of $[\text{Ni}(\text{TAMEisoquin-trisimine})](\text{ClO}_4)_2$ **II.113**.

By simply moving the fused benzo groups to the periphery of the complex intraligand repulsions within the inner coordination sphere of **II.113** are substantially reduced. This was evidenced in the visible-near IR absorbance spectrum of $[\text{Ni}(\text{TAMEisoquin-trisimine})](\text{ClO}_4)_2$ **II.113** (orange spectrum in **Figure 91**). The position of Δ_o for complex **II.113** (795nm (12550cm^{-1}), $\epsilon=39\text{cm}^{-1}\text{M}^{-1}$) has undergone a hypsochromic-shift with respect to the Δ_o for $[\text{Ni}(\text{TAMEquin-trisimine})](\text{ClO}_4)_2$ **II.110** (yellow spectrum in **Figure 91**) by 1500cm^{-1} . Likewise, the position of the spin-forbidden transition ${}^3\text{A}_{2g} \rightarrow {}^1\text{E}_g$ occurs at low energy (ca. 870nm (11450cm^{-1}), $\epsilon=25\text{cm}^{-1}\text{M}^{-1}$) in the ${}^3\text{A}_{2g} \rightarrow {}^3\text{T}_{2g}$ band envelope of the spectrum. The transitions in the spectrum of $[\text{Ni}(\text{TAMEisoquin-trisimine})]^{2+}$ **II.113** are nearly identical in position, shape, and intensity of the corresponding bands in the spectrum of $[\text{Ni}(\text{TAMEpyr-trisimine})]^{2+}$ **I.50** (**Figure 32**). This illustrates that the donor-efficiency of pyridine and isoquinoline are very similar in complexes **I.50** and **II.113**. Unfortunately, the presence of the MLCT band starting at ca. 640nm and proceeding toward the UV region obscured all the other *d-d* transitions expected in the spectrum.

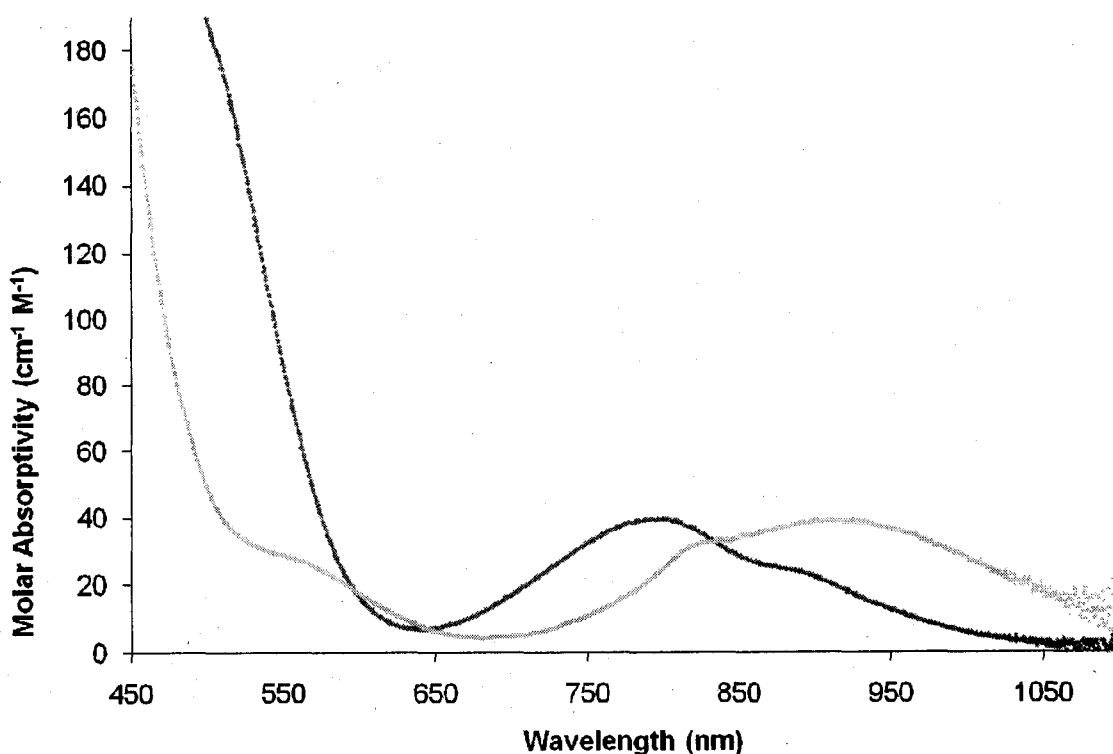


Figure 91 The visible-near IR absorbance spectra of $[\text{Ni}(\text{TAMEisoquin-trisimine})](\text{ClO}_4)_2$ II.113 (orange) and $[\text{Ni}(\text{TAMEquin-trisimine})](\text{ClO}_4)_2$ II.111 (yellow) in MeCN ($T=25^\circ\text{C}$).

X-ray grade single-crystals of $[\text{Ni}(\text{TAMEisoquin-trisimine})](\text{ClO}_4)_2$ II.113 were grown from a 1:1 MeOH:MeCN (v/v) solution via Et_2O diffusion (Table 9). The ORTEP view of the cation $[\text{Ni}(\text{TAMEisoquin-trisimine})]^{2+}$ (Figure 92) clearly demonstrates that the complex possesses a pseudooctahedral geometry.

Table 10 Crystal data and structure refinement for $[\text{Ni}(\text{TAMEisoquin-trisimine})](\text{ClO}_4)_2 \cdot \text{MeCN}$.

Compound	$[\text{Ni}(\text{TAMEisoquin-trisimine})](\text{ClO}_4)_2 \cdot \text{MeCN}$	
Color/shape	Red/blade	
Empirical formula	$\text{C}_{39}\text{H}_{36}\text{Cl}_2\text{N}_8\text{NiO}_8$	
Temperature	100(2) K	
Crystal system	Triclinic	
Space group	P_1	
Unit cell dimensions	$a=9.7915(8)\text{\AA}$	$\alpha=97.1740(10)^\circ$

Table 9 *continued...*

	$b=10.8860(9)\text{\AA}$	$\beta=99.9800(10)^\circ$
	$c=18.4048(16)\text{\AA}$	$\gamma=92.3600(10)^\circ$
Volume	$1913.0(3)\text{\AA}^3$	
Z	2	
Density (calculated)	1.518 Mg/m^3	
Absorption coefficient	0.712mm^{-1}	
Diffractometer/scan	Bruker SMART/CCD area detector	
Radiation/wavelength	Mo $\kappa\alpha$ (graphite monochrom.)/ 0.7107\AA	
F(000)	904	
Crystal size	$0.30\times 0.10\times 0.04\text{mm}$	
θ Range for data collection	2.07 to 25.00°	
Index ranges	$-11\leq h\leq 11$, $-12\leq k\leq 12$, $-21\leq l\leq 21$	
Reflections collected	16878	
Independent reflections	6672	
Observed reflections	5974	
Data/restraints/parameters	6672/0/523	
Goodness-of-fit on F^2	1.101	
Final R indices [$I>2\sigma(I)$]	$R_1=0.0608$, $wR_2=0.1697$	
R indices (all data)	$R_1=0.0657$, $wR_2=0.1740$	
Largest diff. peak and hole	2.840 and -0.706e.\AA^{-3}	

A measured twist angle of $39.8(6)^\circ$ illustrates the restriction the three C=N bonds impose on trigonal twisting about the C_3 axis of the complex. The three five-membered chelate rings are flat (*i.e.* no λ or δ designations can be made) suggesting the three C=N bonds are engaged in extended resonance delocalization with the adjacent heterocycles. This delocalization serves to stabilize the complex cation.

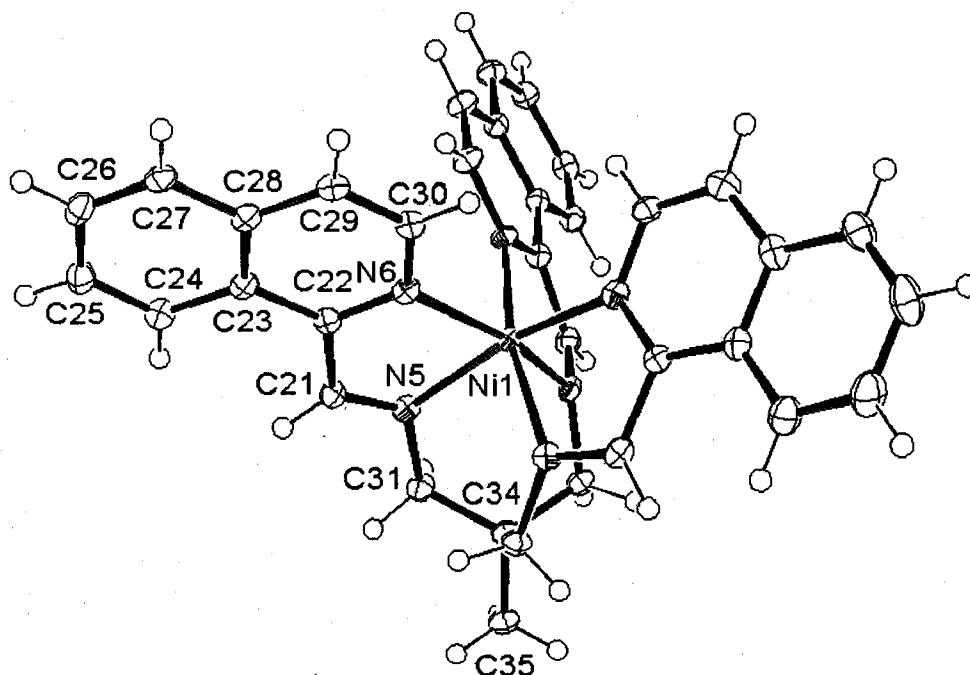


Figure 92 The ORTEP view of the cation $[\text{Ni}(\text{TAMEisoquin-trisimine})]^{2+}$. Note a C_3 axis that is co-linear with atoms C35, C34, and Ni1. The perchlorate anions and MeCN solvate have been eliminated for illustrative clarity.

The absolute configuration of the cation shown in **Figure 92** is Δ . The corresponding Λ isomer (not shown) is also present in the centrosymmetric unit cell ($Z=2$). The striking feature of this structure is the observed “handedness” of the TAME framework as assigned with the conventions developed by Al-Obaidi *et al.*(96) When the pendant arm is saturated, as it is in $[\text{Zn}(\text{TAMEpyr})]^{2+}$ (see **Figure 36**) or $[\text{Fe}(\text{tptMeTAME})]^{2+}$, the energetically preferred conformation of the framework is congruent with the absolute configuration of the complex (*i.e.* $\Delta\delta^{\text{cap}}$ or $\Lambda\lambda^{\text{cap}}$). However, the converse assignment, $\Delta\lambda^{\text{cap}}$ (shown in **Figure 92**) and $\Lambda\delta^{\text{cap}}$ (not shown but present in the unit cell), was observed in the structure of

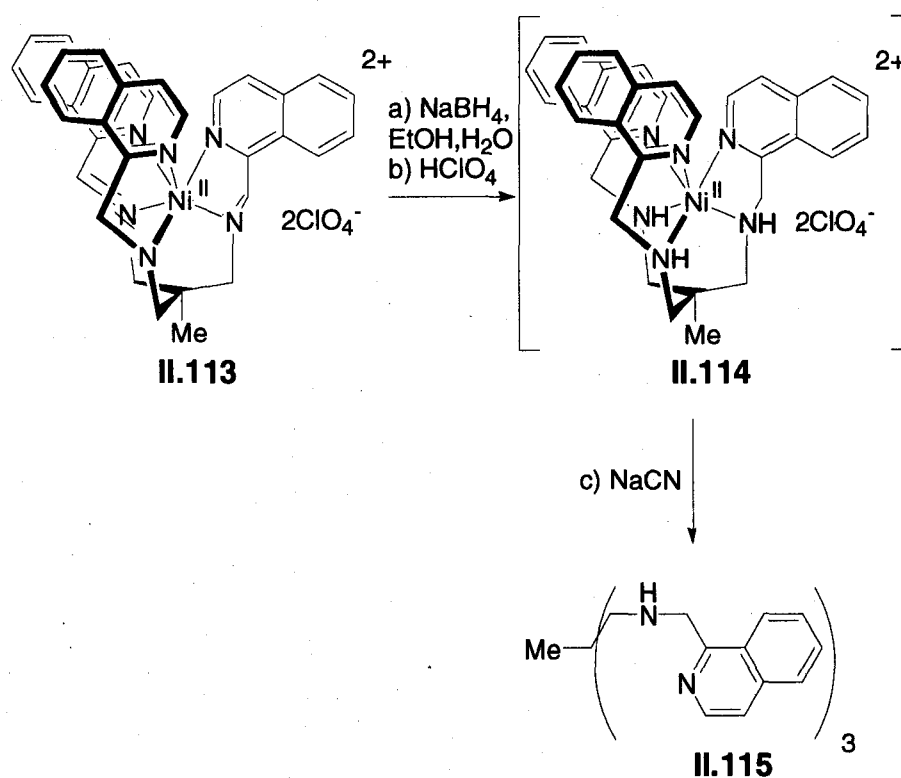
[Ni(TAMEisoquin-trisimine)]²⁺. The rigid nature of the planar five-membered chelate rings prevents the necessary twisting to achieve the desired match between the conformation of the TAME framework and the absolute configuration of the complex. This result further highlights the rigid nature of the TAMEisoquin-trisimine chelator. The average Ni-N_{het} distance (2.084(4)Å) is slightly longer than the average Ni-N_{imine} distance (2.044(8)Å) (Table 10). This may be explained by backbonding of a filled *d*-orbital (*t*_{2g}) on the metal with the antibonding π^* of the C=N group thus strengthening the Ni-N_{imine} bonds. This assertion is corroborated by the presence of the MLCT band starting at ca. 640nm in the absorbance spectrum of this complex (*vide supra*).

Bondlengths (Å)			
Ni-N(imine)	2.035(3)	Ni-N(het)	2.079(3)
Ni-N(imine)	2.048(3)	Ni-N(het)	2.086(3)
Ni-N(imine)	2.050(3)	Ni-N(het)	2.088(3)
C=N(imine)	1.273(5)	N(imine)-C(TAME)	1.461(5)
C=N(imine)	1.272(5)	N(imine)-C(TAME)	1.461(5)
C=N(imine)	1.271(5)	N(imine)-C(TAME)	1.460(5)
C(imine)-C(het)	1.481(5)	C(het)-N(het)	1.331(5)
C(imine)-C(het)	1.471(5)	C(het)-N(het)	1.361(5)
C(imine)-C(het)	1.472(5)	C(het)-N(het)	1.332(5)
		C(het)-N(het)	1.358(5)
		C(het)-N(het)	1.329(5)
		C(het)-N(het)	1.358(5)
Bond angles (°)			
N-Ni-N(chelate)	78.73(12)	N-Ni-N(trans)	162.68(12)
N-Ni-N(chelate)	78.37(12)	N-Ni-N(trans)	159.44(12)
N-Ni-N(chelate)	78.47(12)	N-Ni-N(trans)	162.27(12)

Table 11 Selected bond lengths and bond angles for [Ni(TAMEisoquin-trisimine)](ClO₄)₂·MeCN.

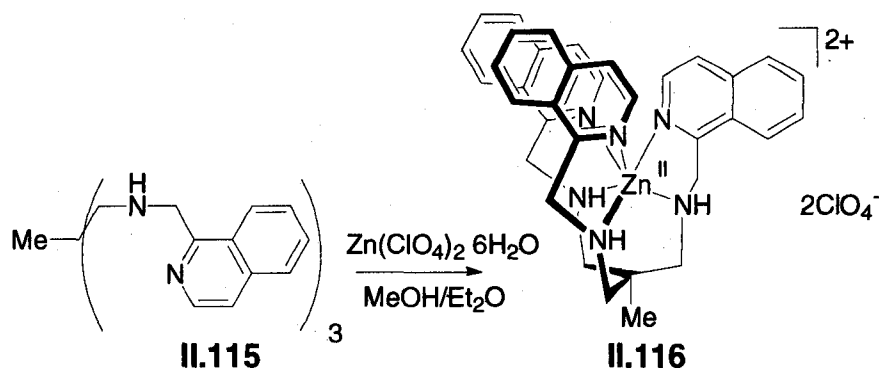
The trisimine complex **II.113** was then reduced to the corresponding triamine complex **II.114** with excess NaBH₄ (Scheme 37). The desired ligand TAMEisoquin **II.115** was liberated from the Ni(II)-complex **II.114** with NaCN and

isolated in nearly quantitative yield (99.0%). The ligand was spectroscopically pure as the free base but needed to be stored as the hydrogen chloride salt (TAMEisoquin·6HCl·H₂O from elemental analysis) to prevent degradation of the moderately light and air sensitive isoquinoline rings.



Scheme 37 The preparation of TAMEisoquin **II.115**.

The liberated chelator TAMEisoquin **II.115** was then ready for complexation studies with a variety of metal ions. The ligand was reacted with Zn(ClO₄)₂·6H₂O in MeOH affording the corresponding [Zn(TAMEisoquin)](ClO₄)₂ complex **II.116** in 91% yield (**Scheme 38**).



Scheme 38 Preparation of [Zn(TAMEisoquin)](ClO₄)₂ II.116.

X-ray quality crystals of [Zn(TAMEisoquin)](ClO₄)₂ II.116 were grown from Et₂O diffusion into a 1:1 MeOH:MeCN (v/v) solution of the complex (Table 11). The structure for this particular complex was difficult to solve. In the asymmetric unit there were four unique complex cations observed resulting in a value for Z of 32. The crystallographers (DiPasquale and Rheingold) labeled the four cations A through D to ease analysis. Each of the unique cations possessed six-coordinate Zn(II) that displayed a distorted octahedral geometry. The twist angles for the cations ranged between 34(2)° and 43.1(8)° (Table 12). The ORETEP view of cation A is shown in Figure 93. As was

Table 12 Crystal data and structure refinement for Zn(TAMEisoquin)](ClO₄)₂·5/3MeCN.

Compound	[Zn(TAMEisoquin)](ClO ₄) ₂ ·5/3MeCN
Color/shape	Colorless/block
Empirical formula	C ₃₅ H ₃₆ N ₆ Zn, Cl ₂ O ₈ , 1.66(C ₂ H ₃ N)
Temperature	208(2) K
Crystal system	Orthorhombic
Space group	<i>Pbca</i>
Unit cell dimensions	a=33.428(3)Å α=90°

Table 11 *continued...*

	b=26.441(3)Å	β=90°
Volume	c=35.580(4)Å	γ=90°
Z	31448(6)Å ³	
Density (calculated)	32	
Absorption coefficient	1.475 Mg/m ³	
Diffractometer/scan	0.823mm ⁻¹	
Radiation/wavelength	Bruker SMART/CCD area detector	
F(000)	Mo Kα (graphite monochrom.)/0.7107Å	
Crystal size	14478	
θ Range for data collection	0.25x0.20x0.10mm	
Index ranges	0.00 to 25.00°	
Reflections collected	0≤h≤39, 0≤k≤31, 0≤l≤42	
Independent reflections	27756	
Observed reflections	27756	
Data/restraints/parameters	27756	
Goodness-of-fit on F ²	27756/0/1933	
Final R indices [I>2σ(I)]	1.038	
R indices (all data)	R ₁ =0.0787, wR ₂ =0.1763	
Largest diff. peak and hole	R ₁ =0.1183, wR ₂ =0.1949	
	1.144 and -0.485e.Å ⁻³	

described for the previous TAME-based crystal structures the stereochemical dispositions of the four cations in the asymmetric unit were analyzed using the conventions of Al-Obaidi *et al.* (96). Because each cation has six chelate rings (three six-membered chelates and three five-membered chelates) and three stereogenic nitrogen centers (*i.e.* the secondary amines) there is the possibility that several isomers of the cation will form. The conformation of the TAME cap in molecule A is δ^{CAP} , meaning the framework is engaged in a clockwise twist about the C₃ axis that passes through atoms C35a, C34a, and Zn1a (see **Figure 93**). The absolute configuration of the three five-membered chelates was determined to be Δ . The chiral nitrogens have been assigned collectively as SSS. Lastly, a shallow pucker in the three five-membered chelate rings was assigned as $\lambda\lambda\lambda$. The stereochemical disposition of the TAMEisoquin ligand in cation A follows as $\Delta\delta^{\text{CAP}}\lambda\lambda\lambda(\text{SSS})$. The remaining cations B through D have been assigned stereochemical designations in **Table 12**.

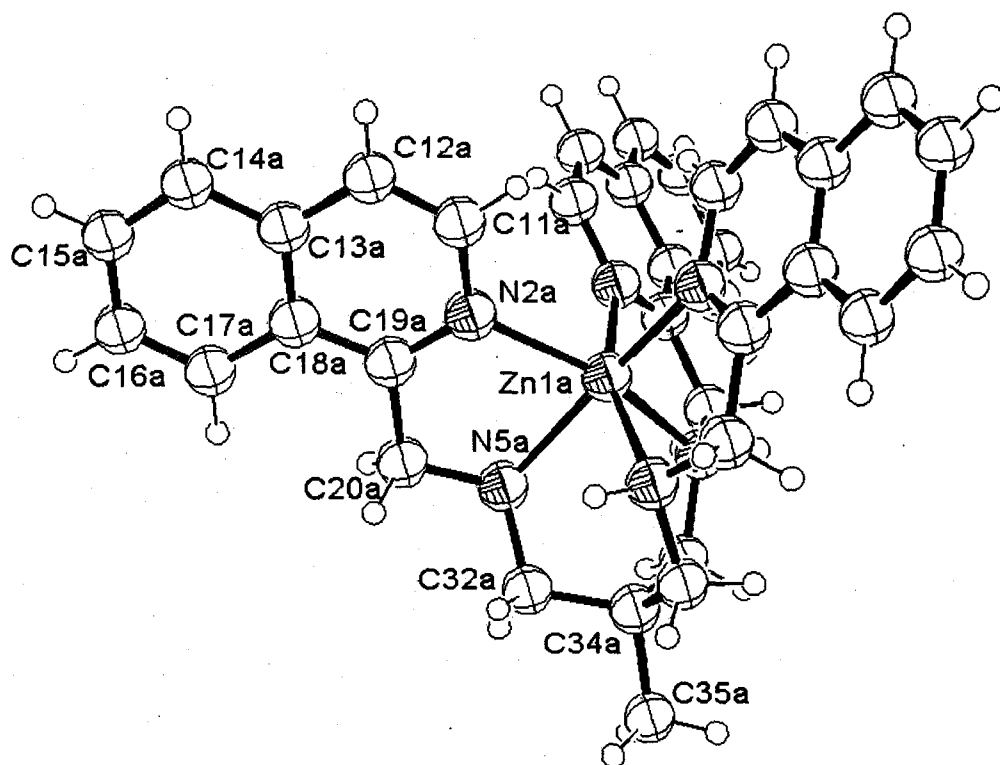


Figure 93 The ORTEP view of cation A for $[\text{Zn}(\text{TAMEisoquin})]^{2+}$. The perchlorate anions and MeCN solvate have been removed for illustrative clarity.

The striking feature of this crystal structure is the range of conformations the ligand possesses in the solid state. This observation illustrates the flexible nature of the TAME framework in this family of chelators. Hydrophobic portions of the complex cation could also associate with nearby molecules possibly interrupting cation-anion interactions. This too may cause the ligand to contort into a variety of conformations, which were evidenced in the crystal data.

Complex	Zn-N(het.) average bond lengths (Å)	Zn-N(amine) average bond lengths (Å)	Twist Angle α (°)	Stereochemical configuration
Cation A	2.16(1)	2.178(4)	34(2)	$\Delta\delta^{\text{CAP}}\lambda\lambda\lambda(\text{SSS})$
Cation B	2.16(1)	2.164(6)	38(2)	$\Lambda\lambda^{\text{CAP}}\delta\delta\delta(\text{RRR})$
Cation C	2.15(1)	2.16(1)	43.1(8)	$\Delta\lambda^{\text{CAP}}\lambda\lambda\lambda(\text{SSS})$
Cation D	2.15(2)	2.16(1)	40(3)	$\Delta\lambda^{\text{CAP}}\lambda\lambda\lambda(\text{SSS})$

Table 13 Selected data from the structure of $[\text{Zn}(\text{TAMEisoquin})]^{2+}$.

The chelator flexibility was further illustrated by dynamic behavior of $[\text{Zn}(\text{TAMEisoquin})]^{2+}$ in solution (Figure 94). The $^1\text{H-NMR}$ spectrum in $\text{DMSO-}d_6$ indicated that the complex maintains an intermediate geometry between a rigid octahedron and trigonal prism. If the chelator was a rigid octahedron then the methylene H's of both the TAME framework and the isoquinolinyl pendant arms would be in unique chemical environments. Therefore, a diastereotopic relationship would exist between the geminal H's of both the pendant arms and the TAME framework. Because of the presence of a C_3 axis each collection of symmetry related methylene H's would possess a doublet-of-doublet spin pattern in the NMR spectrum.(38) However, if the complex cation was a rigid trigonal prism in solution then a C_{3v} symmetry would mandate a simple doublet for the symmetry related TAME methylene H's and a doublet for the isoquinolinyl methylene H's. Thus, the broadening of these resonances in the spectral region between 3.0 and 5.0 ppm indicates isomerization between the helical Λ and Δ configurations. Erosion of the anticipated doublet-of-doublet spin multiplicity also supports a solution phase helical inversion of the cation. This dynamic behavior was enhanced when TAMEisoquin II.115 was exposed to 1.0 equivalent of $\text{Cd}(\text{II})$ (Figure 94). The poor size-match between the binding cavity of the chelator and

the ionic radius of Cd(II) (1.09Å) may enhance helical isomerization by reducing intraligand steric repulsions in the transition state of the twisting cation. This assertion assumes that a Bailar-type twist is the mechanism chosen by the chelator to afford the observed dynamic behavior. Two other plausible mechanisms, namely a rhombic twist or a dissociative pathway, may also play a role in the observed dynamic behavior for both $[\text{Cd}(\text{TAMEisoquin})]^{2+}$ and $[\text{Zn}(\text{TAMEisoquin})]^{2+}$.(47)

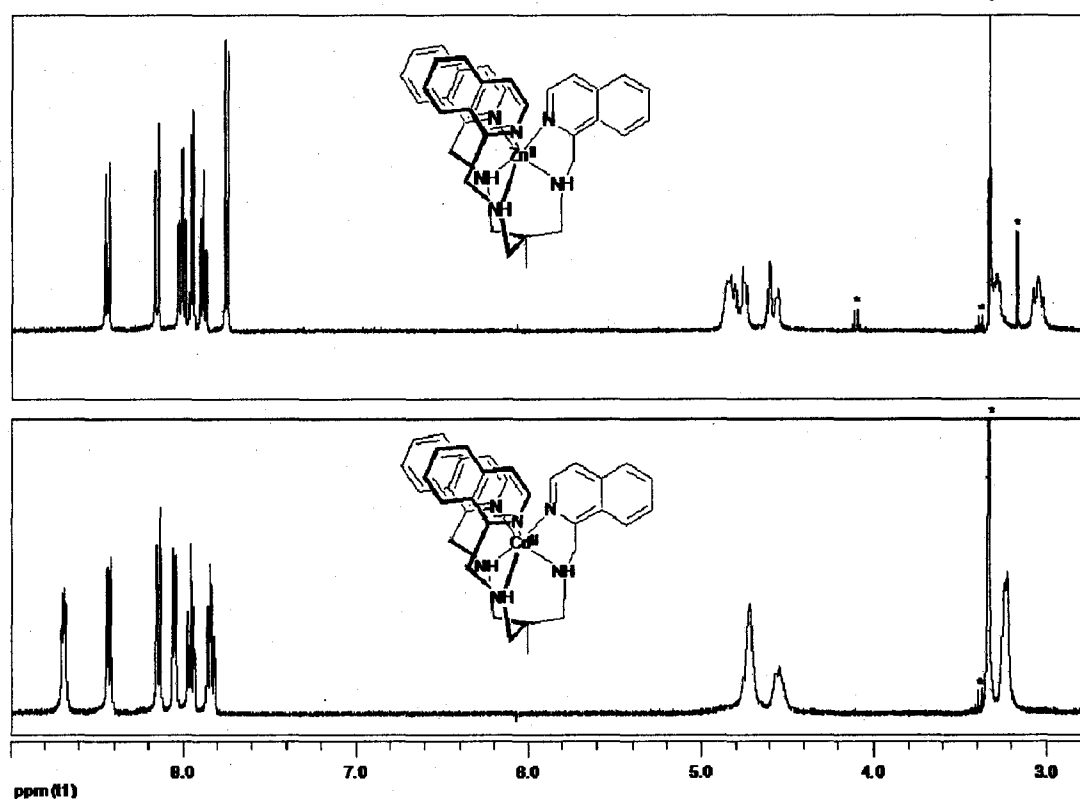
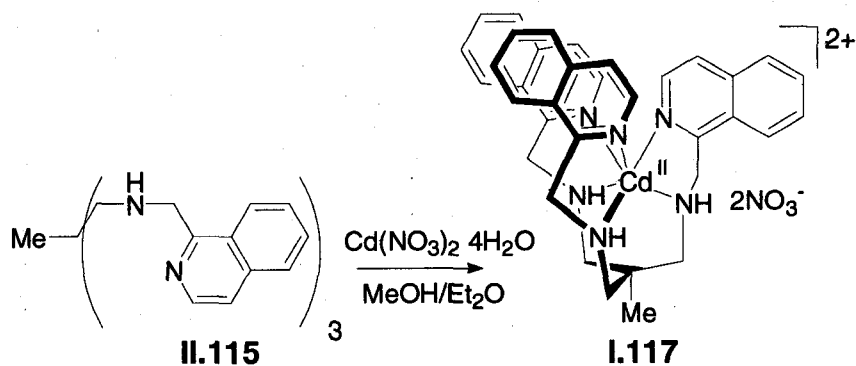


Figure 94 Partial ^1H -NMR spectra of the Zn(II) and Cd(II) complexes of TAMEisoquin. The reader should direct their eyes to the spectral region between 3.0 and 5.0 ppm. Solvent impurities are indicated by an asterisk (*).

To assess the size-fit between Cd(II) and TAMEisoquin the complex was prepared from a MeOH solution of the chelator and $\text{Cd}(\text{NO}_3)_2 \cdot 4\text{H}_2\text{O}$ and isolated in 96.0% yield (Scheme 39). Microcrystals were obtained by Et_2O diffusion into

a 1:1 MeNO₂:MeCN (v/v) solution of the complex. Unfortunately, the crystals did not diffract strongly and as such failed to afford any structural data.



Scheme 39 The preparation of [Cd(TAMEisoquin)](NO₃)₂ I.117.

A computational study was carried out on the [Cd(TAMEisoquin)]²⁺ cation *in lieu* of the desired crystallographic data. A geometry optimization was performed on the cation with DFT at the B3LYP/LANL2DZ level of theory. The computational result is shown in **Figure 95**.

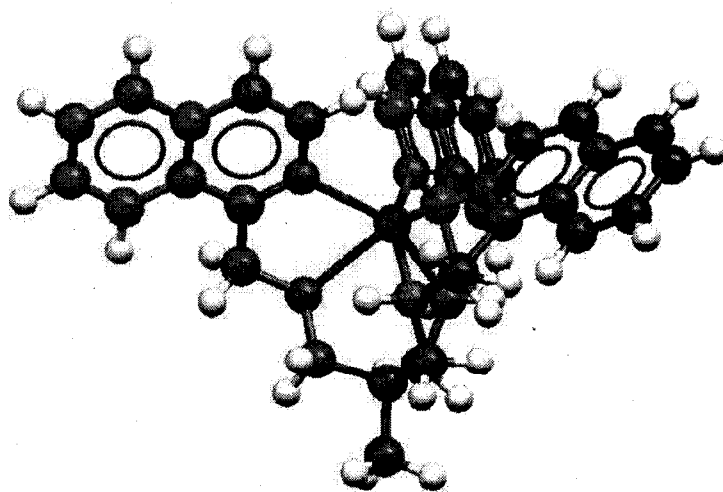
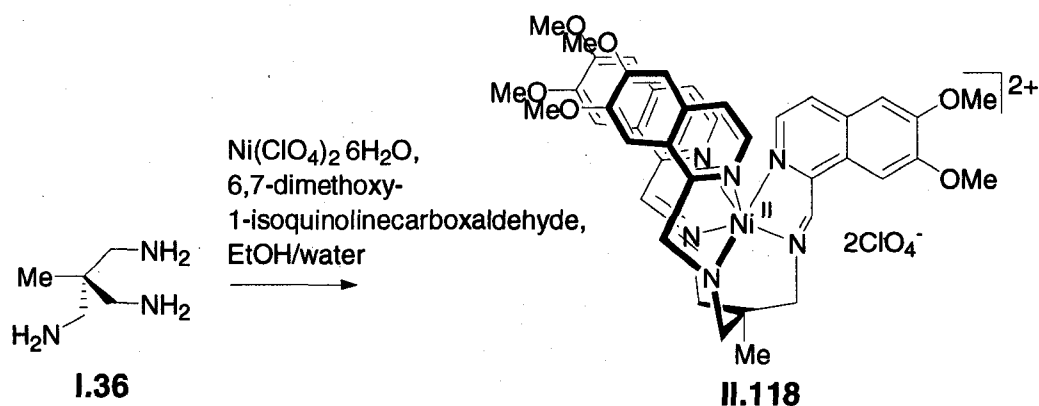


Figure 95 Geometry optimized structure of [Cd(TAMEisoquin)]²⁺ at the B3LYP/LANL2DZ level of theory. Note the splaying of the isoquinoliny groups.

The validity of the computational result was checked by measuring the Cd-N(het.) bond lengths ($2.35 \pm 0.01 \text{ \AA}$) and Cd-N(amine) bond lengths ($2.429 \pm 0.005 \text{ \AA}$). Known CdN₆ complexes have crystallographically measured bond lengths that vary between *ca.* 2.3-2.4 \AA .⁽⁴⁷⁾ This result supports the validity of the computational result. A second check was made on the optimized structure by measuring the computational angle of twist about the C₃ axis of the complex cation and the bite distance between the chelating nitrogens. The computational twist angle of 39(4) $^\circ$ matched the predicted twist angle of 40 $^\circ$ obtained following the method of Kepert.⁽²³⁶⁾ In Kepert's model one only needs the intrachelate bite distances and metal-ligand bond lengths to calculate the twist angle. That structural information that was readily obtained from the geometry optimized structure of [Cd(TAMEisoquin)]²⁺. The conformation of the optimized complex has been assigned as follows: $\Delta\delta^{\text{cap}}\lambda\lambda\lambda(\text{SSS})$. The striking feature of this computational result is that the Cd(II) is beginning to pucker out of the binding cavity of the complex due to the poor size-match between the ligand and the metal. This is perhaps best seen in the splaying the of isoquinoliny groups with respect to the secondary amino groups. The inter-heterocyclic nitrogen distances (3.7(1) \AA) that forms one of the trigonal faces of the distorted octahedron are markedly longer than the inter-amino distances (3.23(9) \AA) that forms the other trigonal face. Ideally, these two distances should be identical, which suggests the ligand undergoes an axial elongation upon coordination to Cd(II).

The closely related azaaromatic 6,7-dimethoxy-1-isoquinolinecarboxaldehyde **II.84** furnished the corresponding trisimine complex **II.118** upon treatment with TAME **I.36** and a Ni(II) salt (**Scheme 40**).



Scheme 40 The preparation of $[\text{Ni}(6,7\text{-DMTI-trisimine})](\text{ClO}_4)_2$ **II.118**.

The ligand was given the trivial name 6,7-DMTI (where 6,7-DMTI=6,7-dimethoxy TAMEisoquin) to simplify chelator nomenclature. The resulting complex formed orange colored needles upon Et_2O diffusion into a 1:1 MeOH:MeCN (v/v) solution. However, no structural data was obtained for this complex. The visible-near IR spectrum in MeCN was nearly identical to the spectrum for $[\text{Ni}(\text{TAMEisoquin-trisimine})](\text{ClO}_4)_2$ (**Table 13**).

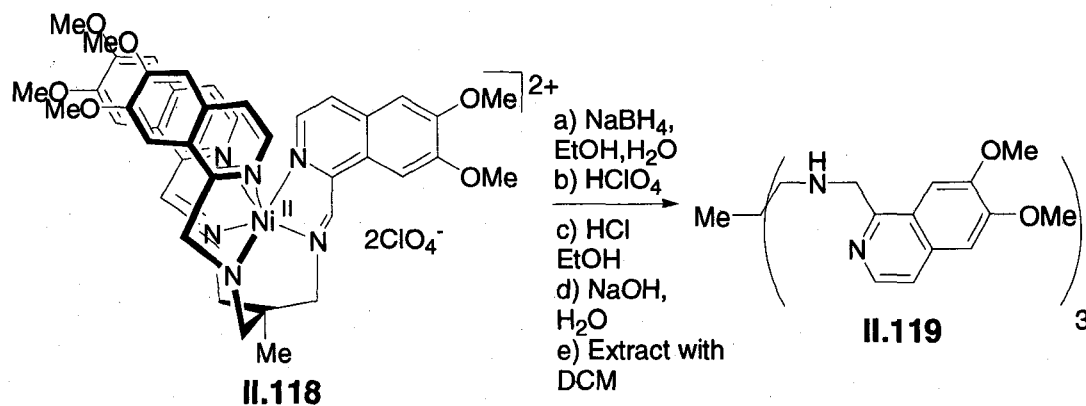
λ_{max} (nm)	$\bar{\nu}$ (cm^{-1})	ϵ ($\text{cm}^{-1}\text{M}^{-1}$)	Assignment
877(sh.)	11400	33.5	${}^3\text{A}_{2g} \rightarrow {}^1\text{E}_{1g}$
805	12400	40.0	${}^3\text{A}_{2g} \rightarrow {}^3\text{T}_{2g}$
ca.640-500	ca.15600-20000	ca.275	MLCT (Ni \rightarrow C=N)
<500	>20000	-	$\pi \rightarrow \pi^*$ (intraligand)

Table 14 Visible-near IR absorbance data for $[\text{Ni}(6,7\text{-DMTI-trisimine})](\text{ClO}_4)_2$ in MeCN at 25°C.

This data suggests that no additional binding-strength was achieved by the presence of the π -donating but inductively withdrawing MeO-groups on the

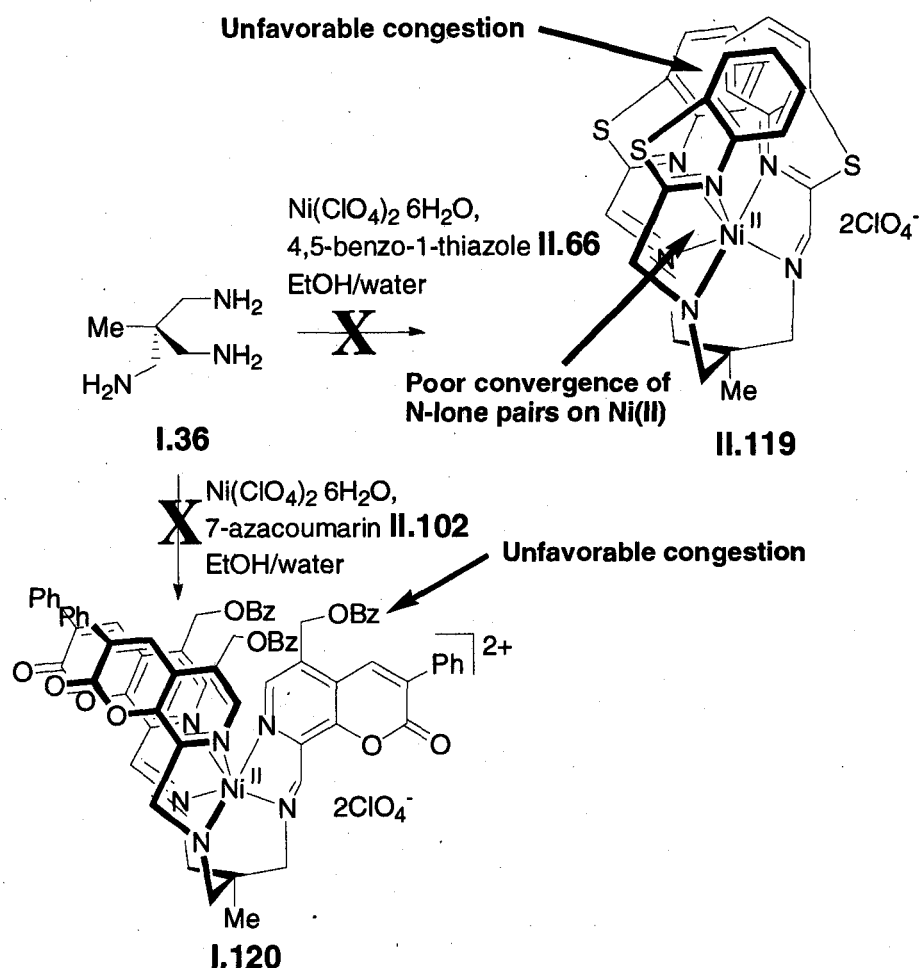
periphery of the complex cation. Moreover, additional steric bulk was minimized in the inner coordination sphere of the complex cation by placing the MeO-groups at the 6 and 7 positions of the heterocyclic ring system.

The three C=N bonds were reduced with excess NaBH₄ in aqueous EtOH but the use of NaCN to liberate 6,7-DMTI **II.119** from the metal center proved unsuccessful. The organic material isolated furnished a complicated ¹H-NMR spectrum (not shown) indicating that the 6,7-dimethoxy-1-isoquinoliny groups were sensitive to the presence of a strong nucleophile like CN⁻. An alternative de-metallation scheme was devised which involved the acidification of crude uncharacterized [Ni(6,7-DMTI)](ClO₄)₂ with concentrated HCl (**Scheme 41**). The resulting protonated chelator was isolated as a precipitate from EtOH and dried under vacuum to afford a white powder. The uncharacterized protonated chelator 6,7-DMTI·xHCl was then dissolved into minimal amounts of water and treated with excess NaOH until a pH≥14 was achieved (evidenced by paper). The free-base 6,7-DMTI **II.119** was then extracted from the basic media with DCM and isolated in 27.2% yield free of impurities. The dismal yield, however, did not hinder subsequent complexation studies with the liberated 6,7-DMTI **II.119** chelator.



Scheme 41 The preparation of 6,7-DMTI **II.119**.

Unfortunately, our tandem Ni(II)-mediated template reaction/tetrahydroborate reduction failed to afford TAME based chelators with either the benzo-fused thiazolecarboxaldehyde **II.66** (see **Scheme 19**) or the 7-azacoumarin **II.102** (see **Scheme 31**). The former thiazole substrate **II.66** only afforded starting material when the corresponding template reaction was carried out. Varying the temperature of the reaction mixture from *ca.* 20°C to reflux did not affect the desired transformation.



Scheme 42 Failed attempts at the preparation of TAME-based trisimine complexes of bulky azaaromatic aldehydes.

The author speculates that steric crowding between the benzo groups working in concert with an unsuitable convergence point of the nitrogen lone pairs in the five-membered chelate rings thwarted the desired reactivity (**Scheme 42**).

In the later case of the 7-azacoumarin aldehyde **II.102**, only the bisazacoumarin complex **II.121** was evidenced in the MALDI-TOF mass spectrum of the crude isolated material (**Figure 96**). The presence of a bulky benzyloxy group on the pyridine ring may have prevented a reaction with the third equivalent of the 7-azacoumarin aldehyde **II.102** substrate. Varying the

solvent and reaction time still only afforded the bisazacoumarin complex **II.121**. Substituting Ni(II) for a larger templating cation could perhaps bias the formation of the desired ligand by bloating the binding cavity thus reducing intraligand steric repulsions.

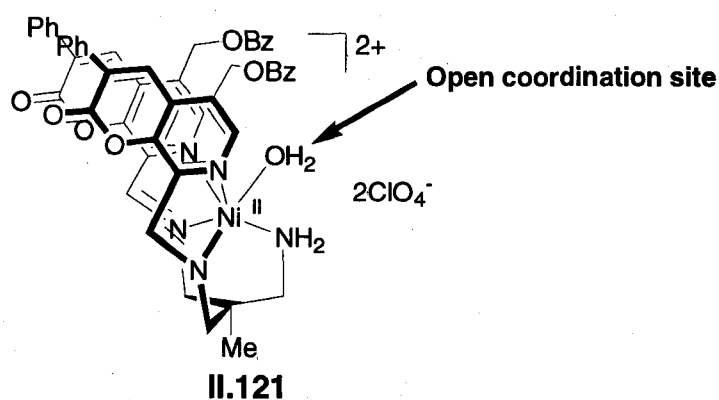
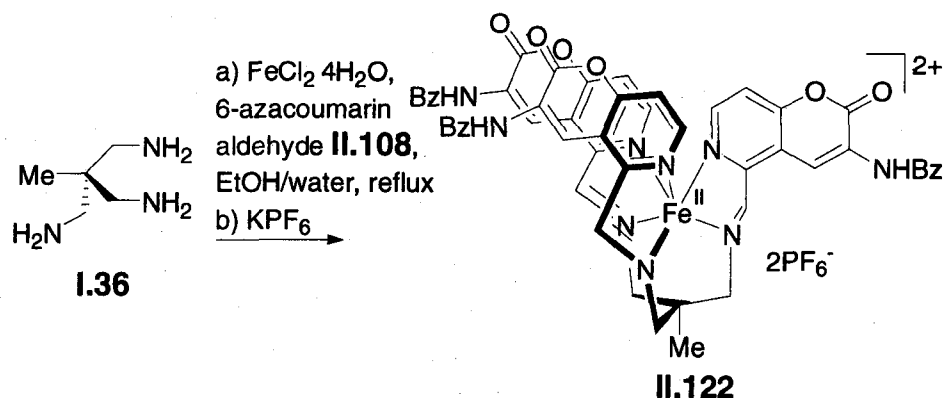


Figure 96 Putative structure of the bisazacoumarin complex II.121.

The impetus for synthesizing the 6-azacoumarin aldehyde **II.108** was partly derived from reducing the steric bulk of the 7-azacoumarin aldehyde **II.102** thus facilitating reaction completion. It was also hypothesized that switching the templating metal to Fe(II) would facilitate reaction completion. The propensity of Fe(II) to achieve a low-spin electronic configuration ($t_{2g}^6 e_g^0$) in the presence of a tris α, α' -diimine ligating set should persuade the reaction equilibria to favor the formation of the desired trischelate instead of a bischelate.⁽⁴²⁾ The reaction of the 6-azacoumarin aldehyde **II.108** with TAME **I.36** in the presence of $\text{FeCl}_2 \cdot 4\text{H}_2\text{O}$ did indeed form the desired trisimine complex **II.122** (Scheme 43).



Scheme 43 The synthesis of the 6-azacoumarin trischelate complex of Fe(II).

The desired complex was isolated as a deep-blue powder from the reaction milieu upon anion exchange with hexafluorophosphate. The desired material was in fact a low-spin species due to the lack of paramagnetic shifting in the ^1H -NMR spectrum. Unfortunately, the reaction mixture was complicated with numerous by-products which elude removal via recrystallization. The azacoumarin substrates **II.102** and **II.108** therefore have limited utility in the metal-mediated template reaction toward the preparation of novel TAME-based chelators. The preparation of an azacoumarin free of excess functionality remains elusive.

2.14. Photophysical properties of TAMEisoquin, and 6,7-DMTI: Zn(II) luminescent sensing

The UV spectra of TAMEisoquin **II.115** and $[\text{Zn}(\text{TAMEisoquin})]^{2+}$ in 50% aqueous DMF exhibit four maxima that have been assigned as intraligand charge-transfer bands (**Figure 97**). The free ligand has maxima at 322 nm ($\log\epsilon_1=3.92\pm 0.01$), 309 nm ($\log\epsilon_2=3.86\pm 0.01$), 283 nm ($\log\epsilon_3=3.96\pm 0.01$), and

272 nm ($\log \epsilon_4 = 4.05 \pm 0.01$). Upon Zn(II)-recognition there was a slight bathochromic shift of *ca.* 2 nm in the UV-spectrum with a concomitant increase in the intensity of the emerging maxima at 324 nm ($\log \epsilon_1 = 3.95 \pm 0.01$) and 312 nm ($\log \epsilon_2 = 3.91 \pm 0.01$) (Figure 97) and attenuation of the maxima at 284 nm ($\log \epsilon_3 = 3.92 \pm 0.01$) and 273 nm ($\log \epsilon_4 = 4.04 \pm 0.01$). The increase in the molar absorptivity has been attributed to the movement of the ${}^1n\pi^*$ state to higher energies upon coordination of the heterocyclic nitrogen to the Zn(II)-cation. There were no spectral changes evidenced when TAMEisoquin II.115 was exposed to >1.0 equivalents of Zn(II), thus supporting a binding stoichiometry of 1:1 M:L under these conditions.

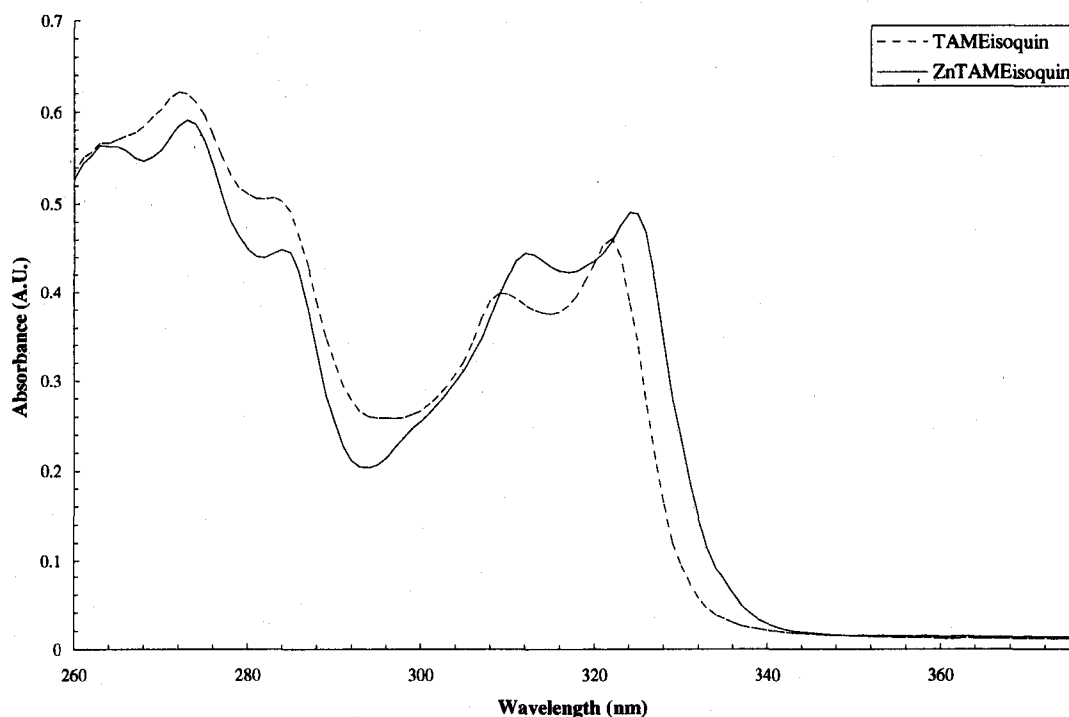


Figure 97 UV spectra of 56 μM TAMEisoquin and $[\text{Zn}(\text{TAMEisoquin})]^{2+}$ in 50% aqueous DMF (v/v) at 25.0°C.

In 1:1 DMF:H₂O (v/v) at 25.0°C the ligand showed very little fluorescence when excited with 321 nm light (**Figure 98**). This result demonstrated that PET was launched at the isoquinolinyl groups via the secondary amines in the absence of the Zn(II) analyte. Limited water solubility of TAMEisoquin II.115 prevented us from studying the efficiency of the PET mechanism as a function of pH. It was speculated that the PET mechanism would be interrupted upon

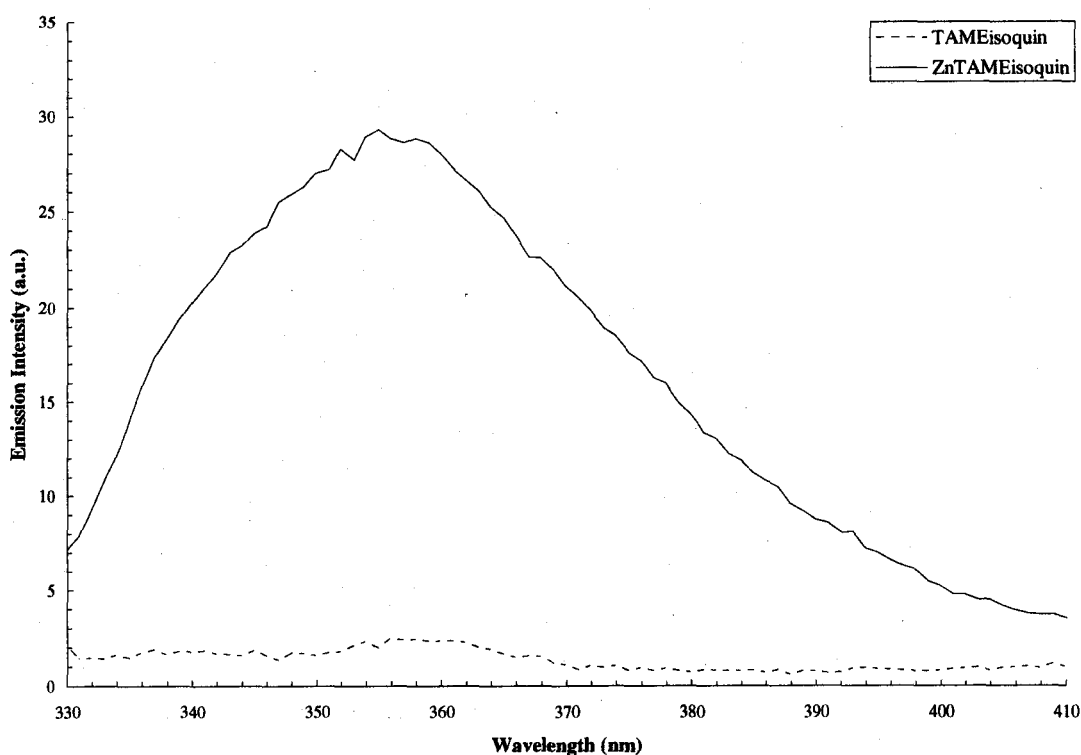


Figure 98 Fluorescence spectra ($\lambda_{ex}=321$ nm) of 14 μ M TAMEisoquin and $[Zn(TAMEisoquin)]^{2+}$ in 50% aqueous DMF at 25.0°C.

protonation of the secondary amines. This in turn would enhance the background emission from the apo-chelator under acidic pH. However, in the presence of Zn(II), a 15-fold enhancement of the emission intensity at 355 nm was observed. The Zn(II)-cation binds to both the secondary amines and the heterocyclic nitrogens (as evidenced in the NMR and X-ray data) of TAMEisoquin

II.115 preventing the PET-mediated quenching of the isoquinolinyl groups. The sensor is then turned-on and the resulting luminescent response amplified via the CEF mechanism.

The emission intensity at 355 nm was linear over a modest concentration range of $[\text{Zn}(\text{TAMEisoquin})]^{2+}$. A nonlinear response emerged in the plot depicted in **Figure 99** when the concentration of the complex reached *ca.* 20 μM . In the linear portion of the plot a slope of $\log K = 6.32 \pm 0.02$, where $F = K \cdot [\text{ZnTAMEisoquin}]$, was calculated by a least-squares fit of the data. Even though the Stoke's shift upon analyte binding was 34 nm (3000 cm^{-1}), overlap of the absorbance and emission spectra at 321 nm likely promoted self-absorption at higher concentrations of $[\text{Zn}(\text{TAMEisoquin})]^{2+}$. (102)

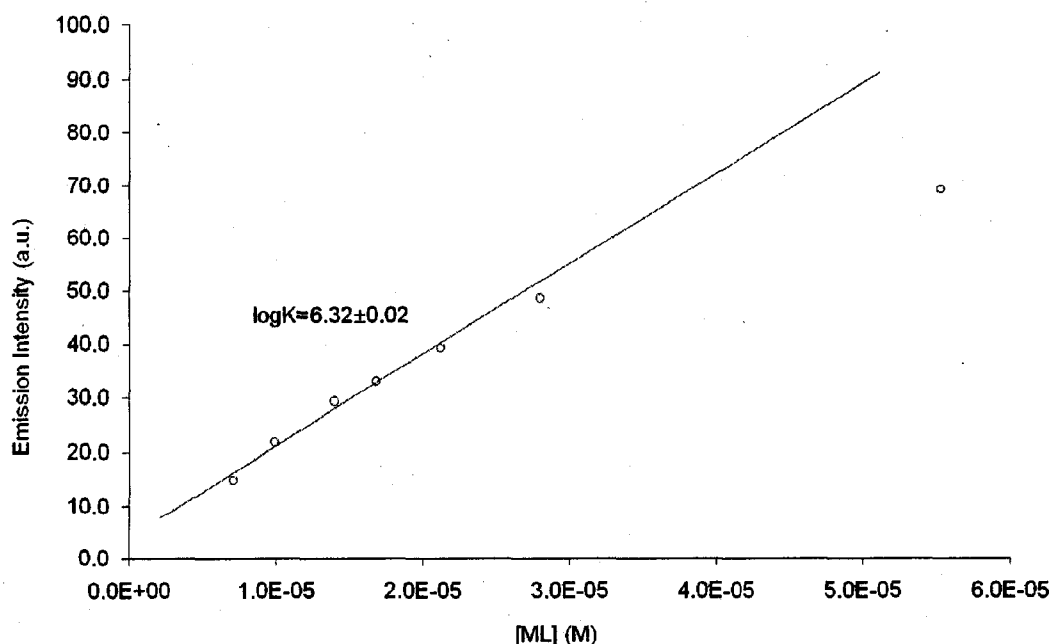


Figure 99 The effect of concentration of $[\text{Zn}(\text{TAMEisoquin})]^{2+}$ on emission intensity (F) at $\lambda_{\text{em}} = 355 \text{ nm}$ in 50% aqueous DMF at 25.0°C.

The quantum yield of $[\text{Zn}(\text{TAMEisoquin})]^{2+}$ was measured to be 1.2% via the use of quinine sulfate as a standard (1N H_2SO_4 $\Phi_{\text{quinine}}=54.6\%$) (Equation II.j). (237) The following relationship was used to calculate $\Phi_{[\text{ZnTAMEisoquin}]}$:

$$\Phi_{[\text{ZnTAMEisoquin}]} = \Phi_{\text{quinine}} \cdot \frac{\text{Gradient}_{[\text{ZnTAMEisoquin}]}}{\text{Gradient}_{\text{quinine}}} \cdot \frac{\eta_{[\text{ZnTAMEisoquin}]}}{\eta_{\text{quinine}}} \quad (\text{II.j})$$

The “gradients” for Equation II.j for both the Zn(II) complex and the standard are the slopes from the plot in Figure 100 (see Chapter 4 for experimental details).

The refractive indices (η) for the solvent systems of both the unknown and standard were neglected.

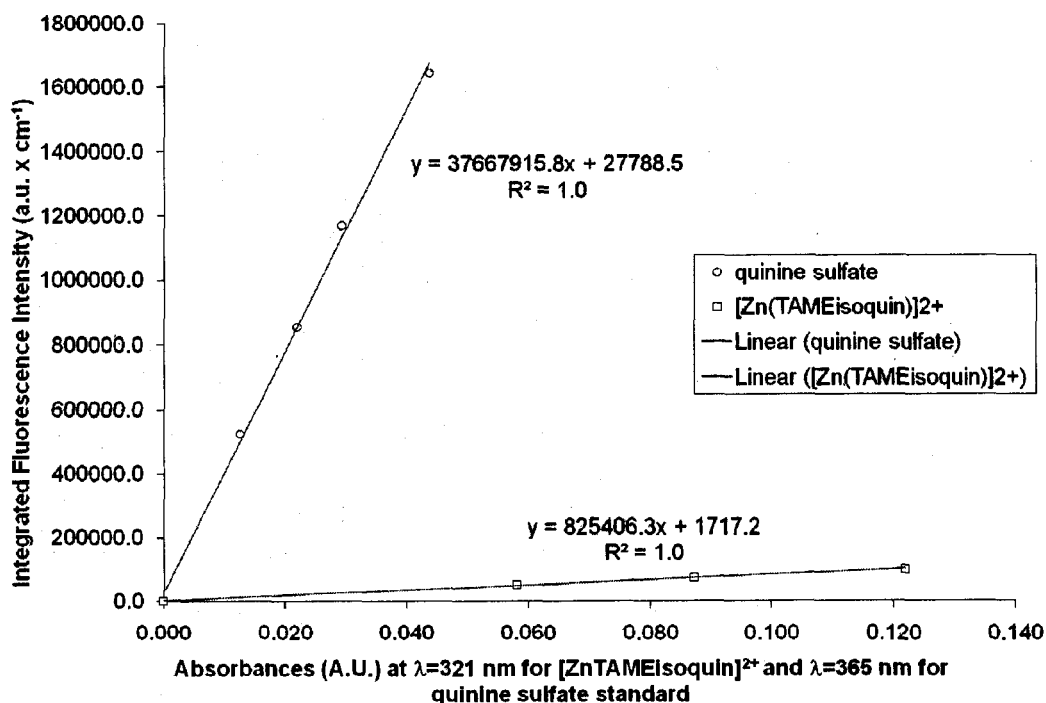


Figure 100 Quantum yield determination of $[\text{Zn}(\text{TAMEisoquin})](\text{ClO}_4)_2$ in 50% aqueous DMF at 25.0°C. Serial dilutions of quinine were prepared in 1N H_2SO_4 .

Dissolved oxygen, which could quench the fluorescence intensity by promoting intersystem crossing, was minimized by purging the solvent systems with nitrogen for *ca.* 1 hr prior to analysis. It is believed that internal conversion arising from the aforementioned trigonal twisting of the complex cation served to attenuate the observed emission intensity. This result may highlight one of the disadvantages of employing the TAME-framework to develop novel Zn(II)-luminescent sensors. Substitution of TAME with the TACH framework could perhaps increase the emission intensity by forming more rigid complexes with the analyte. The crystallographic data of the cation $[\text{Zn}(\text{TAMEisoquin})]^{2+}$ illustrated a number of conformational modes available to the chelator upon analyte recognition (*vide supra*). It is hypothesized that constraining the ligating-architecture may enhance the emission intensity upon analyte recognition by reducing the competing internal-conversion rates. It is hoped that future work on analogous isoquinolinyl ligating systems will confirm this assertion.

The spectroscopic selectivity of TAMEisoquin **II.115** toward Zn(II) was indicated by the luminescent response of **II.115** to other monocationic and dicationic metal ions (**Figure 101**). The fluorescence response was only slightly positive with main group alkali and alkaline earth metal cations. This result highlights the poor-match between the N₆ donor set of TAMEisoquin **II.115** and these oxophilic cations. The response of TAMEisoquin **II.115** to the first row transition-metal ions Mn(II) through Cu(II) was quenching. This was anticipated for the reasons already discussed in this dissertation. Heavier closed-shell metal ions, like Ag(I), also exhibit quenching with TAMEisoquin **II.115** because of

enhanced intersystem crossing rates due to increased spin-orbit coupling with the analyte. The most striking feature observed in this study was that TAMEisoquin II.115 displayed a very feeble fluorescence enhancement in the presence of Cd(II).

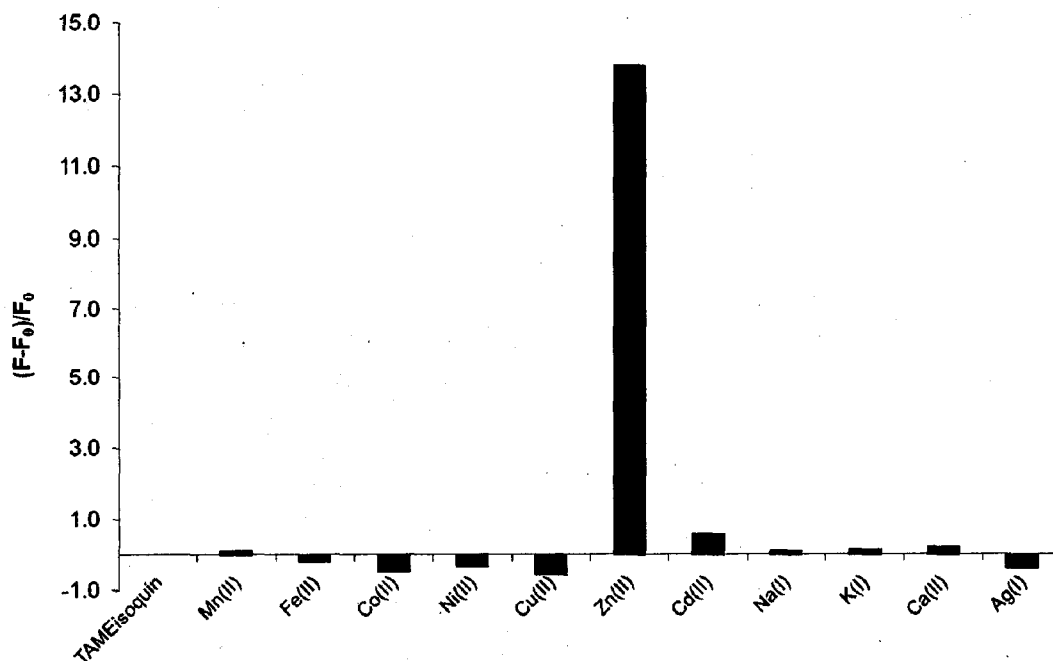
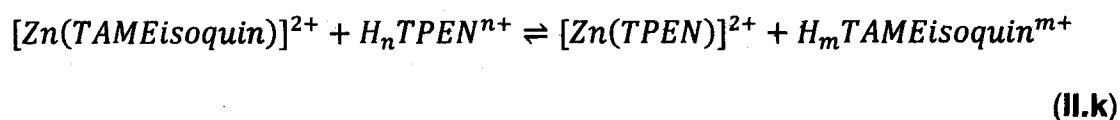


Figure 101 Screening emission enhancements of TAMEisoquin in the presence of 1.0 equivalent of various cationic analytes. The experiments were conducted in 50% aqueous DMF at 25.0°C with [TAMEisoquin]_{Total}=14μM.

This result is particularly noteworthy because Cd(II), as mentioned previously, often interferes with the spectroscopic selectivity of luminescent Zn(II)-sensors. It is believed that Cd(II) not only quenches the emission by the usual heavy-atom effect but it also promotes internal conversion via the aforementioned trigonal twisting of the cation in solution. The observed spectroscopic selectivity for Zn(II) is quite powerful and may prove useful in the development of luminescent sensors for Zn(II). In biological systems Cd(II) is essentially nonexistent,

however, in the analysis of Zn(II) in other arenas, such as hydrometallurgy, environmental chemistry, and materials science the detection of the target analyte may be prone to interference from Cd(II) and Hg(II). (238-241)

An estimation of the binding constant for TAMEisoquin **II.115** to Zn(II) has been carried out by competing the ligand for the metal against TPEN **II.49**, a well-known heavy metal chelator. (242) In the presence of 1.0 equivalent of TPEN **II.49** at pH=7 ($\mu=0.1$ M, see Chapter 4 for experimental details) partial quenching of the emission from $[Zn(TAMEisoquin)]^{2+}$ was achieved, suggesting the metal was partially extracted by TPEN forming the non-luminescent complex $[Zn(TPEN)]^{2+}$ (**Equation II.k**).



The conditional dissociation constant K_d' was calculated from the data to be 1.4 fM, highlighting the strong affinity the chelator TAMEisoquin **II.115** has for the metal.

The UV spectra of the analogous ligand 6,7-DMTI **II.119**, and the corresponding complex $[Zn(6,7-DMTI)]^{2+}$ in 50% aqueous DMF exhibits two well-defined maxima that have been assigned as intraligand charge-transfer bands (**Figure 102**). The free ligand has maxima at 326 nm ($\log\epsilon=3.94\pm0.02$) and 314 nm ($\log\epsilon=3.90\pm0.02$). Upon Zn(II)-recognition there was a slight bathochromic shift of 2 nm in the UV-spectrum with a concomitant increase in the intensity of the emerging maxima at 328 nm ($\log\epsilon=4.03\pm0.02$) and 316 nm ($\log\epsilon=4.04\pm0.02$)

(Figure 102). Likewise, the increase in the molar absorptivity has been attributed to the movement of the ${}^1n\pi^*$ state to higher energies upon coordination of the heterocyclic nitrogen to the Zn(II)-cation. There were no spectral changes evidenced when 6,7-DMTI II.119 was exposed to >1.0 equivalents of Zn(II), thus supporting a binding stoichiometry of 1:1 M:L under these experimental conditions.

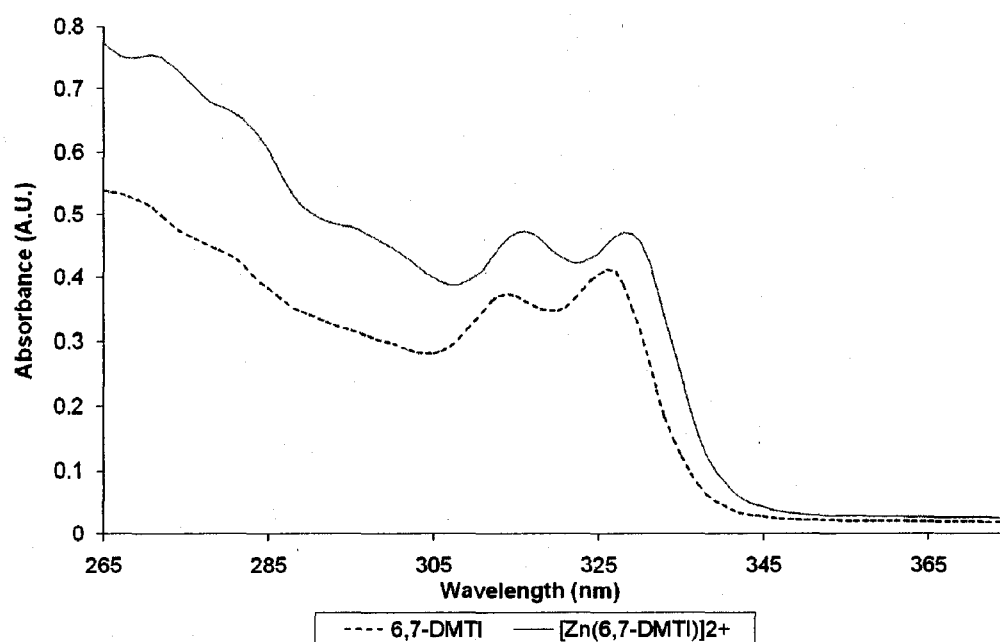


Figure 102 UV spectra of 50 μ M 6,7-DMTI and $[\text{Zn}(6,7\text{-DMTI})]^{2+}$ in 50% aqueous DMF at 25.0°C.

In 50% aqueous DMF at 25.0°C the ligand 6,7-DMTI II.119 showed very little fluorescence when excited with 326 nm light (Figure 103). This result demonstrates that PET was launched at the substituted isoquinolinyl groups via the secondary amines in the absence of the Zn(II) analyte. However, in the presence of Zn(II), a 17-fold enhancement of the emission intensity at 360 nm was observed.

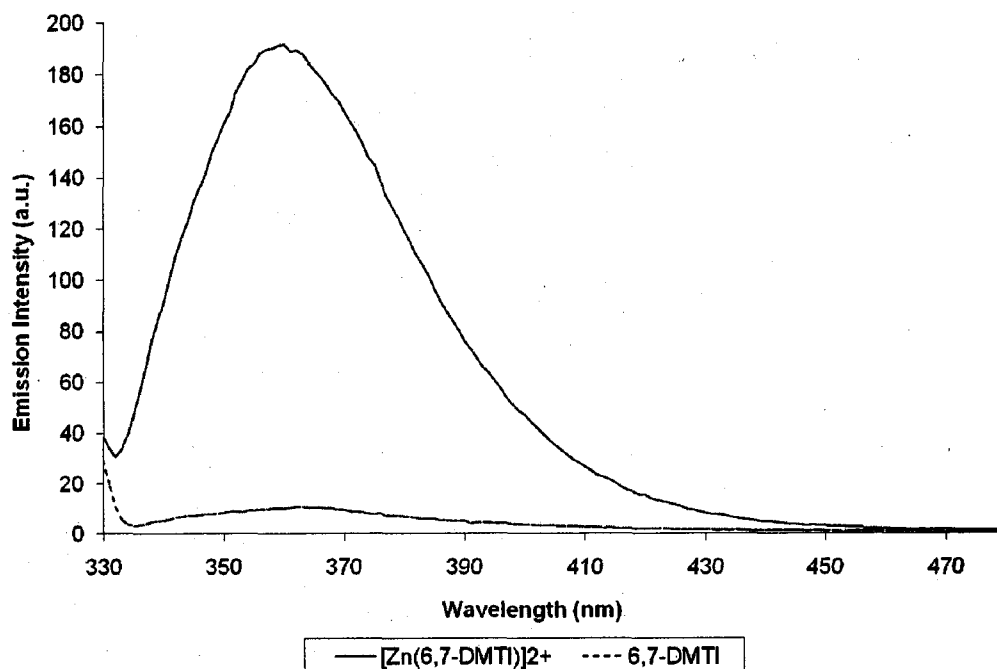


Figure 103 Fluorescence spectra ($\lambda_{\text{ex}}=326$ nm) of $5\mu\text{M}$ 6,7-DMTI and $[\text{Zn}(6,7\text{-DMTI})]^{2+}$ in 50% aqueous DMF at 25.0°C .

The emission intensity at 360 nm was linear over a small concentration range of $[\text{Zn}(6,7\text{-DMTI})]^{2+}$. A nonlinear response emerged in the plot depicted in **Figure 104** when the concentration of the complex reached ca. $30\mu\text{M}$. In the linear portion of the plot a slope of $\log K=7.54\pm 0.03$ was calculated by a least-squares fit of the data. Even though the Stokes' shift upon analyte binding was 34 nm (3000cm^{-1}), overlap of the absorbance and emission spectra at 326nm likely promoted self-absorption at higher concentrations of $[\text{Zn}(6,7\text{-DMTI})]^{2+}$.

Emission of $[\text{Zn}(6,7\text{-DMTI})]^{2+}$ at 360nm

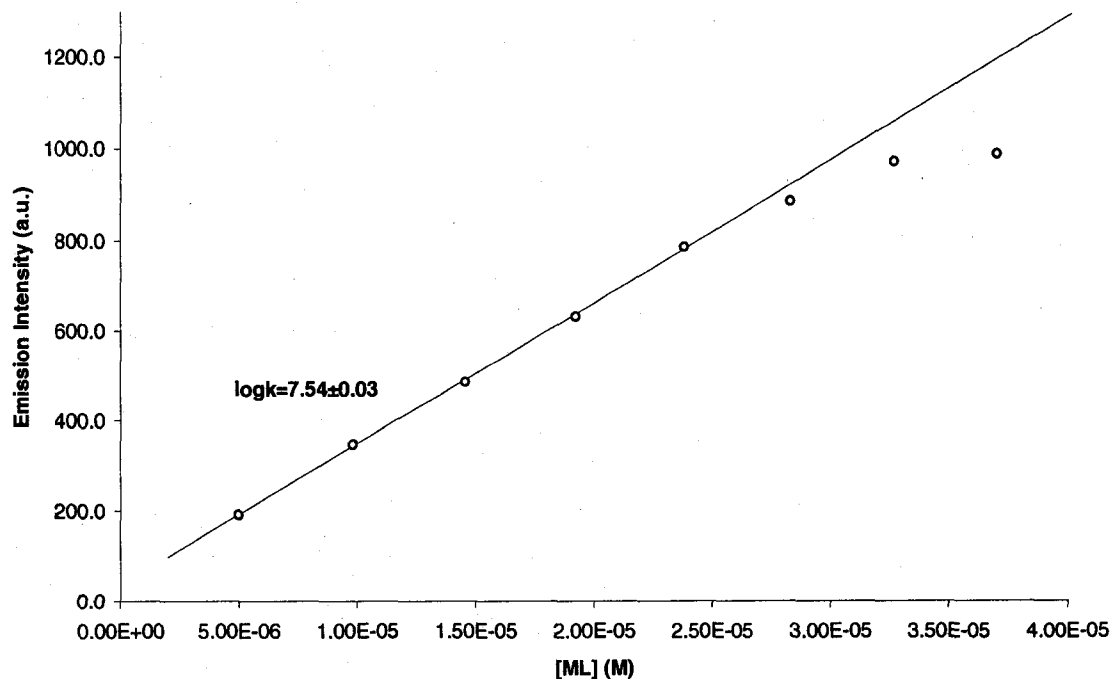


Figure 104 The effect of concentration of $[\text{Zn}(6,7\text{-DMTI})]^{2+}$ on emission intensity (F) at $\lambda_{\text{em}}=360$ nm in 50% aqueous DMF at 25.0°C.

The quantum yield of $[\text{Zn}(6,7\text{-DMTI})]^{2+}$ was measured to be 20% via the use of quinine sulfate as a standard (Figure 105). Analogous to what was observed with the methoxylated TQEN derivatives T(MQ)EN II.50 and T(TMQ)EN II.51 prepared by Mikata *et al.* the quantum yield of $[\text{Zn}(6,7\text{-DMTI})]^{2+}$ was ca.17 times larger than the quantum yield for $[\text{Zn}(\text{TAMEisoquin})]^{2+}$ (*i.e.* 1.2%).(184) The polarizing nature of the electron donating MeO-groups may supply the expected PET/CEF sensing mechanism of 6,7-DMTI II.119 with a modicum of ICT character.

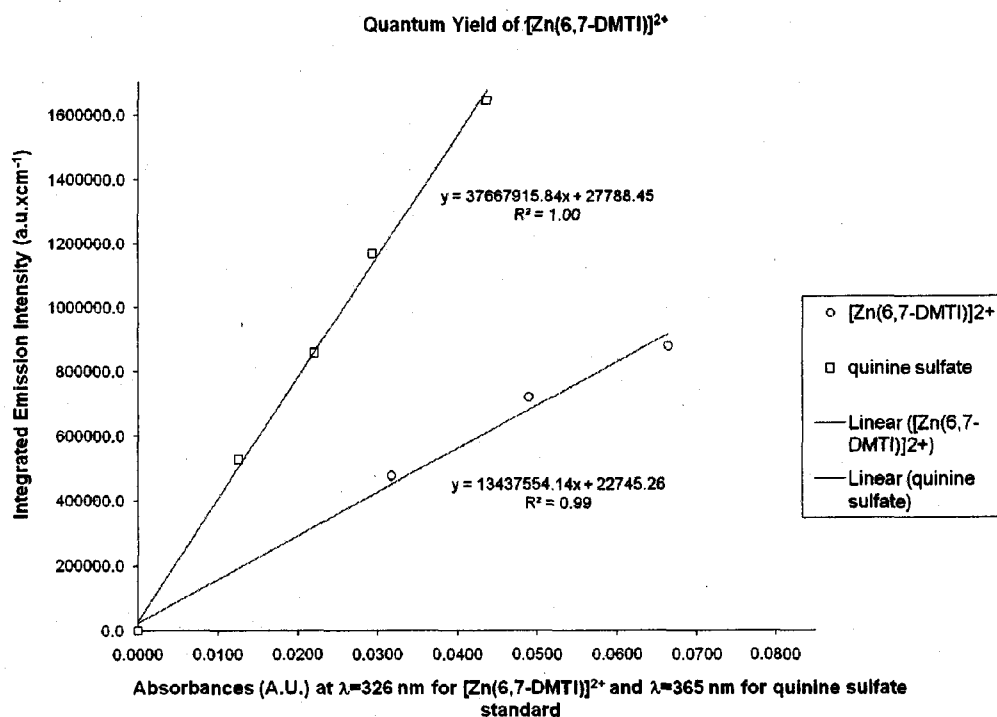


Figure 105 Quantum yield determination of $[\text{Zn}(6,7\text{-DMTI})]^{2+}$ in 50% aqueous DMF at 25.0°C. Serial dilutions of quinine were prepared in 1 N H_2SO_4 .

The spectroscopic selectivity of 6,7-DMTI II.119 toward Zn(II) was indicated by the luminescent response of II.119 to other monocationic and dicationic metal ions (Figure 106). As was seen with TAMEisoquin II.115, the fluorescence response was only slightly positive with main group alkali and alkaline earth metal cations. Likewise, the response of 6,7-DMTI II.119 to the first row transition-metal ions Mn(II) through Cu(II) was quenching. Heavier closed-shell metal ions (*i.e.* Ag(I), Hg(II), and Pb(II)) again exhibited quenching with 6,7-DMTI II.119 because of enhanced intersystem crossing rates due to increased spin-orbit coupling with these analytes. The exquisite spectroscopic selectivity of 6,7-DMTI II.119 for Zn(II) was maintained over Cd(II) highlighting the utility of the TAME-framework in the preparation of size-selective metal-ion sensors.

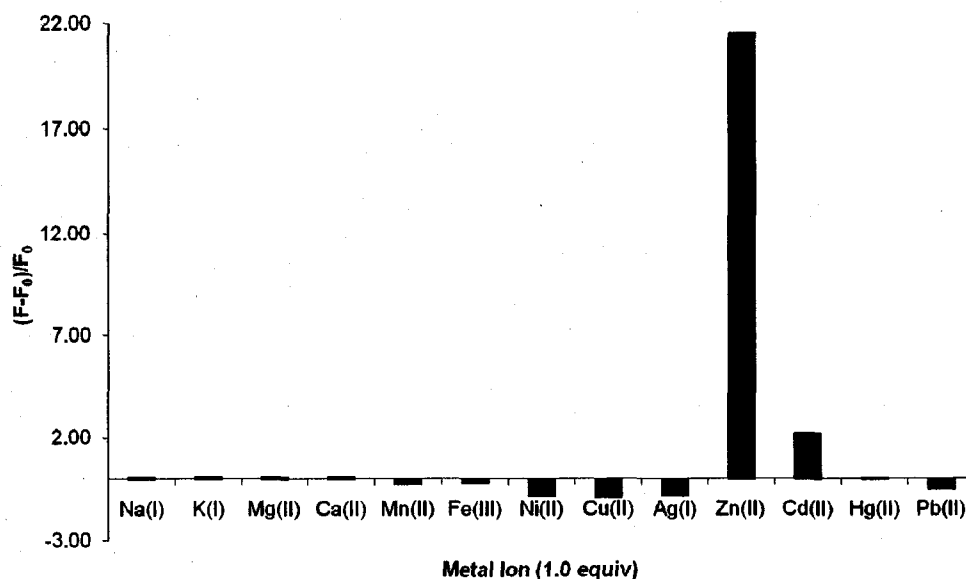


Figure 106 Screening emission enhancements of 6,7-DMTI II.119 in the presence of 1.0 equivalent of various cationic analytes. The experiments were conducted in 50% aqueous DMF at 25.0°C with $[TAMEisoquin]_{Total}=20 \mu M$.

2.15. Conclusions and future work

In sum, the tandem Ni(II)-mediated template reaction/tetrahydroborate reduction developed to prepare the novel chelator TAMEpyr **I.60** has been exploited in the preparation of novel Zn(II)-selective fluorescent sensors. The molecules TAMEisoquin **II.115** and 6,7-DMTI **II.119** possess the fluorophore-spacer-receptor design motif that is evident in many PET-based metal-ion sensors. The isoquinoliny groups allow CEF to work in concert with the PET switching mechanism. Moreover, TAMEisoquin **II.115** and 6,7-DMTI **II.119** display exquisite spectroscopic selectivity for Zn(II) with target-induced fluorescence enhancements of *ca.* 14 and 17 respectively. The measured

quantum yield for $[\text{Zn}(\text{TAMEisoquin})]^{2+}$ was a dismal 1.2%. This was improved, however, to 20% for $[\text{Zn}(6,7\text{-DMTI})]^{2+}$. Unfortunately, the emission maxima for both sensors were embedded in the UV-region of the electromagnetic spectrum. Therefore, these molecules have limited utility in the sensing of biological Zn(II) because of the current instrumental limitations. The thermodynamic stability imparted to the target analyte from the polydentate N_6 -donor set was evidenced in the measured K_d' of 1.4 fM of $[\text{Zn}(\text{TAMEisoquin})]^{2+}$. Unlike many sensors in the literature, the TAME-based chelators display excellent selectivity for Zn(II) over Cd(II). This observation may ultimately play a significant role in the design of second generation molecules. Likewise, the synthetic flexibility of the TAME podand for additional functionalization may facilitate the development of novel bifunctional luminescent sensors (**Figure 107**). It is envisioned that site-selective

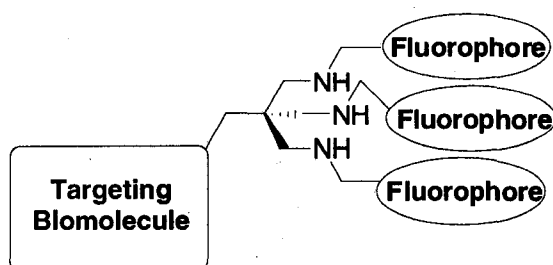


Figure 107 Generic representation of a site-selective TAME-based luminescent sensor for the cellular analysis of Zn(II).

Zn(II) sensing could be accomplished if a targeting biomolecule is attached to the peripheral methyl group of the TAME-framework. Once a visibly-emitting fluorophore is uncovered site-selective luminescent-sensing of Zn(II) in a cellular matrix will ensue

CHAPTER 3

FLUORESCENT RATIO-METRIC INDICATORS FOR TRANSITION METAL IONS: A GENERAL APPROACH

Summary

In this chapter the author will discuss how swelling polymeric networks built from N-isopropylacrylamide (NIPA) have been prepared toward the sensing of Cu(II). This body of work has been a collaborative effort between myself and Dr. Roy Planalp, Dr. W.Rudi Seitz and his student John Osambo (UNH), Dr. Shawn C. Burdette and his student Aaron Atkinson (UCONN). The author's role in this project was to synthesize strongly and weakly binding metal ion receptors to be copolymerized into the polyNIPA network. Fluorescent groups (*e.g.* naphthalyl and anthracenyl) were also copolymerized into this network which acted as luminescent reporters upon analyte recognition. Depending on the charge of the bound metal-receptor complex the polymer either became swollen or shrank. Polymer shrinking brought the donor-acceptor pair closer together such that fluorescence resonance energy transfer (FRET) increased. Conversely, reduction of like charges within the polymeric network caused the polymer to swell thus attenuating the measured FRET. The following discussion

will begin with the phenomenon of polymer swelling citing key literature reports of polymeric based sensors. Then the stage will be set for our work by describing the history of polymeric sensors as explored in the Seitz group. Lastly, the author will discuss the ligating systems he chose to synthesize to be incorporated into the polyNIPA systems and the results obtained for the sensing of Cu(II) will be presented.

3.1. Introduction

The use of polymeric materials in the development of chemical sensors for neutral and ionic analytes has become increasingly popular. Chemically induced polymer swelling is attractive as a transduction strategy because there are many ways to monitor changes in polymer properties that accompany swelling.(243) For example lightly crosslinked polymers can expand or contract with changes in temperature, solvent composition, pH, hydrostatic pressure and by external magnetic and electric fields.(244, 245) When placed in a suitable solvent system the polymer can absorb a portion of the solvent causing swelling.(246, 247) The extent of the swelling depends on two competing processes. Initially, the free energy of mixing will increase the degree of solvation of the polymer and will cause the polymer chains to radiate outward into the solution. However, as the polymer begins to expand the polymer chains will experience an elastic retraction from the cross-linking moieties. The degree of polymeric swelling is also increased by electrostatic repulsions between like-charges that may exist in the polymeric framework (e.g. between two carboxylate residues that are in close proximity to one another when the polymer is in a shrunken state).(243) A steady-state is achieved when the opposing forces of solvation and elastic retraction balance. It is said that volumetric changes within the polymeric network as large as 10-100 times can occur.(248)

Swelling polymeric networks have been exploited in the preparation of novel chemical sensors in the literature. For instance Holtz and Asher

constructed a crystalline array of polymer spheres within a hydrogel that shrink or swell in the presence of certain analytes.(249) The crystalline colloidal array diffracts visible light if the spacing between the polymer spheres increase.(250-252) Upon analyte recognition the diffracted light gives rise to an intense color change which is detectable by the naked eye. The hydrogel contained a molecular recognition group, for instance a crown-ether which demonstrated selective interactions with Pb(II) over Li(I) or K(I) (**Figure 108**). The recognition events cause the gel to swell because of the increased osmotic pressure within the gel due to a Donnan potential arising from mobile counterions to the crown ether bound Pb(II).(244, 247) The swelling increases the mean separation between the colloidal spheres and as such shifts the Bragg peak of the diffracted light to longer wavelengths (*i.e.* red shifts occurred in the visible extinction spectra of the sensing materials in the presence of the analyte).

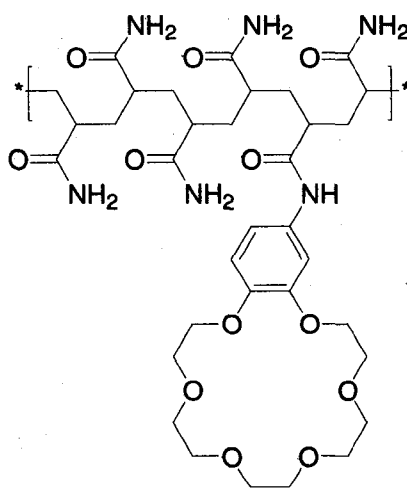


Figure 108 The structure of Holtz and Asher's Pb(II) polymeric sensor.

Optical "turn-off" sensors for the continuous monitoring of O₂ were developed by Lee *et al.* based on the quenching of the stable dye Pt-

octaethylporphyrin (PtOEP) (Figure 109).(253) The d^8 square planar complex PtOEP is a strong room temperature fluorescent dye. However, PtOEP is susceptible to intersystem crossing in the presence of triplet O_2 thus quenching the observable fluorescence. Sensing films were constructed by incorporating PtOEP into polyvinyl chloride, polystyrene or silicone matrices. The response time of the optical sensors varied from 10-100 seconds depending on the type of polymer matrix employed. Presumably the response rate of the sensor is governed by the diffusion of O_2 into the polymeric network where it can interact with the PtOEP dye. The response of the sensor was assessed using Stern-Volmer plots, which describe the emission from PtOEP as a function of O_2 concentration.(101) The sensing films maintained good operational stability. Likewise, there was no significant photo-bleaching of the material as observed over the course of one year. According to the authors the aim of this work was to detect O_2 in aerodynamic environments.

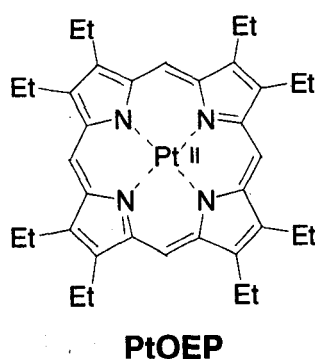


Figure 109 The structure of the luminescent dye PtOEP.

Polymeric sensors other than thin films have also been prepared and described in the literature. For example Chen *et al.* showed that the fluorescence of the water soluble polyanionic conjugated polymer [poly-(2-

methoxy-5-propyloxy sulfonate phenylene vinylene] (MPS-PPV) can be quenched by extremely low concentrations of cationic electron acceptors like *N,N'*-dimethyl-4,4'-bipyridinium (MV^{2+}) in aqueous solutions (**Figure 110**).⁽²⁵⁴⁾

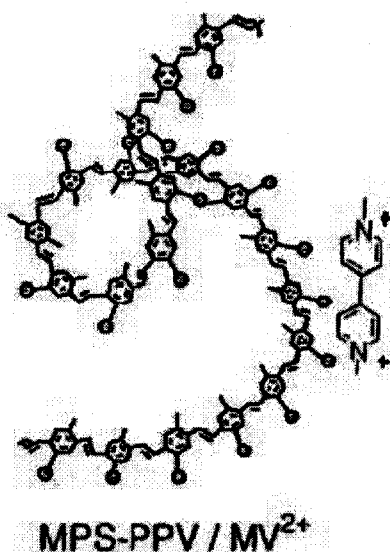


Figure 110 Fluorescence quenching of MPS-PPV with MV^{2+} . The figure was borrowed from reference (254)

Using a combination of steady-state and ultrafast spectroscopy Chen established that the fluorescence quenching arose from a complex that formed between one molecule of the polymer (which contains ~1000 monomer units) with one molecule of MV^{2+} (**Figure 110**). The MV^{2+} is said to be associated with the polymer via π -stacking forces. Transfer of excited state electrons on the polymer chain to MV^{2+} quenches the fluorescence from the polymer. The speed of these electron transfer events was clocked at 650 femtoseconds. The quenching can be selectively reversed (*i.e.* fluorescence “turned-on”) in the presence of a biotinylated derivative of MV^{2+} (**Figure 111**). The biotinylated derivative associates with the polymer in an analogous fashion as the parent MV^{2+} does

effectively quenching all the fluorescence from the polymer. Upon exposure to avidin the biotinylated derivative dissociates from the polymer and forms a strong complex with the analyte. The polymer is now free to fluoresce resulting in a highly selective sensor for avidin. This reversible fluorescence quenching provides the basis for a new class of highly sensitive biological and chemical sensors.

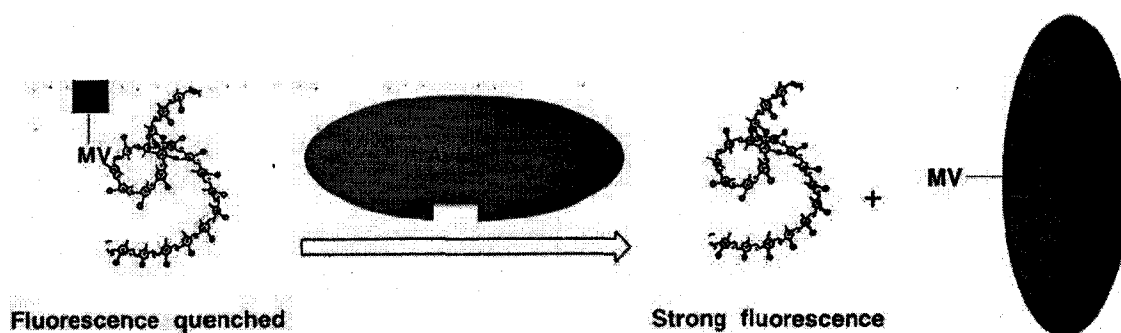


Figure 111 The reversal of MPS-PPV fluorescence quenching upon avidin binding. The functionality labeled "B" is a biotinylated residue on the polymer which has a large affinity for the analyte. The figure was borrowed from reference (254).

3.2. Previous work within the Seitz group

Our collaborators Seitz and coworkers have been interested for some time in preparing and studying swelling polymers for chemical and biological sensing. The seminal paper for this work emerged in the early 1990's with the development of a polymeric sensor that detects changes in the ionic strength of aqueous solutions (Figure 112).(255)

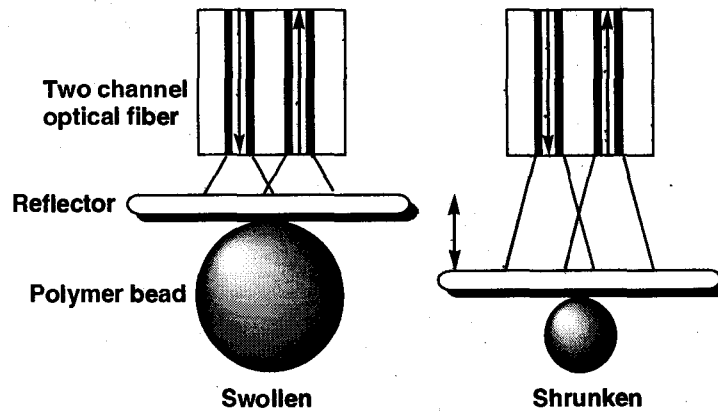


Figure 112 Polymer sensor that detects changes in the ionic strength of aqueous solutions.

The sensor was prepared from commercially available polymeric beads (*i.e.* ion exchange resins) that shrink when the ionic strength of the solution the beads were emerged was increased. The changes in polymer size were attributed to changes in osmotic pressure. As the ionic strength of the solution in contact with the beads increased the degree of solvation within the bead decreased leading to a reduction in the osmotic pressure acting on the bead. This in turn caused the bead to shrink. The polymeric beads were attached to a reflective diaphragm such that changes in polymer size caused a change in the reflector's position (indicated in **Figure 112** by the double-headed arrow). This resulted in a change in the intensity of light reflected back into a two-channel optical fiber. Increased intensity changes were observed as the amount of crosslinking within the beads was decreased. Without the restrictive forces imposed by the crosslinkers the beads were free to shrink to a greater degree allowing more light to be reflected back into the fiber optic channel. Unfortunately, the commercially obtained material was susceptible to cracking with repeated use of the sensor.

This study prompted the Seitz group to synthesize their own polymeric networks so that the physical properties of the swelling material could be tailored for specific applications, which would ultimately result in better performance of the device.(256-258) Polymer beads were constructed from poly(vinyl benzyl chloride) (Poly-VBC) because of the ease with which vinyl benzyl chloride can be polymerized. Moreover, Poly-VBC can be copolymerized with a host of comonomers which allows for the introduction of additional functionality (e.g. a receptor) for selective analyte sensing. Unfortunately, the Poly-VBC beads failed to move the reflective diaphragm shown in **Figure 112** because they did not swell with enough force.(248)

The functionalized Poly-VBC networks were instead directly attached to a fiber optic tip.(256-258) In these systems the intensity of the reflected light from the polymer-substrate interface was measured. As the polymer came in contact with the analyte (e.g. H^+) swelling or shrinking took place which led to changes in the reflected light. The observed changes were attributed to perturbations of the refractive index of the Poly-VBC network. This strategy ultimately proved problematic because of shear forces acting on the polymer-substrate interface during the swelling/shrinking process. These forces caused the delamination of the polymer from surface of the optical tip.

During the course of the aforementioned studies it was shown that functionalized Poly-VBC beads become clear upon swelling and opaque upon shrinking. This observation led to the design of a new sensing scheme. The polymeric beads were instead suspended into a hydrogel forming a cloudy

membrane. Hydrogels themselves are polymer membranes with a high degree of hydrophilicity.(257) When equilibrated in aqueous environments these polymers take up large volumes of water, yet they retain their shape. The intensity of the scattered light within the membrane was measured (Figure 113).

As the beads in the hydrogel became swollen a change

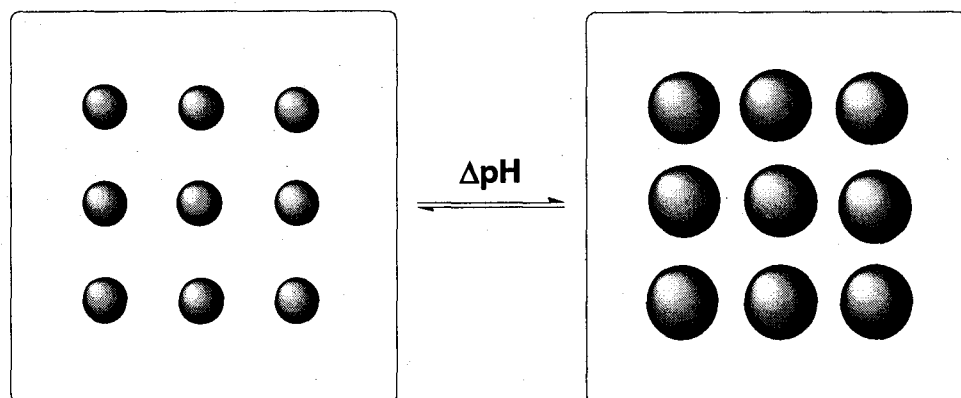


Figure 113 Swelling/shrinking polymeric beads suspended in a hydrogel membrane.

in the refractive index occurred causing changes in the turbidity of the membrane. This phenomenon has proven useful and has been employed by the Seitz group to make new chemical sensors.

In a recent paper Seitz and coworkers demonstrate that lightly crosslinked copolymers of N-isopropylacrylamide (NIPA) that contain a small amount of a recognition comonomer (2% acrylic acid) act as sensors for H^+ , Cu(II) and Pb(II) .(243) They prepared copolymers of NIPA and acrylic acid as microspheres and embedded those spheres into a poly(vinyl alcohol) (PVA) hydrogel membrane. At $\text{pH}=6$ the acrylic acid moieties were deprotonated which caused the spheres to swell because of the increased affinity of the anionic polymer for water. The swelling process was evidenced by measuring a

decrease in the turbidity within the membrane. Upon acidification the carboxylate residues are protonated causing the polymer bead to shrink which increased the turbidity within the membrane. Because it is known that carboxylate groups will coordinate divalent metal ions, thus causing a net decrease in the anionic charge in the polymer bead, Seitz and coworkers found that in the presence of Cu(II) and Pb(II) the embedded polymer beads (that contain 2% w/w acrylic acid) shrank resulting in an increase in the measured refractive index.(259, 260) Because the number of ions needed to induce a large amount of swelling within the polymer was small these membranes are potentially useful for chemical sensing applications. However, greater selectivity for different metal ion analytes needs to be achieved by incorporating comonomers with selective metal binding groups into the polymeric network. The following discussion describes a new approach to selective metal ion sensing.

3.3. Swelling polymeric networks for the detection of Cu(II) (From John Osambo, W. Rudolf Seitz, Daniel P. Kennedy, Roy P. Planalp, Aaron Atkinson, and Shawn Burdette, *submitted for publication*).

Ratiometric sensors utilize analyte-induced changes in absorption maxima, emission maxima, or both to differentiate between the free and bound sensor molecule. Ratiometric emission measurements involve monitoring the fluorescence of the bound and free sensor at a fixed excitation wavelength. The ratio of the intensities from the free and complexed form becomes the measured parameter, provided that the emission maxima for the bound and unbound sensor are sufficiently different. Ratiometric measurements are insensitive to

both the amount of indicator present and instrumental drift factors such as variation in the source intensity. These unique properties make ratiometric measurements the preferred strategy for all sensing applications, particularly intracellular sensing where control of indicator amount becomes impractical.

The limited number of available ratiometric sensors for Cu(II) attests to the difficulty in adapting sensing strategies to metal ions with intrinsic quenching effects. Even though existing small molecule sensors for Cu(II) are capable of ratiometric measurements, these strategies rely on manipulation of extinction coefficients to indirectly increase the emission intensity. The absolute quantum yield of the resulting Cu(II)-complexes often remains relatively low compared to traditional fluorescent sensors for closed-shell metal ions.

An alternative approach to preparing ratiometric sensors for transition metal ions that circumvents fluorescence quenching, involves the use of polymer architecture changes. Herein is reported the design of sensors that take advantage of the thermal phase transition properties of poly-N-isopropylacrylamide (polyNIPA).^(261, 262) Below the lower critical solution temperature (LCST) of 37°C, pure polyNIPA remains soluble in water; however, the polymer precipitates above this temperature. When crosslinked, polyNIPA swells in water below the LCST and contracts at higher temperatures. Copolymerization of NIPA with other monomers shifts the LCST of polyNIPA to lower or higher values depending on the affinity of the other monomers for water. A small percentage of a charged monomer, like a carboxylate unit, can be sufficient to completely disrupt the phase transition, which allows polyNIPA to

remain in solution at temperatures up to the boiling point. Inclusion of a comonomer also introduces heterogeneities along the polymer backbone that cause the phase transition to occur over a range of temperatures. Our approach involves copolymerizing NIPA with a ligand that binds Cu(II) and two fluorophores capable of undergoing fluorescence resonance energy transfer (Figure 114). Ratiometric data can be extrapolated using the relative FRET observed at different concentrations of Cu(II). This report compares two types of

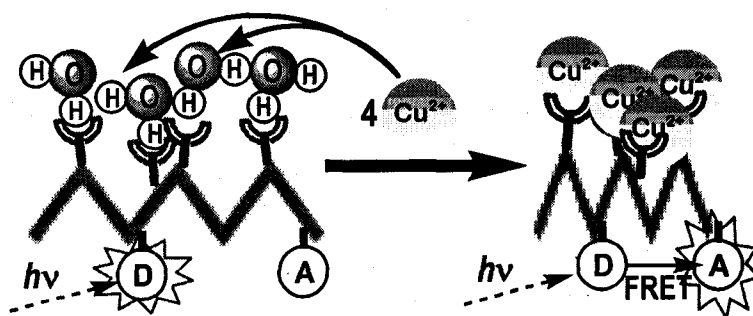


Figure 114 Representation of our novel Cu(II)-sensor.

ligands (Figure 115) with different properties that alter the polymer behavior in aqueous solution. The first ligand III.1, which contains a neutral 2,2'-bipyridyl group in the unbound state, causes the polymer to become charged upon Cu(II) binding. Under these circumstances, binding of the analyte increases the affinity of the polymer for water thus shifting the LCST to higher temperatures. The resulting swelling in the polymer upon metal binding increases the distance between the two fluorophores, which results in decreased FRET. The second ligand III.2, a phenyl iminodiacetate, carries negative charge at pH \geq 6 solutions and forms a neutral complex with the Cu(II) analyte. In contrast to the first approach, complexation reduces the affinity of the polymer for water, thus shifting

the LCST to lower temperatures and causing the polymer to contract. The resulting decrease in distance between the two fluorophores results in increased FRET. In both ligand systems complexation with Cu(II) affects the degree to which the microparticles swell or shrink in water.

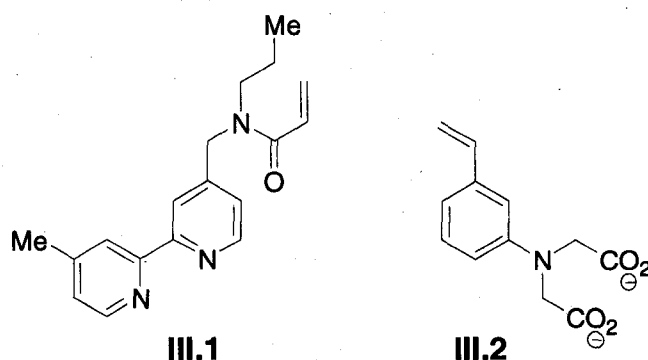


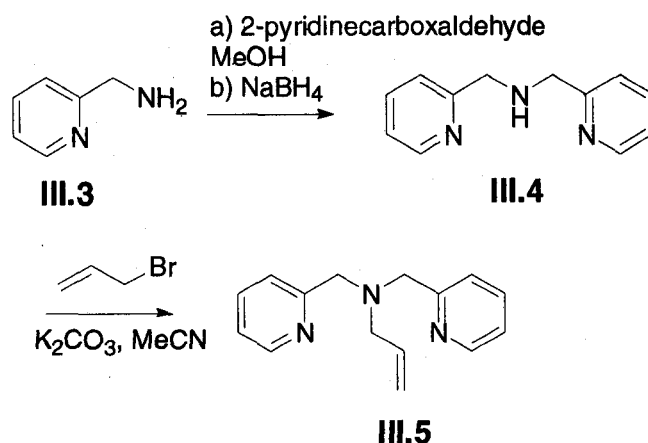
Figure 115 Ligating comonomers for FRET-based Cu(II) sensing.

Results and discussion

3.4. Preparation of metal ion receptors

This chapter describes a collaborative project between the Planalp, Seitz and Burdette groups. The role of the Planalp group was to design and synthesize ligating comonomers, which were incorporated into sensing polymers by the Seitz group.

The first monomer prepared was based on dipicolylamine (DPA) (Scheme 44).

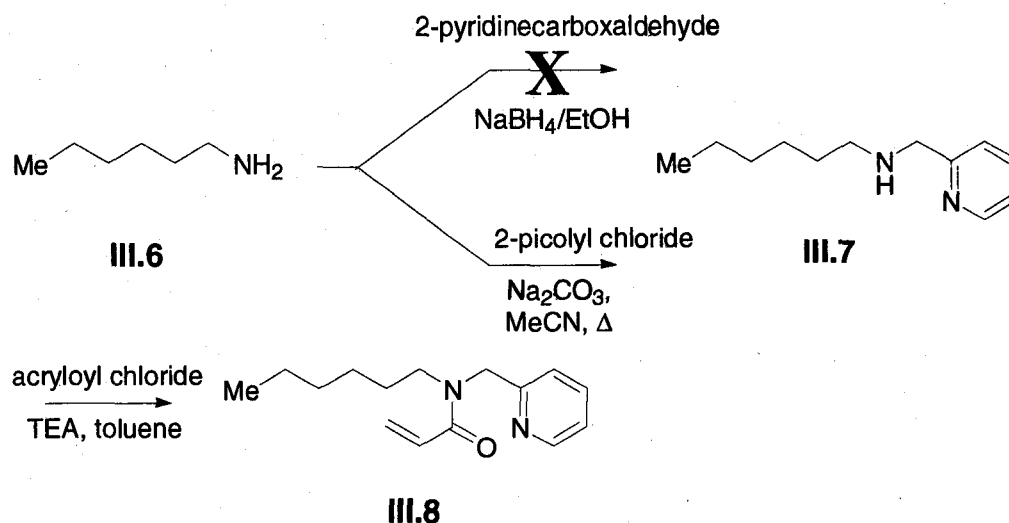


Scheme 44 The preparation of allylated DPA **III.5**.

The choice of DPA as the ligating unit stems from its extensive use as a Zn(II)-receptor in small molecule luminescent sensors.^(126, 135, 136) The short two-step reaction sequence to prepare the allyl DPA began with a condensation between 2-aminomethylpyridine **III.3** and 2-pyridinecarboxaldehyde followed by the *in situ* reduction of the resulting imine intermediate with NaBH₄. A polymerizable allyl tether was appended to the secondary amine of DPA **III.4** via alkylation with allyl bromide. The resulting product required chromatography on basic aluminum oxide to free the desired compound **III.5** from impurities generated during the course of the reaction. Preliminary data from the Seitz group suggested that introduction of allyl DPA into the NIPA framework caused the polymer to expand when it was in the presence of Cu(II) at pH=6. It was reasoned that the monocationic DPA receptor (monoprotonated at pH=6 because $pK_{a1} \sim 10$) will bind Cu(II) displacing a proton and forming a +2 charged complex. This will facilitate polymer swelling because of increased electrostatic repulsions between the bound receptors. The observed polymer swelling resulted in a decrease in the measured FRET between the naphthalene and anthracene

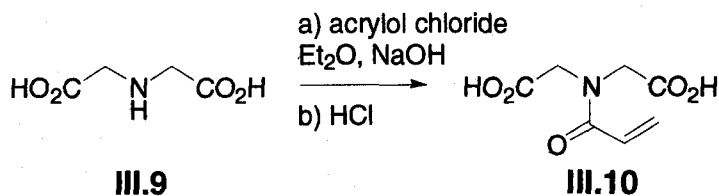
fluorescent groups (data not shown). As mentioned in chapter 2 of this dissertation the FRET phenomenon is heavily dependant on distance between the donor-acceptor pair. Additional data from the Seitz group is needed to complete the analysis.

Another comonomer was synthesized that possessed a lipophilic *n*-hexyl tail (**Scheme 45**). The aliphatic group was selected to increase the distance between the metal binding groups in the polymer. It was envisioned that increasing the distance will attenuate the effect of electrostatic repulsions between bound receptors and thus support the hypothesis that metal binding is principally responsible for polymer swelling. Reductive amination failed to afford the desired synthetic intermediate **III.7** in acceptable yields (*ca.* 10% conversion based on the crude ¹H-NMR). Instead alkylation of *n*-hexylamine with 2-picolyl chloride yielded compound **III.7** which was subsequently purified by reduced pressure distillation (bp=90-93°C, P=95-100mTorr). The secondary amine of compound **III.7** was acylated with acryloyl chloride affording the comonomer **III.8**. No attempts have been made so far on the polymerization of compound **III.8** into the NIPA networks.



Scheme 45 Preparation of a lipophilic comonomer.

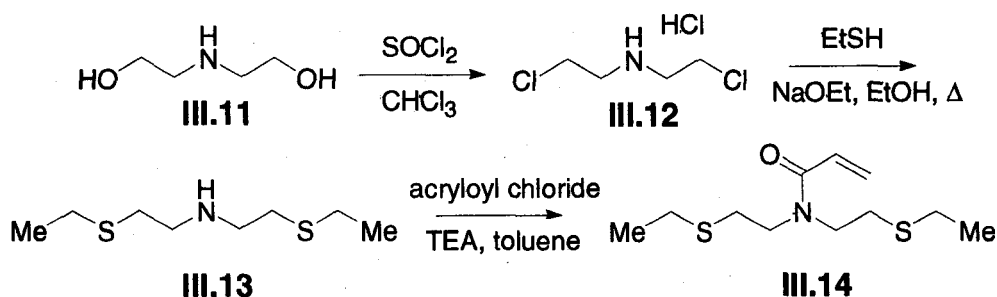
The utility of the iminodiacetate (IDA) group as a cation receptor in small molecule luminescent sensors prompted us to prepare compound **III.10** (Scheme 46). The desired product was easily obtained pure as a white crystalline solid upon neutralization of the reaction mixture. Careful control of the amount of HCl delivered during the workup prevented the polymerization of the isolated product.



Scheme 46 Preparation of acryloyl-IDA.

However, the limited solubility of compound **III.10** proved to be problematic during the polymerization process. As such this compound was not pursued for further study.

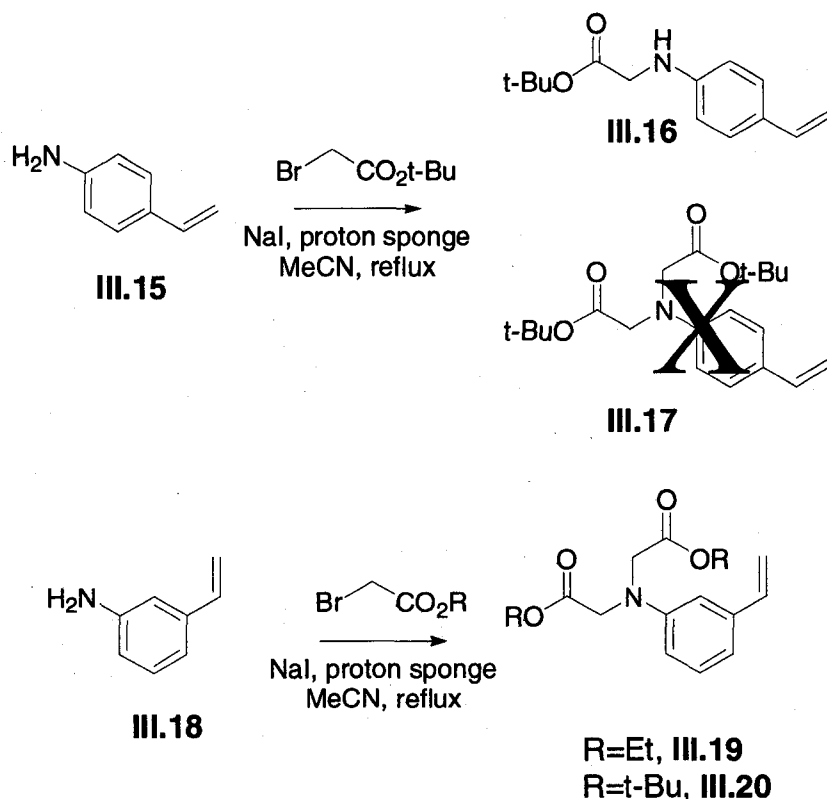
The IDA framework was further exploited in the preparation of a thioether which was envisioned to act as a receptor for softer metal ions like Pb(II) or Hg(II) (**Scheme 47**). The terminal hydroxyl groups of the diethanolamine **III.11**



Scheme 47 Preparation of an acryloyl-thioether receptor for soft metal ions.

substrate were replaced with chlorides using thionyl chloride. The resulting ammonium salt **III.12** then underwent a thioetherification reaction with ethane thiol and sodium ethoxide which afforded the linear dithioether **III.13**. The secondary amino group was acylated with acryloyl chloride affording compound **III.14**.

The IDA receptor was also integrated into a styrenyl scaffold (**Scheme 48**). Attempts at the preparation of compound **III.17** was met with failure. The 4-vinylaniline substrate **III.15** could only be monoalkylated resulting in the production of compound **III.16**. It was hypothesized that both the electron withdrawing vinyl group *para* to the anilino nitrogen working in concert with a steric effect introduced upon monoalkylation prevents the formation of the desired dialkylated product. This prompted us to move the vinyl group *meta* to

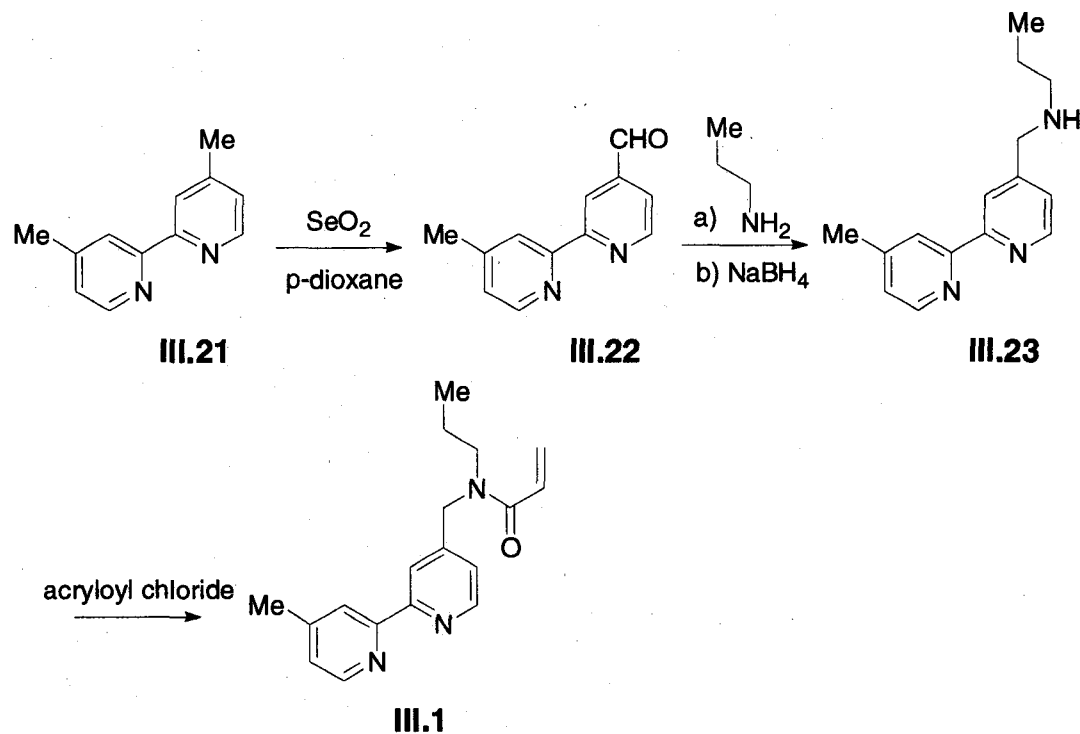


Scheme 48 Preparation of phenyl-IDA ligating comonomers.

the nucleophilic nitrogen which indeed, under identical reaction conditions, furnished the desired dialkylated product. Proton sponge (1,8-bis(dimethylamino)naphthalene) was used because of its relative high pK_a of 12.34 for its conjugate acid in aqueous solution.⁽²⁶³⁾ It is one of the strongest amine bases known where the high basicity is attributed to the relief of strain upon protonation between the nitrogen lone pairs. However, the molecule is sterically hindered, making it a weak nucleophile. Because of this combination of properties, proton sponge has been used in organic synthesis as a highly selective non-nucleophilic base. Both the ethyl ester III.19 and t-butyl ester III.20 were prepared so that multiple deprotection strategies could be tested once the pro-ligating group had been incorporated into the polymeric network. The t-butyl

group can be converted into the corresponding carboxylic acid with trifluoroacetic acid (TFA) whereas the ethyl ester can be hydrolyzed with mineral acids like HCl or H₂SO₄.(264)

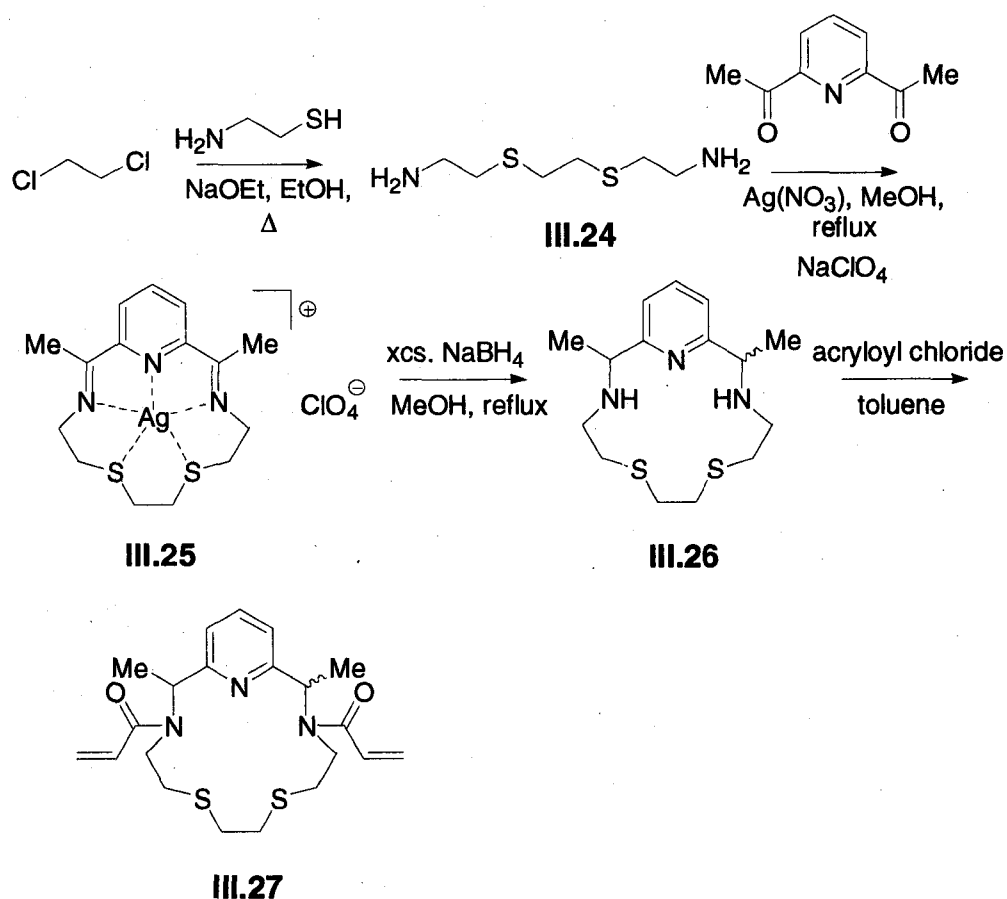
Our collaborator's Burdette and Atkinson prepared a bipyridyl based comonomer. Their synthesis began with a SeO₂ oxidation of the substrate **III.21**. The monoaldehyde **III.22** was isolated from the reaction mixture and reductively aminated with *n*-propylamine giving the secondary amine **III.23** which was then acylated with acryloyl chloride affording the desired compound **III.1**.



Scheme 49 The synthesis of Burdette and Atkinson's 2,2'-bipyridyl comonomer **III.1**.

The results of polymerization and sensor characterization for the *t*-butyl ester **III.2** and the bipy derivative **III.1** are described in the next section.

We are also interested in preparing macrocyclic receptors for Pb(II) and Hg(II). Our first entry into this class of compounds is a diacryloyl derivative of an N_3S_2 macrocycle recently reported by Xiao *et al.*(265) This molecule was chosen because it offers soft (S) and borderline (N) donor groups that are well-suited for Pb(II) and Hg(II) complexation. Molecule **III.27**, however, possesses two complicating features related to rotational isomerism and its expected polymerization behavior.

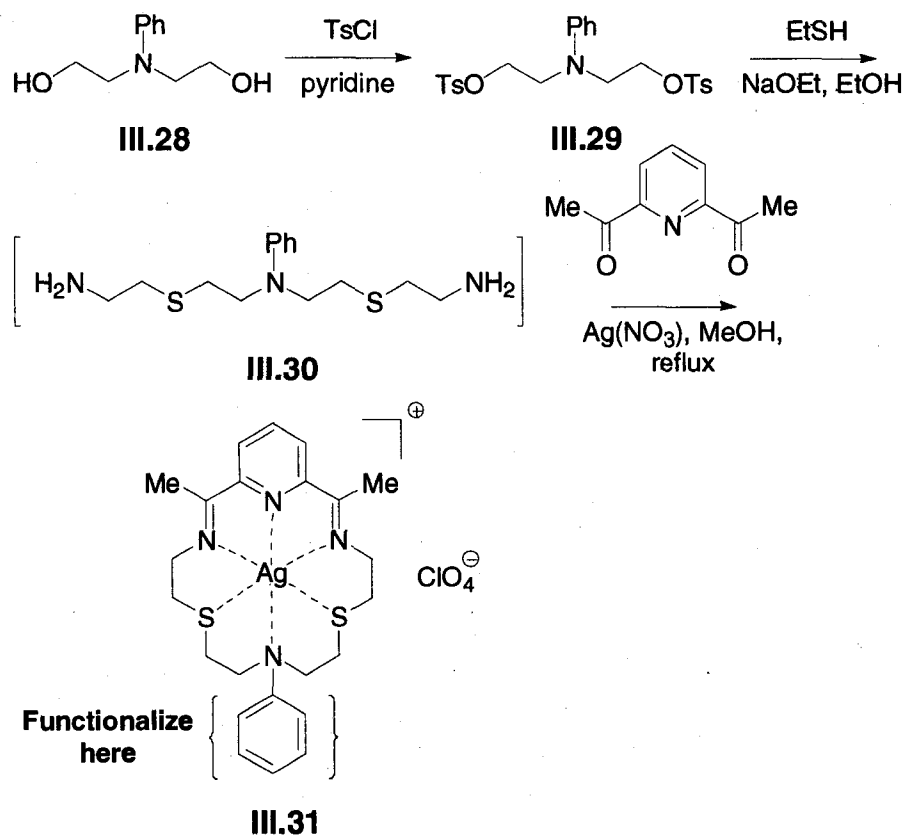


Scheme 50 Preparation of an N_3S_2 macrocycle to serve as a Hg(II) or Pb(II) receptor.

The synthesis began with a thioetherification of 1,2-dichloroethane which afforded the linear diamine **III.24**. The next step of the reaction sequence was a

silver-mediated template reaction of 2,6-diacetylpyridine, which upon anion exchange, gave the desired Schiff-base silver complex **III.25**. The complex was subjected to reductive demetallation conditions to afford three isomers of the N_3S_2 macrocycle (*meso* and D,L pair) **III.26**. The secondary amino groups were acylated with acryloyl chloride to afford the desired monomer **III.27**. This molecule is unique in that the presence of two polymerizable acryloyl groups allows the material to act as both the receptor and cross-linker.

Work is underway in preparing mixed N_xS_y macrocyclic receptors that will possess only one polymerizable functionality. This is envisioned to simplify the polymerization process. A novel model system has been prepared straightforwardly (**Scheme 51**). The synthesis began with tosylation of the *N*-phenyl diethanolamine substrate **III.28**. The tosylates were subsequently displaced by 2-aminoethanethiol in a refluxing mixture of sodium ethoxide and absolute ethanol. The resulting linear triamine **III.30** was used as is in the silver-mediated template reaction of 2,6-diacetylpyridine affording the desired ligating scaffold in complex **III.31**. It is envisioned that introduction of either an acryloyl or vinyl group on the phenyl ring will ultimately grant access to a useful collection of comonomers. No attempts at measuring the metal binding ability of the N_4S_2 or N_3S_2 macrocycles have been made.



Scheme 51 Preparation of a model N₄S₂ macrocycle.

3.5. Sensors prepared with the phenyl-IDA comonomer III.2 and bipyridyl comonomer III.1 (From John Osambo, W. Rudolf Seitz, Daniel P. Kennedy, Roy P. Planalp, Aaron Atkinson, and Shawn Burdette, *submitted for publication*)

The redox active Cu(II) ion was selected as the target analyte for this new approach to metal ion sensing because of its quenching nature. The 2,2'-bipyridyl III.1 and phenyl iminodiacetate III.2 comonomers were selected as the receptors because of the well-studied coordination chemistry of these ligands as well as their changes in charge upon analyte recognition. The bipyridyl ligand III.1 was copolymerized with NIPA via the acryloyl group to make the sensor. The *tert*-butyl ester pro-ligand III.20 was copolymerized with NIPA via the pendant

vinyl group. The ester-containing polymer was treated with acid providing the desired polymer-bound imininodiacetate ligand **III.2**. Naphthalene methacrylate **III.33** and 9-vinyl anthracene **III.32** were included in the polymer formulation to introduce a FRET pair (**Figure 116**). FRET-based systems that utilize naphthalene as the donor and anthracene as the acceptor have been reported previously.^(266, 267) This FRET pair was a convenient option to test our model sensor system because the required monomers are commercially available. Naphthalene and anthracene will shift the LCST to lower values because they are nonpolar, which enhances the FRET in the absence of charged ligands or metal ions since the polymer contracts.

Copolymer microparticles were prepared exclusively by Osambo and Seitz via dispersion polymerization at 60 °C in acetonitrile using azoisobutyrylnitrile

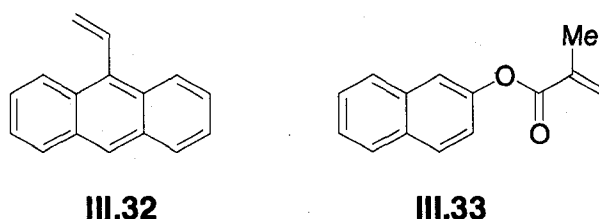


Figure 116 Monomeric FRET pair for incorporation into the swelling polyNIPA polymers. The naphthalene monomer acts as the donor and the anthracene monomer acts as the acceptor.

(AIBN) as the initiator and a styrene/acrylonitrile copolymer as a stabilizer.

Sensors were obtained from polymeric formulations containing ca. 5 mole % ligand, 5 mole % methylenebisacrylamide crosslinker, 90 mole % NIPA, 0.2 mole % naphthalene methacrylate **III.33** and 0.05 mole % vinyl anthracene **III.32**. The concentrations of Cu(II) were determined by excitation of the naphthalene at 260 nm, and measuring the ratio of anthracence emission at 421 nm to naphthalene

emission at 355 nm. This ratio increases as the copolymer shrinks bringing the donor and the acceptor closer together, or decreases when the polymer expands and the distance between the donor and acceptor increases. Fluorescence experiments were carried out at pH=6.0 to prevent the formation of metal hydroxide complexes. The bipyridyl ligand **III.1** is in its neutral form and the phenyliminodiacetate **III.2** is in the dianion form at pH 6, which prevents proton-induced changes in polymer structure.

Figure 117 illustrates how the intensity ratio varies with added Cu(II) for the copolymer prepared using the bipyridyl ligand **III.1**. The intensity ratio decreases with added Cu(II) up to a concentration of approximately 7×10^{-7} M, consistent with decreased FRET as the consequence of particle expansion resulting from charge accumulation on the polymer chain. Depending on the binding constant of the receptor with the target metal ion these sensors can either operate as indicators sampling the matrix for the analyte or as stoichiometric sensors which removes all analyte from the matrix. The intensity ratio does not change at higher concentrations of Cu(II). The sensor behavior reflects a linear relationship between the moles of added Cu(II) and moles of ligand in the copolymer that corresponds to continuing fluorescence ratio decreases up to a saturation point of 1:1 Cu(II):bipyridyl ligand in the polymer particle. At 50 °C, the copolymer particle is initially more compact increasing FRET. As a result of the temperature-dependent change in polymer architecture, the initial intensity ratio is higher, and the magnitude of decrease in the fluorescence ratio when titrated with Cu(II) increases.

9-Vinylanthracene: 2-Naphthylmethacrylate fluorescence intensity ratio vs. concentration of Cu^{2+} solution added to polymer suspension

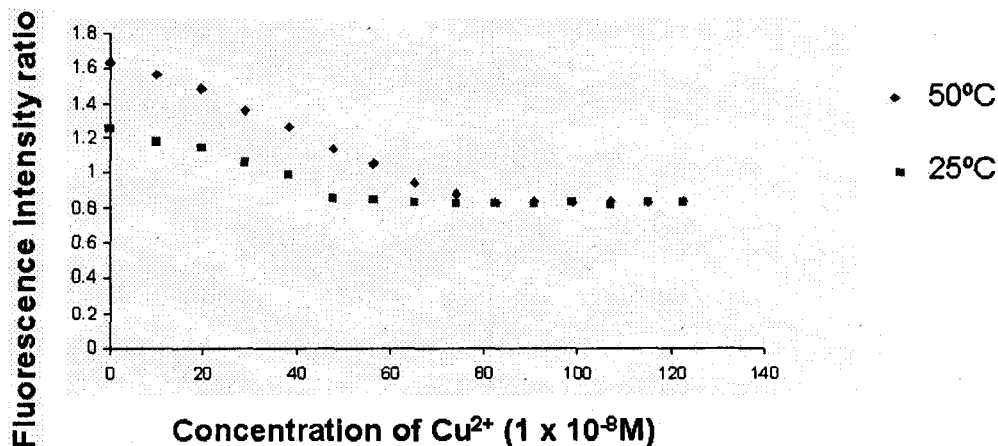


Figure 117 Cu(II) titration of polyNIPA doped with compound III.1

The phenyl iminodiacetate **III.2** containing polymeric sensors also demonstrate architecture driven fluorescence changes, but exhibit different behavior because of the charged metal chelator. **Figure 118** depicts the effects of Cu(II)-binding on the anthracene to naphthalene intensity ratio for the sensor particles. In contrast to the bipyridyl system, the free ligand is charged and the metal complex is neutral. Added Cu(II) neutralizes the charge on the ligand and causes particles to contract, which increases FRET. The ratio increases with added Cu(II) up to *ca.* 5.0×10^{-7} M. Only modest changes in fluorescence intensity are observed upon further addition of Cu(II). The fluorescence changes are consistent with the formation of 1:1 Cu(II):ligand complexes in the polymer particles.

9-Vinylanthracene:2-Naphthylmethacrylate fluorescence Intensity ratio vs. concentration of Cu²⁺ ions added to polymer suspension

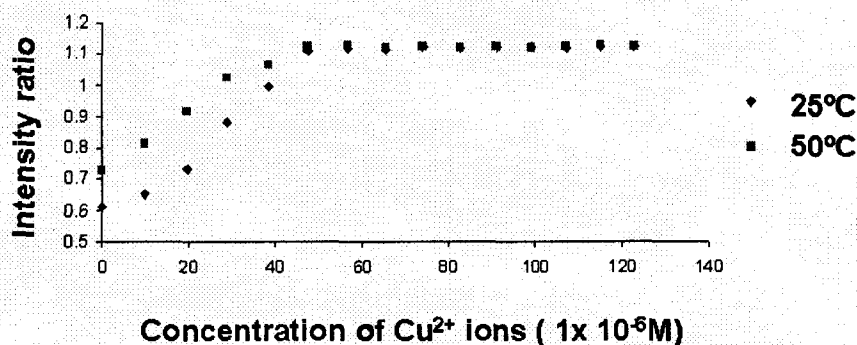


Figure 118 Cu(II) titration of polyNIPA doped with compound III.2

3.6. Conclusions and future work

These experiments demonstrate a general approach to detecting metal ions like Cu(II) that normally quench fluorescence. There is promise that sensitive sensors can be produced, because the fluorescence ratio changes are large, ranging from ca. 0.2 to 0.8 in the case of phenyl iminodiacetate, and from 1.6 down to 1.0 for bipyridyl at 50°C. Future experiments will address shifting the emission wavelengths away from UV wavelengths by examining other FRET pairs. Other ligands will also be screened to address issues of metal ion selectivity and affinity. Ligand selection only requires a change in ligand charge from the free to complexed form, and that backbone modification for copolymerization with NIPA be feasible. Choosing a different acrylate can vary the temperature sensitivity of the sensor particles. Poly(*n*-propylacrylamide) has a LCST of 25°C, 12 degrees lower than polyNIPA, and the LCST can be tuned to any desired temperature by blending acrylamides.(268)

This approach effectively separates the metal ion binding function and the reporting function of the fluorophore into two different parts of the polymer, so that the sensor may bind metal ions without fluorescence quenching. Furthermore, by relying on fluorescence resonance energy transfer, this approach capitalizes on the advantages of ratiometric measurements.

CHAPTER 4

EXPERIMENTAL SECTION

4.1 General methods

Melting points (mp) were recorded on Mel-Temp II capillary melting point apparatus and are reported uncorrected.

Infrared spectra (IR) were recorded on a Nicolet 205 FTIR spectrometer and absorptions are reported in wavenumbers (cm^{-1})

Flash column chromatography was performed with Sorbent Technologies silica gel (32-63 μm).

Thin layer chromatography was performed with Whatman 250 μm silica gel UV₂₅₄ polyester plates (CAT NO 4410 222). The developed plates were also visualized with p-anisaldehyde and phosphomolybdic acid stains.

¹H-NMR spectra were recorded on a Varian *Mercury* 400 MHz NMR spectrometer operating at 399.749 MHz. Chemical shift (δ) values are reported in ppm relative to tetramethylsilane (TMS). Coupling constants are reported in Hertz (Hz).

¹³C-NMR spectra were recorded on a Varian *Mercury* 400 MHz NMR spectrometer operating at 100.516 MHz. Chemical shift (δ) values are reported in

ppm relative to TMS unless otherwise noted. All spectra were obtained decoupled.

Low resolution mass spectra (MS) were recorded on either a Thermo-Finnegan, Finnegan LCQ quadrupole ion-trap mass spectrometer with electrospray ionization for liquid-phase analytes (ESI) with help from Mr. Kevin Bullock or a Shimadzu Group, Kratos Analytical Division, Axima-CFR MALDI-TOF matrix-assisted laser desorption, time-of-flight mass spectrometer (MALDI-TOF) with help from Mrs. Orjana Terova. The methods of ionization are reported for the individual experiments. The matrix used for all the MALDI-TOF measurements was genesic acid. The instrument was calibrated with C_{60} at $m/z=720.0$.

High resolution mass spectra (HR-MS) were conducted by the MS facility at the University of Notre Dame. The method of ionization was fast atom bombardment (FAB) in the positive (+) detection mode. A glycerol matrix was employed in all the measurements.

Elemental analysis (CHN) were performed by Atlantic Microlabs, Inc. using combustion based automatic analyzers.

UV-visible-near infrared absorbance spectra (UV-vis-near IR) were recorded on a Varian Cary 50 spectrophotometer and absorptions are reported in both nanometers (nm) and wavenumbers (cm^{-1}). Molar absorptivities are reported in $cm^{-1}M^{-1}$.

Fluorescence spectra were recorded on a Varian Cary Eclipse Fluorescence spectrometer. Emission wavelengths are reported in nm. Emission intensities were recorded in arbitrary units (a.u.).

Electron Resonance spectra (EPR) were recorded on an X-band (9.5 GHz) Bruker EleXsys E-500 cw-EPR/ENDOR spectrometer with help from professor N. Dennis Chasteen and Dr. Fadi Bou-Abdallah.

X-ray crystallography experiments were carried out by Dr. Arnold Rheingold and Dr. Antonio DiPasquale at the University of California San Diego crystallography facility. Details about each experiment are reported in tables found throughout the text of this dissertation.

Magnetic moments (μ_{eff}) were measured by Evan's NMR method using residual CD_2HCN , $\text{CD}_2\text{HSOCD}_3$ or 5% t-butanol (v/v) as indicator in both the sample and closed capillary.⁽⁶⁷⁾ All magnetic moments are reported in Bohr Magnetons (BM).

4.2. Solvents

Absolute ethanol (EtOH) was obtained from Pharmco Chemical Co. and was used as is.

Acetic anhydride (Ac_2O) was obtained from Mallinckrodt and used as is.

Acetone was obtained from Fischer Chemical Co. and used as is

Acetonitrile (MeCN) was obtained from Aldrich Chemical Co. as spectrophotometric grade.

Chloroform (CHCl₃) was obtained from EMD Chemical Co. and used as is.

Diethylether (Et₂O) was obtained from VWR international and was distilled from Na⁰ and benzophenone prior to use.

Dimethylformamide (DMF) was obtained from Fischer Chemical Co. and was used as is.

Dimethylsulfoxide (DMSO) was obtained from Fischer Chemical Co. and was used as is.

Deuterated NMR solvents (DMSO-*d*₆, CDCl₃, MeCN-*d*₃, D₂O) were obtained from Cambridge Isotope Laboratories and used as is. With the exception of D₂O the remaining solvents were stored in a dessicator that contained a pad of Drierite™ in between use.

Ethylacetate (EtOAc) was obtained from EMD Chemical Co. and was fractionally distilled before use.

Ethylene glycol was obtained from Alfa Aesar and used as is.

Glacial acetic acid (HOAc) was obtained from EM Science and used as is.

Hexanes was obtained from Pharmco Chemical Co. and was fractionally distilled prior to use.

Isopropyl alcohol (*i*PrOH) was obtained VWR and used as is.

Nitromethane (MeNO₂) was obtained from Mallinckrodt and used as is.

Methanol (MeOH) was obtained from Aldrich Chemical Co. as spectrophotometric grade and was used as is.

Methylene Chloride (DCM) was obtained from EMD Chemical Co. and was used as is.

p-Dioxane (1,4-dioxane) was obtained from Aldrich Chemical Co. and was distilled from Na⁰ and benzophenone and stored over 4Å sieves prior to use.

p-Cymene was obtained from Aldrich Chemical Co. and was used as is.

Pyridine was obtained from Fischer Chemical Co. and was distilled and stored over 4Å sieves prior to use.

Tetrahydrofuran (THF) was obtained from EMD Chemical Co. and was distilled from Na⁰ and benzophenone prior to use.

Toluene was obtained from EMD Chemical Co. and was stored over 4Å sieves prior to use.

4.3. Reagents

Table 15 Reagents used and their commercial sources

Reagent	Commercial Source
1,1,1-Tris(hydroxymethyl)ethane	Acros Organics
1,2-Dichloroethane	Fisher Scientific
10% Palladium on active carbon (Pd/C)	Lancaster
1-Isoquinoline carboxylic acid	Alfa Aesar
2,4-Dimethoxybenzaldehyde	Alfa Aesar

Table 14 continued...	
2,4-Pentanedione	Eastman Kodak Co.
2,6-Diacetylpyridine	Aldrich
2-Aminomethylpyridine (AMPY)	Aldrich
2-Aminothiophenol	Aldrich
2'-Hydroxyacetophenone	Acros
2-imidazolecarboxaldehyde	Lancaster
2-Picolyl hydrochloride	Aldrich
2-Pyridinecarboxaldehyde	Aldrich
2-thiazolecarboxaldehyde	Aldrich
3,4-Dimethoxybenzaldehyde	Aldrich
30% hydrogen peroxide (H ₂ O ₂)	EMD
3-Vinylaniline	Aldrich
4-Dimethylaminopyridine (DMAP)	Aldrich
α-Bromo tert-butylacetate	Aldrich
Acryloyl chloride	Aldrich
Allyl bromide	Lancaster
Ammonium acetate (NH ₄ OAc)	J.T. Baker
Ammonium formate (NH ₄ O ₂ CH)	Fisher Scientific
Ammonium hydroxide (NH ₄ OH)	Fisher Scientific
Benzene sulfonylchloride	Acros Organics
Benzoyl chloride (BzCl)	Aldrich
Benzyl bromide (BnBr)	Acros Organics
Benzyl cyanide (BnCN)	Aldrich
Bismuth nitrate pentahydrate (Bi(NO ₃) ₃ ·5H ₂ O)	Alfa Inorganics
Cadium(II) nitrate tetrahydrate (Cd(NO ₃) ₂ ·4H ₂ O)	Fisher Scientific
Celite®	Fisher Scientific
Cetytrimethylammonium bromide (CTABr)	Alfa Products
Chromium chloride hexahydrate (CrCl ₃ ·6H ₂ O)	Mallinckrodt
Cobalt(II) tetrafluoroborate hexahydrate (Co(BF ₄) ₂ ·6H ₂ O)	Aldrich
Copper(II) perchlorate hexahydrate (Cu(ClO ₄) ₂ ·6H ₂ O)	Aldrich
Cysteamine	Sigma-Aldrich
Diethanolamine	Lancaster
Dimethylformamide dimethylacetal (DMFDMA)	Aldrich
Ethanethiol (EtSH)	Aldrich
Ethylene glycol	Alfa Aesar
Formic acid	Aldrich
Hippuric acid	Aldrich
Hydrochloric acid (HCl)	EM Science

Table 14 continued...

Hydroxylamine hydrochloride (NH ₂ OH·HCl)	Acros Organics
Iminodiacetic acid (IDA)	W.R. Grace & Co.
Indium(III) nitrate pentahydrate (In(NO ₃) ₃ ·5H ₂ O)	Alfa Aesar
Iron(II) perchlorate hexahydrate (Fe(ClO ₄) ₂ ·6H ₂ O)	Aldrich
Iron(II) sulfate (FeSO ₄)	Mallinckrodt
Isoquinoline	Eastman Organic Chemical Co.
Lithium aluminum hydride (LiAlH ₄)	Aldrich
Lithium borohydride (LiBH ₄)	Aldrich
Magnesium sulfate (MgSO ₄)	EMD
Manganese(II) perchlorate hexahydrate (Mn(ClO ₄) ₂ ·6H ₂ O)	Aldrich
<i>N,N,N',N'</i> -Tetrakis(2-pyridylmethyl)ethylenediamine (TPEN)	TCI Organics
<i>n</i> -Hexylamine	Aldrich
Nickel perchlorate hexahydrate (Ni(ClO ₄) ₂ ·6H ₂ O)	GFS Chemical Co.
<i>N</i> -Phenyldiethanolamine	Aldrich
Oxalyl chloride	Acros Organics
Paraformaldehyde	Professor Edward Wong
Pentaerythritol	Analabs, Inc.
Pentaerythritol bromide	Fisher Scientific
Perchloric acid (HClO ₄)	Fisher Scientific
Phosphorus tribromide (PBr ₃)	Aldrich
Polyphosphoric acid (82% P ₂ O ₅)	Acros Organics
Potassium bromide (KBr)	Acros
Potassium carbonate (K ₂ CO ₃)	Flinn Scientific, Inc.
Potassium cyanide (KCN)	Mallinckrodt
Potassium hydroxide (KOH)	Fisher Scientific
Potassium iodide (KI)	J.T. Baker
1,8-Bis(dimethylamino)naphthalene (Proton Sponge™)	Aldrich
<i>p</i> -Toluenesulfonamide (pTsNH ₂)	Alfa Aesar
<i>p</i> -Toluenesulfonic acid (pTsOH)	Aldrich
Pyridoxine hydrochloride	Acros Organics
1-Quinolinecarboxylic acid (quinaldic acid)	Alfa Aesar
1,3-dihydroxybenzene (resorcinol)	Fisher Scientific
Salicylaldehyde	Aldrich
Selenium dioxide (SeO ₂)	Aldrich
Silver(I) nitrate (AgNO ₃)	Aldrich
Sodium acetate (NaOAc)	Mallinckrodt

Table 14 continued...	
Sodium azide (NaN ₃)	Matheson Colemann & Bell
Sodium bicarbonate (Na ₂ CO ₃)	Fisher Scientific
Sodium bisulfite (NaHSO ₃)	Fisher Scientific
Sodium borohydride (NaBH ₄)	Aldrich
Sodium carbonate (Na ₂ CO ₃)	Fisher Scientific
Sodium carbonate hydrate (Na ₂ CO ₃ ·H ₂ O)	EM Science
Sodium chloride (NaCl)	Fisher Scientific
Sodium cyanide (NaCN)	Mallinckrodt
Sodium hydroxide (NaOH)	VWR International
Sodium iodide (NaI)	J.T. Baker
Sodium metal (Na ⁰)	Fisher Scientific
Sodium methoxide (NaOMe)	Fisher Scientific
Sodium nitrite (NaNO ₂)	Aldrich
Sodium perchlorate hydrate (NaClO ₄ ·H ₂ O)	Sigma
Sodium sulfate (Na ₂ SO ₄)	EMD
Sulfuric acid (H ₂ SO ₄)	J.T. Baker
Thionyl chloride (SOCl ₂)	Alfa Aesar
T-Hydro®	Aldrich
Triethylamine (TEA)	Aldrich
Trifluoroacetic acid (TFA)	Aldrich
Triphenylphosphine (PPh ₃)	Aldrich
Zinc(II) perchlorate hexahydrate (Zn(ClO ₄) ₂ ·6H ₂ O)	Aldrich

4.4. Synthesis and Characterization

Standard synthetic laboratory techniques were employed in the preparation of the following compounds. Drying was accomplished under a stream of nitrogen or under reduced pressure (*ca.* 10⁻² Torr) with a standard Schlenk line.

Anaerobic manipulations were accomplished under a nitrogen atmosphere in a glovebox (VAC model HE-43 with HE-493 purifier).

Caution: perchlorate salts and organic azides can be explosive and should be handled with care. No explosions occurred during the course of this work.

4.4.1 Chapter 1 Experimentals

1,1,1-Tris(bromomethyl)ethane I.29

To 1,1,1-tris(hydroxymethyl)ethane (11.3 g, 94.0 mmol) was added neat PBr_3 (38.9 g, 144 mmol) via a pressure equalizing funnel over a period of 2 h. The resulting colorless oil was stirred 30 minutes at 100°C . The temperature was then elevated to $170\text{--}180^\circ\text{C}$ and the reaction mixture was stirred for 4 days. The resulting orange oil was cooled to room temperature and suspended in a mixture of 100 mL of tap water and 100 mL of CHCl_3 . The mixture was shaken vigorously and filtered through paper by gravity. The resulting two-phases were separated and the aqueous layer was extracted with additional CHCl_3 (3x25 mL). The pooled organic fractions were then washed with saturated aqueous NaHCO_3 (3x100 mL), brine (3x100 mL) and then dried over excess anhydrous Na_2SO_4 . After decanting away from the drying agent the solvent was removed on a rotary evaporator affording a pale yellow oil that was subsequently distilled (b.p. $119^\circ\text{C}/10\text{ mmHg}$) yielding 8.8 g (64%) of the product as a colorless liquid. $^1\text{H-NMR}$ (CDCl_3): 3.50 (6H, s, methylene H's); 1.29 (3H, s, methyl H's). $^{13}\text{C-NMR}$ (CDCl_3) δ : 39.80, 39.20, 21.79. IR (KBr pellet) $\bar{\nu}$: 2971, 2933, 1459, 1422, 1377, 1269s, 866, 851, 688, 663 cm^{-1} .

1,1,1-Tris(benzenesulfonyloxymethyl)ethane I.31

Into a 500 mL two-way RBF equipped with a Teflon coated stir bar was added 10.0 g (83.2 mmol) of 1,1,1-tris(hydroxymethyl)ethane and 44.0 mL of dry pyridine. The flask was then fit with a pressure equalizing drop funnel and N₂ inlet. The funnel was charged with 38.2 mL (52.9 g, 300 mmol) of benzenesulfonyl chloride and the RBF was immersed in an ice bath. After purging the headspace with N₂ for 10 min the stopcock was cracked and the contents of the funnel were added dropwise to the RBF over the course of 1 hr. The resulting white slurry was then allowed to warm to RT and stand for 16 hr. Into a 1 L Erlenmeyer flask was added 80 mL of H₂O, 160 mL of MeOH and 60 mL of concentrated HCl. The slurry was then poured into the Erlenmeyer flask and the resulting granular solids were stirred vigorously for 0.5 hr. The solid material was filtered through a glass frit via vacuum. The filter cake was recrystallized from boiling absolute EtOH affording 41.5 g (92.3%) of the product as fluffy white needles. ¹H-NMR (CDCl₃): 7.84-7.81 (6H, m, aromatic H's); 7.71-7.66 (3H, m, aromatic H's); 7.59-7.54 (6H, m, aromatic H's); 3.82 (6H, s, methylene H's); 0.91 (3H, s, methyl H's). ¹³C-NMR (CDCl₃) δ: 139.88, 139.24, 134.47, 132.84, 74.81, 44.46, 21.06 ppm. IR (KBr pellet) $\bar{\nu}$: 3068, 2961, 2902, 1587, 1368, 1188, 969, 868 cm⁻¹. mp (104.0-104.5°C).

1,1,1-Tris(aminomethyl)ethane·3HCl I.32

To a slurry of NaN₃ (15.6 g, 240 mmol) and DMF (120 mL) was added 1,1,1-tris(bromomethyl)ethane (6.18 g, 20.0 mmol). The resulting mixture was stirred

under nitrogen at 90-95°C for 16 h, then cooled to room temperature and rapidly poured into 700 mL of tap water giving a clear colorless solution. The aqueous solution was extracted with Et₂O (200 mL, 3x100 mL), the organic fractions were pooled, dried over excess anhydrous MgSO₄ and then filtered through paper by gravity. The colorless ethereal solution was carefully concentrated on a rotary evaporator to 150 mL and subsequently diluted with 200 mL of 1,4-dioxane. The resulting solution was concentrated to 150 mL and then poured into a flask that contained triphenylphosphine (26.2 g, 100 mmol). The resulting yellow solution was then diluted with NH₄OH (100 mL) and stirred at room temperature for 20 hr with signs of gentle effervescence. The mixture was then evaporated to dryness affording a colorless residue. The residue was dissolved into 400 mL of chloroform and then extracted with 2 N HCl (4x100 mL). The acidic aqueous extracts were combined and washed with CHCl₃ (4x20 mL) and then diluted with 25 mL of concentrated HCl. Colorless crystalline material precipitated from solution upon concentration on a rotary evaporator. The mixture was cooled to 4°C overnight, filtered on a glass frit, washed with small portions of cold EtOH and Et₂O, and then dried under vacuum to afford 4.26 g (94%) of the product. ¹H-NMR (D₂O): 3.09 (6H, s, methylene H); 1.14 (3H, s, methyl H); the NH overlaps with the signal from residual water at 4.65. ¹³C-NMR (D₂O) δ: 42.88, 35.44, 17.06. IR (KBr pellet): 2992, 2920, 2788, 2640, 2591, 1602, 1521, 1509, 1470, 1066, 995, 857cm⁻¹.

4-(Hydroxymethyl)-1-methyl-2,6,7-trioxabicyclo[2.2.2]octane **I.38**

Into a 100 mL RBF equipped with a Teflon coated stir bar was added 13.6 g (100 mmol) of pentaerythritol, 10.0 mL of toluene, 18.3 mL (16.2 g, 100 mmol) of triethylorthoacetate and *ca.* 50 mg of *p*-TsOH (acid catalyst). The RBF was fit with a short-path distillation head and the RBF immersed in a hot oil bath. The EtOH (theoretical amount 17.5 mL, 300 mmol) that was produced during the course of the reaction was distilled into a graduated cylinder. The heating was terminated after 6 hr and the resulting glass was sublimed with heating under reduced pressure (*ca.* 10^{-2} Torr) to afford 13.4 g (83.6%) of the product as a white crystalline solid. $^1\text{H-NMR}$ (CDCl_3): 4.03 (6H, s, methylene H's); 3.47 (2H, d, $J=4.8\text{Hz}$, methylene H's); 1.63 (1H, t, $J=4.8\text{Hz}$, OH); 1.46 (3H, s, methyl H's). $^{13}\text{C-NMR}$ (CDCl_3) δ : 108.77, 69.51, 61.57, 35.80, 23.62 ppm. mp (110-111°C).

4-(benzyloxymethyl)-1-methyl-2,6,7-trioxabicyclo[2.2.2]octane **I.39**

Into a 250 mL RBF equipped with a Teflon coated stir bar was added powdered KOH (1.65 g, 29.4 mmol) and 10.0 mL of DMSO. To the resulting suspension was added benzyl bromide (894 μL , 1.29 g, 7.52 mmol) and the substrate **I.38** (1.00 g, 6.24 mmol) which on stirring became exothermic. After 30 min the solution was diluted with 100 mL H_2O and the product was extracted with Et_2O (2x10 mL). The pooled organic fractions were washed sequentially with saturated brine (2 mL), water (2 mL), and then dried over excess anhydrous MgSO_4 . The mixture was filtered and the solvent removed under vacuum affording 973 mg (63.0%) of a colorless oil that solidified on standing. This

material was amenable to trituration with H₂O which aided in the purification of the product. ¹H-NMR(CDCl₃): 7.37-7.25 (5H, m, aromatic H's); 4.45 (2H, s, pseudobenzyl H's); 4.01 (6H, s, methylene H's); 3.19 (2H, s, methylene H's); 1.45 (3H, s, methyl H's). ¹³C-NMR (CDCl₃) δ: 137.70, 128.72, 128.13, 127.63, 108.72, 73.69, 69.73, 68.52, 35.14, 23.66 ppm. mp (83-85°C).

2-[(benzyloxy)methyl]-2-(hydroxymethyl)-1,3-propanediol I.40

Into a 100 mL RBF equipped with a Teflon coated stir bar was added 1.90 g (7.59 mmol) of the substrate **I.39**, 10.0 mL of MeOH and 20.0 mL of 0.01NHCl. The resulting mixture was stirred at RT for 1hr and then neutralized with 708 mg (8.43 mmol) of NaHCO₃. The solvent was removed and the residue suspended in 10.0 mL of MeOH. The suspension was filtered through a glass frit and the filtrate was brought to dryness under vacuum affording 1.73 g (99.0%) of the product as a colorless viscous oil. ¹H-NMR (CDCl₃): 7.38-7.26 (5H, m, aromatic H's); 4.50 (2H, s, benzyl H's); 3.70 (6H, s, methylene H's); 3.49 (2H, s, methylene H's); 2.83 (3H, br.s, OH's).

2-(Benzyloxy)-1,1,1-tris(benzenesulfonyloxymethyl)ethane I.41

Into a 100 mL RBF equipped with a Teflon coated stir bar was added the substrate **I.40** (1.70 g, 7.50 mmol) and 5.0 mL of dry pyridine. The flask was cooled in an ice bath and benzenesulfonyl chloride (3.45 mL, 4.78 g, 27.0 mmol) was added via syringe dropwise to the reaction mixture over the course of 15 min. The reaction was then diluted with 5.0 mL of pyridine and allowed to warm to RT affording a yellow colored precipitate. To the flask was then added water

and the resulting granular solids were broken up with a spatula and then isolated on a glass frit via vacuum. The resulting filter cake was triturated with Et₂O affording 1.23 g (25.3%) of the product as a white crystalline solid. ¹H-NMR (CDCl₃): 7.95-7.10 (20H, m, phenyl H's); 4.27 (2H, s, methylene H's); 3.97 (6H, s, methylene H's); 3.32 (2H, s, methylene H's). ¹³C-NMR (CDCl₃) δ: 135.08, 134.39, 129.63, 128.60, 128.10, 127.61, 73.60, 67.08, 66.45, 44.10 ppm. IR (KBr pellet) $\bar{\nu}$: 3066, 2954, 2891, 1585, 1482, 1448, 1367, 1189, 983, 857, 590 cm⁻¹.

2-(Benzyloxy)-1,1,1-tris(aminomethyl)ethane I.43

Into a 25 mL RBF equipped with a Teflon coated stir bar was added 0.500 g (773 μ mol) of the substrate **I.41**, 1.5 mL of ethylene glycol and 252 mg (3.87 mmol) of NaN₃. The RBF was fit with a reflux condenser equipped with a N₂ inlet and the resulting mixture was brought to reflux in an oil bath thermostated at 130-140°C for 16 hr. The mixture was allowed to cool and then 3.0 mL of H₂O were added. The resulting deep red/brown solution was extracted with Et₂O (2x5 mL) and the pooled organic fractions were dried over excess anhydrous Na₂SO₄. The solution was decanted away from the solids and the solvent was evaporated behind a blast shield in the fume hood affording 142 mg (60.9%) of the crude triazide **I.42** as an amber colored oil. IR (liquid film) $\bar{\nu}$: 3088, 3065, 3031, 2932, 2867, 2533, 2103, 1298 cm⁻¹. Underlined data indicates the presence of the azide.

Into a 100 mL side-armed RBF equipped with a Teflon coated stir bar was added a spatula tip of 10% Pd/C (ca. 2mg) and a 1.0 mL methanolic solution of the triazide **I.42** (141 mg, 471 μmol). The head space was purged with N_2 for 10 min and then a balloon filled with gaseous H_2 was fit to the flask. The mixture was stirred magnetically at RT for 48 hr. The mixture was filtered through a glass frit and the filtrate was brought to dryness under vacuum affording 106 mg (99.9%) of the product as a pale yellow oil.

p-Toluenesulfonamide sodium salt I.45

Into an oven-dried 250 mL RBF was added 1.19 g (51.7 mmol) of metallic sodium followed by 60 mL of dry EtOH resulting in an immediate effervescence. The RBF was fit with a reflux condenser and the heterogeneous mixture was brought to reflux until all the sodium dissolved. To the refluxing mixture was added 8.86 g (51.7 mmol) of p-toluene sulfonamide. The mixture was refluxed for 2 hr resulting in the dissolution of the substrate. On cooling to RT a white precipitate emerged from solution. This material was isolated on a glass frit and dried under vacuum affording 7.11 g (71.0%) of the product as a white powder. IR (KBr pellet) $\bar{\nu}$: 3351, 3306, 3211, 3063, 3033, 3019, 2977, 2917, 2861, 1906, 1642, 1220, 1207, 1152, 1112 cm^{-1} . The $-\text{SO}_2-$ stretching frequencies corresponding to the isolated product (underlined data) have undergone substantial shifting as compared to the starting material. IR (KBr, p-TsNH₂) $\bar{\nu}$: 1326, 1152, 1093 cm^{-1} .

3,3-bis(p-tolylsulfonamidomethyl)-1-p-tolylsulfonyl-azetidine I.48

Into an oven-dried 250 mL RBF was added *ca.* 20 mL of dry DMF, 1.30 g (3.35 mmol) of pentaerythritol bromide, and 3.24 g (16.8 mmol) of the *p*-toluene sulfonamide sodium salt. The resulting mixture was refluxed for 16 hr under the protection of a stream of N₂. The mixture became homogeneous upon reflux followed by the formation of a colorless precipitate. The mixture was allowed to cool to RT and then 100 mL of H₂O was added causing the immediate formation of a white precipitate. The solids were filtered via vacuum and the resulting filter cake returned to the reaction flask. Into the RBF was then added 10 mL of 3:1 acetic acid:H₂O (v/v) and the resulting mixture was boiled for 0.5 hr. The mixture was then filtered hot and the filter cake was recrystallized from absolute EtOH. The resulting crystalline product had a mass of 0.644 g (33.0%). ¹H-NMR (CD₃CN): 7.76 (2H, d, J=8.0Hz, aromatic H's); 7.70 (4H, d, J=8.0Hz, aromatic H's); 7.54 (2H, d, J=8.0Hz, aromatic H's); 7.47 (4H, d, J=8.0Hz, aromatic H's); 5.73 (2H, t, J=7.0Hz, -NHSO₂-); 3.51 (4H, s, ring CH₂'s); 2.80 (4H, d, J=8.0Hz, exo-CH₂'s); 2.55 (3H, s, methyl H's); 2.51 (6H, s, methyl H's). ¹³C-NMR (CDCl₃) δ: 144.65, 144.08, 136.56, 131.13, 130.20, 130.13, 128.60, 127.05 ppm. IR (KBr pellet) $\bar{\nu}$: 3250, 2923, 1598, 1449, 1329, 1162, 1092, 1071, 815, 671, 551 cm⁻¹.

2-Hydroxyl-1,1,1-tris(aminomethyl)ethane·3H₂SO₄ I.49

Into a 250 mL RBF equipped with a Teflon coated stir bar was added 3.00 g (5.19 mmol) of the azetidine substrate **I.48** and 9.0 mL of 70% H₂SO₄ (v/v). The RBF was fit with a reflux condenser equipped with a N₂ inlet and the head space was purged with N₂ for *ca.* 10 min. The mixture was brought to reflux for 2.5 hr affording a brown colored solution. The hot solution was then poured into 100

mL of 30% aqueous EtOH (v/v). The resulting solution was concentrated to 50 mL under vacuum followed by dilution with 100 mL of absolute EtOH affording a granular precipitate. The solids were isolated on a glass frit via vacuum filtration resulting in 1.32 g (60.0%) of the desired product as an off-white powder. $^1\text{H-NMR}$ (D_2O): 4.54 (12H, s, ammonium H's overlapped with the bisulfate H's); 4.02 (1H, s, OH); 3.61 (2H, s, methylene H's); 3.06 (6H, s, methylene H's). $^{13}\text{C-NMR}$ (D_2O) δ : 62.02, 40.26, 39.62 ppm. IR (KBr pellet) $\bar{\nu}$: 3348, 3121, 1630, 1599, 1549, 1186, 1055, 1003, 883, 589 cm^{-1} .

[Ni(TAMEpyr)](ClO₄)₂ I.58

An aqueous solution of NaOH (265 mg, 6.7 mmol) was added to 1,1,1-tris(aminomethyl)ethane·3HCl I.32. The resulting solution was then brought to dryness on a rotary evaporator affording colorless oily solids. Absolute ethanol (25 mL) was then added to the solids, and the mixture was sonicated for 5 minutes and cooled to 4°C for 1hr. The cold ethanolic solution was filtered through a glass frit. The filtrate was then diluted with 100 mL of water and transferred to a flask that contained Ni(ClO₄)₂·6H₂O (808 mg, 2.21 mmol). The resulting sky blue solution was stirred with slow addition of an ethanolic solution (40 mL) 2-pyridinecarboxaldehyde (710 mg, 6.63 mmol). The resulting solution was stirred under nitrogen for 16 hr where a color change from blue to orange took place. The reaction mixture afforded significant amounts of orange colored precipitate, which was collected on a glass frit and dried under vacuum to afford 614 mg of [Ni(TAMEpyr-trisimine)](ClO₄)₂ I.50. To a mixture of 150 mL of doubly distilled water and 20 mL of EtOH was added complex I.50 (0.5 g, 0.8 mmol) and

NaBH₄ (2.2 g, 58 mmol). The reaction mixture was stirred for 16 hr to give a pale pink solution. The pH of the mixture was dropped to *ca.* 6-7 with addition of 70 % HClO₄. The pink precipitate that formed was collected on a glass frit and washed with small portions of Et₂O. The resulting powder was recrystallized by Et₂O diffusion from CH₃CN yielding fuchsia colored prisms. The prisms were isolated and dried under vacuum to give 473 mg (40%) of the product. (Found: C, 42.68; H, 4.71; N, 12.94. C₂₃H₃₀N₆NiCl₂O₈ requires: C, 42.62; H, 4.67; N, 12.97%). MS(ESI/methanol): *m/z* 547 (M-ClO₄). $\mu_{\text{eff}} = 3.2$ BM at 23 °C. $\lambda_{\text{max}}/\text{nm}$ (H₂O) 794 (12.0 cm⁻¹M⁻¹), 510 (15.8 cm⁻¹M⁻¹). IR (Mull): 3275, 1611, 1576, 1095 cm⁻¹.

TAMEpyr I.60

To a sample of [Ni(TAMEpyr)](ClO₄)₂ (50 mg, 80 μmol) was added 5 mL of hot aqueous NaCN (21 mg, 420 μmol). The mixture was shaken for five minutes affording a pale yellow solution. The solution was extracted with methylene chloride (3x5 mL); the organic fractions were combined, and dried over anhydrous Na₂SO₄. The supernatant was decanted and the solvent was removed on a rotary evaporator. The resulting colorless oil was dried further under vacuum to afford 30 mg (96%) of the product. ¹H-NMR (CDCl₃): 8.51 (3H, m, pyridyl H); 7.60 (3H, m, pyridyl H); 7.33 (3H, d, ³J = 7.6 Hz, pyridyl H); 7.13 (3H, m, pyridyl H); 3.91 (6H, s, pseudobenzyl H); 2.62 (6H, s, methylene H); 2.50 (3H, s, NH); 0.95 (3H, s, methyl H). ¹³C-NMR (CDCl₃) δ : 160.61, 149.34, 136.62, 122.37, 122.00, 56.93, 56.16, 38.70, 22.14 ppm.

TAMEsal I.52

The TAME·3HCl salt (237mg, 1.05mmol) and NaOAc (438mg, 3.22mmol) were dissolved into 5.0 mL of H₂O and the resulting solution was added to a 250 mL Erlenmeyer flask. To the flask was then added 40.0 mL of absolute EtOH followed by salicylaldehyde (393mg, 3.22mmol). The bright yellow solution was boiled for 5 min and then cooled to RT. To the flask was then added 20.0 mL of H₂O affording a bright yellow precipitate. The solids were collected on a glass frit via vacuum filtration and the filter cake was recrystallized from boiling EtOH affording 422 mg (93.6%) of the desired compound as a yellow crystalline solid. ¹H-NMR (CDCl₃): 13.37 (3H, s, phenolic H's); 8.38 (3H, s, imine H's); 7.36-7.32 (3H, m, aromatic H's); 7.28-7.25 (3H, m, aromatic H's); 6.99-6.97 (3H, m, aromatic H's); 6.92-6.88 (3H, m, aromatic H's); 3.65 (6H, s, methylene H's); 1.17 (3H, s, methyl H's). ¹³C-NMR (CDCl₃) δ: 166.77, 161.24, 132.77, 131.74, 119.04, 118.86, 117.15, 65.26, 40.43, 21.00 ppm. IR (KBr pellet) $\bar{\nu}$: 3112, 2970, 2886, 2833, 1631, 1579, 1276, 757 cm⁻¹.

[Cr(TAMEsal)]·H₂O I.55

Into a 25 mL RBF equipped with a Teflon coated stir bar was added CrCl₃·6H₂O (124mg, 466μmol), H₂O (1.0 mL), ethylene glycol (1.0 mL) and MeOH (3.0 mL) sequentially. To the resulting forest green solution was added TAMEsal (200 mg, 466μmol) and the resulting mixture was brought to reflux for 0.5 hr. To the refluxing mixture was then added Na₂CO₃·H₂O (51.9 mg, 419μmol) and the resulting solution was refluxed an additional 25 min. The mixture was filtered through a glass frit affording a cranberry colored filtered cake. The crude product

was subsequently recrystallized from MeCN in an Et₂O diffusion chamber to yield 33.2 mg (15.0%) of the desired product as deep red prismatic crystals. (Found: C, 62.74; H, 5.26; N, 8.50. C₂₆H₂₄N₃O₃Cr·H₂O requires: C, 62.90; H, 5.28; N, 8.46 %). $\mu_{\text{eff}} = 3.8$ BM at 23 °C. IR (KBr pellet) $\bar{\nu}$: 3019, 2918, 1619, 1537, 1467, 1445, 1318 cm⁻¹ $\lambda_{\text{max}}/\text{nm}$ (CH₃CN) 500 (20,000 cm⁻¹M⁻¹).

[Ni(TAMEIm-trisimine)](ClO₄)₂ I.56

Into a 250 mL RBF equipped with a Teflon coated stir bar was added 120 mL of MeOH, TAME·3HCl (113 mg, 500 μmol) and NaOMe (162 mg, 3.00 mmol). The resulting suspension was stirred into a solution for 5 min and then Ni(ClO₄)₂·6H₂O (183 mg, 500 μmol) and 2-imidazolecarboxaldehyde (144 mg, 1.50 mmol) were added affording a pale blue solution. The RBF was fit with a reflux condenser equipped with a N₂ inlet and the solution was brought to reflux for 24 hr. The resulting orange colored suspension was filtered through a glass frit via vacuum. The filter cake was recrystallized from MeCN in an Et₂O diffusion chamber affording 83.0 mg (26.0%) of the desired complex as a collection of red needles. (Found: C, 34.35; H, 3.85; N, 20.20. C₁₇H₂₁N₉NiCl₂O₈ requires: C, 34.3; H, 3.60; N, 21.1%). MS(ESI/methanol): m/z 509 (M-ClO₄⁻). IR (KBr pellet): 3126, 2965, 2923, 1635, 1559, 1442, 1109, 624 cm⁻¹. $\lambda_{\text{max}}/\text{nm}$ (CH₃CN) ca. 800 (16 cm⁻¹M⁻¹), 894 (21 cm⁻¹M⁻¹), 534 (45 cm⁻¹M⁻¹).

[Ni(TAMETz-trisimine)](ClO₄)₂ I.57

Into a 250 mL RBF equipped with a Teflon coated stir bar was added 120 mL of MeOH, TAME·3HCl (113 mg, 500 μmol) and NaOMe (162 mg, 3.00 mmol). The

resulting suspension was stirred into a solution for 5 min and then Ni(ClO₄)₂·6H₂O (183 mg, 500 μmol) and 2-thiazolecarboxaldehyde (170 mg, 1.50 mmol) were added affording a pale yellow solution. The RBF was fit with a reflux condenser equipped with a N₂ inlet and the solution was brought to reflux for 24 hr. The resulting orange colored suspension was filtered through a glass frit via vacuum. The filter cake was recrystallized from MeCN in an Et₂O diffusion chamber affording 100 mg (30.3%) of the desired complex as shiny orange colored needles. (Found: C, 31.05; H, 2.80; N, 12.74. C₁₇H₁₈N₆S₃NiCl₂O₈ requires: C, 30.93; H, 2.75; N, 12.73%). IR (KBr pellet): 2932, 2877, 2871, 2807, 2728, 1626, 1496, 1372, 1099, 781, 625 cm⁻¹. λ_{max}/nm (CH₃CN) 814 (35 cm⁻¹M⁻¹), ca. 500 (68 cm⁻¹M⁻¹).

[Fe(TACHTz)](ClO₄)₂

Under the protection of a N₂ atmosphere in the glovebox was mixed a degassed methanolic solution (1.0 mL) of TACHTz (20.0 mg, 47.5 μmol) and a degassed methanolic solution (1.0 mL) of Fe(ClO₄)₂·6H₂O (17.5 mg, 47.5 μmol) immediately forming a forest green solution. To this was then added degassed Et₂O affording copious amounts of a dark green precipitate. The solids were isolated by removing the supernatant via pipet. The resulting crude product was dissolved into 1.0 mL of degassed MeCN and the resulting dark green solution was placed in an Et₂O diffusion chamber for 16hr. The complex crystallized as X-ray grade large red hexagonal prisms. A sample was sent to Dr. Arnold

Rheingold at UCSD for crystallographic analysis (Table 5). IR (Csl pellet): 3256, 3190, 3127, 2900-2850, 1511, 1455, 1098, 624 cm^{-1} .

[Mn(TAMEpyr)](ClO₄)₂ I.65

A colorless methanolic solution (1 mL) of Mn(ClO₄)₂·6H₂O (29 mg, 80 μmol) was added to a colorless methanolic solution (1 mL) of TAMEpyr (31 mg, 80 μmol) resulting in the formation of a colorless precipitate. The mixture was diluted with Et₂O and the solids were collected on a frit and dried under vacuum. The product was recrystallized by ether diffusion from CH₃CN affording nearly colorless needles. The needles were isolated and dried under vacuum to afford 37 mg (72%) of the desired product. (Found: C, 42.41; H, 4.81; N, 12.30. C₂₃H₃₀N₆MnCl₂O₈ requires: C, 42.87; H, 4.69; N, 13.04%). MS(ESI/methanol): *m/z* 544 (M-ClO₄⁻). μ_{eff} = 5.9 BM at 23 °C. IR (Mull): 3266, 1608, 1569, 1094 cm^{-1} .

[Fe(TAMEpyr)](ClO₄)₂ I.66

A pale yellow degassed methanolic solution (1 mL) of Fe(ClO₄)₂·6H₂O (29 mg, 80 μmol) was added to a colorless degassed methanolic solution (1 mL) of TAMEpyr (31 mg, 80 μmol) under the protection of a nitrogen atmosphere. The reaction mixture was allowed to deposit solids for 16 hr. The supernatant was removed and the resulting dark colored crystalline solids were washed with small portions of degassed Et₂O, and then dried under a stream of nitrogen. The solids were then recrystallized by Et₂O diffusion from CH₃CN affording chestnut colored prisms. The crystals of the complex were stable to air indefinitely

whereas a sealed oxygenated aqueous solution of the complex decomposed when incubated at 37°C overnight. ¹H-NMR (CD₃CN degassed): 7.81 (3H, m, pyridyl H); 7.52 (6H, m, pyridyl H); 7.20 (3H, t, ³J = 6.4 Hz, pyridyl H); 4.46 (3H, m, NH); 4.31 (3H, dd, diastereotopic pseudobenzyl H); 4.05 (3H, dd, diastereotopic pseudobenzyl H); 2.97 (3H, dd, diastereotopic methylene H); 2.49 (3H, dd, diastereotopic methylene H); 0.81 (3H, s, methyl H). IR (Csl pellet): 3267, 1615, 1577, 1088, 761, 624 cm⁻¹. (Found: C, 43.10; H, 4.75; N, 13.13. C₂₃H₃₀N₆FeCl₂O₈ requires: C, 42.81; H, 4.69; N, 13.02%).

[Co(TAMEpyr)](BF₄)₂ I.67

A pale red degassed methanolic solution (1 mL) of Co(BF₄)₂·6H₂O (19 mg, 55 μmol) was added to a colorless degassed methanolic solution (1 mL) of TAMEpyr (21 mg, 55 μmol) under the protection of a nitrogen atmosphere. The reaction mixture was then subjected to Et₂O diffusion for 5 days to afford orange colored prismatic crystals. The supernatant was removed and the resulting crystalline solids were washed with small portions of degassed Et₂O, and then dried under a stream of nitrogen to give 21 mg (63%) of the product. The crystals of the complex were stable to air indefinitely but decomposed rapidly in CH₃CN when exposed to air. (Found: C, 44.28; H, 5.05; N, 13.35. C₂₃H₃₀N₆CoB₂F₈ requires: C, 44.34; H, 4.85; N, 13.49%). μ_{eff} = 4.9 BM at 23°C. IR (Csl pellet): 3172m, 1606m, 1565w, 729s, 478s. IR (Mull): 3275, 1611, 1576, 1095 cm⁻¹. λ_{max}/nm (CH₃CN degassed) 939.0 (21.1 cm⁻¹M⁻¹), 472.0 (63.5 cm⁻¹M⁻¹), 400 (28 cm⁻¹M⁻¹).

[Cu(TAMEpyr)](ClO₄)₂ I.68

A pale blue isopropanolic solution (1 mL) of Cu(ClO₄)₂·6H₂O (30 mg, 80 μmol) was added to a colorless isopropanolic solution (1 mL) of TAMEpyr (31 mg, 80 μmol) resulting in the formation of a sky blue powder. The solvent was removed on a rotary evaporator and the resulting powder was recrystallized by Et₂O diffusion from CH₃CN, isolated and dried under vacuum, to afford 47 mg (91%) of the product as royal blue needles. (Found: C, 42.21; H, 4.58; N, 12.77.

C₂₃H₃₀N₆CuCl₂O₈ requires: C, 42.31; H, 4.63; N, 12.87%). MS(ESI/methanol): *m/z* 552 (M-ClO₄⁻). μ_{eff} = 2.1 BM at 23°C. IR (Mull): 3249, 1613, 1574, 1096 cm⁻¹. λ_{max}/nm (CH₃CN) 620 (107 cm⁻¹M⁻¹) asymmetric peak.

[In(TAMEpyr)](NO₃)₃·MeOH I.70

A colorless methanolic solution (0.90 mL) of In(NO₃)₃·5H₂O (8.0 mg, 20 μmol) was added to a colorless methanolic solution (0.90 mL) of TAMEpyr (7.8 mg, 20 μmol) resulting in the formation of a colorless solution. The solution was allowed to stand for 18 hr. The complex was crystallized from solution as feather-like white needles by Et₂O diffusion. The needles were isolated and dried under vacuum to afford 10.1 mg (73%) of the desired product. ¹H-NMR (DMSO-d₆): 8.25-8.21 (3H, m, pyridyl H); 8.04 (3H, s, pyridyl H); 7.79 (3H, d, ³J = 8.0 Hz, pyridyl H); 7.66 (3H, t, ³J = 6.0 Hz, pyridyl H); 5.86 (3H, m, NH); 4.31 (6H, d, ³J = 6.0 Hz, pseudobenzyl H); 3.17 (6H, d, ³J = 7.2 Hz, methylene H); 0.84 (3H, s, methyl H). IR (KBr pellet): 3163, 1609m, 1571w, 1365vs, 1279s. (Found: C,

39.99; H, 4.47; N, 17.72. $C_{23}H_{30}N_6InN_3O_9$ requires: C, 39.85; H, 4.74; N, 17.43%).

[Zn(TAMEpyr)](ClO₄)₂ I.69

A colorless methanolic solution (1 mL) of $Zn(ClO_4)_2 \cdot 6H_2O$ (30 mg, 80 μ mol) was added to a colorless methanolic solution (1 mL) of TAMEpyr (31 mg, 80 μ mol) resulting in the formation of a colorless precipitate. The solvent was diluted with a small portion of Et_2O and the solids were isolated, washed with additional ether, and then recrystallized by Et_2O diffusion from CH_3CN to afford 30 mg (58%) of colorless prisms. 1H -NMR (CD_3CN): 8.07 (3H, m, pyridyl H); 7.88 (3H, d, $^3J = 4.8$ Hz, pyridyl H); 7.57 (3H, d, $^3J = 8$ Hz, pyridyl H); 7.46 (3H, t, $^3J = 6.8$ Hz, pyridyl H); 4.35 (3H, dd, pseudobenzyl H); 3.95 (3H, dd, diastereotopic H); 3.53 (3H, m, NH); 3.32 (3H, dd, diastereotopic methylene H); 2.85 (3H, dd, diastereotopic methylene H); 0.77 (3H, s, methyl H). IR (Mull): 3249, 1613, 1574, 1096 cm^{-1} . (Found: C, 41.90; H, 4.60; N, 12.68. $C_{23}H_{30}N_6ZnCl_2O_8$ requires: C, 42.19; H, 4.62; N, 12.83%). MS(ESI/methanol): m/z 553 ($M-ClO_4^-$). Suitable crystals for X-ray crystallography were prepared by slow Et_2O diffusion into an CH_3CN solution of the complex.

4.4.2 Chapter 2 Experimentals

Methyl-2-quinolinecarboxylate II.53

Into a 250 mL RBF equipped with a Teflon coated stir bar was added 2.01 g (11.6 mmol) of quinaldic acid, 15.0 mL of absolute MeOH, and the resulting

suspension was stirred while immersed in an ice bath for ca. 5min. To the mixture was then added 2.53 mL (4.14 g, 34.8 mmol) of thionyl chloride dropwise. The reaction solution was allowed to warm to room temperature and then refluxed under the protection of N₂ overnight. After ca. 12 hr the solvent was removed under vacuum affording a pale-yellow solid residue. The residue was dissolved into 15 mL of water and the resulting solution treated with excess Na₂CO₃ piecemeal until the effervescence ceased. The resulting solution was extracted with DCM (3x50 mL), the organic fractions pooled and then dried over excess anhydrous Na₂SO₄. The mixture was filtered via gravity and the solvent removed under vacuum. The resulting off-white solid had a mass of 1.74 g (80.0%). The crude product was spectroscopically pure and used as is subsequent reactions. ¹H-NMR (CDCl₃): 8.33-8.31 (2H, m, quinoline H's); 8.21 (1H, d, J=8.4Hz, quinoline H); 7.90-7.88 (1H, m, quinoline H); 7.82-7.78 (1H, m, quinoline H); 7.68-7.64 (1H, m, quinoline H); 4.09 (3H, s, methyl H's). ¹³C-NMR (CDCl₃) δ: 170.10, 148.10, 147.75, 137.56, 130.93, 130.54, 129.57, 128.87, 127.78, 121.25, 53.46 ppm. IR(KBr pellet) $\bar{\nu}$: 3065-3001, 2952, 1714 cm⁻¹.

2-Quinolinecarbinol II.54

Into a 250 mL RBF equipped with a Teflon coated stir bar was added methyl-2-quinolinecarboxylate (1.71g, 9.13mmol), ca. 50 mL of dry Et₂O, and 200 mg (9.13 mmol) of LiBH₄. The head-space was purged with N₂ for 10 min and the resulting heterogeneous mixture refluxed with stirring for 24 hr. The solvent was then removed under vacuum affording a pale yellow solid residue. The residue was dissolved into 50 mL of water and acidified to pH=2 with 1M HCl. The

mixture was made basic to pH=8 with 1M NaOH. The product was extracted with DCM (3x50 mL), the organic fractions pooled and then dried over excess anhydrous Na₂SO₄. The mixture was filtered via gravity and the solvent removed under vacuum affording 1.30 g of a pale yellow oil (90.0%). The crude product was used as is in subsequent reactions. ¹H-NMR (CDCl₃): 8.13 (1H, d, J=8.8Hz, quinoline H); 8.07 (1H, d, J=8.4Hz, quinoline H); 7.82 (1H, d, J=8.0Hz, quinoline H); 7.74-7.52 (1H, m, quinoline H); 7.56-7.52 (1H, m, quinoline H); 7.29 (1H, d, J=8.8Hz, quinoline H); 4.92 (2H, s, methylene H's); ca. 4.5 (1H, s(br.), -OH). IR (liquid film) $\bar{\nu}$: 3345, 3057, 2921, 1619 cm⁻¹.

2-Quinolinecarboxaldehyde II.55

Into a 500 mL three-way RBF equipped with a Teflon coated stir bar, two pressure equalizing drop-funnels, and a N₂ inlet was added 25 mL of dry DCM and 1.55 g (1.07mL, 12.3mmol) of oxalyl chloride. The resulting solution was cooled to -78°C with a dry-ice/acetone bath. The head-space was purged with N₂ for 10 min. One of the drop-funnels was charged with 1.91 g (1.75 mL, 24.5 mmol) of DMSO dissolved in 5 mL of DCM. This solution was added with stirring to the RBF dropwise over a 5 min period. The other funnel was charged with 1.30 g (8.20mmol) of 2-quinolinecarbinol dissolved in ca. 10 mL of DCM. This solution was then added to the reaction mixture dropwise over the course of 5 min. The resulting mixture was stirred an additional 20 min and then TEA (6.20g, 8.51 mL, 61.2 mmol) was added to the RBF dropwise. After waiting an additional 5 min the reaction mixture was warmed to RT. To the mixture was added 50 mL of H₂O. The layers were separated, and the organic phase was washed

sequentially with 5% aqueous NaHCO₃ (50 mL) and 5% aqueous NaCl (50 mL). The organic phase was dried over excess anhydrous Na₂SO₄, filtered via gravity, and the solvent removed under vacuum affording a brown oil. The crude product was purified by column chromatography (R_f=0.80, 1:1 EtOAc:hexanes (v/v)) yielding 1.01 g (77.5%) of a white powder with a sweet aroma. ¹H-NMR (CDCl₃): 10.24 (1H, s, aldehyde H); 8.31 (1H, d, J=8.4Hz, quinoline H); 8.27-8.24 (1H, m, quinoline H); 8.03 (1H, d, J=8.4Hz, quinoline H); 7.92-7.82 (1H, m, quinoline H); 7.85-7.82 (1H, m, quinoline H); 7.71-7.67 (1H, m, quinoline H). ¹³C-NMR (CDCl₃) δ: 194.00, 152.82, 148.16, 137.63, 130.73, 130.66, 130.30, 129.44, 128.10, 117.59 ppm. IR (KBr pellet) $\bar{\nu}$: 3057, 2813, 1711 cm⁻¹.

1-Trioxanyliisoquinoline II.57

Into a 500 mL RBF was added 200 mL of MeCN and 120 g (1.33mol) of 1,3,5-trioxane. To the resulting solution was added sequentially 1.81 g (1.65 mL, 14.0 mmol) of isoquinoline, 1.60 g (1.07 mL, 14.0 mmol) of trifluoroacetic acid, 3.4 mL of 30.0% H₂O₂ (30.0 mmol), and 32.0 mg (0.2 mmol, 0.7 mol%) of FeSO₄. The RBF was fit with a reflux condenser and the mixture refluxed for 5hr. The reaction mixture took on an orange color with heating. The solvent was removed under vacuum, and the resulting solid residue dissolved into 50 mL of 1M NaOH, and the crude product extract with Et₂O (3x50 mL). The pooled organic fractions were dried over excess anhydrous Na₂SO₄, filtered via gravity through paper, and the solvent removed under vacuum. The residue was chromatographed on silica (R_f=0.58, 1:1 EtOAc:hexanes (v/v)) affording 2.30 g (75.6%) of the purified product. ¹H-NMR (CDCl₃): 8.89 (1H, d, J=8.0Hz, isoquinoline H); 8.50 (1H, d,

J=5.6Hz, isoquinoline H); 7.85 (1H, d, J=8.8Hz, isoquinoline H); 7.73-7.64 (3H, m, isoquinoline H); 6.43 (1H, s, methine trioxane H); 5.49 (2H, d, J=6.4Hz, methylene trioxane H's); 5.45 (2H, d, J=6.4Hz, methylene trioxane H's). ¹³C-NMR (CDCl₃) δ: 153.44, 141.40, 137.39, 130.50, 127.70, 127.21, 126.84, 126.32, 122.89, 105.35, 94.27 ppm. IR (KBr) $\bar{\nu}$: 3054, 3006, 2962-2752, 1622, 1331, 1099 cm⁻¹.

Methyl-1-isoquinolinecarboxylate II.60

Into a 250 mL RBF equipped with a Teflon coated stir bar was added 20 mL of MeOH and 3.00 g (17.3mmol) of 1-isoquinolinecarboxylic acid. The RBF was then cooled in an ice bath for 5 min. To the resulting stirred solution was added 6.18 g (3.79 mL, 52.0 mmol) of thionyl chloride dropwise. The mixture was then allowed to warm to RT and after stirring for 30 min the RBF was fit with a reflux condenser and the contents refluxed for 16hr. The solvent was then removed under vacuum and the resulting solid residue was dissolved into 20 mL of H₂O, neutralized by the piecemeal addition of excess Na₂CO₃ until the effervescence ceased. The product was extracted with DCM (4x20 mL), the pooled organic fractions dried over excess Na₂SO₄, filtered via gravity through paper, and the solvent removed under vacuum. The crude product was then distilled under reduced pressure (bp=144-145°C, 700mTorr) affording 1.59 g (49.0%) of a colorless oil. ¹H-NMR (CDCl₃): 8.84 (1H, d, J=8.8Hz, isoquinoline H); 8.63 (1H, d, J=5.6Hz, isoquinoline H); 7.88 (1H, d, J=8.0Hz, isoquinoline H); 7.83 (1H, d, J=5.6Hz, isoquinoline H); 7.76-7.67 (2H, m, isoquinoline H's); 4.10 (3H, s, methyl H's). ¹³C-NMR (CDCl₃) δ: 166.35, 148.24, 141.65, 137.01, 130.65, 128.89,

127.20, 126.99, 126.46, 124.40, 53.06 ppm. IR (liquid film) $\bar{\nu}$: 3055, 2951, 2849, 1720 cm^{-1} .

1-Isoquinolinecarboxaldehyde II.58

Into a 500 mL three-way RBF equipped with a Teflon coated stir bar, a pressure equalizing funnel, and N_2 inlet was added 1.00 g (5.34 mmol) of methyl-1-isoquinolinecarboxylate dissolved in *ca.* 30 mL of dry THF. The funnel was charged with 0.101 g (2.67 mmol) of LiAlH_4 suspended into 10 mL of dry THF. The RBF was cooled in a dry ice/MeOH bath until a temperature of -70°C was achieved. To the RBF was then added the suspension of LiAlH_4 with stirring over the course of 15 min. The resulting brown mixture was stirred an additional 15 min and then the reaction quenched with the addition of excess glacial AcOH (*ca.* 1.5 mL). The resulting reaction mixture was brought to RT and then a few drops of H_2O followed by a few drops of 1M NaOH were added to make the aluminum salts more granular. The resulting heterogeneous mixture was filtered via vacuum through paper and the resulting yellow filtrate brought to dryness under vacuum. The residue was chromatographed on silica with 1:1 EtOAc:hexanes ($R_f=0.79$) affording 0.280 g of the desired product as a white powder with a sweet aroma (33.0%). $^1\text{H-NMR}$ (CDCl_3): 10.40 (1H, s, aldehyde H); 9.34-9.31 (1H, m, isoquinoline H); 8.76 (1H, d, $J=5.6\text{Hz}$, isoquinoline H); 7.93-7.89 (2H, m, isoquinoline H's); 7.79-7.74 (2H, m, isoquinoline H's). $^{13}\text{C-NMR}$ (CDCl_3) δ : 195.63, 149.79, 142.41, 136.85, 130.74, 130.00, 126.91, 126.31, 125.70, 125.45 ppm. IR(KBr pellet) $\bar{\nu}$: 3048, 3033, 2844, 1703 cm^{-1} .

1-isoquinoline carbonitrile II.63

Into a 500 mL RBF equipped with a Teflon coated stir bar was added 16.7 g (256 mmol) of KCN and 130 mL of H₂O. To the resulting stirred solution was added 9.10 g (10.0 mL, 70.4 mmol) of isoquinoline and 27.9 g (20.1 mL, 158 mmol) of benzenesulfonyl chloride sequentially. Approximately 25 mL of DCM was added to the gummy reaction mixture and the resulting biphasic solution was stirred for 4 hr at RT. The organic layer was then removed with a separatory funnel and the remaining aqueous layer was extracted with DCM (3x50 mL). The pooled organic fractions were washed with H₂O (100 mL), 3N HCl (50 mL), H₂O (100 mL), 1N NaOH (50 mL), and H₂O (100 mL) sequentially. The organic fraction was dried over excess anhydrous Na₂SO₄ and filtered via gravity through paper. The solvent was removed under vacuum affording 8.60 g (41.0%) of crude 2-phenylsulfonyl-1,2-dihydroisoquinoline-1-carbonitrile **II.62**. ¹H-NMR (CDCl₃): 7.91-7.88 (2H, m, aromatic H's); 7.65-7.61 (1H, m, aromatic H); 7.57-7.52 (2H, m, aromatic H's); 7.35-7.25 (2H, m, aromatic H's); 7.20-7.18 (1H, m, aromatic H); 7.14-7.12 (1H, m, aromatic H); 6.78-6.76 (1H, m, 4H of the isoquinolinyl group); 6.18 (1H, d, J=8.0Hz, 3H of the isoquinolinyl group); 6.14 (1H, s, 1H of the isoquinolinyl group).

Into a large beaker was added 200mL of EtOH and 7.20 g (24.4 mmol) of 2-phenylsulfonyl-1,2-dihydroisoquinoline-1-carbonitrile. To the stirred suspension was added 0.920 g (24.4 mmol) of NaBH₄ causing the heterogeneous reaction mixture to effervesce gently. After 2 hr of stirring the resulting yellow solution was evaporated to dryness and the residue partitioned between CHCl₃ (100 mL)

and H₂O (100mL). The organic layer was isolated and then washed sequentially with 3N HCl (50 mL), H₂O (100 mL), 1N NaOH (50 mL), and H₂O (100 mL). The organic phase was then dried over excess anhydrous Na₂SO₄, filtered via gravity through paper and the solvent removed under vacuum affording 2.32 g (62.0%) of the product as a white powder. The overall yield of the product starting from isoquinoline was 21.0%. ¹H-NMR (CDCl₃): 8.65 (1H, d, J=5.6Hz, isoquinoline H); 8.36-8.33 (1H, m, isoquinoline H); 7.97-7.95 (1H, m, isoquinoline H); 7.92-7.90 (1H, m, isoquinoline H); 7.86-7.79 (2H, m, isoquinoline H's). ¹³C-NMR (CDCl₃) δ: 143.51, 136.11, 135.03, 131.95, 130.08, 129.56, 127.54, 125.52, 124.65, 116.06 ppm. IR (KBr pellet) $\bar{\nu}$: 3059, 2228, 1622 cm⁻¹.

2-Hydroxymethyl benzothiazole II.65

Into a 100mL RBF was added 9.49 g (125 mmol) of glycolic acid and 12.5 g (10.7 mL, 100 mmol) of 2-aminothiophenol and the resulting mixture was heated neat in a sand bath to a gentle boil. The theoretical amount of H₂O (ca. 3.0 mL) evolved after 1.5 hr of heating. The resulting orange colored oil was cooled to RT and then 120 mL of 3N HCl was added affording a yellow suspension. The suspension was cooled in an ice bath and 60 mL of 20% NaOH (w/v) was added. The resulting solids were collected via filtration and washed with 1 L of cold H₂O. The granular solids were dried under vacuum affording 9.19 g (56.0%) of the product as a yellow powder. ¹H-NMR (CDCl₃): 7.97 (1H, d, J=8.4Hz, benzo H); 7.87 (1H, d, J=8.0Hz, benzo H); 7.46 (1H, t, J=8.0Hz, benzo H); 7.37 (1H, t, J=8.0Hz, benzo H); 5.08 (2H, s, methylene H's); 3.96 (1H, s, -OH). ¹³C-NMR

(CDCl₃) δ : 172.87, 152.95, 134.86, 126.39, 125.31, 122.94, 122.03, 62.71 ppm.

IR (KBr pellet) $\bar{\nu}$: 3161, 2902, 2831, 1611 cm⁻¹.

2-Benzothiazolecarboxaldehyde II.66

Into a 100mL RBF equipped with a Teflon coated stir bar was added 5.00 g (30.3 mmol) of 2-hydroxymethyl benzothiazole, 3.40 g (30.6 mmol) of SeO₂, 25.0 mL of p-dioxane and 1.0 mL of H₂O. The RBF was fit with a reflux condenser equipped with a N₂ inlet and the resulting suspension was brought to reflux for 0.5 hr. The mixture was cooled to RT and then filtered via vacuum through paper into 200 mL of cold H₂O. The product was extracted with DCM (4x100 mL) and the pooled organic fractions dried over excess anhydrous Na₂SO₄. The mixture was filtered and the solvent removed under vacuum affording 3.40 g of the crude product (69.0% crude) as a brown powder. The product was purified by sublimation affording 1.67 g (34.0%) of a white crystalline solid with a sweet aroma. ¹H-NMR (CDCl₃): 10.17 (1H, s, aldehyde H); 8.24 (1H, d, J=8.4Hz, aromatic H); 8.00 (1H, d, J=8.0Hz, aromatic H); 7.59 (2H, m, aromatic H's). ¹³C-NMR (CDCl₃) δ : 185.65, 165.50, 152.71, 136.56, 128.61, 127.58, 125.97, 122.84 ppm.

2'-Hydroxyacetophenone oxime II.68

Into a 100 mL RBF equipped with a Teflon coated stir bat was massed 2.78 g (40.0 mmol) of hydroxylamine hydrochloride. To the RBF was added 40 mL of absolute EtOH and 10 mL of H₂O. The resulting mixture was stirred into a solution followed by the addition of 2.72 g (2.41 mL, 20.0 mmol) of 2'-hydroxy

acetophenone. The RBF was fit with a reflux condenser and the mixture was brought to reflux. To the refluxing solution was added 5.44 g (40.0 mmol) of NaOAc·H₂O dissolved in 10 mL of H₂O. The resulting solution was refluxed for 2.5 hr and then cooled to -10°C. The cold solution was then poured slowly into 200 mL of H₂O affording a white crystalline precipitate. The product was collected in a Büchner funnel and washed with cold H₂O. The resulting solids were dried under vacuum affording 2.00 g (66.0%) of the desired product. ¹H-NMR (CDCl₃): 11.64 (1H, s, phenolic H); 8.09 (1H, s, oxime H); 7.45-7.43 (1H, m, phenyl H); 7.29-7.25 (1H, m, phenyl H); 7.00-6.90 (2H, m, phenyl H's); 2.36 (3H, s, methyl H's). ¹³C-NMR (CDCl₃) δ: 159.73, 157.57, 131.03, 127.86, 119.56, 118.80, 117.47, 11.01 ppm.

2'-Hydroxyacetophenone acetoxime II.69

Into a 50mL RBF equipped with a Teflon coated stir bar was added 2.00 g (13.2 mmol) of 2'-hydroxyacetophenone oxime followed by 4.0 mL of Ac₂O which immediately caused the evolution of heat. An additional 1.0 mL aliquot of Ac₂O was added to the RBF followed by 50 mL of H₂O. The resulting white precipitate was isolated on a Büchner funnel and the resulting filter cake was washed with small portions of cold H₂O. The resulting solids were dried under vacuum affording 2.33 g (91.0%) of the product. ¹H-NMR (CDCl₃): 11.28 (1H, s, phenolic H); 7.48-7.45 (1H, m, aromatic H); 7.35-7.31 (1H, m, aromatic H); 7.04-7.01 (1H, m, aromatic H); 6.93-6.89 (1H, m, aromatic H); 2.44 (3H, s, methyl H's); 2.25 (3H, s, methyl H's). ¹³C-NMR δ: 167.02, 164.24, 158.80, 132.59, 128.67, 119.32, 118.33, 117.41, 19.46, 13.11 ppm.

3-Methyl-1,2-benzisoxazole II.70

Into a 100mL RBF equipped with a Teflon coated stir bar was added 2.30 g (11.9 mmol) of 2'-hydroxyacetophenone acetoxime and 25 mL of dry pyridine. The RBF was fit with a reflux condenser equipped with a N₂ inlet and the contents of the RBF were brought to reflux with stirring for 3.5 hr. The reaction mixture was allowed to cool to RT and then it was poured into 50 mL of 1N HCl. The product was extracted with DCM (3x50 mL), the organic fractions were pooled and then dried over excess anhydrous MgSO₄. The mixture was filtered via gravity through paper and the filtrate was brought to dryness under vacuum. The resulting product was purified by reduced pressure distillation (bp=56°C, 210mTorr) affording 1.21 g (76.6%) of the product as a colorless oil. ¹H-NMR (CDCl₃): 7.65-7.62 (1H, m, aromatic H); 7.55-7.54 (2H, m, aromatic H); 7.33-7.29 (1H, m, aromatic H); 2.59 (3H, s, methyl H's). ¹³C-NMR (CDCl₃) δ: 163.03, 155.22, 129.95, 123.39, 122.46, 121.38, 110.05, 10.33 ppm.

3,4-Dimethoxy-β-nitrostyrene II.73

Into a 250 mL RBF equipped with a Teflon coated stir bar was added 33.0 g (199 mmol) of 3,4-dimethoxybenzaldehyde and 83.0 mL (93.5 g, 1.53 mol) of MeNO₂. To the resulting orange solution was added 5.00 g (64.9 mmol) of NH₄OAc and the RBF was fit with a reflux condenser equipped with a N₂ inlet. After purging the head space for ca. 10 min the mixture was brought to reflux. After 1 hr at reflux the red colored solution was poured carefully into 330 mL of ice cold 70% aqueous isopropyl alcohol (v/v). The resulting bright yellow suspension was

allowed to stand for 15 min and then the yellow precipitate was isolated via vacuum on a Büchner funnel. The filter cake was washed with ca. 170 mL of 70% aqueous isopropyl alcohol until the emerging filtrate was colorless. The filter cake was then recrystallized from boiling EtOH and dried under vacuum to afford 28.1 g (67.7%) of the product as a bright yellow crystalline solid. $^1\text{H-NMR}$ (CDCl_3): 7.97 (1H, d, $J=13.6\text{Hz}$, alkene H); 7.44 (1H, d, $J=13.6\text{Hz}$, alkene H); 7.18 (1H, dd, $J_1=8.0\text{Hz}$, $J_2=2.0\text{Hz}$, aromatic H at C6); 7.02 (1H, d, $J=2.0\text{Hz}$, aromatic H at C2); 6.92 (1H, d, $J=8.0\text{Hz}$, aromatic H at C5); 3.95 (3H, s, methyl H's); 3.93 (3H, s, methyl H's). $^{13}\text{C-NMR}$ (CDCl_3) δ : 153.03, 149.77, 139.53, 135.38, 124.84, 123.01, 111.55, 110.46, 56.30, 56.23 ppm. IR (KBr pellet) $\bar{\nu}$: 3124, 3082-2839, 1627, 1598, 978 cm^{-1} . mp: 134-136°C.

3,4-Dimethoxy- β -nitroethylbenzene II.74

Into a 500 mL RBF equipped with a Teflon coated stir bar was added 80 mL of absolute EtOH. The RBF was then emerged in an ice water bath and stirred under the protection of N_2 for ca. 10 min. To the cold solvent was then added 7.24 g (191 mmol) of NaBH_4 and the RBF was then fit with a pressure equalizing funnel charged with a saturated solution of 10.0 g (47.8 mmol) of 3,4-dimethoxy- β -nitrostyrene in 175 mL of dry THF. The substrate was added dropwise to the RBF over the course of 90 min. After 90 min the resulting colorless reaction mixture was poured into 200 mL of cold H_2O . To the resulting mixture was then added 50 mL of glacial acetic acid. The resulting pale yellow solution was allowed to cool to RT. The product was isolated from the aqueous mixture with

Et₂O (3x100 mL) and the pooled organic fractions were dried over excess anhydrous MgSO₄, filtered via gravity through paper, and the solvent removed under vacuum affording 7.93 g (78.5%) of the crude product as a pale yellow oil. This material was used as is in subsequent chemistries. ¹H-NMR (CDCl₃): 6.82 (1H, d, J=8.0Hz, aromatic H at C5); 6.75 (1H, dd, J₁=8.2Hz, J₂=2.0Hz, aromatic H at C6); 6.71 (1H, d, J=2.0Hz, aromatic H at C2); 4.59 (2H, t, J=7.2Hz, methylene H's adjacent to arene); 3.87 (3H, s, methyl H's); 3.86 (3H, s, methyl H's); 3.26 (2H, t, J=7.2Hz, methylene H's adjacent to nitro group). ¹³C-NMR (CDCl₃) δ: 149.40, 148.56, 128.28, 120.84, 111.93, 111.73, 76.75, 56.09, 33.35 ppm. There was coincidental overlap of the MeO-groups. IR (KBr pellet) $\bar{\nu}$: 3003, 2960-2837, 1608, 1592, 1552, 1379 cm⁻¹.

3,4-Dimethoxy-β-phenethylamine II.75

Into a 250 mL RBF that contained 7.50 g (35.5 mmol) of crude 3,4-dimethoxy-β-nitroethylbenzene was added 65 mL of absolute MeOH and a Teflon coated stir bar. To the resulting stirred yellow solution was added a slurry of 10% Pd/C (250 mg, 0.235 mmol, 0.670 mol%) in 20 mL of MeOH. To the resulting black suspension was added 9.87 g (156 mmol) of ammonium formate and the RBF was fit with a reflux condenser and N₂ inlet. The head space was purged with N₂ for ca. 10 min and the mix brought to reflux for 16 hr. The mixture was cooled to RT, filtered via vacuum through a pad of Celite® and then the pale yellow filtrate brought to dryness under vacuum. The residue was dissolved into 60 mL of H₂O and made basic with 20% NaOH (w/v) until a pH of ca. 14 was achieved (paper

indicator). The basic solution was extracted with DCM (60 ml followed by 2x30 mL). The pooled organic fractions were dried over excess anhydrous MgSO_4 , filtered via gravity through paper, and the solvent removed under vacuum affording 5.58 g (86.7%) of the product as a clear orange colored oil. This material was purified by suspending the isolated oil into ca. 100 mL of Et_2O and adding concentrated H_2SO_4 dropwise yielding a white precipitate. The mixture was sonicated, triturated with additional Et_2O , and then isolated on a glass frit. The white powder was dried under vacuum and then stored long-term in a dessicator. $^1\text{H-NMR}$ ($\text{DMSO-}d_6$) 8.32 (2H, br.s, H_2SO_4); 7.77 (2H, br.s, NH_2^-); 6.89 (1H, d, $J=8.4\text{Hz}$, aromatic H at C5); 6.87 (1H, d, $J=2.0\text{Hz}$, aromatic H at C2); 6.76 (1H, dd, $J_1=8.4\text{Hz}$, $J_2=2.0\text{Hz}$, aromatic H at C6); 3.76 (3H, s, methyl H's); 3.73 (3H, s, methyl H's); 3.03 (2H, m, methylene H's adjacent to amine); 2.80 (2H, t, $J=7.2\text{Hz}$, methylene H's adjacent to arene). $^{13}\text{C-NMR}$ (CDCl_3) δ : 149.42, 148.29, 130.23, 121.23, 113.19, 112.63, 56.16, 56.07, 40.90, 33.20 ppm.

6,7-Dimethoxy-1,2,3,4-tetrahydroisoquinoline-oxalate II.76

Into a 50 mL RBF equipped with a Teflon coated stir bar was added 5.00 g (27.6 mmol) of free-base 3,4-dimethoxy- β -phenethylamine and 30.0 mL of formic acid. To the resulting brown colored solution was added 850 mg (28.3 mmol) of paraformaldehyde and the resulting heterogeneous mixture was sealed and heated with stirring at $50.0\pm 0.1^\circ\text{C}$ in a thermostated temperature bath for 16 hr. The solvent was then removed under vacuum and the resulting red/orange oil dissolved into 100 mL of EtOH saturated with oxalic acid (ca. 5 g) affording a white fluffy precipitate. The heterogeneous mixture was cooled to 4°C for 16 hr

and then the white solids isolated via vacuum filtration yielding 7.35 g (94.0%) of the product as the oxalate salt. $^1\text{H-NMR}$ (DMSO- d_6): 6.74 (1H, s, aromatic H); 6.69 (1H, s, aromatic H); 4.62 (3H, s, NH+oxalate H's); 4.13 (2H, s, methylene H's at C1); 3.67 (3H, s, methyl H's); 3.66 (3H, s, methyl H's); 3.32 (2H, t, $J=6.0\text{Hz}$, methylene H's); 2.89 (2H, t, $J=6.0\text{Hz}$, methylene H's). $^{13}\text{C-NMR}$ (DMSO- d_6) δ : 165.81, 148.04, 147.38, 124.22, 120.11, 111.94, 109.76, 55.85, 44.17, 41.76, 23.23 ppm. There was coincidental overlap of the MeO-groups. IR (KBr pellet) $\bar{\nu}$: 3422, 3001-2590, 1917, 1723, 1615, 1520 cm^{-1} . mp (uncorrected): 196-197°C.

Fremy's salt II.80

Into a 1L beaker equipped with a large Teflon coated stir bar was added ca. 250g of crushed ice. The beaker was immersed in ice water bath and 15.0g (217mmol) of NaNO_2 were added. The mixture was stirred with a glass rod followed by the addition of 41.6g (400mmol) of NaHSO_3 and 22.5mL (23.6g, 393mmol) of glacial acetic acid. The resulting mixture was agitated with a glass rod and then stirred magnetically for 90min. The resulting solution was checked with potassium iodide-starch paper (negative) and pH paper (pH~5). To the beaker was added 50.0g (472mmol) of Na_2CO_3 and 250mL of H_2O resulting in a pH=11 solution of the inorganic hydroxylamine **II.81**. Into the solution was then immersed a homemade stainless steel electrode fabricated from 15.0cm of 0.064" stainless wire. The electrode was connected to a full-wave bridge rectifier and isolation transformer (**Figure 119**). The circuit was completed with 40.0cm of coiled 0.064" stainless steel wire immersed in a porous cup (cathode). The cup

was then suspended in the 1L beaker and filled with 10% aqueous Na_2CO_3 (w/v). The voltage was ramped with a Variac until a current of 2.00A was observed. The solution within the beaker turned a deep purple color indicating the formation of the nitrosodisulfonate radical **11.79**. After 3hr an aliquot of the solution was analyzed at $\lambda=544\text{nm}$ indicating the oxidation was 83.7% complete. Into the purple colored solution was added 76.6g (1.03mol) KCl causing an orange colored fluffy solid to precipitate from solution. The mixture was filtered on a glass frit via vacuum and the filter cake was washed with 100mL of 1M KOH. The damp filter cake was stored in a Nalgene® bottle at 4°C indefinitely. The identity of the isolated material was verified qualitatively with EPR (see Chapter 2).

Preparation of Fremy's Salt

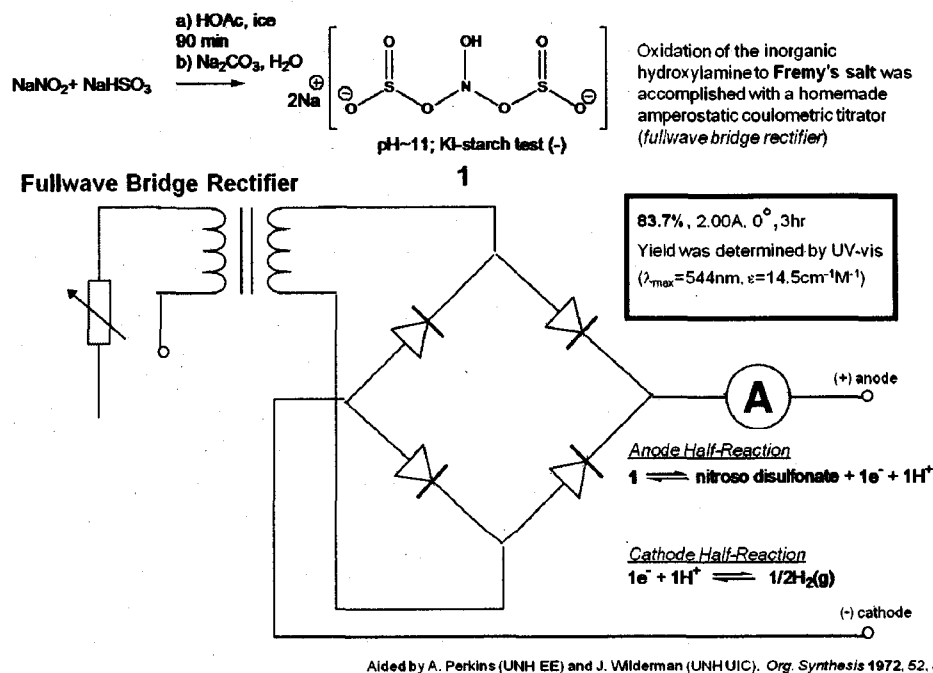


Figure 119 Schematic of the homemade amperostatic coulometric titrator.

6,7-Dimethoxyisoquinoline II.77

Into a 500 mL Erlenmeyer flask equipped with a Teflon coated stir bar was added 16 g (151mmol) Na_2CO_3 and 400mL of H_2O . To the solution was added ca. 6.1g of damp Fremy's salt and 2.47 g (8.70 mmol) of 6,7-dimethoxy-1,2,3,4-tetrahydroisoquinoline-oxalate resulting in a deep-purple colored solution. The resulting solution was stirred at RT for 2 days. An excess of Fremy's salt was maintained by adding small aliquots periodically over the course of the reaction. The aqueous solution was extracted with DCM (100 mL, followed by 2x50 mL portions) and the pooled organic fractions were dried over excess anhydrous MgSO_4 . The mixture was filtered via gravity through paper and the solvent removed under vacuum affording 1.06 g (64.5%) of the crude product. TLC (silica, 1:1 MeOH:EtOAc) indicated the presence of two compounds ($R_f=0.61$, 6,7-dimethoxyisoquinoline II.77; $R_f=0.39$, 3,4-dihydro-6,7-dimethoxyisoquinoline II.77b). The $^1\text{H-NMR}$ spectrum was used to quantify the ratio of the desired compound II.77 to II.77b: 0.89:0.11. The desired product was isolated via column chromatography (1:1 MeOH:EtOAc). $^1\text{H-NMR}$ of II.77b (CDCl_3): 9.04 (1H, s, aromatic H at C1); 8.39 (1H, d, $J=5.6\text{Hz}$, aromatic H); 7.50 (1H, d, $J=5.6\text{Hz}$, aromatic H); 7.19 (1H, s, aromatic H); 7.06 (1H, s, aromatic H); 4.04 (6H, s, methyl H's). $^1\text{H-NMR}$ of II.77 (CDCl_3): 8.23 (1H, s, imine H at C1); 6.81 (1H, s, aromatic H); 6.67 (1H, s, aromatic H); 3.92 (3H, s, methyl H's); 3.90 (3H, s, methyl H's); 3.73 (2H, t, $J=8.0\text{Hz}$, CH_2 adjacent to aromatic ring); 2.68 (2H, t, $J=8.0\text{Hz}$, CH_2 adjacent to N). $^{13}\text{C-NMR}$ of II.77 (CDCl_3) δ : 153.20, 150.51,

150.19, 142.25, 132.71, 124.96, 119.40, 105.49, 104.75, 56.29, 56.23 ppm. IR of II.77 (KBr pellet) $\bar{\nu}$: 3059, 3014, 2966-2585, 1620, 1575, 1506 cm^{-1} .

3,4-Dihydro-6,7-dimethoxy-1-methylisoquinoline II.82

Into a thermostated cell was added 5.0 mL of DCM, 1.09 g (6.00 mmol) of 3,4-dimethoxy- β -phenethylamine, 517 μL (9.00 mmol) of glacial acetic acid and approximately 5 mL of polyphosphoric acid (82% P_2O_5). The resulting viscous mixture was brought to $80.0 \pm 0.1^\circ\text{C}$ with periodic stirring with a glass rod. After 4 hr the viscous brown mixture was poured over excess cracked ice and the resulting red-colored solution was brought to pH=10 with the slow addition of excess Na_2CO_3 . The resulting solution was extracted with DCM (3x75 mL) and the pooled organic fractions dried over excess anhydrous MgSO_4 , filtered via gravity through paper and then brought to dryness under vacuum. The mass of the isolated product was 1.00 g (82.0%) of a pale yellow solid. $^1\text{H-NMR}$ (CDCl_3): 6.99 (1H, s, aromatic H); 6.69 (1H, s, aromatic H); 3.92 (3H, s, methyl H's); 3.91 (3H, s, methyl H's); 3.63 (2H, triplet of quartets, $J_1=7.4\text{Hz}$, $J_2=1.6\text{Hz}$, methylene H's); 2.64 (2H, m, methylene H's); 2.36 (3H, t, $J=1.6\text{Hz}$, methyl H's). $^{13}\text{C-NMR}$ (CDCl_3) δ : 163.84, 151.06, 147.68, 131.37, 122.75, 110.48, 109.28, 56.46, 56.20, 47.28, 25.99, 23.68 ppm. IR (KBr pellet) $\bar{\nu}$: 2994-2839, 1627, 1604, 1573, 1514 cm^{-1} .

6,7-Dimethoxy-1-methylisoquinoline II.83

Into a 250mL RBF equipped with a Teflon coated stir bar was added 1.00 g (4.87 mmol) of 3,4-dihydro-6,7-dimethoxy-1-methylisoquinoline, 50 mL of p-cymene,

and 0.500 g (0.470 mmol, 0.1 mol%) of 10% Pd/C. The RBF was fit with a reflux condenser and a N₂ inlet and the head space was purged for 10 min and then the mixture was brought to reflux for 27 hr. The mixture was filtered hot through a pad of Celite® and the filtrate was brought to dryness under vacuum. The product was isolated via column chromatography (silica, 1:1 MeOH:EtOAc, R_f=0.60) as 0.530 g (53.5%) of a yellow crystalline solid. ¹H-NMR (CDCl₃): 8.27 (1H, d, J=6.0Hz, aromatic H); 7.37 (1H, d, J=6.0Hz, aromatic H); 7.27 (1H, s, aromatic H); 7.05 (1H, s, aromatic H); 4.04 (3H, s, methyl H's); 4.03 (3H, s, methyl H's); 2.89 (3H, s, methyl H's at C1). ¹³C-NMR (CDCl₃) δ: 156.13, 152.73, 150.05, 141.18, 132.87, 123.44, 118.40, 105.49, 104.04, 56.24, 56.20, 22.73 ppm. IR (KBr pellet) $\bar{\nu}$: 3055, 3026, 2969-2840, 1619, 1569, 1506, 1481 cm⁻¹.

6,7-Dimethoxyisoquinoline-1-carboxaldehyde II.84

Into a 250 mL RBF equipped with a Teflon coated stir bar was added 0.530 g (2.61 mmol) of 6,7-dimethoxy-1-methylisoquinoline, 30 mL of dry p-dioxane and 0.500 g (4.51 mmol) SeO₂. The RBF was fit with a reflux condenser equipped with a N₂ inlet and the head space was purged for 10 min. The heterogeneous mixture was brought to reflux for 2 hr and then filtered hot through a pad of Celite®. The filtrate was brought to dryness and the desired product purified with column chromatography (silica, 1:1 MeOH:EtOAc, R_f=0.65) affording 0.196 g (34.6%) of the pure compound as a light tan crystalline solid with a sweet aroma. ¹H-NMR (CDCl₃): 10.36 (1H, s, aldehyde H); 8.74 (1H, s, aromatic H); 8.62 (1H, s, aromatic H); 7.73 (1H, d, J=5.6Hz, aromatic H); 7.12 (1H, s, aromatic H); 4.10 (3H, s, methyl H's); 4.05 (3H, s, methyl H's). ¹³C-NMR (CDCl₃) δ: 196.66,

153.36, 153.09, 147.48, 141.84, 134.65, 124.21, 123.42, 104.98, 103.66, 56.50, 56.26 ppm. IR (KBr pellet): 2997-2811, 1695, 1653, 1616, 1582, 1560, 1506 cm^{-1} .

2,4-Dimethoxy- β -nitrostyrene II.86

Into an oven dried 250 mL RBF was added 8.15 g (49.0 mmol) of 2,4-dimethoxybenzaldehyde, a Teflon coated stir bar and 20.5 mL (23.1 g, 378 mmol) of MeNO_2 . The RBF was fit with a reflux condenser and N_2 inlet and the heterogeneous mixture was refluxed for 1 hr. The resulting red solution was poured into 70% aqueous isopropyl alcohol causing a precipitation of fluffy yellow solids. The crude product was isolated on a Büchner funnel and the filter cake was washed with 70% isopropyl alcohol until the emerging filtrate was colorless. The product was recrystallized from boiling EtOH affording 7.89 g (76.6%) of a crystalline yellow solid. $^1\text{H-NMR}$ (CDCl_3): 8.08 (1H, d, $J=13.6\text{Hz}$, alkene H); 7.82 (1H, d, $J=13.6\text{Hz}$, alkene H); 7.38 (1H, d, $J=8.8\text{Hz}$, aromatic H at C6); 6.56 (1H, dd, $J_1=8.4\text{Hz}$, $J_2=2.4\text{Hz}$, aromatic H at C5); 6.49 (1H, d, $J=2.4\text{Hz}$, aromatic H at C3); 3.93 (3H, s, methyl H's); 3.87 (3H, s, methyl H's). $^{13}\text{C-NMR}$ (CDCl_3) δ : 164.61, 161.44, 136.24, 135.93, 134.56, 112.63, 106.13, 98.87, 55.86 ppm.

There is coincidental overlap of the methyl C's.

2,4-Dimethoxy- β -nitroethylbenzene II.87

Into a 250 mL RBF equipped with a Teflon coated stir bar was added 30 mL of absolute EtOH and 3.62 g (95.6 mmol) of NaBH_4 and the RBF was fit with a pressure equalizing funnel and N_2 inlet. The funnel was charged with 5.00 g

(23.9 mmol) of 2,4-dimethoxy- β -nitrostyrene dissolved in 50 mL of dry THF. The RBF was immersed in an ice bath and the solution was added to the RBF over the course of 90 min. The resulting colorless mixture was poured into 100 mL of H₂O and 40 mL of concentrated HCl was added slowly to the aqueous mixture affording vigorous effervescence. The solution was allowed to cool and then extracted with Et₂O (3x50 mL). The pooled organic fractions were dried over excess anhydrous MgSO₄, filtered via gravity through paper, and the solvent removed under vacuum yielding 4.39 g (86.9%) of a clear orange oil. ¹H-NMR (CDCl₃): 7.03 (1H, d, J=8.0Hz, aromatic H at C6); 6.45 (1H, d, J= 2.4Hz, aromatic H at C3); 6.41 (1H, dd, J₁=8.0Hz, J₂=2.4Hz, aromatic H at C3); 4.55 (2H, t, J=7.2Hz, methylene H's); 3.81 (3H, s, methyl H's); 3.79 (3H, s, methyl H's); 3.23 (t, J=7.2Hz, methylene H's). ¹³C-NMR (CDCl₃) δ : 160.69, 158.59, 131.25, 116.41, 104.37, 98.85, 75.25, 55.59, 55.49, 28.81 ppm. IR (KBr pellet) $\bar{\nu}$: 3003, 2940-2838, 1614, 1588, 1552, 1508 cm⁻¹.

2,4-Dimethoxy- β -phenethylamine II.88

Into a 250 mL RBF that contained 4.39 g (20.8 mmol) of crude 2,4-dimethoxy- β -nitroethylbenzene was added 40 mL of absolute MeOH and a Teflon coated stir bar. To the resulting stirred yellow solution was added a slurry of 10% Pd/C (146 mg, 0.137 mmol, 0.670 mol%) in 10 mL of MeOH. To the resulting black suspension was added 5.77 g (91.5 mmol) of ammonium formate and the RBF was fit with a reflux condenser and N₂ inlet. The head space was purged with N₂ for ca. 10 min and the mix brought to reflux for 16 hr. The mixture was cooled to

RT and then filtered via vacuum through a pad of Celite® and the pale yellow filtrate brought to dryness under vacuum. The residue was dissolved into 40 mL of H₂O and made basic with 20% NaOH (w/v) until a pH of *ca.* 14 was achieved (paper indicator). The basic solution was extracted with DCM (3x40 mL). The pooled organic fractions were dried over excess anhydrous MgSO₄, filtered via gravity through paper, and the solvent removed under vacuum affording 3.32 g (88.2%) of the product as an orange colored oil. ¹H-NMR (CDCl₃) 7.03 (1H, d, J=8.0Hz, aromatic H); 6.45 (1H, d, J=2.4Hz, aromatic H); 6.42 (1H, dd, J₁=8.0Hz, J₂=2.4Hz, aromatic H); 3.78 (8H, br.s, NH₂ overlapped with methyl H's); 2.87 (2H, t, J=6.8Hz, methylene H's); 2.68 (2H, t, J=6.8Hz, methylene H's). ¹³C-NMR (CDCl₃) δ: 159.52, 158.62, 130.79, 120.59, 103.93, 98.67, 55.43, 55.34, 42.48, 34.30 ppm. IR (liquid film) $\bar{\nu}$: 3367, 3296, 3262, 3177, 3073, 2999-2836, 1612, 1587, 1507 cm⁻¹.

7-Hydroxy-4-methylcoumarin II.94

Into 20 mL scintillation vial equipped with a Teflon coated stir bar was added 121 mg (0.250 mmol) of Bi(NO₃)₃·5H₂O, 651 mg (637 μL, 5.00 mmol) of ethyl acetoacetate, and 550 mg (5.00 mmol) of 1,3-dihydroxybenzene (resorcinol). The resulting mixture was brought to 75.0±0.1°C in a thermostated cell for 1 hr. The resulting heterogeneous mixture was cooled to RT and then small amounts of ice were added to the mixture affording a gummy off-white solid. The mixture was centrifuged and the supernatant decanted. The solid plug was recrystallized from boiling absolute EtOH and the product was isolated on a glass frit via vacuum. The mass of the resulting product was 756 mg (85.8%) of a white

crystalline solid. $^1\text{H-NMR}$ ($\text{DMSO-}d_6$): 10.52 (1H, br.s, phenolic H); 7.59 (1H, d, $J=8.8\text{Hz}$, aromatic H at C5); 6.81 (1H, dd, $J_1=8.8\text{Hz}$, $J_2=2.4\text{Hz}$, aromatic H at C6); 6.71 (1H, d, $J=2.4\text{Hz}$, aromatic H at C8); 6.13 (1H, d, $J=1.2\text{Hz}$, H at C3); 2.37 (3H, d, $J=1.2\text{Hz}$, methyl H's). $^{13}\text{C-NMR}$ ($\text{DMSO-}d_6$) δ : 161.83, 160.95, 155.51, 154.21, 127.29, 113.53, 112.69, 110.92, 102.85, 18.77 ppm. IR (KBr pellet) $\bar{\nu}$: 3116, 2820, 2425, 1671, 1605, 1515 cm^{-1} .

5-(Hydroxymethyl)-8-methyl-3-phenyl-2H-pyrano[2,3-c]pyridin-2-one II.100

Into a 100 mL RBF equipped with a Teflon coated stir bar was added 30 mL of H_2O and then 5.00 g (24.3 mmol) of pyridoxine-HCl. To the resulting vigorously stirred colorless solution was added 21.2 g (243 mmol) of MnO_2 followed by 30 mL of H_2O and 1.35 mL (24.3 mmol) of concentrated H_2SO_4 . The resulting heterogeneous mixture was stirred under the protection of N_2 for 2 hr at ca. 70°C in a warm oil bath. The resulting dark brown heterogeneous mixture was cooled to RT and then filtered via vacuum through a glass frit and the filtrate was transferred to a 250 mL RBF, checked with pH paper (~5), and then diluted with 50 mL of H_2O . To the brown solution was added 3.60 g (90.0 mmol) of NaOH affording copious amounts of a precipitate. The pH was checked again (~11-12) and then 2.85 g (2.80 mL, 24.3 mmol) of benzyl cyanide and 886 mg (2.43 mmol) of cetyl trimethyl ammonium bromide (CTABr) were added sequentially. The resulting orange colored heterogeneous mixture was stirred vigorously at ca. 90°C under the protection of N_2 in a warm oil bath for 0.5 hr. The resulting heterogeneous brown mix was then cooled at $1-2^\circ\text{C}$ for 16 hr. The resulting precipitate as isolated on a glass frit and washed with cold H_2O and acetone.

The filter cake was recrystallized from boiling 1:1 acetone:H₂O affording 2.47 g (38.1%) of the product as colorless needles. ¹H-NMR (DMSO-*d*₆): 8.34 (1H, s, azacoumarin H at C6); 8.26 (1H, s, azacoumarin H at C4); 7.76 (2H, m, phenyl H's); 7.50 (3H, m, phenyl H's); 5.50 (1H, t, J=5.5Hz, -OH); 4.82 (2H, d, J=5.5Hz, pseudobenzyl H's); 2.60 (3H, s, methyl H's). ¹³C-NMR (DMSO-*d*₆) δ: 159.22, 147.21, 146.43, 143.17, 136.52, 134.93, 131.99, 131.72, 129.89, 129.44, 128.96, 123.06, 58.64, 19.15 ppm. IR (KBr pellet) $\bar{\nu}$: 3168, 2902, 2840, 2731, 2642, 1722, 1601, 1558, 1505 cm⁻¹.

5-(Benzyloxymethyl)-8-methyl-3-phenyl-2H-pyrano[2,3-*c*]pyridin-2-one II.102

Into a 50 mL RBF equipped with a Teflon coated stir bar was added the 7-azacoumain II.100 (267 mg, 1.00 mmol) and 4.0 mL of DCM. To the resulting stirred suspension was added 12.0 mg (0.100 mmol) of DMAP, 167 μ L (121 mg, 1.20 mmol) of TEA and 128 μ L (155 mg, 1.10 mmol) of benzoyl chloride and the mixture was stirred at RT for 24 hr under the protection of N₂. To the heterogeneous mixture was added 30 mL of EtOAc, the reaction mixture was washed sequentially with 30mL of H₂O, 30mL of saturated aqueous NaHCO₃, 30mL of saturated NH₄Cl and then 30mL of H₂O. The isolated organic fraction was diluted with 30 mL of EtOAc, dried over excess anhydrous MgSO₄, filtered through paper via gravity, and the solvent removed under vacuum affording 250 mg (89.0%) of the product as a pale yellow solid. ¹H-NMR (CDCl₃): 8.53 (1H, s, coumarin H at C6); 8.11 (1H, s, coumarin H at C4); 8.03 (2H, m, phenyl H's); 7.69 (2H, m, phenyl H's); 7.58 (1H, m, phenyl H); 7.45 (5H, m, phenyl H's); 5.61 (2H, s, pseudobenzyl H's); 2.77 (3H, s, methyl H's). ¹³C-NMR (CDCl₃) δ: 166.20,

158.97, 149.30, 147.39, 144.98, 134.36, 134.15, 133.87, 133.73, 130.00, 129.89, 129.49, 128.89, 128.76, 124.65, 123.53, 61.17, 19.27 ppm. IR (KBr pellet) $\bar{\nu}$: 3064, 2967, 2921, 2853, 1716, 1654, 1597 cm^{-1} . HR-MS (FAB+): $m/z=372.1243$ ($M+H^+$).

5-(Benzyloxymethyl)-3-phenyl-2H-pyrano[2,3-c]pyridin-2-one-8-carboxaldehyde II.102

Into a 10mL quartz reaction tube equipped with a Teflon coated stir bar was added 100 mg (0.269 mmol) of the benzyloxy-7-azacoumarin **II.101**, 4.0 mL of dry p-dioxane and 50.7 mg (0.457 mmol) of SeO_2 . The resulting mixture was irradiated in a CEMS microwave oven for 0.5 hr in a closed vessel at 200°C and 40 psi. The power of the irradiation was controlled manually to achieve and maintain the reaction temperature (see attached plot). The resulting yellow solution was cooled to RT and then chromatographed on silica with 1:1 hexanes:EtOAc (v/v) ($R_f=0.61$) affording 216 mg (83.3%) of the desired product as a white powder with a sweet aroma. $^1\text{H-NMR}$ (CDCl_3): 10.57 (1H, s, aldehyde H); 8.84 (1H, s, azacoumarin H at C6); 8.17 (1H, s, azacoumarin H at C4); 8.05 (2H, m, phenyl H's); 7.71 (2H, m, phenyl H's); 7.60 (1H, m, phenyl H); 7.47 (5H, m, phenyl H's); 5.70 (2H, s, pseudobenzyl H's). $^{13}\text{C-NMR}$ (CDCl_3) δ : 187.98, 166.06, 157.34, 150.02, 146.01, 139.83, 134.78, 134.07, 133.59, 133.03, 131.51, 130.57, 129.98, 129.05, 128.94, 125.95, 60.75 ppm. IR (KBr pellet) $\bar{\nu}$: 3061, 2921, 2850, 1740, 1716, 1599, 1584 cm^{-1} . HR-MS (FAB+): $m/z=386.1042$ ($M+H^+$).

***N*-(5-acetyl-6-methyl-2-oxo-2H-pyran-3-yl)-benzamide II.106**

Into a 250 mL RBF equipped with a Teflon coated stir bar was added 20 mL of dry toluene, 3.09 mL (3.00 g, 30.0 mmol) of 2,4-pentanedione and 4.50 mL (4.04 g, 33.9 mmol) of DMFDMA. The RBF was fit with a reflux condenser equipped with a N₂ inlet and the head space was purged for 10 min. The reaction mixture was brought to reflux for 2 hr. The resulting orange solution was cooled to RT and the solvent was removed under vacuum. To the red colored oil was added 30 mL of Ac₂O and 5.37 g (30.0 mmol) of hippuric acid. The resulting mixture was brought to reflux for 40 min affording a deep red colored solution. The solvent was then removed under vacuum and the solid residue was recrystallized from boiling absolute EtOH affording 3.59 g (44.1%) of long, fibrous, tan colored needles. ¹H-NMR (CDCl₃): 8.91 (1H, s, pyran-2*H*-one H at C4); 8.60 (1H, br.s, NH); 7.90 (2H, m, benzoyl H's); 7.61 (1H, m, benzoyl H); 7.53 (2H, m, benzoyl H's); 2.62 (3H, s, methyl H's); 2.55 (3H, s, methyl H's). ¹³C-NMR (CDCl₃) δ: 196.15, 166.47, 162.11, 158.76, 133.49, 132.90, 129.22, 127.29, 123.67, 122.77, 116.81, 29.53, 20.13 ppm. IR (KBr) $\bar{\nu}$: 3342, 3111, 3003, 1725, 1681, 1665, 1623, 1602, 1527 cm⁻¹.

3-Benzoylamino-5-methyl-2*H*-pyrano[3,2-*c*]pyridine-2-one II.108

Into a 250 mL RBF equipped with Teflon coated stir bar was added 2.71 g (10.0 mmol) of substrate **II.106** and 20 mL of dry toluene. To the resulting stirred suspension was added 1.50 mL (1.35 g, 11.3 mmol) of DMFDMA and the RBF fit with a reflux condenser equipped with a N₂ inlet and the head space was purged

for ca. 10 min. The contents of the RBF were brought to reflux for 3 hr. An additional 10 mL aliquot of toluene was added to prevent burning the emerging precipitate. The solvent was removed under vacuum affording and the red crystalline residue was dissolved into 50 mL of AcOH. To the solution was added 1.54 g (20.0 mmol) of NH₄OAc and the reflux condenser equipped with a N₂ inlet was reattached to the RBF. The head space was purged for 10 min and then the contents of the flask were brought to reflux for 1 hr. The RBF was cooled in an ice bath and the resulting precipitate was isolated on a glass frit via vacuum. The filter cake was recrystallized from 45 mL of boiling absolute EtOH affording 617 mg (22.0%) of the product as a yellow crystalline solid. ¹H-NMR (DMSO-*d*₆): 9.83 (1H, s, pyran-2-one H at C4); 8.72 (1H, br.s, NH); 8.46 (1H, d, J=5.6Hz, pyridine H at C7); 7.97 (2H, m, phenyl H's); 7.64 (1H, m, phenyl H); 7.56 (2H, m, phenyl H's); 7.32 (1H, d, J=5.6Hz, pyridine H at C8); 2.70 (3H, s, methyl H's). ¹³C-NMR (DMSO-*d*₆) δ: 166.75, 157.56, 157.46, 156.30, 149.69, 133.91, 132.97, 129.25, 128.31, 125.51, 123.36, 114.66, 110.05, 21.94 ppm. IR (KBr pellet) $\bar{\nu}$: 3401, 3345, 3151, 2925, 1723, 1670, 1627, 1589, 1565, 1523 cm⁻¹.

3-Benzoylamino-2*H*-pyrano[3,2-*c*]pyridine-2-one-5-carboxaldehyde II.109

Into a 10 mL quartz reaction tube equipped with a Teflon coated stir bar was added 400 mg (1.43 mmol) of 3-benzoylamino-5-methyl-2*H*-pyrano[3,2-*c*]pyridine-2-one, 5.0 mL of dry p-dioxane and 317 mg (2.85 mmol) of SeO₂. The resulting mixture was irradiated in a CEMS microwave oven for 0.5 hr in a closed vessel at 175°C and 30 psi. The power of the microwave was controlled

manually to achieve and maintain the desired reaction temperature. The resulting yellow solution was cooled to RT and then chromatographed on silica with EtOAc ($R_f=0.61$) affording 290 mg (69.0%) of the desired product as a white powder with a sweet aroma. $^1\text{H-NMR}$ (CDCl_3): 10.15 (1H, s, aldehyde H); 9.90 (1H, br.s, NH); 9.67 (1H, s, azacoumarin H at C4); 8.84 (1H, d, $J=5.6\text{Hz}$, azacoumarin H at C7); 7.98 (2H, m, phenyl H's); 7.75 (1H, d, $J=5.6\text{Hz}$, azacoumarin H at C8); 7.67 (1H, m, phenyl H); 7.58 (2H, m, phenyl H's). $^{13}\text{C-NMR}$ (CDCl_3) δ : 195.27, 166.85, 156.89, 156.64, 150.01, 148.30, 133.92, 133.13, 129.34, 128.73, 128.48, 119.49, 116.47, 115.01 ppm. IR (KBr pellet) $\bar{\nu}$: 3406, 3127, 2922, 2852 1730, 1703, 1672, 1624, 1586, 1560, 1528 cm^{-1} . HR-MS (FAB+): $m/z=295.0712$ ($\text{M}+\text{H}^+$).

[Ni(TAMEquin-trisimine)](ClO_4) $_2 \cdot 1/2\text{H}_2\text{O}$ II.110

Into a 20 mL scintillation vial equipped with a Teflon coated stir bar was added 30.0 mg (0.256 mmol) of TAME dissolved in 2.3 mL of absolute EtOH. To the stirred solution was then added 11.6 mL of H_2O and 93.6 mg (0.256 mmol) of $\text{Ni}(\text{ClO}_4)_2 \cdot 6\text{H}_2\text{O}$ dissolved in 3.9 mL of H_2O affording a violet colored solution. To this solution was then added 121 mg (0.768 mmol) of 2-quinolinecarboxaldehyde dissolved in 3.0 mL of EtOH. The resulting mixture changed color from green to orange which was then followed by precipitation of an orange colored powder. The heterogeneous mixture was stirred for 16 hr at RT. The resulting mixture was cooled to $1-2^\circ\text{C}$ for 1 hr affording copious amounts of an orange colored powder. This material was then isolated on a glass frit via vacuum filtration. The resulting filter cake was recrystallized from MeCN in an Et_2O diffusion chamber

affording 61.7 mg (30.0%) of the desired product as orange colored needles. (Found: C, 52.46; H, 3.85; N, 10.49. $C_{35}H_{30}N_6NiCl_2O_8 \cdot 1/2H_2O$ requires: C, 52.47; H, 3.90; N, 10.49%). IR (KBr pellet) $\bar{\nu}$: 3073, 2969, 2931, 2874, 1665, 1621, 1597, 1512, 1100, 623 cm^{-1} . UV-vis (MeCN, 25°C): 11050 (39 $cm^{-1}M^{-1}$); ca. 12100 (32 $cm^{-1}M^{-1}$); ca. 18000 (28 $cm^{-1}M^{-1}$). MS (ESI): m/z 692 (M-ClO₄).

TAMEquin II.112

Into a 20 mL scintillation vial equipped with a Teflon coated stir bar was added 40.9 mg (51.6 μ mol) of [Ni(TAMEquin-trisimine)](ClO₄)₂ followed by 9.7 ml of H₂O and 1.3 mL of EtOH. To the stirred suspension was added 142 mg (376 mmol) of NaBH₄ and the resulting mixture was stirred for 42 hr at RT. A black granular solid formed from solution. The mixture was then quenched with the dropwise addition of concentrated HClO₄ until all the effervescence had ceased. A cream colored solid emerged from solution which was subsequently isolated via centrifugation. To the residue was added 5.0 mL of H₂O followed by a few spatula tips of NaCN immediately affording a white solid. The solid was extracted with DCM (3x5 mL), the pooled organic fractions dried over excess anhydrous Na₂SO₄, and the organic layer decanted into another vial. The solvent was removed under vacuum affording 18.9 mg (68.0%) of the product as a pale yellow solid. ¹H-NMR (CDCl₃): 7.98 (6H, t, J=8.8Hz, quinolinylnyl H's); 7.73 (3H, d, J=8.8Hz, quinolinylnyl H's); 7.65-7.61 (3H, m, quinolinylnyl H's); 7.49-7.45 (6H, m, quinolinylnyl H's); 4.11 (6H, s, pseudobenzyl H's); 2.70 (6H, s, methylene H's); ca. 2.5 (3H, br.s, NH's); 0.98 (3H, s, methyl H's). ¹³C-NMR (CDCl₃) δ : 161.34,

147.85, 136.49, 129.51, 127.73, 127.47, 126.09, 120.68, 57.12, 56.82, 38.84,
22.25 ppm.

[Ni(TAMEisoquin-trisimine)](ClO₄)₂·MeCN II.113

To a solution of TAME (30.9 mg, 264 μmol) in EtOH (2.3 mL) was added Ni(ClO₄)₂·6H₂O (93.6 mg, 256 μmol) dissolved in H₂O (4.0 mL). The resulting pale blue solution was titrated with 1-isoquinolinecarboxaldehyde (121 mg, 770 μmol) dissolved in EtOH (3.0 mL). A finely divided orange powder precipitated from solution immediately. The heterogeneous reaction mixture was allowed to stir at RT for 16 hr. The solids were filtered on a glass frit, washed with portions of Et₂O (3x10 mL), and dried under vacuum. The crude trisimine complex was recrystallized from 1:1 MeOH:MeCN (v/v) via Et₂O diffusion as large, lustrous orange needles (137 mg, 62%). IR(KBr pellet): 3256, 2964, 2933, 1623, 1589, 1458, 1322, 1093cm⁻¹. λ/cm⁻¹ (MeCN) 12550 (39cm⁻¹M⁻¹); 11450 (sh, 25cm⁻¹M⁻¹); ~19800 (~180cm⁻¹M⁻¹). (Found: C, 53.06; H, 3.99; N 11.54.

C₃₅H₃₀N₆NiCl₂O₈·C₂H₃N requires: C, 53.33; H, 3.99; N, 11.77%). Crystals suitable for X-ray crystallography were obtained by slow Et₂O diffusion into a 1:1 MeCN:MeOH (v/v) solution of the complex.

TAMEisoquin II.115

To a suspension of [Ni(TAMEisoquin-trisimine)](ClO₄)₂·2MeCN (50 mg, 63 μmol) in H₂O (10 mL) was added NaBH₄ (151 mg, 4.00 mmol). The resulting mixture was briefly sonicated and then shaken to afford copious amounts of a pale pink precipitate. The mix was stirred at RT for 3 hr. The reaction was then quenched

with the addition of concentrated HClO_4 ($\text{pH}=6$). The mixture was centrifuged and the supernatant was decanted away from the solid plug. The solids were washed with Et_2O (2x20 mL) and then dried under vacuum. The resulting pale pink solids were dissolved into MeOH (3 mL). To the solution was added excess NaCN (19.1 mg, $391\mu\text{mol}$) dissolved in H_2O (1 mL). The mixture was shaken vigorously and then extracted with DCM (3x3 mL). The organic fractions were combined, dried over Na_2SO_4 , decanted, and the solvent was removed under vacuum to afford TAMEisoquin as a pale yellow oil (34.0 mg, 99%). $^1\text{H-NMR}(\text{CDCl}_3)$: 8.39 (3H, d, $J=6.0\text{Hz}$); 8.21 (3H, d, $J=8.8\text{Hz}$); 7.77 (3H, d, $J=8.0\text{Hz}$); 7.60 (3H, m); 7.50 (3H, d, $J=6.0\text{Hz}$); 7.46 (3H, m); 4.36 (6H, s); 2.77 (6H, s); 2.53 (3H, br.s); 1.02 (3H, s). $^{13}\text{C-NMR}(\text{CDCl}_3)$: 159.54, 141.85, 136.31, 130.01, 127.35, 127.15, 127.06, 125.38, 120.06, 57.09, 54.04, 39.22, 21.95 ppm. The ligand was also prepared as a hydrochloride salt by dissolving the free amine into EtOH and adding conc. HCl dropwise. The resulting white precipitate was isolated, washed with Et_2O , and dried under vacuum. (Found: C, 54.31; H, 5.74; N, 10.86. $\text{C}_{35}\text{H}_{36}\text{N}_6 \cdot 6\text{HCl} \cdot \text{H}_2\text{O}$ requires: C, 54.07; H, 5.70; N, 10.81%).

$[\text{Zn}(\text{TAMEisoquin})](\text{ClO}_4)_2 \cdot 2\text{H}_2\text{O} \cdot 1/2\text{MeCN II.116}$

To a solution of TAMEisoquin (28.3 mg, $52.3\mu\text{mol}$) in MeOH (3 mL) was added $\text{Zn}(\text{ClO}_4)_2 \cdot 6\text{H}_2\text{O}$ (19.5 mg, $52.3\mu\text{mol}$) dissolved in MeOH (mL). The mixture was allowed to stand for 5min, and then Et_2O (20 mL) was added affording copious amounts of a white precipitate. The heterogeneous mixture was centrifuged and the supernatant was decanted. The solid plug was washed with Et_2O and then dried under vacuum affording the desired complex as a white

powder (38.4 mg, 91%). $^1\text{H-NMR(DMSO-}d_6)$: 8.44 (3H, d, $J=8.8\text{Hz}$); 8.15 (3H, d, $J=8.0\text{Hz}$); 8.01 (3H, t, $J=6.8\text{Hz}$); 7.95 (3H, d, $J=6.0\text{Hz}$); 7.89 (3H, t, $J=7.2\text{Hz}$); 7.75 (3H, d, $J=6.0\text{Hz}$); 4.83 (3H, m); 4.75 (3H, m); 4.58 (3H, m); 3.28 (3H, m); 3.05 (3H, m); 0.76 (3H, s). IR(KBr): 3280, 3070, 2920, 1627, 1598, 1101 cm^{-1} . (Found: C, 50.83; H, 4.59; N, 10.10. $\text{C}_{35}\text{H}_{36}\text{N}_6\text{ZnCl}_2\text{O}_8 \cdot 2\text{H}_2\text{O} \cdot 1/2\text{MeCN}$ requires: C, 50.19; H, 4.85; N, 10.57%). Crystals suitable for X-ray analysis were obtained via Et_2O diffusion into a 1:1 MeOH:MeCN (v/v) solution of the complex.

[Cd(TAMEisoquin)](NO₃)₂·2H₂O II.117

To a solution of TAMEisoquin (43.7 mg, 80.8 μmol) in MeOH (1.5 mL) was added $\text{Cd(NO}_3)_2 \cdot 4\text{H}_2\text{O}$ (22.9 mg, 74.2 μmol) dissolved MeOH (1.5 mL). The mixture was allowed to stand for 5 min, and then Et_2O (20 mL) was added affording copious amounts of a white precipitate. The heterogeneous mixture was centrifuged and the supernatant was decanted. The solid plug was washed with Et_2O and then dried under vacuum affording the desired complex as a white powder (55.9 mg, 96%). Microcrystals were obtained via Et_2O diffusion into a 1:1 MeNO₂:MeCN (v/v) solution of the complex. $^1\text{H-NMR(DMSO-}d_6)$: 8.69 (3H, d, $J=6.0\text{Hz}$); 8.43 (3H, d, $J=8.4\text{Hz}$); 8.14 (3H, d, $J=8.0\text{ Hz}$); 8.05 (3H, d, $J=6.0\text{Hz}$); 7.96 (3H, t, $J=7.6\text{Hz}$); 7.84 (3H, t, $J=7.2\text{Hz}$); 4.72 (6H, s); 4.55 (3H, m); 3.24 (6H, m); 0.89 (3H, s). IR(KBr pellet): 3219, 3065, 2919, 2869, 1625, 1381, 1346, 1312 cm^{-1} . (Found: C, 51.83; H, 4.64; N, 13.93. $\text{C}_{35}\text{H}_{36}\text{N}_6\text{CdN}_2\text{O}_6 \cdot 2\text{H}_2\text{O}$ requires: C, 51.70; H, 4.96; N, 13.78%).

[Ni(6,7-DMTI-trisimine)](ClO₄)₂·3H₂O II.118

To a solution of TAME (32.4 mg, 276 μmol) in EtOH (2.0 mL) was added Ni(ClO₄)₂·6H₂O (101 mg, 276 μmol) dissolved in H₂O (10 mL). The resulting pale blue solution was titrated with 6,7-dimethoxy-1-isoquinolinecarboxaldehyde II.84 (180 mg, 829 μmol) dissolved in EtOH (3.0 mL). The heterogeneous reaction mixture was refluxed for 16 hr. The yellow/orange solids were filtered on a glass frit, washed with portions of Et₂O (3x10 mL), and dried under vacuum. The crude trisimine complex was recrystallized from 1:1 MeOH:MeCN (v/v) via Et₂O diffusion as thin, red/orange needles (260 mg, 97.0%). IR (KBr pellet): 3135, 3079, 2938, 2844, 1648, 1620, 1560, 1511, 1489, 1094, 623 cm⁻¹. λ/nm (MeCN) 877 (33 cm⁻¹M⁻¹); 805 (40 cm⁻¹M⁻¹); ca. 640-500 (~275 cm⁻¹M⁻¹). (Found: C, 47.66; H, 4.70; N, 8.11. C₄₁H₄₂N₆O₆NiCl₂O₈·3H₂O requires: C, 47.97; H, 4.71; N, 8.19%).

6,7-DMTI II.119

To a suspension of [Ni(6,7-DMTI-trisimine)](ClO₄)₂ (114 mg, 117 μmol) in H₂O (20 mL) was added NaBH₄ (284 mg, 7.51 mmol) and 1.0 mL of absolute EtOH. The resulting mixture was briefly sonicated and then shaken to afford copious amounts of a pale pink precipitate. The mix was stirred at RT for 3 hr. The reaction was then quenched with the addition of concentrated HClO₄ (pH=6). The mixture was centrifuged and the supernatant was decanted away from the solid plug. The solids were washed with Et₂O (2x20 mL) and then dried under vacuum. The resulting pale pink triamine complex was dissolved into MeOH (3

mL). To the solution was added excess NaCN (19.1 mg, 391 μmol) dissolved in H_2O (1 mL). The mixture was shaken vigorously and then extracted with DCM (3x3 mL). The organic fractions were combined, dried over Na_2SO_4 , decanted, and the solvent was removed under vacuum to afford TAMEisoquin as a pale yellow oil (34.0 mg, 99%). $^1\text{H-NMR}(\text{CDCl}_3)$: 8.39 (3H, d, $J=6.0\text{Hz}$); 8.21 (3H, d, $J=8.8\text{Hz}$); 7.77 (3H, d, $J=8.0\text{Hz}$); 7.60 (3H, m); 7.50 (3H, d, $J=6.0\text{Hz}$); 7.46 (3H, m); 4.36 (6H, s); 2.77 (6H, s); 2.53 (3H, br.s); 1.02 (3H, s). $^{13}\text{C-NMR}(\text{CDCl}_3)$: 159.54, 141.85, 136.31, 130.01, 127.35, 127.15, 127.06, 125.38, 120.06, 57.09, 54.04, 39.22, 21.95 ppm. The ligand was also prepared as a hydrochloride salt by dissolving the free amine into EtOH and adding concentrated HCl dropwise. The resulting white precipitate was isolated, washed with Et_2O , and dried under vacuum. (Found: C, 54.31; H, 5.74; N, 10.86. $\text{C}_{35}\text{H}_{36}\text{N}_6 \cdot 6\text{HCl} \cdot \text{H}_2\text{O}$ requires: C, 54.07; H, 5.70; N, 10.81%).

PHOTOPHYSICAL AND BINDING CONSTANT EXPERIMENTALS

Stock solutions of the ligands TAMEisoquin **II.115** and 6,7-DMTI **II.119** with various metal ions were prepared in 1:1 DMF: H_2O (v/v). These stock solutions were then used to prepare various $\sim\mu\text{M}$ 1:1 M:L solutions. All spectral measurements were carried out in a 3 cm^3 cuvette with a 1 cm path-length. The fluorescence spectra were conducted with an excitation wavelength (λ_{ex}) of 321nm for TAMEisoquin **II.115** and 326nm for 6,7-DMTI **II.119**.

The quantum yield of the Zn(II)-complexes were determined by comparing with a quinine sulfate standard measured in 1N H₂SO₄. The formula used to calculate the quantum yield of the Zn(II) complex is:

$$\Phi_x = \Phi_{st} \frac{Grad_x}{Grad_{st}} \cdot \frac{\eta_x^2}{\eta_{st}^2}$$

(II.j)

The subscripts 'x' and 'st' refer to the experimental sample and the standard, respectively, and Grad refers to the slope of a least-squares straight line through a plot of integrated fluorescence intensity vs. absorbance. The refractive indices, η , were neglected in the computation and may introduce a small amount of error in the quantum yields reported herein.

The binding constant of TAMEisoquin for Zn(II) was assessed using a ligand exchange reaction with the strongly binding chelator TPEN. Stock solutions of [Zn(TAMEisoquin)]²⁺ and TPEN were prepared in 50mM HEPES buffered at pH = 7.2 with 0.1M KNO₃ as ionic strength adjuster. A 14 μ M solution of [Zn(TAMEisoquin)]²⁺ with 1.0 equiv of TPEN was prepared in the HEPES buffer. A decrease in the emission intensity at 355nm was monitored over the course of three weeks (T=25°C). A 14 μ M solution of [Zn(TAMEisoquin)]²⁺ without the competing ligand was also monitored as a control for photobleaching. A decrease of approximately 50% of the original emission intensity remained constant after 1 week. From this data a conditional dissociation constant K_d of 1.4 fM was calculated. The reaction was repeated with 2.0 equivalents of

competing TPEN and a K_d of 1.4 fM was calculated after the reaction obtained equilibrium.

4.4.3 Chapter 3 Experimentals

Dipicolylamine (DPA) III.4

Into a 25 mL RBF equipped with a Teflon coated stir bar was added 2-pyridinecarboxaldehyde (1000 μ L, 1.126 g, 10.5 mmol), 2.1 mL of MeOH and 2-aminomethylpyridine III.3 (1073 μ L, 1.125 g, 10.4 mmol) sequentially. The resulting solution was stirred at RT for 1 hr and then NaBH_4 was added (143 mg, 3.70 mmol) affording copious effervescence. The mixture was stirred for 16 hr and then the solvent was removed under vacuum. The residue was dissolved into H_2O (10 mL), acidified to pH=4 with concentrated HCl (evidenced by paper) and then the solution washed with CHCl_3 (2x10 mL). To the solution was added 1 M NaOH until the pH=11 and then the product was extracted with CHCl_3 (5x15 mL). The pooled organic fractions were dried over excess MgSO_4 , filtered via gravity through paper and the solvent removed under vacuum yielding 1.50 g (72.0%) of the desired product as a yellow oil. $^1\text{H-NMR}$ (CDCl_3): 8.57-8.55 (2H, m, pyridyl H's); 7.66-7.62 (2H, m, pyridyl H's); 7.36 (2H, d, $J=4.0\text{Hz}$, pyridyl H's); 7.17-7.14 (2H, m, pyridyl H's); 3.98 (4H, s, pseudobenzyl H's); 2.60 (1H, br.s, NH). $^{13}\text{C-NMR}$ (CDCl_3) δ : 159.90, 149.50, 136.64, 122.46, 122.12, 54.99 ppm. IR (liquid film) $\bar{\nu}$: 3304, 3053, 3009, 2913, 2836, 1591, 1570, 1473 cm^{-1} .

***N*-allyl-dipicolylamine III.5**

Into a 250 mL RBF equipped with a Teflon coated stir bar was added DPA III.4 (1.50 g, 7.53 mmol), 100 mL of MeCN and the K_2CO_3 (10.4 g, 75.3 mmol). To the vigorously stirred heterogeneous mixture was then added allyl bromide (2.73 g, 22.6 mmol) dropwise via pipet. The resulting mixture was sealed and stirred at RT for 16 hr. The mixture was then filtered via vacuum through a glass frit and the filtrate was brought to dryness under vacuum affording 1.69 g (94.0% crude) of the product as a dark brown oil. The crude oil was chromatographed on aluminum oxide with 4:1 hexanes:EtOAc (v/v) and the fractions that contained the compound with $R_f=0.4$ were pooled and brought to dryness under vacuum affording the desired compound as a yellow oil. 1H -NMR ($CDCl_3$): 8.52 (2H, m, pyridyl H's); 7.65 (2H, m, pyridyl H's); 7.54 (2H, d, $J=8.0$ Hz, pyridyl H's); 7.14 (2H, m, pyridyl H's); 5.94 (1H, m, allyl H); 5.24 (1H, m, allyl H); 5.16 (1H, m, allyl H); 3.82 (4H, s, pseudobenzyl H's); 3.19 (2H, m, allylic H's). ^{13}C -NMR ($CDCl_3$) δ : 160.03, 149.26, 136.57, 135.64, 123.01, 122.08, 118.11, 60.15, 57.55 ppm. IR (liquid film) $\bar{\nu}$: 3070, 3009, 2977, 2922, 2817, 1642, 1590, 1570, 1473 cm^{-1} .

***N*-hexyl-2-pyridinemethanamine III.7**

Into a 250 mL RBF equipped with a Teflon coated stir bar was added Na_2CO_3 (15.0 g, 141 mmol), 2-picolylchloride·HCl (8.20 g, 50.0 mmol) and 100 mL of MeCN. To the stirred mixture was then added *n*-hexylamine III.6 (13.2 mL, 10.1 g, 100 mmol). The RBF was fit with a reflux condenser equipped with a N_2 inlet and the contents of the flask were brought to reflux for 18 hr. The mixture was

then filtered via gravity through paper and the solvent removed under vacuum. The oil was distilled under reduced pressure (bp=90-93°C, 95-100 mTorr) affording 493 mg (5.0%) of the desired product as a yellow oil. The remainder of the crude product was set aside for future distillations. ¹H-NMR (CDCl₃): 8.55 (1H, m, pyridyl H); 7.63 (1H, m, pyridyl H); 7.31 (1H, m, pyridyl H); 7.15 (1H, m, pyridyl H); 3.90 (2H, s, pseudobenzyl H's); 2.65 (2H, t, J=7.2Hz, α-CH₂); 2.07 (1H, s, NH); 1.53 (2H, p, J=6.4Hz, β-CH₂); 1.29 (6H, m, γ,δ,ε-CH₂'s); 0.88 (3H, t, J=6.8Hz, terminal methyl H's). ¹³C-NMR (CDCl₃) δ: 160.14, 149.48, 136.58, 122.45, 122.05, 55.57, 49.97, 31.98, 30.33, 27.24, 22.81, 14.25 ppm.

***N*-acryloyl-*N*-hexyl-2-pyridinemethanamine III.8**

Into a 100 mL RBF equipped with a Teflon coated stir bar was massed the substrate III.7 (400 mg, 2.08 mmol) followed by the addition of 4.0 mL of dry toluene. The RBF was cooled in an ice bath and then the acryloyl chloride (169 μL, 188 mg, 2.08 mmol) and TEA (319 μL, 232 mg, 2.29 mmol) were added sequentially. The resulting heterogeneous mixture was stirred for 30 min under the protection of a N₂ atmosphere. The mixture was then filtered through a glass frit and the filtrate brought to dryness under vacuum affording 459 mg (90.0%) of the product as a yellow oil. ¹H-NMR (CDCl₃, rotational isomers were evidenced in the spectrum resulting in the doubling of each resonance): 8.58, 8.52 (1H, m, pyridyl H); 7.66 (2H, m, pyridyl H's); 7.32, 7.20 (1H, m, pyridyl H); 6.64, 6.51 (1H, dd, J₁=10.0Hz, J₂=16.6Hz, AMX acryloyl H); 6.44, 6.38 (1H, dd, J₁=2.0Hz, J₂=16.6Hz, AMX acryloyl H); 5.75, 5.64 (1H, dd, J₁=2.0Hz, J₂=10.0Hz, AMX

acryloyl H); 4.77, 4.71 (2H, s, pseudobenzyl H's); 3.27, 3.41 (2H, t, $J=7.6\text{Hz}$, $\alpha\text{-CH}_2$); 1.59 (2H, m, $\beta\text{-CH}_2$); 1.27 (6H, m, $\gamma,\delta,\epsilon\text{-CH}_2$'s); 0.87 (3H, m, terminal methyl H's). $^{13}\text{C-NMR}$ (CDCl_3) δ : 166.98, 166.53, 158.00, 157.63, 149.90, 149.19, 137.27, 137.01, 128.74, 128.64, 128.01, 127.53, 122.70, 122.65, 122.50, 120.64, 53.46, 51.81, 48.61, 47.47, 31.76, 31.64, 29.42, 27.76, 27.20, 26.87, 26.62, 22.73, 14.22, 14.17 ppm.

[Carboxymethyl-(acryloyl)-amino]acetic acid III.10

Into a 100 mL RBF equipped with a Teflon coated stir bar was added iminodiacetic acid (1.00 g, 7.51 mmol), 6.0 mL of 10% NaOH (w/v) and Et_2O (6.0 mL). The resulting biphasic mixture was cooled in an ice bath followed by the addition of acryloyl chloride (617 μL , 688 mg, 7.60 mmol). The mixture was allowed to warm to RT and then stirred under the protection of a N_2 atmosphere for 16 hr. To the mixture was then added concentrated HCl until a pH=3 was achieved. The aqueous layer was isolated, washed with CHCl_3 (2x5 mL), and then brought to dryness under vacuum. The residue was suspended in MeOH and diluted with EtOAc until a finely divided white powder formed. The powder was isolated on a glass frit via filtration and brought to dryness under vacuum affording 1.20 g (85.0%) of the desired product as a white powder. $^1\text{H-NMR}$ (D_2O): 6.35 (1H, dd, $J_1=10.4\text{Hz}$, $J_2=17.0\text{Hz}$, AMX acryloyl H), 6.03 (1H, dd, $J_1=1.6\text{Hz}$, $J_2=16.8\text{Hz}$, AMX acryloyl H); 5.65 (1H, dd, $J_1=1.6\text{Hz}$, $J_2=10.4\text{Hz}$, AMX acryloyl H); 3.99 (2H, s, CH_2); 3.91 (2H, s, CH_2). $^{13}\text{C-NMR}$ (D_2O) δ : 175.90,

175.04, 170.01, 129.92, 126.70, 53.17, 51.63 ppm. IR (KBr pellet) $\bar{\nu}$: 3568, 3446, 2991, 2950, 1649, 1608, 1466 cm^{-1} .

2,2'-Dichlorodiethylamine·HCl III.12

Into a 100 mL RBF equipped with a Teflon coated stir bar was added diethanolamine **III.11** (1.17 g, 11.1 mmol) and 10.0 mL of CHCl_3 . To the stirred solution was added SOCl_2 (2.44 mL, 3.98 g, 33.4 mmol) via syringe and then the RBF was fit with a reflux condenser and brought to reflux for 1.5 hr. The solvent was removed under vacuum and the residue suspended into Et_2O and sonicated. The resulting white powder was isolated on a glass frit and brought to dryness under vacuum affording 1.05 g (53.0%) of the desired product. $^1\text{H-NMR}$ ($\text{DMSO-}d_6$): 9.78 (2H, br.s, NH's); 3.97 (4H, t, $J=6.4\text{Hz}$, $\text{CH}_2\text{-N}$); 3.36 (4H, t, $J=6.4\text{Hz}$, Cl-CH_2 -). $^{13}\text{C-NMR}$ ($\text{DMSO-}d_6$) δ : 48.55, 39.66 ppm.

3,9-Dithia-6-monoazaundecane III.13

Into a 50 mL RBF equipped with a Teflon coated stir bar was added metallic sodium (644 mg, 28.0 mmol) and 25 mL of absolute EtOH . To the effervescing warm solution was then added ethanethiol (1.24 mL, 1.04 g, 16.8 mmol) and substrate **III.12** (1.00 g, 5.60 mmol). The mixture was refluxed for 2 hr under the protection of a N_2 atmosphere. The RBF was then cooled in ice and the solvent removed under vacuum. The residue was dissolved into 80 mL of H_2O and the product was extracted with DCM (3x40 mL). The pooled organic fractions were dried over excess anhydrous MgSO_4 , filtered via gravity through paper and the solvent removed under vacuum affording 800 mg (73.0%) of the desired product

as a yellow foul smelling liquid. $^1\text{H-NMR}$ (CDCl_3): 2.83 (4H, t, $J=6.0\text{Hz}$, 5,7- CH_2 's); 2.70 (4H, t, $J=6.0\text{ Hz}$, 4,8- CH_2 's); 2.55 (4H, q, $J=7.2\text{Hz}$, 2,10- CH_2 's); 1.75 (1H, br.s, NH); 1.27 (6H, t, $J=7.2\text{Hz}$, terminal methyl H's). $^{13}\text{C-NMR}$ (CDCl_3) δ : 48.52, 32.10, 26.03, 15.07 ppm.

***N*-acryloyl-3,9-dithia-6-undecanamide III.14**

Into a 50 mL RBF equipped with a Teflon coated stir bar was added the substrate III.13 (600 mg, 3.10 mmol) and 5.0 mL of dry toluene. The RBF was immersed in an ice bath and under the protection of a N_2 atmosphere the acryloyl chloride (252 μL , 281 mg, 3.10 mmol) and TEA (476 μL , 345 mg, 3.41 mmol) were added sequentially via syringe. The resulting heterogeneous mixture was stirred for 30 min. The mixture was filtered through a glass frit and the solvent removed under vacuum affording 768 mg (99.9%) of the desired product as an oily film. $^1\text{H-NMR}$ (CDCl_3): 6.56 (1H, dd, $J_1=10.4\text{Hz}$, $J_2=16.6\text{Hz}$, AMX acryloyl H); 6.38 (1H, dd, $J_1=2.0\text{Hz}$, $J_2=16.6\text{Hz}$, AMX acryloyl H); 5.73 (1H, dd, $J_1=2.0\text{Hz}$, $J_2=10.4\text{Hz}$, AMX acryloyl H); 3.59 (4H, m, 5,7- CH_2 's); 2.72 (4H, m, 2,10- CH_2 's); 2.59 (4H, m, 4,8- CH_2 's); 1.28 (6H, m, terminal methyl H's). $^{13}\text{C-NMR}$ (CDCl_3) δ : 166.23, 128.80, 127.34, 49.13, 47.57, 30.98, 29.31, 26.51, 26.23, 15.03, 14.97 ppm.

[*Tert*-butoxycarbonyl methyl-(3-vinyl-phenyl)-amino]acetic acid *tert*-butyl ester III.20

To 15.0 mL of MeCN was added 3-vinylaniline (476 μL , 4.20 mmol), proton sponge (1.98 g, 9.24 mmol), and NaI (0.316 g, 2.11 mmol) sequentially. The resulting mixture was stirred magnetically for 5 min at RT affording a nearly colorless solution. To the solution was then added *tert*-butyl bromoacetate (1.30

mL, 8.82 mmol) resulting in the immediate formation of a white ppt. The mixture was refluxed under a N₂ atmosphere for 51 hr. The heterogeneous mixture was then cooled and poured into 100 mL of EtOAc and then filtered via vacuum through a glass frit. The filtrate was collected and washed with an equal volume of brine. The organic phase was isolated, dried over excess MgSO₄, filtered via gravity through paper, and the solvent removed under vacuum. The resulting yellow oil was chromatographed on silica (2:1 hexanes:EtOAc (v/v), R_f=0.6) to remove the residual proton sponge. The purified product was a colorless oil and had a mass of 1.24 g (85.0%). ¹H-NMR (CDCl₃): 7.16 (1H, m, aromatic H); 6.83 (1H, m, aromatic H); 6.65 (1H, dd, J_{AX}=11.0Hz, vinyl AMX H, J_{MX} is obscured due to overlapping resonances); 6.61 (1H, m, aromatic H); 6.51 (1H, m, aromatic H); 5.67 (1H, dd, J_{MX}=17.6Hz, J_{AM}=0.8Hz, vinyl AMX H); 5.19 (1H, dd, J_{AX}=11.0Hz, J_{AM}=0.8Hz, vinyl AMX H); 4.02 (4H, s, methylene H's); 1.46 (18H, s, methyl H's). ¹³C-NMR (CDCl₃): 170.39, 148.52, 138.56, 137.68, 129.43, 116.40, 113.54, 112.30, 110.47, 81.84, 54.86, 28.26ppm. IR (liquid film): 3084.6, 2977.7, 1741.7, 1599.6, and 1151.2cm⁻¹. HR/EM (theory: m/z=347.2097; observed: m/z=347.2117).

2,2'-[1,2-Ethanediybis(thio)]bis-ethanamine III.24

Into a 50 mL RBF equipped with a Teflon coated stir bar was added 2-aminoethanethiol (3.09 g, 40.0 mmol) and 20 mL of absolute EtOH. To the stirred suspension was added metallic sodium (1.15 g, 50.0 mmol) and the effervescing suspension was stirred into a solution. The RBF was fit with a reflux condenser and 1,2-dichloroethane (1.58 mL, 1.98 g, 20.0 mmol) was added to the reaction

mixture dropwise resulting in a violent reaction that spontaneously refluxed. Once the addition was complete the mixture was gently refluxed for 16 hr. The solution was concentrated under vacuum and the resulting residue dissolved into 50 mL of H₂O and the product extracted with DCM (3x25 mL). The pooled organic fractions were dried over excess anhydrous MgSO₄, filtered via gravity through paper, and the solvent removed under vacuum affording 767 mg (21.2%) of the product as a waxy pale yellow solid. ¹H-NMR (CDCl₃): 2.89 (4H, t, J=6.4Hz, 2,9-CH₂'s); 2.73 (4H, s, 5,6-CH₂'s); 2.66 (4H, t, J=6.4Hz, 3,8-CH₂'s); 1.37 (4H, br.s, NH's). ¹³C-NMR (CDCl₃) δ: 41.43, 36.62, 32.18 ppm. IR (KBr pellet) $\bar{\nu}$: 3352, 3287, 2920, 2863, 1580, 1473 cm⁻¹.

[Ag (2,13-Dimethyl-6,9-dithia-3,12,18-triazabicyclo[12.3.1]octadeca-1(18),2,12,14,16-pentaene-κN3,κN12,κN18,κS6,κS9)] (ClO₄) III.25

Into a 500 mL three-way RBF equipped with two-pressure equalizing drop funnels and a reflux condenser fit with a N₂ inlet was added a large Teflon coated stir bar and 100 mL of MeOH. To the stirred solvent was then added Ag(NO₃) (799 mg, 4.70 mmol). One funnel was charged with a methanolic solution (10.0 mL) of 2,6-diacetylpyridine (767 mg, 4.70 mmol) and the other was charged with a methanolic solution (10.0 mL) of substrate **III.24** (848 mg, 4.70 mmol). The head space of the apparatus was purged with N₂ for 10 min. To the RBF was then added sequentially the 2,6-diacetylpyridine and substrate **III.24**. The resulting yellow mixture was brought to reflux in the dark for 16 hr. Within minutes of boiling a black granular solid precipitated from the reaction mixture indicative of the formation of Ag⁰. The mixture was then filtered through a glass frit and the bright yellow filtrate was diluted with a methanolic solution (10 mL) of

NaClO₄·H₂O (1.41 g, 10.0 mmol). The resulting yellow solids were sonicated into a yellow powder, isolated on a glass frit and brought to dryness under vacuum affording 899 mg (35.9 %) of the desired product as a yellow powder. ¹H-NMR (DMSO-*d*₆): 8.27 (3H, m, pyridyl H's); 3.65 (4H, m, N-CH₂'s); 3.33 (2H, s, H₂O); 3.22 (4H, t, J=5.2Hz, S-CH₂-CH₂-N's); 3.03 (4H, br.s, S-CH₂CH₂-S); 2.55 (6H, s, methyl H's). ¹³C-NMR (DMSO-*d*₆) δ: 166.15, 150.53, 141.47, 125.16, 47.54, 39.34, 34.67, 16.86 ppm. IR (KBr pellet) $\bar{\nu}$: 3429, 3145, 3102, 2965, 2921, 1636, 1581, 1417, 1089 cm⁻¹. $\lambda_{\text{max}}/\text{nm}$ (CH₃CN) 291.0 (4300 cm⁻¹M⁻¹) π - π^* , 336 (2975 cm⁻¹M⁻¹) MLCT.

2,13-Dimethyl- 6,9-dithia-3,12,18-triazabicyclo[12.3.1]octadeca-1(18),14,16-triene III.26

Into a 250 mL RBF equipped with a Teflon coated stir bar was added 100 mL of MeOH and substrate III.25 (800 mg, 1.50 mmol). To the stirred suspension was added NaBH₄ (567 mg, 15.0 mmol) and the resulting mixture was refluxed under the protection of a N₂ atmosphere for 2 hr. The reaction mixture was cooled to RT and the granular black solids (Ag⁰) were filtered on a glass frit and the filtrate was brought to dryness under vacuum. The residue was suspended into 20 mL of H₂O and ca. 10 g of NaOH was added to make the mixture basic. The product was extracted with CHCl₃ (3x50 mL), the pooled organic fractions washed with H₂O (2x25 mL), dried over excess anhydrous MgSO₄ and filtered through paper via gravity. The filtrate was brought to dryness under vacuum affording 458 mg (82.3%) of the desired product as a pale yellow oil. ¹H-NMR (CDCl₃ a mixture of a *D,L* pair and a *meso*-compound were evidenced in the spectrum): 7.60 (2H, m, pyridyl H's); 7.09 (4H, m, pyridyl H's); 3.92 (2H, q, J=6.8Hz, methine H's); 3.84

(2H, q, J=6.4Hz, methine H's); 2.62 (2H, m, methylene H's); 2.27 (4H, br.s, NH's); 1.40 (6H, d, J=1.6Hz, methyl H's); 1.39 (6H, d, J=1.6Hz, methyl H's). ¹³C-NMR (CDCl₃) δ: 164.26, 164.03, 137.15, 136.90, 120.71, 119.94, 59.33, 59.15, 47.74, 47.39, 33.89, 33.73, 32.79, 32.47, 23.18, 22.99 ppm. IR (liquid film) $\bar{\nu}$: 3293, 3058, 2966, 2922, 2845, 2715, 1590, 1574, 1466 cm⁻¹.

12,18-Diacryloyl-2,13-dimethyl- 6,9-dithia-3,12,18-triazabicyclo[12.3.1]octadeca-1(18),14,16-triene III.27

Into a 50 mL RBF equipped with a Teflon coated stir bar was added the substrate III.26 (458 mg, 1.23 mmol) and 5.0 mL of dry toluene. The RBF was immersed in an ice bath and under the protection of a N₂ atmosphere the acryloyl chloride (251 μ L, 279 mg, 3.09 mmol) and TEA (464 μ L, 337 mg, 3.33 mmol) were added sequentially via syringe. The resulting heterogeneous mixture was stirred for 30 min. The mixture was diluted with 25 mL of EtOAc and then filtered through a glass frit. The filtrate was brought to dryness under vacuum affording 516 mg (99.9%) of the desired product as an oily film. Because of the presence of rotational isomers the NMR spectra were essentially uninterpretable. IR (liquid film) $\bar{\nu}$: 3062, 2978, 2932, 2853, 2240, 1793, 1729, 1643, 1611, 1590, 1575, 1446 cm⁻¹. HR-MS (FAB+): m/z=420.1762 (M+H⁺).

N-phenyldiethanolamine ditosylate III.29

Into a 250 mL RBF equipped with a Teflon coated stir bar was added N-phenyldiethanolamine (25.0 g, 138 mmol) and 50 mL of dry pyridine. The RBF was fit with a pressure equalizing drop funnel equipped with a N₂ inlet and charged with a pyridine solution (25 mL) of p-toluenesulfonyl chloride (52.6 g,

276 mmol). After chilling the RBF in an ice bath the stopcock to the drop funnel was cracked and the reagents were mixed slowly over the course of 1 hr. The RBF was allowed to warm to RT and the heterogeneous mixture was stirred for 3 hr. The mixture was then poured into 500 mL of ice water and the resulting solids were isolated on a glass frit. A portion of the crude material was recrystallized from boiling 1:1 H₂O:EtOH (v/v) affording 3.35 g (ca. 5%) of the desired product as a white crystalline solid. The remainder of the crude was stored for later recrystallizations. ¹H-NMR (CDCl₃): 7.71 (4H, AA'XX' of the tosyl H's); 7.27 (4H, AA'XX' of the tosyl H's); 7.13 (2H, apparent t, J= 7.6Hz, phenyl H's); 6.70 (1H, apparent t, J=7.2Hz, phenyl H); 6.43 (2H, apparent d=8.4Hz, phenyl H's); 4.09 (4H, t, J=6.0Hz, O-CH₂'s); 3.55 (4H, t, J=6.0Hz, N-CH₂'s); 2.42 (6H, s, methyl H's). ¹³C-NMR (CDCl₃) δ: 145.91, 145.20, 132.77, 130.10, 129.68, 128.04, 117.77, 112.18, 66.77, 50.36, 21.86 ppm. There is coincidental overlap of two of the aromatic resonances.

[Ag(N₄S₂-macrocycle)](ClO₄)₂ III.31

Into a 50 mL RBF equipped with a Teflon coated stir bar was added 2-amino ethanethiol (945 g, 12.2 mmol) and 50 mL of absolute EtOH. To the stirred suspension was added metallic sodium (352 mg, 15.3 mmol) and the effervescing suspension was stirred into a solution. The RBF was fit with a reflux condenser and substrate **III.29** (3.00 g, 6.13 mmol) was added to the reaction mixture dropwise resulting in a violent reaction that spontaneously refluxed. Once the addition was complete the mixture was gently refluxed for 16 hr. The solution was concentrated under vacuum and the resulting residue dissolved into

20 mL of H₂O and the product extracted with DCM (3x30 mL). The pooled organic fractions were dried over excess anhydrous MgSO₄, filtered via gravity through paper, and the solvent removed under vacuum affording 1.55 mg (84.5%) of the product as a pale orange oil. The material was used as is in the subsequent chemistry without characterization.

Into a 500 mL three-way RBF equipped with two-pressure equalizing drop funnels and a reflux condenser fit with a N₂ inlet was added a large Teflon coated stir bar and 100 mL of MeOH. To the stirred solvent was then added Ag(NO₃) (854 mg, 5.03 mmol). One funnel was charged with a methanolic solution (10.0 mL) of 2,6-diacetylpyridine (821 mg, 5.03 mmol) and the other was charged with a methanolic solution (10.0 mL) of substrate **III.30** (1.506 g, 5.03 mmol). The head space of the apparatus was purged with N₂ for 10 min. To the RBF was then added sequentially the 2,6-diacetylpyridine and substrate **III.30**. The resulting yellow mixture was brought to reflux in the dark for 16 hr. Within minutes of boiling a black granular solid precipitated from the reaction mixture indicative of the formation of Ag⁰. The mixture was then filtered through a glass frit and the bright yellow filtrate was diluted with a methanolic solution (10 mL) of NaClO₄·H₂O (1.41 g, 10.0 mmol). The resulting yellow solids were sonicated into a yellow powder, isolated on a glass frit and brought to dryness under vacuum affording 1.65 g (51.9 %) of the desired product as a yellow powder. Small aliquots were recrystallized by Et₂O diffusion into a 1:1 MeCN:X (v/v, where X=MeNO₂ or MeOH) solution of the complex. ¹H-NMR (DMSO-*d*₆): 8.23 (3H, m, pyridyl H's); 7.10 (2H, m, phenyl H's); 6.89 (2H, apparent d, J=8.0Hz, phenyl

H's); 6.68 (1H, apparent t, J=7.2Hz, phenyl H); 3.75 (4H, apparent t, J=5.2Hz, methylene H's); 3.58 (4H, apparent t, J=6.0Hz, methylene H's); 3.11 (4H, apparent t, J=5.6Hz, methylene H's); 3.05 (4H, apparent t, J=5.6Hz, methylene H's); 2.43 (6H, s, methyl H's). $^{13}\text{C-NMR}$ (DMSO- d_6) δ : 166.20, 151.23, 141.08, 129.57, 125.32, 118.96, 115.88, 110.00, 51.20, 48.59, 34.84, 31.91, 16.89 ppm. IR (KBr pellet) $\bar{\nu}$: 2927, 1649, 1598, 1582, 1502, 1353, 1086, 806, 759, 621 cm^{-1} . $\lambda_{\text{max}}/\text{nm}$ (CH_3CN) 291.0 ($6500 \text{ cm}^{-1}\text{M}^{-1}$) $\pi-\pi^*$.

APPENDIX

ASPECTS OF THE IRON COORDINATION CHEMISTRY OF CURCUMIN AND THE SYNTHETIC DERIVATIVE DMCU

Summary

In appendix I the author of this dissertation will describe the work he conducted on the natural product curcumin and a synthetic derivative dimethoxycurcumin (DMCU). First a case will be created for the biological significance of curcumin. Then our interest in curcumin as a novel cellular iron chelator will be discussed citing a recent publication from our collaborators Dr. Suzy Torti, Dr. Frank Torti and their respective students at the Wake Forest University. Then the discussion will segue into what is known about the aqueous speciation of curcumin with Fe(II/III) followed by a description of the studies carried out by the author with the help of Dr. Fadi Bou-Abdallah and Dr. N. Dennis Chasteen (UNH) that show how curcumin mediates a one electron reduction of Fe(III) under basic conditions. The section will then end with conclusions and proposed future work.

Introduction

Curcumin is a naturally occurring yellow pigment found in the rhizome *Curcuma longa*, which has been used for centuries as a spice and coloring agent in eastern cuisine.(269) Characterized as a polyphenol, curcumin possesses a diverse array of functional groups (Figure 120).

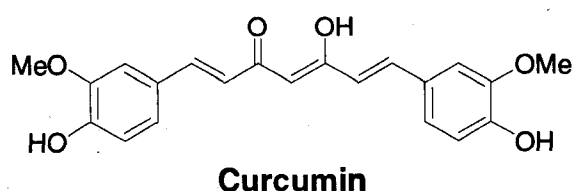


Figure 120 The structure of curcumin.

Imbedded in the core of curcumin is a β -diketone which is reminiscent of the chelating groups found in the well-known ligands acetoacetate (acac) and salen. The enol tautomer of curcumin is drawn in the figure because it dominates in both solution and the solid phase.(270) On the periphery of curcumin exists substituted phenolic groups which are appended to the diketone via alkene spacers. The presence of these olefinic groups is important because they allow curcumin to act as a Michael-acceptor.(271) This effect has been implicated in the ability of curcumin to modify biological targets like the glutathione transferase family of enzymes (GST's), which may partially explain the observed antioxidant behavior of curcumin.

There are numerous reports on the medicinal benefits of curcumin, which include its anti-inflammatory, antioxidant and anticancer properties, cardiopreventive effects and its use to treat various skin disorders.(272)

Likewise, the striking effects of curcumin on those who suffer from diabetes, rheumatoid arthritis, multiple sclerosis, Alzheimer's disease, inflammatory bowel disease, cystic fibrosis and HIV have been reported.(272) It is believed from the ample evidence available in the literature that curcumin will interact and modify gene expression, transcription factors, numerous enzymes and protein kinases.(272)

Because we are inorganic chemists we have focused our attention on the coordination chemistry of curcumin, with a particular emphasis on iron. Our underlying hypothesis in this work is that curcumin is a cellular iron chelator. Iron is both toxic and essential to biological systems.(273) Ferritin, the major iron storage protein, plays a key role in maintaining iron homeostasis by capturing and buffering the intracellular labile iron pool.(269) Work conducted on the synthetic chemopreventive agent *oltipraz* shows that ferritin plays a role in the antioxidant (phase II) response pathway.(274) Levels of ferritin are regulated both transcriptionally by oxidants and cytokines and post-transcriptionally by the labile iron in cells.(269) When cellular iron content is high, mRNA-binding ferritin repressor proteins (IRPs) are inactivated and ferritin translation is increased. Dr. Suzy Torti, Dr. Frank Torti and their coworkers have noted that *oltipraz* induced ferritin mRNA in concert with other proteins involved in the antioxidant response pathway.(274) However, the effect exhibited by curcumin was an unprecedented dissociation between the mRNA and protein regulation. They note that as ferritin mRNA increased (an effect associated with the electrophilic or antioxidant response) the amount of ferritin decreased.(269) Iron chelators are known to

bind intracellular iron and thus activate ferritin translational repressors that repress ferritin at the translational level.(275) What this means for curcumin is that, according to the Torti's, curcumin is acting as both an iron chelator and antioxidant enzyme inducer within the cell. Working closely with the Torti group we are currently interested in understanding the fundamental coordination chemistry of curcumin and its synthetic derivatives. We hope that these studies will, in part, aid in explaining some of the aforementioned biological effects.

Reported Iron Coordination Chemistry of Curcumin

There are two potential metal binding sites in curcumin, namely the β -diketone moiety and the catecholic 3-methoxy-4-hydroxy site. The diketone is the thermodynamically preferred site of metal-ion binding. This is due to the steric accessibility and the quasi-aromatic nature of the resulting chelate ring. There is scant structural evidence in the literature of transition-metal complexes of curcumin with the notable exceptions of *biscurcumin* complexes of Cu(II), which are said to be tetrahedral in geometry, and a unique $[(\eta^6\text{-p-cymene})(\text{Cl})\text{Ru}(\text{curcumin})]$ complex that is our opinion biologically irrelevant.(276, 277) Both the Cu(II) and Ru(II) species are chelated by the diketone group of the ligand. A lack of structural data in the literature provides the investigator with an impetus to obtain crystallographic information on synthetic iron-curcumin chelates to better understand the binding properties of the ligand.

However, there does exist a literature report that describes the aqueous speciation of curcumin with Fe(II/III).⁽²⁷⁸⁾ The thermodynamic data is consistent with curcumin acting as an Fe(III) chelator, which is best evidenced in the calculation of the pM values for both Fe(II) and Fe(III) at pH=7.4, 1 μ M iron, 10 μ M curcumin (Table 15).

Model	logK _{aH}	log β Fe(II)	log β Fe(III)	pM
HCurcumin ²⁻ =LH	10.51	-	-	-
H ₂ Curcumin ¹⁻ =LH ₂	9.88	-	-	-
H ₃ Curcumin=LH ₃	8.38	-	-	-
[Fe ^{II} (OH)] ⁺ =FeH-1	-	-9.3	-	-
[Fe ^{II} (OH) ₂ H ₂ Curcumin] ⁻ =LFe	-	9.20	-	-
[Fe ^{II} (OH)H ₂ Curcumin]=LFeH	-	19.76	-	-
[Fe ^{II} H ₂ Curcumin] ⁺ =LFeH ₂	-	28.11	-	-
[Fe ^{III} (OH)] ²⁺ =FeH-1	-	-	-3.5	-
[Fe ^{III} (OH) ₂] ⁺ =FeH-2	-	-	-6.37	-
[Fe ^{III} H ₂ Curcumin] ²⁺ =LFe	-	-	22.25	-
[Fe ^{III} (OH)H ₂ Curcumin] ⁺ = LFeH-1	-	-	12.14	-
Fe(II)-Curcumin	-	-	-	7.7
Fe(III)-Curcumin	-	-	-	16.7
Fe(III)-deferiprone	-	-	-	20
Fe(III)-desferrioxamine	-	-	-	26

Table 16 Reported protonation and binding constants of curcumin with iron.⁽²⁷⁸⁾

The larger the pM value is ($pM = -\log[Fe]_{free}$) the lower the concentration of free iron, which means more of the metal is bound by the chelator. The nine-decade difference between the pM values for curcumin with Fe(II) and Fe(III) (7.7 vs. 16.7) has been attributed to the better match, in terms of HSAB theory, between the oxygen donor atoms of the chelator and Fe(III). Curcumin's selectivity for Fe(III) in fact occurs across a wide-range of pH values. If one calculates the pM

value as a function of pH for curcumin the selectivity for ferric ion increases starting at ca. pH=3 (Figure 121). The plot below clearly demonstrates that curcumin will preferentially bind Fe(III) over Fe(II). As a comparison the pM values at pH=7.4, 1 μ M Fe(III), 10 μ M chelator were calculated for the well known chelators deferiprone and desferrioxamine (Table 15).(269)

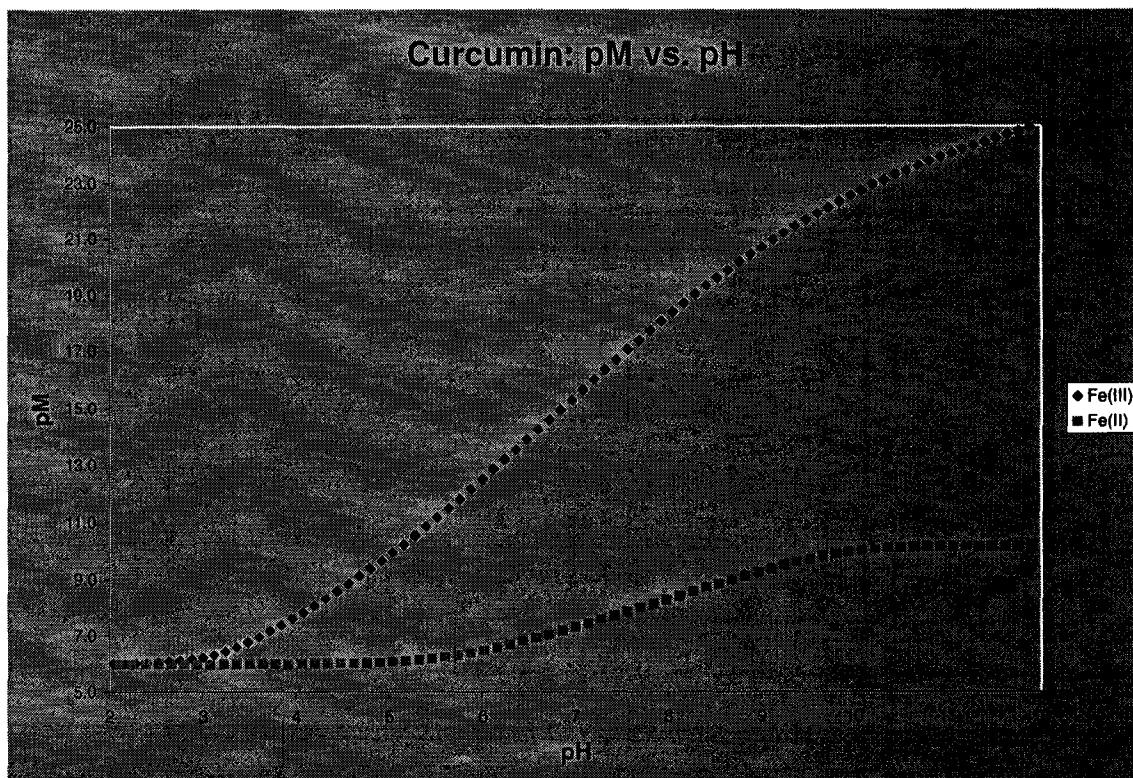


Figure 121 Calculated pM values for curcumin with Fe(III) (blue curve) and Fe(II) (pink curve) as a function of pH.

The reduced pM for curcumin as compared to these iron chelators, which are typically used to treat iron overload, is related to its reduced denticity (*i.e.* curcumin is bidentate and deferiprone and desferrioxamine are tetra- and hexadentate respectively). However, the pM value for curcumin compares favorably to the iron chelator nitrilotriacetic acid (NTA) and many other iron chelators and as such is consistent with chelation activity *in vivo*.(34, 269)

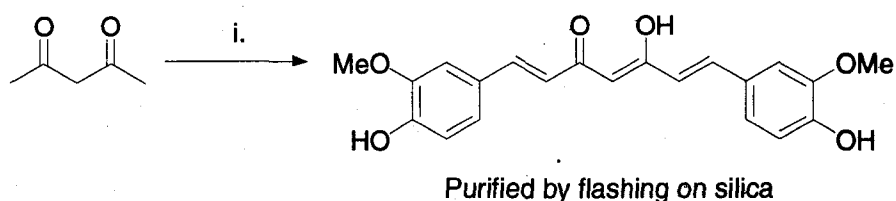
The Challenge of Curcumin

Drawing inspiration from the studies carried out by the Torti group at Wake Forest University we decided to further explore the iron coordination chemistry of curcumin to better understand the structure and reactivity of the proposed metal complexes. A major challenge when working with curcumin is its limited water solubility, so one goal of this particular project is to create synthetic derivatives of curcumin that possess enhanced water solubility as compared to the native compound. These modifications, however, cannot sacrifice the functionality that is responsible for the aforementioned biological activity. Another goal of this project is to better understand the observed effects curcumin has on iron metabolism. Because there was a lack of structural information for Fe-curcumin complexes in the literature we initially attempted to synthesize metal complexes of the ligand and characterize their structures with X-ray crystallography. These efforts were not met with any success. The following discussion, however, describes what was learned from our studies.

Ligand Preparation and Iron Complexation Experiments

The ligands curcumin, prepared by our coworker Joon Cho, and the synthetic derivative DMCU, prepared by the author, can be synthesized straightforwardly in one step taking advantage of the chemistry developed by Pedersen *et al* (Scheme 52).⁽²⁷⁹⁾ The reaction sequence began by treating acetoacetate (acac) with B_2O_3 affording a 2:1 acac:boron complex *in situ*. This step served to protect the interstitial methine against unfavorable Knoevenagel

condensations upon treatment of the reaction mixture with the benzaldehyde derivative and $B(OiPr)_3$ (*i.e.* to make curcumin the benzaldehyde derivative needs to be vanillin and to make DMCU the benzaldehyde derivative is 3,4-dimethoxybenzaldehyde). The resulting mixture is then made basic with TEA and then heated overnight resulting in a regioselective aldol condensation on the terminal methyls of the boron bound acac groups. The resulting chelated curcumin is liberated from the boron center upon acidification and the isolated crude product is purified with flash column chromatography on silica. This afforded spectroscopically pure curcumin in low to modest yields (*ca.* 10-30%). The advantage of this synthetic strategy is the limited number of steps and the ease with which curcumin derivatives can be prepared. In fact, the derivative DMCU was prepared under identical conditions by simply switching the vanillin substrate with 3,4-dimethoxybenzaldehyde.



i. a) 0.7 equiv B_2O_3 , EtOAc 40°C, 30 min b) 2.0 equiv vanillin, 2.0 equiv $B(OiPr)_3$, EtOAc, 40°C, 30 min c) 1.5 equiv TEA, EtOAc, dropwise addition over 15 min, 40°C, 18 hr d) 1.2N HCl, 60°C, 1 hr

Scheme 52 The preparation of curcumin.

With the ligands in hand complexation studies with iron ensued. We were initially hoping to see 1:2 or even 1:3 metal complexes of curcumin (depending on the oxidation state of the iron employed). However, from the aforementioned

speciation data only 1:1 complexes were reported in aqueous solvent systems. Work carried out by Saladini *et al.* on glycosyl-curcuminoid derivatives show 1:2 complexes with both Ga(III) and Fe(III) in water.(280) In our studies when one equivalent of $\text{FeCl}_3 \cdot 6\text{H}_2\text{O}$ was mixed with two equivalents of curcumin and two equivalents of NaOH (used to deprotonate the enolic proton to aid in complexation) in methanol a brown precipitate emerged from solution. This material was centrifuged, isolated and dried under vacuum. The MALDI-TOF mass spectrum (matrix: gentisic acid 10mg/mL in 450/50 MeCN/water+0.01%TFA. Fullerene was used in the calibration) of this isolated material reveals the presence of a 2:1 curcumin:iron complex ($m/z=790$) (**Figure 122**).

Date: dkh84 -2 shots0001.P2 3 Nov 2006 8:49 Cal: David 9 Sep 2006 13:48
Kratos PC Axima CFRplus V2.3.4: Mode reflectron, Power: 164, P.Ext. @ 1400 (bin 128)

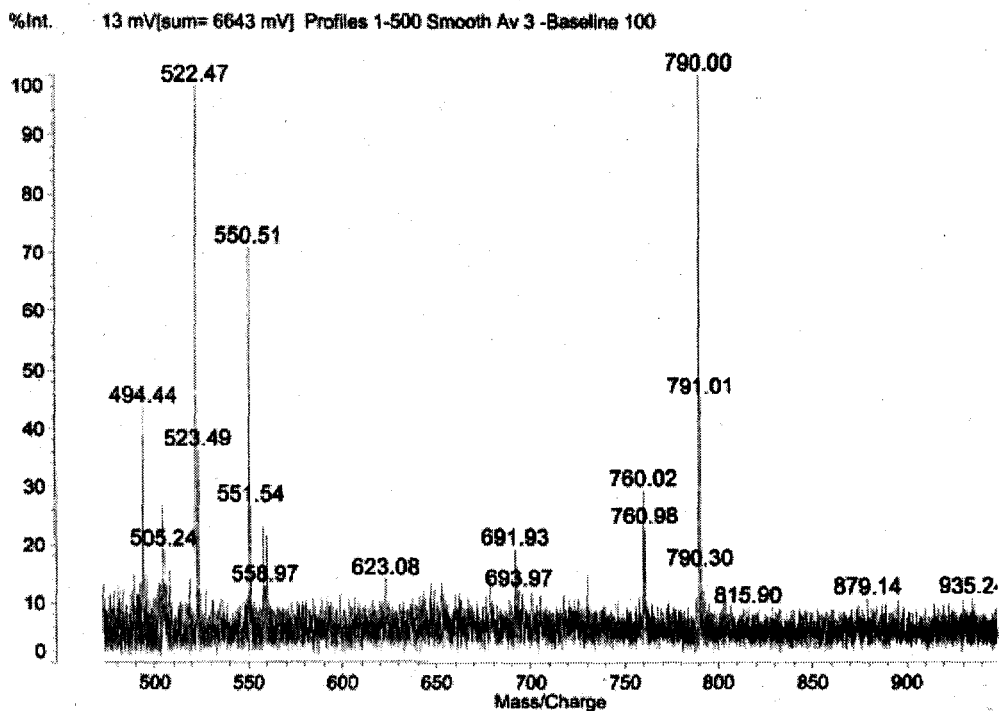


Figure 122 The MALDI-TOF MS of the isolated brown powder.

One argument invoked to explain the coordination unsaturation in the speciation data is based on interligand steric congestion within the inner coordination sphere of higher order Fe-curcumin complexes. Repulsions may lead to attenuated binding affinities resulting in the reported 1:1 complexes with curcumin. The author of this dissertation believes that poor solubility is the reason a 1:2 complex of curcumin with iron has failed to be accounted for in the speciation data.

To further study this chemistry the author worked closely with Dr. Fadi Bou-Abdallah and Dr. N. Dennis Chasteen. Mixing $\text{FeCl}_3 \cdot 6\text{H}_2\text{O}$, curcumin and NaOH in a 1:1:2 ratio in MeOH did not afford the brown precipitate but instead

gave a dark colored solution which could be studied with EPR spectroscopy (Figure 123).

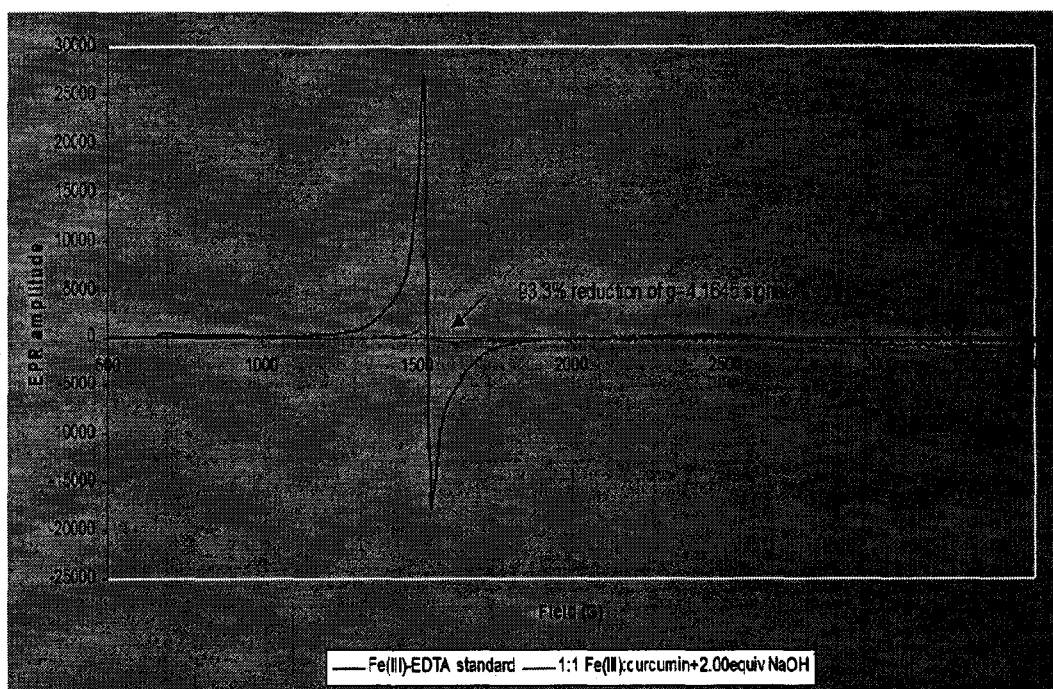


Figure 123 EPR spectra of standard Fe(III)-EDTA and Fe(III)-curcumin.

A standard Fe(III)-EDTA sample in pH=7 water was provided and checked by the Chasteen lab. Both the standard and the sample were analyzed at $[\text{Fe(III)}]_{\text{tot}}=100\text{mM}$. The Fe-curcumin sample was prepared by adding 2.0 equiv of commercially available standardized 1.000N NaOH (EM science) to a methanol solution of commercially available curcumin (Acros, 98%). To the resulting crimson red solution (presumably a dianionic curcumin species) was added 1.0 equiv of $\text{FeCl}_3 \cdot 6\text{H}_2\text{O}$ dissolved in methanol. The resulting solution was shaken and then analyzed frozen at 77K using X-band EPR (frequency=9.156951GHz). The instrumental parameters were set as the following:

modulation frequency=10G; modulation amplitude=100kHz; receiver gain= 60dB; time constant=655.36ms; sweep time=335.54s; conversion time=81.92ms; power=17.09mW; attenuation=11dB; number of scans=1; centerfield=2000G, sweep-width=3000G, number of data points=4096.

Aggregation within the sample was checked by analyzing at the following $[\text{Fe(III)}]_{\text{tot}}$ concentrations: 5mM, 1mM, 0.5mM, 0.1mM. Quantitation at the $g\sim 4.3$ signal was accomplished via double integration of this feature.

The EPR data suggests that in the presence of base curcumin will reduce the oxidation state of Fe(III) to Fe(II). Loss of intensity at the $g=4.3$ feature as compared to the Fe-EDTA standard is consistent with either aggregation within the sample or reduction of the oxidation state. Aggregation was ruled out as a possibility by running serial dilutions of the sample and plotting the double integral as a function of total Fe(III) concentration. This resulted in a linear relationship (not shown). An EPR spectrum is not expected for Fe(II) species because of the even number of unpaired electrons for a HS d^6 metal in an octahedral field. This results in a loss of the so-called Kramer's degeneracy.(87)

To confirm if redox chemistry was taking place between curcumin and Fe(III) NMR was used to measure the magnetic susceptibility of various mixtures of iron and curcumin (Table 16).(281)

Sample	χ_m' (cm ³ mol ⁻¹)	n	μ_{eff} (B.M.)
FeCl ₃ ·6H ₂ O alone	0.01374	4.8	5.7
1:1 Fe-curcumin no NaOD added	0.01380	4.8	5.7
1:1 Fe-curcumin +2.00 equiv NaOD	0.01066	4.2	5.1
1:1 Fe-DMCU +2.00 equiv NaOD	0.01622	5.2	6.2

Table 17 Measured magnetic moments for various solutions of curcumin and Fe(III).

The experiments were carried out at room temperature ($T=296\text{K}$) with $[\text{Fe(III)}]_{\text{tot}}=5\text{-}10\text{ mM}$ in $\text{MeOH-}d_4$ containing $^t\text{BuOH}$ (5% v/v). To the samples was added a sealed capillary tube containing the solvent system alone. Quantitation of the magnetic susceptibility was done using the following expression:

$$\chi_m = 477 \frac{\Delta\nu}{2 \cdot \nu_1 \cdot c}$$

where the difference in frequency of the $^t\text{BuOH}$ resonance in contact with the paramagnetic material and the $^t\text{BuOH}$ in the capillary tube is $\Delta\nu$, the field strength of the NMR instrument is ν_1 (400 MHz); and the concentration of the sample is c (given in mol L⁻¹). The corrected magnetic susceptibility (χ_m') was calculated using the diamagnetic contributions from: 1) the metal core electrons (-13·10⁻⁶ cm³mol⁻¹); 2) the chloride anions (3x-23·10⁻⁶ cm³mol⁻¹); 3) the hydration sphere of the ferric chloride reagent (6x-13·10⁻⁶ cm³mol⁻¹); 4) the curcumin (-180·10⁻⁶ cm³mol⁻¹, estimated from Pascal's constants).⁽⁶⁷⁾ The number of unpaired electrons (n) per metal ion and the magnetic moments (μ_{eff}) were calculated from the NMR data using the following expressions:

$$8 \cdot \chi'_m \cdot T = n \cdot (n + 2)$$

$$\mu_{eff} = \sqrt{8 \cdot \chi'_m \cdot T}$$

The data in the table shows that Fe(III) is being reduced to Fe(II) when the stoichiometry of the reaction solution was 1:1:2 in curcumin:Fe(III):NaOH.

Another striking feature observed from the data was that DMCU did not afford a reduction with Fe(III) suggesting that the phenolic group, present only in curcumin, is responsible for the observed redox behavior.

Conclusions and Future Work

From the data the author of this dissertation has proposed a mechanism for the redox activity of curcumin with Fe(III) (**Figure 124**).

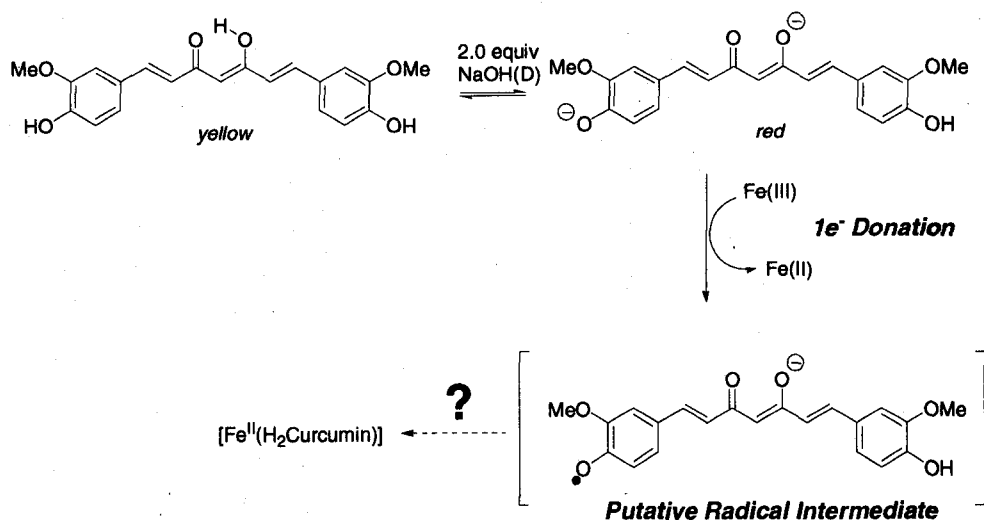


Figure 124 Proposed mechanism for curcumin mediated reduction of Fe(III).

The proposed mechanism involves the intermediacy of a radical curcumin species. It is believed that extended delocalization of the unpaired spin density accounts for the relative longevity of this species. Somehow the damaged

curcumin radical needs to be repaired at the expense of something in solution before it can form a complex with Fe(II). The details for this specific reaction remain elusive. In the case of DMCU the phenol is not present and as such the methoxy group on the 3-position of the aromatic ring does not reduce Fe(III). To further support this proposed mechanism stopped-flow and freeze-quench experiments needed to be conducted to intercept and characterize the fleeting intermediates.

In summary, curcumin acts both as an antioxidant enzyme inducer and cellular iron chelator. Moreover, curcumin is an Fe(III) chelator and does form higher order complexes with iron (*i.e.* 1:2 and perhaps 1:3 Fe:curcumin species). Lastly, curcuminoids that bear phenolic groups participate in redox chemistry with iron. Work is currently being conducted by Joon Cho with the help of the Chasteen lab to further support the curcumin mediated reduction of Fe(III) to Fe(II).

Dimethoxycurcumin (DMCU)

Into a 100 mL RBF equipped with a Teflon coated stir bar was added acetoacetate (1.00 g, 1.03 mL, 10.0 mmol), 10 mL of EtOAc and B₂O₃ (50 mg, 7.00 mmol). The flask was then fit with a Claisen adapter equipped with a rubber septum and N₂ inlet. The head space was purged with N₂ for 10 min and then the RBF was immersed in a thermostated bath at 40°C for 0.5 hr. A milky white suspension formed in the RBF. To the RBF was added a solution of 3,4-dimethoxybenzaldehyde (3.32 g, 20.0 mmol) dissolved in 5 mL of EtOAc followed

by neat $B(OiPr)_3$ (3.76 g, 4.61 mL, 20.0 mmol) via syringe. The resulting homogeneous orange colored solution was stirred an additional 0.5 hr at 40°C. To the solution was then added TEA (887 mg, 1.28 mL, 15.0 mmol) dissolved in 10 mL of EtOAc. After 15 min the solution developed a rich red color. After stirring for nearly 19 hr the temperature of the thermostated bath was raised to 60°C and to the reaction mixture was added 1.5 mL of concentrated HCl and 8.5 mL of H₂O. After 1 hr the resulting biphasic mixture was allowed to cool to RT followed by isolation of the organic layer. The aqueous layer was extracted with additional portions of EtOAc (3x10 mL) and the combined organic fractions were washed with saturated brine and dried over excess anhydrous MgSO₄. The mixture was filtered via gravity through paper and the solvent removed under vacuum leaving 3.51 g (88.0% crude yield) of a red glass. The crude mixture was chromatographed on silica with 2:3 Et₂O:hexanes (v/v) and the fractions that contained the compound with $R_f=0.30$ were pooled and brought to dryness. The resulting orange powder was the desired compound and proved to be spectroscopically pure. ¹H-NMR (CDCl₃): 7.61 (2H, J=16.0 Hz, alkene H's); 7.14 (2H, dd, J₁=2.0Hz, J₂=8.4Hz, aromatic H's); 7.08 (2H, d, J=2.0Hz, aromatic H's); 6.88 (2H, d, J=8.4Hz, aromatic H's); 6.50 (2H, d, J=15.6Hz, alkene H's); 5.82 (1H, s, methine H); 3.94 (6H, s, methoxy H's); 3.92 (6H, s, methoxy H's). ¹³C-NMR (CDCl₃): 183.46, 151.25, 149.44, 140.61, 128.27, 122.85, 122.24, 111.33, 109.94, 101.51, 56.20, 56.12 ppm.

REFERENCES

1. Martell, A. E., Perutka, J., and Kong, D. (2001) Dinuclear metal complexes and ligands: stabilities and catalytic effects, *Coordination Chemistry Reviews* 216-217, 55-63.
2. Curtis, N. F. (1968) Macrocyclic coordination compounds formed by condensation of metal-amine complexes with aliphatic carbonyl compounds, *Coordination Chemistry Reviews* 3, 3-47.
3. Alexander, V. (1995) Design and Synthesis of Macrocyclic Ligands and Their Complexes of Lanthanides and Actinides, *Chemical Reviews (Washington, D. C.)* 95, 273-342.
4. Okawa, H., Furutachi, H., and Fenton, D. E. (1998) Heterodinuclear metal complexes of phenol-based compartmental macrocycles, *Coordination Chemistry Reviews* 174, 51-75.
5. Lindoy, L. F. (1989) The development of mixed donor macrocyclic systems for metal-ion discrimination, *Pure and Applied Chemistry* 61, 1575-1580.
6. Guerriero, P., Tamburini, S., and Vigato, P. A. (1995) From mononuclear to polynuclear macrocyclic or macroacyclic complexes, *Coordination Chemistry Reviews* 139, 17-243.
7. Kahn, O. (1995) Magnetism of heterobimetallics: toward molecular-based magnets, *Advances in Inorganic Chemistry* 43, 179-259.
8. Murray, K. S. (1995) The magnetochemistry of homo- and hetero-tetranuclear first-row d-block complexes, *Advances in Inorganic Chemistry* 43, 261-358.
9. Akita, M., and Hikichi, S. (2002) Inorganic chemistry based on Tp ligands -from dioxygen complexes to organometallic systems, *Bulletin of the Chemical Society of Japan* 75, 1657-1679.
10. Amendola, V., Fabbrizzi, L., and Pallavicini, P. (2001) Controlling the assembling/disassembling process of metal-containing superstructures, *Coordination Chemistry Reviews* 216-217, 435-448.
11. Beer, P. D., and Smith, D. K. (1997) Anion binding and recognition by inorganic based receptors, *Progress in Inorganic Chemistry* 46, 1-96.
12. Brooker, S. (2001) Complexes of thiophenolate-containing Schiff-base macrocycles and their amine analogues, *Coordination Chemistry Reviews* 222, 33-56.
13. Abeysinghe, R. D., Greene, B. T., Haynes, R., Willingham, M. C., Turner, J., Planalp, R. P., Brechbiel, M. W., Torti, F. M., and Torti, S. V. (2001) p53-independent

apoptosis mediated by tachpyridine, an anti-cancer iron chelator, *Carcinogenesis FIELD Full Journal Title: Carcinogenesis* 22, 1607-1614.

14. Greene, B. T., Thorburn, J., Willingham, M. C., Thorburn, A., Planalp, R. P., Brechbiel, M. W., Jennings-Gee, J., Wilkinson, J. I. V., Torti, F. M., and Torti, S. V. (2002) Activation of caspase pathways during iron chelator-mediated apoptosis, *Journal of Biological Chemistry* 277, 25568-25575.
15. Torti, S. V., Torti, F. M., Whitman, S. P., Brechbiel, M. W., Park, G., and Planalp, R. P. (1998) Tumor cell cytotoxicity of a novel metal chelator, *Blood* 92, 1384-1389.
16. Bowen, T., Planalp, R. P., and Brechbiel, M. W. (1996) An improved synthesis of cis,cis-1,3,5-triaminocyclohexane. Synthesis of novel hexadentate ligand derivatives for the preparation of gallium radiopharmaceuticals, *Bioorganic & Medicinal Chemistry Letters* 6, 807-810.
17. Ward, M. D. (2001) Supramolecular coordination chemistry, *Annual Reports on the Progress of Chemistry, Section A: Inorganic Chemistry* 97, 293-329.
18. Vigato, P. A., and Tamburini, S. (2004) The challenge of cyclic and acyclic Schiff bases and related derivatives, *Coordination Chemistry Reviews* 248, 1717-2128.
19. Richardson, D. R., Tran, E. H., and Ponka, P. (1995) The potential of iron chelators of the pyridoxal isonicotinoyl hydrazone class as effective antiproliferative agents, *Blood* 86, 4295-4306.
20. Schaus, S. E., Brandes, B. D., Larrow, J. F., Tokunaga, M., Hansen, K. B., Gould, A. E., Furrow, M. E., and Jacobsen, E. N. (2002) Highly Selective Hydrolytic Kinetic Resolution of Terminal Epoxides Catalyzed by Chiral (salen)Co(III) Complexes. Practical Synthesis of Enantioenriched Terminal Epoxides and 1,2-Diols, *Journal of the American Chemical Society* 124, 1307-1315.
21. Carey, F. A., Sundberg, R. J., and Editors (2000) *Advanced Organic Chemistry, Part A: Structure and Mechanisms, Fourth Edition*.
22. Busch, D. H. (1963) Reactions of ligands in metal complexes, *Advances in Chemistry Series* 37, 1-18.
23. Blinn, E. L., and Busch, D. H. (1968) Reactions of coordinated ligands. XV. Demonstration of the kinetic coordination template effect, *Inorganic Chemistry* 7, 820-824.
24. Costisor, O., Linert, W., and Editors (2004) *Metal Mediated Template Synthesis of Ligands*.
25. Cook, D. H., Fenton, D. E., Drew, M. G. B., Rodgers, A., McCann, M., and Nelson, S. M. (1979) Mononuclear and homobinuclear lead(II) complexes of macrocyclic Schiff

- bases, *Journal of the Chemical Society, Dalton Transactions: Inorganic Chemistry (1972-1999)*, 414-419.
26. Cook, D. H., and Fenton, D. E. (1979) Alkaline earth metal complexes of macrocyclic Schiff bases derived from furan-2,5-dicarbaldehyde, *Journal of the Chemical Society, Dalton Transactions: Inorganic Chemistry (1972-1999)*, 810-813.
27. Cook, D. H., and Fenton, D. E. (1979) Calcium, strontium, and barium complexes of pyridyl-containing macrocyclic Schiff bases, *Journal of the Chemical Society, Dalton Transactions: Inorganic Chemistry (1972-1999)*, 266-272.
28. Wulfsberg, G. (2000) *Inorganic Chemistry*, 1 ed., University Science Books, Sausalito.
29. Shannon, R. D. (1976) Revised effective ionic radii and systematic studies of interatomic distances in halides and chalcogenides, *Acta Crystallographica, Section A: Crystal Physics, Diffraction, Theoretical and General Crystallography A32*, 751-767.
30. Herrera, A. M., Staples, R. J., Kryatov, S. V., Nazarenko, A. Y., and Rybak-Akimova, E. V. (2003) Nickel(II) and copper(II) complexes with pyridine-containing macrocycles bearing an aminopropyl pendant arm: synthesis, characterization, and modifications of the pendant amino group, *Dalton Transactions*, 846-856.
31. Lin, H.-K., Wang, X., Su, X.-C., Zhu, S.-R., and Chen, Y.-T. (2002) Synthesis and thermodynamic properties of novel tripod ligands and their cobalt(II), nickel(II), copper(II) and zinc(II) complexes, *Transition Metal Chemistry (Dordrecht, Netherlands)* 27, 384-389.
32. Bollinger, J. E., Mague, J. T., and Roundhill, D. M. (1994) Lipophilic Hexadentate Aluminum, Gallium, Indium, and Iron Complexes of a New Phenolate-Derivatized Cyclohexanetriamine Ligand, *Inorganic Chemistry* 33, 1241-1242.
33. Lions, F., and Martin, K. V. (1957) Sexadentate chelate compounds. IX, *Journal of the American Chemical Society* 79, 1572-1575.
34. Hancock, R. D., and Martell, A. E. (1989) Ligand design for selective complexation of metal ions in aqueous solution, *Chemical Reviews (Washington, DC, United States)* 89, 1875-1914.
35. Pearson, R. G. (1963) Hard and soft acids and bases, *Journal of the American Chemical Society* 85, 3533-3539.
36. Gillum, W. O., Wentworth, R. A. D., and Childers, R. F. (1970) Hindered ligand systems. IV. Complexes of cis,cis-1,3,5-tris(pyridine-2-carboxaldimino)cyclohexane. Trigonal-prismatic vs. octahedral coordination, *Inorganic Chemistry* 9, 1825-1832.

37. Fleischer, E. B., Gebala, A. E., and Swift, D. R. (1971) Single-crystal structure of [cis,cis-1,3,5-tris(2-pyridinealdimino)cyclohexane]nickel(II) perchlorate, *Journal of the Chemical Society [Section] D: Chemical Communications*, 1280-1281.
38. Hilfiker, K. A., Brechbiel, M. W., Rogers, R. D., and Planalp, R. P. (1997) Tricationic Metal Complexes ([ML][NO₃]₃, M = Ga, In) of N,N',N''-Tris(2-pyridylmethyl)-cis-1,3,5-triaminocyclohexane: Preparation and Structure, *Inorganic Chemistry* 36, 4600-4603.
39. Park, G., Ye, N., Rogers, R. D., Brechbiel, M. W., and Planalp, R. P. (2000) Effect of metal size on coordination geometry of N,N',N''-tris(2-pyridylmethyl)-cis,cis-1,3,5-triaminocyclohexane: synthesis and structure of [MIII](ClO₄)₂ (M = Zn, Cd and Hg), *Polyhedron* 19, 1155-1161.
40. Park, G., Lu, F. H., Ye, N., Brechbiel, M. W., Torti, S. V., Torti, F. M., and Planalp, R. P. (1998) Novel iron complexes and chelators based on cis,cis-1,3,5-triaminocyclohexane: iron-mediated ligand oxidation and biochemical properties, *JBIC, Journal of Biological Inorganic Chemistry* 3, 449-457.
41. Park, G. (September 2000) Transition Metal Complexes of Novel Ligands Derived from the Cis,Cis-1,3,5-Triaminocyclohexane (TACH) Framework: Structural and Biological Studies, in *Chemistry*, p 503, University of New Hampshire, Durham.
42. Childers, M. L. (May 2007) I. Complexation of Fe(II), Co(II), Ni(II), and Cu(II) by Hexadentate Tripodal Aminopyridyl Chelators II. Binding Preferences for Zn(II) Relative to Ni(II) and Cu(II) in Novel Tetradentate Aminopyridyl Chelators, in *Chemistry*, p 154, University of New Hampshire, Durham.
43. Park, G., Przyborowska, A. M., Ye, N., Tsoupas, N. M., Bauer, C. B., Broker, G. A., Rogers, R. D., Brechbiel, M. W., and Planalp, R. P. (2003) Steric effects caused by N-alkylation of the tripodal chelator N,N',N''-tris(2-pyridylmethyl)-cis,cis-1,3,5-triaminocyclohexane (tachpyr): structural and electronic properties of the Mn(II), Co(II), Ni(II), Cu(II) and Zn(II) complexes, *Dalton Transactions*, 318-324.
44. Childers, M. L., Su, F., Przyborowska, A. M., Bishwokarma, B., Park, G., Brechbiel, M. W., Torti, S. V., Torti, F. M., Broker, G., Alexander, J. S., Rogers, R. D., Ruhlandt-Senge, K., and Planalp, R. P. (2005) Pyridine-ring alkylation of cytotoxic r-1,c-3,c-5-tris[(2-pyridylmethyl)amino]cyclohexane chelators: Structural and electronic properties of the MnII, FeII, NiII, CuII and ZnII complexes, *European Journal of Inorganic Chemistry*, 3971-3982.
45. Wieghardt, K., Schoeffmann, E., Nuber, B., and Weiss, J. (1986) Syntheses, properties and electrochemistry of transition-metal complexes of the macrocycle 1,4,7-tris(2-pyridylmethyl)-1,4,7-triazacyclononane (L). Crystal structures of [NiL](ClO₄)₂, [MnL](ClO₄)₂, and [PdL](PF₆)₂ containing a distorted-square-base-pyramidal PdIIN5 core, *Inorganic Chemistry* 25, 4877-4883.

46. Christiansen, L., Hendrickson, D. N., Toftlund, H., Wilson, S. R., and Xie, C. L. (1986) Synthesis and structure of metal complexes of triaza macrocycles with three pendant pyridylmethyl arms, *Inorganic Chemistry* 25, 2813-2818.
47. Cotton, F. A., Wilkinson, G., Bochmann, M., and Murillo, C. (1998) *Advanced Inorganic Chemistry, 6th Edition*.
48. Tsukube, H., Yamashita, K., Iwachido, T., and Zenki, M. (1989) Triazamacrocycle having pyridine-pendant arms as a new sodium ion-selective ionophore, *Tetrahedron Letters* 30, 3983-3986.
49. Tsukube, H., Yamashita, K., Iwachido, T., and Zenki, M. (1991) Sodium-selective macrocyclic polyamine carriers having pyridine-functionalized sidearms, *Journal of the Chemical Society, Perkin Transactions 1: Organic and Bio-Organic Chemistry (1972-1999)*, 1661-1665.
50. Jackson, W. G., McKeon, J. A., Hockless, D. C. R., and Willis, A. C. (2006) The Reversible and Stereoselective N- to C-bonded Rearrangement of Tris(2-pyridylmethyl)-1,4,7-triazacyclononane-cobalt(III), *Inorganic Chemistry* 45, 4119-4135.
51. Hohn, A., Geue, R. J., Sargeson, A. M., and Willis, A. C. (1989) Stabilization of an unusual conformation of an encapsulated metal ion cobalt(methylarsasarcophagine): synthesis and structure, *Journal of the Chemical Society, Chemical Communications*, 1648-1649.
52. Geue, R. J., Petri, W. R., Sargeson, A. M., and Snow, M. R. (1992) Metal ion cages: capping reactions with bifunctional methylene compounds and formaldehyde, *Australian Journal of Chemistry* 45, 1681-1703.
53. Hohn, A., Geue, R. J., and Sargeson, A. M. (1990) A new strategy for the metal template synthesis of organic metal ion cages, *Journal of the Chemical Society, Chemical Communications*, 1473-1475.
54. Hohn, A., Geue, R. J., Sargeson, A. M., and Willis, A. C. (1989) Phospha-capped cobalt(III) cage molecules: synthesis, properties, and structure, *Journal of the Chemical Society, Chemical Communications*, 1644-1645.
55. Korybut-Daszkiewicz, B., Hartshorn, R. M., and Sargeson, A. M. (1989) Pyruvate imine cobalt(III) complex as a reagent for metal encapsulation, *Journal of the Chemical Society, Chemical Communications*, 1375-1376.
56. Mannich, C., and Kroesche, W. (1912) Condensation product of formaldehyde, ammonia, and antipyrine, *Archiv der Pharmazie (Weinheim, Germany)* 250, 647-667.
57. Hollingshed, G. K., Lawrance, G. A., Maeder, M., and Rossignoli, M. (1991) Polyamine complexation-I. Stability constants for metal ion complexation of 5-(4'-amino-2'-azabutane)-5-methyl-3,7-diazanonane-1,9-diamine, *Polyhedron* 10, 409-413.

58. Irving, H. M., and Williams, R. J. P. (1953) Stability of transition metal complexes, *Journal of the Chemical Society*, 3192-3210.

59. Weare, W. W., Dai, X., Byrnes, M. J., Chin, J. M., Schrock, R. R., and Mueller, P. (2006) Catalytic reduction of dinitrogen to ammonia at a single molybdenum center, *Proceedings of the National Academy of Sciences of the United States of America* 103, 17099-17106.

60. Deroche, A., Morgenstern-Badarau, I., Cesario, M., Guilhem, J., Keita, B., Nadjo, L., and Houee-Levin, C. (1996) A Seven-Coordinate Manganese(II) Complex Formed with a Single Tripodal Heptadentate Ligand as a New Superoxide Scavenger, *Journal of the American Chemical Society* 118, 4567-4573.

61. Hirobe, M., Hirano, T., and Nagano, T. (1989) Ethylenediamine derivative-iron complexes as active oxygen removers, p 10 pp, (Lederle (Japan), Ltd., Japan).
Application: JP

JP.

62. Nagano, T., Hirano, T., and Hirobe, M. (1989) Superoxide dismutase mimics based on iron in vivo, *Journal of Biological Chemistry* 264, 9243-9249.

63. Hirobe, M., Hirano, T., and Nagano, T. (1989) Active oxygen-removing agents containing chelating agents, p 7 pp, (Lederle (Japan), Ltd., Japan). Application: JP

JP.

64. Mohamadou, A., and Gerard, C. (2001) Synthesis and characterisation of zinc(II) complexes of tripodal N7 ligands involving pyridine and amine or amide nitrogen donors. Crystal structure of a zinc(II) complex, *Journal of the Chemical Society, Dalton Transactions*, 3320-3328.

65. Hartman, J. R., Vachet, R. W., and Callahan, J. H. (2000) Gas, solution, and solid state coordination environments for the nickel(II) complexes of a series of aminopyridine ligands of varying coordination number, *Inorganica Chimica Acta* 297, 79-87.

66. Hartman, J. R., Vachet, R. W., Pearson, W., Wheat, R. J., and Callahan, J. H. (2003) A comparison of the gas, solution, and solid state coordination environments for the copper(II) complexes of a series of aminopyridine ligands of varying coordination number, *Inorganica Chimica Acta* 343, 119-132.

67. Earnshaw, A. (1968) *Introduction to Magnetochemistry*.

68. Brewer, G., Luckett, C., May, L., Beatty, A. M., and Scheidt, W. R. (2004) Synthesis and characterization of tripodal iron(II) complexes prepared from 2-pyridinecarboxaldehyde and 1-methyl-2-imidazolecarboxaldehyde: stabilization of iron(II) cations with N6 donor sets, *Inorganica Chimica Acta* 357, 2390-2396.

69. Ge, Q.-C., Guo, Y.-H., Lin, H., Lin, H.-K., and Zhu, S.-R. (2003) Stoichiometrical coordination behaviour of hexaza tripodal ligands towards zinc(II), copper(II), nickel(II) and cobalt(II), *Transition Metal Chemistry (Dordrecht, Netherlands)* 28, 572-578.
70. Constable, E. C., and Thompson, A. M. W. C. (1992) A new ligand for the self assembly of starburst coordination oligomers and polymers, *Journal of the Chemical Society, Chemical Communications*, 617-619.
71. Donaldson, P. B., Tasker, P. A., and Alcock, N. W. (1977) Trigonal prismatic versus octahedral coordination. Part 2. X-ray structure determinations of manganese(II), cobalt(II), and nickel(II) complexes of intermediate geometry derived from the ligand 1,1,1-tris(pyridine-2-aldiminomethyl)ethane, *Journal of the Chemical Society, Dalton Transactions: Inorganic Chemistry (1972-1999)*, 1160-1165.
72. Fleischer, E. B., Gebala, A. E., Swift, D. R., and Tasker, P. A. (1972) Trigonal prismatic-octahedral coordination. Complexes of intermediate geometry, *Inorganic Chemistry* 11, 2775-2784.
73. Kennedy, D. P., DiPasquale, A. G., Rheingold, A. L., and Planalp, R. P. (2007) Ni(II)-mediated synthesis of the novel tripodal aminopyridyl ligand tamepyr: Coordination geometry and rigidity of complexes with the divalent 3d metals Fe-Zn and with In(III), *Polyhedron* 26, 197-203.
74. Derfer, J. M., Greenlee, K. W., and Boord, C. E. (1949) New synthesis of monoalkylcyclobutanes: reduction of neopentyl type tribromides, *Journal of the American Chemical Society* 71, 175-182.
75. Doering, W. v. E., and Levy, L. K. (1955) d-Orbital resonance. I. The acidity of bridgehead α -hydrogen in a bicyclic trisulfone, *Journal of the American Chemical Society* 77, 509-513.
76. Staudinger, H., and Meyer, J. (1919) New organic compounds of phosphorus. III. Phosphinemethylene derivatives and phosphinimines, *Helvetica Chimica Acta* 2, 635-646.
77. Martin, V. V., Lex, L., and Keana, J. F. W. (1995) A safe and convenient procedure for the synthesis of polyamines via azide intermediates, *Organic Preparations and Procedures International* 27, 117-120.
78. Fleischer, E. B., Gebala, A. E., Levey, A., and Tasker, P. A. (1971) Conversion of aliphatic and alicyclic polyalcohols to the corresponding primary polyamines, *Journal of Organic Chemistry* 36, 3042-3044.
79. Dunn, M. P. (2007) Synthesis and characterization of new iron (II) chelating agents to resist oxidation based on the tachpyr/tamepyr framework, in *Chemistry*, p 47, University of New Hampshire, Durham.

80. Geue, R. J., and Searle, G. H. (1983) Cation-exchange chromatography and selective complexation in the isolation of branched acyclic polyamines: syntheses of ethyldinetris(methanamine) [tame], 2,2-bis(aminomethyl)propan-1-ol [hmmpp], 4,4',4''-ethyldinetris(3-azabutan-1-amine) [sen] and 5,5',5''-ethyldinetris(4-azapentan-1-amine) [stn], *Australian Journal of Chemistry* 36, 927-935.
81. Dunn, T. J., Neumann, W. L., Rogic, M. M., and Woulfe, S. R. (1990) Versatile methods for the synthesis of differentially functionalized pentaerythritol amine derivatives, *Journal of Organic Chemistry* 55, 6368-6373.
82. Litherland, A., and Mann, F. G. (1938) Amino derivatives of pentaerythritol. I. Preparation, *Journal of the Chemical Society*, 1588-1595.
83. Dwyer, F. P., Gill, N. S., Gyrfas, E. C., and Lions, F. (1957) Sexadentate chelate compounds. VIII, *Journal of the American Chemical Society* 79, 1269-1272.
84. Durham, D. A., Hart, F. A., and Shaw, D. (1967) Structure of the condensation product of 1,1,1-tris(aminomethyl)ethane with pyridine-2-carboxaldehyde, its complexes with lanthanide nitrates, and its isomerization in the presence of ferrous ion, *Journal of Inorganic and Nuclear Chemistry* 29, 509-516.
85. Edwards, A., and Webb, G. A. (1978) NMR studies on some 1,3,5-triazaadamantane derivatives, *Organic Magnetic Resonance* 11, 103-105.
86. Diebler, H., Eigen, M., Ilgenfritz, G., Maass, G., and Winkler, R. (1969) Kinetics and mechanism of reactions of main group metal ions with biological carriers, *Pure and Applied Chemistry* 20, 93-115.
87. Cowan, J. A. (1997) *Inorganic Biochemistry An Introduction*, Second ed., Wiley-VCH, New York.
88. Onggo, D., Scudder, M. L., Craig, D. C., and Goodwin, H. A. (2000) Structural and Mossbauer spectral studies of iron(II) complexes of thiazole-containing bidentates, *Australian Journal of Chemistry* 53, 153-158.
89. Fitzpatrick, L. J., and Goodwin, H. A. (1982) Coordination of conjugated imine systems with Group VIII metals. I. Iron and ruthenium complexes of 2-(2-pyridyl)thiazole, *Inorganica Chimica Acta* 61, 229-233.
90. Childs, B. J., Craig, D. C., Scudder, M. L., and Goodwin, H. A. (1998) Structural and electronic studies of the coordination of 6-(thiazol-2-yl)-2,2'-bipyridine and related systems to Fe(II), Co(II) and Ni(II), *Inorganica Chimica Acta* 274, 32-41.
91. Widlicka, D. W., Wong, E. H., Weisman, G. R., Lam, K. C., Sommer, R. D., Incarvito, C. D., and Rheingold, A. L. (2000) A prestrained tricyclic biimidazole ligand adaptable to diverse coordination modes, *Inorganic Chemistry Communications* 3, 648-652.

92. Yoon, N. M., and Gyoung, Y. S. (1985) Reaction of diisobutylaluminum hydride with selected organic compounds containing representative functional groups, *Journal of Organic Chemistry* 50, 2443-2450.
93. Childers, R. F., and Wentworth, R. A. D. (1973) Hindered ligand systems. VII. Crystal field spectrum of *cis,cis*-1,3,5-tris(pyridine-2-carboxaldimino)cyclohexanenickel(II), *Inorganic Chemistry* 12, 2778-2782.
94. Miessler, G. L., and Tarr, D. A. (1999) *Inorganic Chemistry, Second Edition*.
95. Robinson, M. A., Curry, J. D., and Busch, D. H. (1963) Complexes derived from strong field ligands. XVII. Electronic spectra of octahedral nickel(II) complexes with ligands of the α -diimine and closely related classes, *Inorg. Chem.* 2, 1178-1181.
96. Al-Obaidi, A. H. R., Jensen, K. B., McGarvey, J. J., Toftlund, H., Jensen, B., Bell, S. E. J., and Carroll, J. G. (1996) Structural and Kinetic Studies of Spin Crossover in an Iron(II) Complex with a Novel Tripodal Ligand, *Inorganic Chemistry* 35, 5055-5060.
97. Tamura, M., Urano, Y., Kikuchi, K., Higuchi, T., Hirobe, M., and Nagano, T. (2000) Synthesis and superoxide dismutase activity of novel iron complexes, *Journal of Organometallic Chemistry* 611, 586-592.
98. Goto, M., Koga, N., Ohse, Y., Kurosaki, H., Komatsu, T., and Kuroda, Y. (1994) Dependence of dehydrogenation of amines towards coordination geometry: oxidation products of tricyano[di(2-pyridylmethyl)amine]ferrate(II) from *mer* and *fac* isomers, *Journal of the Chemical Society, Chemical Communications*, 2015-2016.
99. Ye, N., Park, G., Przyborowska, A. M., Sloan, P. E., Clifford, T., Bauer, C. B., Broker, G. A., Rogers, R. D., Ma, R., Torti, S. V., Brechbiel, M. W., and Planalp, R. P. (2004) Nickel(II), copper(II) and zinc(II) binding properties and cytotoxicity of tripodal, hexadentate tris(ethylenediamine)-analogue chelators, *Dalton Transactions*, 1304-1311.
100. Ignacio Tinoco, J. K. S. J. C. W. J. D. P. (2002) *Physical Chemistry Principles and Applications in Biological Sciences*, Fourth ed., Prentice Hall, New Jersey.
101. Harris, D. C., and Bertolucci, M. D. (1989) *Symmetry and Spectroscopy. An Introduction to Vibrational and Electronic Spectroscopy*.
102. Skoog, D. A., West, D. M., and Holler, F. J. (1988) *Fundamentals of Analytical Chemistry. 5th Ed.*
103. Fox, M. A. C., M. (1988) *Photoinduced Electron Transfer*, Elsevier, Amsterdam.
104. Mattay, J., and Editor (1990) *Topics in Current Chemistry, 158: Photoinduced Electron Transfer II*.
105. Mattay, J., and Editor (1992) *Photoinduced Electron Transfer IV. [In: Top. Curr. Chem., 1992; 163]*.

106. Kavarnos, G. J. (1993) *Fundamentals of Photoinduced Electron Transfer*.
107. Siegeman, H. (1975) Oxidation and reduction half-wave potentials of organic compounds, *Techniques of Chemistry (New York) 5, Pt. 2*, 667-1056.
108. Callan, J. F., de Silva, A. P., and Magri, D. C. (2005) Luminescent sensors and switches in the early 21st century, *Tetrahedron 61*, 8551-8588.
109. Zang, L., Liu, R., Holman, M. W., Nguyen, K. T., and Adams, D. M. (2002) A Single-Molecule Probe Based on Intramolecular Electron Transfer, *Journal of the American Chemical Society 124*, 10640-10641.
110. Fahrni, C. J., Yang, L., and VanDerveer, D. G. (2003) Tuning the photoinduced electron-transfer thermodynamics in 1,3,5-triaryl-2-pyrazoline fluorophores: X-ray structures, photophysical characterization, computational analysis, and in vivo evaluation, *Journal of the American Chemical Society 125*, 3799-3812.
111. Prasanna de Silva, A., Gunaratne, H. Q. N., and Sandanayake, K. R. A. S. (1990) A new benzo-annelated cryptand and a derivative with alkali cation-sensitive fluorescence, *Tetrahedron Letters 31*, 5193-5196.
112. de Silva, A. P., Gunaratne, H. Q. N., Gunnlaugsson, T., and Nieuwenhuizen, M. (1996) Fluorescent switches with high selectivity towards sodium ions: correlation of ion-induced conformation switching with fluorescence function, *Chemical Communications (Cambridge)*, 1967-1968.
113. Tian, H., Gan, J., Chen, K., He, J., Song, Q. L., and Hou, X. Y. (2002) Positive and negative fluorescent imaging induced by naphthalimide polymers, *Journal of Materials Chemistry 12*, 1262-1267.
114. Geue, J. P., Head, N. J., Ward, A. D., and Lincoln, S. F. (2003) The formation of fluorescent alkaline earth complexes by 4-{2-[10-(2-morpholinoethyl)-9-anthryl]methyl}morpholine and its -ethyl}morpholine and -propyl}morpholine analogues in acetonitrile, *Australian Journal of Chemistry 56*, 301-307.
115. Geue, J. P., Head, N. J., Ward, A. D., and Lincoln, S. F. (2003) The Formation of Fluorescent Alkali Metal and Alkaline Earth Complexes by 1-(2-[10-[2-Piperazinoethyl]-9-anthryl]ethyl)piperazine and Alkaline Earth Complexes by 4-(2-[10-[2-(1,4-Thiazinan-4-yl)ethyl]-9-anthryl]ethyl)thiomorpholine in Acetonitrile, *Australian Journal of Chemistry 56*, 917-922.
116. Geue, J. P., Head, N. J., Ward, A. D., and Lincoln, S. F. (2003) Complexation of alkali metal and alkaline earth ions by anthracene based fluorophores with one and two appended monoaza coronand receptors, *Dalton Transactions*, 521-526.

117. Kenmoku, S., Urano, Y., Kanda, K., Kojima, H., Kikuchi, K., and Nagano, T. (2004) Rational design of novel photoinduced electron transfer type fluorescent probes for sodium cation, *Tetrahedron* **60**, 11067-11073.
118. De Silva, A. P., and Sandanayake, K. R. A. S. (1989) Fluorescent PET (photo-induced electron transfer) sensors for alkali metal ions with improved selectivity against protons and with predictable binding constants, *Journal of the Chemical Society, Chemical Communications*, 1183-1185.
119. Gunnlaugsson, T., Bichell, B., and Nolan, C. (2004) Fluorescent PET chemosensors for lithium, *Tetrahedron* **60**, 5799-5806.
120. DiCesare, N., and Lakowicz, J. R. (2001) Fluorescent probe for monosaccharides based on a functionalized boron-dipyrromethene with a boronic acid group, *Tetrahedron Letters* **42**, 9105-9108.
121. Beer, G., Daub, J., and Rurack, K. (2001) Chiral discrimination with a fluorescent boron-dipyrromethene dye, *Chemical Communications (Cambridge, United Kingdom)*, 1138-1139.
122. Baki, C. N., and Akkaya, E. U. (2001) Boradiazaindacene-Appended Calix[4]arene: Fluorescence Sensing of pH Near Neutrality, *Journal of Organic Chemistry* **66**, 1512-1513.
123. Cha, N. R., Moon, S. Y., and Chang, S.-K. (2003) New ON-OFF type Ca²⁺-selective fluoroionophore having boron-dipyrromethene fluorophores, *Tetrahedron Letters* **44**, 8265-8268.
124. Gee, K. R., Rukavishnikov, A., and Rothe, A. (2003) New Ca²⁺ fluoroionophores based on the BODIPY fluorophore, *Combinatorial Chemistry and High Throughput Screening* **6**, 363-366.
125. Tsien, R. Y. (1980) New calcium indicators and buffers with high selectivity against magnesium and protons: design, synthesis, and properties of prototype structures, *Biochemistry* **19**, 2396-2404.
126. Tsien, R. Y. (1994) Fluorescence imaging creates a window on the cell, *Chemical & Engineering News* **72**, 34-44.
127. Pearson, A. J., and Hwang, J.-J. (2001) Crown-annelated p-phenylenediamine derivatives as electrochemical and fluorescence-responsive chemosensors: cyclic voltammetry studies, *Tetrahedron Letters* **42**, 3541-3543.
128. Pearson, A. J., and Xiao, W. (2003) Fluorescence and NMR Binding Studies of N-Aryl-N'-(9-methylanthryl)diaza-18-crown-6 Derivatives, *Journal of Organic Chemistry* **68**, 5369-5376.

129. Pearson, A. J., Hwang, J. J., and Ignatov, M. E. (2001) Crown-annelated p-phenylenediamine derivatives as electrochemical and fluorescence responsive chemosensors: fluorescence studies, *Tetrahedron Letters* **42**, 3537-3540.
130. Martin, M. M., Plaza, P., Meyer, Y. H., Badaoui, F., Bourson, J., Lefevre, J.-P., and Valeur, B. (1996) Steady-State and Picosecond Spectroscopy of Li⁺ or Ca²⁺ Complexes with a Crowned Merocyanine. Reversible Photorelease of Cations, *Journal of Physical Chemistry* **100**, 6879-6888.
131. Nakahara, Y., Kida, T., Nakatsuji, Y., and Akashi, M. (2004) A novel fluorescent indicator for Ba²⁺ in aqueous micellar solutions, *Chemical Communications (Cambridge, United Kingdom)*, 224-225.
132. Fendler, J. H. (1982) *Membrane Mimetic Chemistry: Characterizations and Applications of Micelles, Microemulsions, Monolayers, Bilayers, Vesicles, Host-Guest Systems, and Polyions*.
133. Bissell, R. A., Bryan, A. J., Prasanna de Silva, A., and McCoy, C. P. (1994) Fluorescent PET (photoinduced electron transfer) sensors with targeting/anchoring modules as molecular versions of submarine periscopes for mapping membrane-bounded protons, *Journal of the Chemical Society, Chemical Communications*, 405-407.
134. Katerinopoulos Haralambos, E. (2004) The coumarin moiety as chromophore of fluorescent ion indicators in biological systems, *Curr Pharm Des FIELD Full Journal Title:Current pharmaceutical design* **10**, 3835-3852.
135. Chang, C. J., Nolan, E. M., Jaworski, J., Burdette, S. C., Sheng, M., and Lippard, S. J. (2004) Bright Fluorescent Chemosensor Platforms for Imaging Endogenous Pools of Neuronal Zinc, *Chemistry & Biology* **11**, 203-210.
136. Walkup, G. K., Burdette, S. C., Lippard, S. J., and Tsien, R. Y. (2000) A New Cell-Permeable Fluorescent Probe for Zn²⁺, *Journal of the American Chemical Society* **122**, 5644-5645.
137. Bissell, R. A., Prasanna de Silva, A., Gunaratne, H. Q. N., Lynch, P. L. M., Maguire, G. E. M., and Sandanayake, K. R. A. S. (1992) Molecular fluorescent signalling with 'fluor-spacer-receptor' systems: approaches to sensing and switching devices via supramolecular photophysics, *Chemical Society Reviews* **21**, 187-195.
138. Valeur, B., and Editor (2000) *Molecular Fluorescence - An Introduction: Principles and Applications, 1st Edition 2000*.
139. Lim, N. C., and Brueckner, C. (2004) DPA-substituted coumarins as chemosensors for zinc(II): modulation of the chemosensory characteristics by variation of the position of the chelate on the coumarin, *Chemical Communications (Cambridge, United Kingdom)*, 1094-1095.

140. Woodrooffe Carolyn, C., and Lippard Stephen, J. (2003) A novel two-fluorophore approach to ratiometric sensing of Zn(2+), *J Am Chem Soc FIELD Full Journal Title:Journal of the American Chemical Society* 125, 11458-11459.
141. Bhattacharya, S., and Gulyani, A. (2003) First report of Zn²⁺ sensing exclusively at mesoscopic interfaces, *Chemical Communications (Cambridge, United Kingdom)*, 1158-1159.
142. Gunnlaugsson, T., Lee, T. C., and Parkesh, R. (2003) A highly selective and sensitive fluorescent PET (photoinduced electron transfer) chemosensor for Zn(ii), *Organic & Biomolecular Chemistry* 1, 3265-3267.
143. Gunnlaugsson, T., Lee, T. C., and Parkesh, R. (2003) Cd(II) Sensing in Water Using Novel Aromatic Iminodiacetate Based Fluorescent Chemosensors, *Organic Letters* 5, 4065-4068.
144. Gunnlaugsson, T., Lee, T. C., and Parkesh, R. (2004) Highly selective fluorescent chemosensors for cadmium in water, *Tetrahedron* 60, 11239-11249.
145. Nolan, E. M., and Lippard, S. J. (2003) A "Turn-On" Fluorescent Sensor for the Selective Detection of Mercuric Ion in Aqueous Media, *Journal of the American Chemical Society* 125, 14270-14271.
146. Rurack, K., Kollmannsberger, M., Resch-Genger, U., and Daub, J. (2000) A Selective and Sensitive Fluoroionophore for HgII, AgI, and CuII with Virtually Decoupled Fluorophore and Receptor Units, *Journal of the American Chemical Society* 122, 968-969.
147. de Silva, A. P., Gunaratne, H. Q. N., and McCoy, C. P. (1997) Molecular Photoionic AND Logic Gates with Bright Fluorescence and "Off-On" Digital Action, *Journal of the American Chemical Society* 119, 7891-7892.
148. Guo, X., Qian, X., and Jia, L. (2004) A Highly Selective and Sensitive Fluorescent Chemosensor for Hg²⁺ in Neutral Buffer Aqueous Solution, *Journal of the American Chemical Society* 126, 2272-2273.
149. de Silva, A. P., Gunaratne, H. Q. N., Gunnlaugsson, T., Huxley, A. J. M., McCoy, C. P., Rademacher, J. T., and Rice, T. E. (1997) Signaling Recognition Events with Fluorescent Sensors and Switches, *Chemical Reviews (Washington, D. C.)* 97, 1515-1566.
150. Benniston, A. C., Harriman, A., Lawrie, D. J., Mayeux, A., Rafferty, K., and Russell, O. D. (2003) A general purpose reporter for cations: absorption, fluorescence and electrochemical sensing of zinc(II), *Dalton Transactions*, 4762-4769.
151. Descalzo, A. B., Martinez-Manez, R., Radeaglia, R., Rurack, K., and Soto, J. (2003) Coupling Selectivity with Sensitivity in an Integrated Chemosensor Framework: Design of a Hg²⁺-Responsive Probe, Operating above 500 nm, *Journal of the American Chemical Society* 125, 3418-3419.

152. Metivier, R., Leray, I., and Valeur, B. (2003) A highly sensitive and selective fluorescent molecular sensor for Pb(II) based on a calix[4]arene bearing four dansyl groups, *Chemical Communications (Cambridge, United Kingdom)*, 996-997.
153. Fletcher, M. H., White, C. E., and Sheftel, M. S. (1946) Determination of beryllium in ores. Fluorometric method, *Industrial and Engineering Chemistry, Analytical Edition 18*, 179-183.
154. Capitan, F., Roman, M., and Guiraum, A. (1974) Spectrofluorometric determination of aluminum(III) by sodium 2-quinizarinsulfonate, *Anales de Quimica (1968-1979) 70*, 508-514.
155. Quinti, L., Allen, N. S., Edge, M., Murphy, B. P., and Perotti, A. (2003) A study of the luminescent complexes formed by the dye 1,4-dihydroxyanthraquinone (quinizarin) and Ga(III) and In(III), *Journal of Photochemistry and Photobiology, A: Chemistry 155*, 93-106.
156. Jimenez, D., Martinez-Manez, R., Sancenon, F., and Soto, J. (2004) Electro-optical triple-channel sensing of metal cations via multiple signalling patterns, *Tetrahedron Letters 45*, 1257-1259.
157. Xiao, Y., and Qian, X. (2003) Novel highly efficient fluoroionophores with a perieffect and strong electron-donating receptors: TICT-promoted PET and signaling response to transition metal cations with low background emission, *Tetrahedron Letters 44*, 2087-2091.
158. Balasubramaniyan, V. (1966) Peri interaction in naphthalene derivatives, *Chemical Reviews (Washington, DC, United States) 66*, 567-641.
159. Prasanna de Silva, A., Gunaratne, H. Q. N., Habib-Jiwan, J.-L., McCoy, C. P., Rice, T. E., and Soumillion, J.-P. (1995) New fluorescent model compounds for the study of photoinduced electron transfer: the influence of a molecular electric field in the excited state, *Angewandte Chemie, International Edition in English 34*, 1728-1731.
160. Morozumi, T., Hiraga, H., and Nakamura, H. (2003) Intramolecular charge-transfer behavior of 1-pyrenyl aromatic amides and its control through the complexation with metal ions, *Chemistry Letters 32*, 146-147.
161. Forster, T. (1948) Intermolecular energy transference and fluorescence, *Ann. Physik [6 Folge] 2*, 55-75.
162. Arduini, M., Felluga, F., Mancin, F., Rossi, P., Tecilla, P., Tonellato, U., and Valentiniuzzi, N. (2003) Aluminium fluorescence detection with a FRET amplified chemosensor, *Chemical Communications (Cambridge, United Kingdom)*, 1606-1607.
163. De Costa, M. D. P., De Silva, A. P., and Pathirana, S. T. (1987) Two dimensional fluorescent sensors. Different dependences of the fluorescence band position and the

fluorescence quantum yield of 1,5-diphenyl-3-vinyl-D2-pyrazoline upon solvent dipolarity and hydrogen-bond acidity, *Canadian Journal of Chemistry* 65, 1416-1419.

164. De Costa, M. D. P., and Jayasinghe, W. A. P. A. (2004) Detailed studies on complexation behavior and mechanism of fluorescence quenching of naphthalene linked hydroxamic acid with transition metal ions by UV-visible and fluorescence spectra, *Journal of Photochemistry and Photobiology, A: Chemistry* 162, 591-598.

165. Fabbrizzi, L., Licchelli, M., Pallavicini, P., Perotti, A., Taglietti, A., and Sacchi, D. (1996) Fluorescent sensors for transition metals based on electron-transfer and energy-transfer mechanisms, *Chemistry--A European Journal* 2, 75-82.

166. Licchelli, M., Biroli, A. O., Poggi, A., Sacchi, D., Sangermani, C., and Zema, M. (2003) Excimer emission induced by metal ion coordination in 1,8-naphthalimide-tethered iminopyridine ligands, *Dalton Transactions*, 4537-4545.

167. Lakowicz, J. R. (1983) *Principles of Fluorescence Spectroscopy*.

168. Turro, N. J. (1978) *Modern Molecular Photochemistry*.

169. Kawakami, J., Kimura, H., Nagaki, M., Kitahara, H., and Ito, S. (2004) Intramolecular exciplex formation and complexing behavior of 1-(2-naphthalenecarboxy)-n-(p-substituted benzenecarboxy)oxaalkanes as fluorescent chemosensors for calcium and barium ions, *Journal of Photochemistry and Photobiology, A: Chemistry* 161, 141-149.

170. Kopecky, J. (1992) *Organic Photochemistry: A Visual Approach*.

171. Barltrop, J. A., and Coyle, J. D. (1975) *Excited States in Organic Chemistry*.

172. Snyder, R., and Testa, A. C. (1984) Influence of electron-donor-acceptor complexation on electronic relaxation of quinoline, *Journal of Physical Chemistry* 88, 5948-5950.

173. Hiratani, K., Nomoto, M., Sugihara, H., and Okada, T. (1990) Specific fluorescence detection of lithium ion with 2,9-disubstituted 1,10-phenanthroline derivatives, *Chemistry Letters*, 43-46.

174. Hiratani, K., Nomoto, M., Ohuchi, S., and Taguchi, K. (1990) Fluorescence behavior of 3,3-bis(8-quinolyloxymethyl)oxetane: effects of solvents, carrier-concentration, and metal ions on the fluorescence intensity, *Bulletin of the Chemical Society of Japan* 63, 1349-1353.

175. Mahadevan, I. B., Kimber, M. C., Lincoln, S. F., Tiekink, E. R. T., Ward, A. D., Betts, W. H., Forbes, I. J., and Zalewski, P. D. (1996) The synthesis of zinquin ester and zinquin acid, zinc(II)-specific fluorescing agents for use in the study of biological zinc(II), *Australian Journal of Chemistry* 49, 561-568.

176. Zalewski, P. D., Forbes, I. J., and Betts, W. H. (1993) Correlation of apoptosis with change in intracellular labile zinc(II) using zinquin [(2-methyl-8-p-toluenesulfonamido-6-quinolyloxy)acetic acid], a new specific fluorescent probe for zinc(II), *Biochemical Journal* 296, 403-408.
177. Frederickson, C. J., Kasarskis, E. J., Ringo, D., and Frederickson, R. E. (1987) A quinoline fluorescence method for visualizing and assaying the histochemically reactive zinc (bouton zinc) in the brain, *Journal of Neuroscience Methods* 20, 91-103.
178. Savage, D. D., Montano, C. Y., and Kasarskis, E. J. (1989) Quantitative histofluorescence of hippocampal mossy fiber zinc, *Brain Research* 496, 257-267.
179. Zalewski, P. D., Forbes, I. J., Seamark, R. F., Borlinghaus, R., Betts, W. H., Lincoln, S. F., and Ward, A. D. (1994) Flux of intracellular labile zinc during apoptosis (gene-directed cell death) revealed by a specific chemical probe, Zinquin, *Chemistry & Biology* 1, 153-161.
180. Fahrni, C. J., and O'Halloran, T. V. (1999) Aqueous Coordination Chemistry of Quinoline-Based Fluorescence Probes for the Biological Chemistry of Zinc, *Journal of the American Chemical Society* 121, 11448-11458.
181. Koh, J.-Y., Suh, S. W., Gwag, B. J., He, Y. Y., Hsu, C. Y., and Choi, D. W. (1996) The role of zinc in selective neuronal death after transient global cerebral ischemia, *Science (Washington, D. C.)* 272, 1013-1016.
182. Di Virgilio, F., Steinberg, T. H., and Silverstein, S. C. (1990) Inhibition of Fura-2 sequestration and secretion with organic anion transport blockers, *Cell Calcium* 11, 57-62.
183. Mikata, Y., Wakamatsu, M., and Yano, S. (2005) Tetrakis(2-quinolinylmethyl)ethylenediamine (TQEN) as a new fluorescent sensor for zinc, *Dalton Trans FIELD Full Journal Title: Dalton transactions (Cambridge, England : 2003)*, 545-550.
184. Mikata, Y., Wakamatsu, M., Kawamura, A., Yamanaka, N., Yano, S., Odani, A., Morihiro, K., and Tamotsu, S. (2006) Methoxy-Substituted TQEN Family of Fluorescent Zinc Sensors, *Inorganic Chemistry* 45, 9262-9268.
185. Nicolaou, K. C., Safina, B. S., Funke, C., Zak, M., and Zecri, F. J. (2002) Stereocontrolled synthesis of the quinaldic acid macrocyclic system of thiostrepton, *Angewandte Chemie, International Edition* 41, 1937-1940.
186. Mancuso, A. J., Huang, S.-L., and Swern, D. (1978) Oxidation of long-chain and related alcohols to carbonyls by dimethyl sulfoxide \"activated\" by oxalyl chloride, *Journal of Organic Chemistry* 43, 2480-2482.
187. Huang, S. L., Omura, K., and Swern, D. (1976) Oxidation of sterically hindered alcohols to carbonyls with dimethyl sulfoxide-trifluoroacetic anhydride, *Journal of Organic Chemistry* 41, 3329-3331.

188. Huang, S. L., Omura, K., and Swern, D. (1978) Further studies on the oxidation of alcohols to carbonyl compounds by dimethyl sulfoxide/trifluoroacetic anhydride, *Synthesis*, 297-299.
189. Giordano, C., Minisci, F., Vismara, E., and Levi, S. (1986) A general, selective, and convenient procedure of homolytic formylation of heteroaromatic bases, *Journal of Organic Chemistry* 51, 536-537.
190. Fenton, H. J. H. (1894) Oxidation of tartaric acid in presence of iron, *Journal of the Chemical Society, Transactions* 65, 899-910.
191. Rutner, H., and Spoerri, P. E. (1963) Lithium aluminum hydride reductions of pyrazinecarboxylic esters. Synthesis of pyrazine carboxaldehyde from methyl pyrazinoate, *Journal of Organic Chemistry* 28, 1898-1899.
192. Reissert, A. (1905) Introduction of benzoyl groups into tertiary cyclic bases, *Berichte der Deutschen Chemischen Gesellschaft* 38, 3415-3435.
193. Jones, R. C. F., Smallridge, M. J., and Chapleo, C. B. (1990) Tetrahydrofolate coenzyme models: synthesis of tetrahydroimidazoisoquinolines and tetrahydroimidazoquinolines, *Journal of the Chemical Society, Perkin Transactions 1: Organic and Bio-Organic Chemistry (1972-1999)*, 385-391.
194. Campaigne, E., Thompson, R. L., and Van Werth, J. E. (1959) Some heterocyclic aldehyde thiosemicarbazones possessing antiviral activity, *Journal of Medicinal & Pharmaceutical Chemistry* 1, 577-600.
195. Stokker, G. (1983) Preparation of 1,2-benzisoxazoles from salicylaloximes via trichloroacetyl isocyanate, *Journal of Organic Chemistry* 48, 2613-2615.
196. Jain, M., and Kwon, C.-H. (2003) 1,2-Benzisoxazole Phosphorodiamidates as Novel Anticancer Prodrugs Requiring Bioreductive Activation, *Journal of Medicinal Chemistry* 46, 5428-5436.
197. Tagawa, Y., Yamashita, K., Higuchi, Y., and Goto, Y. (2003) Improved oxidation of an active methyl group of N-heteroaromatic compounds by selenium dioxide in the presence of tert-butyl hydroperoxide, *Heterocycles* 60, 953-957.
198. Kornblum, N., Jones, W. J., and Anderson, G. J. (1959) A new and selective method of oxidation. Conversion of alkyl halides and alkyl tosylates to aldehydes, *Journal of the American Chemical Society* 81, 4113-4114.
199. Markovac, A., Stevens, C. L., Ash, A. B., and Hackley, B. E., Jr. (1970) Synthesis of oximes. III. Iodine dimethyl sulfoxide reaction with methylpyridines, *Journal of Organic Chemistry* 35, 841-843.

200. Henry, L. (1895) Nitro-alcohols, *Comptes Rendus Hebdomadaires des Seances de l'Academie des Sciences* 120, 1265-1268.
201. Kodukulla, R. P. K., Trivedi, G. K., Vora, J. D., and Mathur, H. H. (1994) Synthesis, chemical transformation and antimicrobial activity of a novel class of nitroolefins: 1,3-diaryl-2-nitroprop-1-enes, *Synthetic Communications* 24, 819-832.
202. Clemmensen, E. (1912) Reduction of Ketones to the Corresponding Hydrocarbons with Amalgamated Zinc and Hydrochloric Acid, *Orig. Com. 8th Intern. Congr. Appl. Chem.* 6, 68-76.
203. Battersby, A. R., LeCount, D. J., Garratt, S., and Thrift, R. I. (1961) Synthetic applications of 1,2-dihydroisoquinolines. Synthesis of (+)-coreximine, *Tetrahedron* 14, 46-53.
204. Kohno, M., Sasao, S., and Murahashi, S. (1990) Synthesis of phenethylamines by hydrogenation of *p*-nitrostyrenes, *Bulletin of the Chemical Society of Japan* 63, 1252-1254.
205. Ramirez, F. A., and Burger, A. (1950) The reduction of phenolic *p*-nitrostyrenes by lithium aluminum hydride, *Journal of the American Chemical Society* 72, 2781-2782.
206. Pictet, A., and Spengler, T. (1911) Formation of Isoquinoline Derivatives by the Action of Methylal on Phenylethylamine, Phenylalanine and Tyrosine, *Berichte der Deutschen Chemischen Gesellschaft* 44, 2030-2036.
207. Ruchirawat, S., Chaisupakitsin, M., Patranuwatana, N., Cashaw, J. L., and Davis, V. E. (1984) A convenient synthesis of simple tetrahydroisoquinolines, *Synthetic Communications* 14, 1221-1228.
208. Strombom, J., and Bruhn, J. G. (1978) Alkaloids of *Pachycereus pecten-aboriginum*, a Mexican cactus of ethnopharmacologic interest, *Acta Pharmaceutica Suecica* 15, 127-132.
209. Mata, R., and McLaughlin, J. L. (1980) Cactus alkaloids. XLII: 3,4-Dimethoxy-*p*-phenethylamine and heliamine from the Mexican cereoid *Backebergia militaris*, *Journal of Pharmaceutical Sciences* 69, 94-95.
210. Murahashi, S., Naota, T., and Taki, H. (1985) Ruthenium-catalyzed oxidation of secondary amines to imines using *tert*-butyl hydroperoxide, *Journal of the Chemical Society, Chemical Communications*, 613-614.
211. Michelson, A. M., Szabo, L., and Todd, A. R. (1956) Nucleotides. XXXVI. Adenosine-2' uridine-5' phosphate, *Journal of the Chemical Society*, 1546-1549.
212. Teuber, H. J., and Benz, S. (1967) Reactions with nitrosodisulfonate. XXXVI. Quinoline-5,6-quinones from 5-hydroxyquinolines, *Chemische Berichte* 100, 2918-2929.

213. Wehrli, P. A., and Pigott, F. (1972) Oxidation with the nitrosodisulfonate radical. I. Preparation and use of disodium nitrosodisulfonate. Trimethyl-p-benzoquinone, *Organic Syntheses* 52, 83-88.
214. Wehrli, P. A., and Schaer, B. (1974) Isoquinolines from tetrahydroisoquinolines. Novel aromatization reaction with Fremy's salt, *Synthesis*, 288-289.
215. Narita, E., Sato, T., Shioya, T., Ikari, M., and Okabe, T. (1984) Formation of hydroxylamidobis(sulfate) ion by the absorption of nitric oxide in aqueous solutions of sodium sulfite containing iron(II)-EDTA complex, *Industrial & Engineering Chemistry Product Research and Development* 23, 262-265.
216. Rosen, G. M., Britigan, B. E., Halpern, H. J., and Pou, S. (1999) *Free Radicals: Biology and Detection by Spin Trapping*.
217. Bales, B. L. (1971) EPR of frozen aqueous solutions of Fremy's salt. Resolution enhancement of polycrystalline spectra, *Chemical Physics Letters* 10, 361-364.
218. Griffith, O. H., and Waggoner, A. S. (1969) Nitroxide free radicals: spin labels for probing biomolecular structure, *Accounts of Chemical Research* 2, 17-24.
219. Bischler, A., and Napieralski, B. A new synthesis of isoquinoline, *Berichte der Deutschen Chemischen Gesellschaft* 26, 1903-1908.
220. Venkov, A. P., and Ivanov, I. I. (1996) Synthesis of isoquinolines from 2-phenylethylamines, amides, nitriles and carboxylic acids in polyphosphoric acid, *Tetrahedron* 52, 12299-12308.
221. Postaire, E., Martinez, D., Viel, C., Chastagnier, M., and Hamon, M. (1988) Vanadic oxidation of papaverine in 2.5 M and 5 M sulfuric acid, *Bulletin de la Societe Chimique de France*, 982-988.
222. Balczewski, P., Mallon, M. K. J., Street, J. D., and Joule, J. A. (1990) A synthesis of aaptamine from 6,7-dimethoxy-1-methylisoquinoline, *Journal of the Chemical Society, Perkin Transactions 1: Organic and Bio-Organic Chemistry (1972-1999)*, 3193-3198.
223. Sundberg, F. A. C. R. J. (2000) *Advanced Organic Chemistry*, Fourth ed., Kluwer Academic/ Plenum Publishers, New York.
224. Atkins, R. L., and Bliss, D. E. (1978) Substituted coumarins and azacoumarins. Synthesis and fluorescent properties, *Journal of Organic Chemistry* 43, 1975-1980.
225. Schimitschek, E. J., Trias, J. A., Hammond, P. R., and Atkins, R. L. (1974) Laser performance and stability of fluorinated coumarin dyes, *Optics Communications* 11, 352-355.

226. Hammond, P. R., Fletcher, A. N., Henry, R. A., and Atkins, R. L. (1975) Search for efficient, near uv lasing dyes. I. Substituent effects on bicyclic dyes, *Applied Physics (Berlin)* 8, 311-314.
227. De, S. K., and Gibbs, R. A. (2005) An efficient and practical procedure for the synthesis of 4-substituted coumarins, *Synthesis*, 1231-1233.
228. Brufola, G., Fringuelli, F., Piermatti, O., and Pizzo, F. (1997) Efficient one-pot synthesis of 7-azacoumarins by Knoevenagel reaction using water as reaction medium, *Heterocycles* 45, 1715-1721.
229. Heyl, D. (1948) Vitamin B6. V. Conversion of pyridoxine to the lactone of 4-pyridoxic acid, *Journal of the American Chemical Society* 70, 3434-3436.
230. Knoevenagel, E., Baebenroth, F., and Wollweber, O. (1898) Condensation of malonic acid with aromatic aldehydes by means of ammonia and amines, *Berichte der Deutschen Chemischen Gesellschaft* 31, 2596-2619.
231. Svete, J., Cadez, Z., Stanovnik, B., and Tisler, M. (1990) Methyl 2-(benzoylamino)-3-(dimethylamino)propenoate in the synthesis of heterocyclic systems. The synthesis of substituted 3-benzoylamino-2H-pyran-2-ones, *Synthesis*, 70-72.
232. Strah, S., Svete, J., and Stanovnik, B. (1996) The synthesis of 5-substituted 3-(benzoylamino)-6-[2-(substituted amino)ethenyl]-2H-pyran-2-ones and their transformation into 2H-pyrano[3,2-c]pyridine derivatives, *Journal of Heterocyclic Chemistry* 33, 751-756.
233. Strah, S., Svete, J., and Stanovnik, B. (1996) Rearrangements of 5-acetyl-3-benzoylamino-6-(2-dimethylamino-1-ethenyl)-2H-pyran-2-one and 3-benzoylamino-6-(2-dimethylamino-1-ethenyl)-5-ethoxycarbonyl-2H-pyran-2-one into 1-aminopyridine, pyrano[2,3-b]pyridine and isoxazole derivatives, *Journal of Heterocyclic Chemistry* 33, 1303-1306.
234. Park, G. (2005) Zn(II) complex of tachquin, N,N',N''-tris(2-quinolinylmethyl)-cis,cis-1,3,5-triaminocyclohexane; Synthesis and X-ray structure of [Zn(tachquin)](ClO₄)₂·H₂O, *Bulletin of the Korean Chemical Society* 26, 1849-1852.
235. Larsen, E., LaMar, G. N., Wagner, B. E., Parks, J. E., and Holm, R. H. (1972) Three-dimensional macrocyclic encapsulation reactions. III. Geometrical and electronic features of tris(diimine) complexes of trigonal-prismatic, antiprismatic, and intermediate stereochemistry, *Inorganic Chemistry* 11, 2652-2668.
236. Kepert, D. L. (1972) Stereochemistry of tris(bidentate) complexes, *Inorganic Chemistry* 11, 1561-1563.
237. Miller, J. N. (1981) *Techniques in Visible and Ultraviolet Spectrometry, Vol. 2: Standards in Fluorescence Spectrometry*.

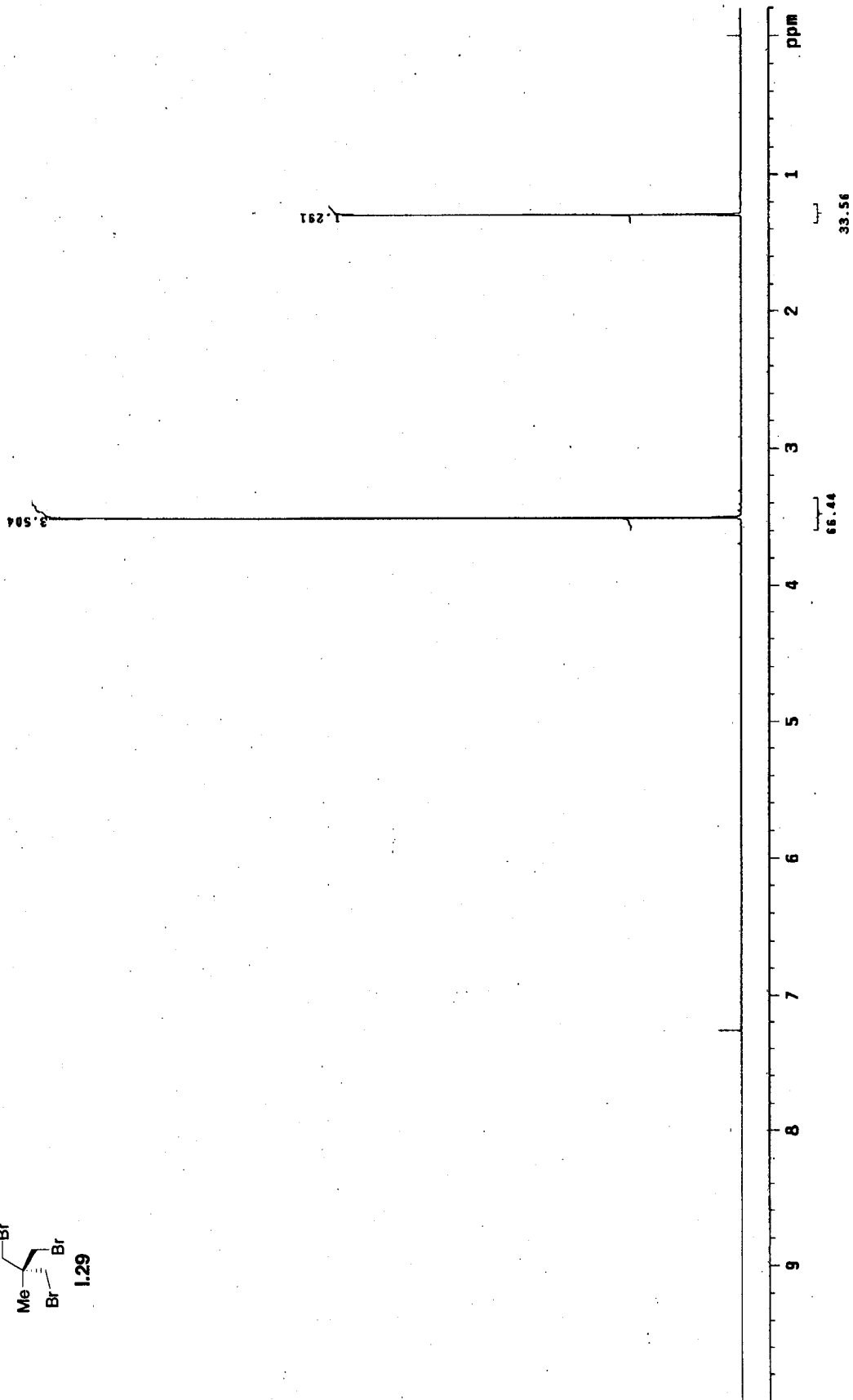
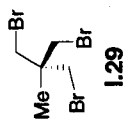
238. Ali, S. T., Reddy, R. C., Munirathnam, N. R., Sudheer, C., Anil, G., and Prakash, T. L. (2006) A novel in-situ technique of ultra purification of cadmium for electronic applications, *Separation and Purification Technology* 52, 288-294.
239. Edlin, C. D., Parker, D., Perry, J. J. B., Chartroux, C., and Gloe, K. (1999) Selective solvent extraction of tetrahedrally-coordinating transition metal ions from acidic aqueous media using benzimidazole-phosphinate ligands: specificity for zinc(II) over copper(II), *New Journal of Chemistry* 23, 819-826.
240. Ma, L. Q., and Rao, G. N. (1997) Chemical fractionation of cadmium, copper, nickel, and zinc in contaminated soils, *Journal of Environmental Quality* 26, 259-264.
241. Xie, H., and Nie, X. (2006) Determination of trace impurities in high-purity cadmium by high-resolution inductively coupled plasma mass spectrometry, *Analytical Sciences* 22, 1371-1374.
242. Anderegg, G., Hubmann, E., Podder, N. G., and Wenk, F. (1977) Pyridine derivatives as complexing agents. XI. Thermodynamics of metal complex formation with bis-, tris- and tetrakis[(2-pyridyl)methyl]amines, *Helvetica Chimica Acta* 60, 123-140.
243. Oktar, O., Caglar, P., and Seitz, W. R. (2005) Chemical modulation of thermosensitive poly(N-isopropylacrylamide) microsphere swelling: a new strategy for chemical sensing, *Sensors and Actuators, B: Chemical* B104, 179-185.
244. Tanaka, T. (1978) Collapse of gels and the critical endpoint, *Physical Review Letters* 40, 820-823.
245. Flory, P. J., and Rehner, J., Jr. (1943) Statistical mechanics of cross-linked polymer networks. II. Swelling, *Journal of Chemical Physics* 11, 521-526.
246. Flory, P. J., and Rehner, J., Jr. (1943) Statistical mechanics of cross-linked polymer networks. I. Rubberlike elasticity, *Journal of Chemical Physics* 11, 512-520.
247. Flory, P. J. (1953) *Principles of Polymer Chemistry*.
248. Kaval, N. (2002) IMPROVED SWELLABLE POLYMER MICROSPHERES FOR CHEMICAL SENSING, in *Chemistry*, p 173, University of New Hampshire, Durham.
249. Holtz, J. H., and Asher, S. A. (1997) Polymerized colloidal crystal hydrogel films as intelligent chemical sensing materials, *Nature (London)* 389, 829-832.
250. Carlson, R. J., and Asher, S. A. (1984) Characterization of optical diffraction and crystal structure in monodisperse polystyrene colloids, *Applied Spectroscopy* 38, 297-304.
251. Asher, S. A., Flaugh, P. L., and Washinger, G. (1986) Crystalline colloidal Bragg diffraction devices: the basis for a new generation of Raman instrumentation, *Spectroscopy (Duluth, MN, United States)* 1, 26-31.

252. Rundquist, P. A., Photinos, P., Jagannathan, S., and Asher, S. A. (1989) Dynamical Bragg diffraction from crystalline colloidal arrays, *Journal of Chemical Physics* 91, 4932-4941.
253. Lee, S.-K., and Okura, I. (1998) Photoluminescent determination of oxygen using metalloporphyrin-polymer sensing systems, *Spectrochimica Acta, Part A: Molecular and Biomolecular Spectroscopy* 54A, 91-100.
254. Chen, L., McBranch, D. W., Wang, H.-L., Helgeson, R., Wudl, F., and Whitten, D. G. (1999) Highly sensitive biological and chemical sensors based on reversible fluorescence quenching in a conjugated polymer, *Proceedings of the National Academy of Sciences of the United States of America* 96, 12287-12292.
255. McCurley, M. F., and Seitz, W. R. (1991) Fiber-optic sensor for salt concentration based on polymer swelling coupled to optical displacement, *Analytica Chimica Acta* 249, 373-380.
256. Rooney, M. T. (1996) Polymer substrates for optical chemical sensing, in *Chemistry*, p 184, University of New Hampshire, Durham.
257. Doherty, S. D. (2000) Swellable polymer substrates for use in magnetochemical and optical chemical sensing, in *Chemistry*, p 291, University of New Hampshire, Durham.
258. Conway, V. (1994) Polymer substrates for use in fiber optic sensors : suspension polymerization of Kraton G1652 modified poly(vinylbenzyl chloride), in *Chemistry*, p 136, University of New Hampshire, Durham.
259. Ricka, J., and Tanaka, T. (1985) Phase transition in ionic gels induced by copper complexation, *Macromolecules* 18, 83-85.
260. Li, W., Zhao, H., Teasdale, P. R., John, R., and Zhang, S. (2002) Synthesis and characterisation of a polyacrylamide-polyacrylic acid copolymer hydrogel for environmental analysis of Cu and Cd, *Reactive & Functional Polymers* 52, 31-41.
261. Hirotsu, S., Hirokawa, Y., and Tanaka, T. (1987) Volume-phase transitions of ionized N-isopropylacrylamide gels, *Journal of Chemical Physics* 87, 1392-1395.
262. Boutris, C., Chatzi, E. G., and Kiparissides, C. (1997) Characterization of the LCST behavior of aqueous poly(N-isopropylacrylamide) solutions by thermal and cloud point techniques, *Polymer* 38, 2567-2570.
263. Alder, R. W., Bowman, P. S., Steele, W. R. S., and Winterman, D. R. (1968) The remarkable basicity of 1,8-bis(dimethylamino)naphthalene, *Chemical Communications (London)*, 723-724.

264. Greene, T. W., and Wuts, P. G. M. (1991) *Protective Groups in Organic Synthesis*. 2nd Ed.
265. Xiao, H., Liu, R., Craig, D. C., and Baker, A. T. (2003) Complexes of a New N3S2 Macrocyclic: Synthesis, Structure and Electropray Mass Spectrometry, *Journal of Coordination Chemistry* 56, 923-932.
266. Moore, E. G., Bernhardt, P. V., Pigliucci, A., Riley, M. J., and Vauthey, E. (2003) Rates of Electronic Energy Transfer in Conformationally Flexible Bichromophoric Macrocyclic Complexes: a Combined Experimental and Molecular Modeling Study, *Journal of Physical Chemistry A* 107, 8396-8403.
267. Jiang, H., and Xu, H.-J. (2001) Using energy transfer to probe solvent dependent conformational changes in a D-A podand, *Wuli Huaxue Xuebao* 17, 1092-1096.
268. Maeda, Y., Nakamura, T., and Ikeda, I. (2001) Changes in the Hydration States of Poly(N-alkylacrylamide)s during Their Phase Transitions in Water Observed by FTIR Spectroscopy, *Macromolecules* 34, 1391-1399.
269. Jiao, Y., Wilkinson, J., Pietsch, E. C., Buss, J. L., Wang, W., Planalp, R., Torti, F. M., and Torti, S. V. (2006) Iron chelation in the biological activity of curcumin, *Free Radical Biology & Medicine* 40, 1152-1160.
270. Suo, Q., Huang, Y., Weng, L., He, W., Li, C., Li, Y., and Hong, H. (2006) Purification and molecular crystal structure of natural curcumin, *Shipin Kexue (Beijing, China)* 27, 27-30.
271. Adams, B. K., Cai, J., Armstrong, J., Herold, M., Lu, Y. J., Sun, A., Snyder, J. P., Liotta, D. C., Jones, D. P., and Shoji, M. (2005) EF24, a novel synthetic curcumin analog, induces apoptosis in cancer cells via a redox-dependent mechanism, *Anti-Cancer Drugs* 16, 263-275.
272. Shishodia, S., Sethi, G., and Aggarwal, B. B. (2005) Curcumin: getting back to the roots, *Annals of the New York Academy of Sciences* 1056, 206-217.
273. Hershko, C., Link, G., and Cabantchik, I. (1998) Pathophysiology of iron overload, *Annals of the New York Academy of Sciences* 850, 191-201.
274. Pietsch, E. C., Chan, J. Y., Torti, F. M., and Torti, S. V. (2003) Nrf2 mediates the induction of ferritin H in response to xenobiotics and cancer chemopreventive dithiolethiones, *Journal of Biological Chemistry* 278, 2361-2369.
275. Pietsch, E. C., Hurley, A. L., Scott, E. E., Duckworth, B. P., Welker, M. E., Leone-Kabler, S., Townsend, A. J., Torti, F. M., and Torti, S. V. (2003) Oxathiolene oxides: a novel family of compounds that induce ferritin, glutathione S-transferase, and other proteins of the phase II response, *Biochemical Pharmacology* 65, 1261-1269.

276. Valapatukutikadan, D. J., and Krishnankutty, K. (2005) Synthesis, characterization and antitumor activities of some synthetic curcuminoid analogues and their copper complexes, *Transition Metal Chemistry (Dordrecht, Netherlands)* 30, 229-233.
277. Kuhlwein, F., Polborn, K., and Beck, W. (1997) Metal complexes of dyes. Part 9. Transition metal complexes of curcumin and derivatives, *Zeitschrift fuer Anorganische und Allgemeine Chemie* 623, 1211-1219.
278. Bernabe-Pineda, M., Ramirez-Silva, M. T., Romero-Romo, M. A., Gonzalez-Vergara, E., and Rojas-Hernandez, A. (2004) Spectrophotometric and electrochemical determination of the formation constants of the complexes Curcumin-Fe(III)-water and Curcumin-Fe(II)-water, *Spectrochimica Acta, Part A: Molecular and Biomolecular Spectroscopy* 60A, 1105-1113.
279. Pedersen, U., Rasmussen, P. B., and Lawesson, S. O. (1985) Synthesis of naturally occurring curcuminoids and related compounds, *Liebigs Annalen der Chemie*, 1557-1569.
280. Arezzini, B., Ferrali, M., Ferrari, E., Grandi, R., Monti, S., and Saladini, M. (2004) Glycosyl-curcuminoids as potential new chelating agents in iron overload chelation therapy, *European Journal of Inorganic Chemistry*, 646-652.
281. Evans, D. F. (1959) The determination of the paramagnetic susceptibility of substances in solution by nuclear magnetic resonance, *Journal of the Chemical Society*, 2003-2005.

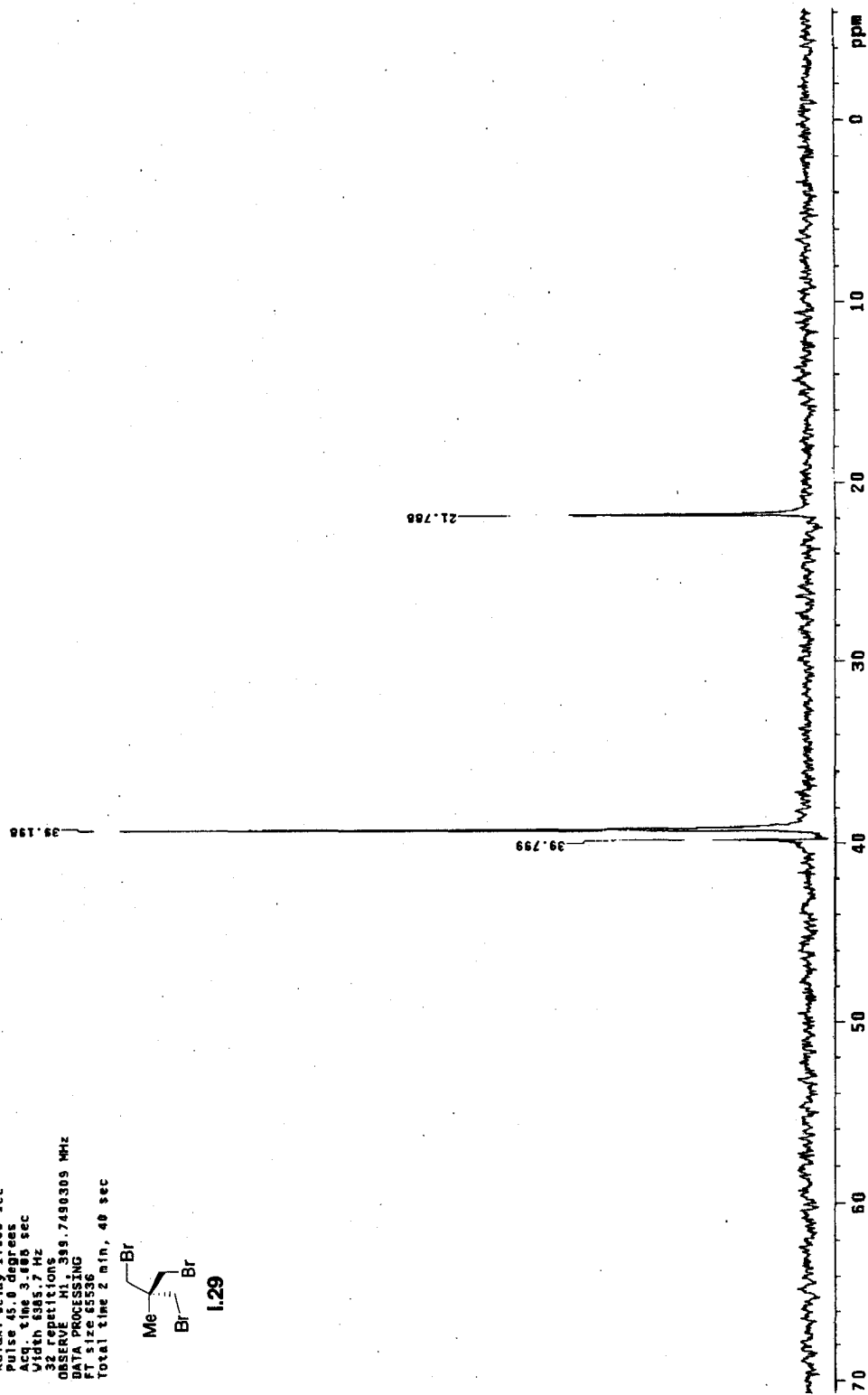
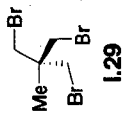
SELECTED SPECTRA



Archive directory: /export/home/kennedy/vmarsys/data
Sample directory: dk40_1_07Jun2004

Pulse Sequence: s2pu1
Solvent: CCl₄
Ambient temperature
File: PROTON
Mercury-88888 "1y1station"

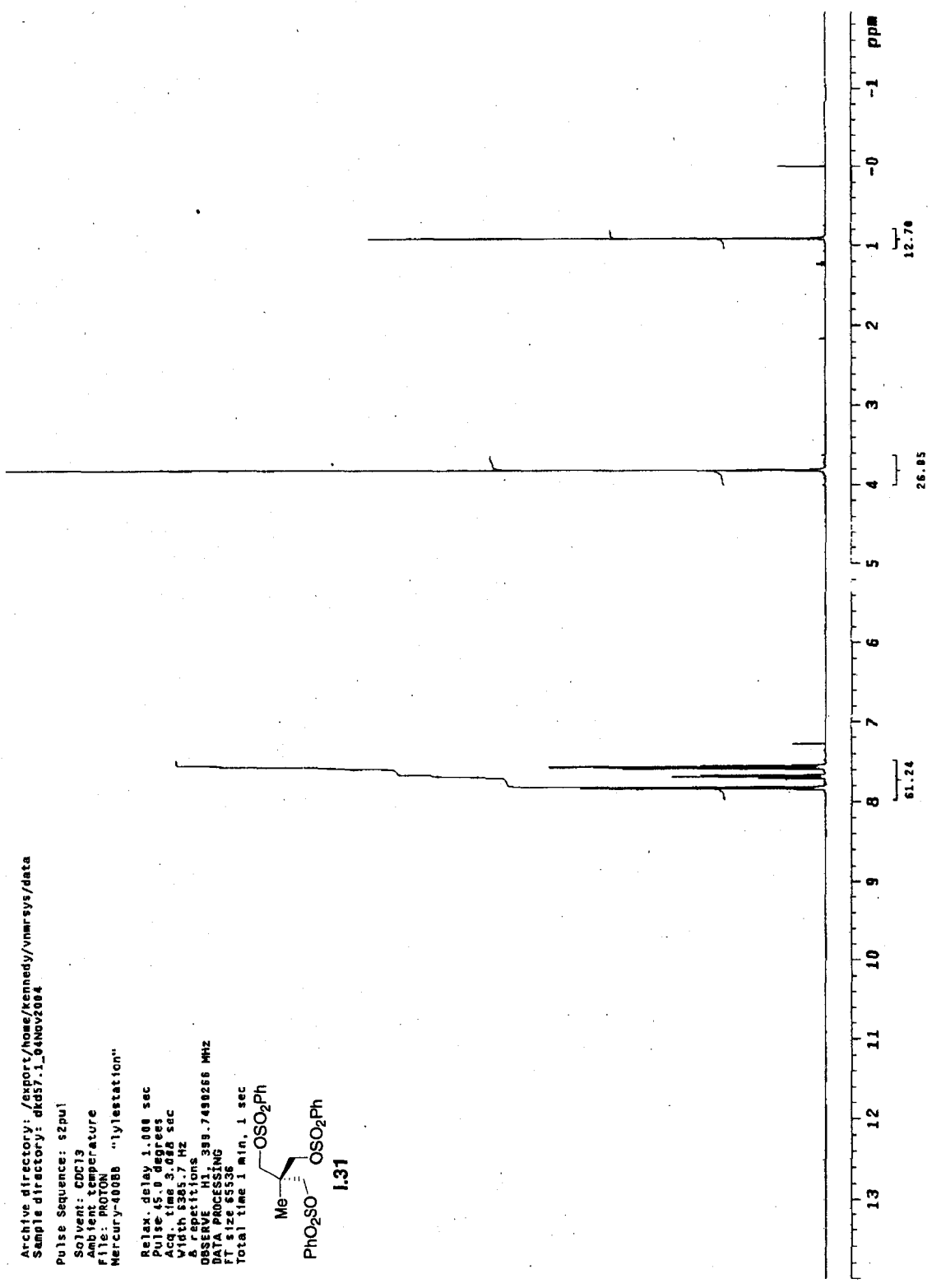
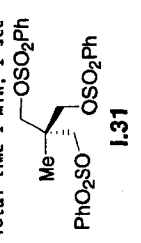
Relax. delay 1.000 sec
Pulse 45.0 degrees
Acq 4.000 sec
Width 6345.7 Hz
32 repetitions
OBSERVE H1 399.7490309 MHz
DATA PROCESSING
FT size 65536
Total time 2 min, 40 sec



Archive directory: /export/home/kennedy/vnmr/sys/data
Sample directory: dkds7.1_04Nov2004

Pulse Sequence: s2pul
Solvent: CDCl3
Ambient temperature
File: PROTON
Mercury-400BB "1ylestation"

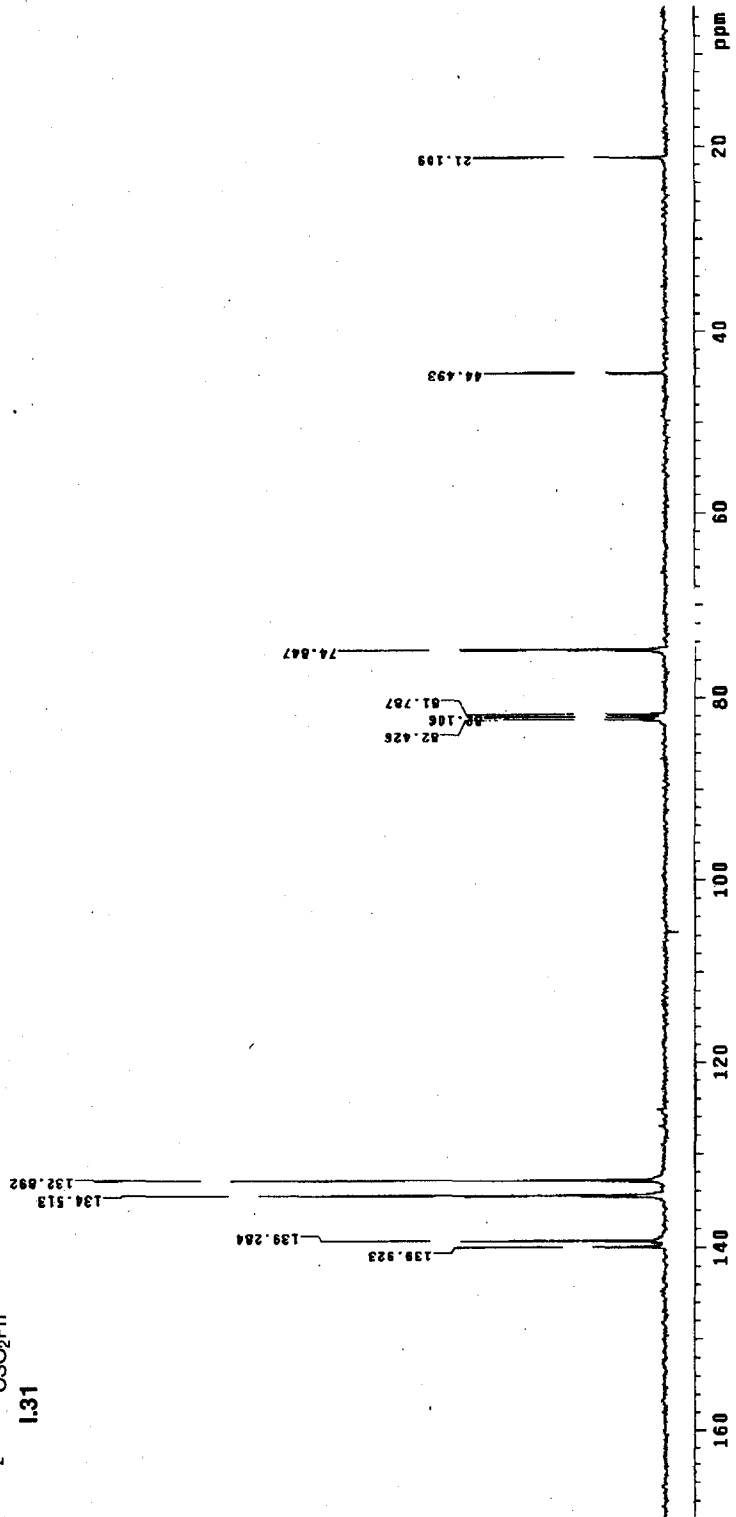
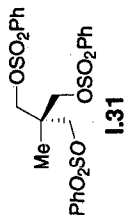
Relax. delay 1.000 sec
Pulse 15.0 degree
Acq. time 3.000 sec
Width 6395.7 Hz
repetitions
OBSERVE H1 399.7490266 MHz
DATA PROCESSING
FT size 6536
Total time 1 min, 1 sec



Archive directory: /export/home/kennedy/vmarsys/data
 Sample directory: dkds7_1_94Nov2804

Pulse Sequence: szpul
 Solvent: CDC13
 Ambient temperature
 File: PHOTON
 Mercury-400BB "lytestation"

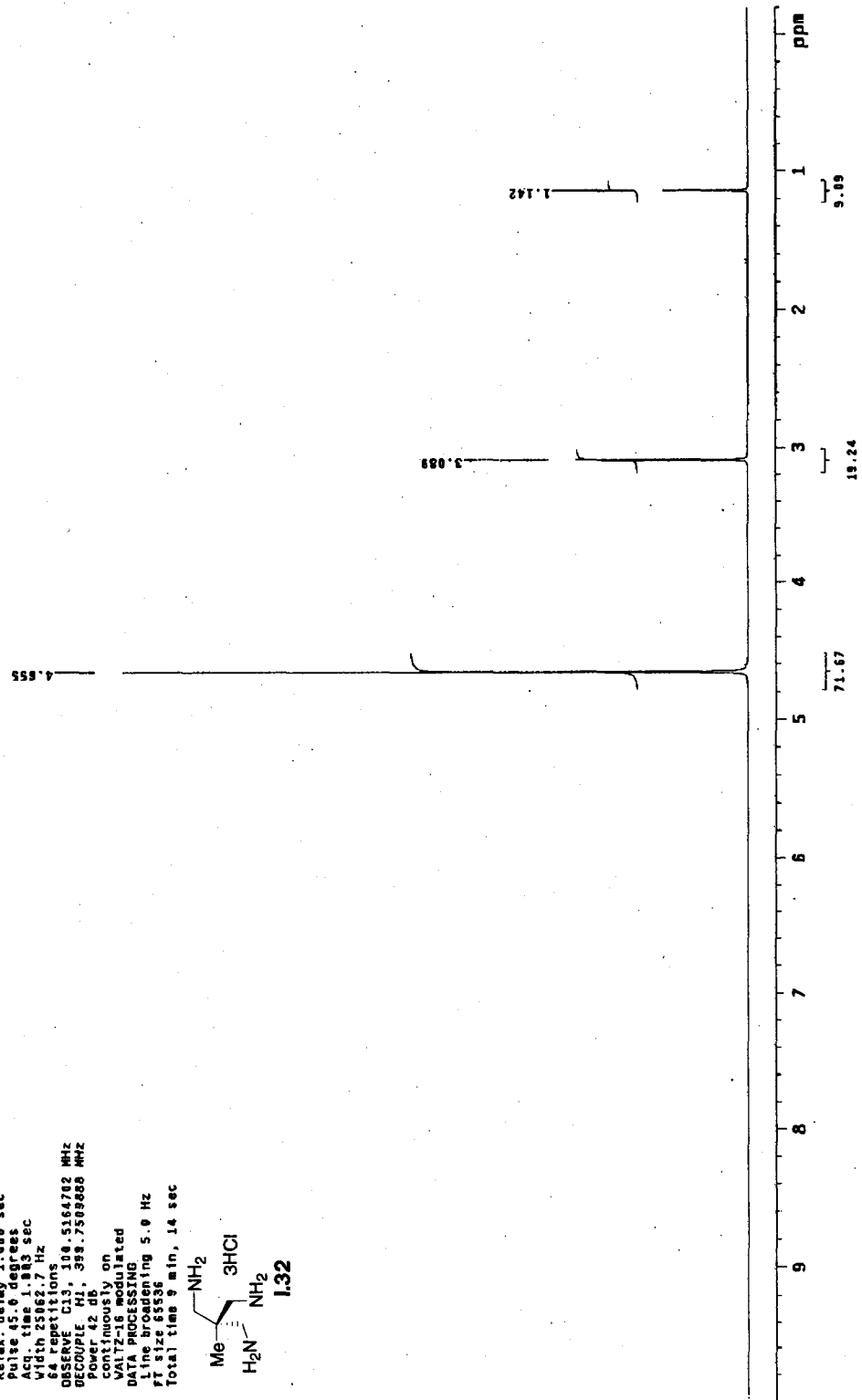
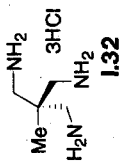
Relax. delay 1.008 sec
 Pulse 45.0 degrees
 Width 6365.2 Hz
 Width 6365.2 Hz
 8 repetitions
 OBSERVE HL 399.7490266 MHz
 DATA PROCESSING
 FT size 65536
 Total time 1 min, 1 sec



Archive directory: /export/home/kennedy/vmrsys/data
Sample directory: dkds7.2_04Nov2004

Pulse Sequence: szpu1
Solvent: CDCl3
Ambient temperature
File: CARBON
Mercury-40000 "lytstation"

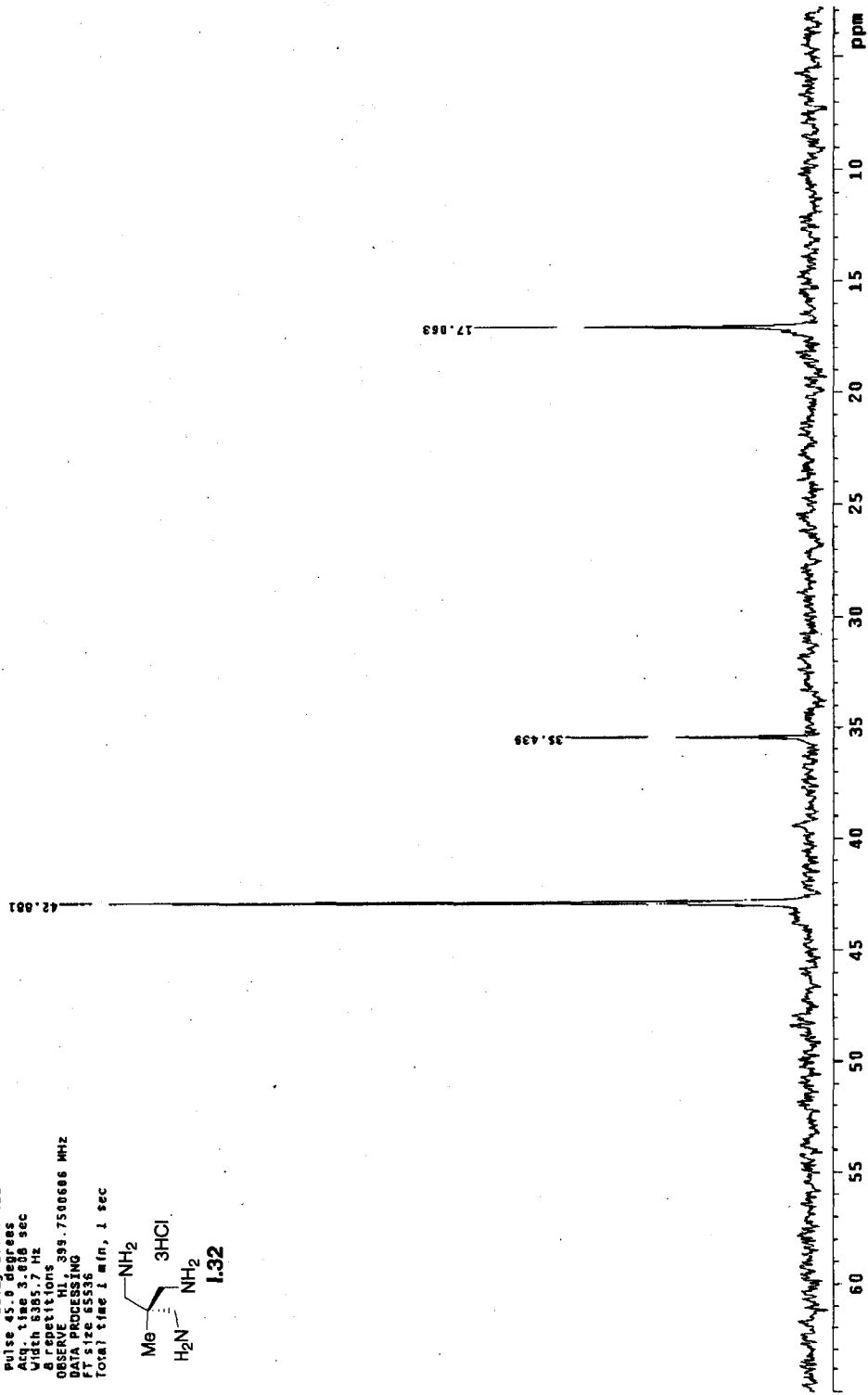
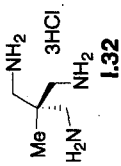
Relax. delay 1.000 sec
Pulse 45.0 degrees
Acq. time 1.983 sec
Width 25062.7 Hz
64 repetitions
OBSERVE CH, 100.5164702 MHz
DECOUPLE CH, 598.7509666 MHz
continuously on
WALTZ-16 modulated
DATA PROCESSING
Line broadening 5.0 Hz
FT size 65536
Total time 9 min, 14 sec



Archive directory: /export/home/kennedy/vmarsys/data
Sample directory: dkc44.1_12Jun2004-12:42:07

Pulse Sequence: s2pu1
Solvent: D2O
Ambient temperature
F1: Mercury
Mercury: 49998 "lylestation"

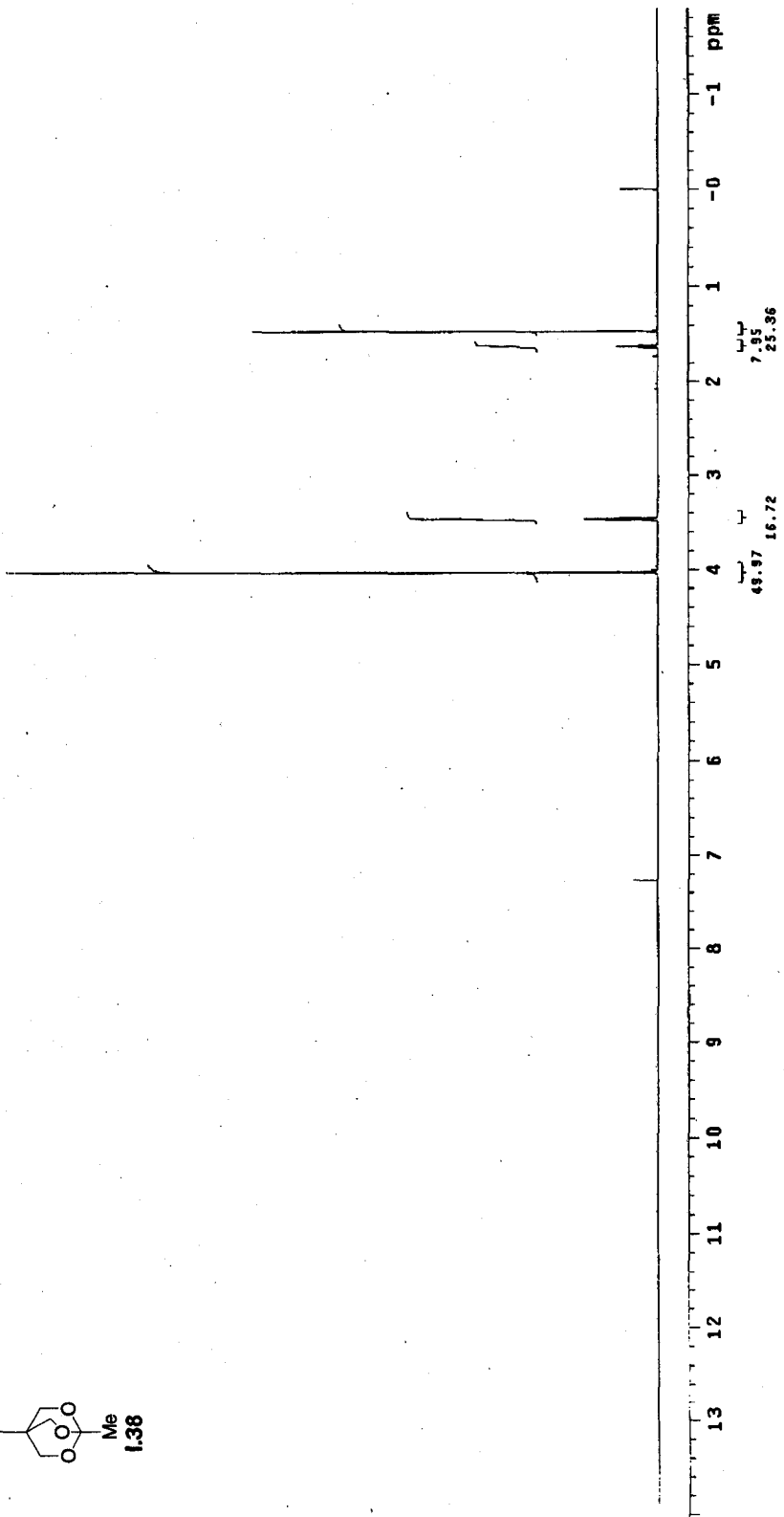
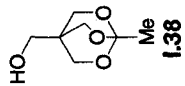
Relax. delay 1.000 sec
Puls. prog. 1.000 sec
Acq. time 3.606 sec
Width 6385.7 Hz
repetitions
OBSERVE H1, 399.750066 MHz
DATA PROCESSING
FT size 65536
Total time 1 min, 1 sec



Archive directory: /export/home/kennedy/vmarsys/data
Sample directory: dkd66.2_09Nov2004

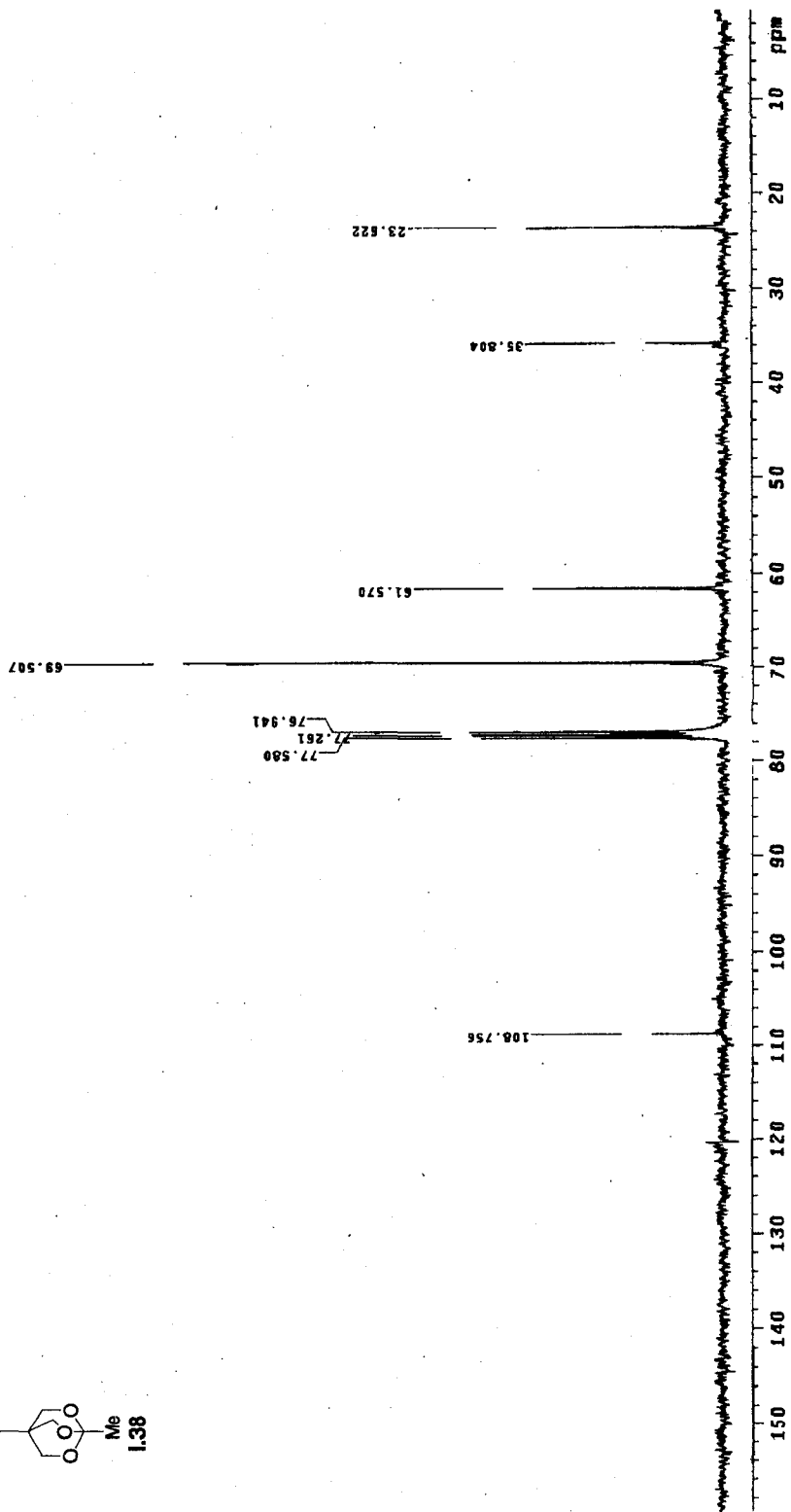
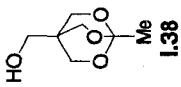
Pulse Sequence: szpu1
Solvent: CDCl3
Acquisition Temperature
File: PROTON
Mercury-400BB "lylestation"

Relax. delay 1.000 sec
Pulse 45.0 degrees
Acq. time 3.900 sec
Width 833.7 Hz
OBSERVE 1H 399.7430000 MHz
DATA PROCESSING
FT size 65336
Total time 1 min, 1 sec



Archive directory: /export/home/kennedy/vnmrsys/data
Sample directory: dkde0.2_09Nov2004

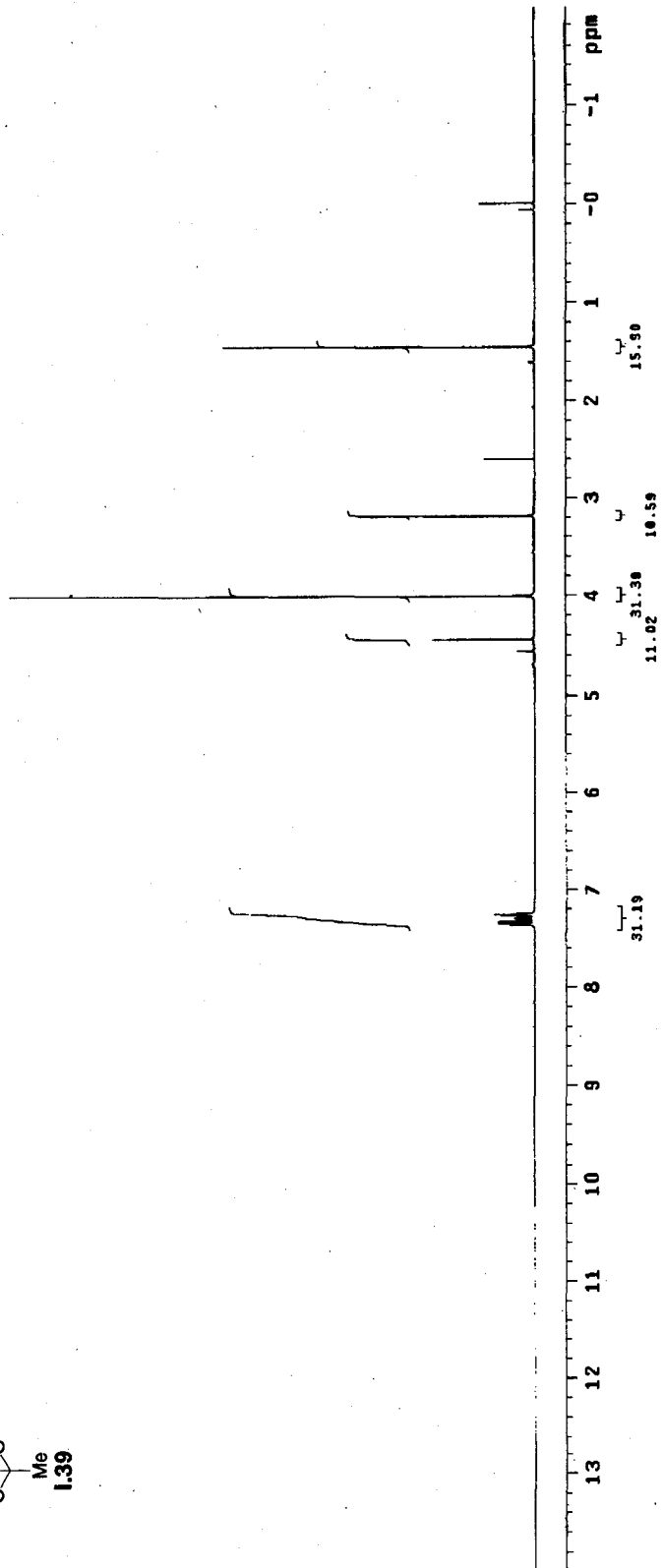
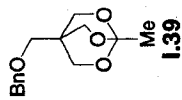
Pulse Sequence: s2pu1
Solvent: CDCl3
Ambient temperature
File: PROTON
Mercury-40000 "lytestation"
Relax. delay 1.000 sec
Pulse 45.0 degrees
Acq. time 3.000 sec
Width 6885.7 Hz
Repetitions
Observed F1 399.7450889 MHz
Reference F1 50.1300000 MHz
F2 size 65536
Total time 1 min, 1 sec



Archive directory: /export/home/kennedy/vnmrSYS/data
Sample directory: dkd66_3_89NOV2004-15:34:48

Pulse Sequence: szpul
Solvent: CDCl3
Ambient temperature
File: CARBON
Mercury-40sBB "lylestation"

Relax. delay 1.880 sec
Pulse 45.6 degrees
Acq. time 1.883 sec
Width 25062.7 Hz
256 repetitions
OBSERVE C13, 100.5164504 MHZ
DECOUPLE H1, 399.7508666 MHZ
Power 42 dB
continuously on
WALTZ-16 modulated
DATA PROCESSING
Line broadening 5.0 Hz
Ft size 65536
Total time 3 min, 14 sec



Archive directory: /export/home/kennedy/vnarsys/data
Sample directory: dkd64_2_1UNOV2864

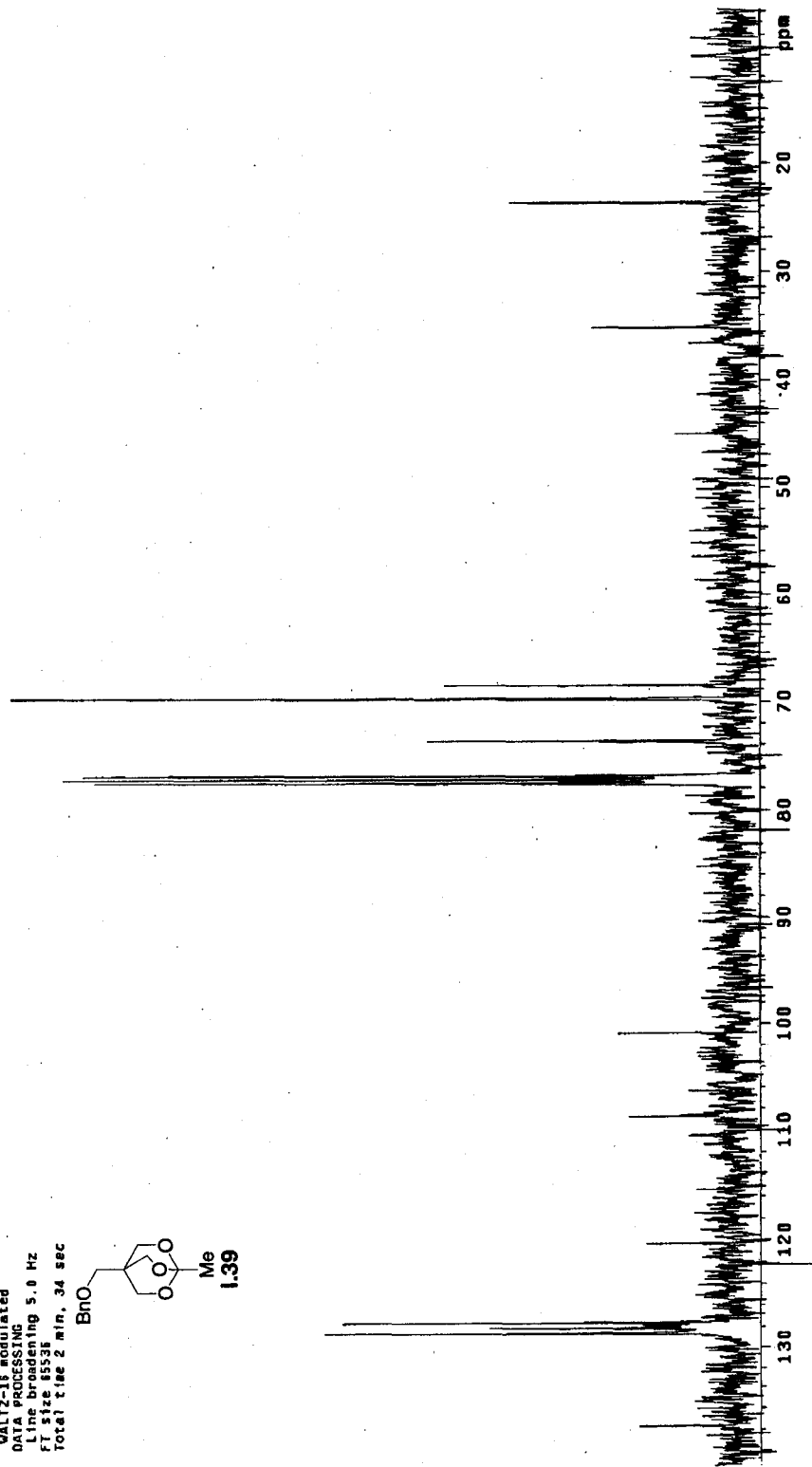
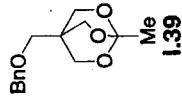
Pulse Sequence: s2pul

Solvent: CDCl3
Ambient temperature
File: CARBON
Mercury-400B5 "lytestation"

Relax. delay 1.000 sec
Pulse 45.0 degrees
Acq. time 1.803 sec
Width 25062.7 Hz
64 repetitions

OBSERVE C13, 100.518594 MHz
DECUPLE H1, 399.759366 MHz

Power 42 dB
Sensitivity on
MATHS on
MULTIPLICATED
DATA PROCESSING
Line broadening 5.0 Hz
FT size 65535
Total time 2 min, 34 sec



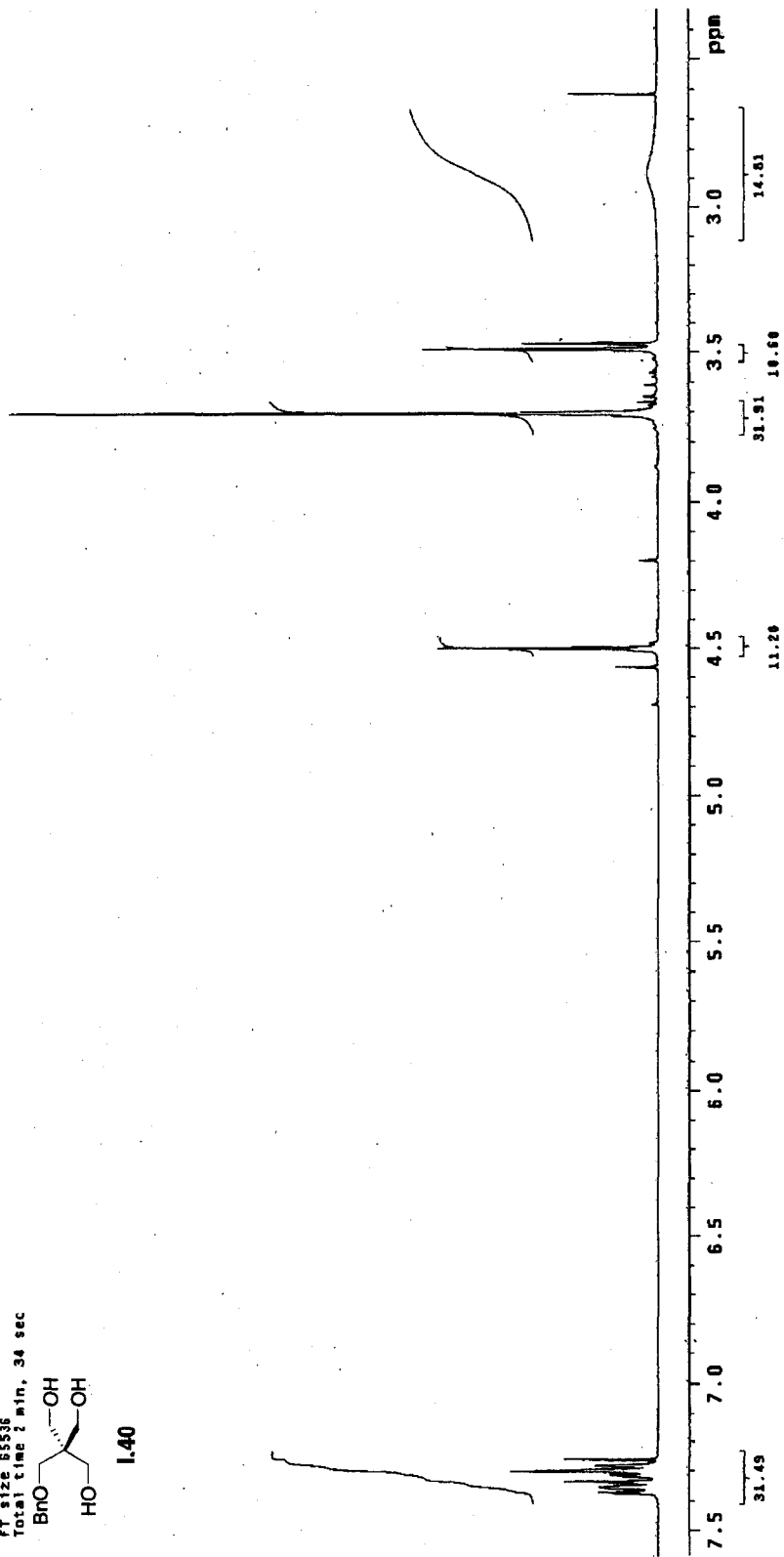
Archive directory: /export/home/kennedy/vnarsys/data
Sample directory: dkd64.2_10Nov2004

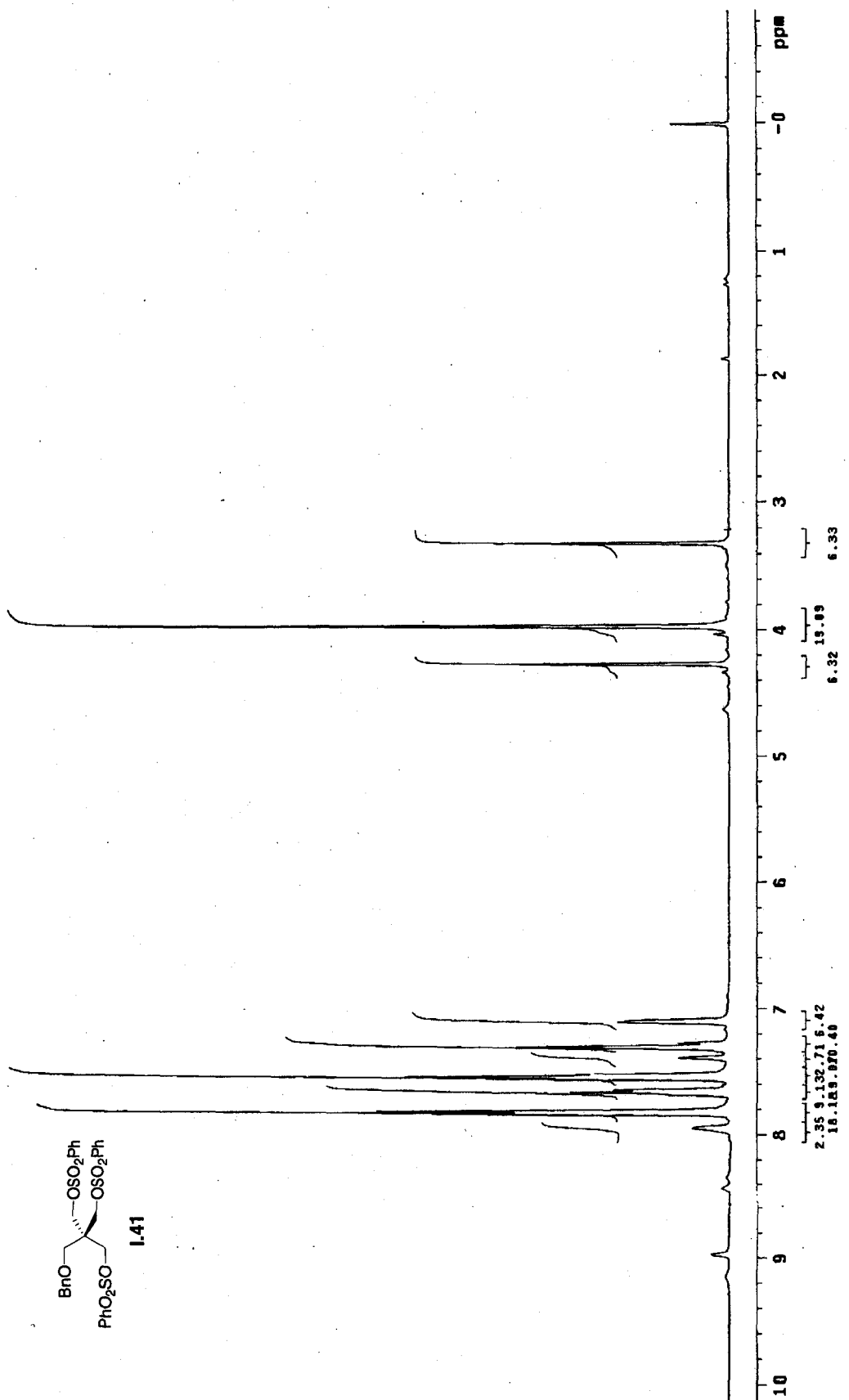
Pulse sequence: s2pu1
Solvent: CDCl3
Ambient temperature
File: CARBON
Mercury-40000 "lytestation"

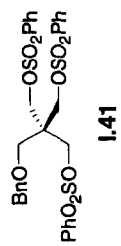
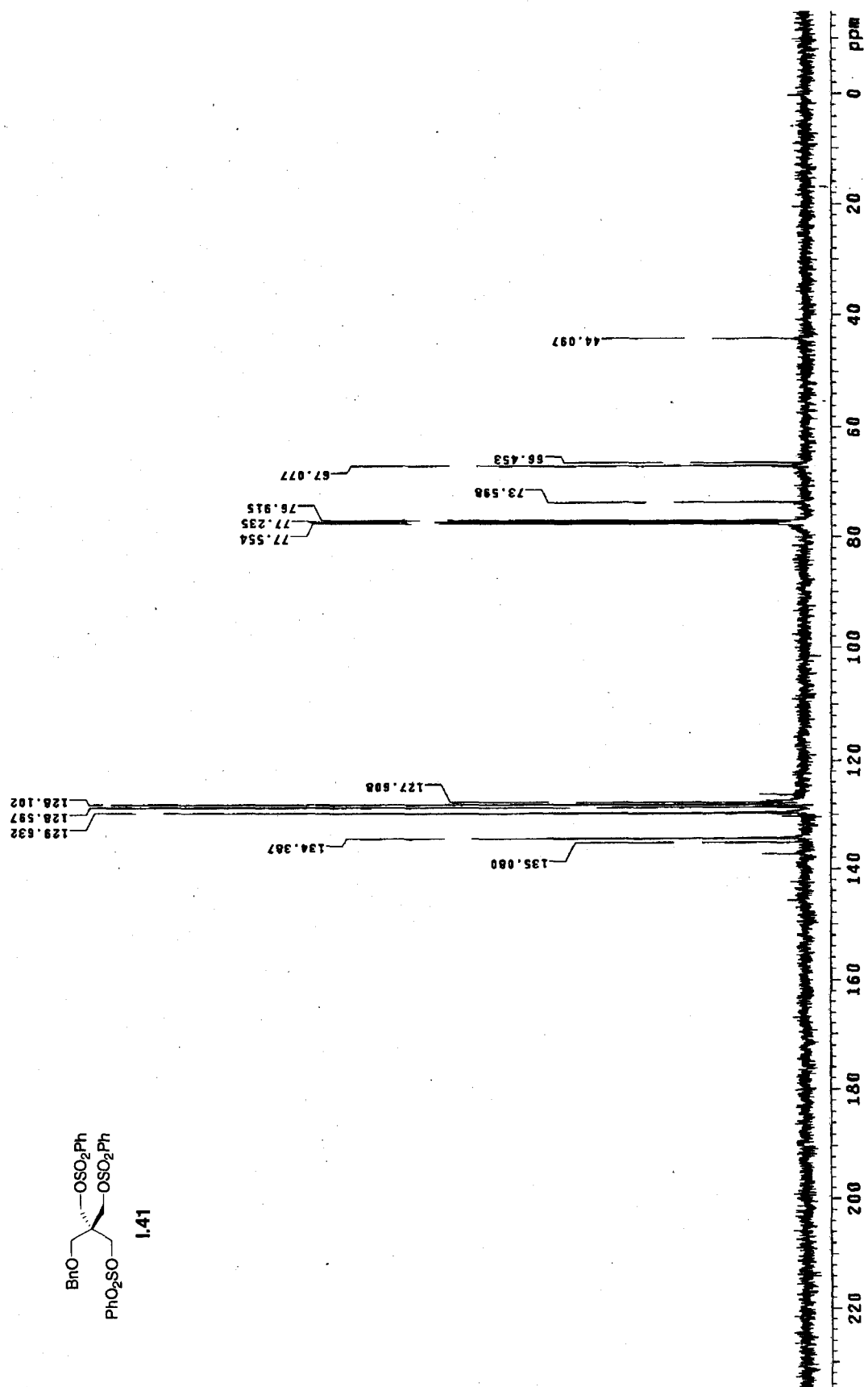
Relax. delay 1.000 sec
Pulse 45.0 degrees
Acq. time 1.003 sec
Width 25062.7 Hz
64 repetitions
OBSERVE C13, 100.5169504 MHz
DECOUPLE H1, 399.7509060 MHz
Power 42 dB
continuously on
WALTZ-16 modulated
DATA PROCESSING
F1 line broadening 5.0 Hz
SI 1.000000
Total time: 1 min, 34 sec

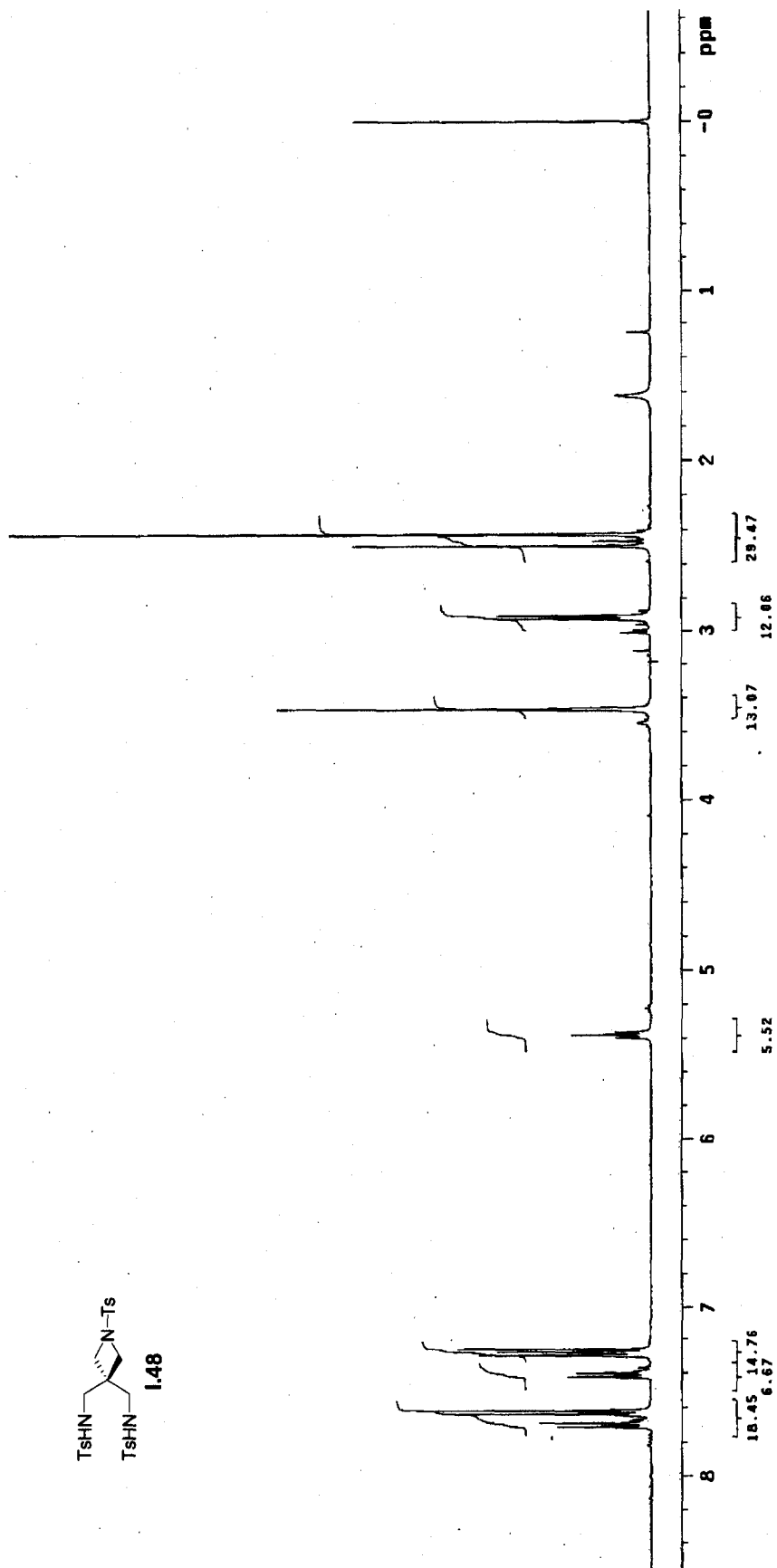
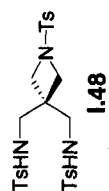


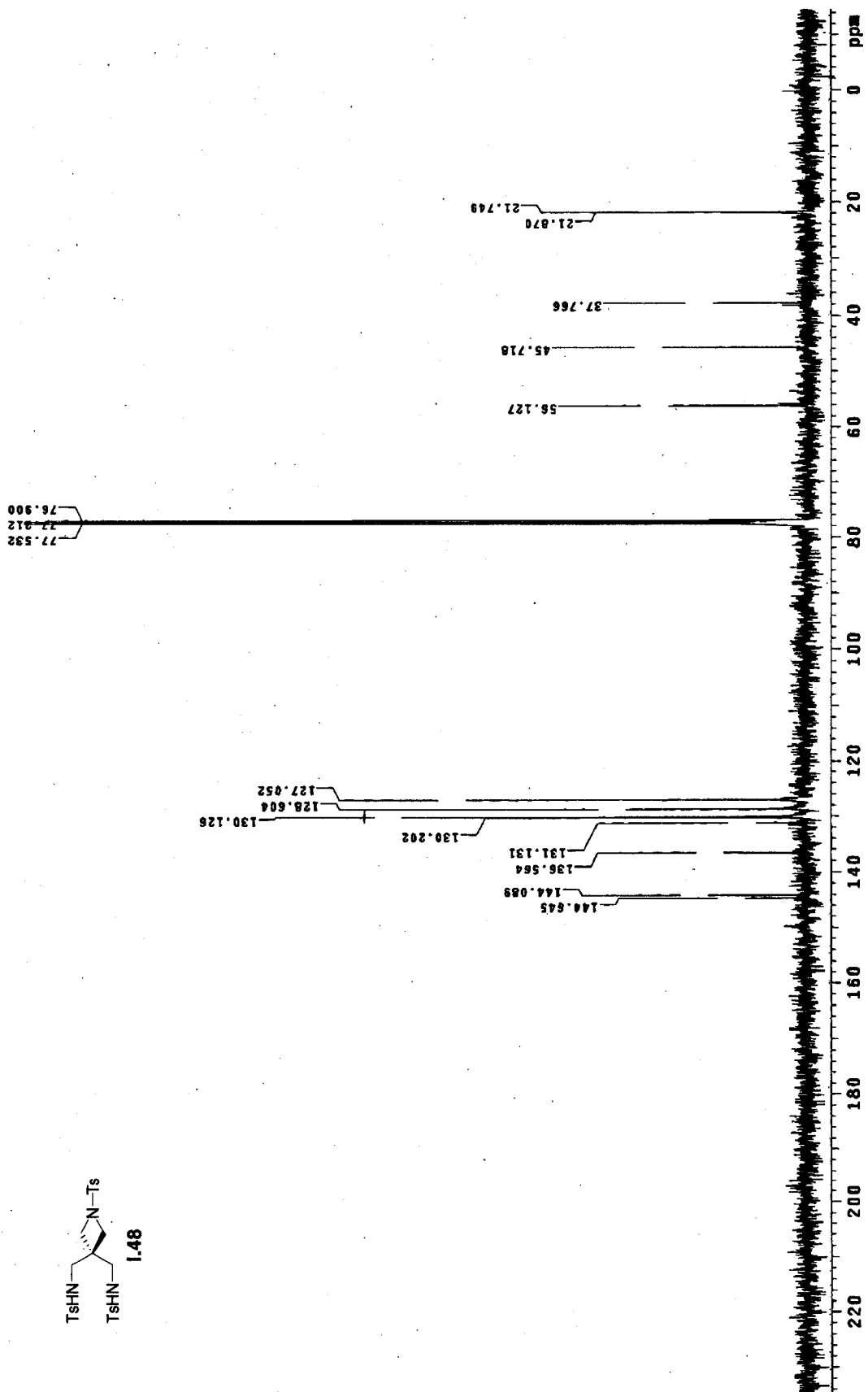
1.40









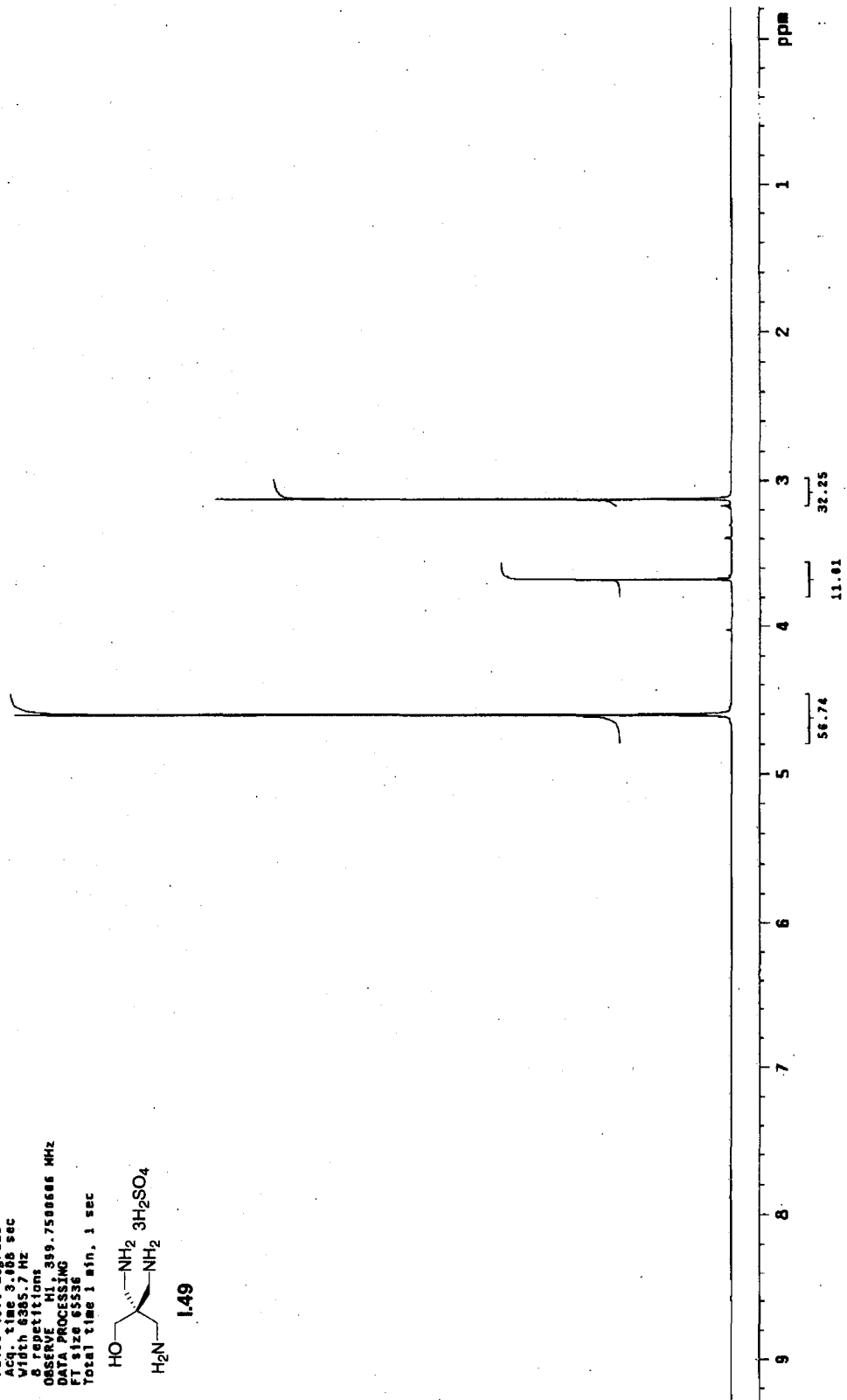
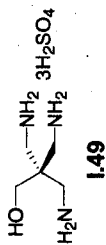


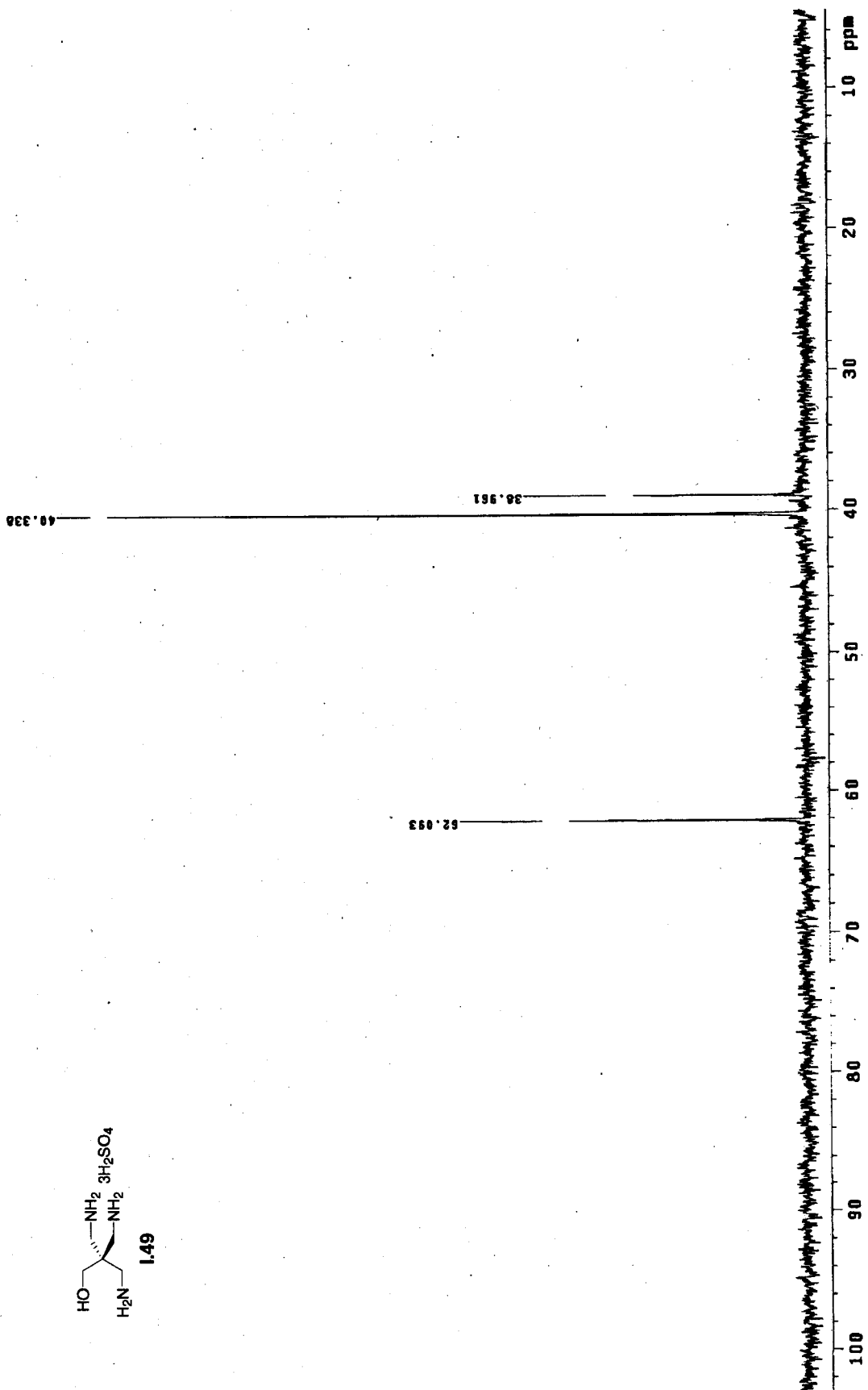
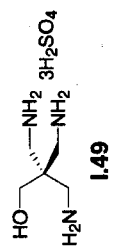
Archive directory: /export/home/kennedy/vmarsys/data
Sample directory: dk768_1_29Jun2007-11:09:16
File: PKDT0N

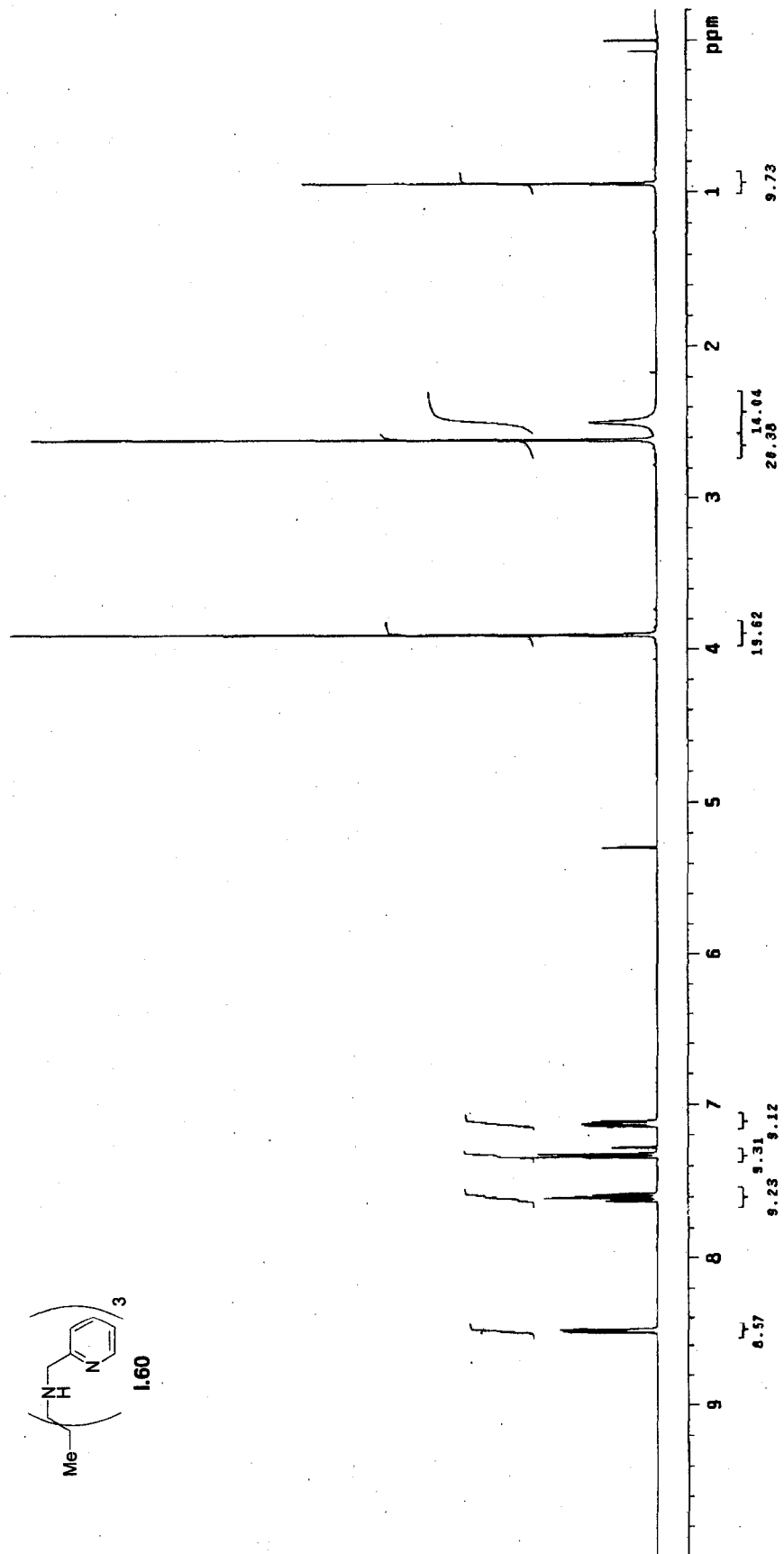
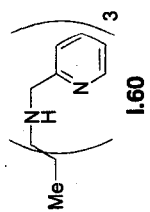
Pulse Sequence: szpul

Solvent: D2O
Ambient temperature
Mercury-400BB "lyl64.unh.edu"

Relax. delay 1.000 sec
Pulse 45.0 degrees
Acq. time 3.000 sec
Width 6305.7 Hz
6 repetitions
OBSERVE HI, 399.758068 MHz
DATA PROCESSING
FI size 65536
Total time 1 min, 1 sec

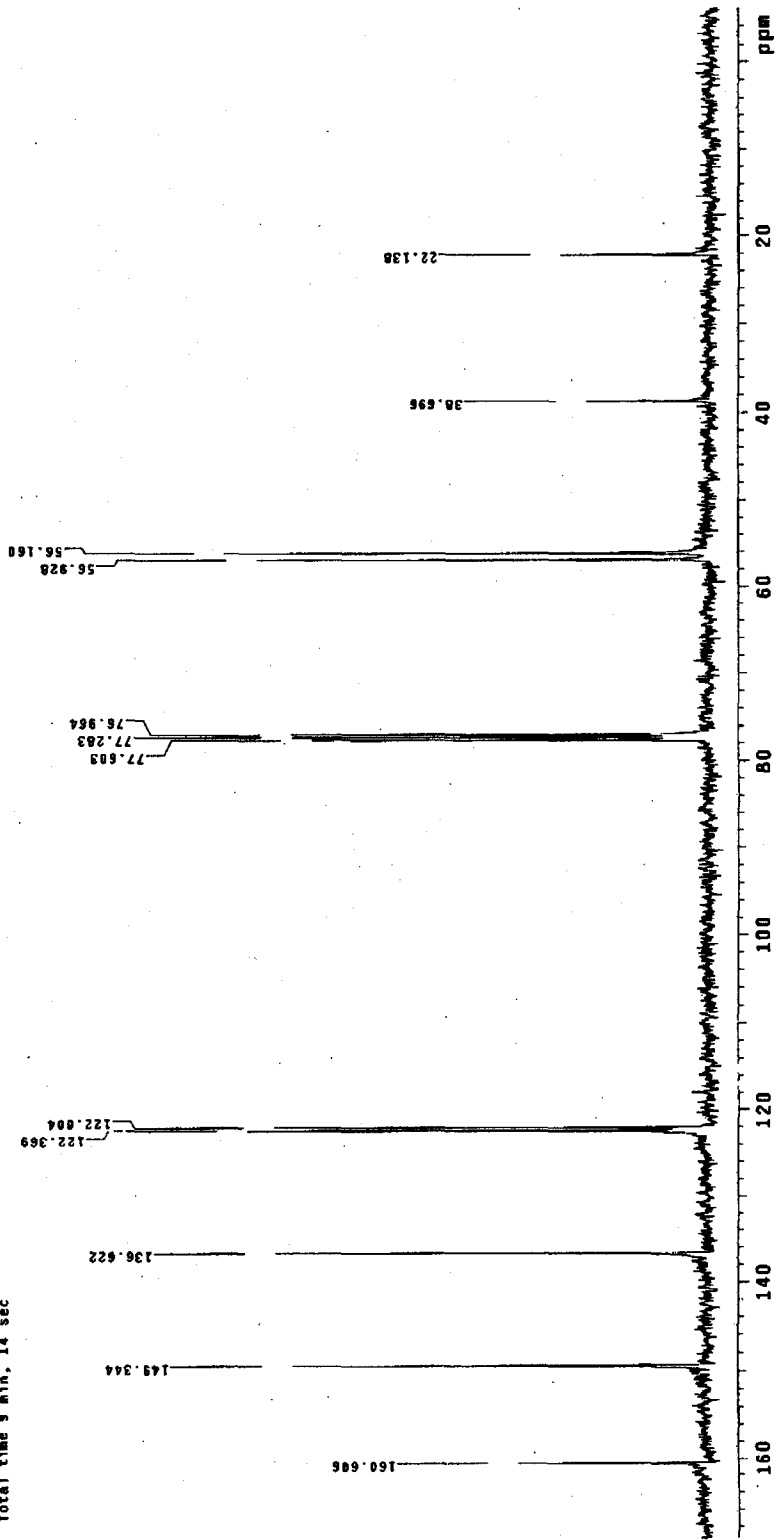
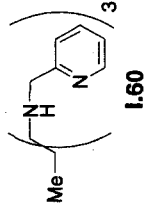






Archive directory: /export/home/kennedy/vnmrSYS/data
 Sample directory: dkc66_3_23jun2004

Pulse Sequence: s2pul
 Solvent: CDCl3
 Ambient temperature
 File: CARBON
 Mercury-400MB "lylestation"
 Relax. delay 1.000 sec
 Pulse 45.0 degrees
 Acq. time 1.003 sec
 Width 23002.7 Hz
 OBSERVE CH1 FREQ0 5163584 MHz
 DECOUPLE CH2 339.7500000 MHz
 Power 42 dB
 continuously on
 WALTZ-16 modulated
 DATA PROCESSING
 Line broadening 5.0 Hz
 Ft size 65536
 Total time 9 min, 14 sec

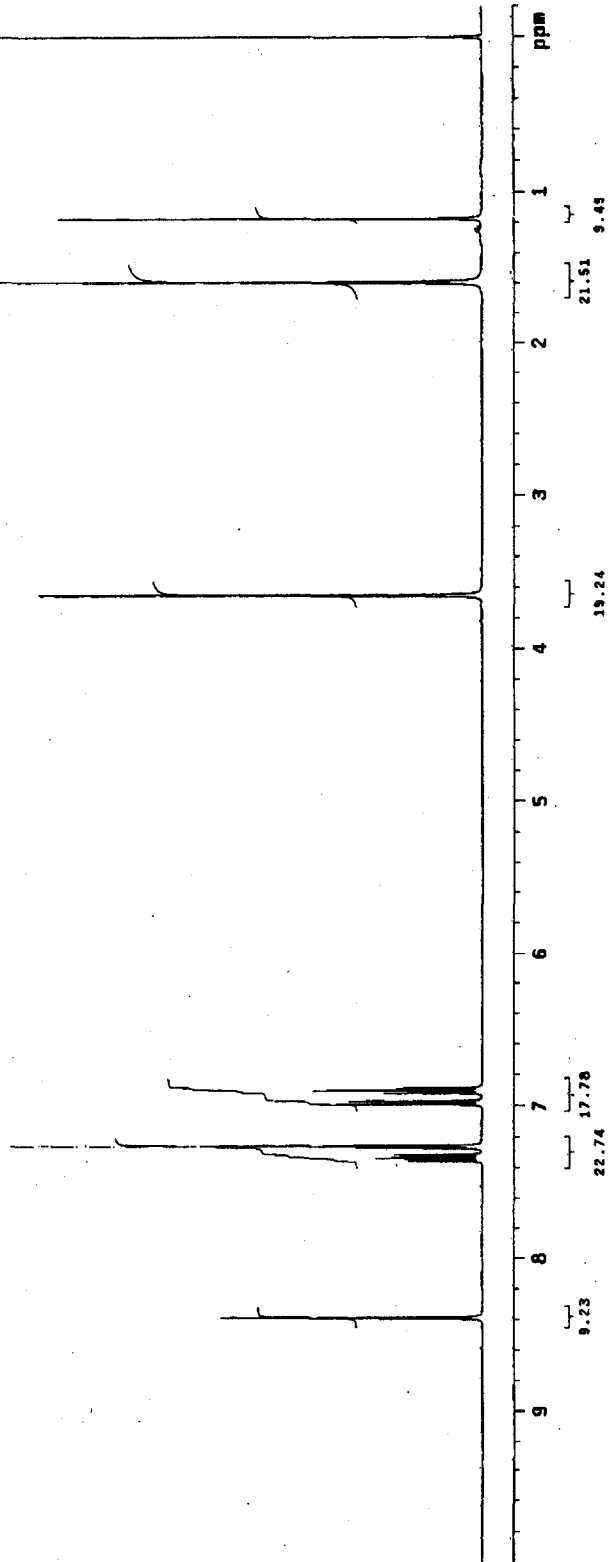
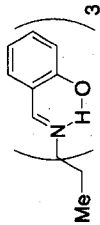


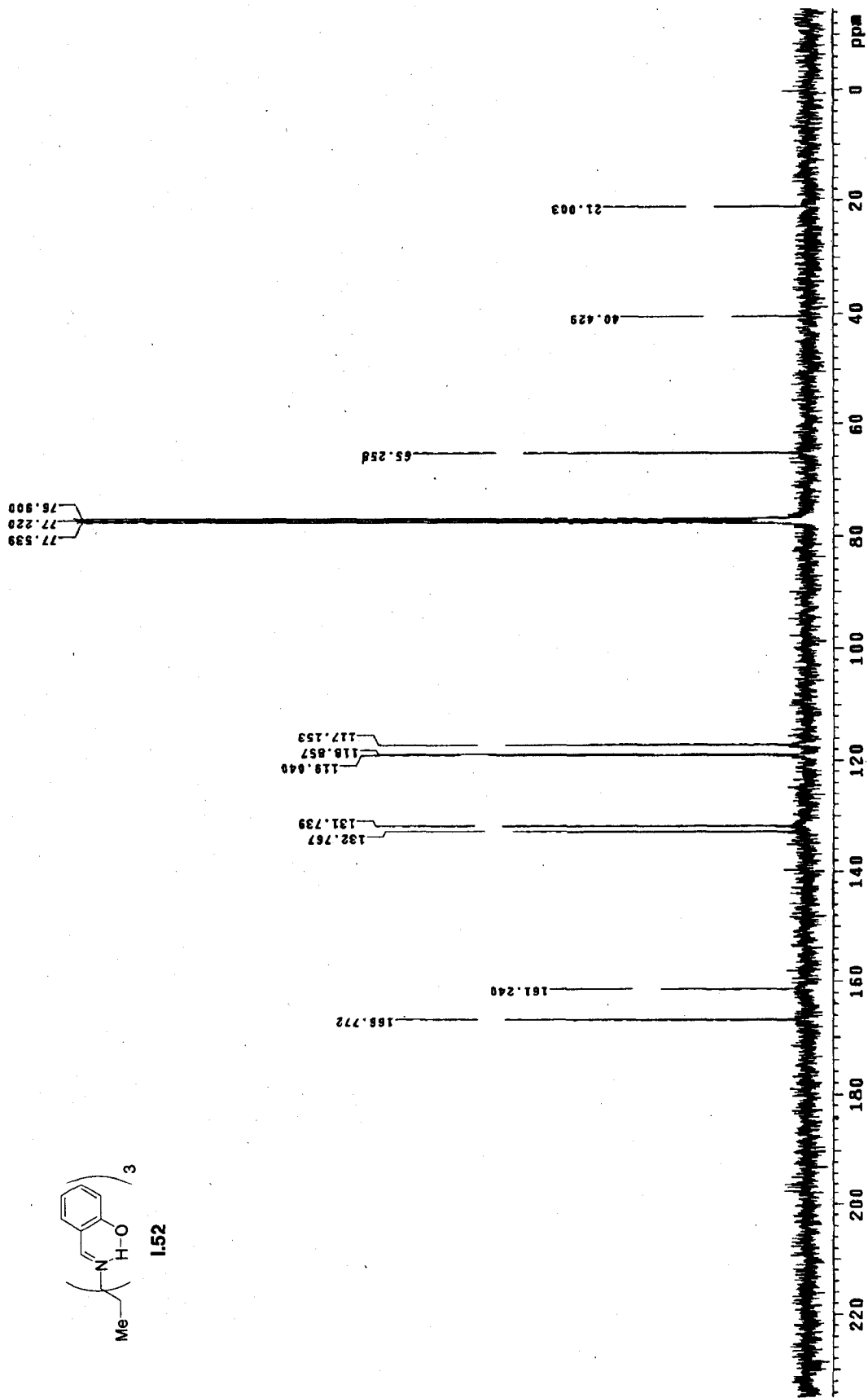
Archive directory: /export/home/kennedy/vmrsys/data
Sample directory: dcd8.5_23jun2000

Pulse Sequence: s2pu1

Solvent: CDCl3
Ambient temperature
File: CAC008 "lylestafon"

Relax. delay 1.000 sec
Pulse 45.0 degrees
Acq. time 2.303 sec
Width 20411.0 Hz
256 scans
OBSERVE C13, 100.5189584 MHz
DECOUPLE H1, 399.7509888 MHz
Power 42 dB
continuously on
VOLTAGE-16 modulated
DATA PROCESSING
Line broadening 5.0 Hz
FT size 65536
Total time 3 min, 14 sec

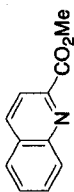




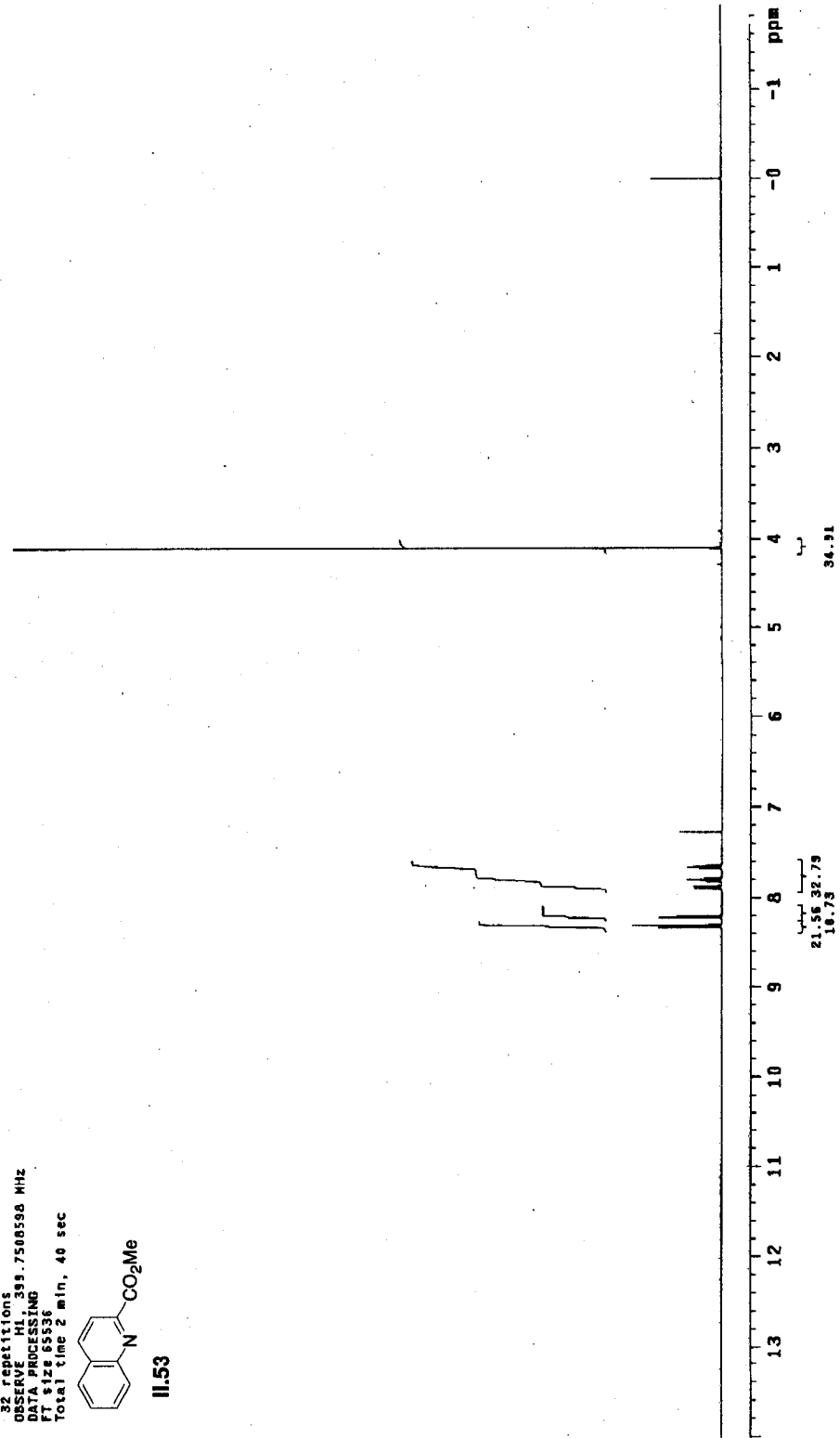
Archive directory: /export/home/kennedy/vnarsys/data
Sample directory: dke12.1.22Dec2004

Pulse Sequence: szpul
Solvent: DMSO
Ambient temperature
File: PROTON
Mercury-40086 "lyTestation"

Relax. delay 1.000 sec
Pulse 45.0 degrees
Acq. time 3.000 sec
Width 6365.7 Hz
32 repetitions
QZ: 0.00000000
QZ: 0.00000000
QZ: 0.00000000
PT 612.65536
Total time 2 min, 40 sec



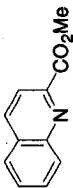
11.53



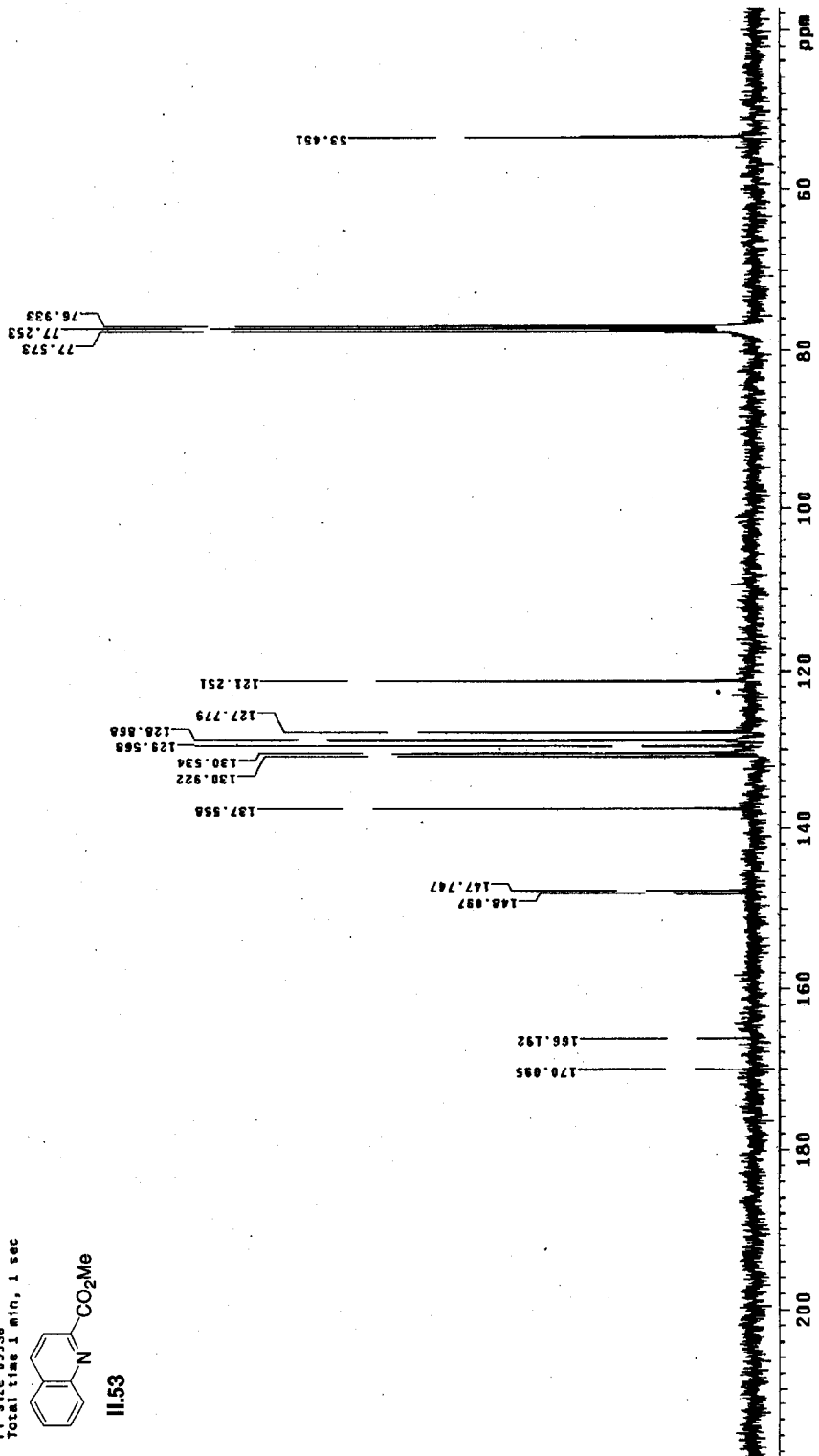
Archive directory: /export/home/kennedy/vnmrsvs/data
Sample directory: dk746_1_02Feb2006

Pulse Sequence: s2pul
Solvent: CDCl3
Ambient temperature
File: PROTON
Mercury-40000 "lytestation"

Relax. delay 1.000 sec
Pulse 45.0 degrees
Acq. time 3.000 sec
Width 6305.7 Hz
repetitions 8
OBSERVE HI, 399.7490214 MHz
DATA PROCESSING
F1 size 85336
Total time 1 min, 1 sec



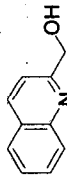
11.53



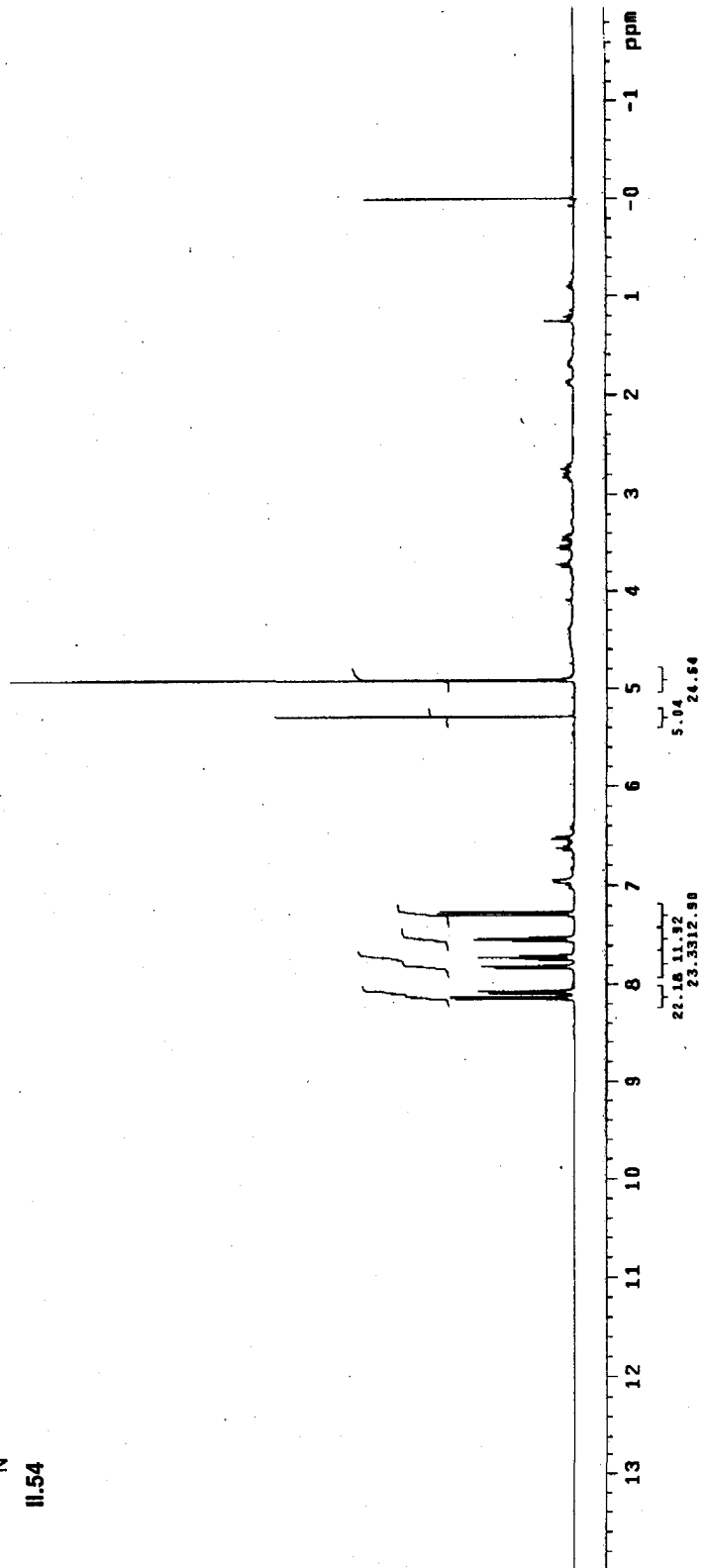
Archive directory: /export/home/kennedy/vnmrSYS/data
Sample directory: dkf46.2_02Feb2006

Pulse sequence: s2pul
Solvent: CDCl3
Ambient temperature
File: CARBON
Mercury-40005 "lylestation"

Relax. delay 1.000 sec
Pulse 45.0 degrees
Acq. time 1.003 sec
Width 25062.7 Hz
256 repetitions
OBSERVE Ch. 100.5163504 MHz
DECOUPLE H1, 339.7509888 MHz
Power 41 dB
Sensitivity ON
VALZ-16
DATA PROCESSING
Line broadening 3.0 Hz
FT size 65536
Total time 1 min, 14 sec



11.54



Archive directory: /export/home/kennedy/vmarsys/data
Sample directory: dk748_1_03feb2008

Pulse Sequence: szpu1

Solvent: CDCl3

Acq. temperature

File: PROTON

Mercury-40008 "lylestation"

Relax. delay 1.000 sec

Pulse 45.0 degrees

Acq. time 3.008 sec

Width 6583.7 Hz

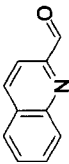
8

Observer: jms 399.7490329 MHz

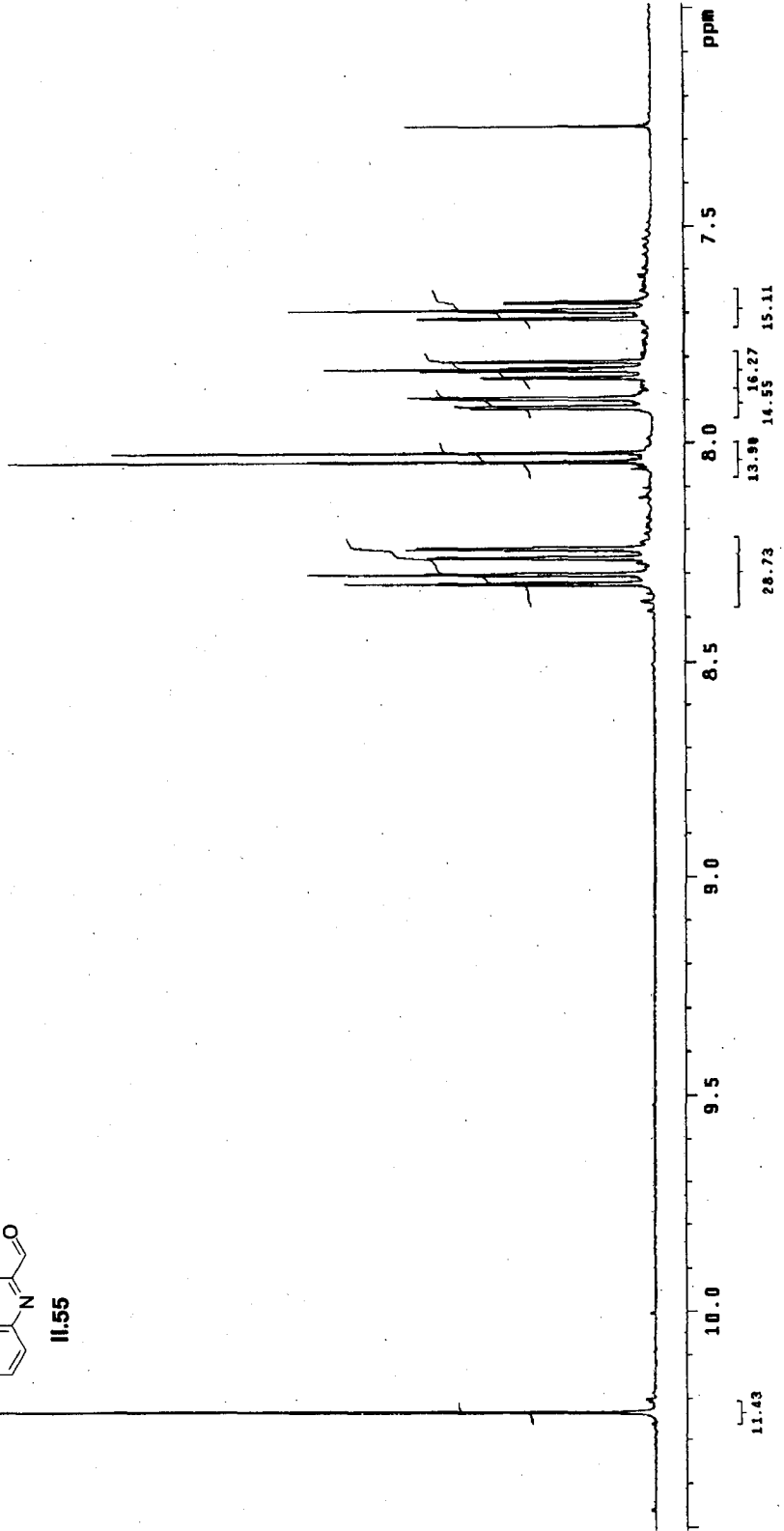
DATA PROCESSING

FT size 15436

Total time: 1 min, 1 sec

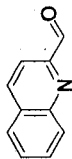


11.55

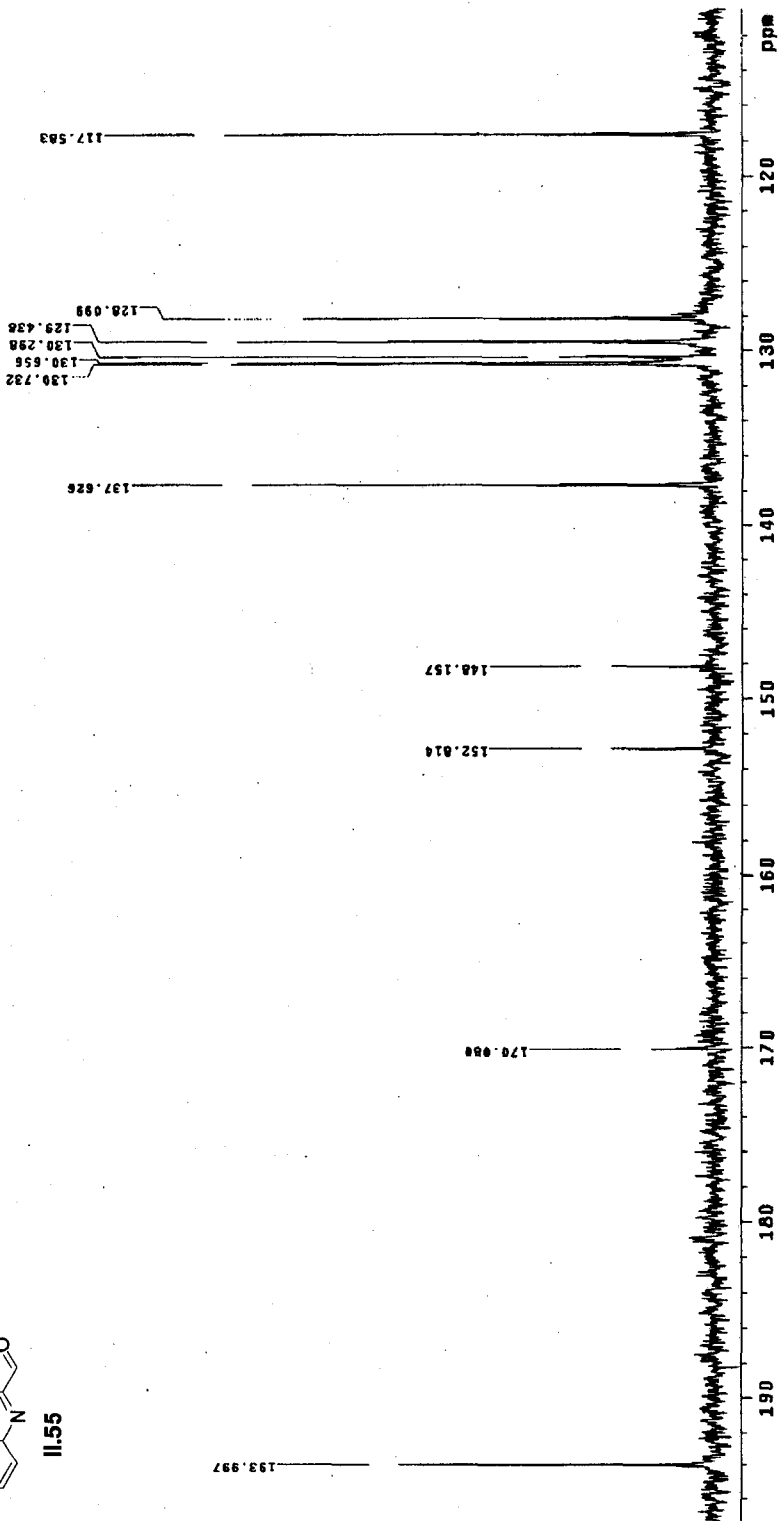


Archive directory: /export/home/kennedy/vmarsys/data
Sample directory: ekf51.2_08Feb2006

Pulse Sequence: s2pul
Solvent: CDCl3
Ambient temperature
File: PROTON
Mercury-300BB "lylestation"
Relax. delay 1.000 sec
Pulse 45.0 degrees
Acq. time 3.000 sec
Width 6385.7 Hz
SFO 300.136 MHz
QPCPCP14.ms 399.7490292 MHz
DATA PROCESSING
FT size 65536
Total time 1 min, 1 sec



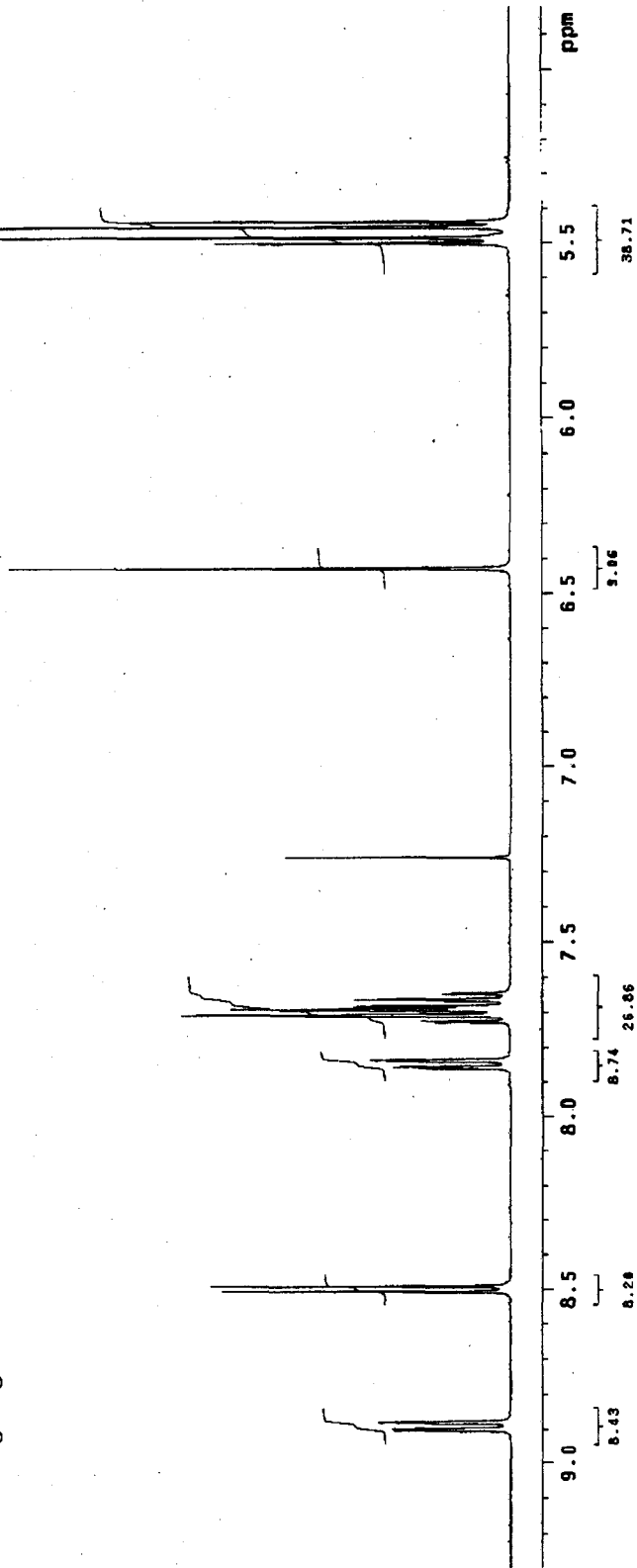
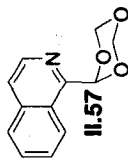
11.55



Archive directory: /export/home/kennedy/vmrsys/data
Sample directory: dkf51.3_08Feb2008

Pulse Sequence: s2pul
Solvent: CDCl3
Acquire temperature
File: CARBON "lylstaton"
Mercury-40088

Relax. delay 1.000 sec
Acq. time 4.188 sec
Acq. date 08Feb2008
Width 25862.7 Hz
256 repetitions
OBSERVE C13 100.5169504 MHz
DECUPLE H1 399.7509660 MHz
Power 41 dB
continuously on
WALTZ-16 modulated
DATA PROCESSING
Line broadening 3.0 Hz
FT size 65536
Total time 9 min, 14 sec



Archive directory: /export/home/kennedy/vnmrSYS/data

Sample directory: dk475_1_08Mar2006

Pulse Sequence: s2pu1

Solvent: CDCl3

Temp: 25.0 C / 298.1 K

File: PROTON

Mercury-40005 "lylestation"

Relax. delay 1.000 sec

Pulse 45.0 degrees

Acq. time 3.000 sec

Width 6385.7 Hz

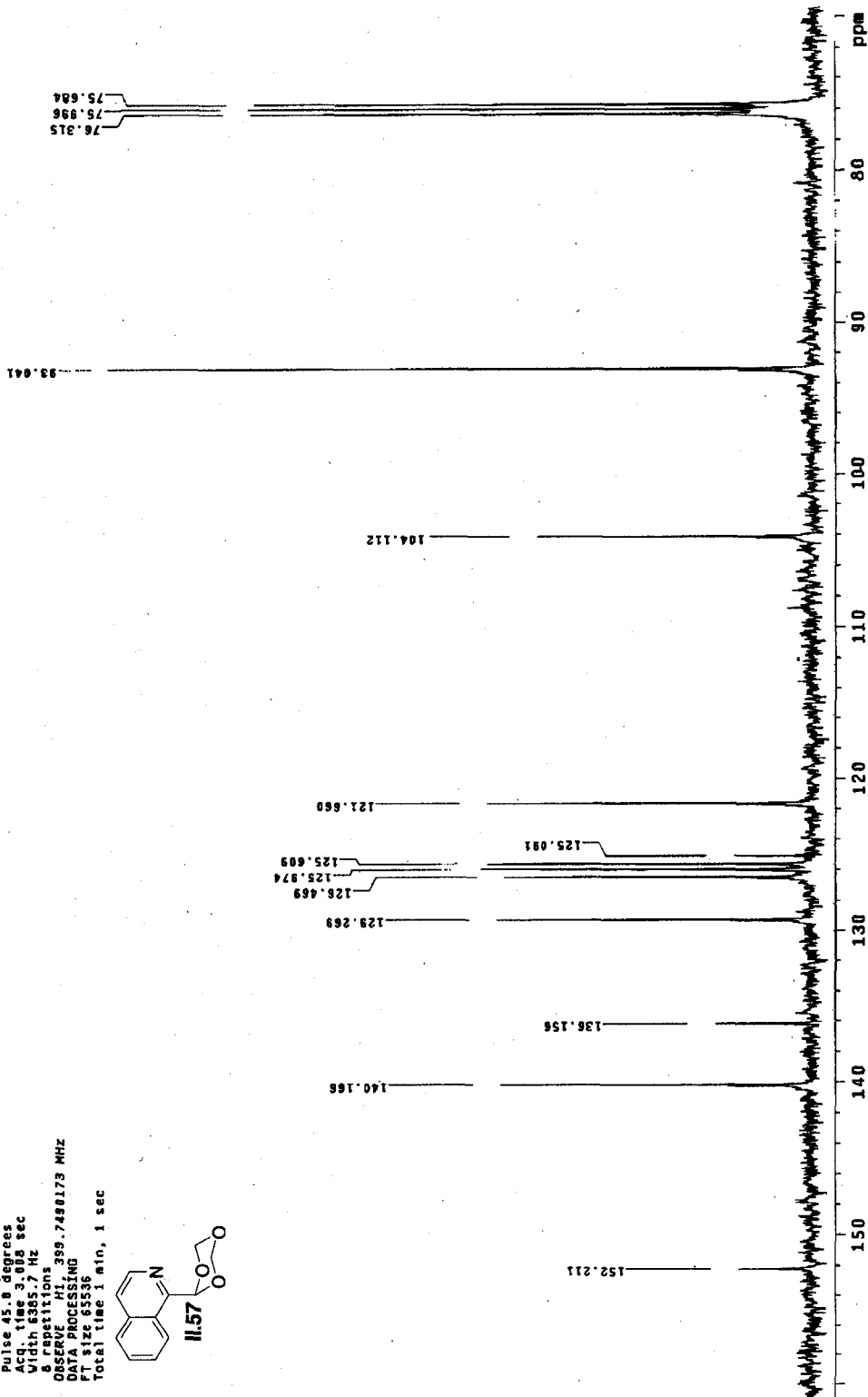
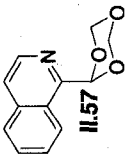
8 repetitions

OBSERVE F1: 399.7480173 MHz

DATA PROCESSING

FT size 65536

Total time 1 min, 1 sec

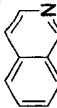


Archive directory: /export/home/kennedy/vnarsys/data
Sample directory: dkf79_1_06Mar2006

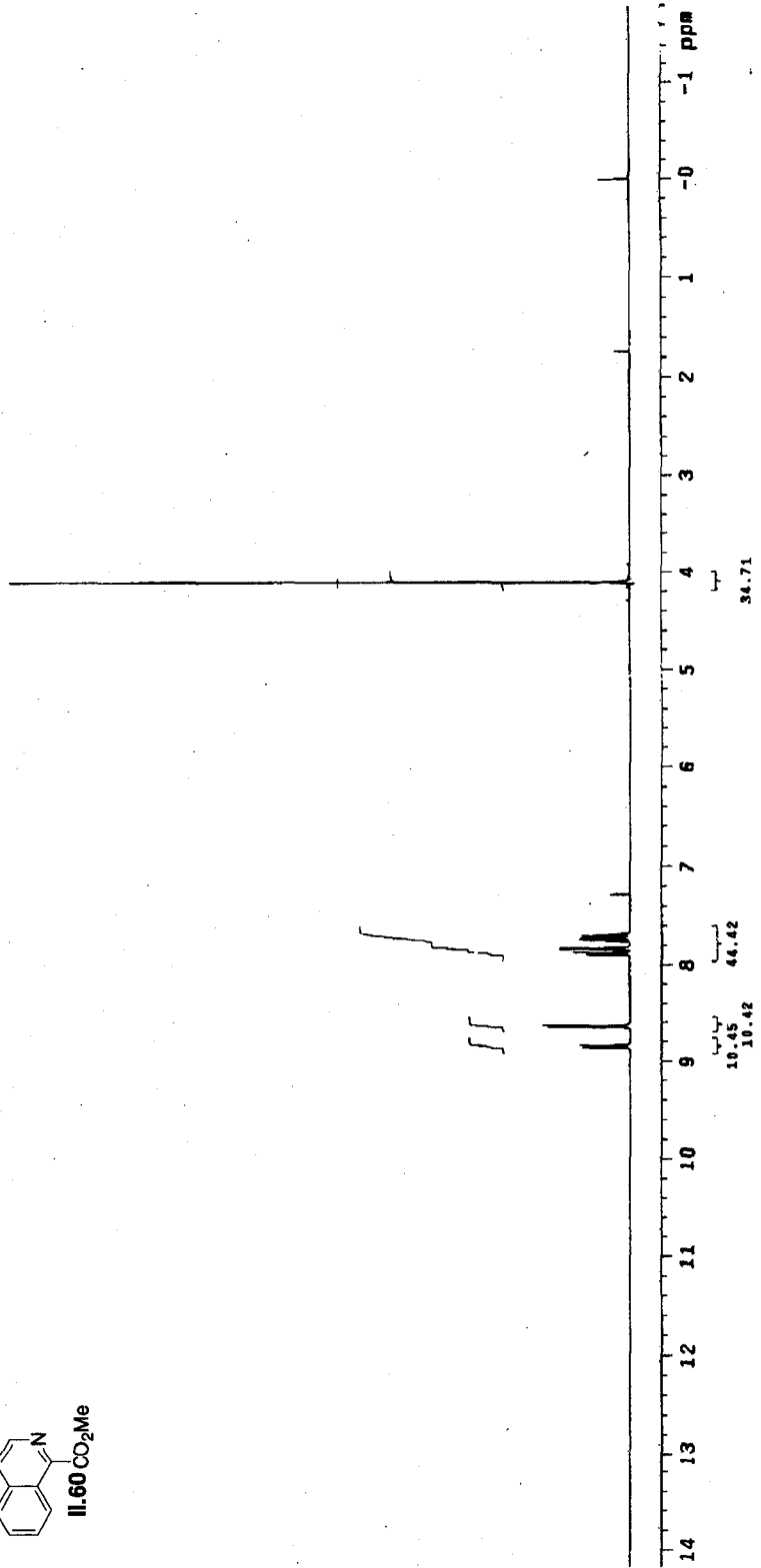
Pulse Sequence: s2pul

Solvent: CDCl3
Temp: 25.0 C / 296.1 K
File: CARBON
Mercury-400BB "lylestation"

Relax. delay 1.000 sec
Pulse 45.0 degrees
Acq. time 1.993 sec
Width 25862.7 Hz
S12 repetitions
OBSERVE CH3, 100.5170737 MHz
DECUPLE H1, 399.7509866 MHz
Power 43.85
C13 pulse delay on
VAL2=16 calculated
DATA PROCESSING
Line broadening 3.0 HZ
FT size 65536
Total time 18 min, 7 sec



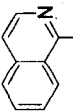
11.60 CO₂Me



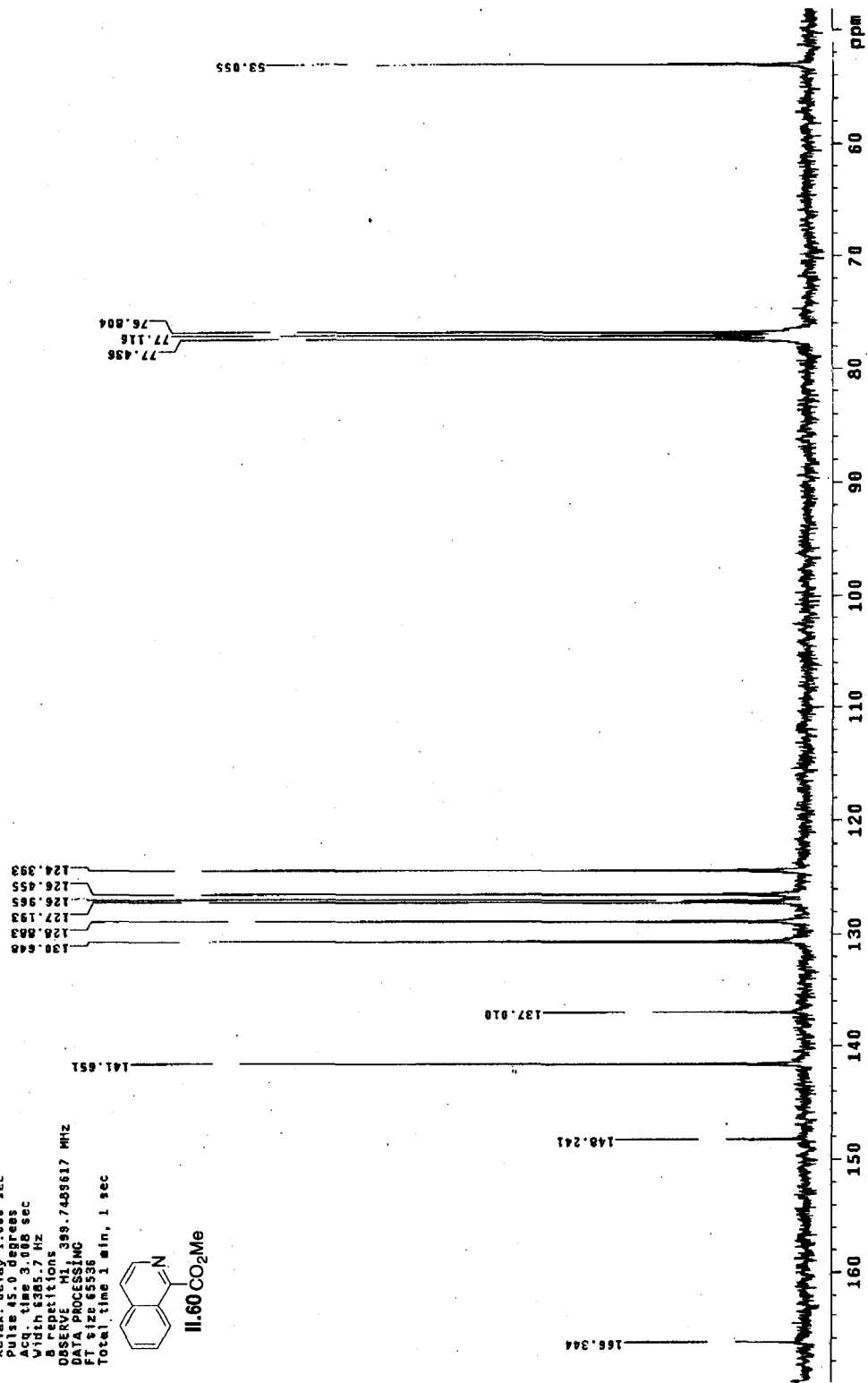
Archive directory: /export/home/kennedy/vnmrSYS/data
Sample directory: dkf81.1_03Mar2086

Pulse Sequence: s2pu1
Solvent: CDCl3
Temp: 25.0 C / 298.1 K
File: PROTON
Mercury-40088 "lytestation"

Relax. delay 1.000 sec
Pulse 45.0 degrees
Acq. time 3.000 sec
Width 385.7 Hz
Repetitions 8
DECOR 0.000000
DPC 0.000000
FT size 65536
Total time 1 min, 1 sec



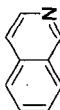
II.60 CO₂Me



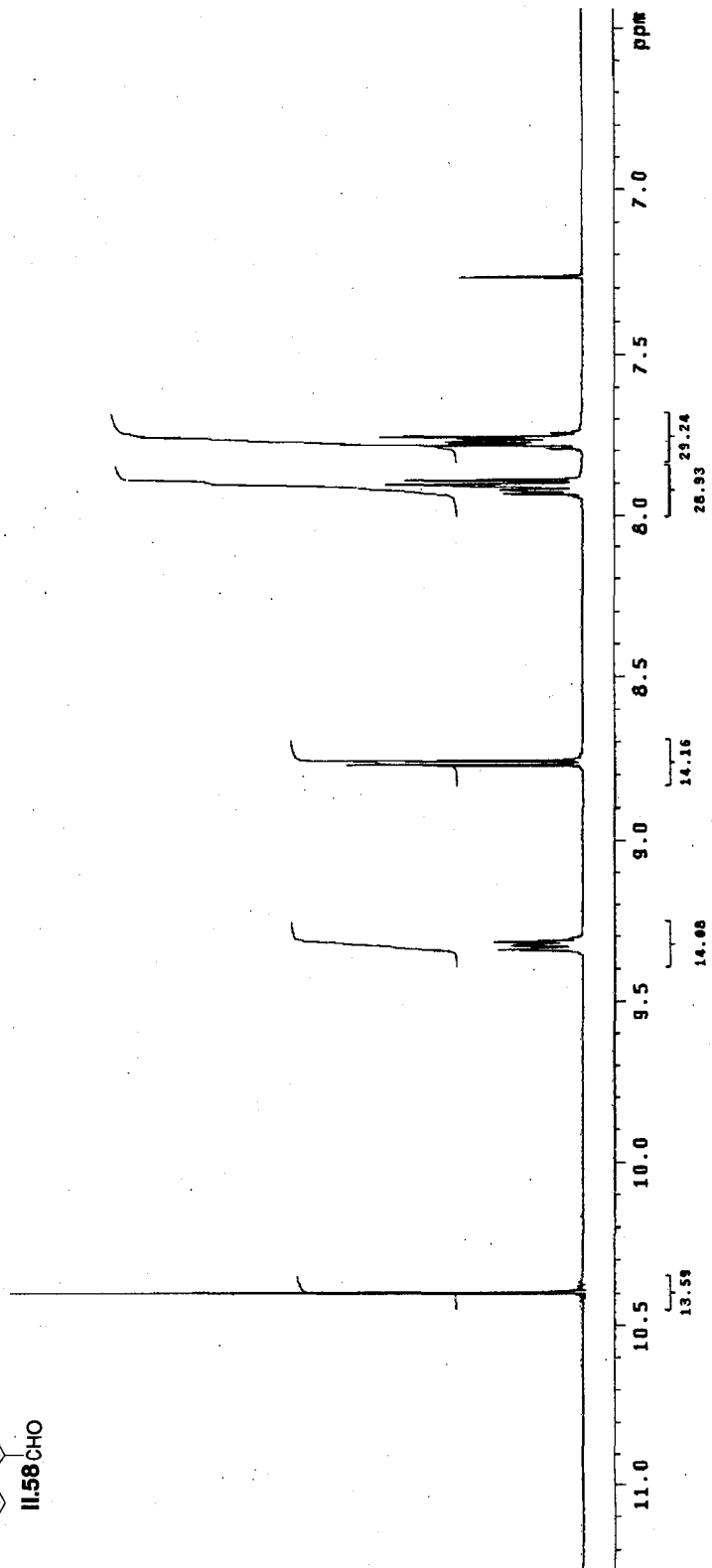
Archive directory: /export/home/kennedy/vmarsys/data
Sample directory: dkf81.2_89Mar2006

Pulse Sequence: s2pul
Solvent: CDCl3
Temp: 25.0 C / 298.1 K
File: CARBON
Mercury-4:HB5 "lytestation"

Relax. delay 1.000 sec
Pulse 45.0 degrees
Acq. Time 1.000 sec
Width 25002.7 Hz
Observed Splittings
ORSEPR C13, 5168804 MHz
DECOUPLE C11, 399.750000 MHz
Power 41 dB,
continuously on
WALTZ-16 modulated
DATA PROCESSING
Line broadening 3.0 Hz
FT size 65536
Total time 18 min, 7 sec



11.58 CHO

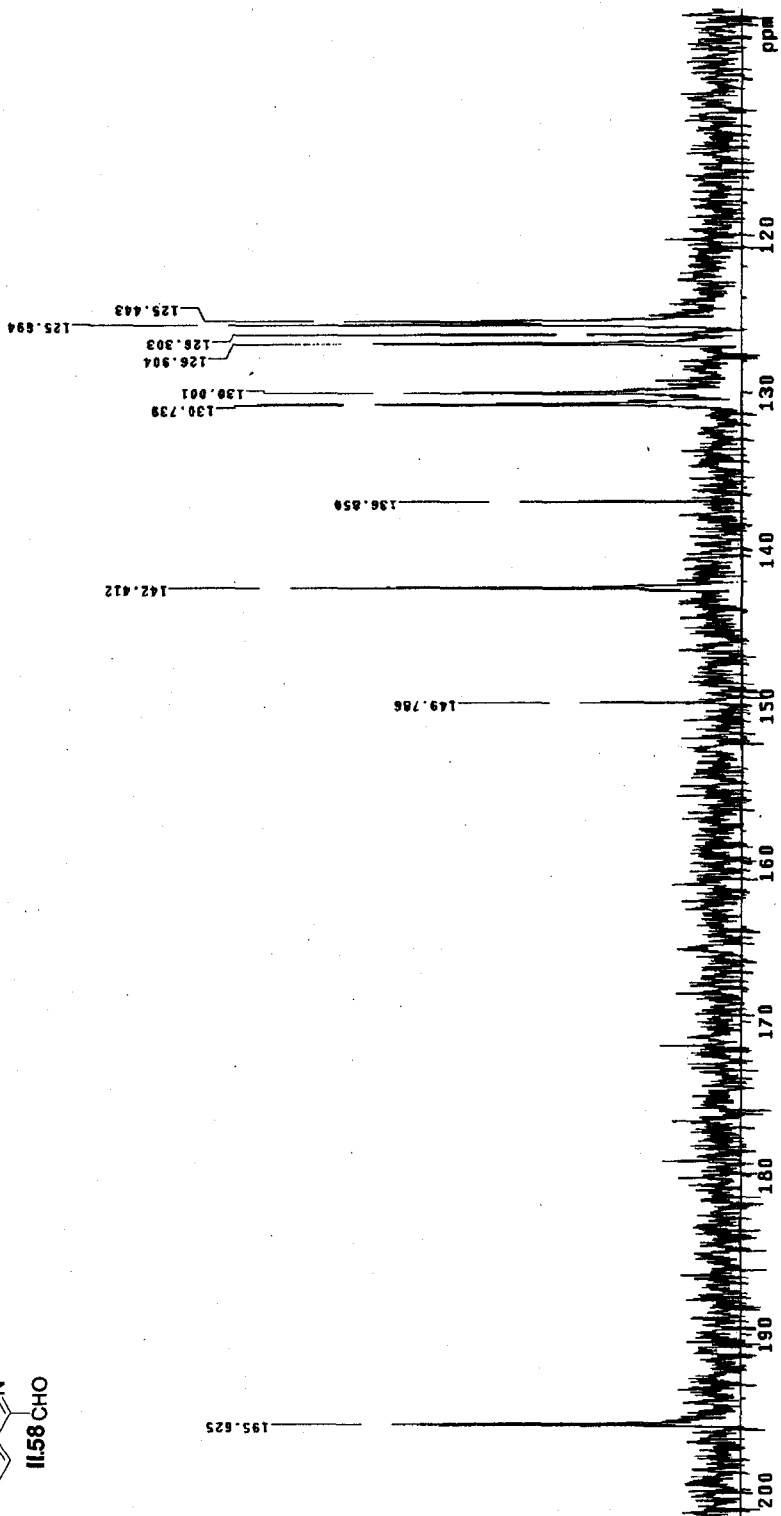
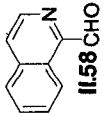


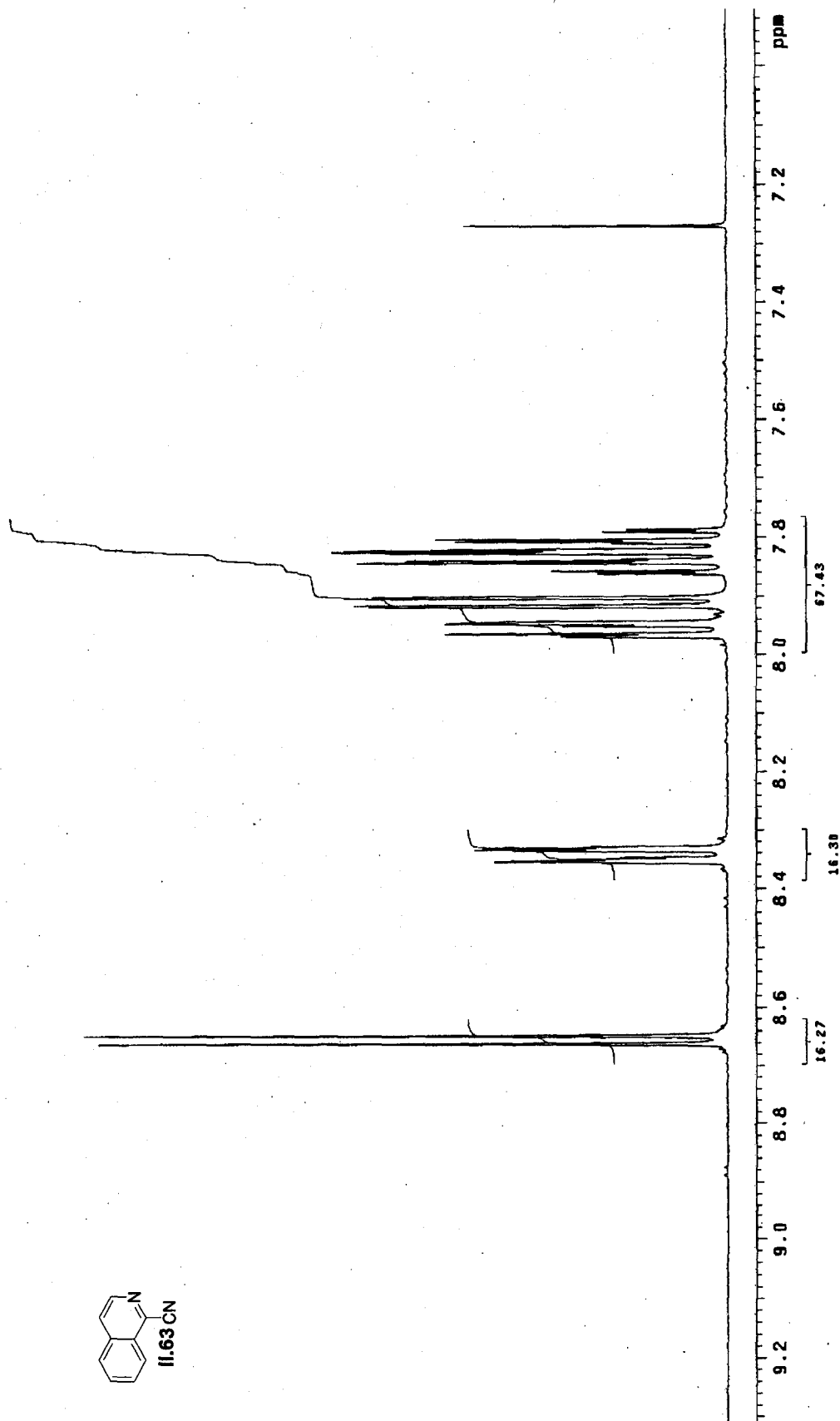
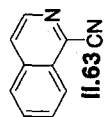
Archive directory: /export/home/kennedy/vmrSYS/data
Sample directory: dk783_1_18Mar2006

Pulse Sequence: s2pul

Solvent: CDCl3
Ambient temperature
File: PRONON
Mercury-40000 "lytestation"

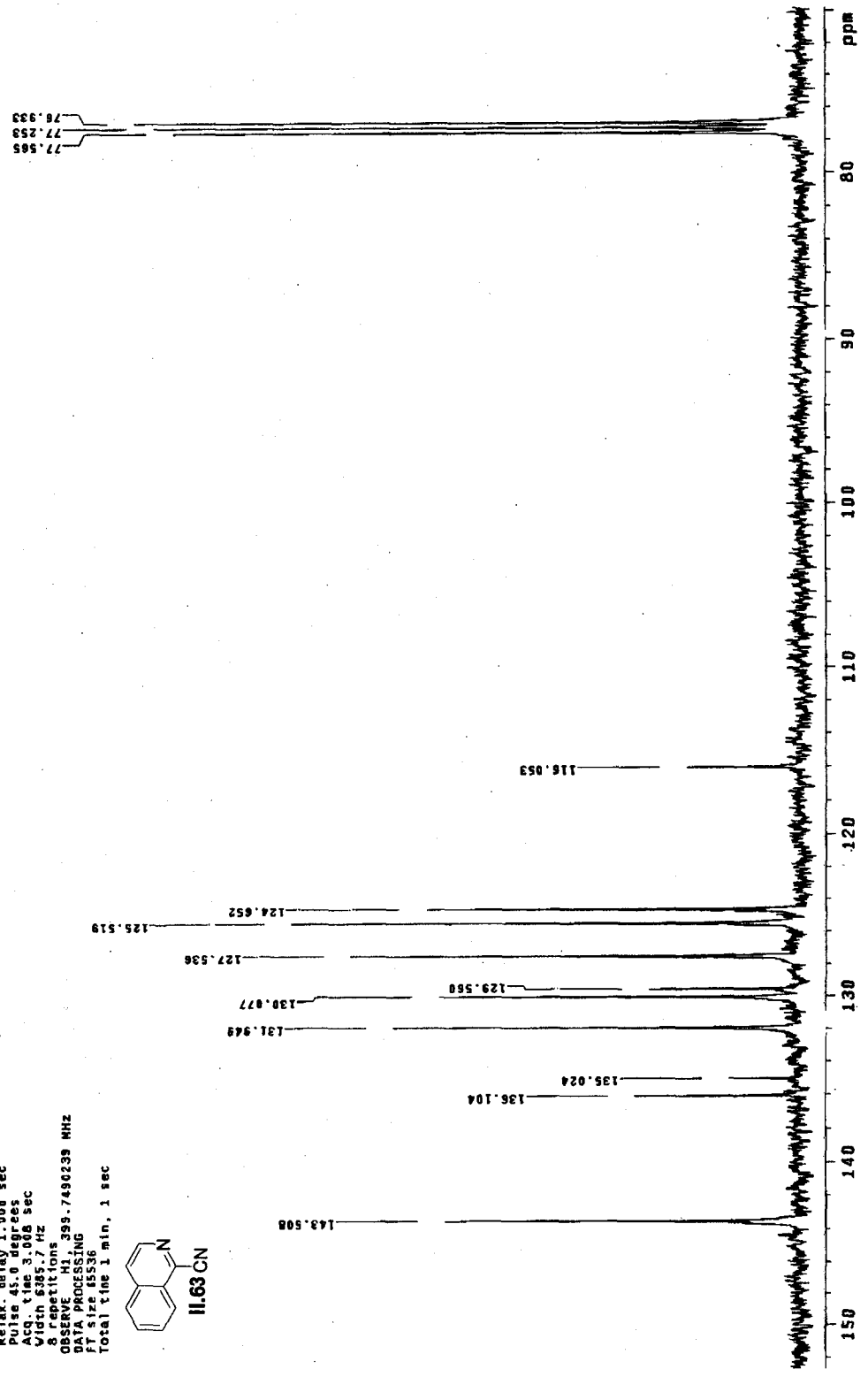
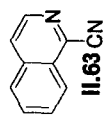
Relax. delay 1.000 sec
Pulse 45.8 degrees
Urch 1.000 sec
Urch 1.000 sec
Urch 1.000 sec
A 1.000 sec
OBSERVE HD 399.748235 MHZ
DATA PROCESSING
FT size 65536
Total time 1 min, 1 sec





Archive directory: /export/home/kennedy/vnmrsws/data
Sample directory: dkf9211_1_21Mar2006

Pulse Sequence: s2pul
Solvent: CDCl3
Temp: 25.0 C / 298.1 K
File: PROTON
Mercury-40000 "lylestation"
Relax. delay 1.000 sec
Pulse 45.0 degrees
Acq. time 3.000 sec
Width 6385.7 Hz
8 repetitions
OBSERVE: H1, 299.7490239 MHz
DATA PROCESSING
File: dkf9211_1_21Mar2006
Total time 1 min, 1 sec

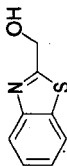


Archive directory: /sxnmt/home/kennedy/vnarsys/data
Sample directory: dk9311_2_21Mar2006

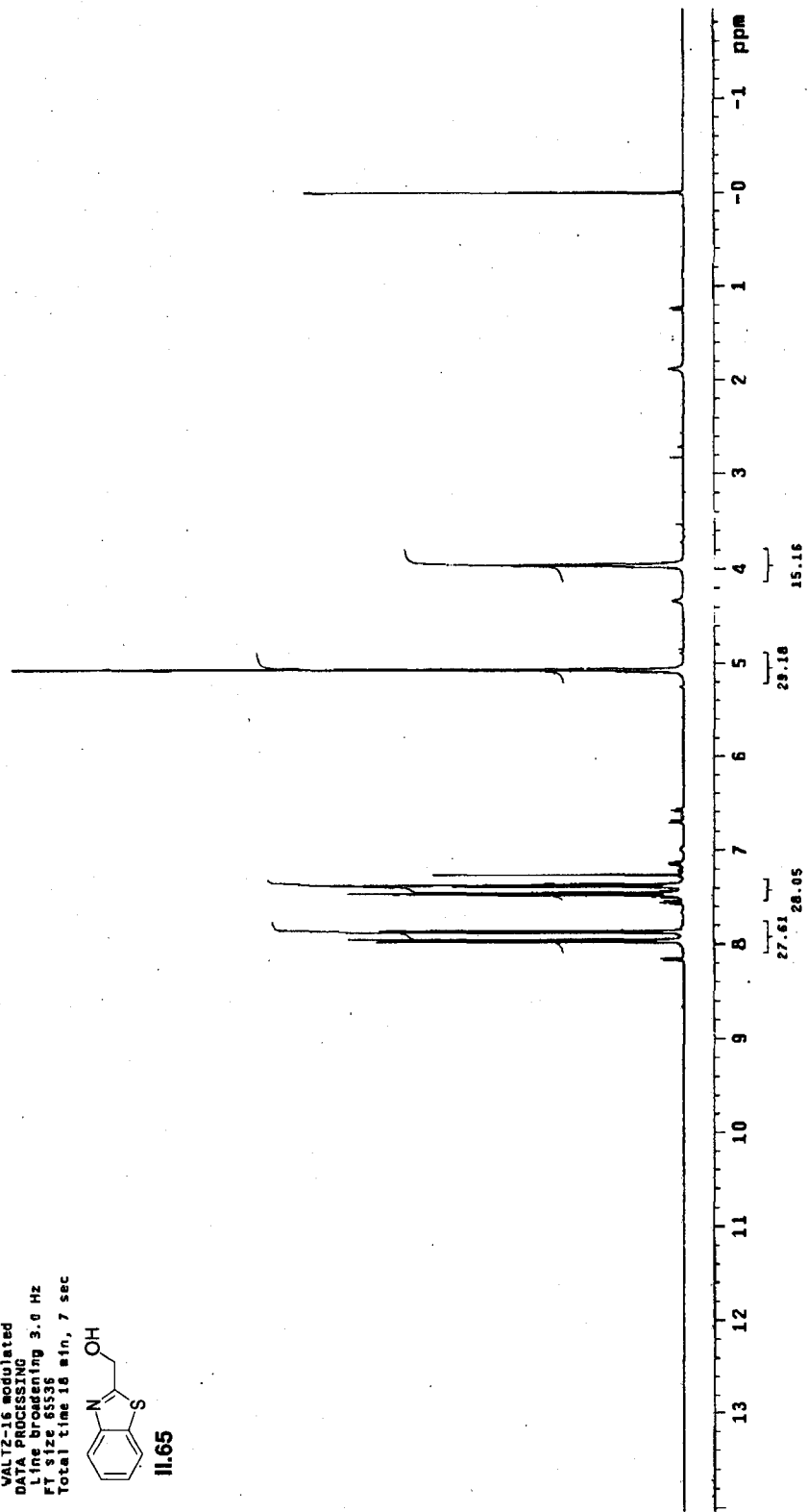
Pulse Sequence: s2pul

Solvent: CDCl3
Temp: 65.00 C / 298.1 K
F1: 65.00 MHz
Mercury-40088 "lytestation"

Relax. delay 1.000 sec
Pulse 15.0 degrees
Acq. time 1.00 sec
Width 2562.7 Hz
S12 repetitions
OBSERVE C13, 100.518584 MHz
DECUPLE H1, 399.750888 MHz
Power 41 dB
continuously on
VALTZ-16 modulated
DATA PROCESSING
Line broadening 3.0 Hz
FT size 65536
Total time 18 min, 7 sec



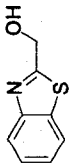
11.65



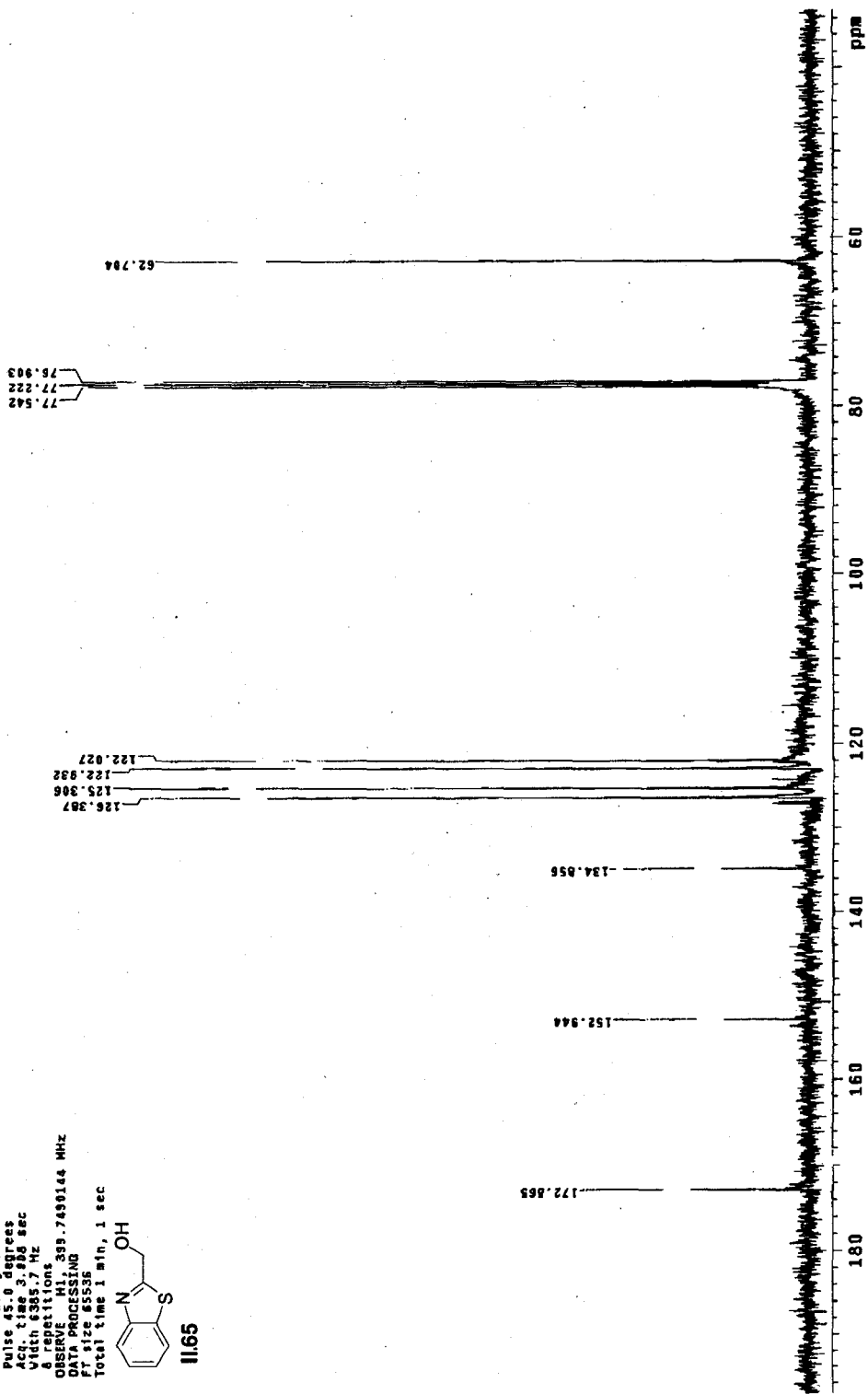
Archive directory: /export/home/kennedy/nmrsvy/data
Sample directory: dk813_1_6Apr2008

Pulse Sequence: szpul
Solvent: CDCl3
Ambient temperature
File: PROTON "lylestation"
Mercury-400BB

Relax. delay 1.000 sec
Pulse 45.0 degrees
Acq. time 3.000 sec
Width 6385.7 Hz
6 repetitions
OBSERVE F1 399.7490144 MHz
DATA PROCESSING
F1 size 65536
Total time 1 min, 1 sec



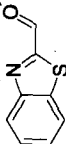
11.65



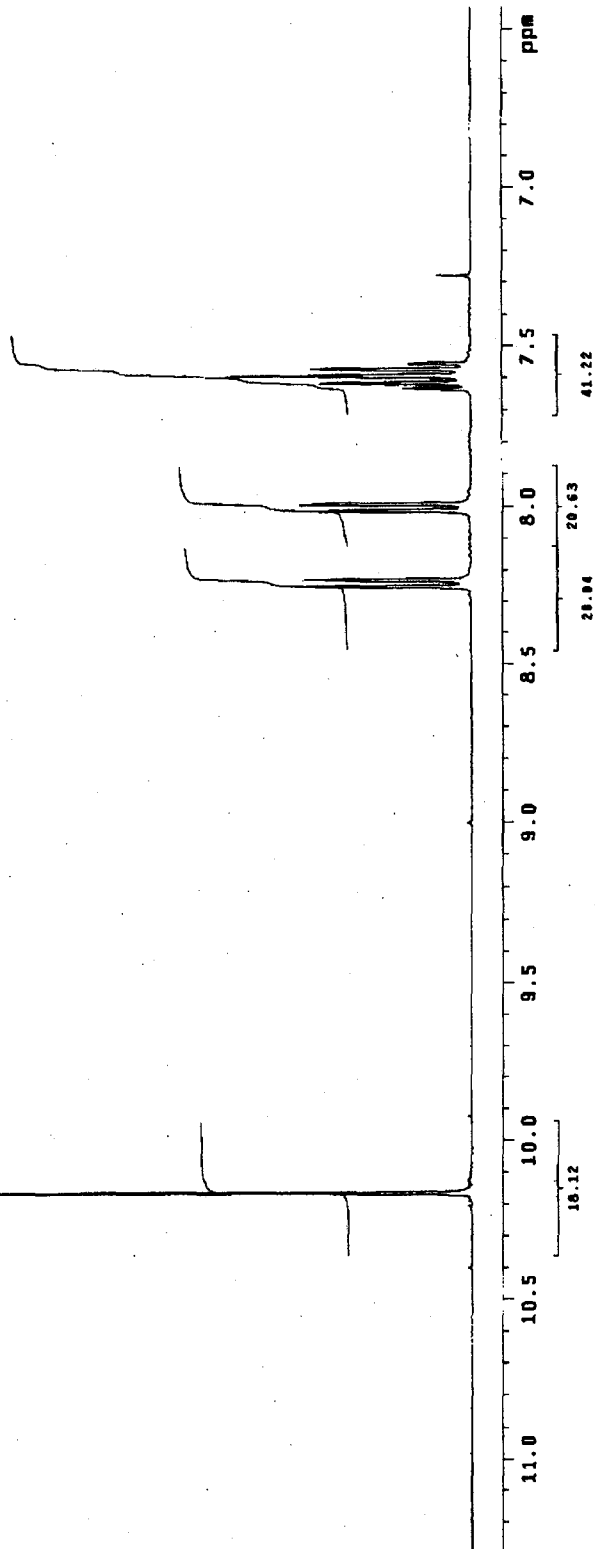
Archive directory: /export/home/kennedy/vmarsys/data
Sample directory: dfg13.2_86Apr2006

Pulse Sequence: s2pu1
Solvent: CDCl3
Ambient temperature
File: CARBON
Mercury-40000 "1ylestation"

Relax. delay 1.000 sec
Pulse 45.0 degrees
Acq. time 1.000 sec
Width 25062.7 Hz
512 repetitions
OBSERVE C13, 100.6189504 MHz
DECOUPLE H1, 399.7509866 MHz
Power 41 dB
continuously on
WALTZ16 is modulated
J Modulation
File: R002321WD
Line: 100.6189504 MHz
FT size 65536
Total time 16 min. 7 sec



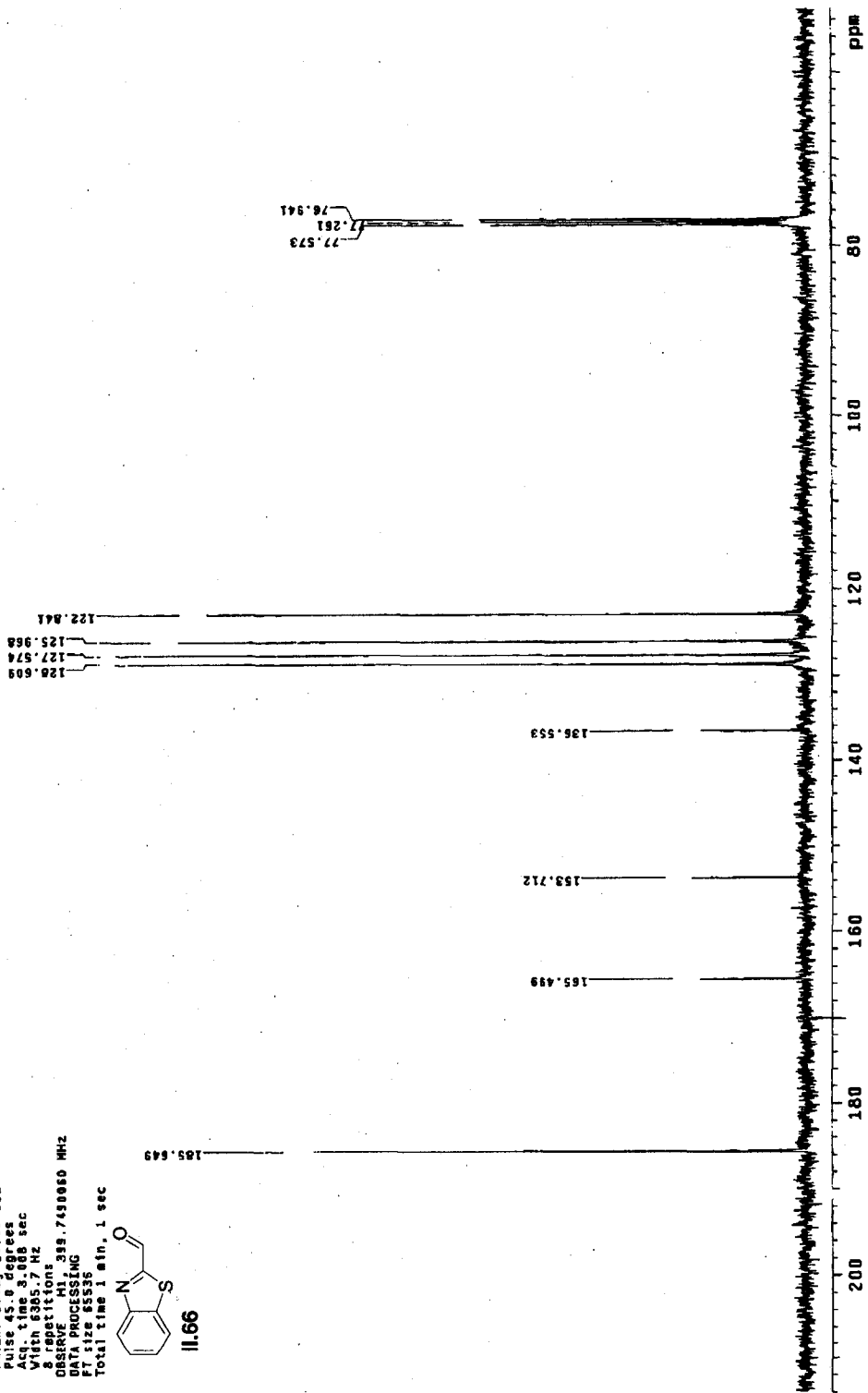
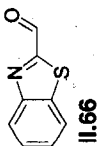
11.66



Archive directory: /export/home/kennedy/vmrcsys/data
Sample directory: dk915.1_06Apr2006

Pulse Sequence: s2pul
Solvent: CCl3
Ambient temperature
File: PROTON
Mercury-40000 "lylestation"

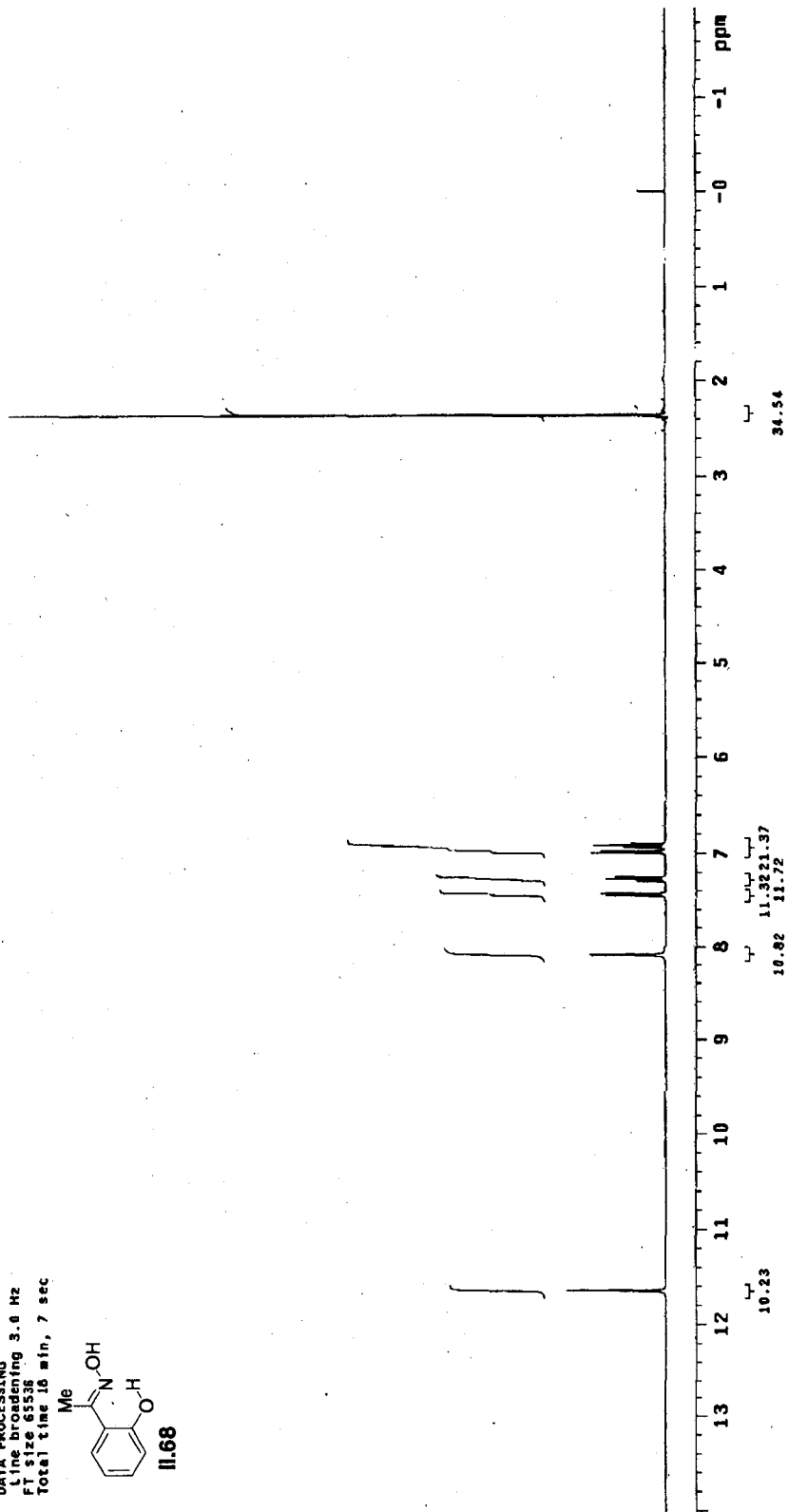
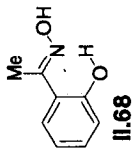
Relax. delay 1.000 sec
Pulse 45.0 degrees
Acq. time 3.000 sec
Width 6305.7 Hz
repetitions 333.7430060 MHz
DATE_ ACQUISITION
PT size 65535
Total time 1 min. 1 sec



Archive directory: /export/home/kennedy/vnmr/sys/data
Sample directory: dkg15_2_86Apr2806

Pulse Sequence: szpu1
Solvent: CDCl3
Ambient temperature
File: CARBON
Mercury-40088 "lytestation"

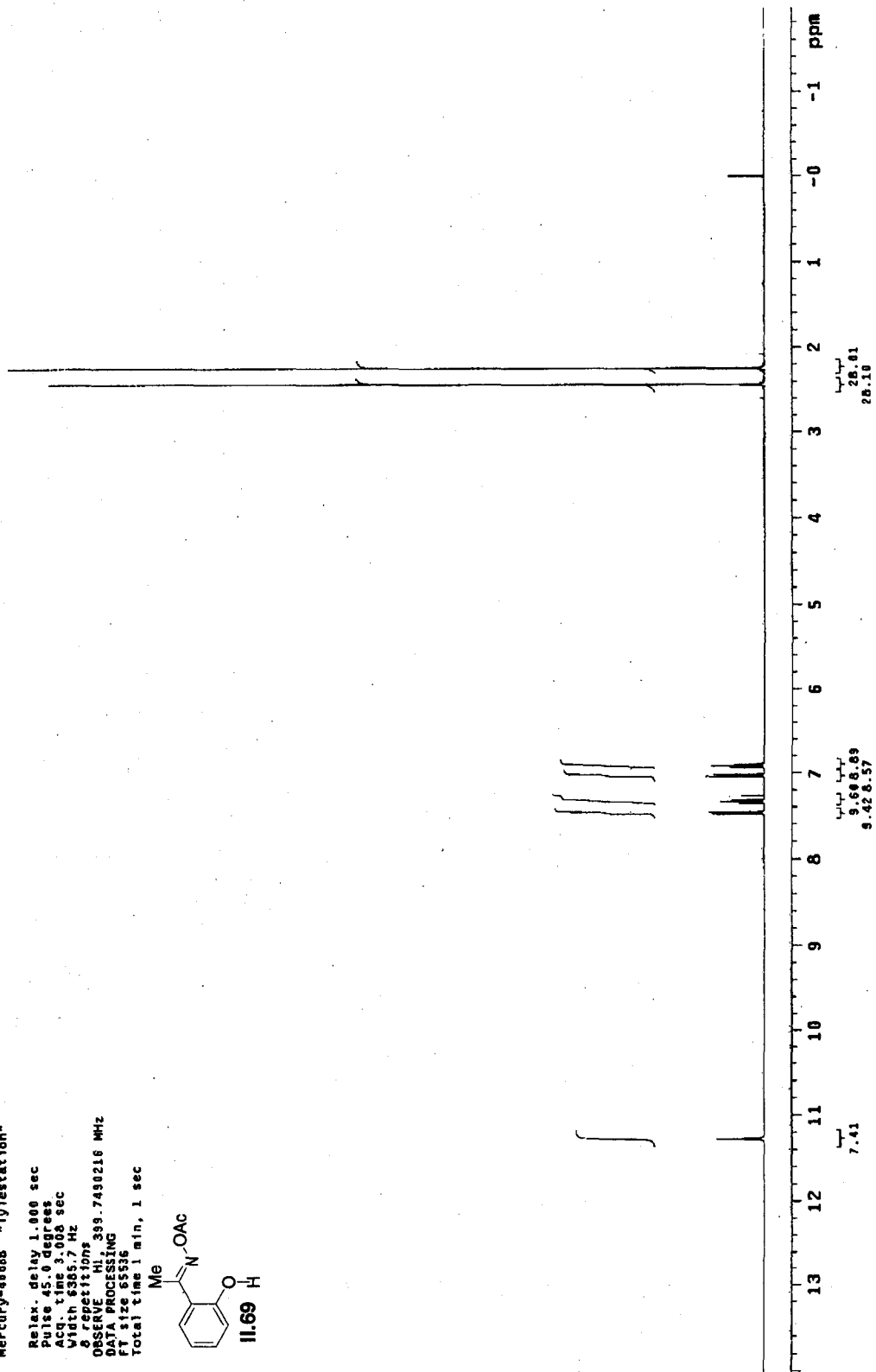
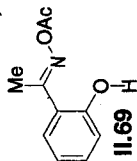
Relax. delay 1.000 sec
Pulse 45.0 degrees
Acq. time 1.603 sec
Width 25862.7 Hz
192 repetitions
OBSERVE C13, 100.519564 MHz
DECOUPLE H1, 399.759566 MHz
Power 42.0 dB
Sensitivity on
VMT-16 modulated
DATA PROCESSING
Line broadening 3.0 Hz
FT size 65536
Total time 18 min, 7 sec



Archive directory: /export/home/kennedy/vmarsys/data
Sample directory: dk919_1_11Apr2006

Pulse sequence: s2put
Solvent: CMC13
Ambient temperature
File: PROTON
Mercury-40006 "lytestation"

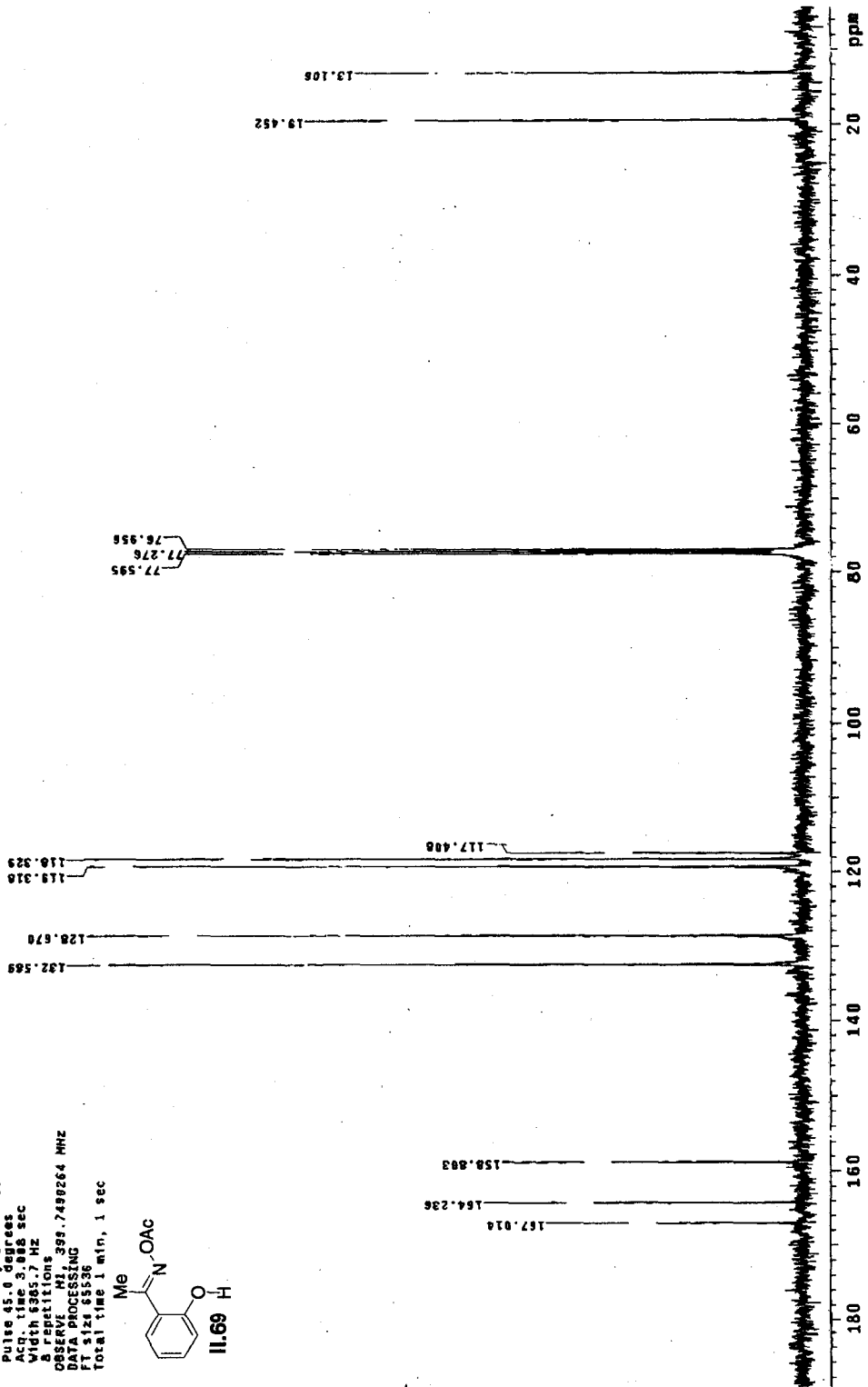
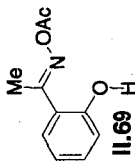
Relax. delay 1.000 sec
Pulse 15.0 degrees
Width 536.7 Hz
A repetition
OBSERVE HI 399.7490216 MHz
DATA PROCESSING
FT size 65536
Total time 1 min, 1 sec



Archive directory: /export/home/kennedy/vnmr-ssys/data
Sample directory: dk921.1_12Apr2086

Pulse Sequence: s2pul
Solvent: CDCl3
Ambient temperature
File: MCOB8
Mercury-400WB "ylestation"

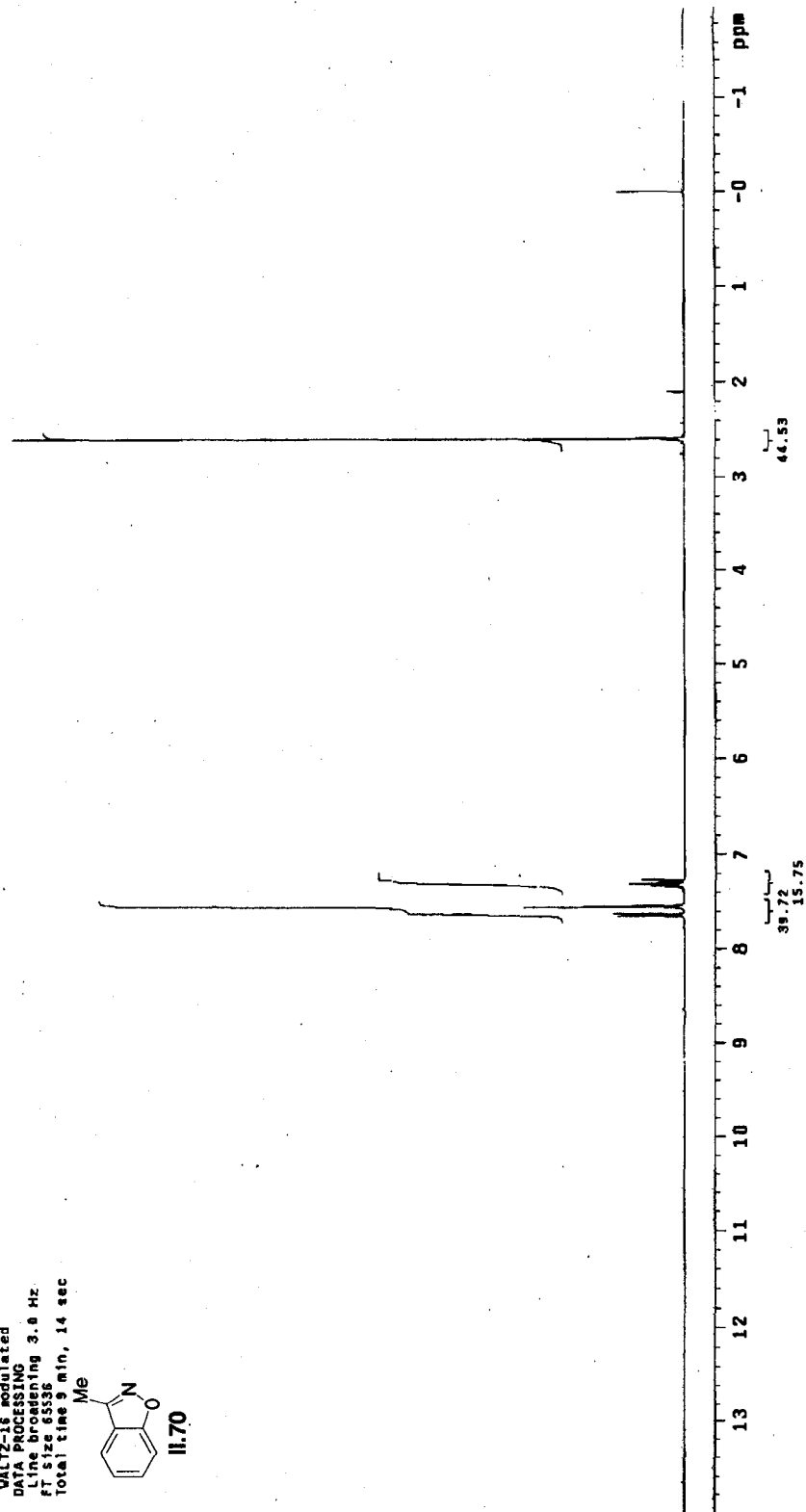
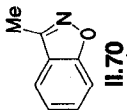
Relax delay 1.000 sec
Acq 45.4 degrees
Width 6985.7 Hz
S F 800.136 MHz
S F 200.136 MHz
S F 100.628 MHz
OBSERVE M1 399.7490264 MHz
DATA PROCESSING
FT size 65536
Total time 1 min, 1 sec



Archive directory: /export/home/kennedy/vmarsys/data
Sample directory: dkg21.2_12Apr2008

Pulse Sequence: s2pul
Solvent: CDCl3
Acquire temperature
File: CARBON
Mercury-4000B "1ylestation"

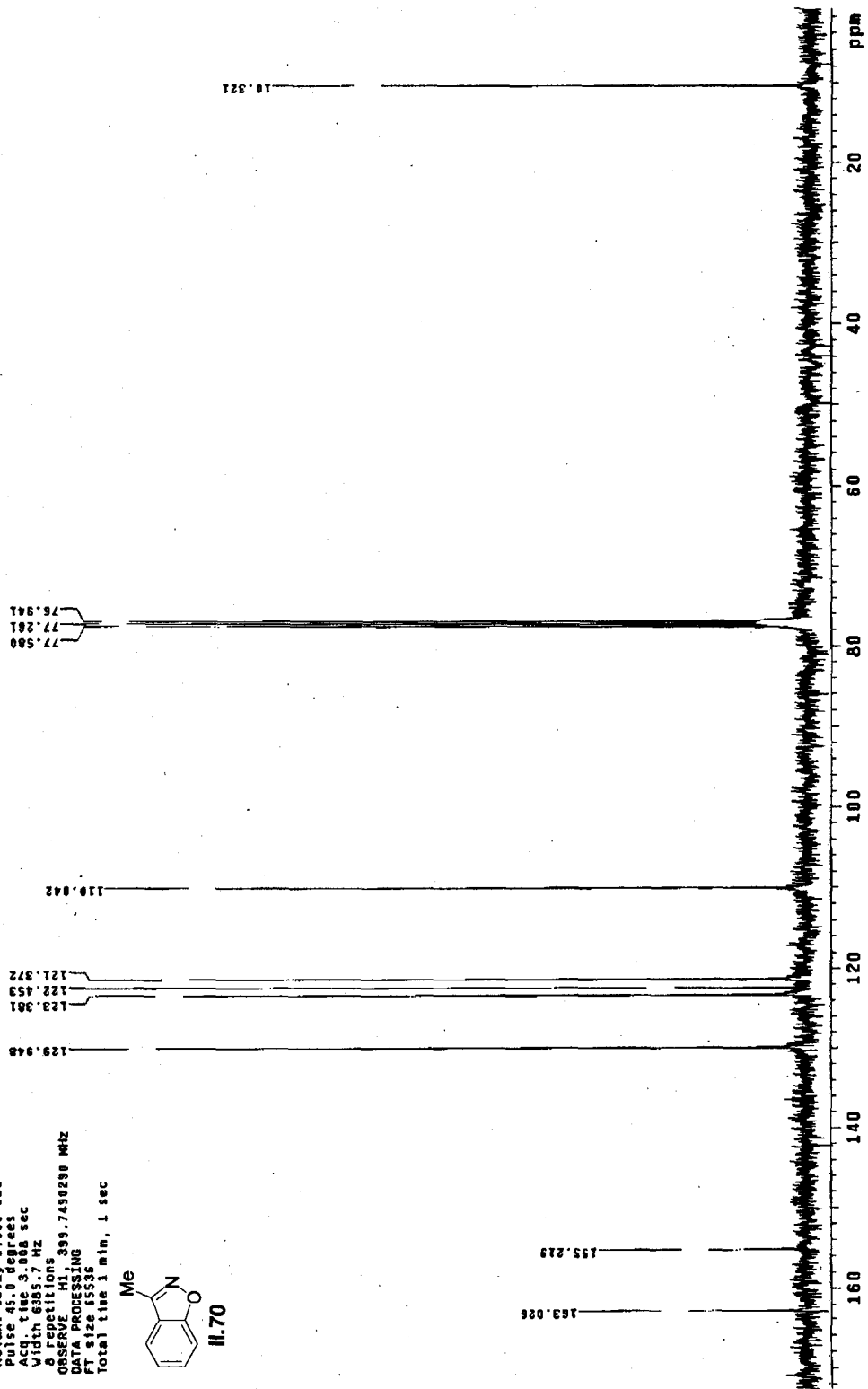
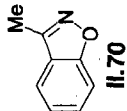
Relax. delay 1.000 sec
Pulse 45.0 degrees
Acq. time 1.083 sec
Width 25062.7 Hz
256 repetitions
OBSERVE C13, 100.5169504 MHz
DECOUPLE H1, 399.7509888 MHz
Power 41 dB
continuously on
WALTZ-16 modulated
DATA PROCESSING
Line broadening 3.0 Hz
F2 size 65536
Total time 9 min, 14 sec



Archive directory: /export/home/kennedy/vmarsys/data
Sample directory: dkg22_1_13Apr2006

Pulse Sequence: s2pu1
Solvent: CDCl3
Ambient temperature
File: PROTON
Mercury-40888 "lylestation"

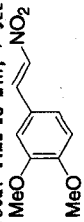
Relax. delay 1.008 sec
Pulse 45.0 degrees
Acq. time 3.008 sec
Width 6305.7 Hz
8 repetitions
OBSERVE H1, 399.7430290 MHz
DATA PROCESSING
FT size 65536
Total time 1 min, 1 sec



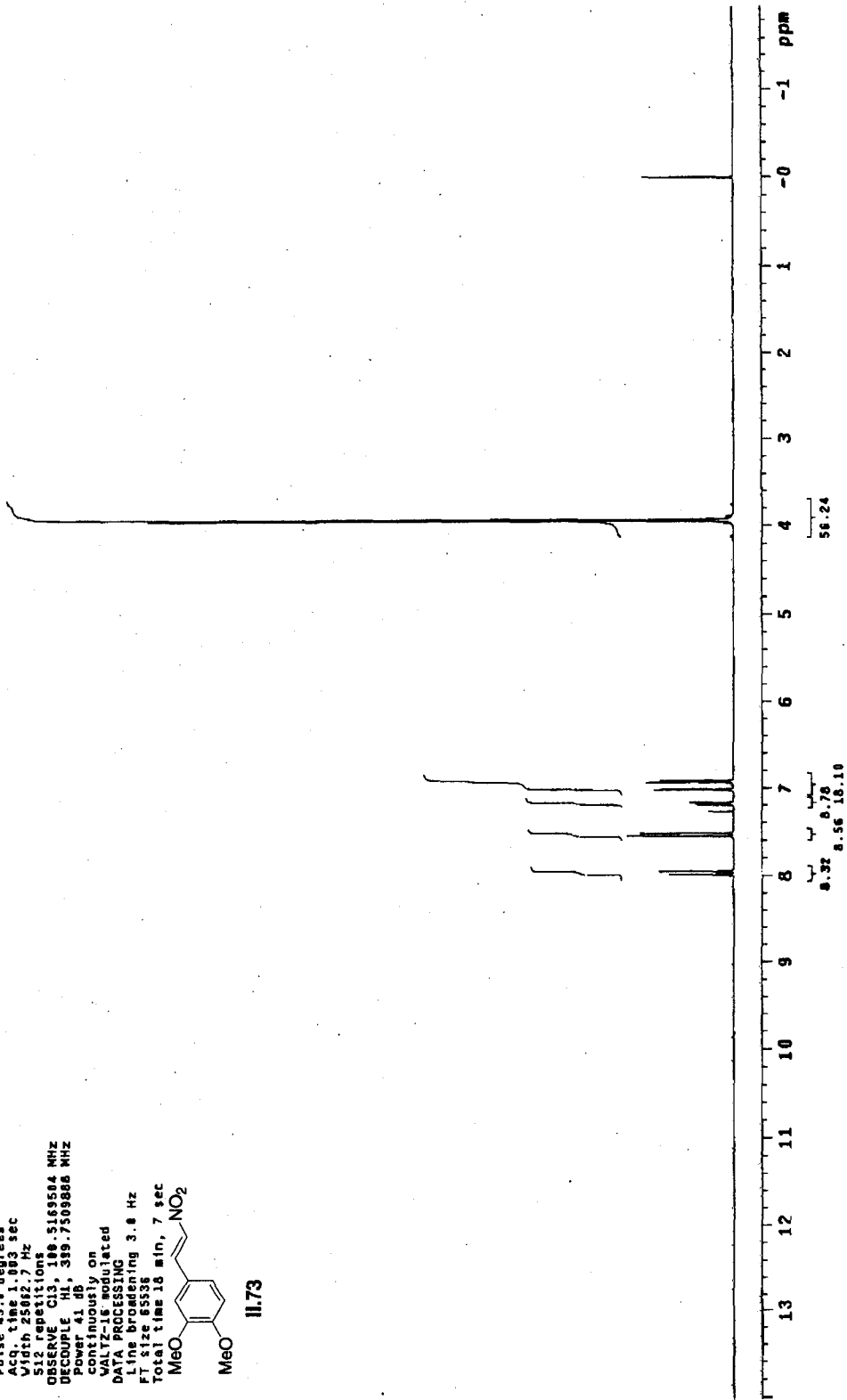
Archive directory: /export/home/kennedy/vnmrSYS/data
Sample directory: dk922.2_13Apr2006

Pulse Sequence: s2pul
Solvent: CDCl3
Ambient temperature
File: CARBON
Mercury-4006 "lylestation"

Relax. delay 1.000 sec
Pulse 45.0 degrees
Acq. time 1.003 sec
Width 25002.7 Hz
Siz repetitions
OBSERVE C13, 100.5169504 MHz
DECOUPLE H1, 399.7509806 MHz
Coupling on
WALTZ-16 modulated
DATA PROCESSING
Line broadening 3.0 Hz
FT size 65536
Total time 18 min, 7 sec



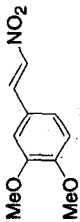
11.73



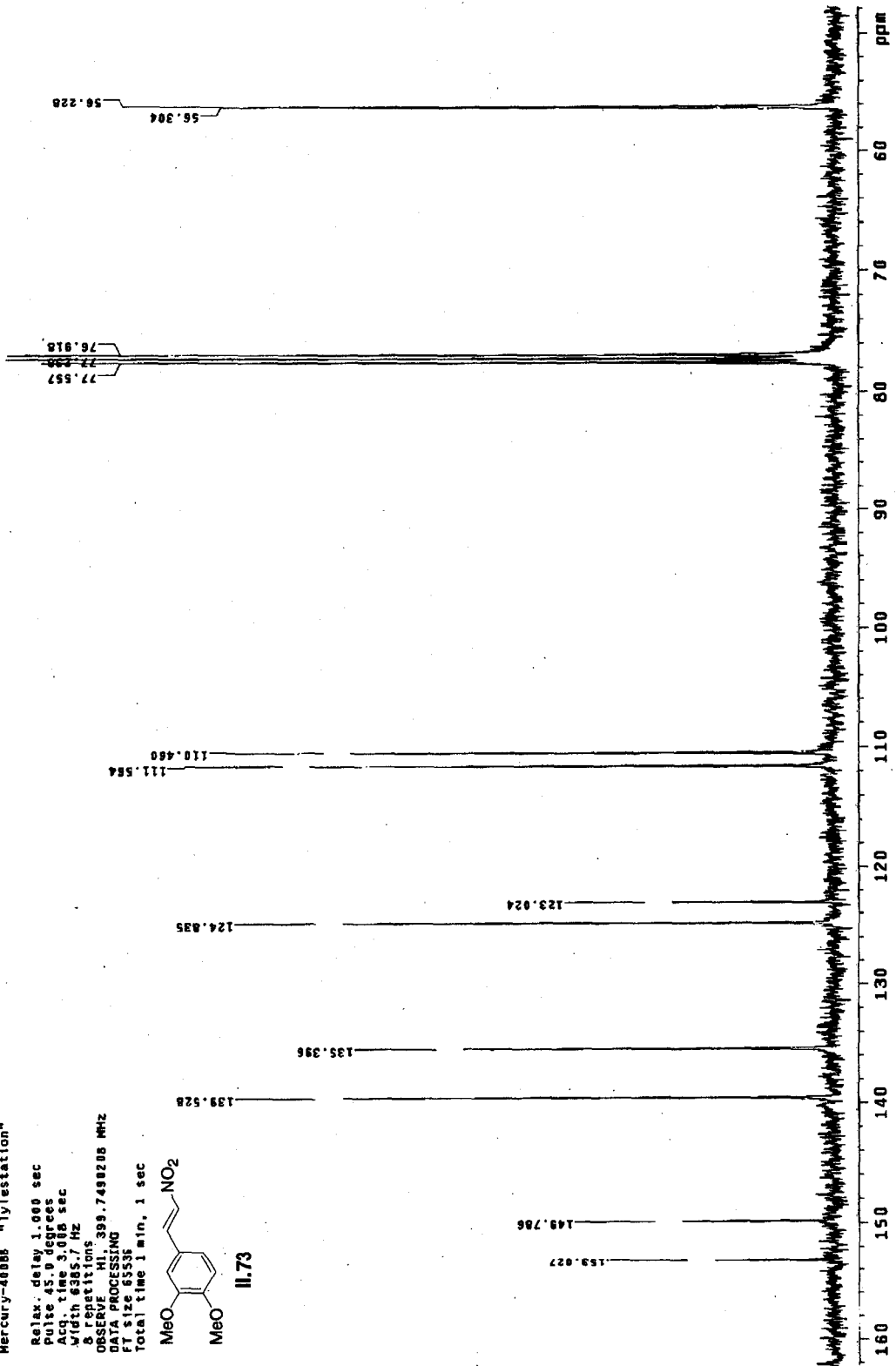
Archive directory: /export/home/kennedy/vnarsys/data
Sample directory: dkht3.1_12Nov2006

Pulse Sequence: szpu1
Solvent: CDCl3
Temp: 25.0 C / 298.1 K
File: PROTON
Mercury-40000 "1ylestation"

Relax. delay 1.000 sec
Acq. time 3.000 sec
Acq. file 3.000 sec
Width 6385.7 Hz
& Resolutions
OBSERVE HI 399.7498208 MHz
DATA PROCESSING
FT size 65536
Total time 1 min, 1 sec



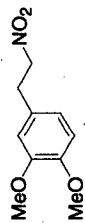
11.73



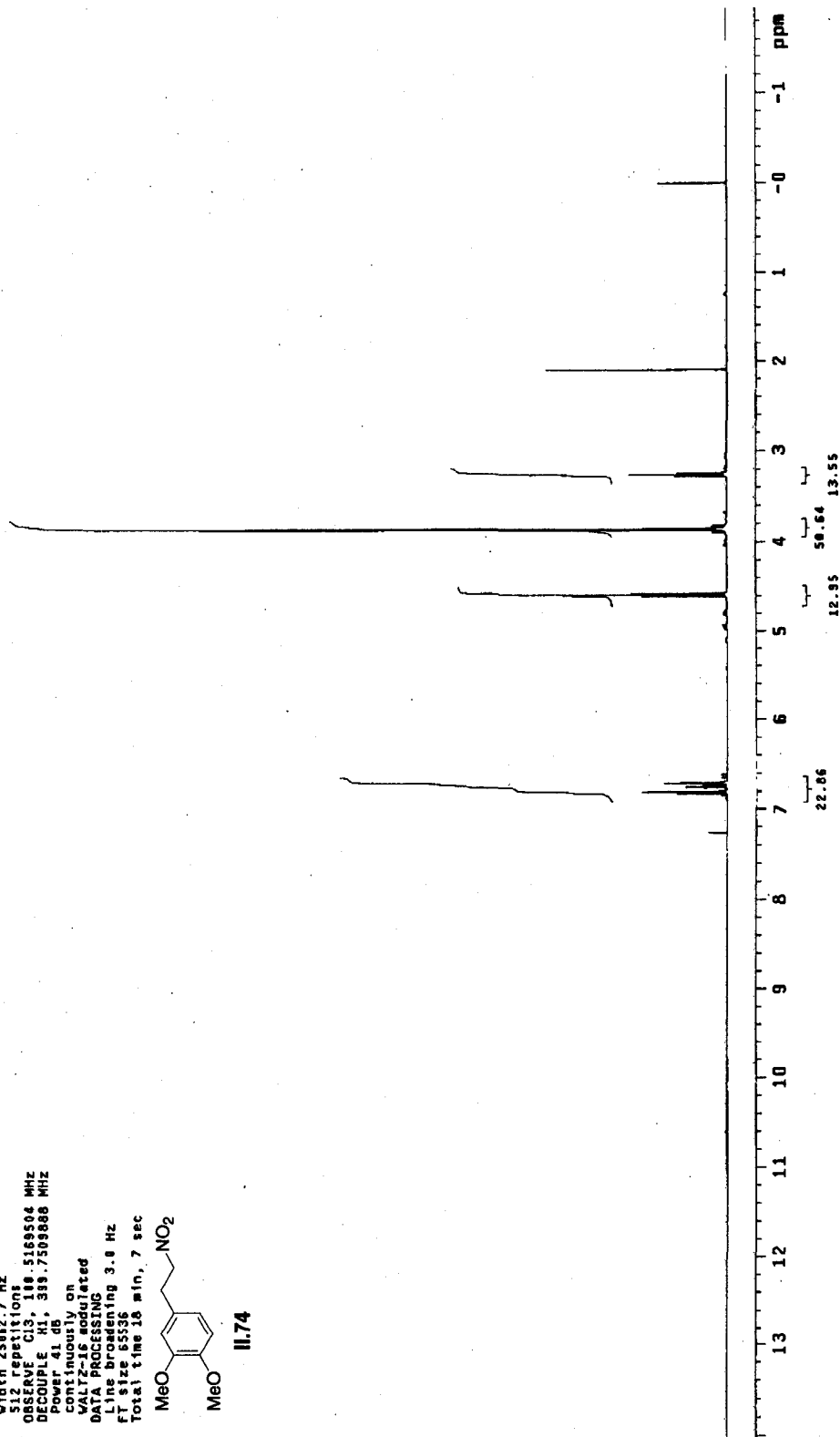
Archive directory: /export/home/kennedy/vnarsys/data
Sample directory: dkh73.5_12Nov2066

Pulse Sequence: s2pu1
Solvent: CDCl3
Temp: 25.1 C / 296.1 K
File: CARBON
Mercury-40985 "jylestation"

Relax. delay 1.000 sec
Pulse 45.0 degrees
Acq. time 1.903 sec
Width 25042.7 Hz
Siz 1024
Siz repetition 1
DECUPLE C13, 399.5169564 MHz
Power 41 dB
continuity on
WALTZ-16 modulated
DATA PROCESSING
Line broadening 3.0 Hz
FT size 65536
Total time 18 min, 7 sec



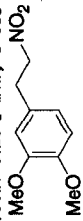
11.74



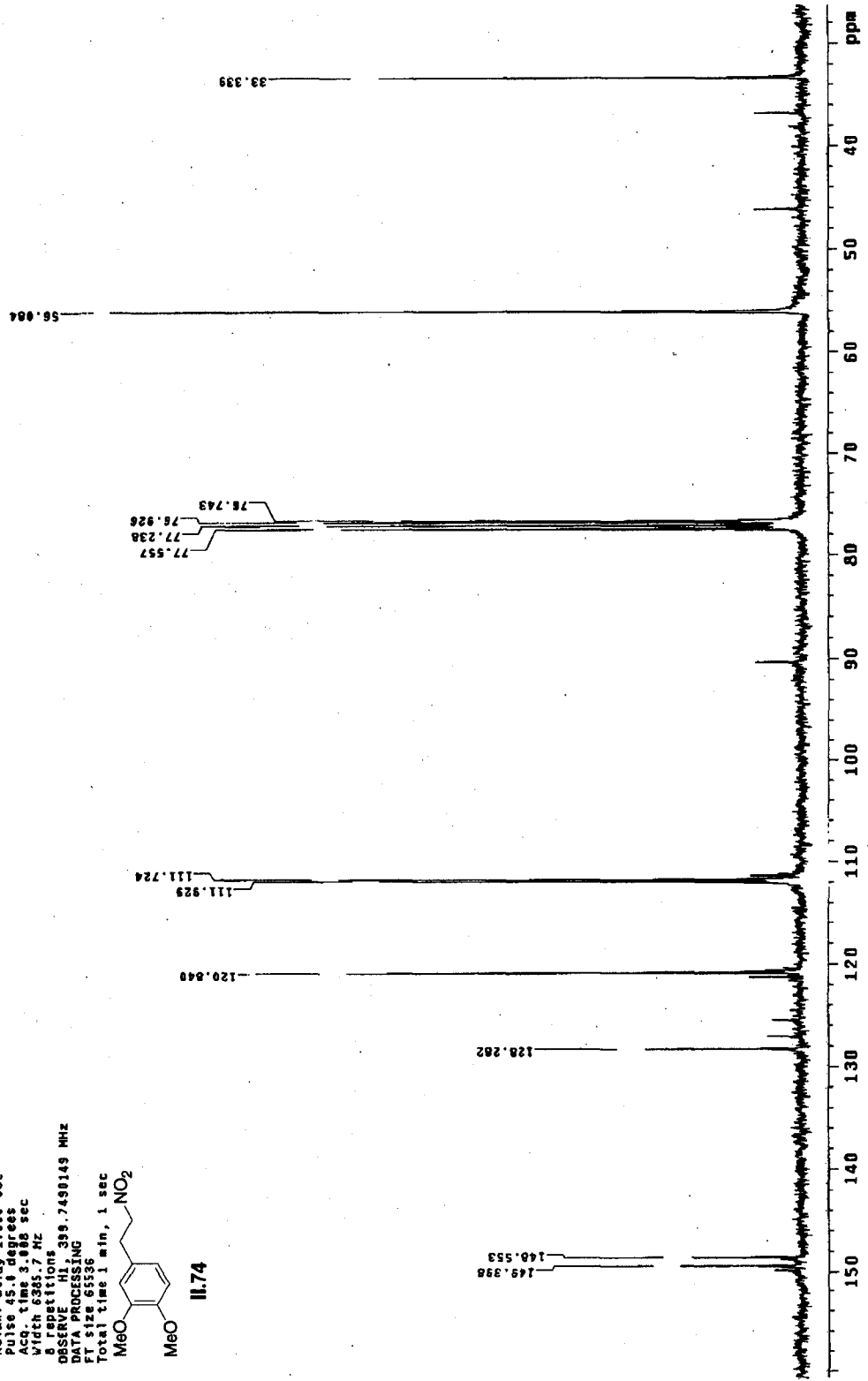
Archive directory: /export/home/kennedy/vmrsys/data
Sample directory: dkh86_1_28Nov2006

Pulse sequence: s2pu1
Solvent: CDCl3
Temp: 25.0 C / 298.1 K
File: PROTON
Mercury-400BB "lyltestation"

Relax. delay 1.000 sec
Pulse 45.0 degrees
Acq. time 3.000 sec
Width 6385.7 Hz
8 repetitions
OBSERVE HI, 399.7490149 MHz
DATA PROCESSING
FT size 65536
Total time 1 min, 1 sec



II.74

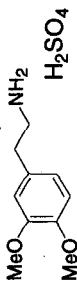


Archive directory: /export/home/kennedy/vnarsys/data
Sample directory: dkh66.2_28Nov2066

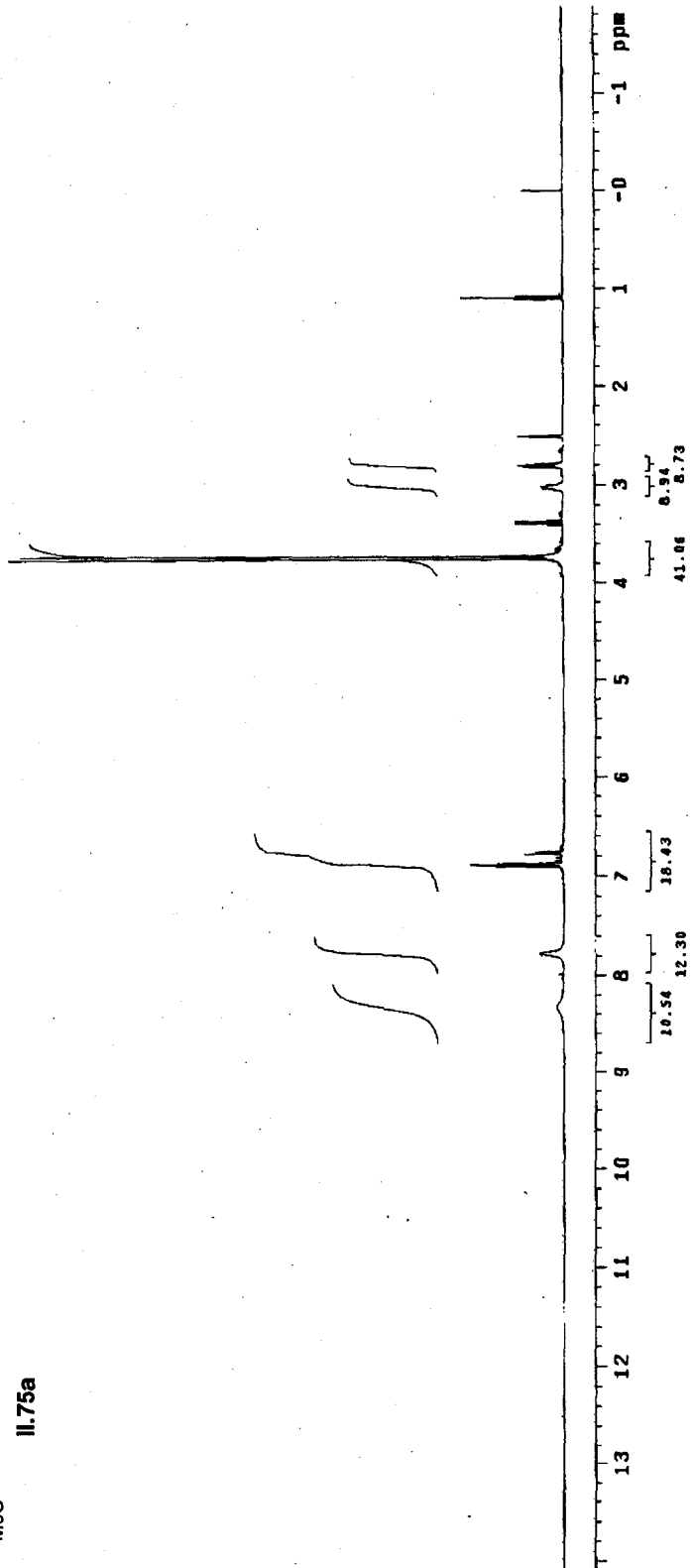
Pulse Sequence: szpu

Solvent: CDCl3
Temp. 25.0 C / 298.1 K
File: CARBON
Mercury-40068 "1ylestation"

Relax. delay 1.000 sec
Pulse 45.0 degrees
Acq. time 1.003 sec
Width 25062.7 Hz
512 repetitions
OBSERVE C13, 100.5169504 MHz
DECOUPLE H1, 399.7509888 MHz
Power 41 dB
continuously on
WALTZ-16 modulated
DATA PROCESSING
F1 line broadening 3.0 Hz
F2 size 65536
Total time 18 min, 7 sec



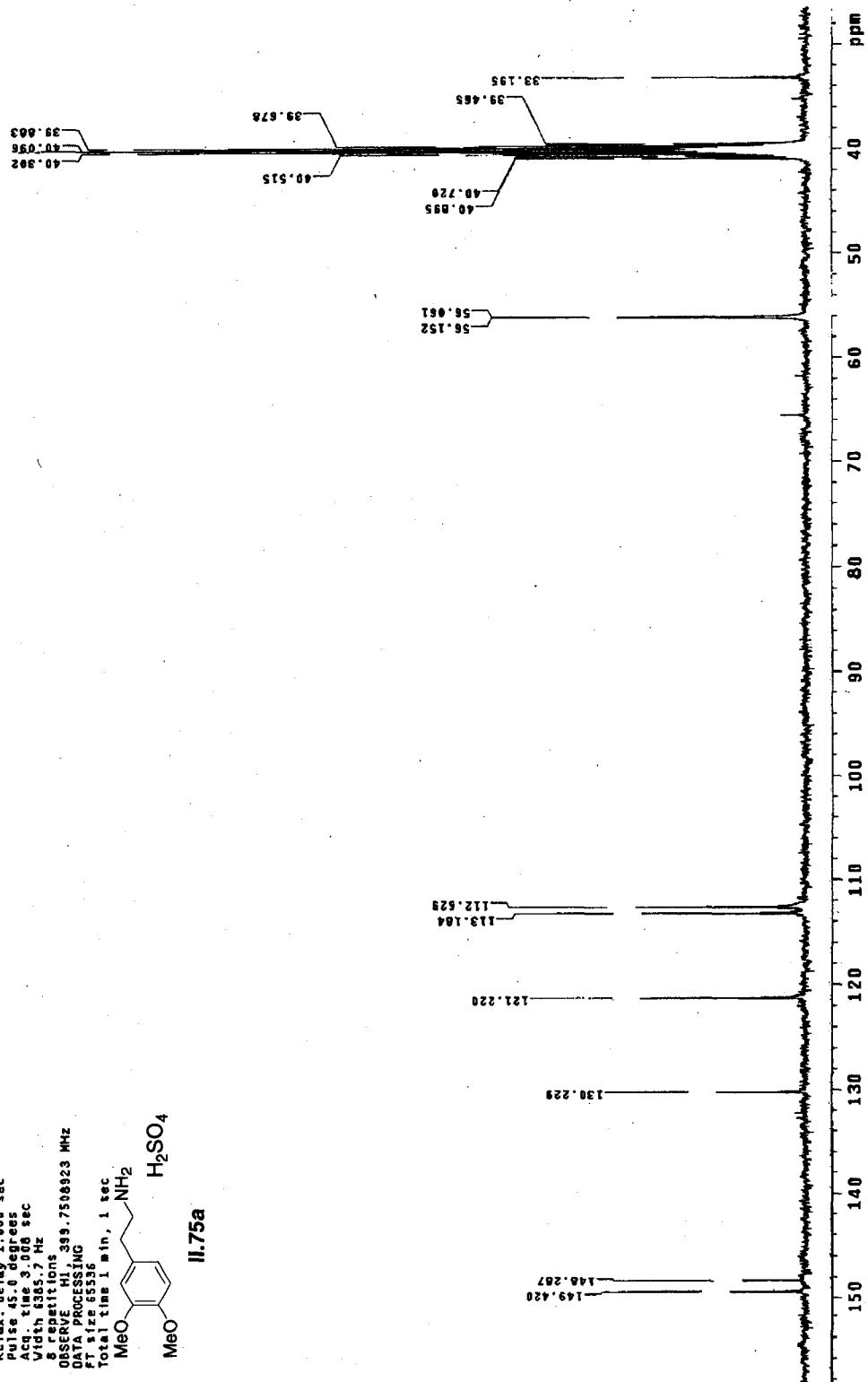
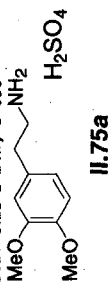
11.75a



Archive directory: /export/home/tenney/vmarsys/data
 Sample directory: dkhs3.1_3Nov2086

Pulse Sequence: s2pul
 Solvent: DMSO
 Temp: 25.0 C / 298.1 K
 Fil: 9000M "1ylestation"

Relax. delay: 1.000 sec
 Acq. time: 3.000 sec
 Width: 685.7 Hz
 S. repetitions: 8
 OBSERVE: H1, 399.7508923 MHz
 DATA PROCESSING
 FT size: 65536
 Total time: 1 min, 1 sec



Archive directory: /export/home/kennedy/vnarsys/data
Sample directory: dkn93_2_30Nov2006

Pulse Sequence: s2pu1

Solvent: DMSO
Temp: 25.0 C / 298.1 K
File: CARBON
Mercury-400066 "lytestation"

Relax. delay 1.000 sec

Pulse 45.0 degrees

Acq. time 1.003 sec

Width 25062.7 Hz

SIZ repetitions

OBSERVE C13, 100.5174278 MHz

DECUPLE H1, 399.7526676 MHz

Power 10.00 dB

Carrier 100.625131 MHz

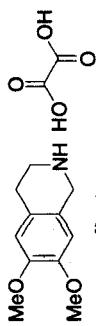
WALTZ-16 modulated

DATA PROCESSING

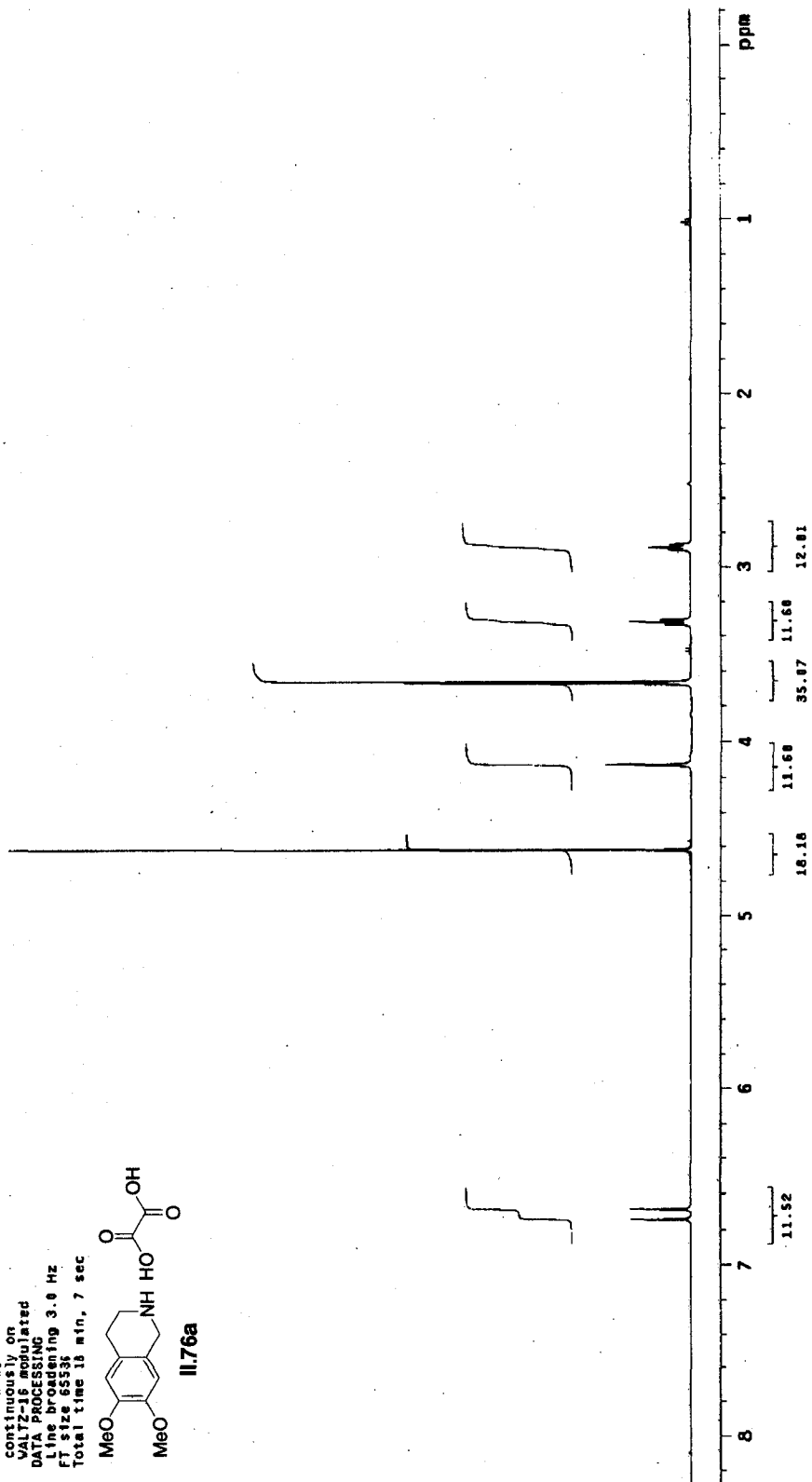
Line broadening 3.0 Hz

FT size 65536

Total time 18 min, 7 sec



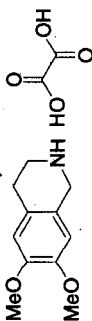
II.76a



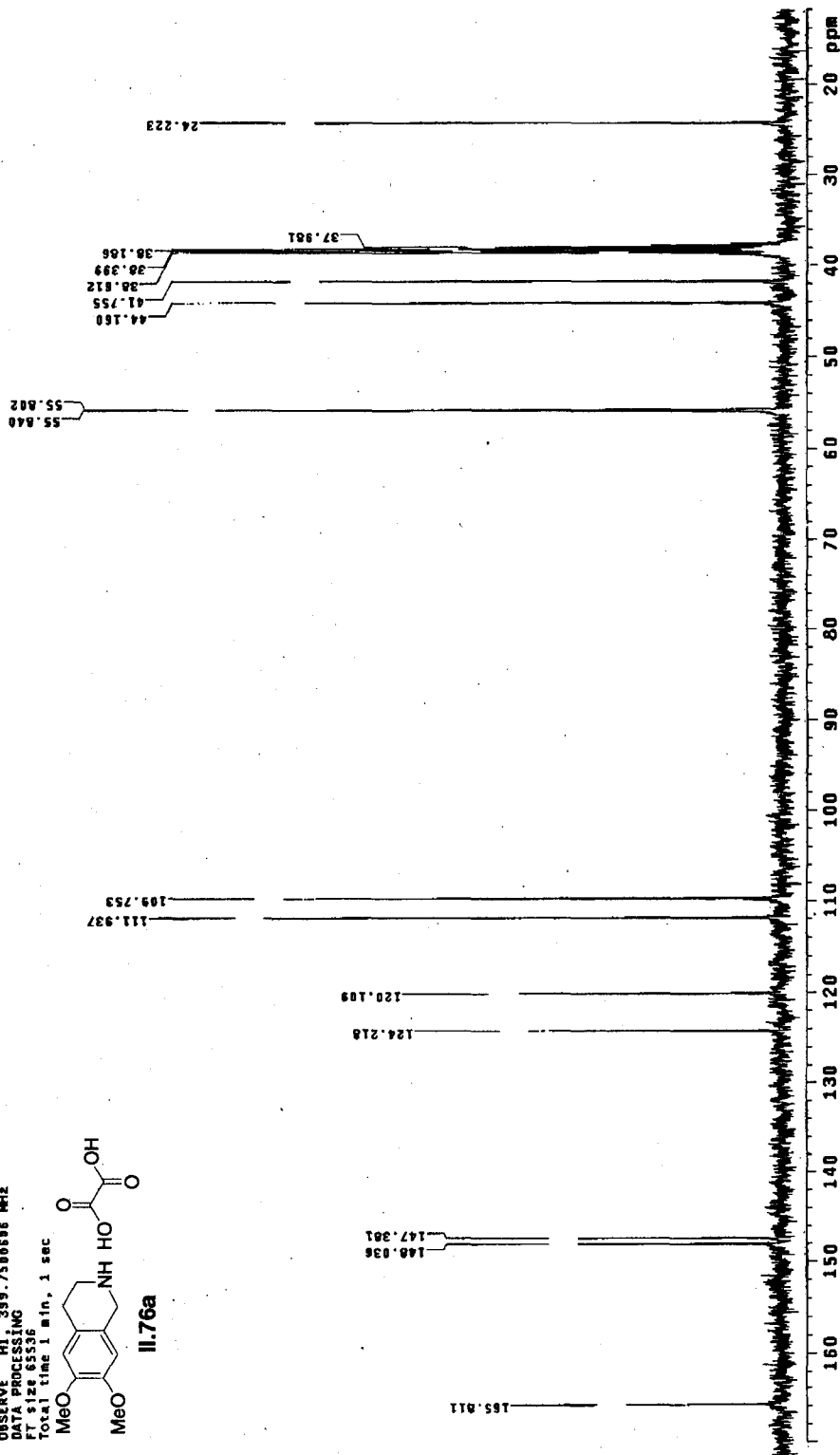
Archive directory: /export/home/kennedy/vnmrSYS/data
Sample directory: dK102.2_95Dec2006

Pulse Sequence: szput
Solvent: D2O
Temp: 25.9 C / 299.1 K
File: PROTON
Nucleus: 13C
Mercury: 49888 "lytestation"

Relax. delay 1.000 sec
Pulse 45.0 degrees
Acq. time 3.000 sec
Width 6385.7 Hz
repetitions 399.7500000 MHz
DATE_ 06/23/06
DAT_ 06/23/06
FT_ 124 65336
Total time 1 min, 1 sec



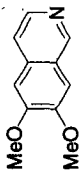
II.76a



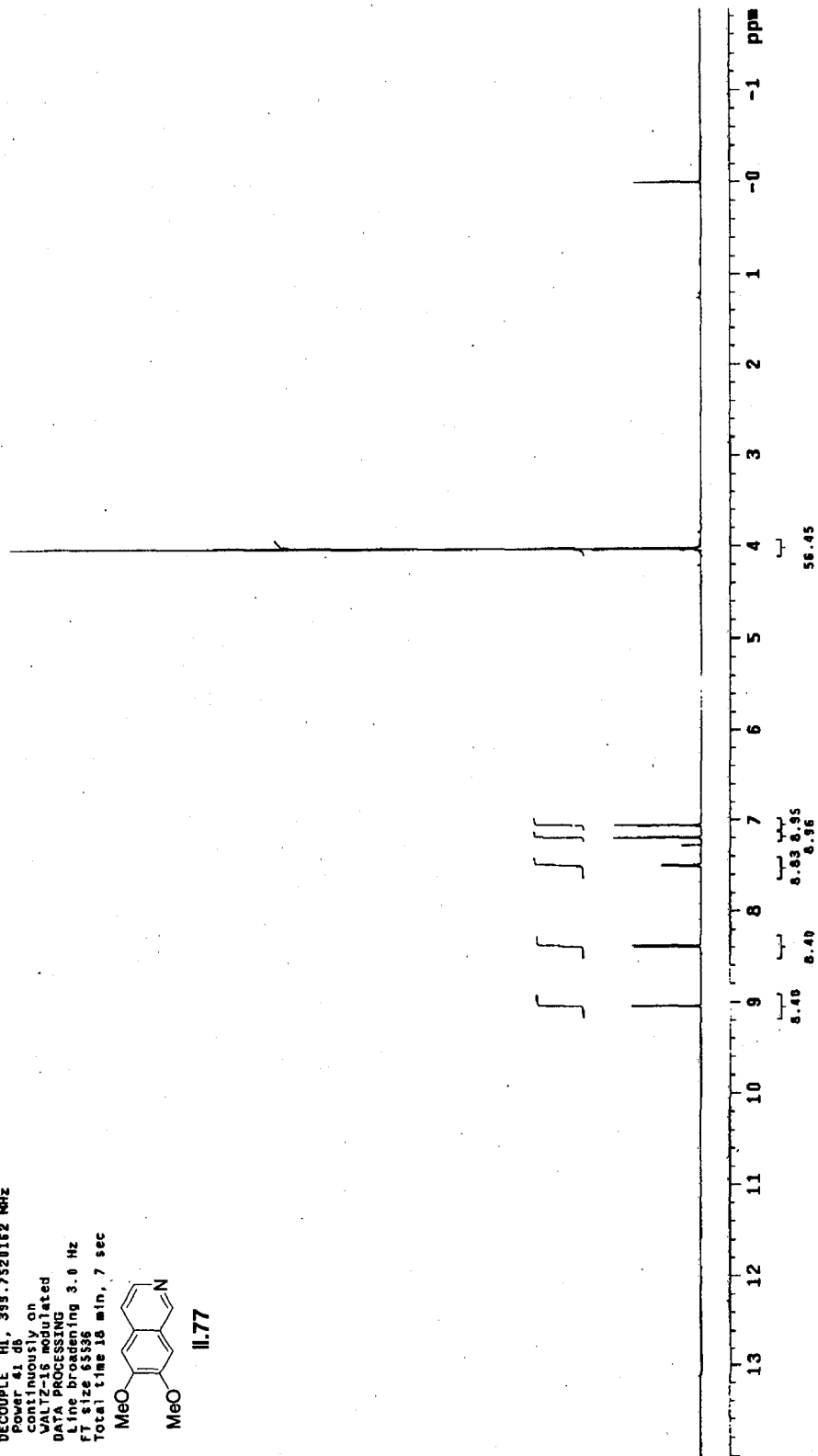
Archive directory: /export/home/kennedy/vnarsys/data
Sample directory: dk102_3_050ec206

Pulse Sequence: s2pul
Solvent: D2O
Temp: 25.0 C / 298.1 K
File: CARBON
Mercury-4000 "jylestation"

Relax. delay 1.000 sec
Pulse 45.0 degrees
Acq. time 1.053 sec
Width 25062.7 Hz
Siz 2 repetitions
OBSERVE C13, 100.5172087 MHz
DECOUPLE H1, 395.7520162 MHz
Power 41 db
continuously on
WALTZ-16 modulated
DATA PROCESSING
Line broadening 3.0 Hz
FT size 65536
Total time 18 min, 7 sec



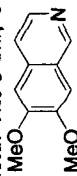
11.77



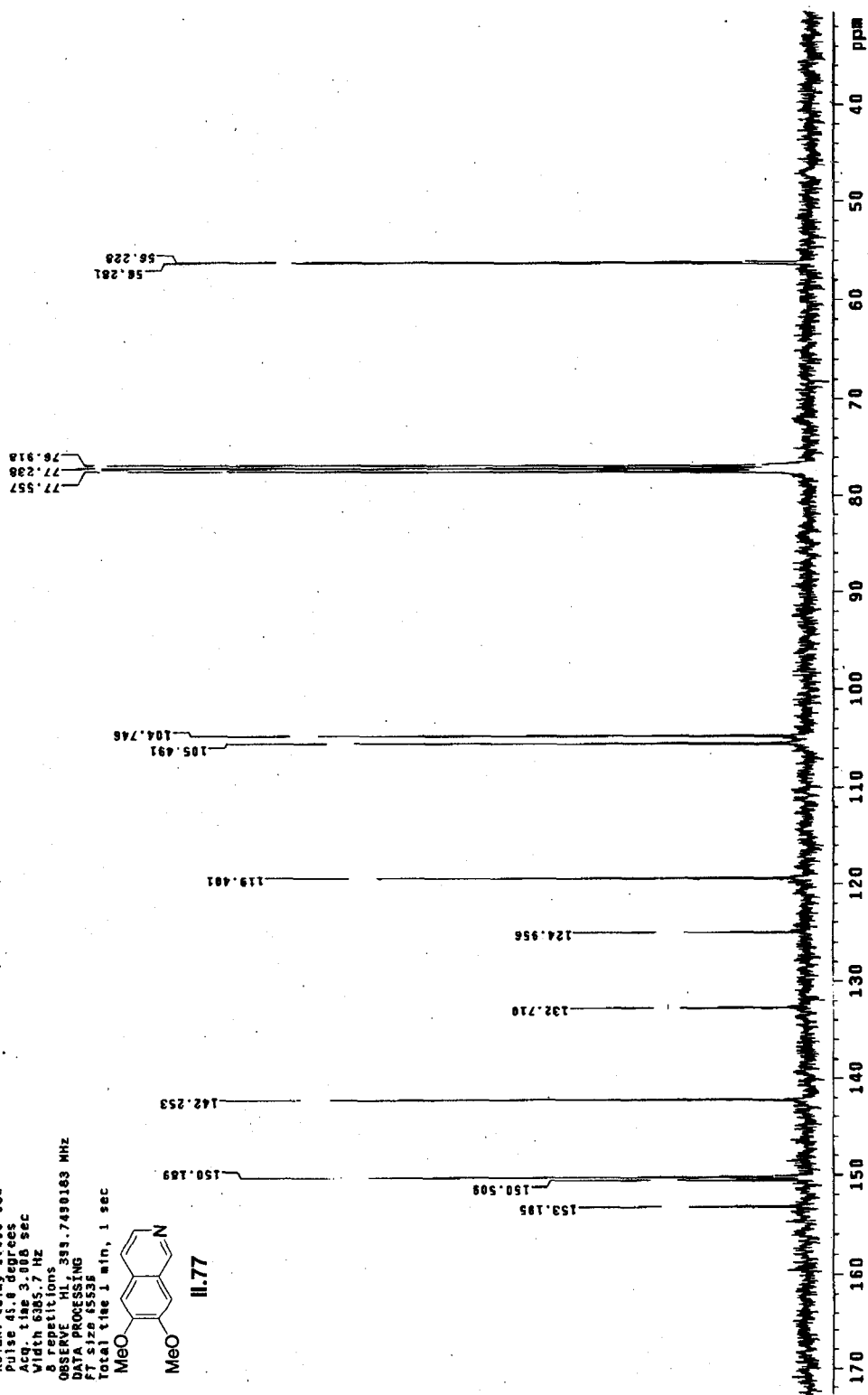
Archive directory: /export/home/kennedy/vnarsys/data
Sample directory: d6108_3_110ac286

Pulse Sequence: s2pu1
Solvent: CDCl3
Temp: 25.0 C / 296.1 K
File: PROTON
Mercury-40888 "lylestation"

Relax. delay 1.000 sec
Puls. 45.000 sec
Acq. time 3.000 sec
Width 6395.7 Hz
& repetitions
OBSERVE HL 399.7490163 MHz
DATA PROCESSING
FT size 65535
Total time 1 min, 1 sec



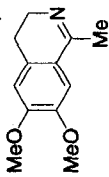
II.77



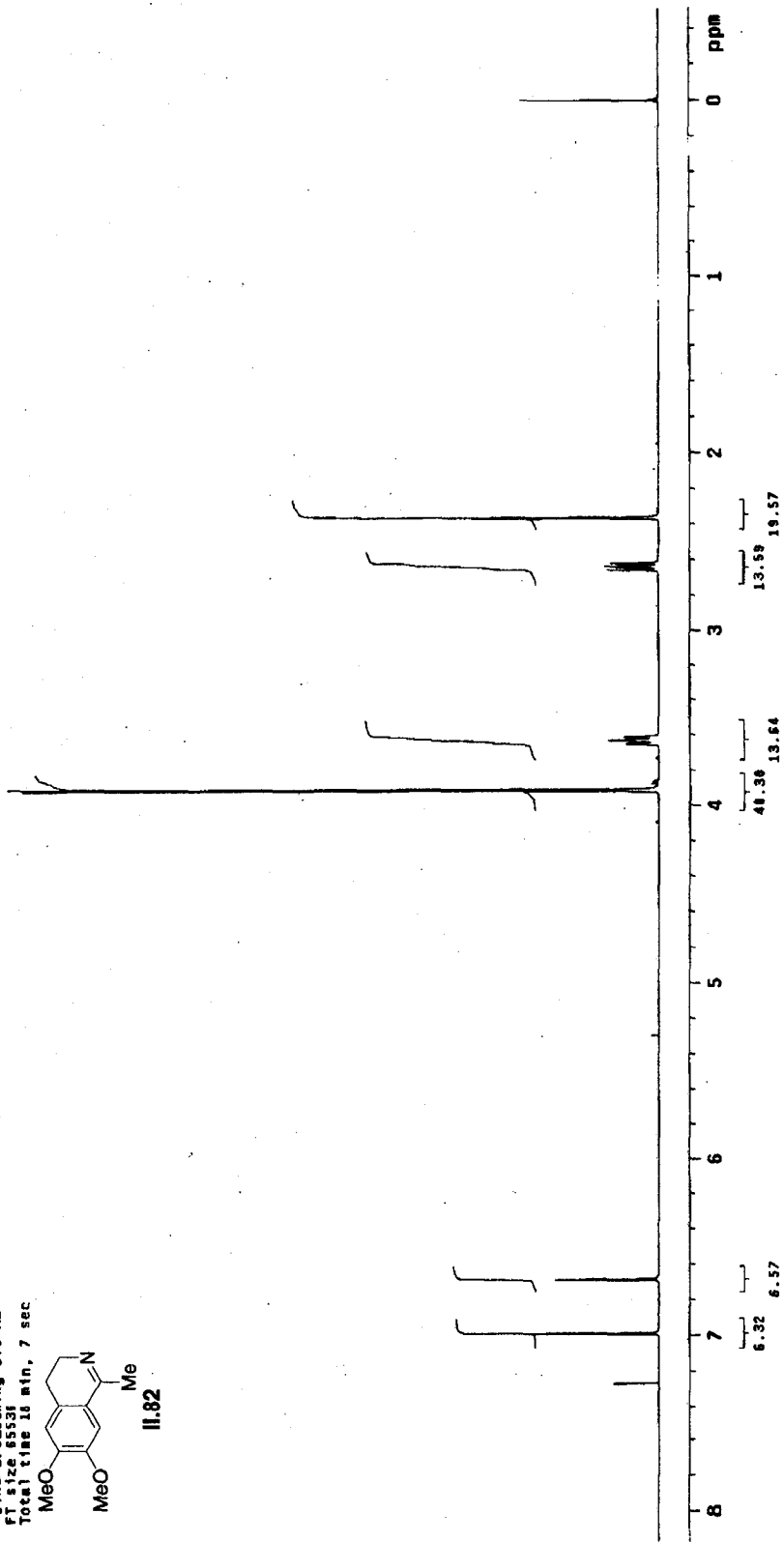
Archive directory: /export/home/kennedy/vmarsys/data
Sample directory: dk109.4_110ac2005

Pulse Sequence: s2pul
Solvent: CDCl3
Temp: 25.0 C / 298.1 K
File: CARBON
Mercury-400BB "1ylestation"

Relax. delay 1.000 sec
Pulse 45.0 degree
Acq time 1.093 sec
Width 25627 Hz
S12 repetitions
OBSERVE C13 100.5165504 MHz
DECUPLE H1 399.7509008 MHz
Power 41 dB
continuously on
VAL72-16 modulated
DATA PROCESSING
Line broadening 3.0 Hz
FT size 65536
Total time 18 min, 7 sec



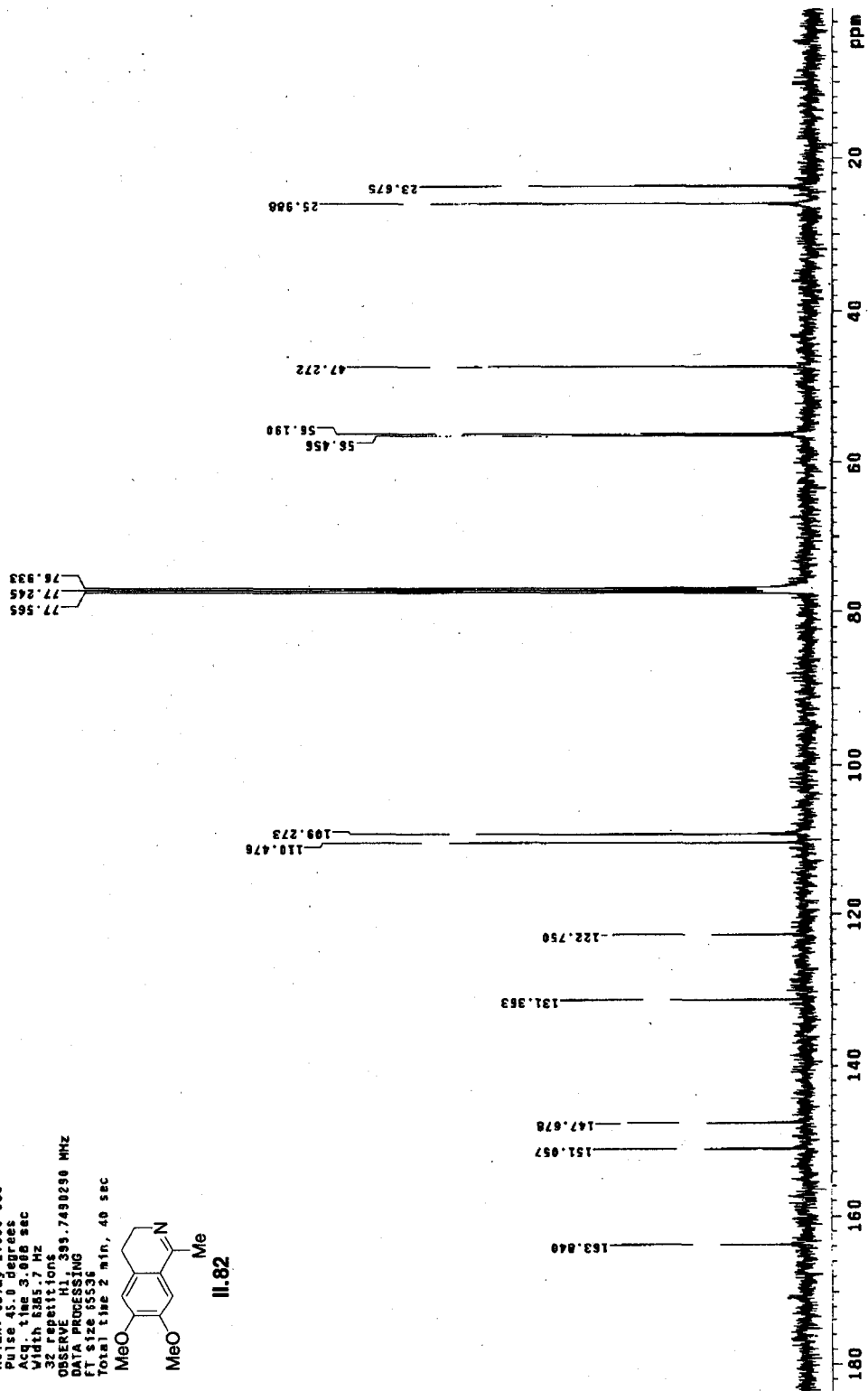
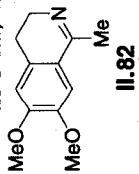
11.82



Archive directory: /export/home/kennedy/vnarsys/data
Sample directory: dk124_1_20Dec2006

Pulse Sequence: s2pul
Solveht: CDC13
Temp: 25.0 C / 298.1 K
File: PROTON
Mercury-100BB "1ylestation"

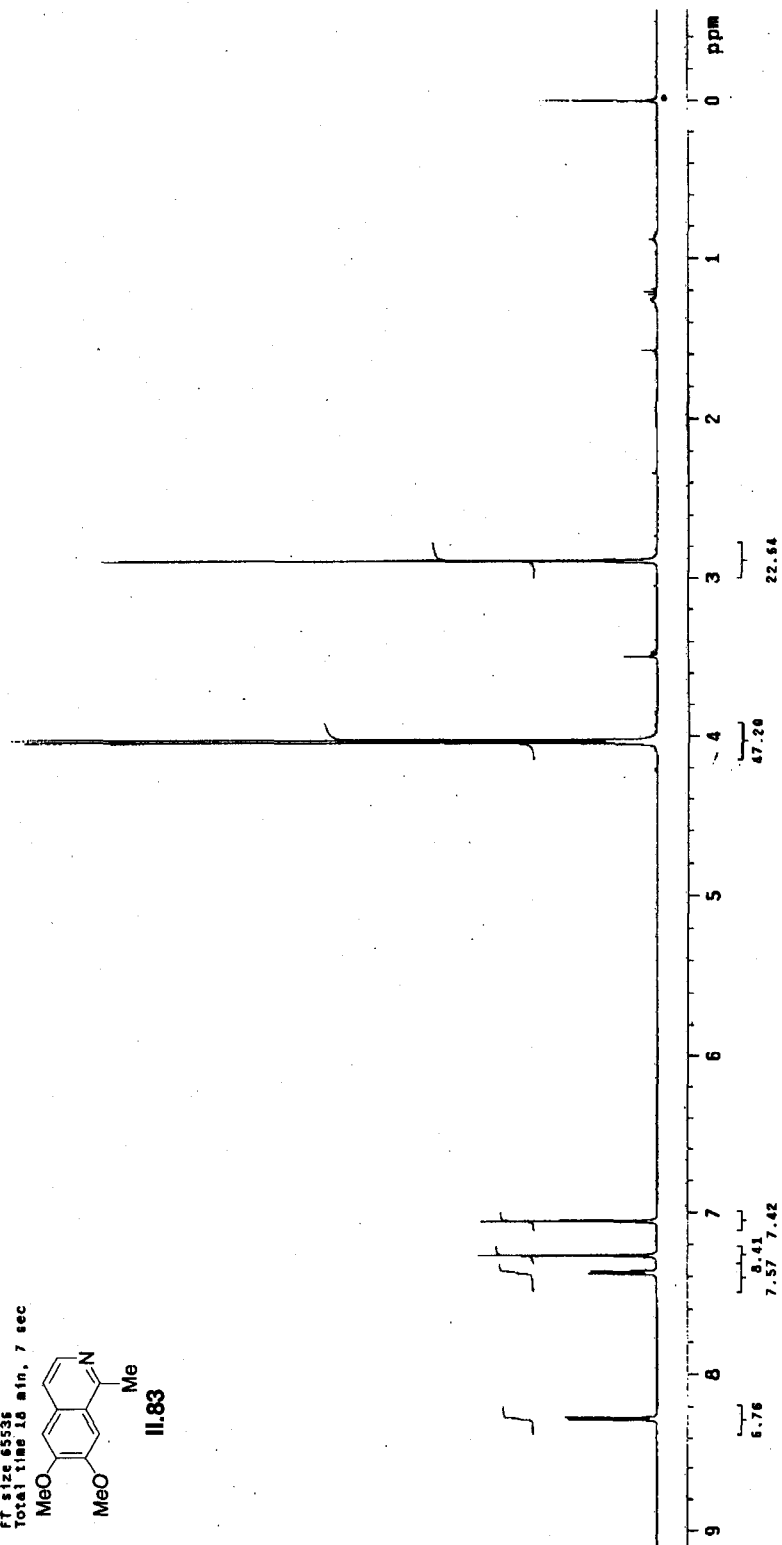
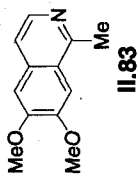
Relax. delay 1.800 sec
Pulse 45.0 degrees
Acq. time 3.088 sec
Width 8263.7 Hz
Observer
OPERATION: 395.7490290 MHz
DATA PROCESSING
FT size 15536
Total time 2 min, 40 sec



Archive directory: /export/home/kennedy/vmarsys/data
Sample directory: dk124_2_28Dec2006

Pulse Sequence: s2pu1
Solvent: CDCl3
Temp: 25.0 C / 298.1 K
File: CARBON
Mercury-40000 "lylestation"

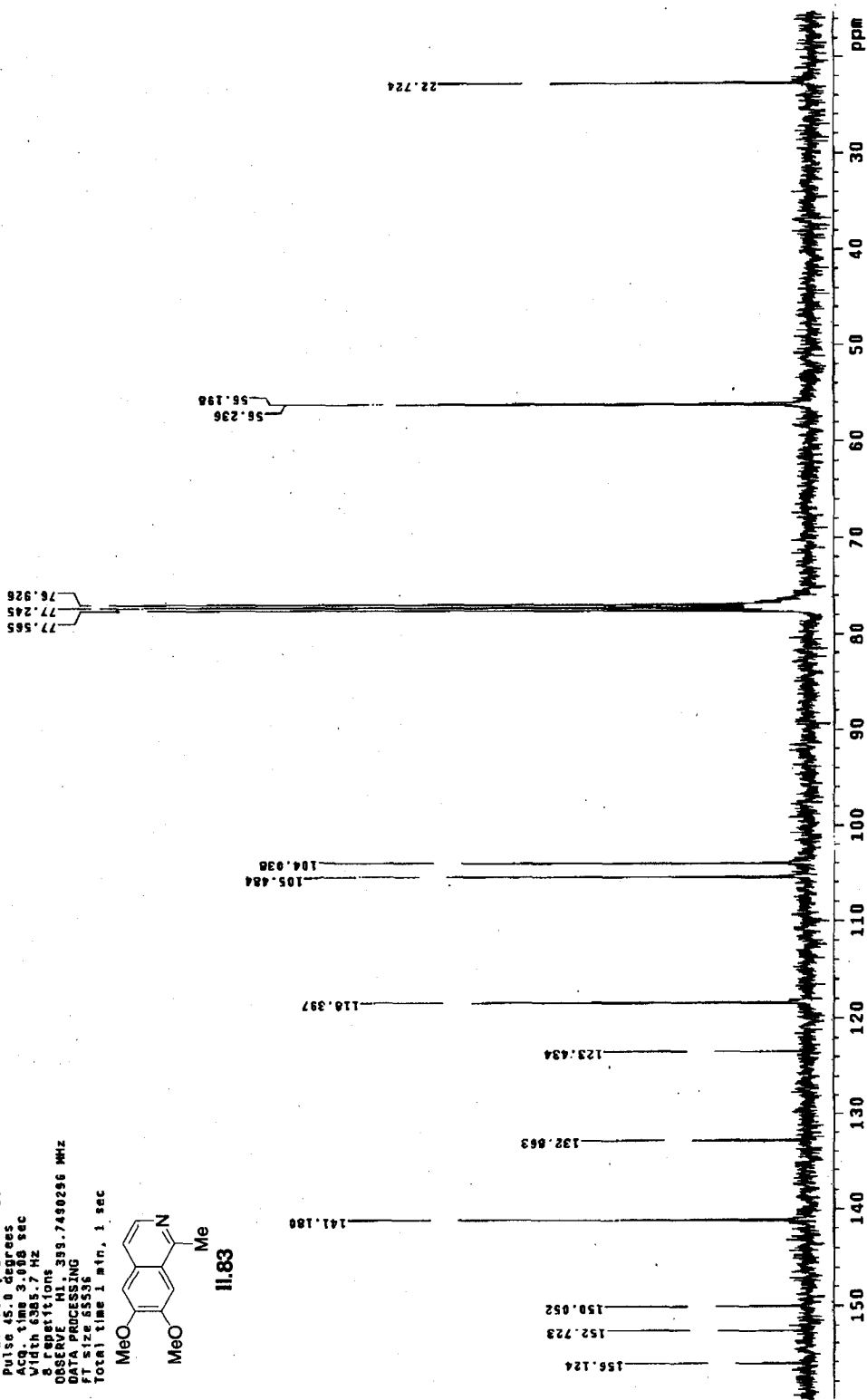
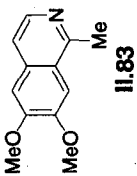
Relax. delay 1.000 sec
Pulse 45.0 degrees
Acq. time 1.903 sec
Width 25062.7 Hz
512 Repetitions
OBSERVE C13, 100-518954 MHz
DECOUPLE H1, 399.759968 MHz
Power 41 dB
Continuously on
Waltz16 Modulated
DATA PROCESSING
Line broadening 3.0 Hz
FT size 65536
Total time 18 min. 7 sec



Archive directory: /export/home/kennedy/vmrfsys/data
 Sample directory: dR226-1_21dec2000

Pulse Sequence: szpu1
 Solvent: CDCl3
 Temp: 25.0 C / 298.1 K
 F1In: PROTON
 Mercury: 40000 "lytestation"

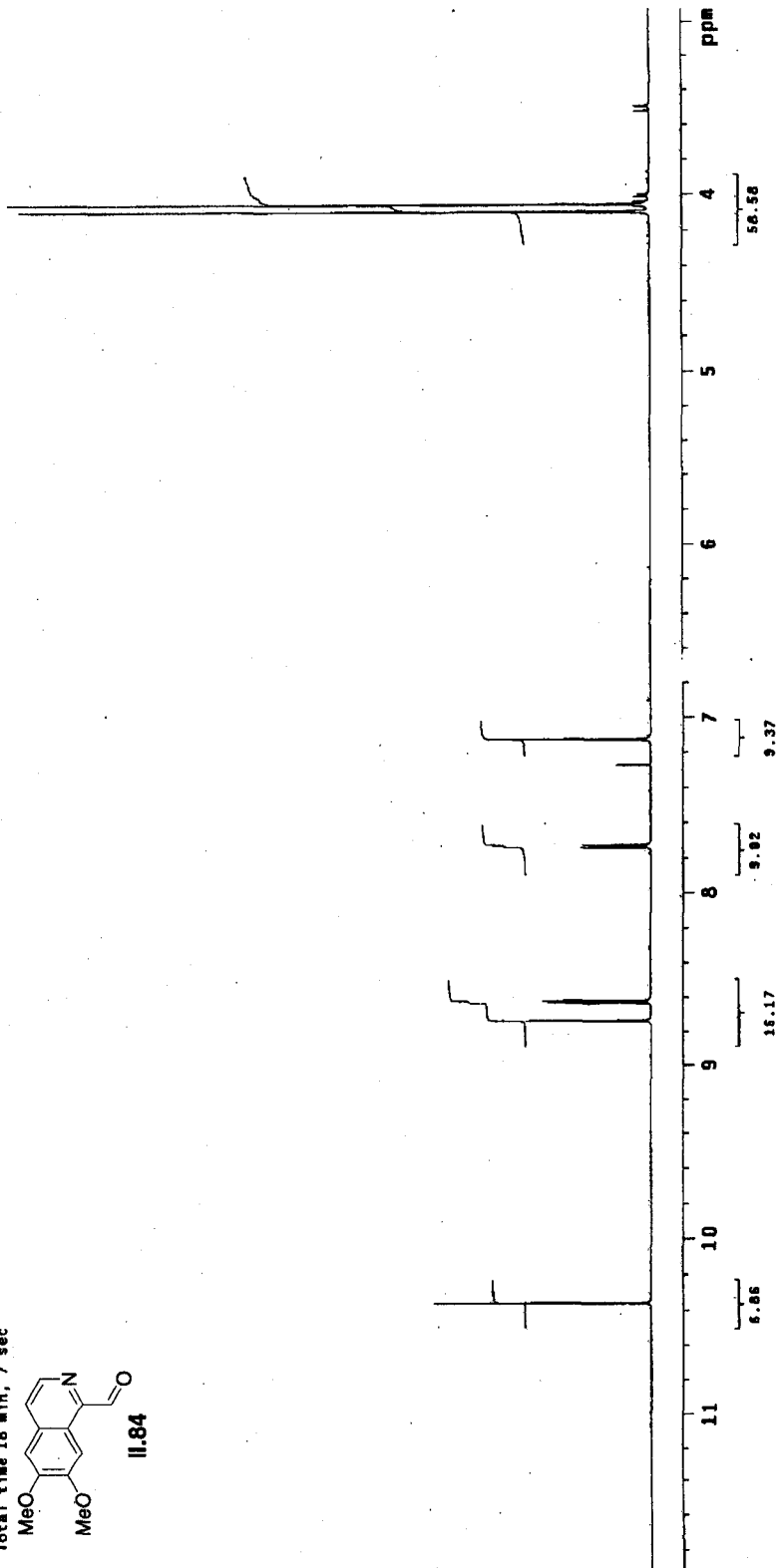
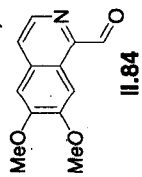
Relax delay: 1.000 sec
 Pulprog: zgpg30
 Acq time: 3.000 sec
 Width: 6385.7 Hz
 S Freq: 400.146 MHz
 8 FIDST11010
 OBSERVE H1, 399.7490286 MHz
 DATA PROCESSING
 FT size 65536
 Total time 1 min, 1 sec



Archive directory: /export/home/kennedy/vmarsys/data
Sample directory: dk126.2_210ec2086

Pulse Sequence: s2pu1
Solvent: CDCl3
Temp: 25.1 C / 298.1 K
File: CARBON
Mercury-400BB "1y]estation"

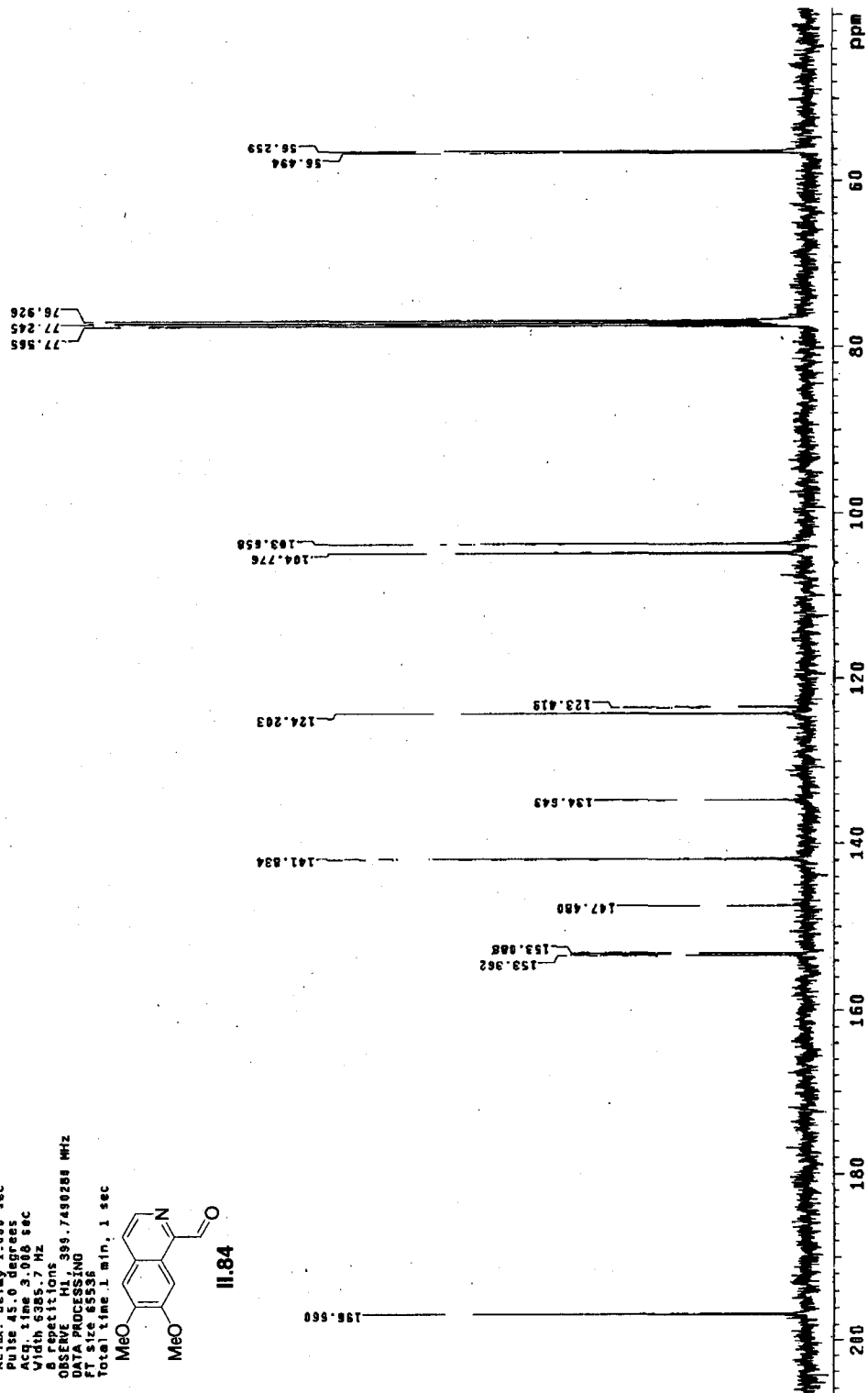
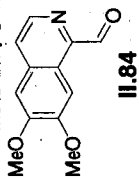
Relax. delay 1.000 sec
Pulse 45.0 degrees
Acq. time 1.000 sec
Width 2582.7 Hz
512 repetitions
OBSERVE C13, 148.5169504 MHz
DECOUPLE H1, 399.7598666 MHz
Power 01.05
Continuously on
Sensitivity limited
DATA PROCESSING
Line broadening 3.0 Hz
FT size 65536
Total time 16 min, 7 sec



Archive directory: /export/home/kennedy/vmr/sys/data
 Sample directory: dk126_1_02Jan88

Pulse Sequence: s2pul
 Solvent: CDCl3
 Temp: 25.0 C / 298.1 K
 File: PROTON
 Mercury-400BB "lytestation"

Relax. delay 1.000 sec
 Pulse 45.0 degrees
 Acq. time 3.000 sec
 Width 6385.7 Hz
 Obs. frequency 399.749288 MHz
 Obs. resolution
 DATA PROCESSING
 FT size 65536
 Total time 1. min, 1. sec



Archive directory: /export/home/kennedy/vmarsys/data
Sample directory: dk128.1_02Jan2007

Pulse Sequence: szpu1

Solvent: CDCl3

Temp. 25.0 C / 298.1 K

File: CARBON

Mercury-4000B "lylestation"

Relax. delay 1.000 sec

Pulse 45.0 degrees

Acq. time 1.003 sec

Width 25862.7 Hz

512 repetitions

OBSERVE C13, 100.5169504 MHz

DECOUPLE H1, 399.7509868 MHz

Power 41 dB

continuously on

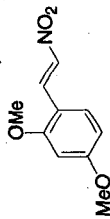
VALZ-16 modulated

DATA PROCESSING

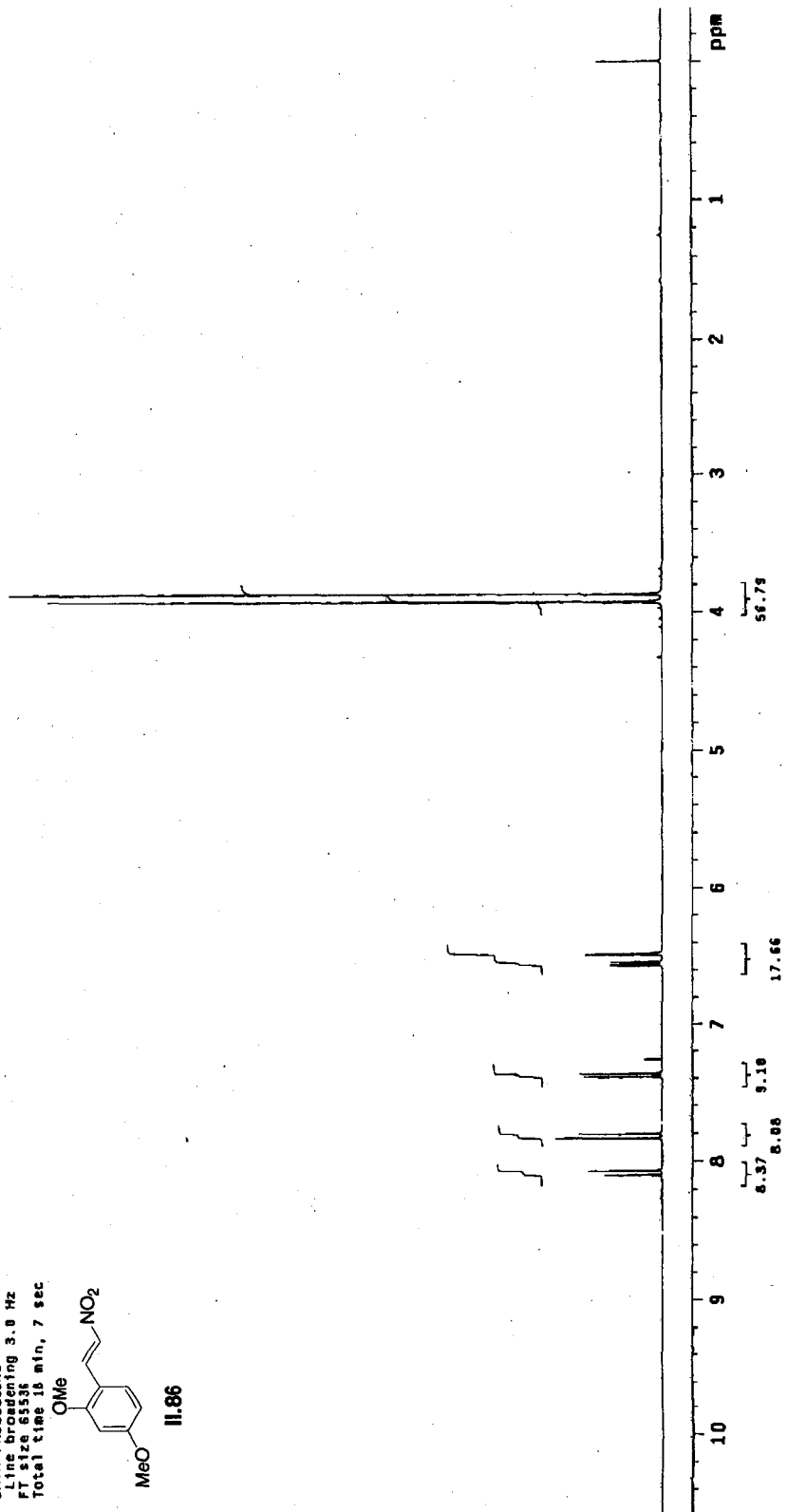
Line broadening 3.0 Hz

FT size 65536

Total time 18 min, 7 sec



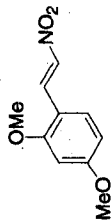
11.86



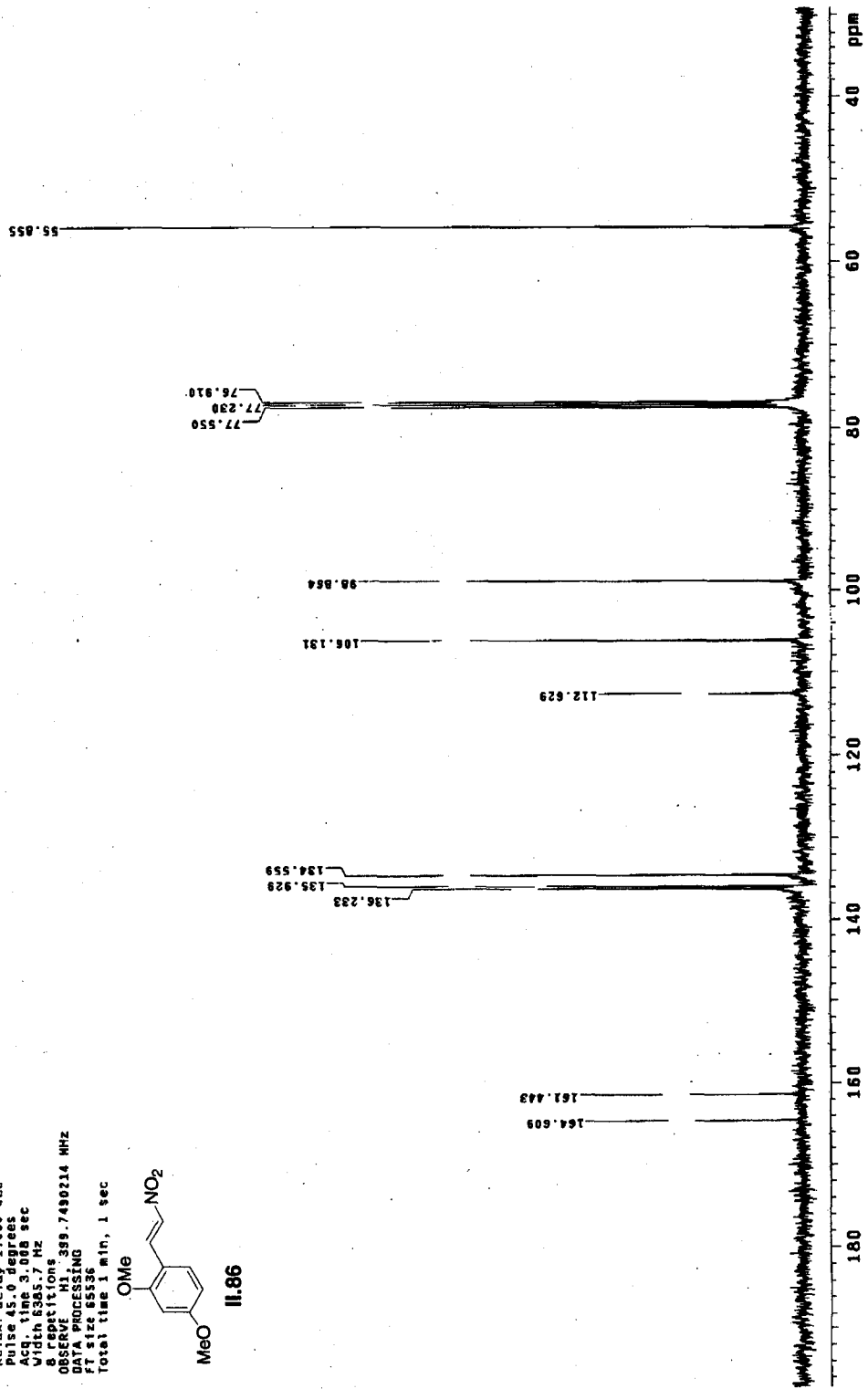
Archive directory: /export/home/kennedy/vnmrSYS/data
Sample directory: dkh85.1_27Nov2005

Pulse Sequence: s2pul
Solvent: CDCl3
Temp: 25.0 C / 288.1 K
File: PROTON
Mercury-400BB "lylestation"

Relax. delay 1.000 sec
Pulse 45.0 degrees
Acq. time 3.068 sec
Width 6385.7 Hz
Observed F1 300.7490214 MHz
Spectrum 1
DATE ACQUISITION
DATA PROCESSING
FT size 65536
Total time 1 min, 1 sec



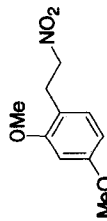
11.86



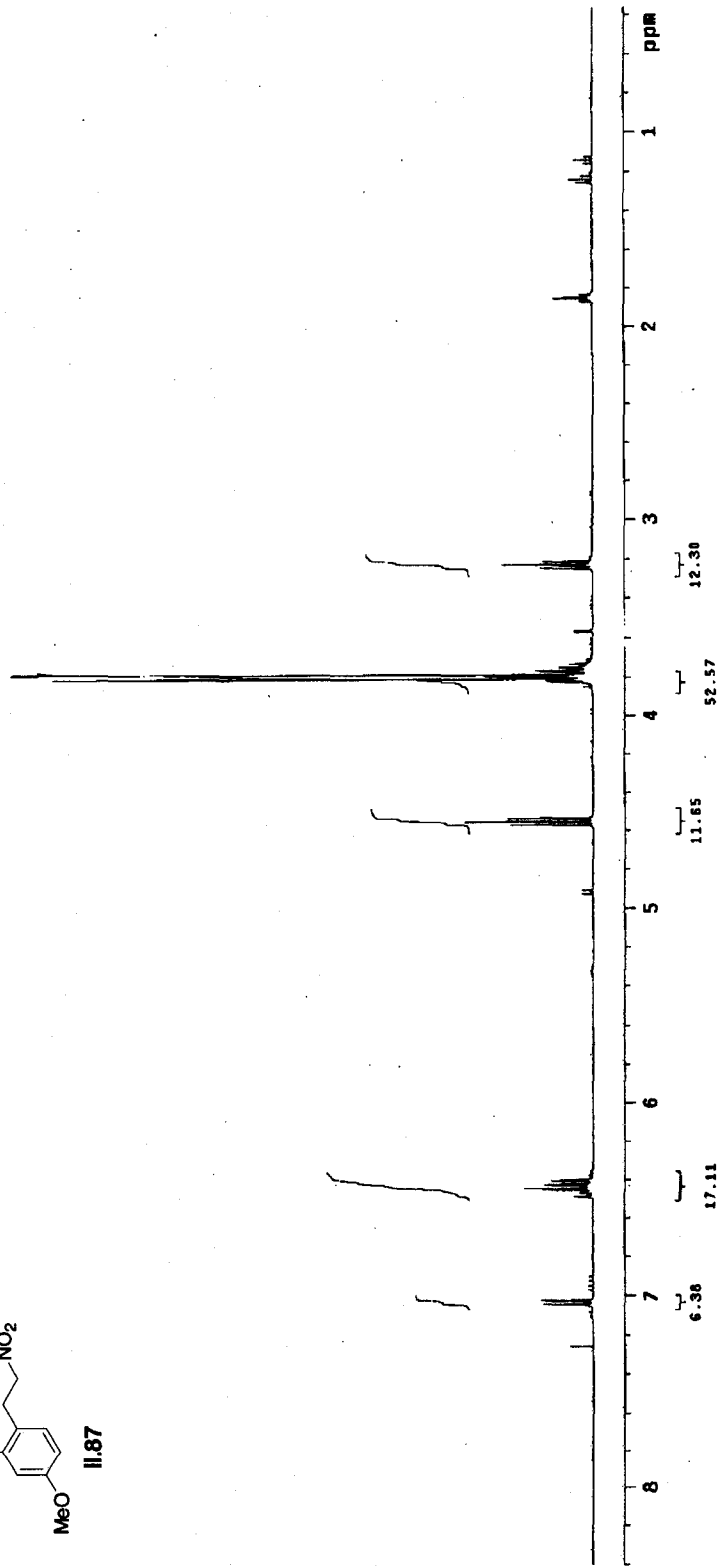
Archive directory: /export/home/kennedy/vmarsys/data
Sample directory: dkh95_3_30Nov2006

Pulse Sequence: s2pu1
Solvent: CDCl3
Temp. 25.0 C / 298.1 K
File: CARBON
Mercury-40006 "lylestation"

Relax. delay 1.000 sec
Pulse 45.0 degrees
Acq. time 1.883 sec
Width 25002.7 Hz
512 repetitions
OBSERVE C13, 180.5169584 MHz
DECOUPLE H1, 399.7589868 MHz
Power 41 dB
Continuously on
WALTZ-16 modulated
DATA PROCESSING
Line broadening 3.0 Hz
F1 size 63396
Total time 20 min. 7 sec



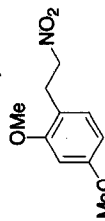
II.87



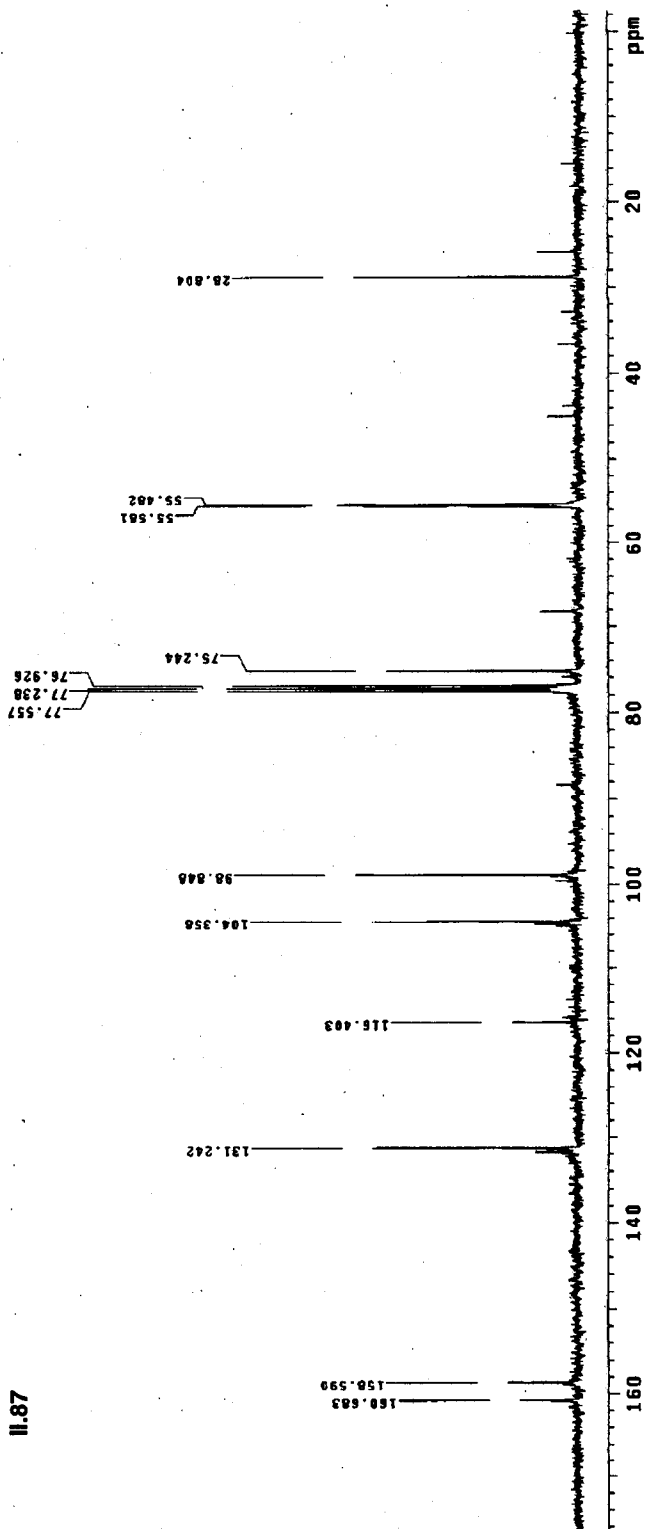
Archive directory: /export/home/kennedy/vnarsys/data
Sample directory: dkmb6_2_27Nov2006

Pulse Sequence: s2pul
Solvent: CDCl3
Temp: 25.0 C / 298.1 K
File: CARSON
Mercury-41088. "lytestation"

Relax. delay 1.800 sec
Pulse 45.0 degrees
Acq. time 1.700 sec
Vct 12861.70 Hz
328 repetitions
OBSERVE C13, 100.5165584 MHz
DECUPLE H1, 399.7503868 MHz
Power 41 dB
continuously on
VAlTz-16 modulated
DATA PROCESSING
Line broadening 3.0 Hz
F2 size 65536
Total time 18 min, 7 sec



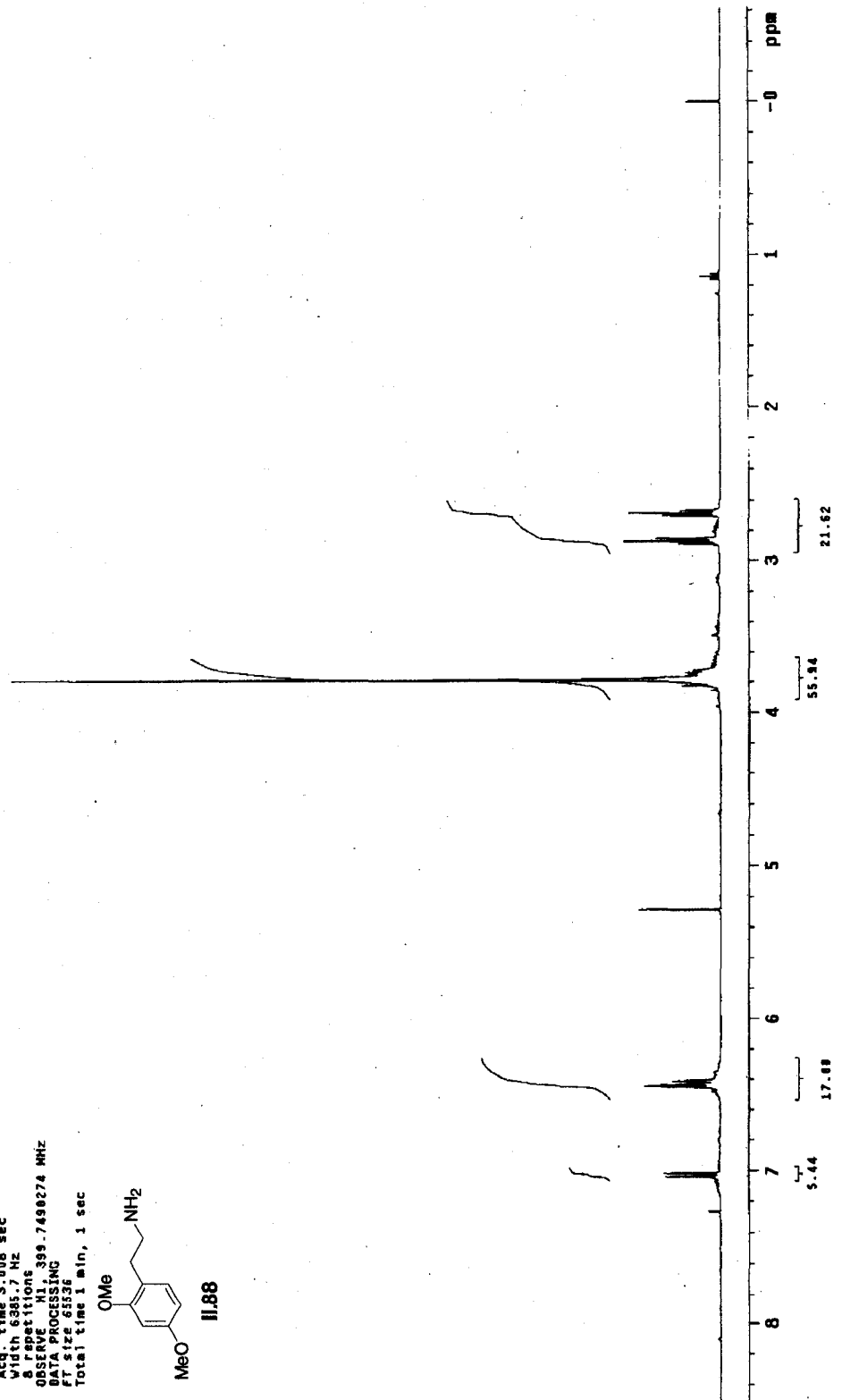
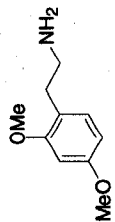
II.87



Archive directory: /export/hoas/kennedy/vmr/sys/data
Sample directory: dkh55.2_31Nov2005

Pulse Sequence: s2pul
Solvent: CDCl3
Temp: 25.0 C / 298.1 K
File: PROTON
Mercury-400BB "lylestation"

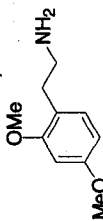
Relax. delay 1.000 sec
Pulse 45.0 degrees
Acq. time 3.000 sec
Width 6385.7 Hz
8 repetitions
OBSERVE M1, 399.7490274 MHz
DATA PROCESSING
FT size 65536
Total time 1 min, 1 sec



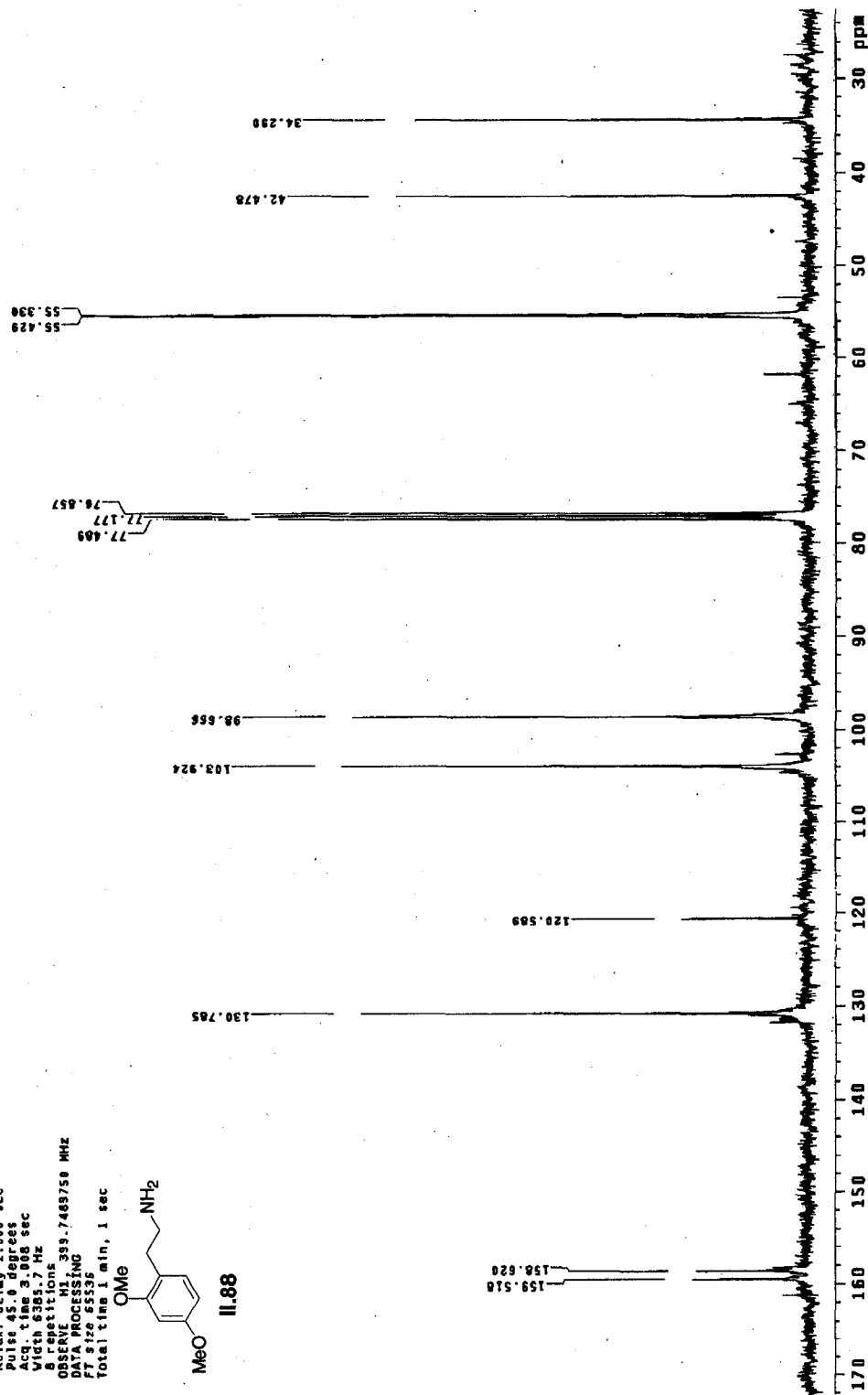
Archive directory: /export/home/kennedy/vmrsys/data
Sample directory: dkh97_1_03Dec2088

Pulse Sequence: szpul
Solvent: CDCl3
Temp: 25.8 C / 298.1 K
File: PRGTON
Mercury-488B "lylestation"

Relax. delay 1.000 sec
Pulse 45.0 degrees
Acq. time 3.000 sec
Width 6303.7 Hz
Observed F1 (nu) 39.7469750 MHz
DATA PROCESSING
FT size 65536
Total time 1 min, 1 sec



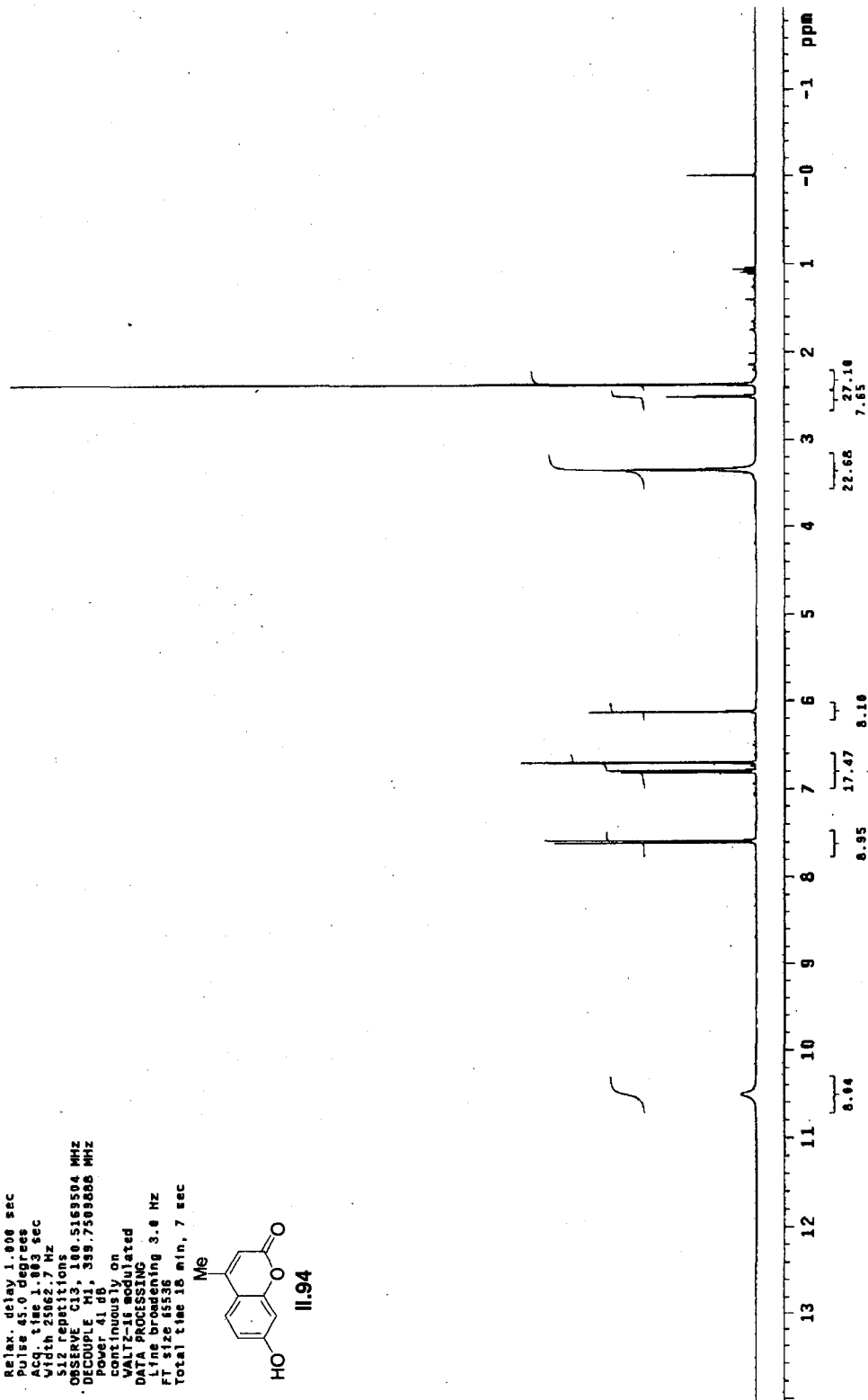
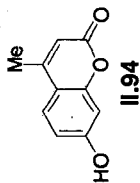
II.88



Archive directory: /export/home/kennedy/vnarsys/data
Sample directory: dch97.2_30dec206

Pulse Sequence: szpul
Solvent: CDCl3
Temp: 25.0 C / 298.1 K
File: CARBON
Mercury-400BB "1ylestation"

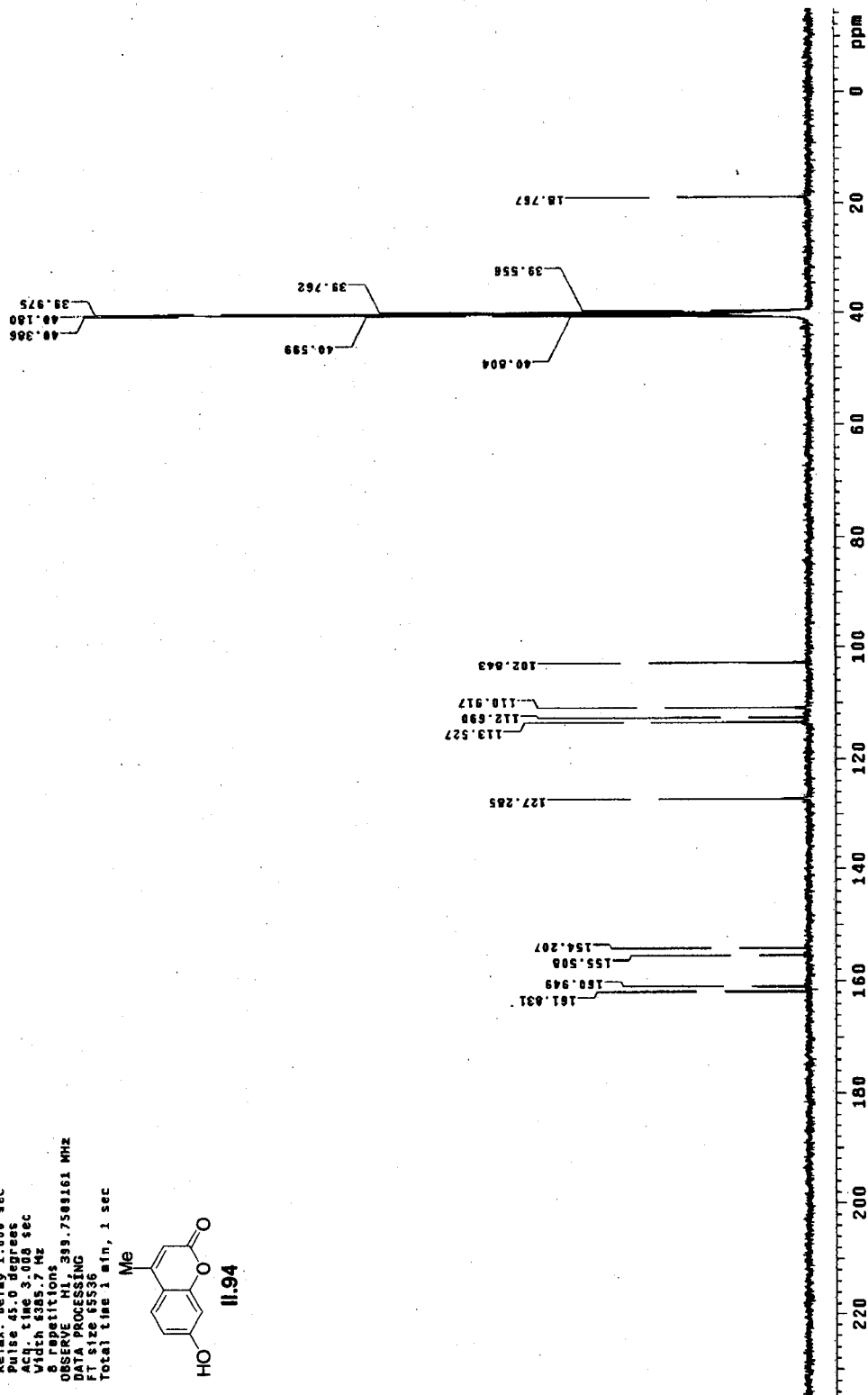
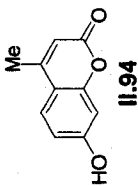
Relax. delay 1.000 sec
Pulse 45.0 degrees
Acq. time 1.003 sec
Width 25062.7 Hz
512 repetitions
OBSERVE C13, 100-5169504 MHz
DECOUPLE H1, 399.7509868 MHz
Power 41 dB
continuously on
with the magnet
DATA PROCESSING
Line broadening 3.6 Hz
FT size 65536
Total time 18 min, 7 sec



Archive directory: /export/home/kennedy/vnmrsys/data
Sample directory: dK183.1_12Feb2007

Pulse Sequence: s2pu1
Solvent: DMSO
Temp: 30 C / 298.1 K
File: PROTON
Mercury-400BB "1ylestation"

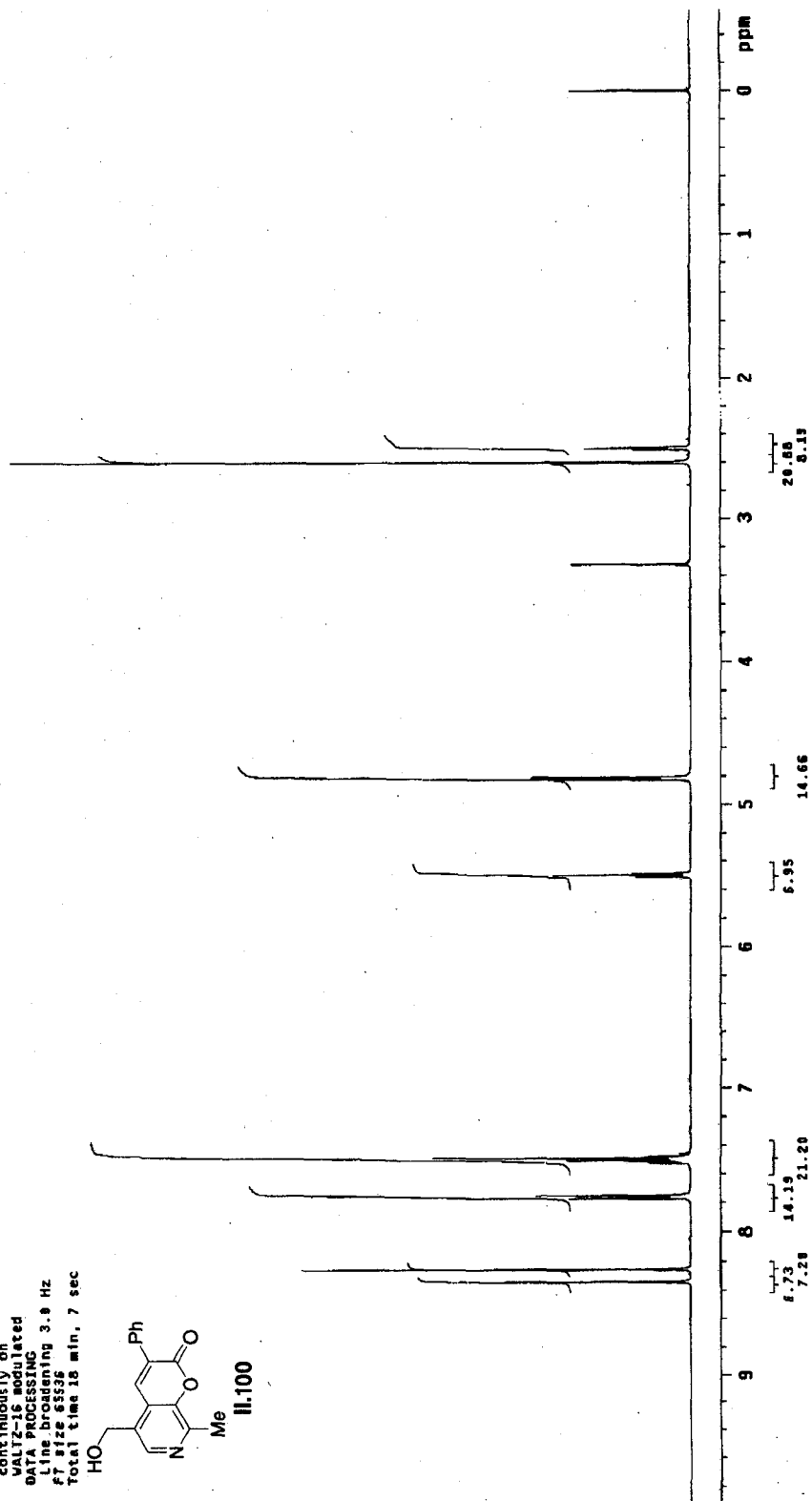
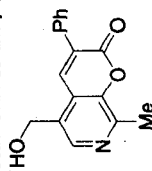
Refer-delay 1.000 sec
Pulse 40.000 sec
Acq time 3.000 sec
Vid 325.7 MHz
8 repetitions
OBSERVE H1, 399.7503161 MHz
DATA PROCESSING
FT size 65536
Total time 1 min, 1 sec



Archive directory: /export/home/kennedy/vnarsys/data
Sample directory: dk163.2_12Feb2007

Pulse Sequence: szpu1
Solvent: DMSO
Temp. 25.1 C / 296.1 K
File: CARBON
Mercury-40185 "1y1estation"

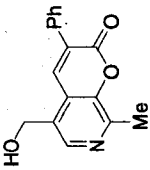
Relax. delay 1.000 sec
Pulse 45.0 degrees
Acq. time 1.003 sec
Width 25062.7 Hz
512 repetitions
OBSERVE C13, 130.5174276 MHz
DECOUPLE H1, 399.7528076 MHz
Power 41 dB
continuously on
WALTZ-16 modulated
DATA PROCESSING
Line broadening 3.9 Hz
FT size 65536
Total time 16 min, 7 sec



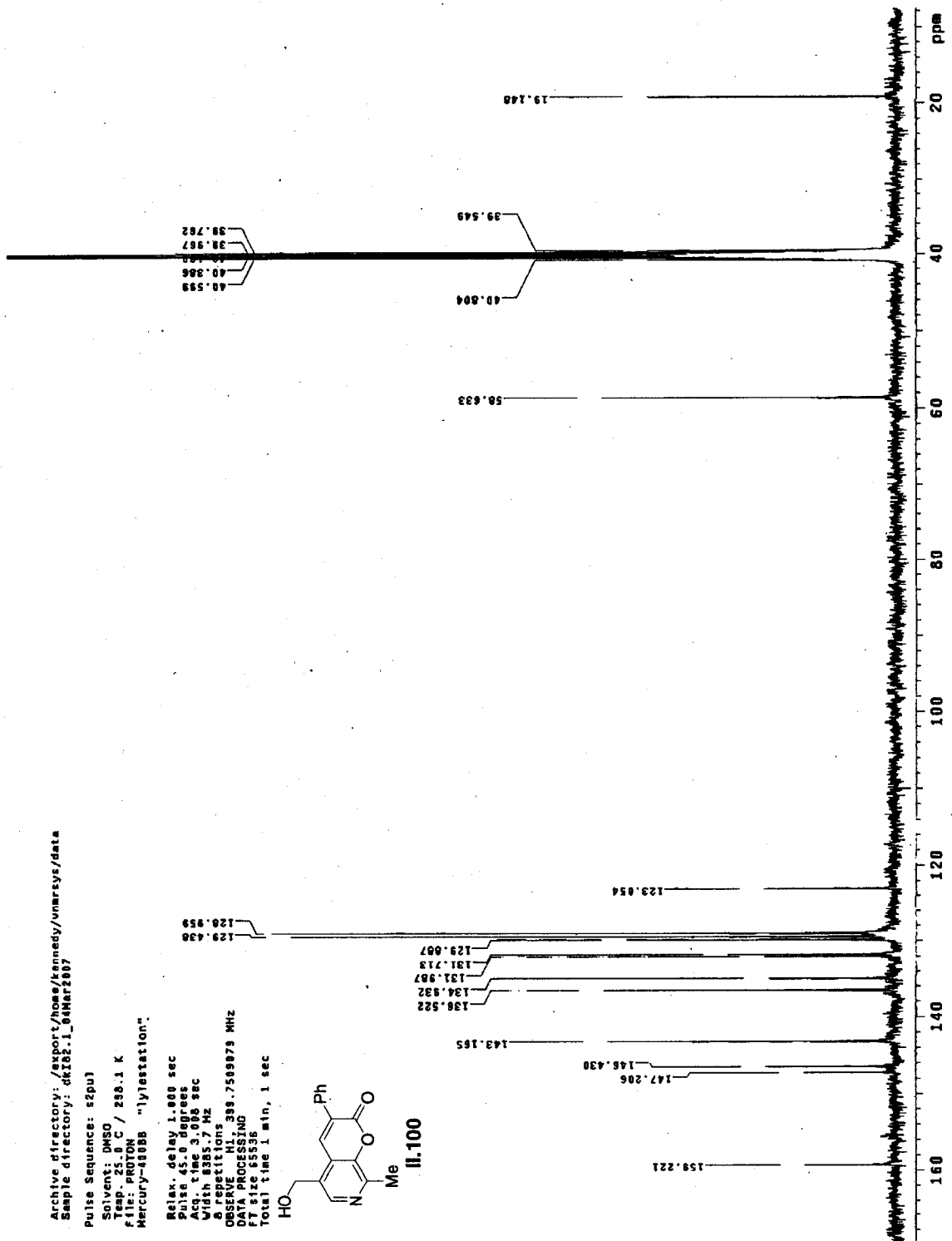
Archive directory: /export/home/kennedy/unarsys/data
Sample directory: dk182_1_04Mar2007

Pulse Sequence: szpul
Solvent: DMSO
Temp: 25.0 C / 298.1 K
File: PROTON
Mercury-400BB "lytstation"

Relax. delay 1.000 sec
Pulse 45.0 degrees
Acq. time 3.008 sec
Width 8000.7 Hz
Observer HJ
OBSERVE F1 398.759879 MHz
DATA PROCESSING
FT size 65536
Total time 1 min, 1 sec



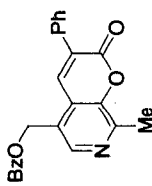
II.100



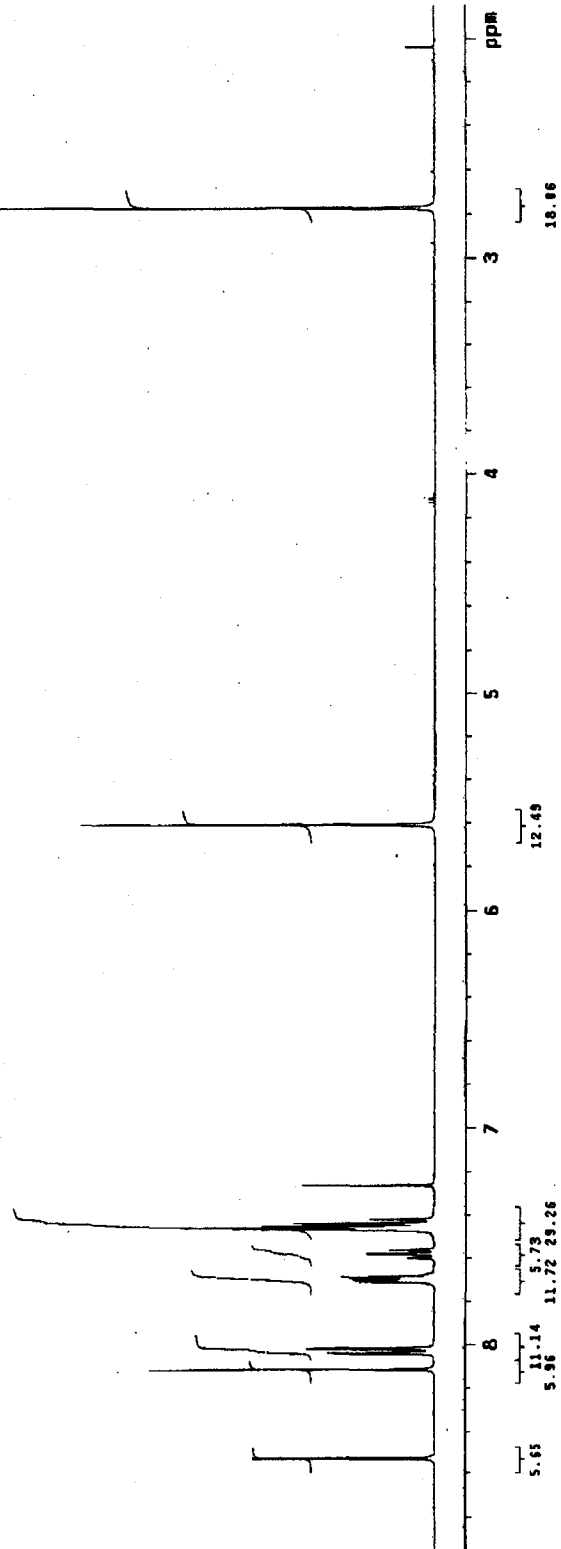
Archive directory: /export/home/kennedy/vnarsys/data
Sample directory: dki62_2_04Mar2007

Pulse Sequence: s2pul
Solvent: DMSO
Temp: 25.0 C / 298.1 K
File: CARBON
Mercury-400BBB "1j1astation"

Relax. delay 1.000 sec
Pulse 45.0 degrees
Acq. time 1.003 sec
Width 25062.7 Hz
1000 repetitions
OBSERVE C13, 100.5174278 MHz
DECOUPLE H1, 399.7528076 MHz
Power 41.0 dB
Continuously on
Waltz16
DATA PROCESSING
Line broadening 3.0 Hz
FT size 65536
Total time 35 min. 5 sec

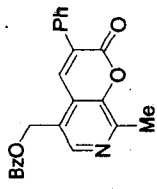


II.101

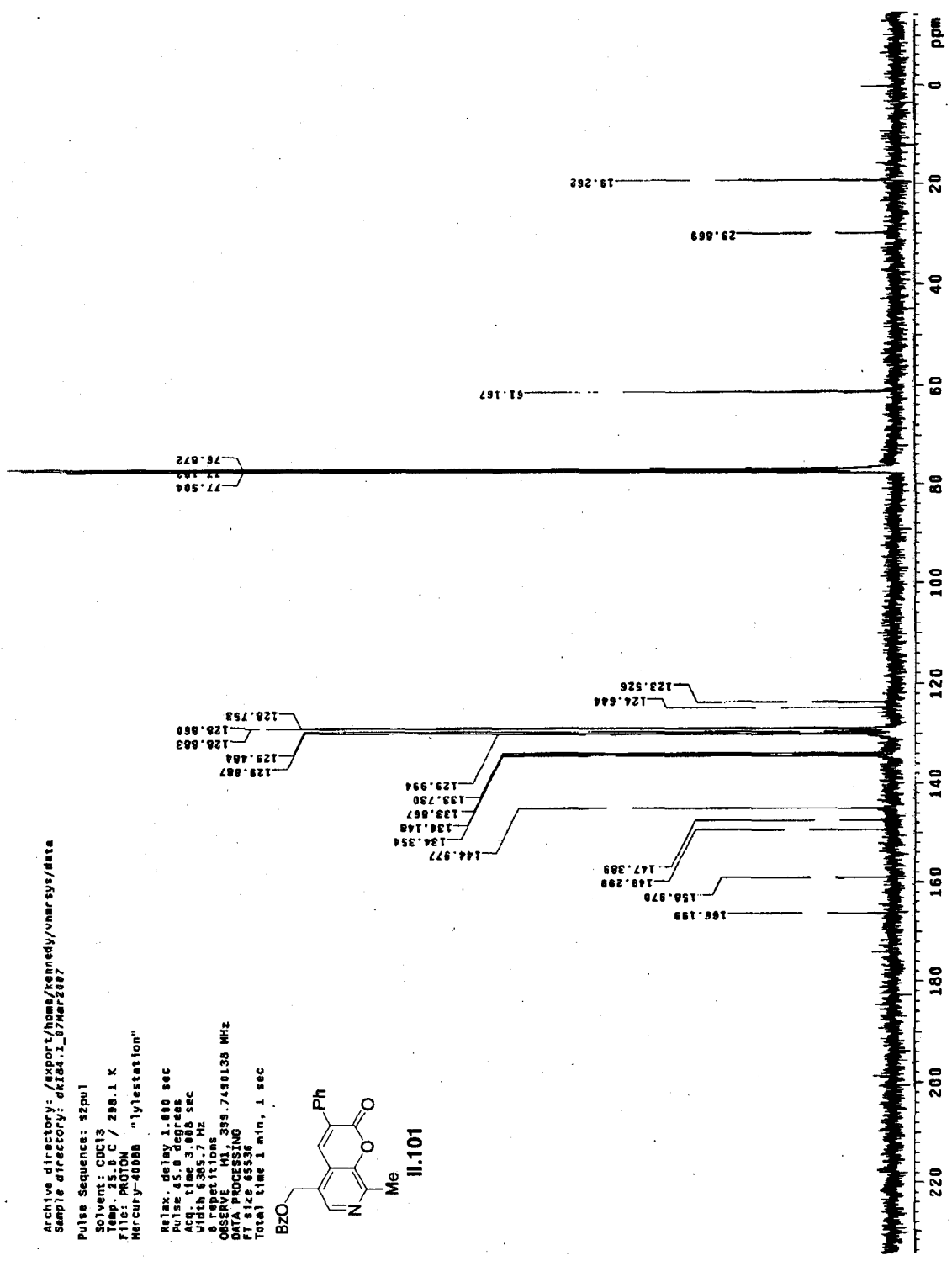


Archive directory: /export/home/kennedy/nmr/sus/data
 Sample directory: dk184_1_07Mar2007

Pulse Sequence: szpul
 Solvent: CDCl3
 Temp: 25.0 C / 298.1 K
 File: PROTON
 Mercury-40000 "lylestation"
 Relax. delay 1.000 sec
 Pulse 45.0 degrees
 Acq. time 3.000 sec
 Width 6385.7 Hz
 6 repetitions
 Observed 11350.7490138 MHz
 Observed 400.141990000 MHz
 File 4536
 Total time 1 min, 1 sec



II.101

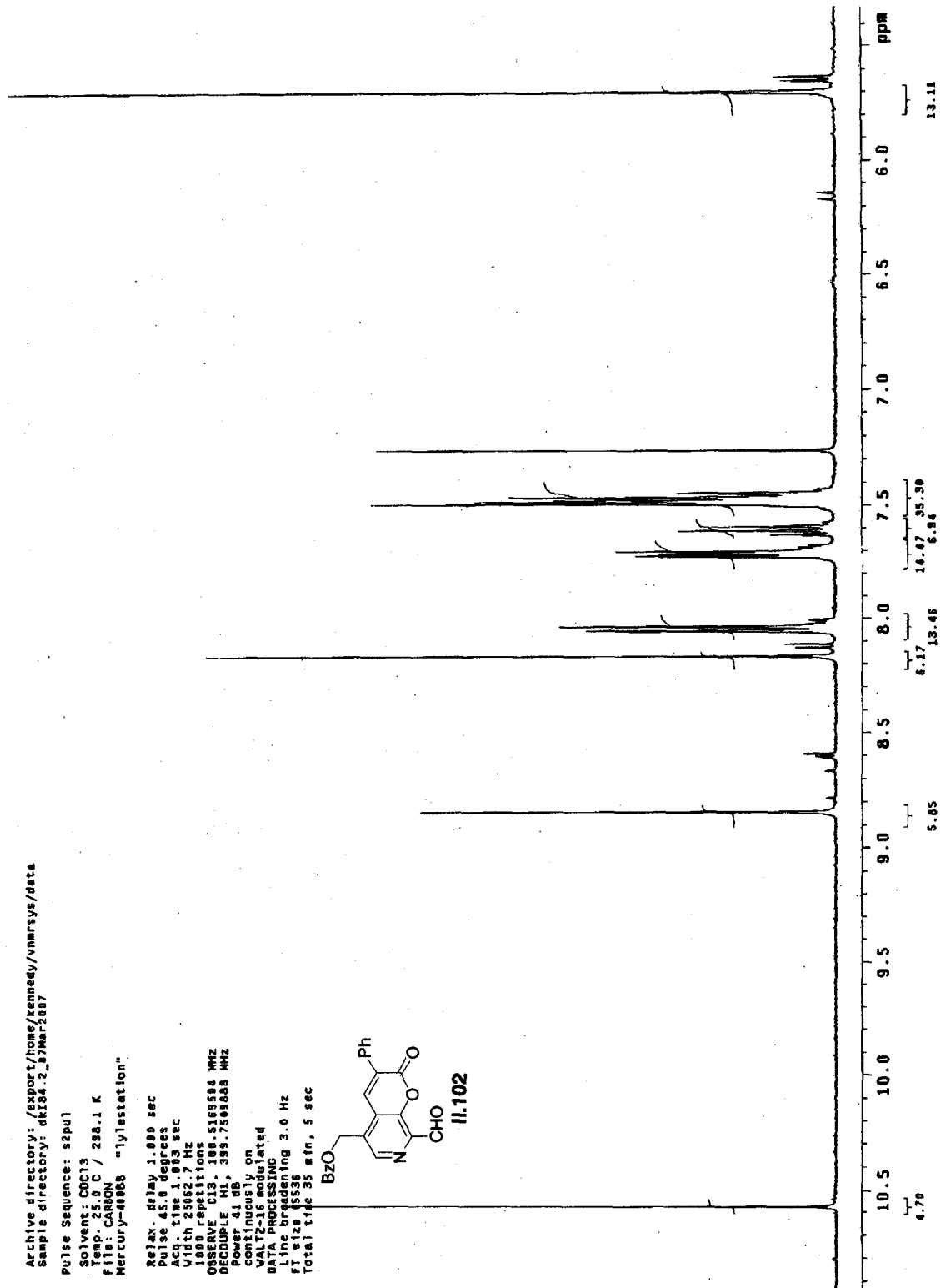
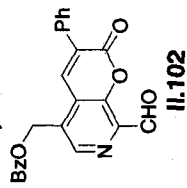


Archive directory: /export/home/kennedy/vmarsys/data
Sample directory: dki84_2_87Mar2007

Pulse Sequence: s2pul

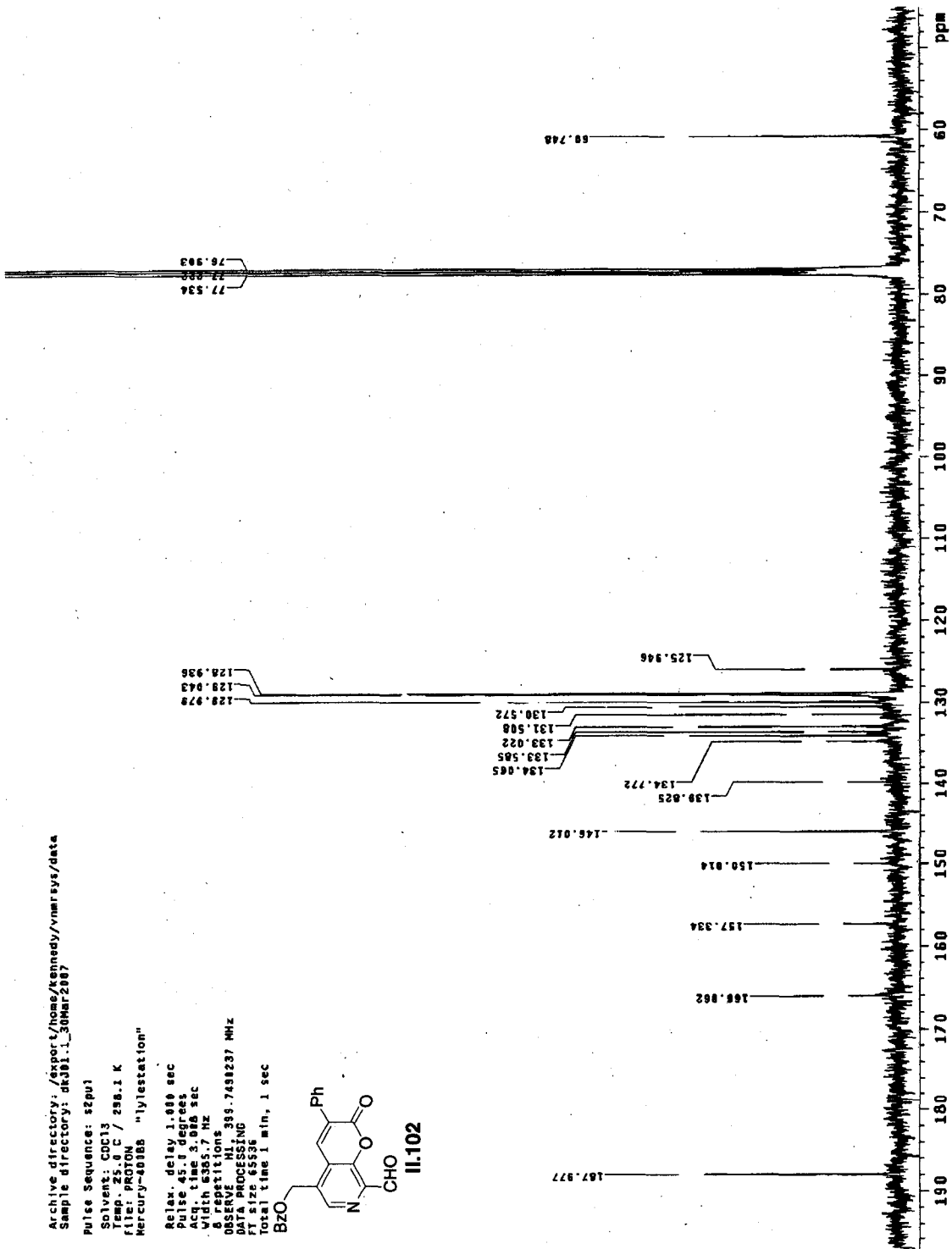
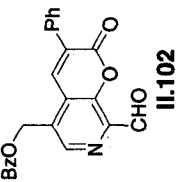
Solvent: CDCl3
Temp: 25.0 C / 298.1 K
File: CARON
Mercury-40006 "lylstaton"

Relax. delay 1.000 sec
Pulse 45.0 degrees
Acq. time 1.003 sec
Width 25062.7 Hz
1000 repetitions
OBSERVE CH, 100.6189584 MHz
DECODE CH, 399.7598888 MHz
Power 41 dB
continuously on
VOLTAGE modulated
DATA PROCESSING
Line broadening 3.0 Hz
FT size 45536
Total time 35 min, 5 sec



Archive directory: /snp/4/home/keaney/vnmrsvs/data
Sample directory: d5391_1_30mar2007

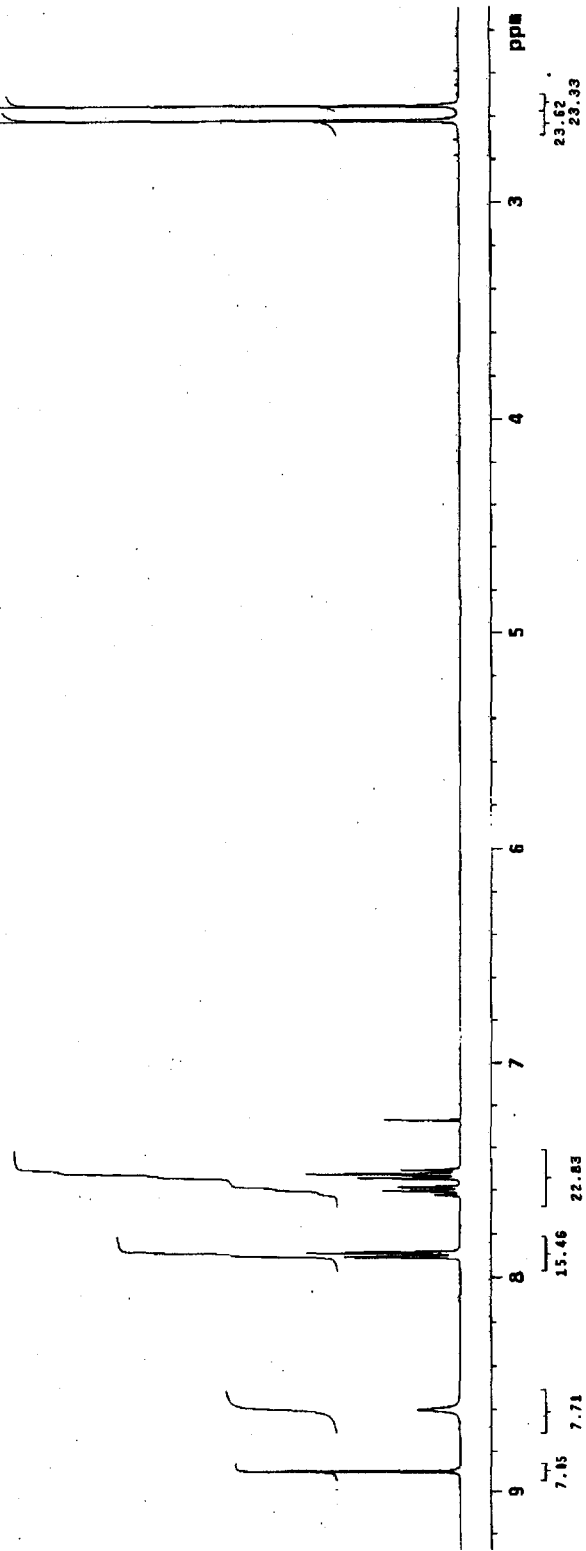
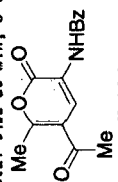
Pulse Sequence: s2pu1
Solvent: CDCl3
Temp: 25.0 C / 298.1 K
File: PROTON
Mercury-40188 "lylstation"
Relax. delay 1.000 sec
Pulse 45.0 degrees
Acq. time 3.000 sec
Width 6395.7 Hz
Spectrum 399.749237 MHz
6 repetitions
DATA PROCESSING
FT size 65536
Total time 1 min, 1 sec



Archive directory: /support/home/tenmedy/vmarsys/data
Sample directory: sf01.2_30Mar2007

Pulse Sequence: s2pu1
Solvent: CDCl3
Temp: 25.0 C / 298.1 K
File: CARBON
Mercury-40000 "lytestation"

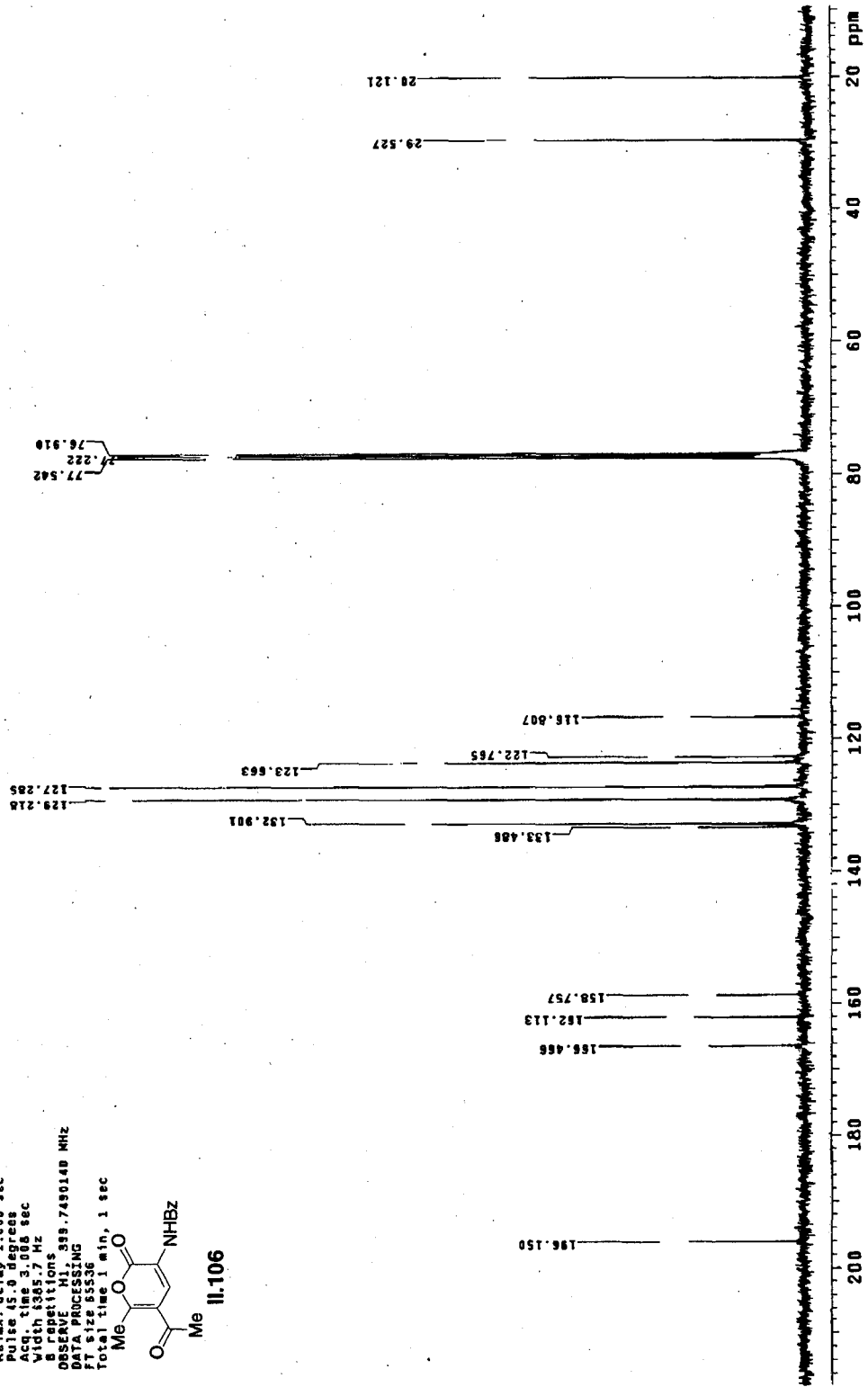
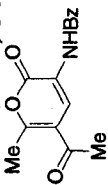
Relax. delay 1.000 sec
Pulse 45.0 degrees
Acq. time 1.003 sec
Sweep 23002.7 Hz
100% resolution
OBSERVE F13, 100.6189504 MHz
DECOUPLE H1, 399.7609866 MHz
Power 41.00
continuously on
WALTZ-16 modulated
DATA PROCESSING
Line broadening 3.0 Hz
F1 size 65536
Total time 35 min, 5 sec



Archive directory: /export/home/kennedy/vmrsys/data
 Sample directory: dkj15.1_28Apr2007

Pulse Sequence: s2pul
 Solvent: CDCl3
 Ambient temperature
 File: PROTON
 Mercury-40000 "lylstaton"

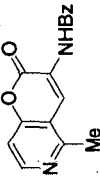
Relax. delay 1.000 sec
 Pulse 45.0 degree
 Acq. time 3.000 sec
 Width 1365.7 Hz
 8 repetitions
 OBSERVE: H1, 399.7490140 MHz
 DATA PROCESSING
 FI size 55536
 Total time 1 min, 1 sec



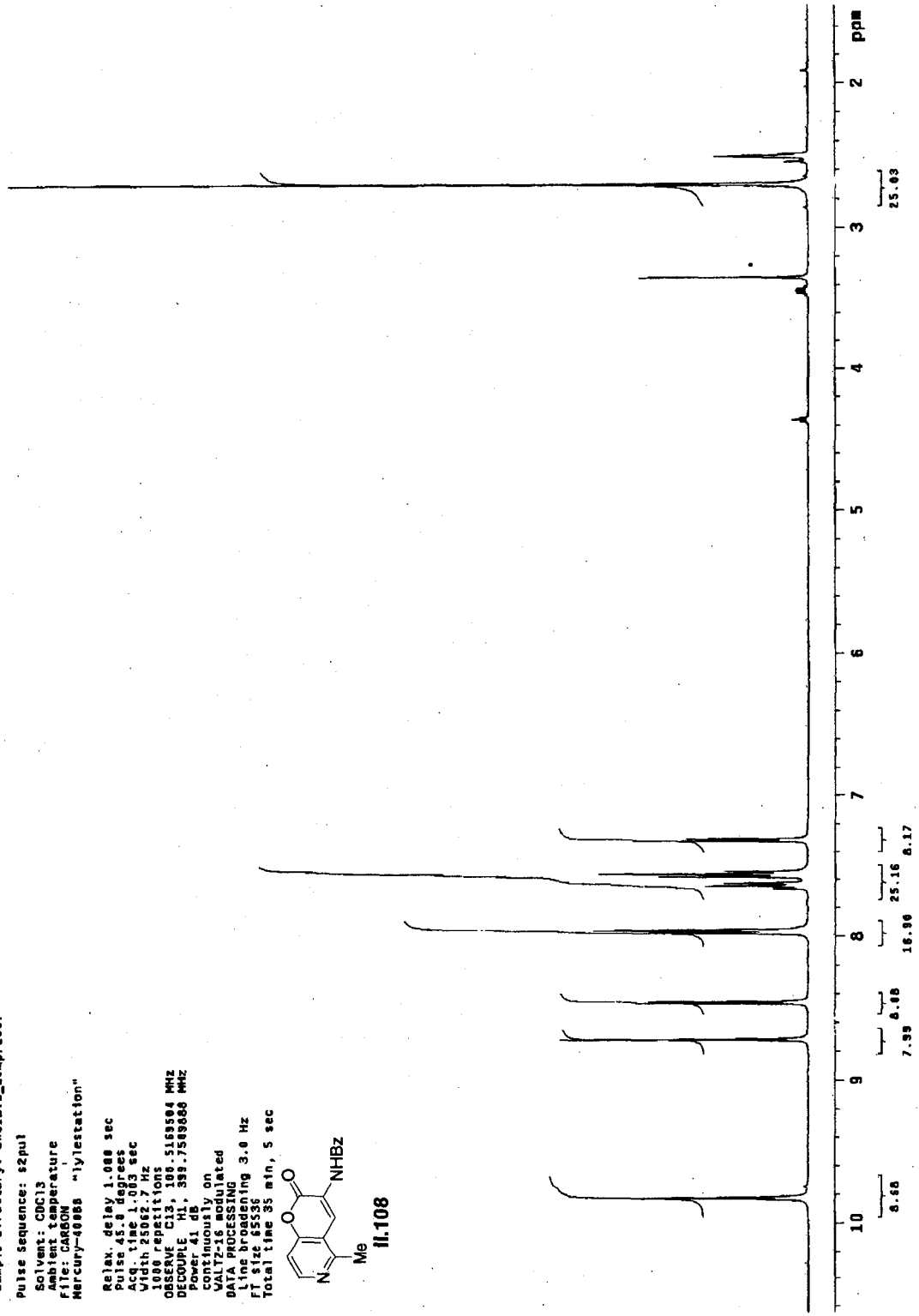
Archive directory: /export/home/kennedy/vmarsys/data
Sample directory: dk318_2_23Apr2007

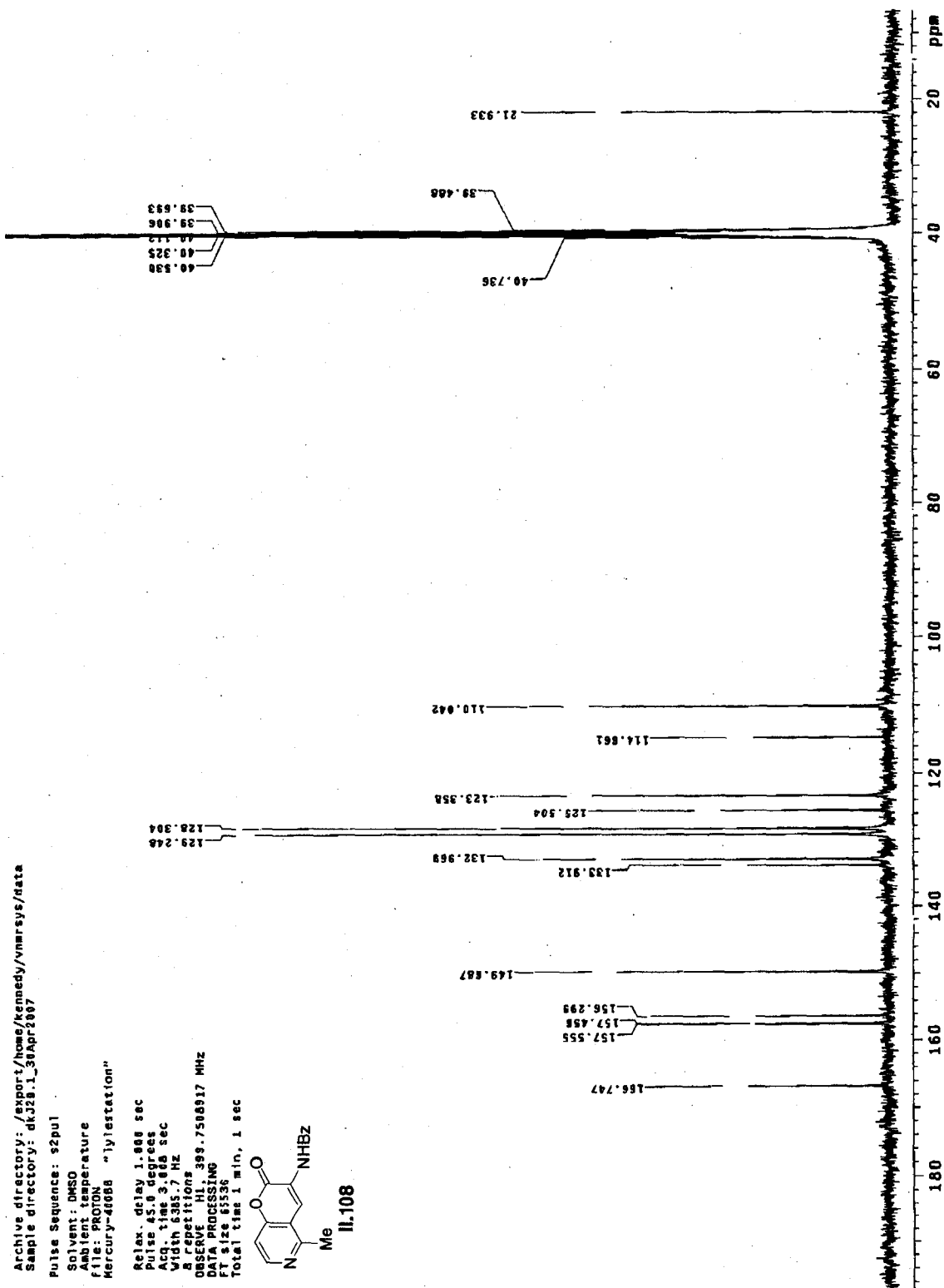
Pulse sequence: s2pul
Solvent: CDCl3
Ambient temperature
File: CARCON
Mercury-40000 "lylestation"

Relax. delay 1.000 sec
Pulse 45.8 degrees
Acq. time 1.083 sec
Width 25062.7 Hz
1000 repetitions
OBSERVE C13, 100.5169504 MHz
DECOUPLE H1, 339.7589666 MHz
continuously on
VOLTAGE-16 modulated
DATA PROCESSING
Line broadening 3.0 Hz
FT size 65536
Total time 35 min, 5 sec



II.108



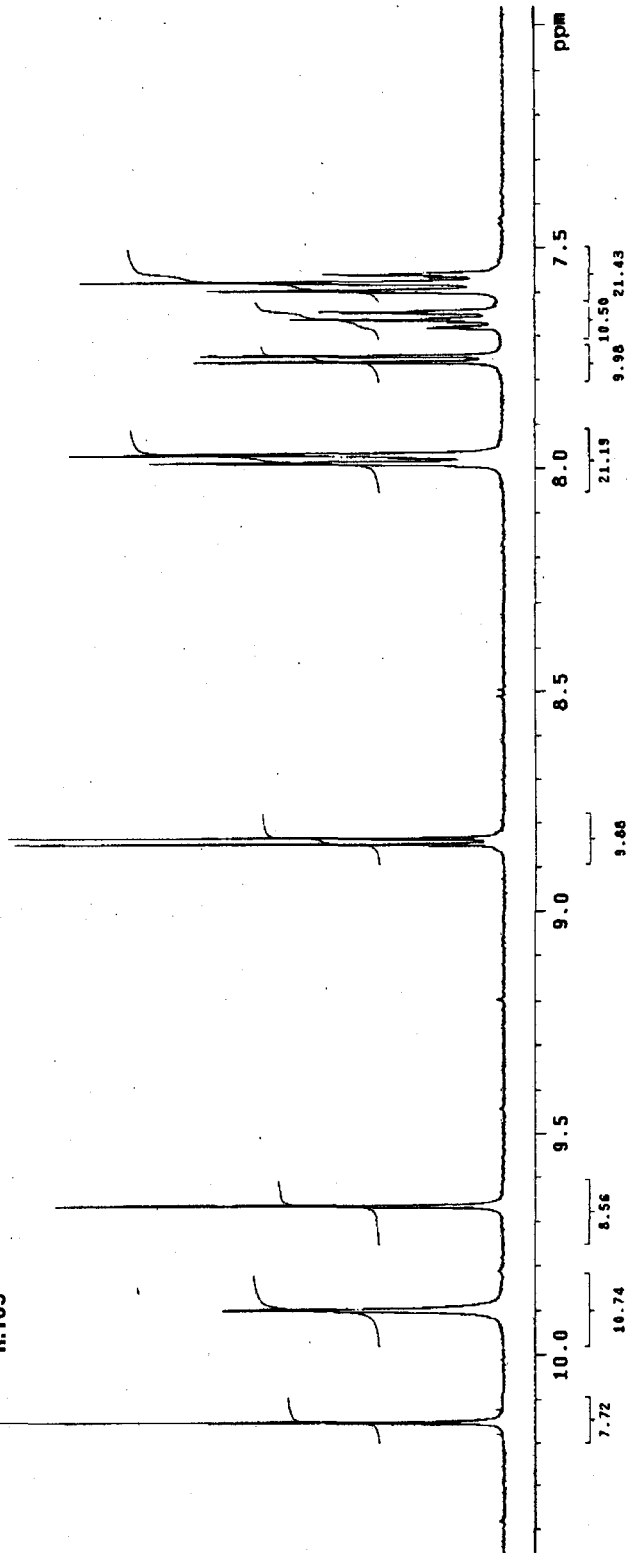
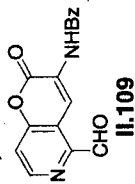


Archive directory: /export/home/kennedy/vnarsys/data
Sample directory: dk328.2_01May2187

Pulse Sequence: s2pul

Solvent: DMSO
Ambient temperature
File: CARBON
Mercury-48888 "lyletstation"

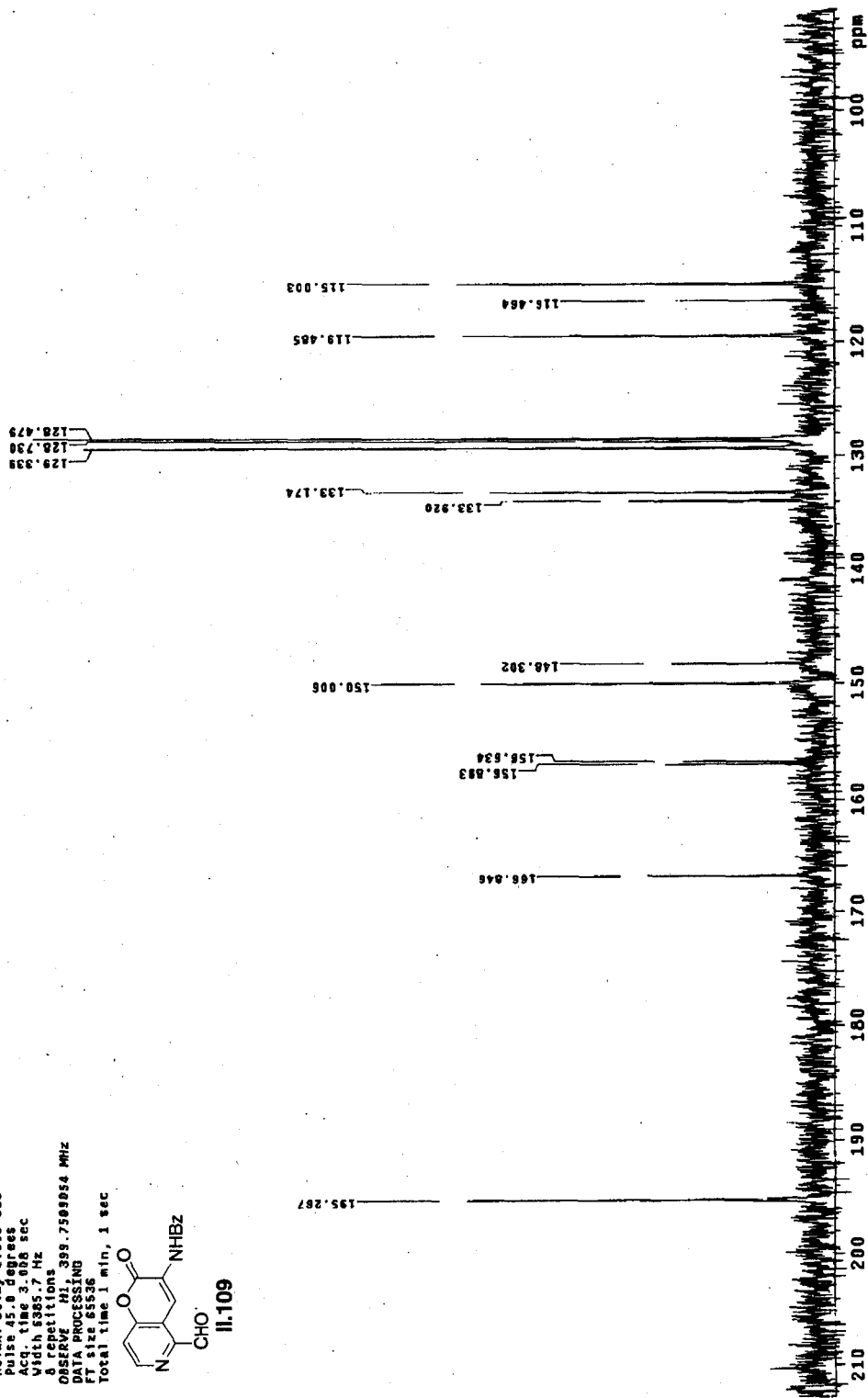
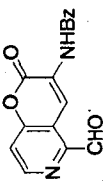
Relax. delay 1.888 sec
Pulse 45.0 degrees
Acq. time 1.083 sec
Width 25862.7 Hz
1000 repetitions
OBSERVE C13, 100.5174276 MHz
DECOUPLE H1, 399.7528876 MHz
Power 41 dB
continuously on
VOLT2-18 modulated
DATA PROCESSING
FI length 8535
FI size 8535
Total time 35 min, 5 sec



Archive directory: /export/hose/kennedy/vmarsys/data
 Sample directory: akj23.1_01May2007

Pulse Sequence: s2pul
 Solvent: DMSO
 Ambient temperature
 File: PROTON
 Mercury-400BB "lyltestation"

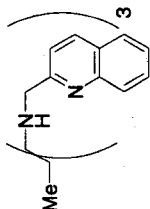
Relax. delay 1.000 sec
 Pulse 45.0 degrees
 Acq. time 3.000 sec
 Width 9985.7 Hz
 8 repetitions
 OBSERVE F1: 399.7509054 MHz
 DATA PROCESSING
 Total time 1 min, 1 sec



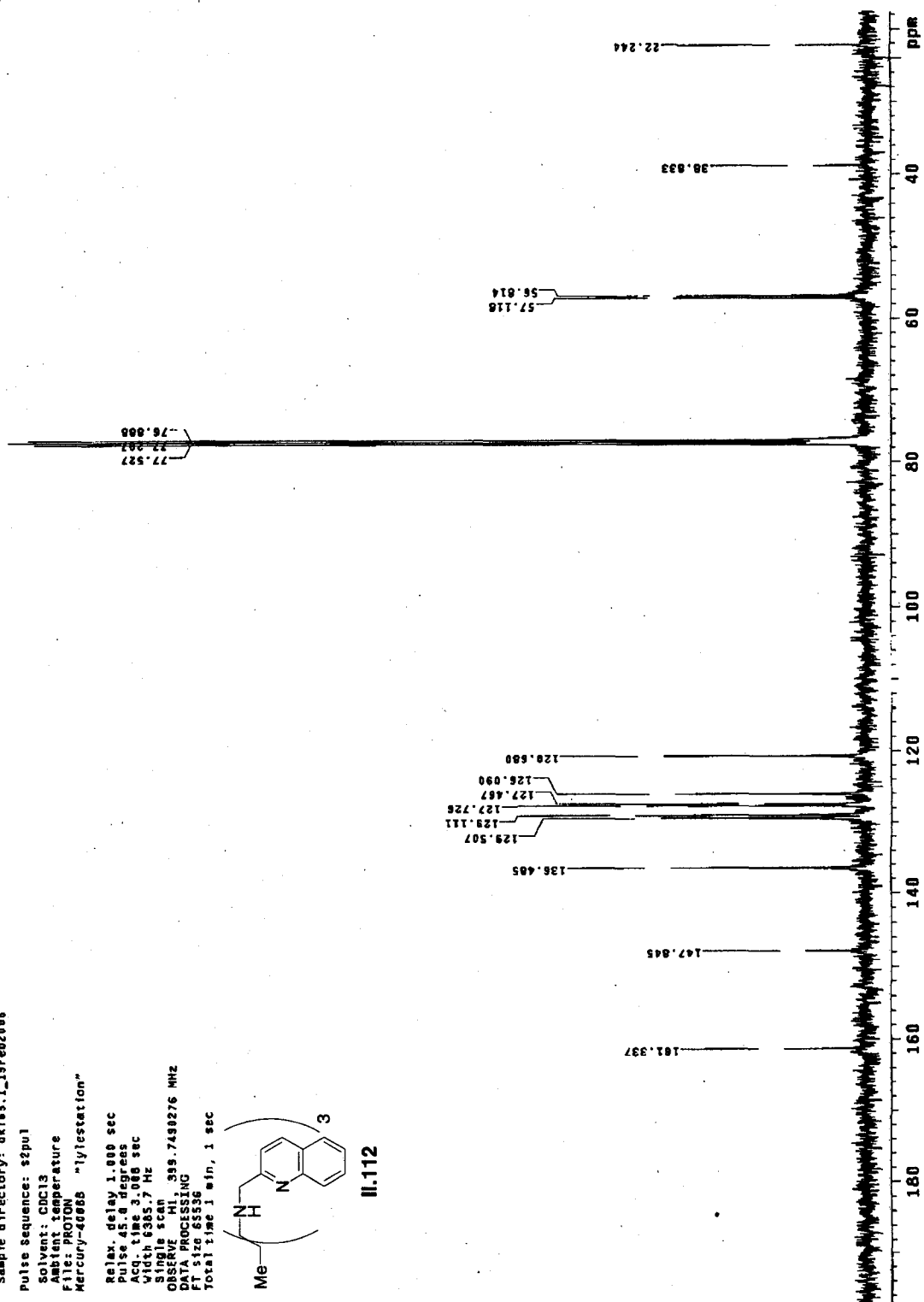
Archive directory: /export/home/kennedy/vnmrsys/data
Sample directory: dk185.1_19Feb2086

Pulse Sequence: s2pu1
Solvent: CDCl3
Ambient temperature
File: PROTON
Mercury-40888 "lytestation"

Relax. delay 1.000 sec
Pulse 45.0 degrees
Acq. time 3.086 sec
Width 6365.7 Hz
SINGLE scan
OBSERVE H1, 399.7490276 MHz
DATA PROCESSING
F1 size 85336
Total time 1 min, 1 sec



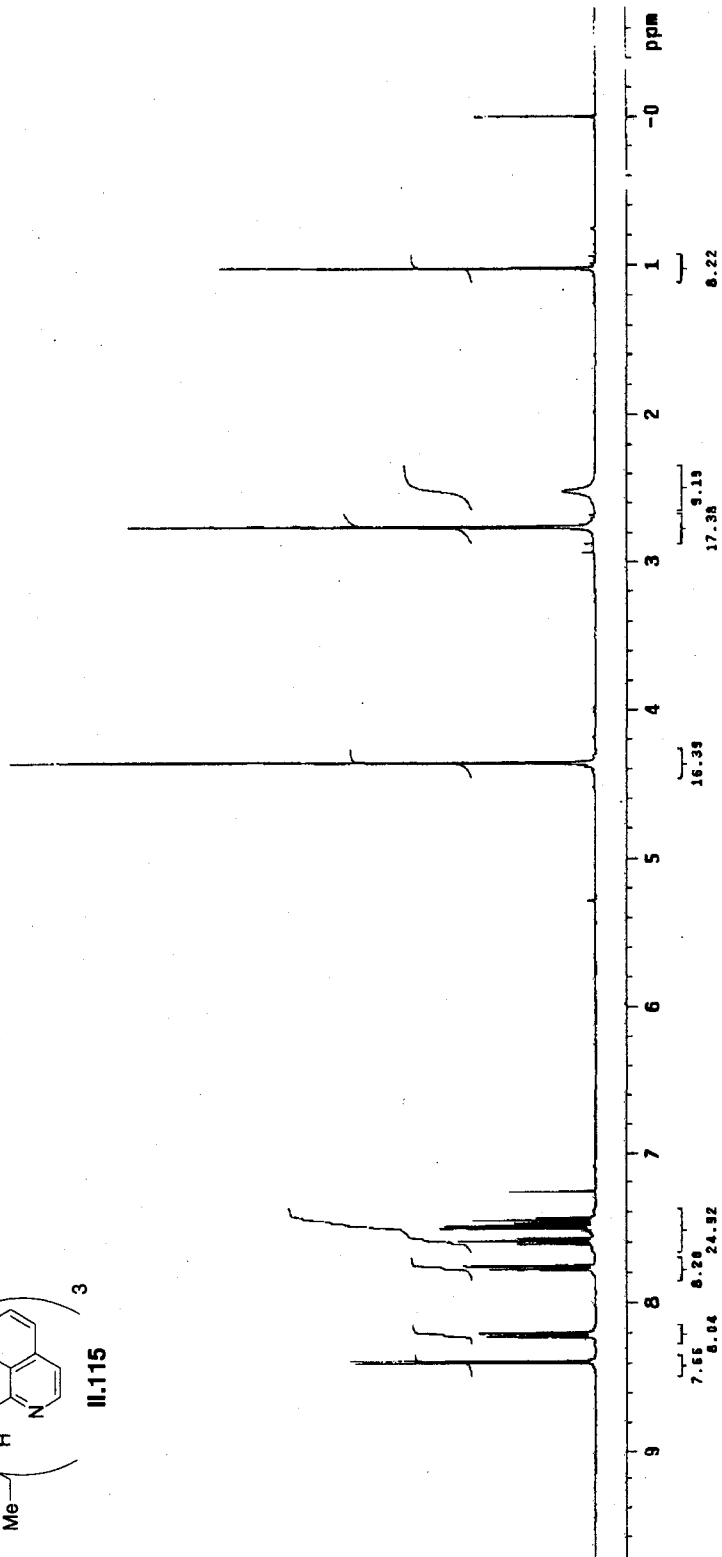
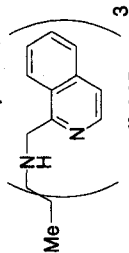
II.112



Archive directory: /export/home/kennedy/vnarsys/data
Sample directory: dkf65.2_18feb2866

Pulse Sequence: szpu1
Solvent: CDCl3
Ambient Temperature
File: CARION
Mercury-4000 "lylestation"

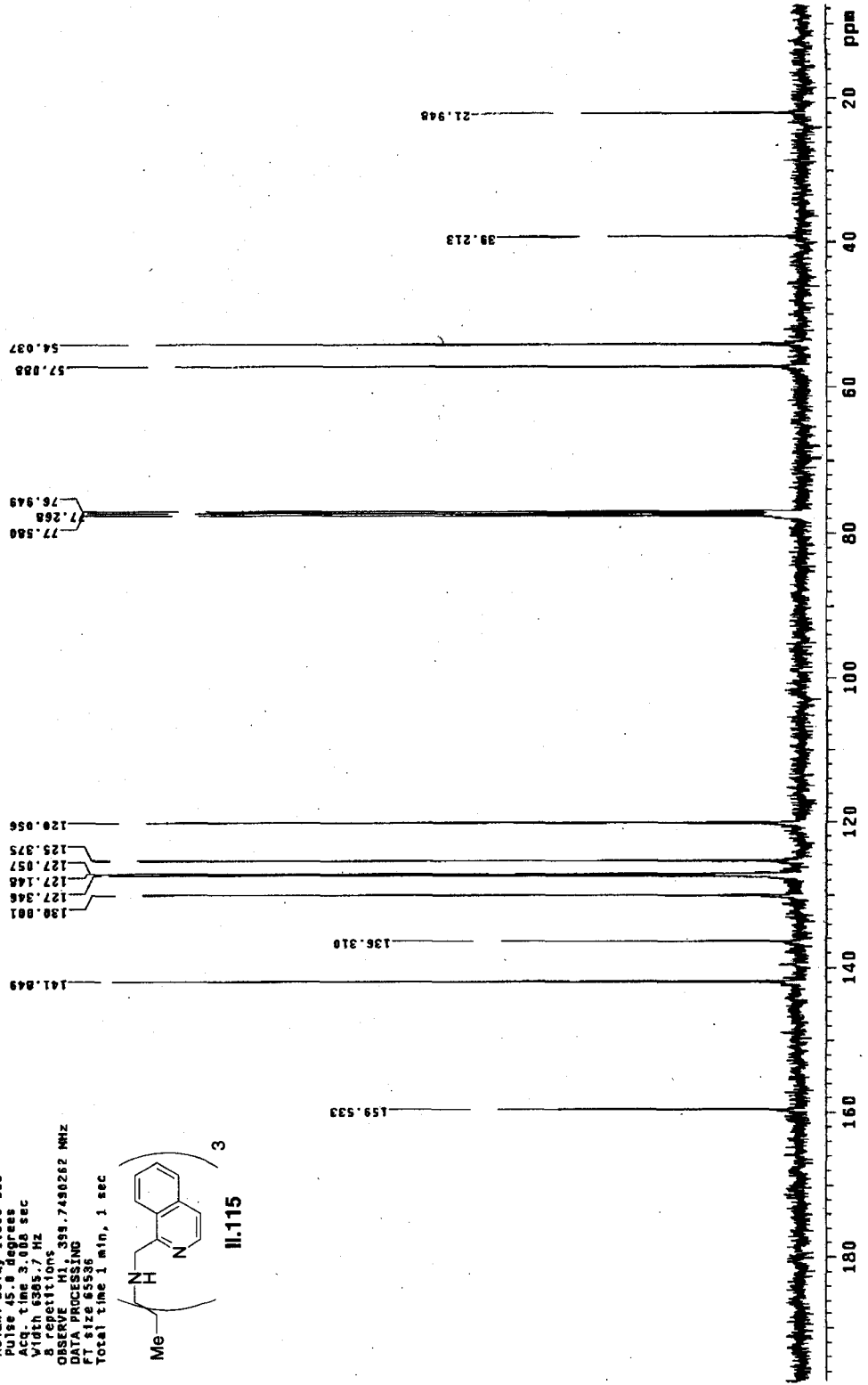
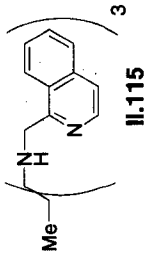
Relax. delay 1.000 sec
Pulse 45.0 degrees
Acq. time 1.003 sec
Width 25662.7 Hz
Siz 2048
Siz Repetitions
OBSERVE C13, 100.5163584 MHz
DECOUPLE H1, 399.7509886 MHz
Power 41 dB
Continuously on
Data processed
DATA PROCESSING
Line broadening 3.0 Hz
FT size 65536
Total time 18 min, 7 sec



Archive directory: /export/home/kennedy/vnmr/sys/data
Sample directory: dkg02.1_28Mar2006

Pulse Sequence: szpul
Solvent: CDCl3
Ambient temperature
File: PROTON
Mercury-400BB "lylestation"

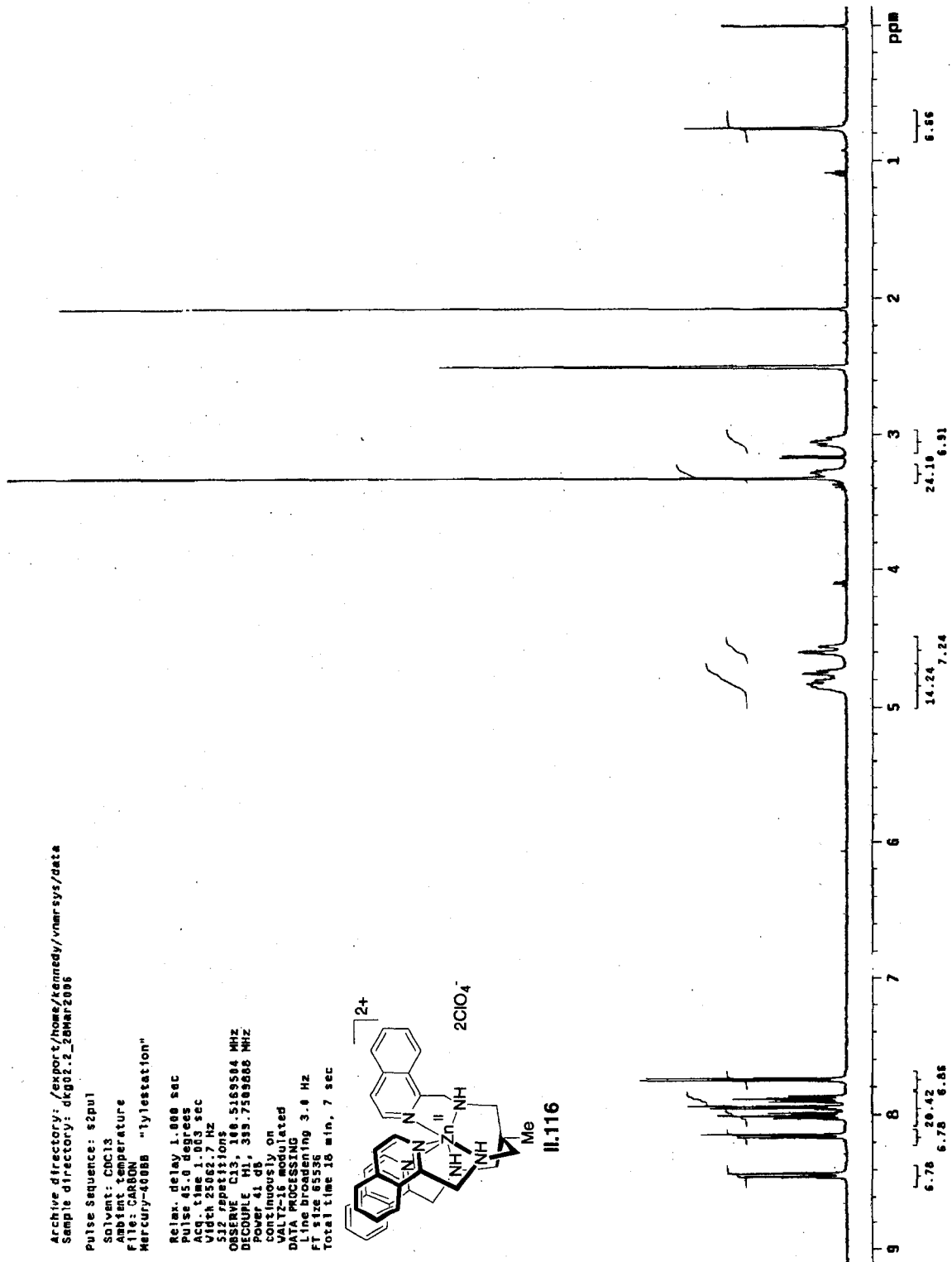
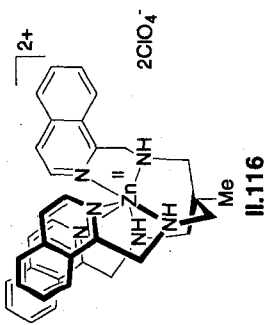
Relax. delay 1.000 sec
Pulse 45.9 degrees
Acq. time 3.000 sec
Width 6387.7 Hz
ORSECF 11.000 Hz 399.7490262 MHz
DATA PROCESSING
FT size 65536
Total time 1 min, 1 sec



Archive directory: /export/home/Kennedy/vnarsys/data
Sample directory: dkg02_2_28Mar2006

Pulse sequence: s2pu1
Solvent: CDCl3
Ambient temperature
File: CARBON
Mercury-400BB "tyltestation"

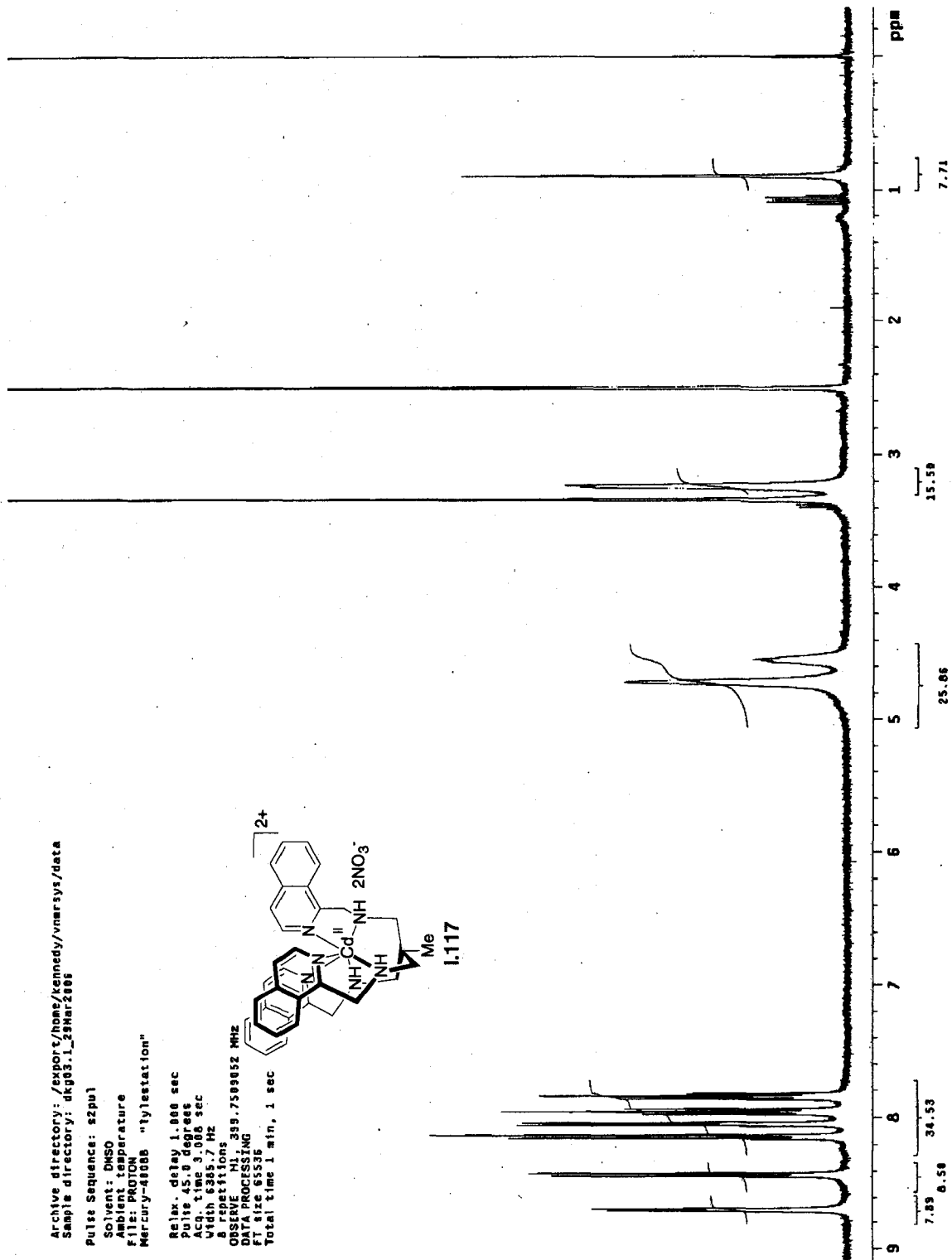
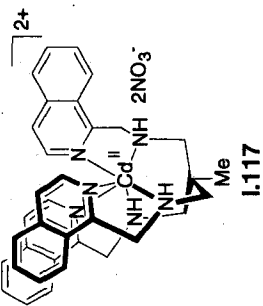
Relax. delay 1.000 sec
Pulse 45.0 degrees
Acq. time 1.063 sec
Width 25062.7 Hz
512 repetitions
OBSERVE C13, 100.5165504 MHz
DECOUPLE H1, 399.7509600 MHz
Power 41 dB
continuously on
VALZ-16 modulated
DATA PROCESSING
File processing 3.0 Hz
FT size 65536
Total time 18 min, 7 sec

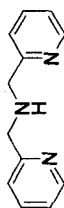


Archive directory: /export/home/kennedy/vnarsys/data
Sample directory: dkg03_1_29Mar2006

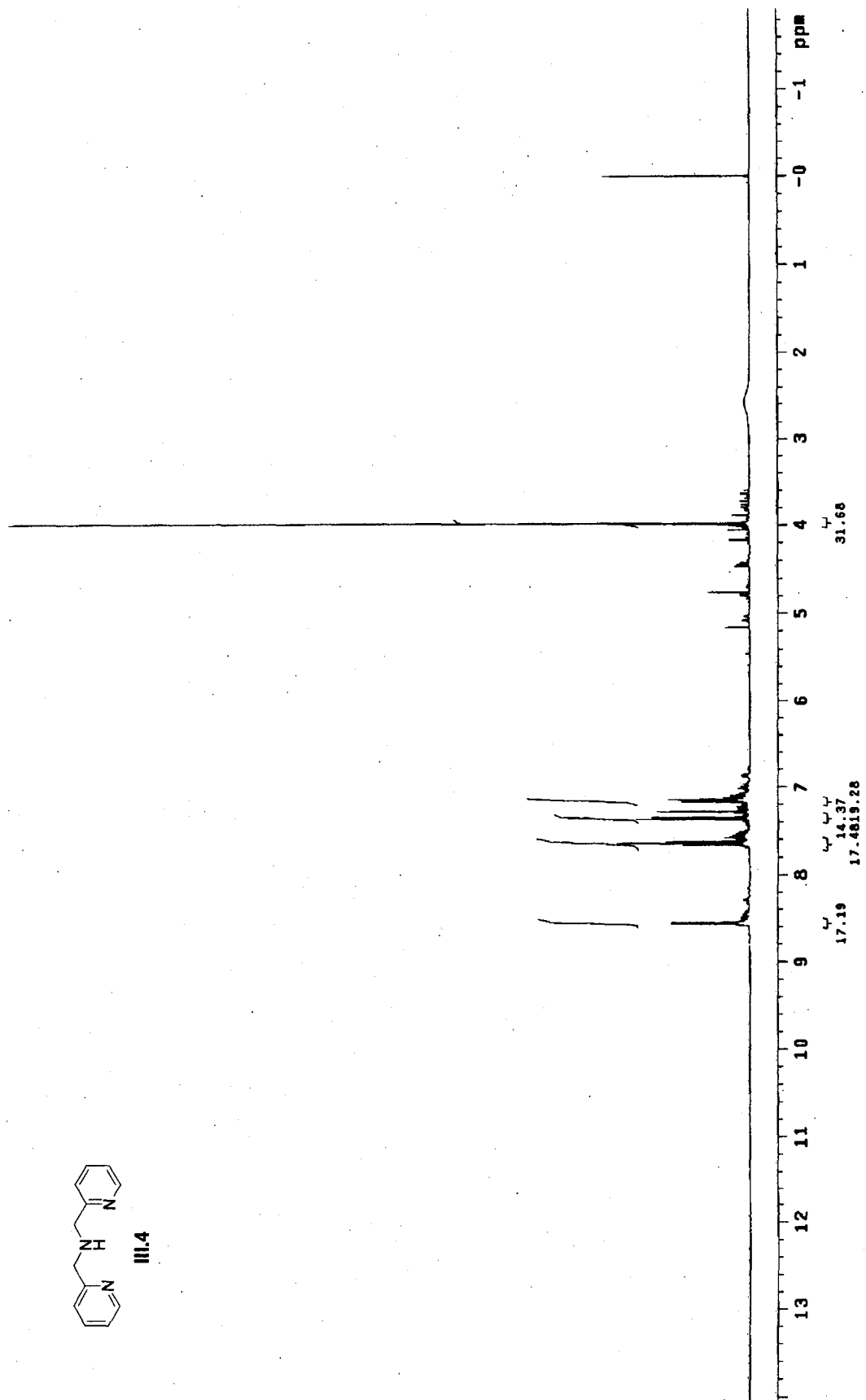
Pulse Sequence: szpul
Solvent: DMSO
Ambient temperature
File: PNOION
Mercury-4000B "tyltestatton"

Relax. delay 1.000 sec
Pulse 45.0 degrees
Width 6365.7 Hz
A repetitions
OBSERVE M1 399.7509032 MHz
DATA PROCESSING
FT size 65536
Total time 1 min, 1 sec





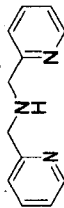
III.4



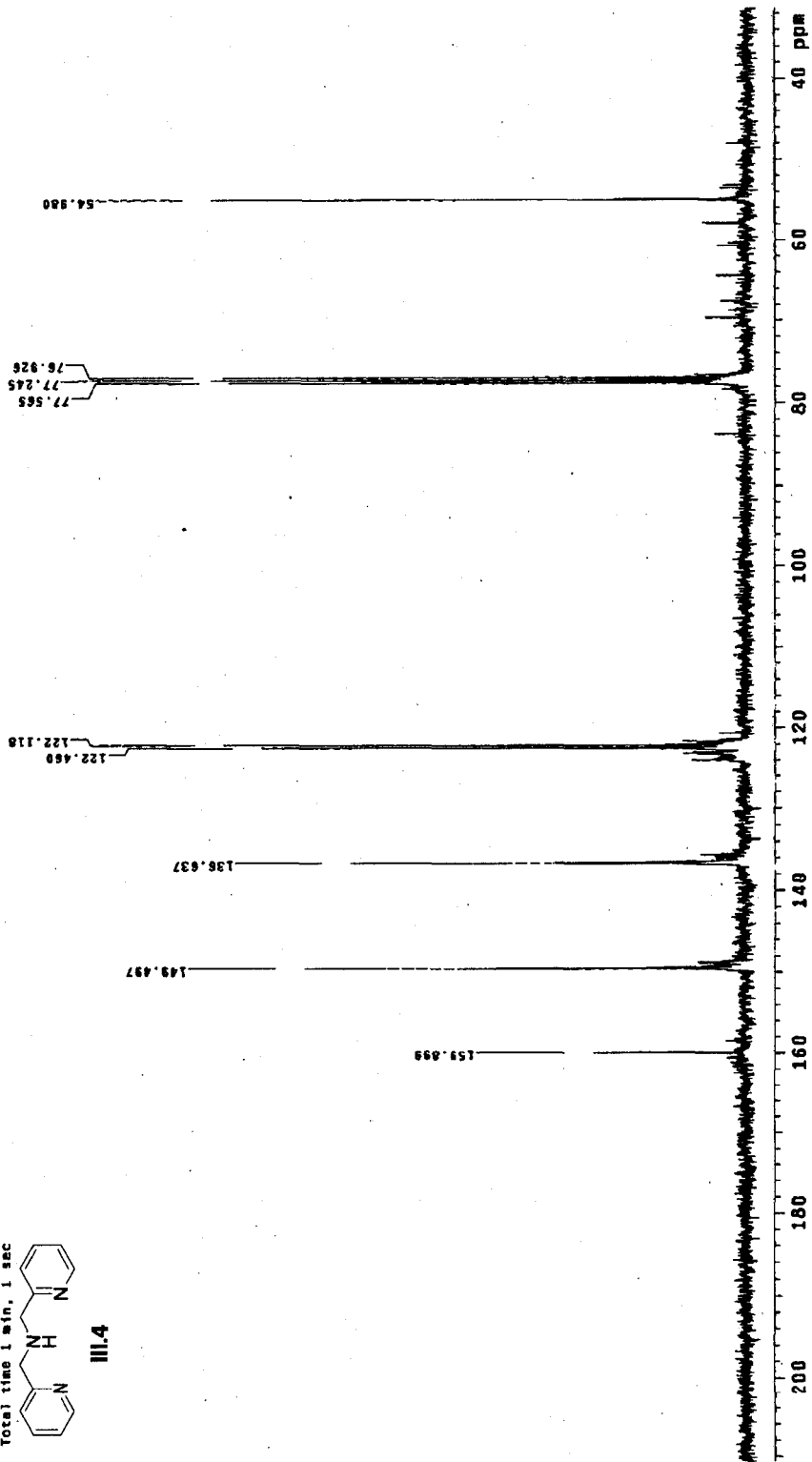
Archive directory: /export/home/kennedy/vmrsys/data
Sample directory: d864_1_130n266

Pulse sequence: s2pu1
Solvent: CDCl3
Ambient temperature
File: PROTON
Mercury-400BB "ylestation"

Relax delay 1.000 sec
Pulse AS 0 degrees
Acq. time 3.000 sec
Width 6385.7 Hz
8 repetitions
OBSERVE H1, 399.7490095 MHz
DATA PROCESSING
FT size 65536
Total time 1 min, 1 sec



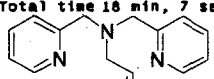
III.4



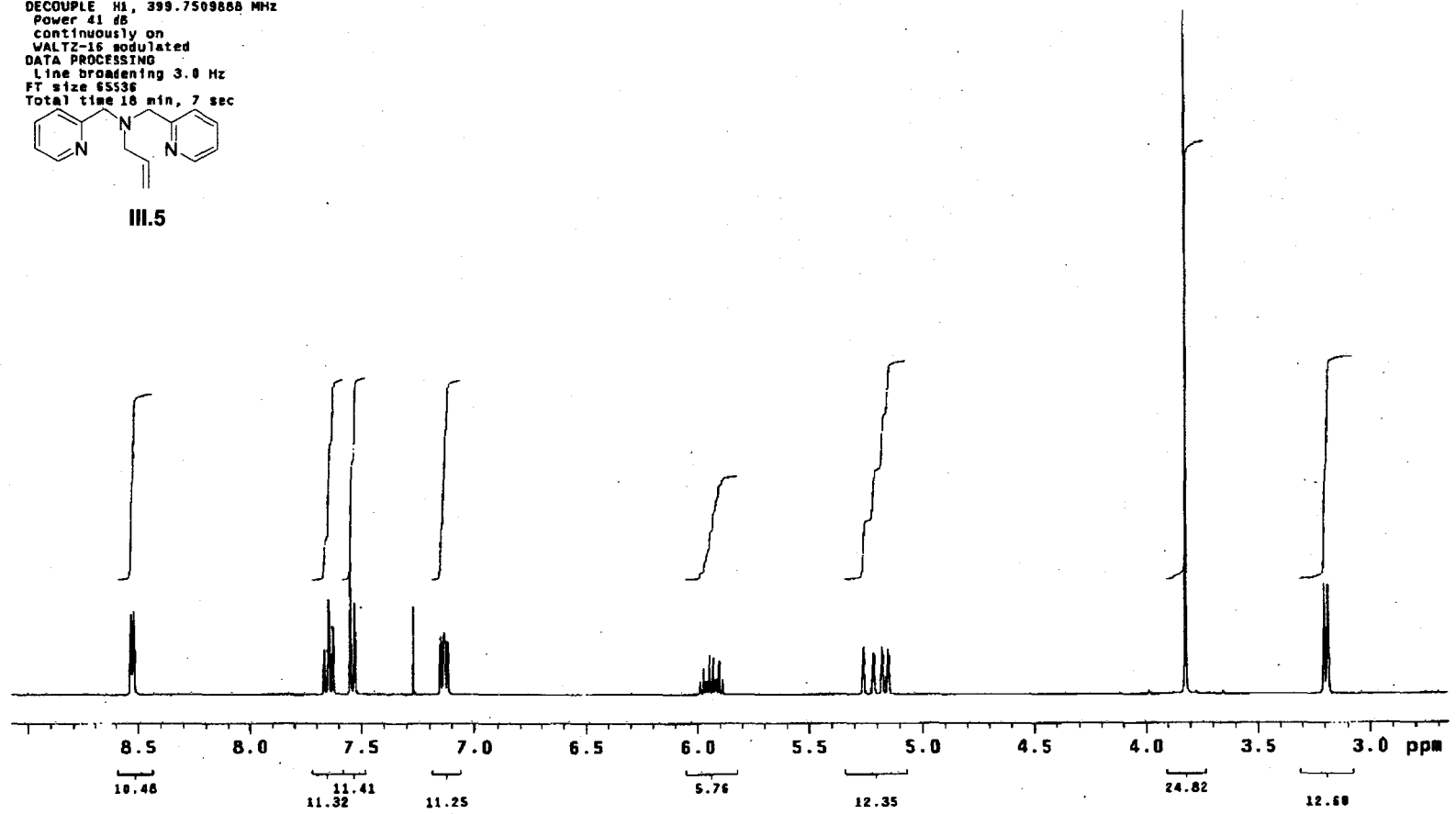
Archive directory: /export/home/kennedy/vnmrsys/data
Sample directory: dkg64.2_13Jun2006

Pulse Sequence: s2pu1
Solvent: CDCl3
Ambient temperature
File: CARBON
Mercury-400BB "lylestation"

Relax. delay 1.000 sec
Pulse 45.0 degrees
Acq. time 1.003 sec
Width 25062.7 Hz
512 repetitions
OBSERVE C13, 100.5169504 MHz
DECOUPLE H1, 399.7509868 MHz
Power 41 dB
continuously on
WALTZ-16 modulated
DATA PROCESSING
Line broadening 3.0 Hz
FT size 65536
Total time 16 min, 7 sec



III.5

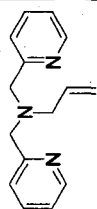


Archive directory: /export/home/tenney/vmarsys/data
Sample directory: dkg66_3_23Jun2006-21:32:34

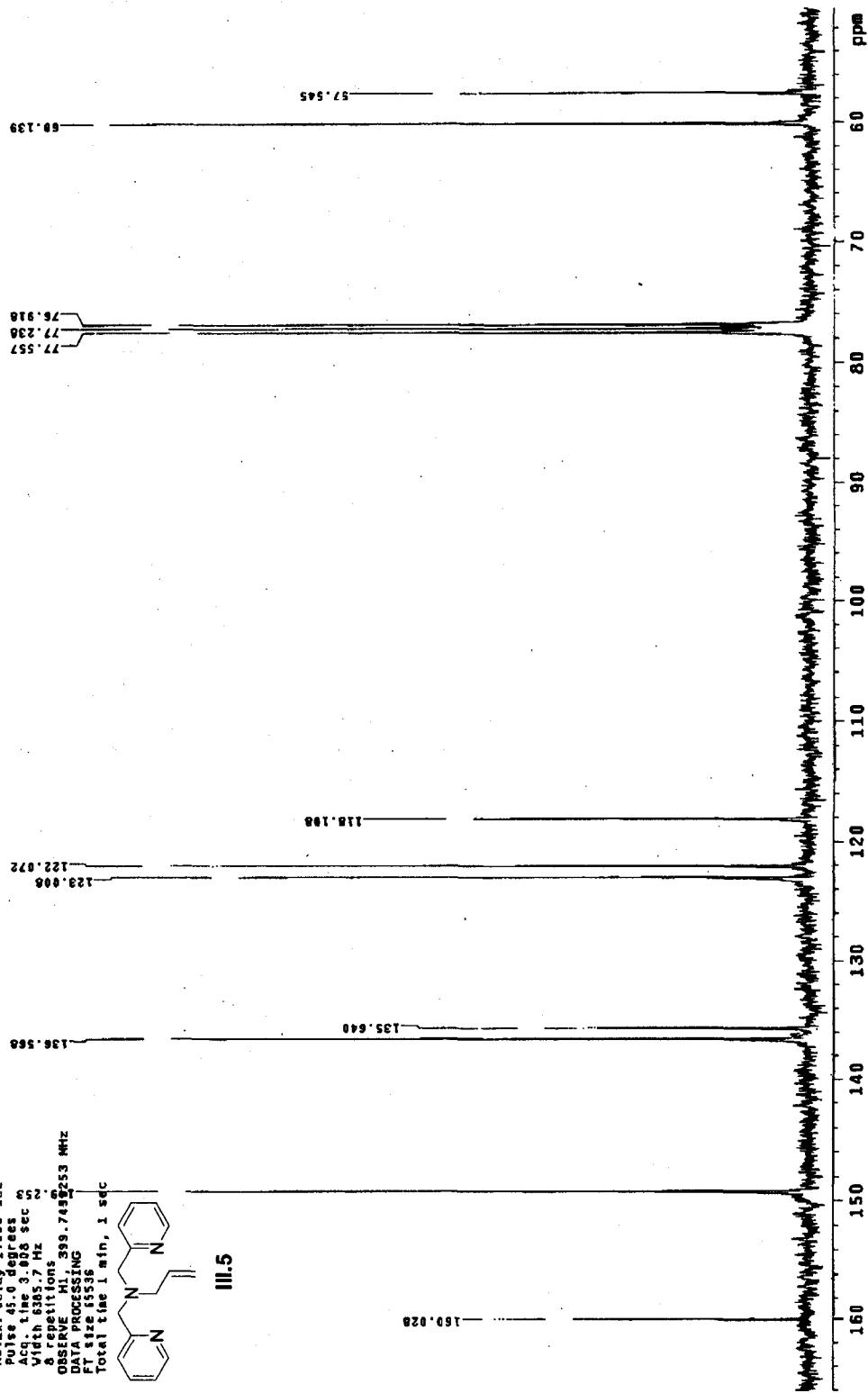
Pulse Sequence: s2pu1

Solvent: CDCl3
Temp: 25.8 C / 288.1 K
File: PROTON
Mercury-40488 "lytestation"

Relax. delay 1.680 sec
Pulse 45.0 degrees
Acq. time 3.906 sec
V1 pulse 7.00 Hz
A 4.00 Hz
OBSERVE H1 399.749253 MHz
DATA PROCESSING
FT size 65536
Total time 1 min, 1 sec



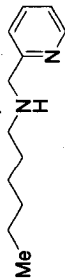
III.5



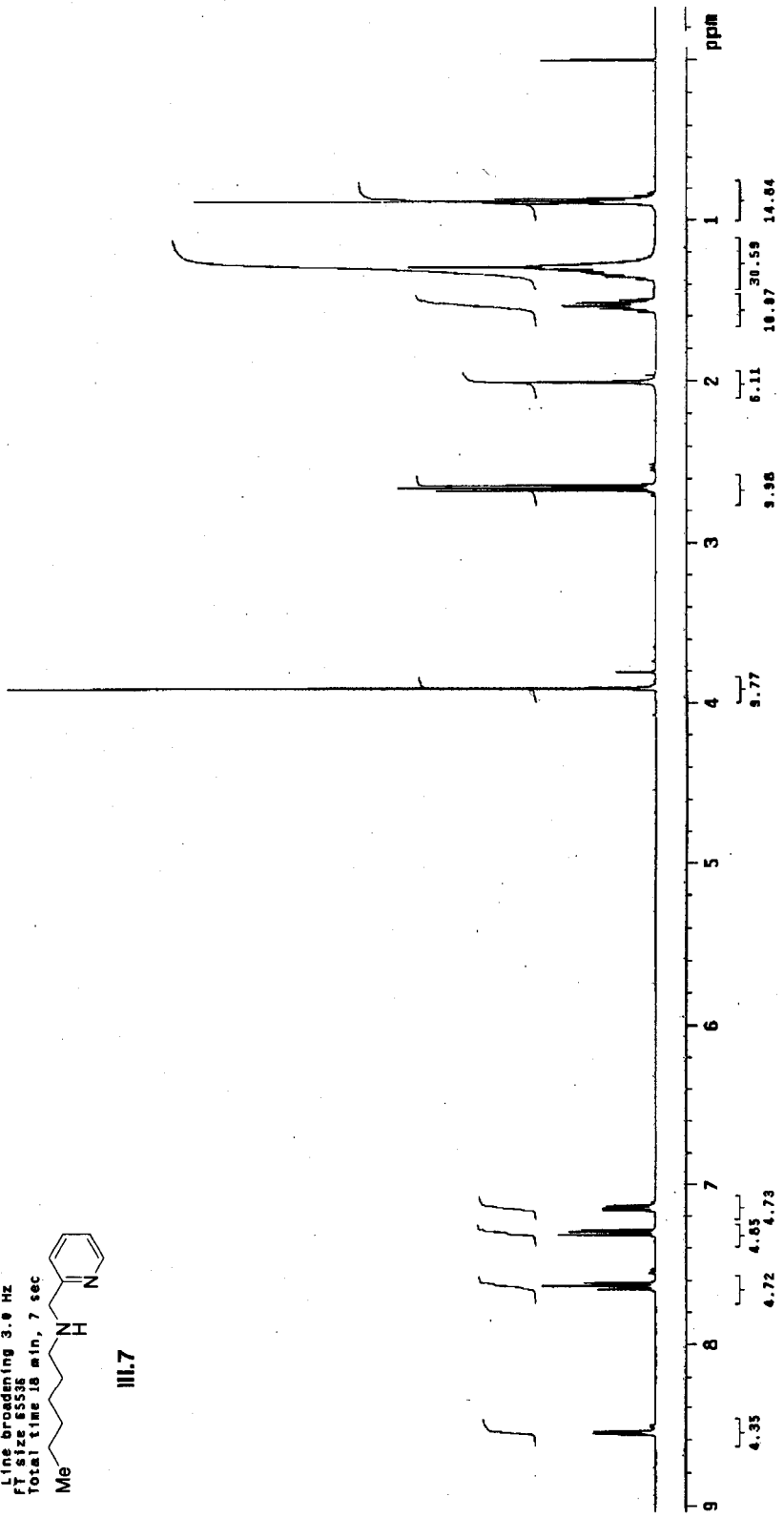
Archive directory: /export/home/kennedy/vnmrsys/data
Sample directory: dk96.3_230un2096

Pulse Sequence: e2pu1
Solvent: CDCl3
Temp: 25.0 C / 298.1 K
File: CARBON
Mercury-40088 "lylestation"

Relax. delay 1.000 sec
Pulse 45.0 degrees
Acq. time 1.003 sec
Width 25882.7 Hz
312 repetitions
OBSERVE CH1, 108.518566 MHz
PULSE CH1, 399.738888 MHz
continuously on
WALTZ-16 modulated
DATA PROCESSING
Line broadening 3.0 Hz
FT size 65536
Total time 18 min, 7 sec



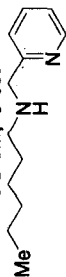
III.7



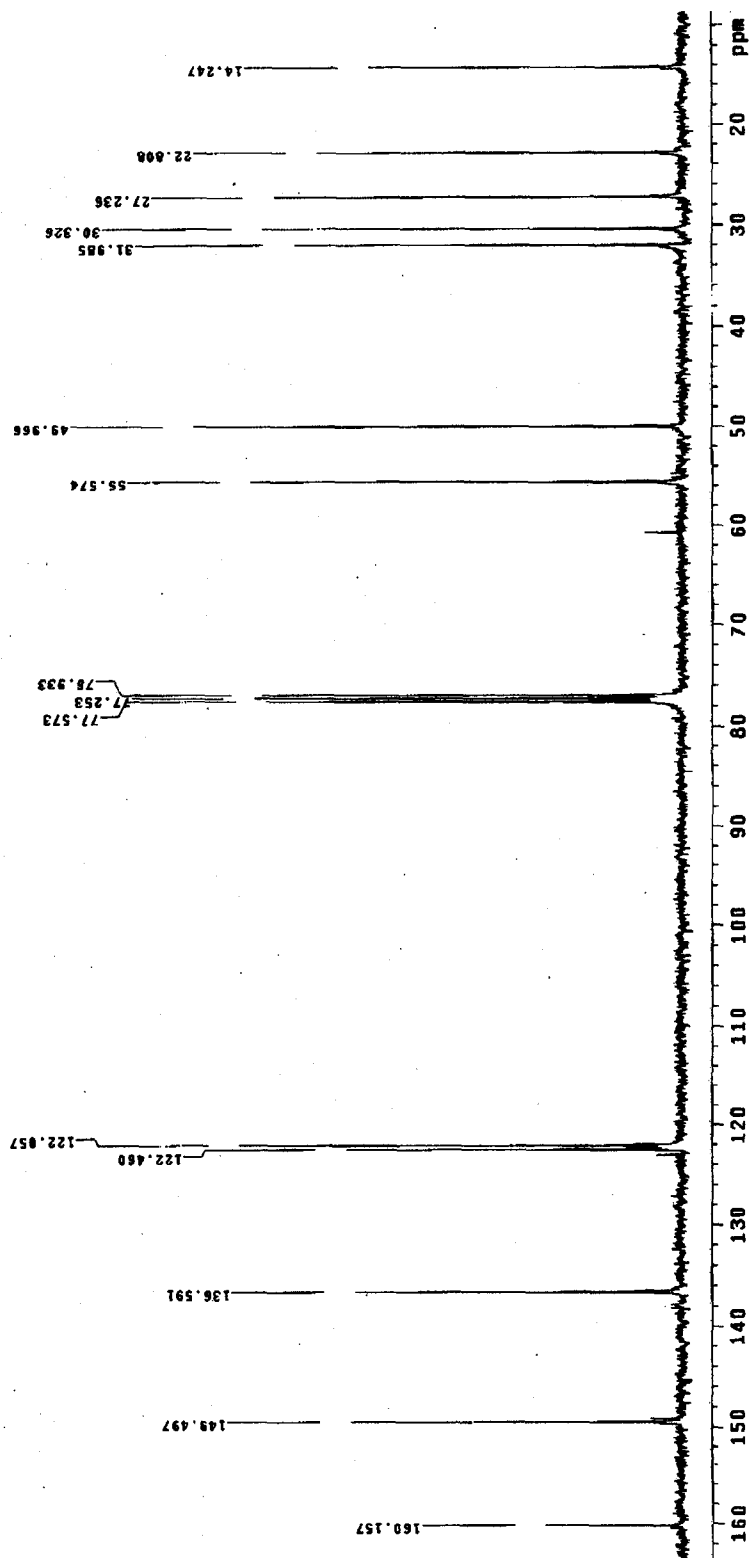
Archive directory: /export/home/kennedy/vmr/sys/data
Sample directory: dkq77_1_23jun2006

Pulse sequence: zgpg30
Solvent: CDCl3
Temp: 25.0 C / 298.1 K
File: PRDTON
Mercury-40086 "lylestation"

Relax. delay: 1.000 sec
Pulse: 9.000 sec
Acq. time: 3.000 sec
Width: 6305.7 Hz
S. Repetitions: 8
OBSERVE: H1, 399.7498192 MHz
DATA PROCESSING
FT size: 65536
Total time: 1 min, 1 sec



III.7



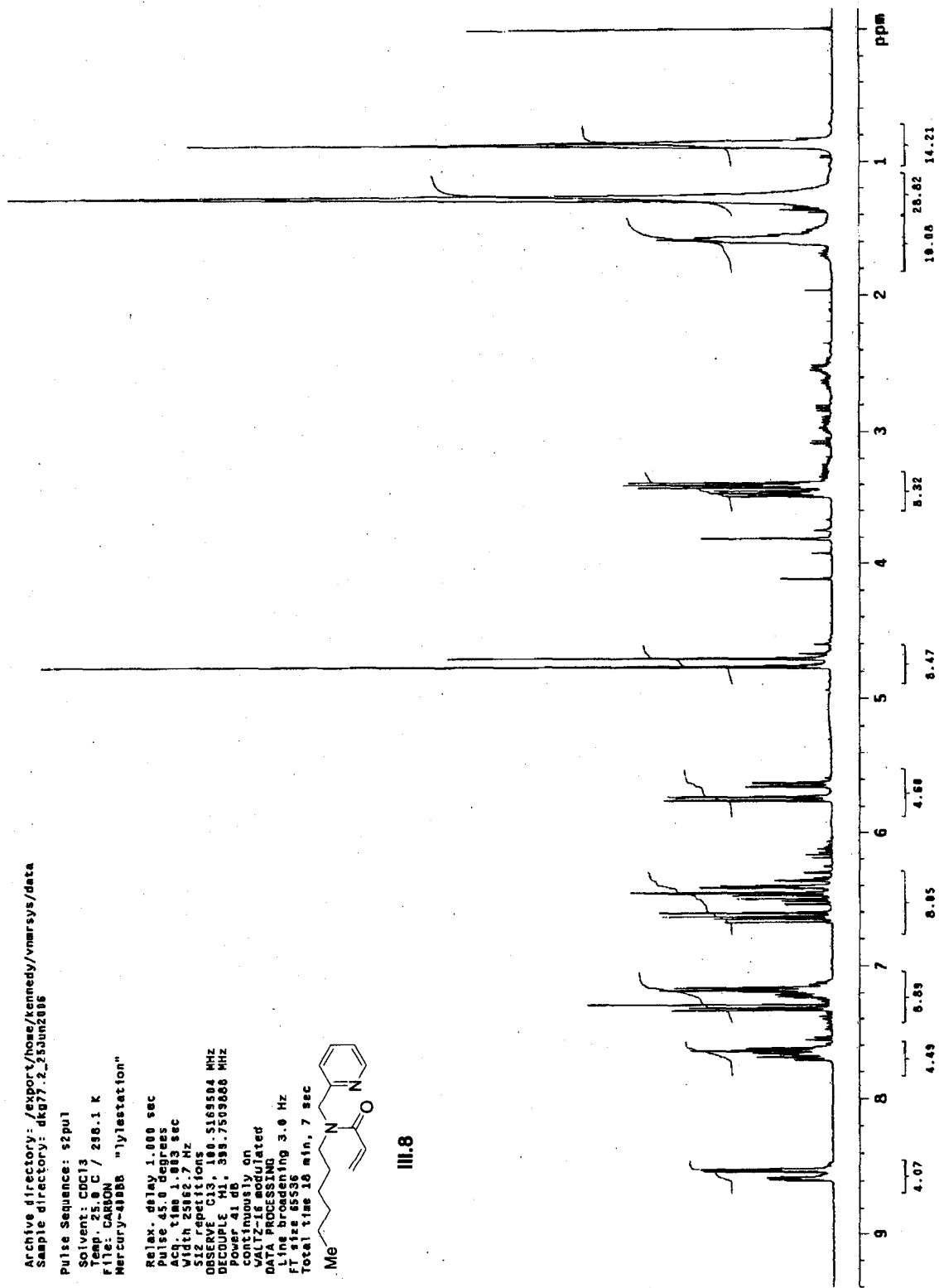
Archive directory: /export/rose/kennedy/vmrSYS/data
Sample directory: dk877_2_20unz886

Pulse Sequence: s2pul
Solvent: CDCl3
Temp: 25.0 C / 298.1 K
File: CARBON
Mercury-49888 "lylestation"

Relax. delay 1.000 sec
Pulse 45.0 degrees
Acq. time 1.883 sec
Width 25842.7 Hz
Z-Envelope 1.000000
OBSERVE C13 50.169504 MHz
DECUPLE H1 398.750366 MHz
Power 41 dB
continuously on
WALTZ-16 modulated
DATA PROCESSING
Line broadening 3.0 Hz
FT size 65536
Total time 18 min, 7 sec



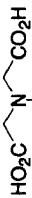
III.8



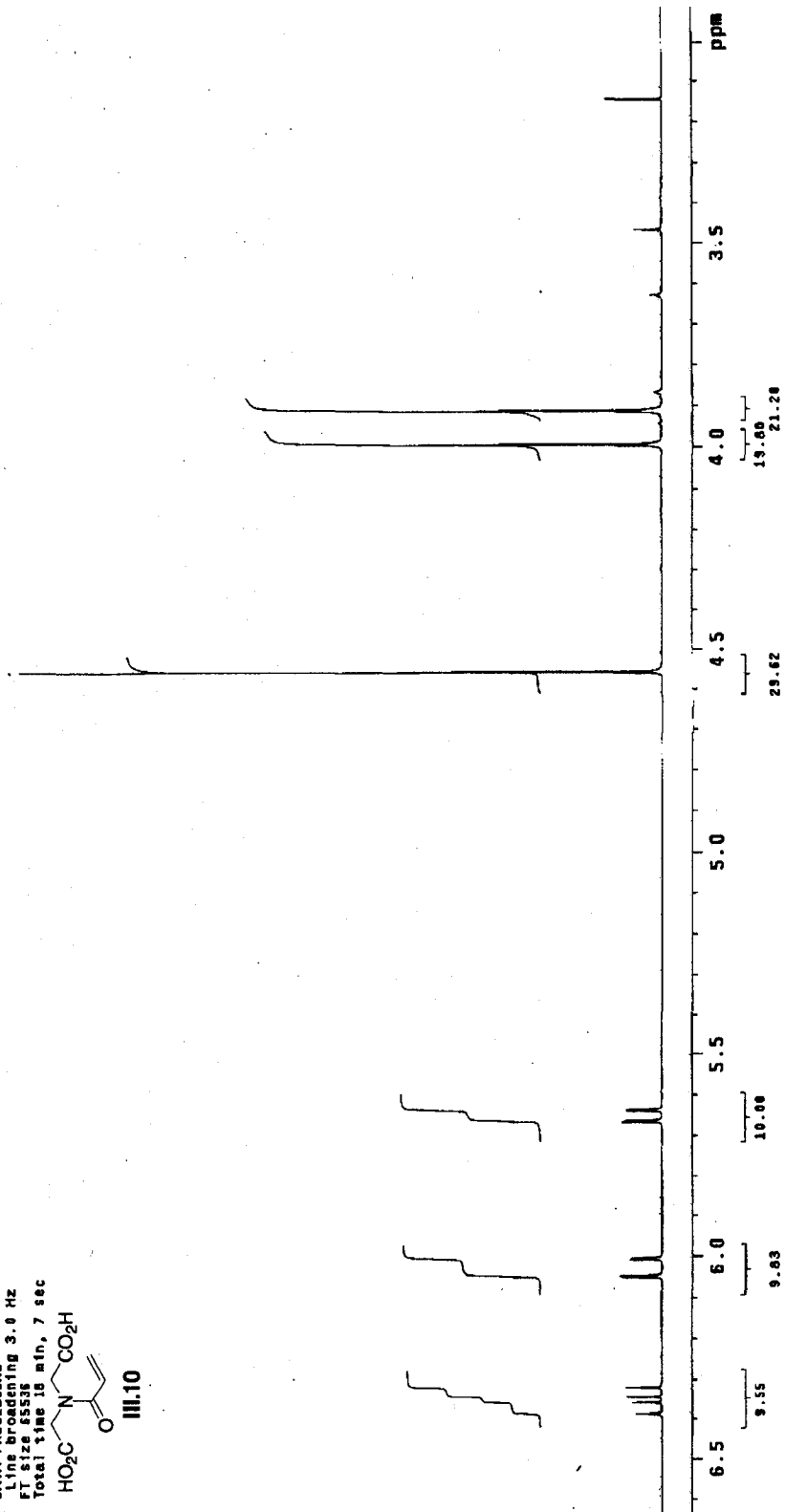
Archive directory: /export/home/kennedy/vmarsys/data
Sample directory: dk979_2_26Jun2005

Pulse Sequence: s2pul
Solvent: COCl₂
Ambient temperature
File: CARBON
Mercury-400DB "lylestation"

Relax. delay 1.000 sec
Pulse 45.0 degrees
Acq. time 1.003 sec
Width 25062.7 Hz
512 repetitions
OBSERVE C13, 100.5163504 MHz
DECOUPLE H1, 399.7509886 MHz
Power 41 dB
continuously on
JWALTZ-16 modulated
DATA PROCESSING
F1 size 65536
FT size 65536
Total time 18 min, 7 sec



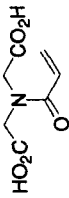
III.10



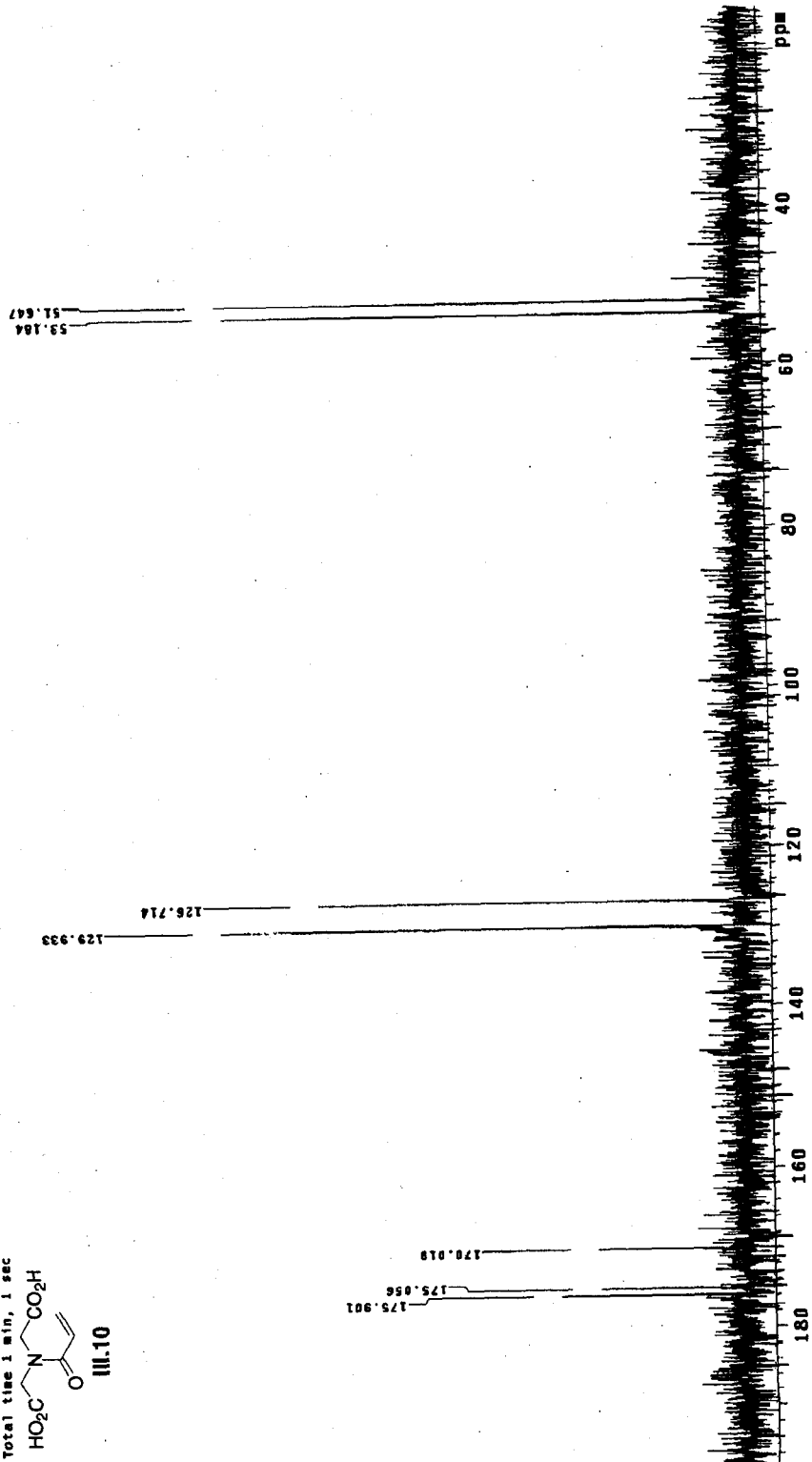
Archive directory: /export/home/kennedy/vnmr/sys/data
Sample directory: dk9/3.5_22jun788

Pulse Sequence: s2pul
Solvent: D2O
Temp: 25.8 C / 298.1 K
File: PHOTON
Mercury-400DB "lylestation"

Relax. delay 1.888 sec
Pulse 45.0 degrees
Vcd. 1135.100 sec
S. 4135.100 sec
S. 4135.100 sec
S. 4135.100 sec
OBSERVE H1 399.7589606 MHz
DATA PROCESSING
FT size 65535
Total time 1 min, 1 sec



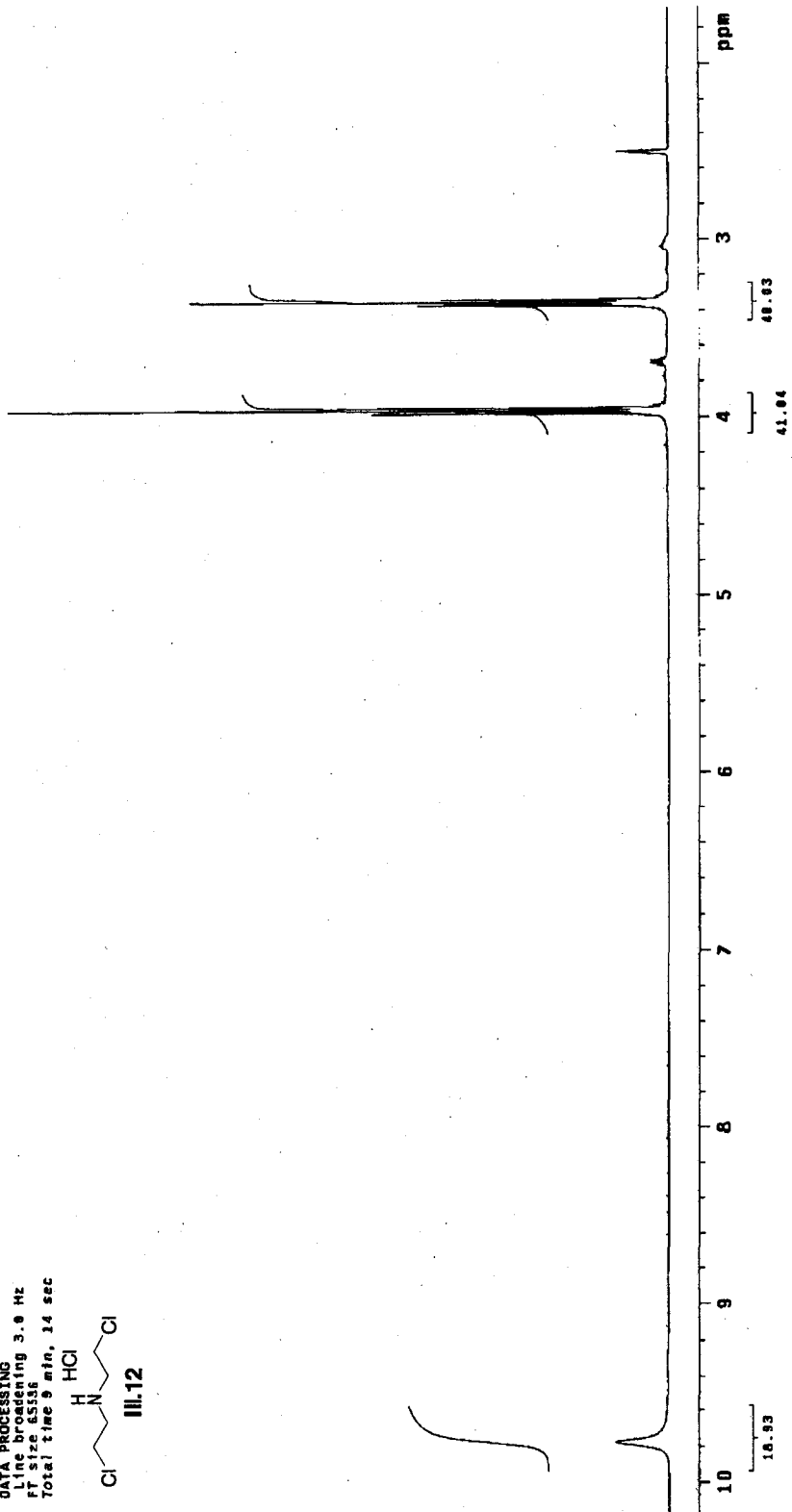
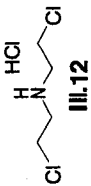
III.10



Archive directory: /export/home/kennedy/vnmrSYS/data
Sample directory: dkg73.4_22Jun86B

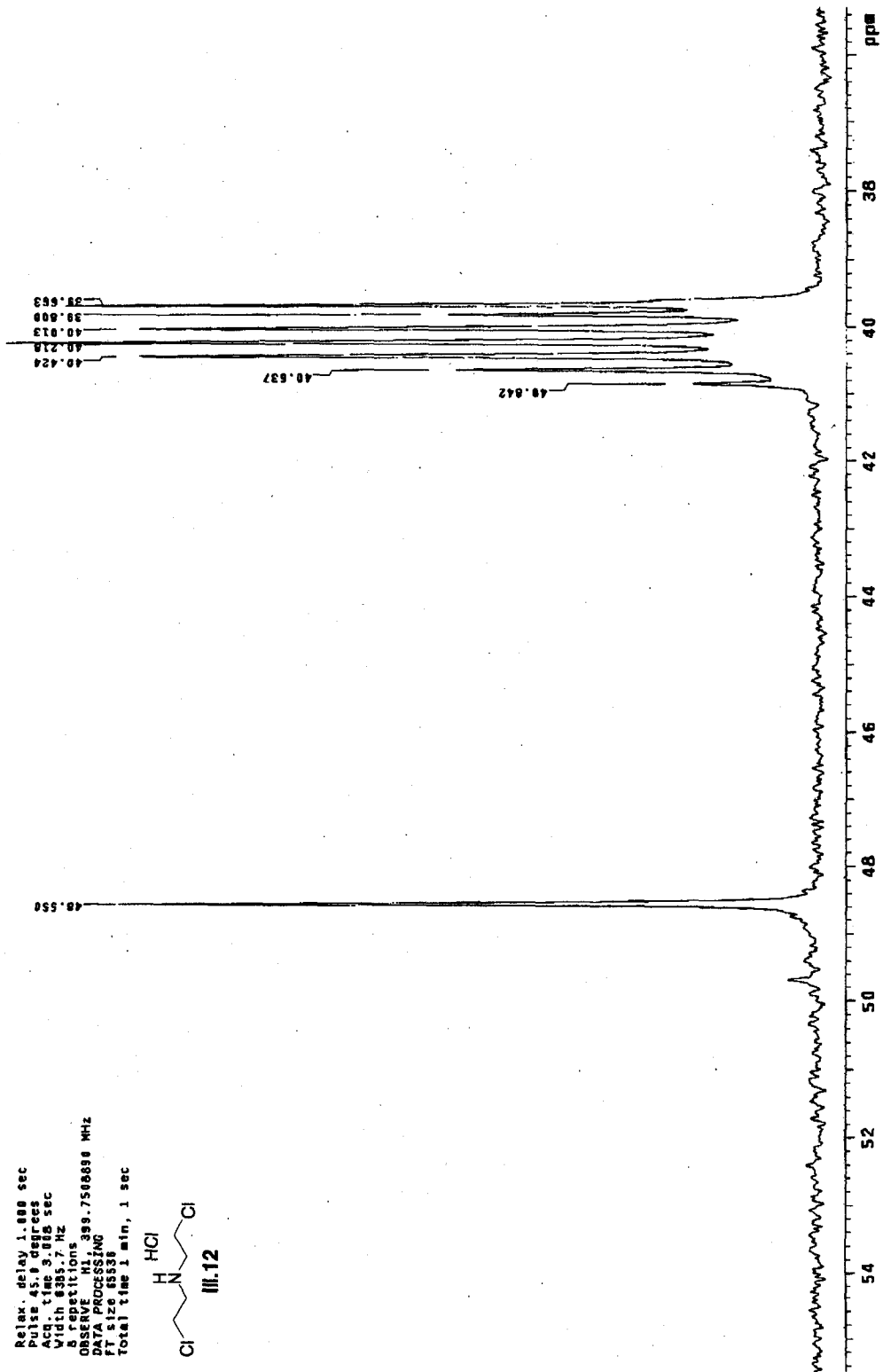
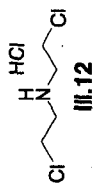
Pulse Sequence: szpul
Solvent: D2O
Temp: 25.0 C / 298.1 K
File: CARBON
Mercury-40866 "lylestation"

Relax. delay 1.000 sec
Pulse 45.0 degrees
Acq. time 1.003 sec
Width 2302.7 Hz
Observed F1 100.628100 MHz
Observed F2 517288.7 MHz
Decouple F1 399.7520162 MHz
Power 61 dB
continuously on
WALTZ-16 modulated
DATA PROCESSING
Line broadening 3.0 Hz
FT size 6556
Total time 9 min. 14 sec



Archive directory: /export/home/kennedy/vnmrSYS/data
Sample directory: ak604.1_30Jun2006

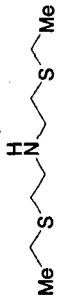
Pulse Sequence: szpu1
Solvent: DMSO
Temp: 35.0 C / 308.1 K
File: PROTON
Mercury-40888 "1ylestetion"
Relax. delay: 1.000 sec
Pulse: 45.0 degrees
Acq. time: 3.888 sec
Width: 835.7 Hz
8 repetitions
OBSERVE: H1, 399.750889 MHz
DATA PROCESSING
FT size: 65536
Total time: 1 min, 1 sec



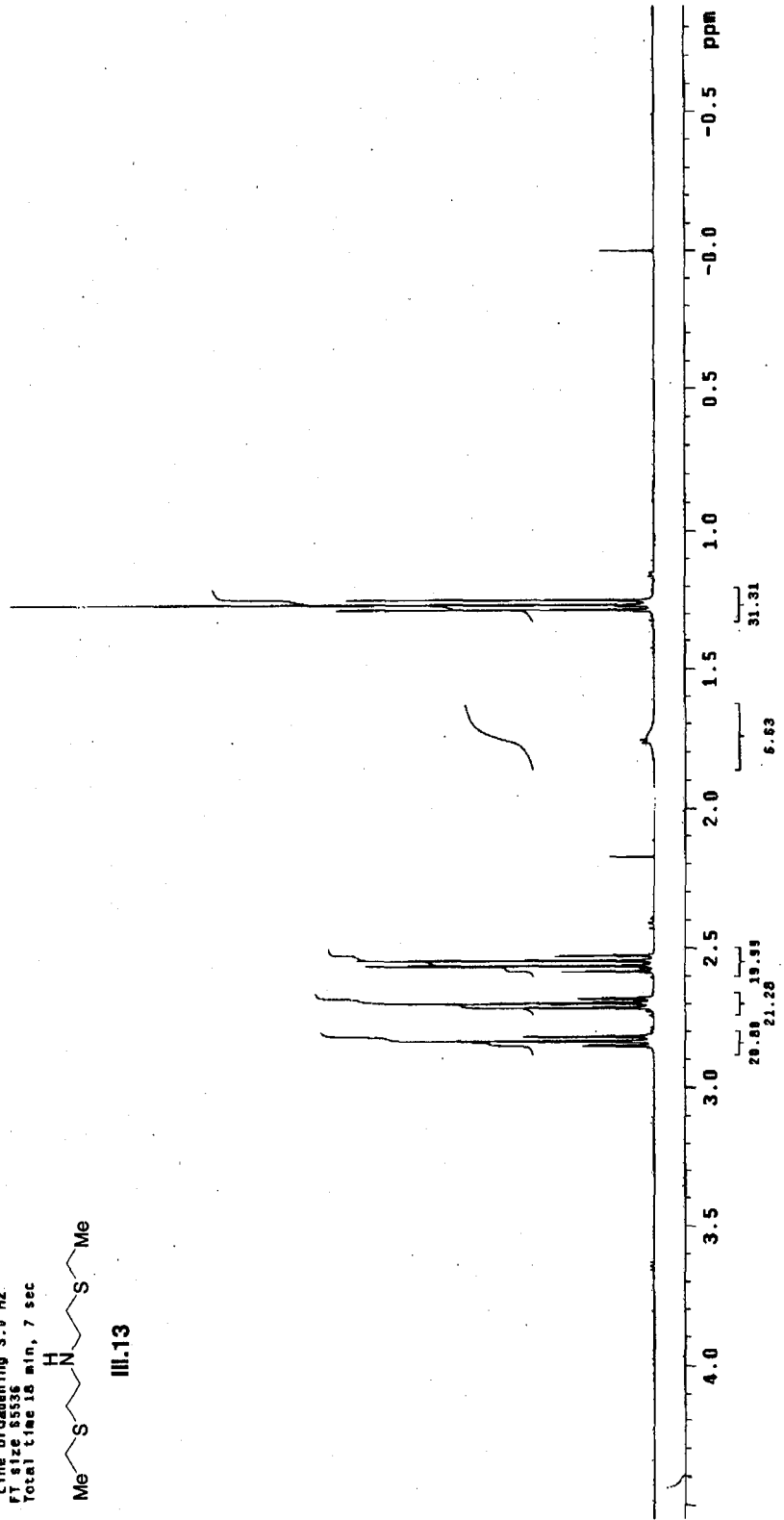
Archive directory: /export/home/kennedy/vmarsys/data
Sample directory: dkgal.2_30Jun2008

Pulse Sequence: s2pu1
Solvent: DM60
Temp: 30.0 C / 300.1 K
File: C3850M
Mercury-40000 "1ylestation"

Relax. delay 1.000 sec
Pulse 45.0 degrees
Acq. time 1.935 sec
400 MHz
256 repetitions
OBSERVE C13, 100.5174278 MHz
DECUPLE H1, 399.7528876 MHz
Power 41 dB
continuously on
WALTZ-16 modulated
DATA PROCESSING
Line broadening 3.0 Hz
FT size 5536
Total time 18 min, 7 sec



III.13



Archive directory: /export/home/kennedy/vmr/sys/data
Sample directory: dk086_1_03012006

Pulse Sequence: s2pu1

Solvent: CDCl3

Ambient temperature

File: PROTON

Mercury-40000 "lylestation"

Relax. delay 1.000 sec

Pulse 45.0 degrees

Acq. time 3.000 sec

Width 6385.7 Hz

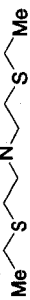
8 repetitions

OBSERVE H1, 399.7490134 MHz

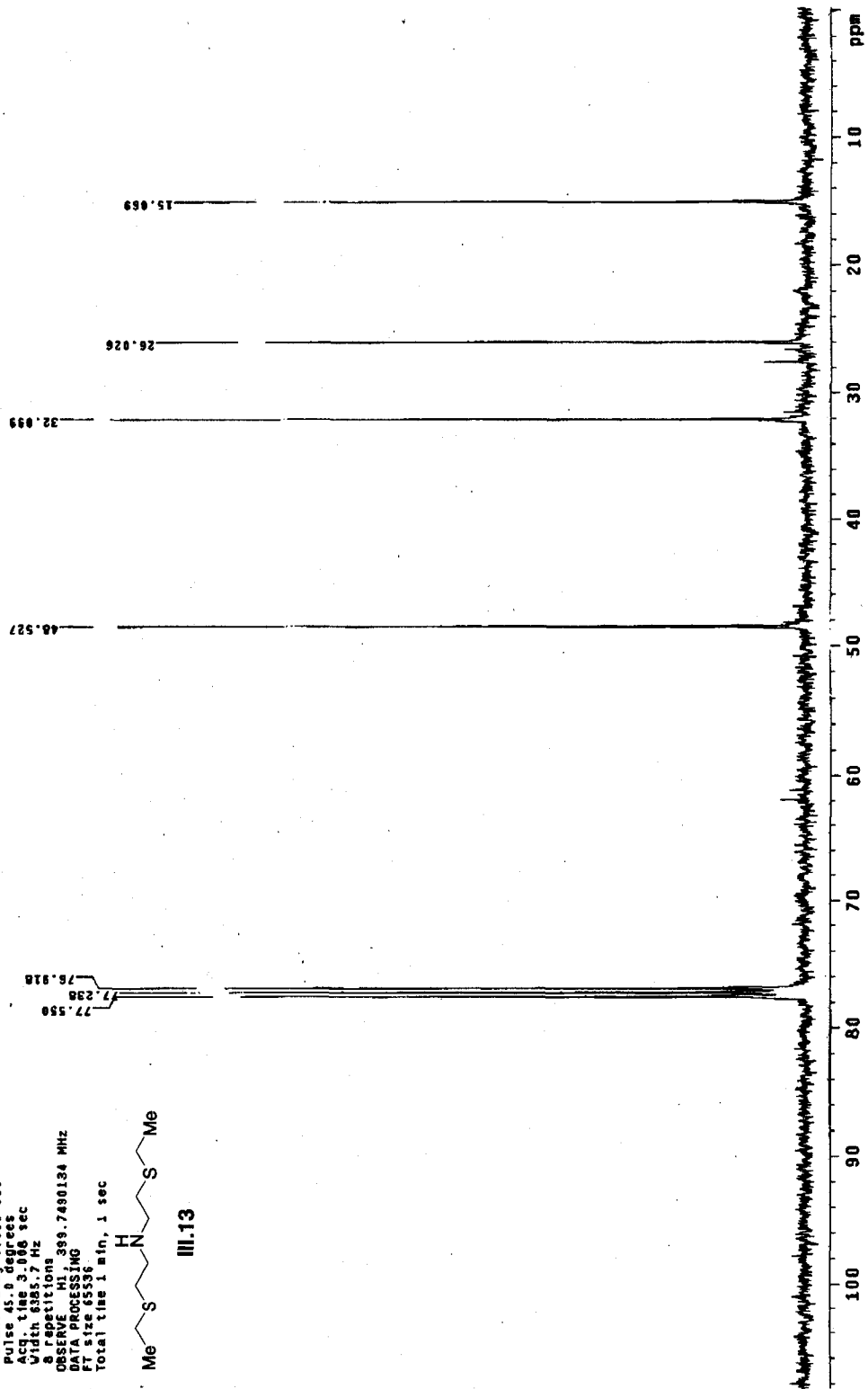
DATA PROCESSING

FT size 65536

Total time 1 min, 1 sec



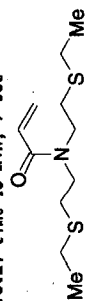
III.13



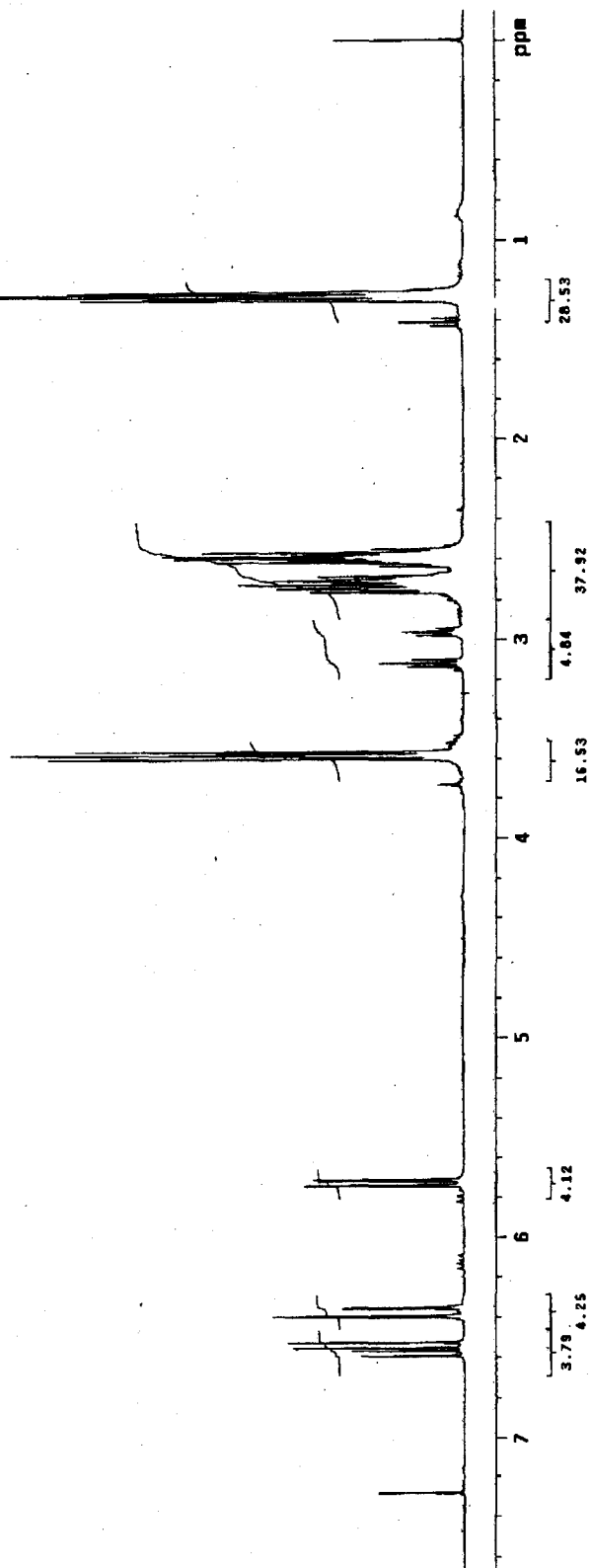
Archive directory: /export/home/kennedy/vmrsys/data
Sample directory: dk988_2_03012006

Pulse Sequence: s2pu1
Solvent: CDCl3
Ambient temperature
File: CAG80M "lytestation"

Relax. delay 1.000 sec
Pulse 45.0 degrees
Acq. time 1.903 sec
Width 23862.7 Hz
S12 repetitions
OBSERVE CH3, 100.5165594 MHz
DECOUPLE H1, 399.7509866 MHz
Power 81 dB
Spectrum on
VATZ microcalculated
DATA PROCESSING
Line broadening 3.0 Hz
FT size 65536
Total time 18 min, 7 sec



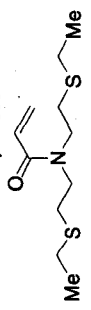
III.14



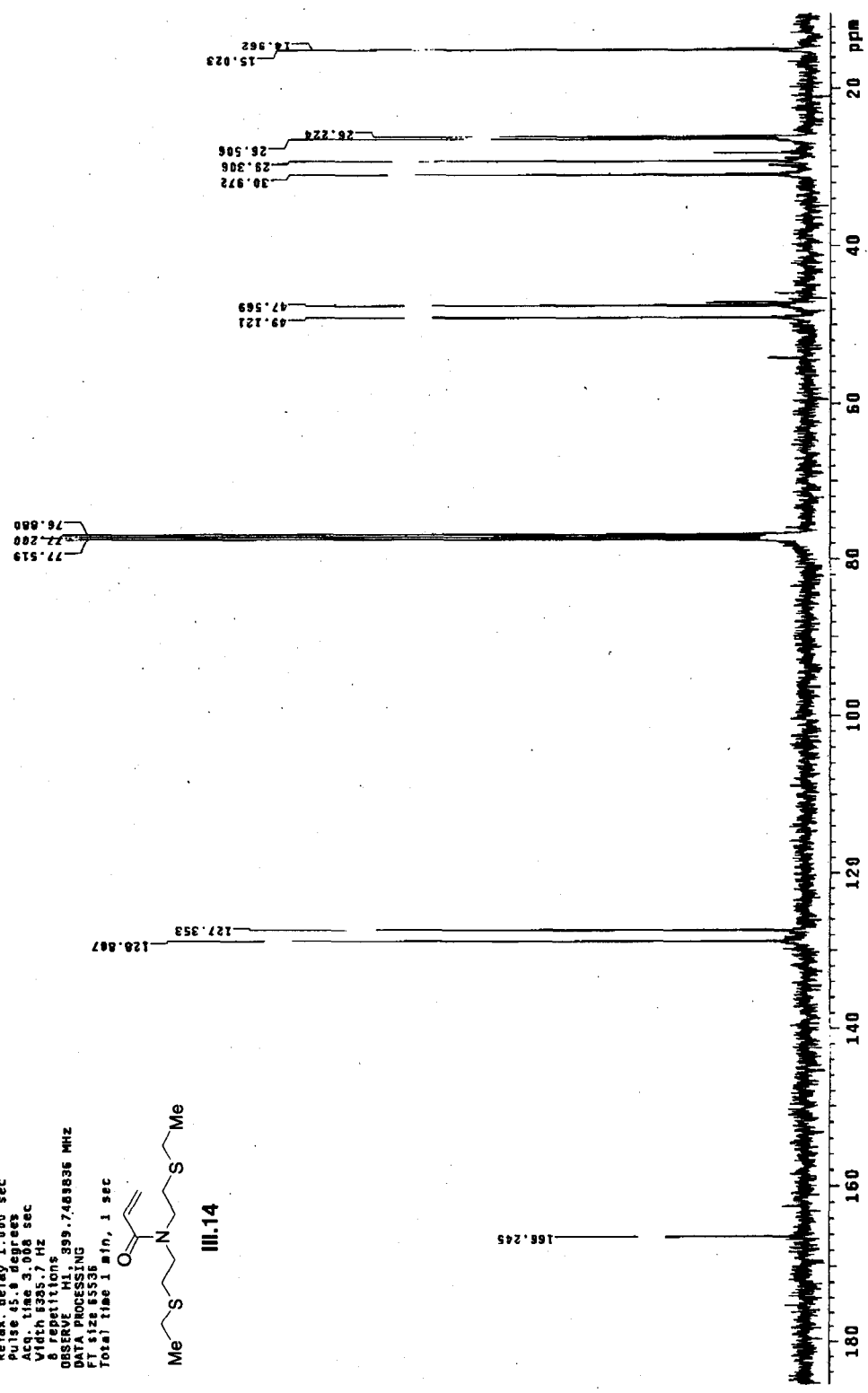
Archive directory: /export/home/kennedy/vnarsys/data
Sample directory: dk988.1_643072895

Pulse Sequence: s2pul
Solvent: CDCl3
Ambient temperature
File: PHOTON
Mercury-48888 "lylestation"

Relax. delay 1.000 sec
Pulse 45.0 degrees
Acq. time 3.008 sec
Width 5385.7 Hz
8 repetitions
OBSERVE HI, 399.7488836 MHz
DATA PROCESSING
F1 size 83536
Total time 1 min, 1 sec



III.14



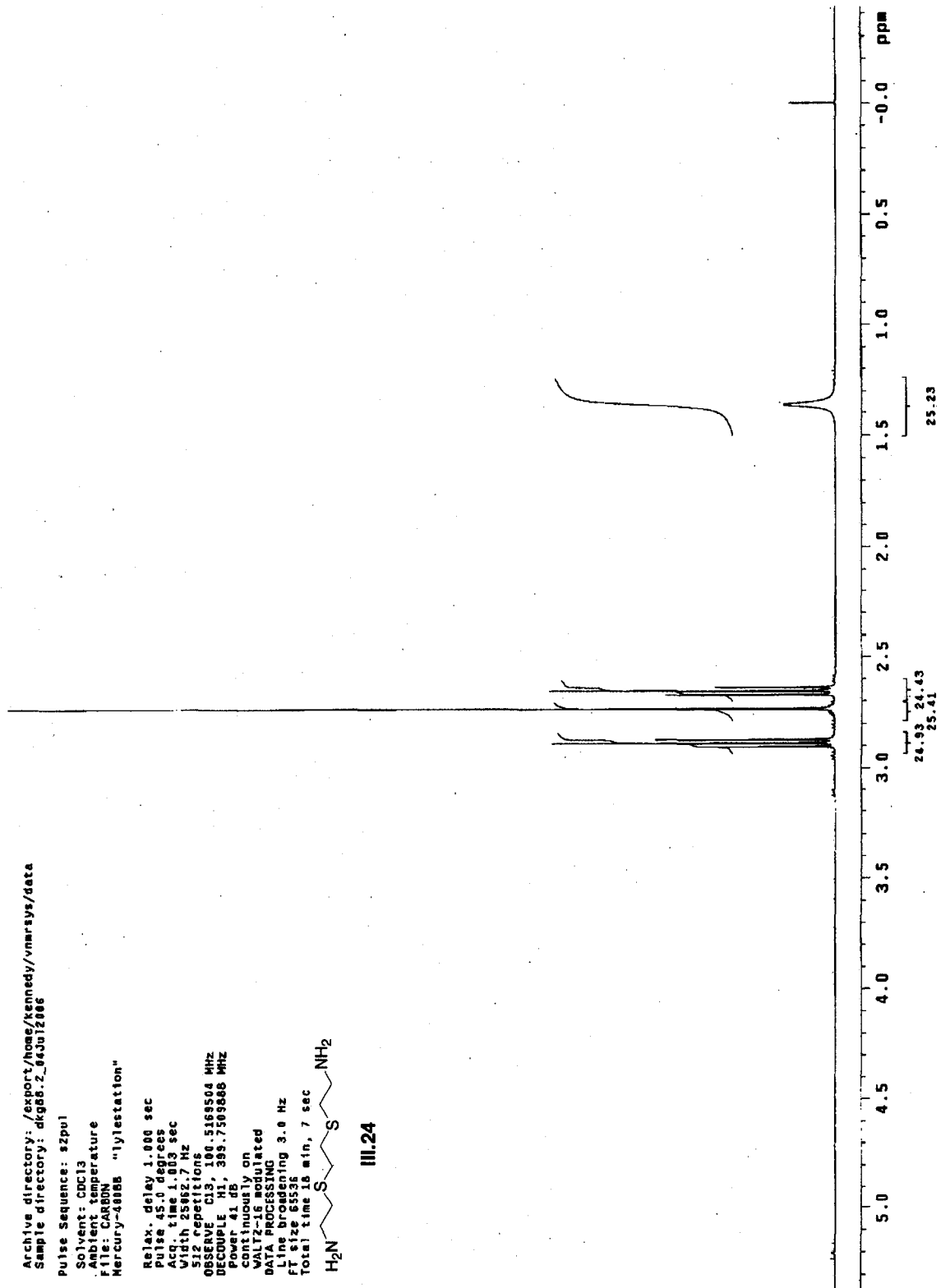
Archive directory: /export/home/kennedy/vmrays/data
Sample directory: dkg88.2_643u208

Pulse Sequence: szpul
Solvent: CDC13
Acq time: 1.003 sec
File: CARBON
Mercury-400BB "lylestation"

Relax. delay: 1.000 sec
Pulse: 0.0 deg, 0.0 sec
Acq. time: 1.003 sec
Width: 25462.7 Hz
512 repetitions
OBSERVE C13, 100.5169504 MHz
DECUPLE H1, 399.7509865 MHz
Power: 41 dB
continuously on
WALTZ-16 modulated
DATA PROCESSING
Line broadening: 3.0 Hz
FT size: 65536
Total time: 26 min, 7 sec



III.24



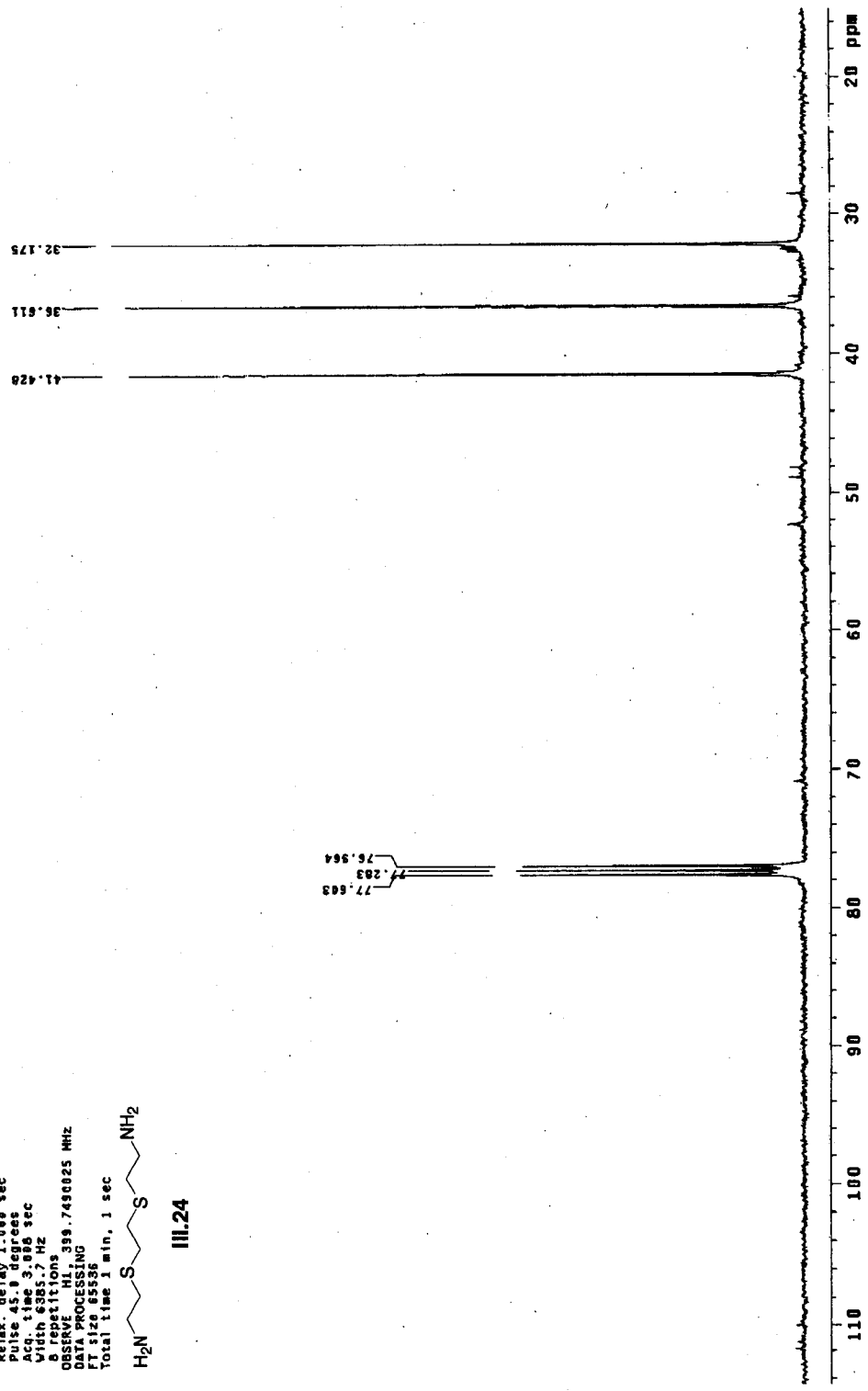
Archive directory: /export/home/kennedy/vmrssys/data
Sample directory: dk329_1_19May2007

Pulse Sequence: s2pu1
Solvent: CDCl3
File Name: Temperature
File Path: /P01008
Mercury-40086 "Iylestation"

Relax. delay 1.000 sec
Pulse AS 8 degrees
Acc. time 3.000 sec
Width 8385.7 Hz
0 repetitions
OBSERVE H1, 399.749025 MHz
DATA PROCESSING
FT size 65536
Total time 1 min, 1 sec



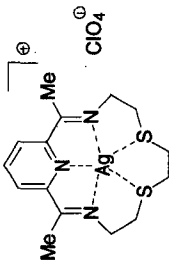
III.24



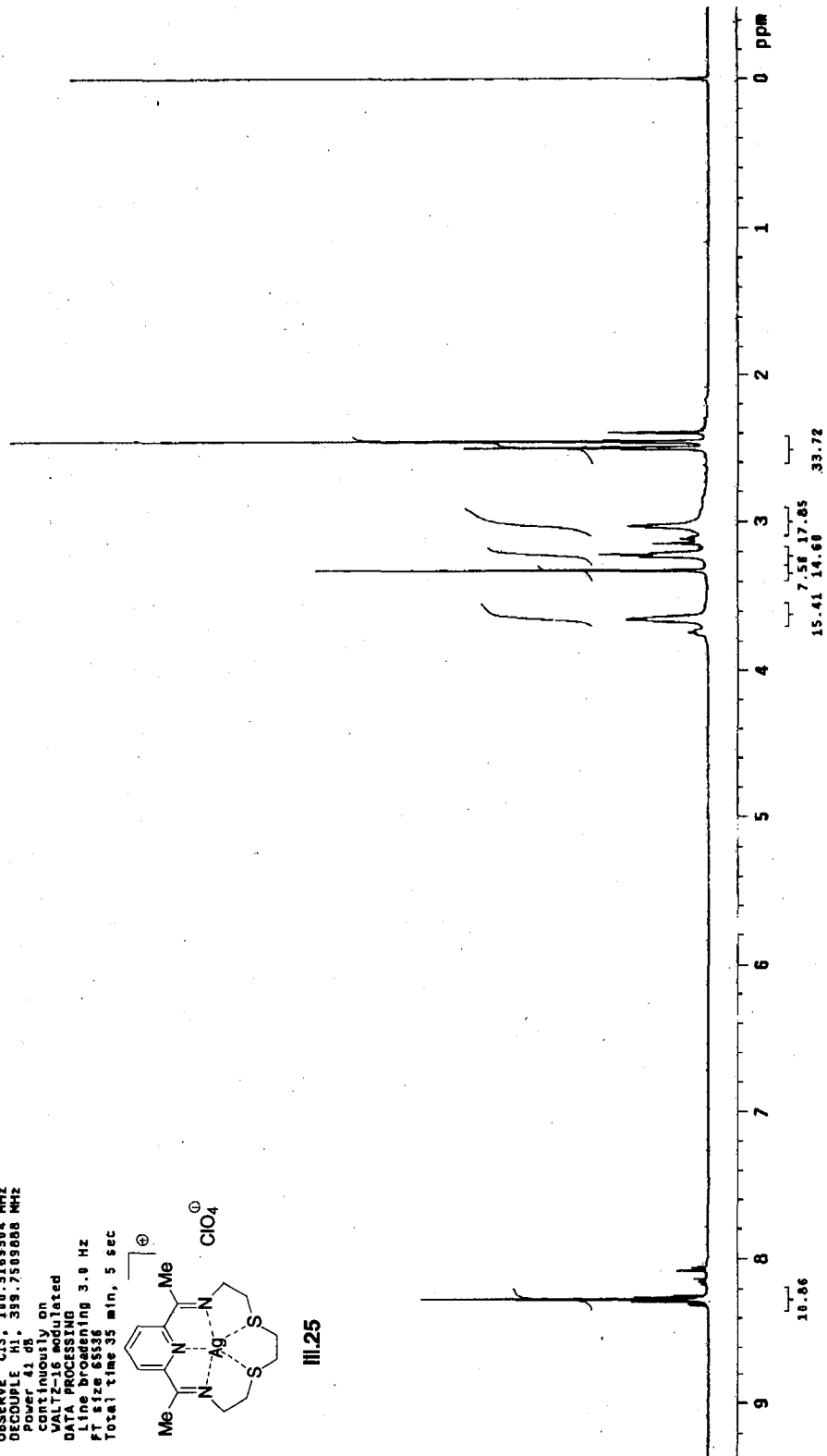
Archive directory: /export/home/kennedy/vmrcs/data
Sample directory: dkj29.2_10May2007

Pulse Sequence: s2pu1
Solvent: CDCl3
Ambient temperature
File: CARBON
Mercury-4918B "jylestation"

Relax. delay 1.000 sec
Pulse 45.0 degrees
Acq. time 1.003 sec
Width 25062.7 Hz
1000 repetitions
OBSERVE C13, 100.5169504 MHz
DECOUPLE H1, 399.7509086 MHz
Power 41 dB
continuously on
WALTZ-16 modulated
DATA PROCESSING
F1 size 65536
F2 size 65536
Total time 35 min, 5 sec



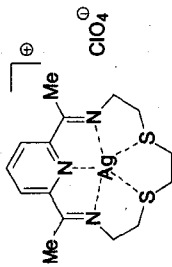
III.25



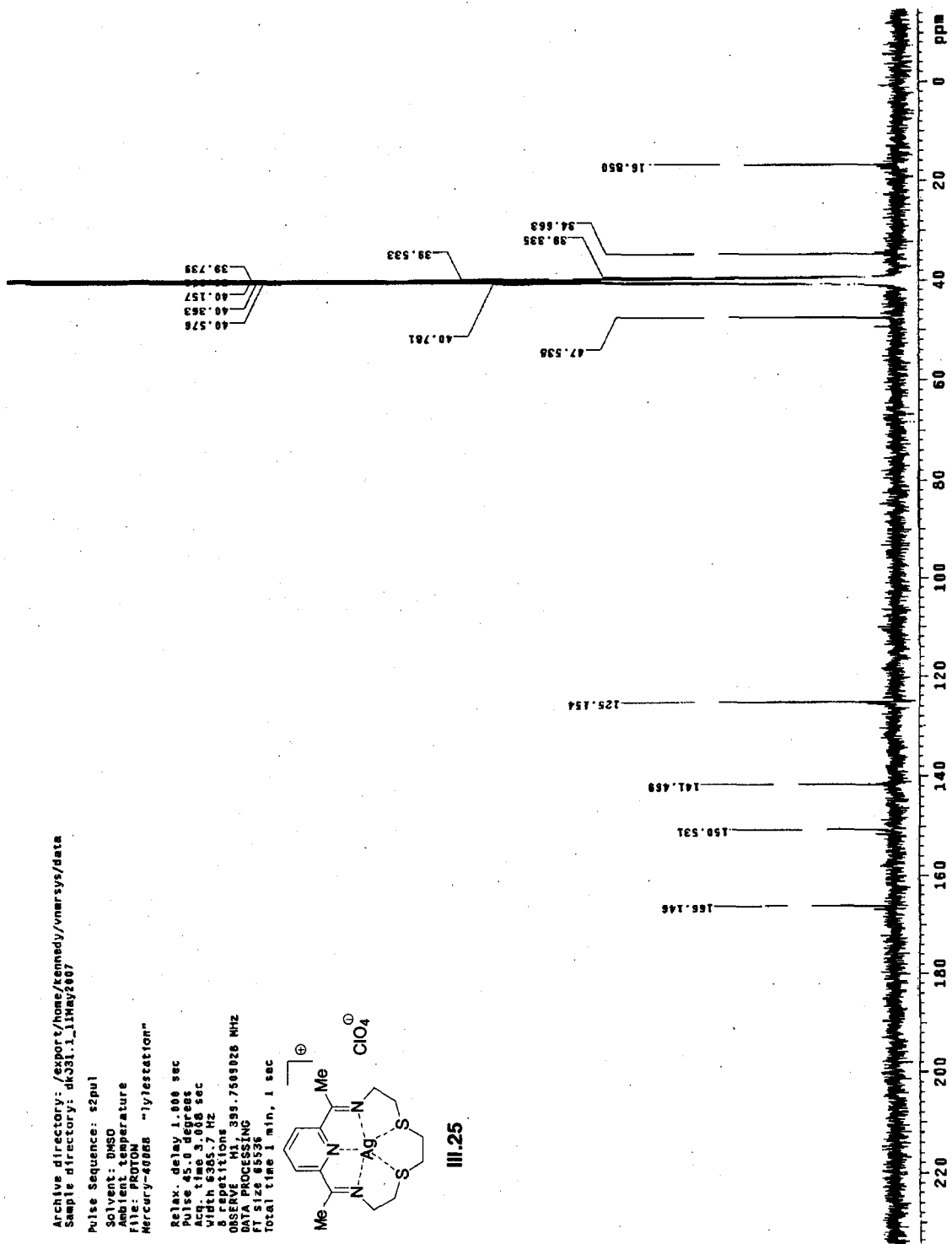
Archive directory: /export/home/kennedy/vnmrsys/data
Sample directory: dk331_1_11May2007

Pulse Sequence: s2pul
Solvent: DMSO
Ambient temperature
File: PROTON
Mercury-400BB "lytestation"

Relax. delay 1.000 sec
Pulse 45.0 degrees
Pulse width 12.000 sec
Pulse delay 1.000 sec
Sweep rate 435.7 MHz
S repetitions
OBSERVE H1 399.7509028 MHz
DATA PROCESSING
FT size 65536
Total time 1 min, 1 sec



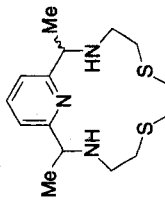
III.25



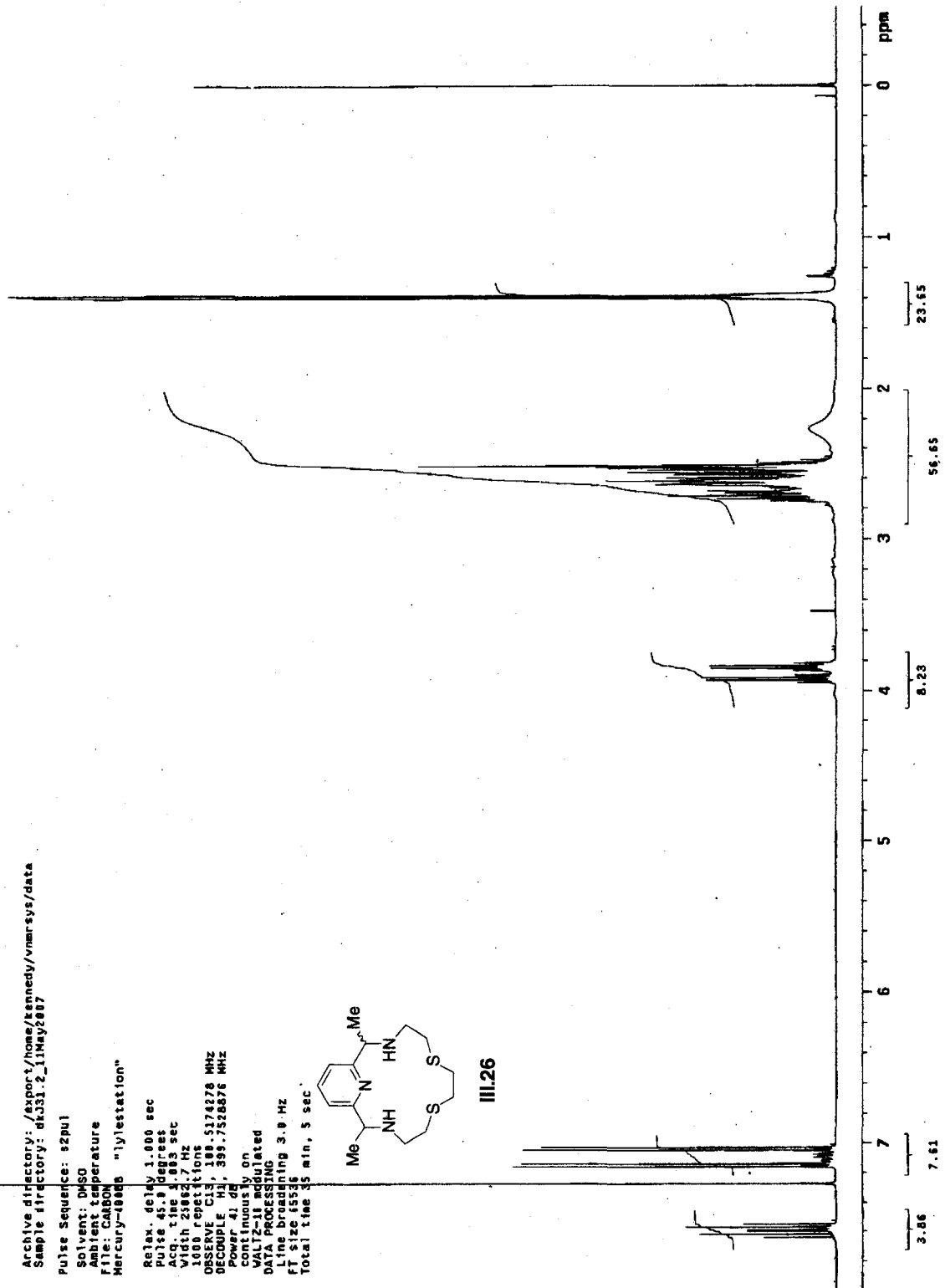
Archive directory: /export/home/kennedy/vnmr/sys/data
Sample directory: dk331.2_11May2007

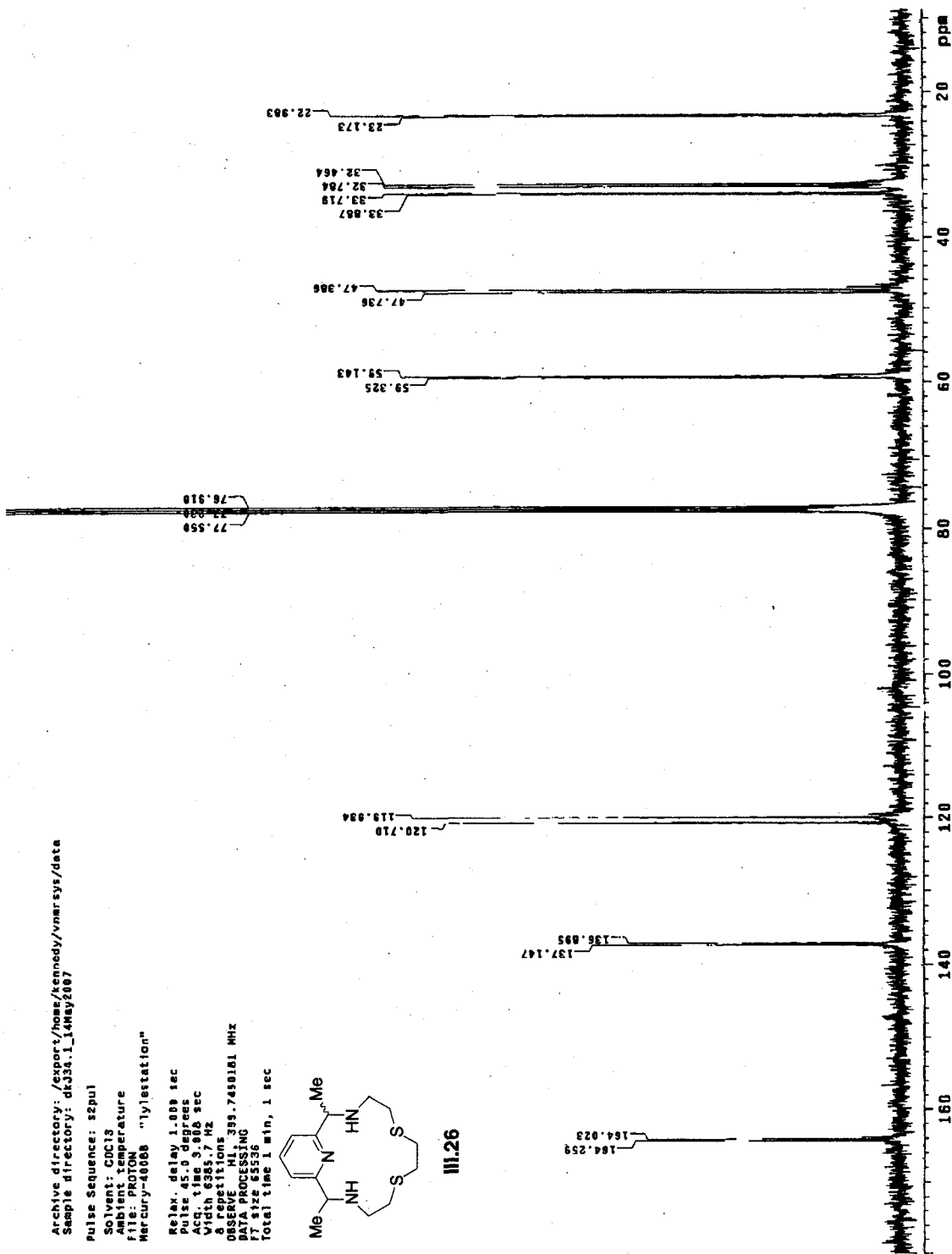
Pulse Sequence: szpu1
Solvent: DMSO
Ambient temperature
File: CARBON
Mercury-100dB "1ylestation"

Relax. delay 1.000 sec
Pulse 45.0 degrees
Acq. time 3.003 sec
Width 25882.7 Hz
1000 repetitions
OBSERVE Ch1, 100.6174278 MHz
DECOUPLE Ch2, 399.7328876 MHz
coupling on
continuously
VOLTAGE II regulated
DATA PROCESSING
Line broadening 3.0 Hz
FT size 45536
Total time 35 min, 5 sec



III.26

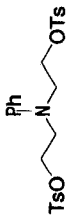




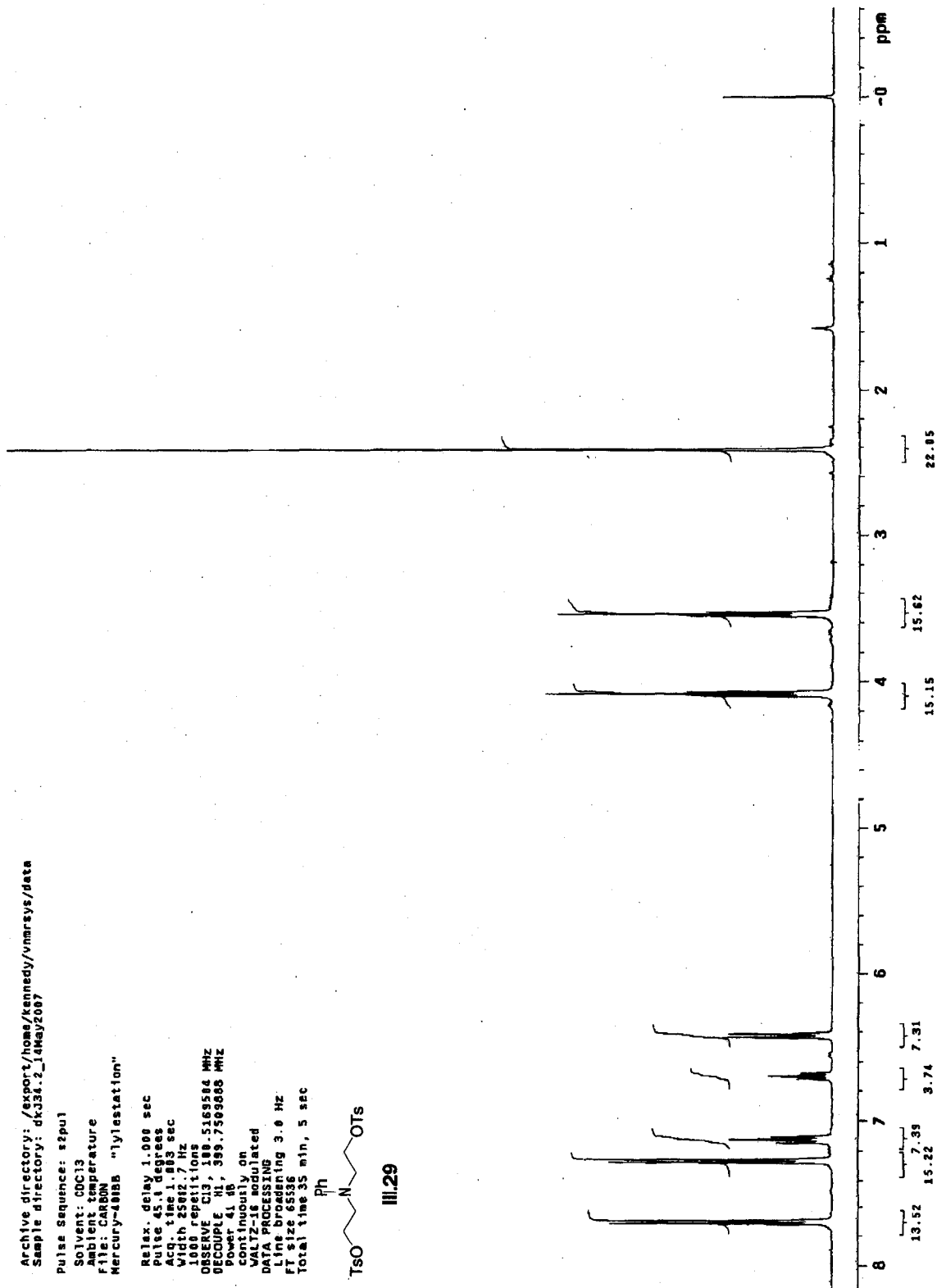
Archive directory: /export/home/kennedy/vnmr.sys/data
Sample directory: dk334.2_14May2007

Pulse Sequence: szpul
Solvent: CDCl3
Acquire Temperature
File: CARBON
Mercury-400B "Jytestation"

Relax. delay 1.000 sec
Pulse 45.1 degrees
Width 2592.7 Hz
1000 repetitions
OBSERVE C13 100.516584 MHz
DECUPLE H1 399.750868 MHz
Power 41 dB
continuously on
WALTZ-16 modulated
DATA PROCESSING
Line broadening 3.0 Hz
FT size 65536
Total time 35 min, 5 sec



III.29



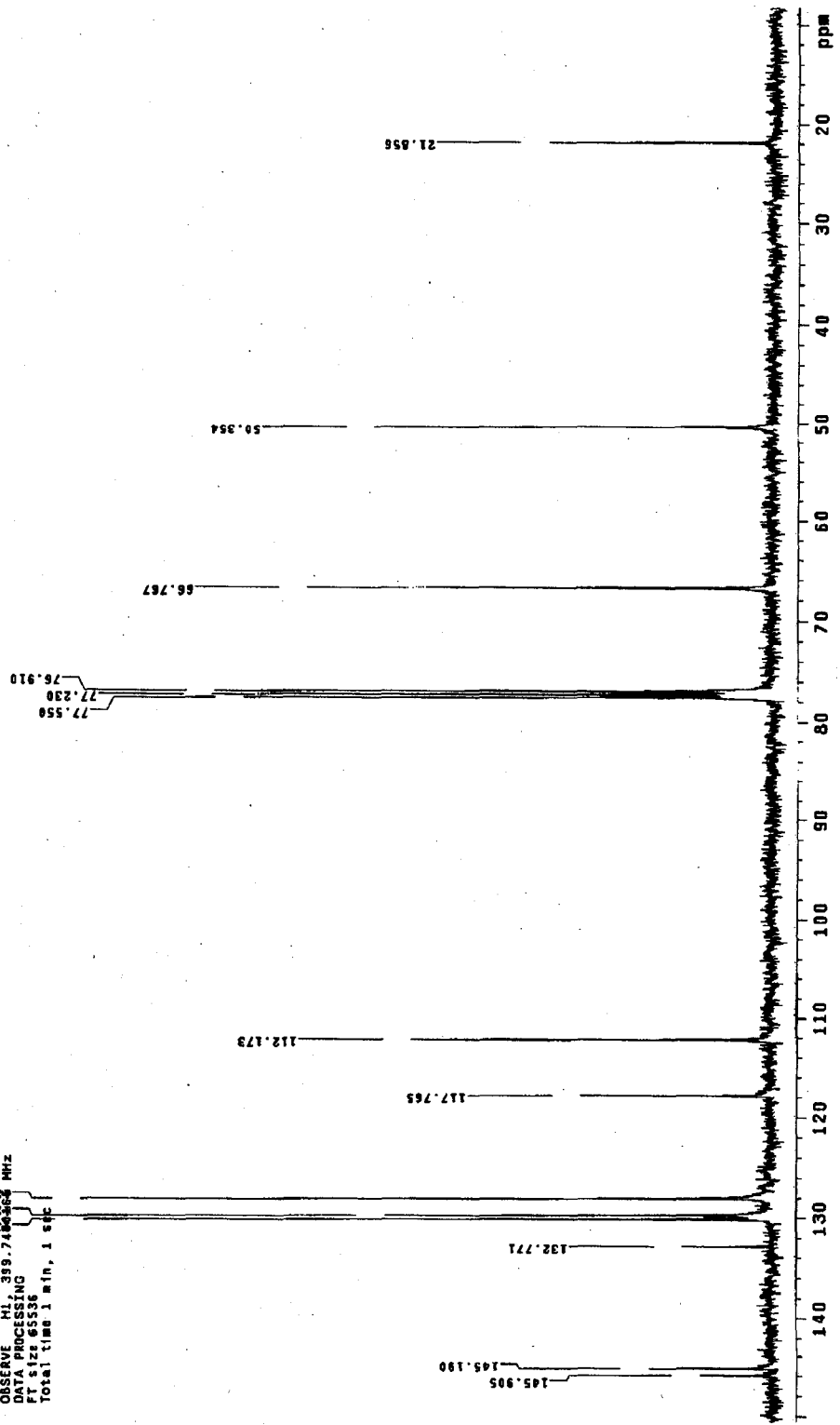
Archive directory: /export/home/kennedy/vmrsys/data
 Sample directory: dk342.1_86Jun287

Pulse Sequence: szpu1
 Solvent: CDCl3
 Ambient temperature
 File: PROTON
 Mercury-4000B "lylestation"



III.29

Relax. delay 1.000 sec
 Pulse 45.0 degrees
 Acq. time 3.986 sec
 Width 8385.7 Hz
 # repetitions 6
 OBSERVED F2 399.7400000 MHz
 PROCESSOR 1
 FT 165534
 Total time 1 min, 1 sec

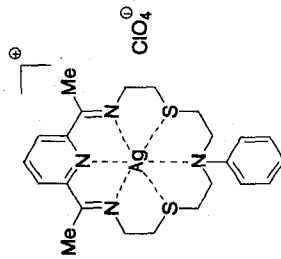


Archive directory: /export/home/kennedy/vnarsys/data
 Sample directory: dk345_1_25Jun2007
 File: PROTON

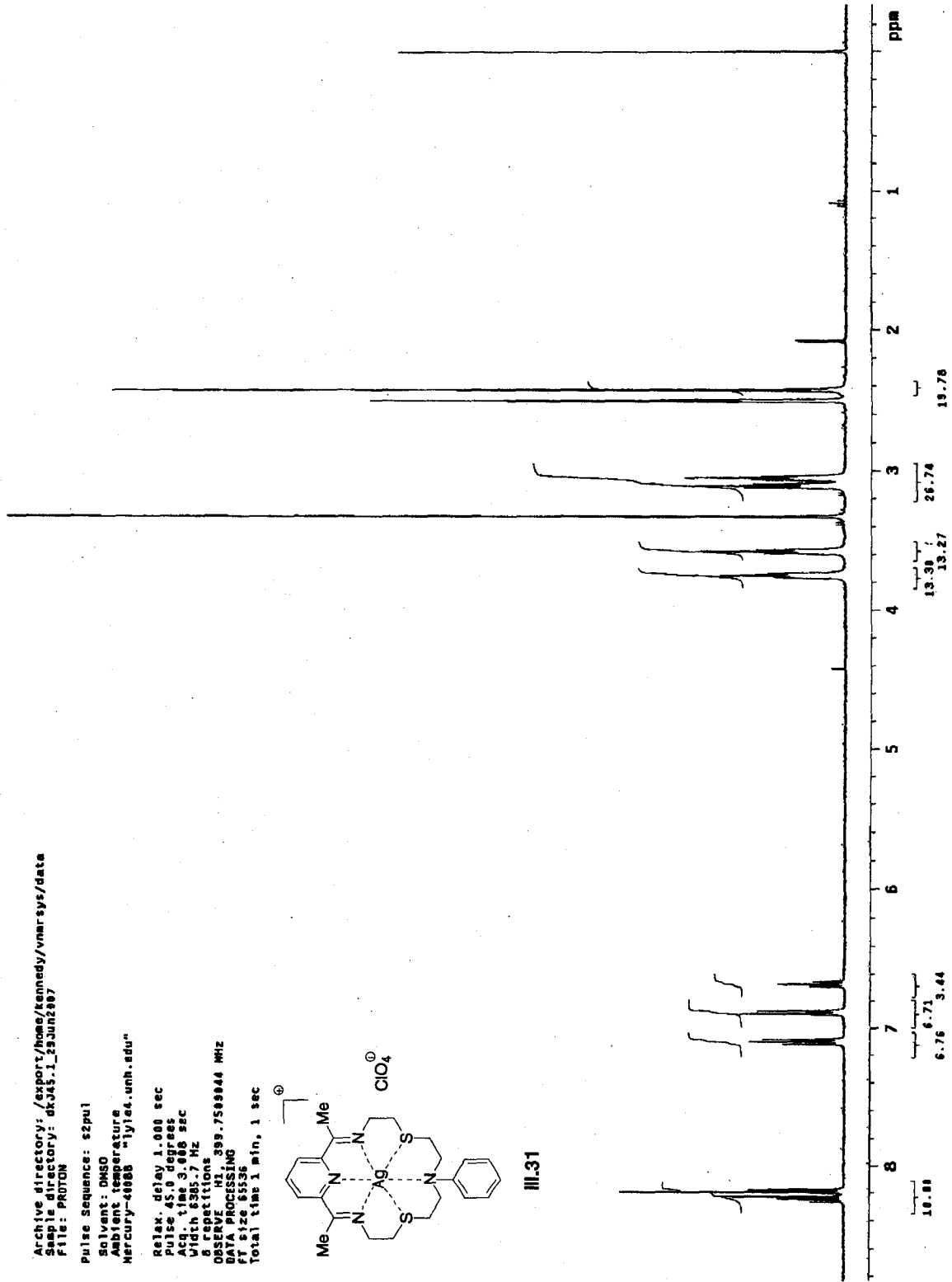
Pulse Sequence: s2pu1

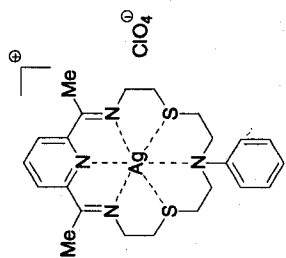
Solvent: DMSO
 Ambient temperature
 Mercury-40000 "lyfak.unh.edu"

Relax. delay 1.000 sec
 Pulse 45.0 degrees
 Acq. time 3.000 sec
 Width 6365.7 Hz
 8 repetitions
 OBSERVE Hz: 399.7589044 MHz
 DATA PROCESSING
 F1 size 65736
 Total time 1 min, 1 sec



III-31





III.31

